

SPRINGER SERIES ON FLUORESCENCE

09

Series Editor O. S. Wolfbeis

Volume Editor A. P. Demchenko

Advanced Fluorescence Reporters in Chemistry and Biology II

Molecular Constructions, Polymers
and Nanoparticles

 Springer

9

Springer Series on Fluorescence

Methods and Applications

Series Editor: O.S. Wolfbeis

For further volumes:
<http://www.springer.com/series/4243>

Springer Series on Fluorescence

Series Editor: O.S. Wolfbeis

Recently Published and Forthcoming Volumes

Advanced Fluorescence Reporters in Chemistry and Biology II

Molecular Constructions, Polymers and Nanoparticles

Volume Editor: A.P. Demchenko

Vol. 9, 2010

Advanced Fluorescence Reporters in Chemistry and Biology I

Fundamentals and Molecular Design

Volume Editor: A.P. Demchenko

Vol. 8, 2010

Lanthanide Luminescence

Photophysical, Analytical and Biological Aspects

Volume Editors: P. Hänninen and H. Härmä

Vol. 7

Standardization and Quality Assurance in Fluorescence Measurements II

Bioanalytical and Biomedical Applications

Volume Editor: Resch-Genger, U.

Vol. 6, 2008

Standardization and Quality Assurance in Fluorescence Measurements I

Techniques

Volume Editor: U. Resch-Genger

Vol. 5, 2008

Fluorescence of Supermolecules, Polymeres, and Nanosystems

Volume Editor: M.N. Berberan-Santos

Vol. 4, 2007

Fluorescence Spectroscopy in Biology

Volume Editor: M. Hof

Vol. 3, 2004

Fluorescence Spectroscopy, Imaging and Probes

Volume Editor: R. Kraayenhof

Vol. 2, 2002

New Trends in Fluorescence Spectroscopy

Volume Editor: B. Valeur

Vol. 1, 2001

Advanced Fluorescence Reporters in Chemistry and Biology II

Molecular Constructions, Polymers and Nanoparticles

Volume Editor: Alexander P. Demchenko

With contributions by

G. Bergamini · S.M. Borisov · P. Ceroni · J. Chen ·
A.P. Demchenko · A.B. Descalzo · I. Díez · T. Fischer ·
M. Grabolle · M.A. Habeeb Muhammed · Y. Jin · C.L. John ·
I. Klimant · O.P. Klochko · S. Liang · B. Liu · M.Yu.
Losytskyy · E. Marchi · T. Mayr · G. Mistlberger · T. Nann ·
R. Nilsson · R. Nitschke · L.D. Patsenker · K. Peter ·
T. Pradeep · K.-Y. Pu · R.H.A. Ras · U. Resch-Genger ·
M.A. Reppy · K. Rurack · R.A. Simon · W. Tan ·
A.L. Tatarets · E.A. Terpetschnig · S. Xu · V.M. Yashchuk ·
H. Yao · Q. Yuan · J.X. Zhao · S. Zhu

Volume Editor

Prof. Dr. Alexander P. Demchenko
Palladin Institute of Biochemistry
National Academy of Sciences of Ukraine
Kyiv 01601
Ukraine
alexdem@ukr.net

ISSN 1617-1306

e-ISSN 1865-1313

ISBN 978-3-642-04699-5

e-ISBN 978-3-642-04701-5

DOI 10.1007/978-3-642-04701-5

Springer Heidelberg Dordrecht London New York

Library of Congress Control Number: 2010934374

© Springer-Verlag Berlin Heidelberg 2010

This work is subject to copyright. All rights are reserved, whether the whole or part of the material is concerned, specifically the rights of translation, reprinting, reuse of illustrations, recitation, broadcasting, reproduction on microfilm or in any other way, and storage in data banks. Duplication of this publication or parts thereof is permitted only under the provisions of the German Copyright Law of September 9, 1965, in its current version, and permission for use must always be obtained from Springer. Violations are liable to prosecution under the German Copyright Law.

The use of general descriptive names, registered names, trademarks, etc. in this publication does not imply, even in the absence of a specific statement, that such names are exempt from the relevant protective laws and regulations and therefore free for general use.

Cover design: WMXDesign GmbH, Heidelberg, Germany

Printed on acid-free paper

Springer is part of Springer Science+Business Media (www.springer.com)

Series Editor

Prof. Dr. Otto S. Wolfbeis

Institute of Analytical Chemistry

Chemo- and Biosensors

University of Regensburg

93040 Regensburg

Germany

otto.wolfbeis@chemie.uni-regensburg.de

Aims and Scope

Fluorescence spectroscopy, fluorescence imaging and fluorescent probes are indispensable tools in numerous fields of modern medicine and science, including molecular biology, biophysics, biochemistry, clinical diagnosis and analytical and environmental chemistry. Applications stretch from spectroscopy and sensor technology to microscopy and imaging, to single molecule detection, to the development of novel fluorescent probes, and to proteomics and genomics. The *Springer Series on Fluorescence* aims at publishing state-of-the-art articles that can serve as invaluable tools for both practitioners and researchers being active in this highly interdisciplinary field. The carefully edited collection of papers in each volume will give continuous inspiration for new research and will point to exciting new trends.

Preface

A variety of fluorescent and luminescent materials in the form of molecules, their complexes, and nanoparticles are available for implementation as reporting units into sensing technologies. Increasing demands from these application areas require development of new fluorescence reporters based on association and aggregation of fluorescence dyes and on their incorporation into different nanostructures. Interactions between these dyes and their incorporating matrices lead to new spectroscopic effects that can be actively used for optimizing the sensor design. One of these effects is a spectacular formation of J-aggregates with distinct and very sharp excitation and emission bands. By incorporation into nanoparticles, organic dyes offer dramatically increased brightness together with improvement of chemical stability and photostability. Moreover, certain dyes can form nanoparticles themselves so that their spectroscopic properties are improved. Semiconductor quantum dots are the other type of nanoparticles that possess unique and very attractive photophysical and spectroscopic properties. Many interesting and not fully understood phenomena are observed in clusters composed of only several atoms of noble metals. In conjugated polymers, strong electronic conjugation between elementary chromophoric units results in dramatic effects in quenching and in conformation-dependent spectroscopic behavior.

Possessing such powerful and diverse arsenal of tools, we have to explore them in novel sensing and imaging technologies that combine increased brightness and sensitivity in analyte detection with simplicity and low cost of production. The present book overviews the pathways for achieving this goal. In line with the discussion on monomeric fluorescence reporters in the accompanying book (Vol. 8 of this series), an insightful analysis of photophysical mechanisms behind the fluorescence response of composed and nanostructured materials is made. Based on the progress in understanding these mechanisms, their realization in different chemical structures is overviewed.

Demonstrating the progress in an interdisciplinary field of research and development, this book is primarily addressed to specialists with different background – physicists, organic and analytical chemists, and photochemists – to those who develop and apply new fluorescence reporters. It will also be useful to specialists in bioanalysis and biomedical diagnostics.

Kyiv, Ukraine
June 2010

Alexander P. Demchenko

Contents

Part I General Aspects

Nanocrystals and Nanoparticles Versus Molecular Fluorescent Labels as Reporters for Bioanalysis and the Life Sciences: A Critical Comparison	3
Ute Resch-Genger, Markus Grabolle, Roland Nitschke, and Thomas Nann	
Optimization of the Coupling of Target Recognition and Signal Generation	41
Ana B. Descalzo, Shengchao Zhu, Tobias Fischer, and Knut Rurack	
Collective Effects Influencing Fluorescence Emission	107
Alexander P. Demchenko	

Part II Encapsulated Dyes and Supramolecular Constructions

Fluorescent J-Aggregates and Their Biological Applications	135
Mykhaylo Yu. Losytskyy and Valeriy M. Yashchuk	
Conjugates, Complexes, and Interlocked Systems Based on Squaraines and Cyanines	159
Leonid D. Patsenker, Anatoliy L. Tatars, Oleksii P. Klochko, and Ewald A. Terpetschnig	

Part III Dye-Doped Nanoparticles and Dendrimers

Dye-Doped Polymeric Particles for Sensing and Imaging	193
Sergey M. Borisov, Torsten Mayr, Günter Mistlberger, and Ingo Klimant	

Silica-Based Nanoparticles: Design and Properties	229
Song Liang, Carrie L. John, Shuping Xu, Jiao Chen, Yuhui Jin, Quan Yuan, Weihong Tan, and Julia X. Zhao	
Luminescent Dendrimers as Ligands and Sensors of Metal Ions	253
Giacomo Bergamini, Enrico Marchi, and Paola Ceroni	
Prospects for Organic Dye Nanoparticles	285
Hiroshi Yao	
Part IV Luminescent Metal Nanoclusters	
Few-Atom Silver Clusters as Fluorescent Reporters	307
Isabel Díez and Robin H.A. Ras	
Luminescent Quantum Clusters of Gold as Bio-Labels	333
M.A. Habib Muhammed and T. Pradeep	
Part V Conjugated Polymers	
Structure, Emissive Properties, and Reporting Abilities of Conjugated Polymers	357
Mary A. Reppy	
Optical Reporting by Conjugated Polymers via Conformational Changes	389
Rozalyn A. Simon and K. Peter R. Nilsson	
Fluorescence Reporting Based on FRET Between Conjugated Polyelectrolyte and Organic Dye for Biosensor Applications	417
Kan-Yi Pu and Bin Liu	
Index	455

Part I

General Aspects

Nanocrystals and Nanoparticles Versus Molecular Fluorescent Labels as Reporters for Bioanalysis and the Life Sciences: A Critical Comparison

Ute Resch-Genger, Markus Grabolle, Roland Nitschke, and Thomas Nann

Abstract At the core of photoluminescence techniques are suitable fluorescent labels and reporters, the spectroscopic properties of which control the limit of detection, the dynamic range, and the potential for multiplexing. Many applications including recent developments in intracellular labeling rely on well established molecular chromophores such as small organic dyes or fluorescent proteins. However, one of the most exciting – but also controversial – advances in reporter technology, the emerging development and application of luminescent nanoparticles with unique optical properties, yet complicated surface chemistry paves new roads for fluorescence imaging and sensing as well as for in vitro and in vivo labeling. Here, we compare and evaluate the differences in physico-chemical properties of common fluorophores, focusing on traditional organic dyes and luminescent nanocrystals with size-dependent features. The ultimate goal is to provide a better understanding of the advantages and limitations of both classes of chromophores, facilitate fluorophore choice for users of fluorescence techniques, and address future challenges in the rational design and manipulation of nanoparticulate labels and probes.

Keywords Amplification · Fluorescent reporter · Fluorophore · FRET · In vitro · In vivo · Labeling · Lanthanide chelate · Multiplexing · Nanoparticle · Quantum dot · Transition metal complex

U. Resch-Genger (✉) and M. Grabolle
BAM Federal Institute for Materials Research and Testing, Richard-Willstaetter-Str. 11, 12489
Berlin, Germany
e-mail: Ute.resch@bam.de

R. Nitschke
Life Imaging Center, Center of Biological Systems Analysis, Albert-Ludwigs-University
Freiburg, Habsburgerstr. 49, 79104 Freiburg, Germany
Center for Biological Signaling Studies (bioss), Albertstrasse 19, 79104 Freiburg, Germany

T. Nann
School of Chemistry, University of East Anglia (UEA), Norwich NR4 7TJ, UK

Contents

1	Introduction	4
2	Properties of Molecular and Nanoparticulate Labels and Reporters	6
2.1	Spectroscopic Properties	6
2.2	Solubility and Aggregation	17
2.3	Thermal and Photochemical Stability	18
2.4	Cyto- and Nanotoxicity	19
3	Application of Molecular and Nanoparticulate Fluorophores	21
3.1	Coupling Chromophores to Biomolecules	21
3.2	Extra- and Intracellular Targeting of Biomolecules	23
3.3	Interactions Between Chromophores and their Microenvironment	24
3.4	Exploitation of Förster Resonance Energy Transfer	26
3.5	Multiplexing Detection Schemes	27
3.6	Strategies for Signal Amplification	29
3.7	Reproducibility, Quality Assurance and Limitations	29
4	Applications of Nanoparticles: State-of-the-Art and Future Trends	31
5	Conclusions	33
	References	33

1 Introduction

The investigation of many fundamental processes in the life sciences requires straightforward tools for the fast, sensitive, reliable, and reproducible detection of the interplay of biomolecules with one another and with various molecular or ionic species. One of the best suited and most popular methods to meet these challenges presents the use of photoluminescence or fluorescence techniques in conjunction with functional dyes and labels [1–3]. Advantages of fluorescence methods, which range from fluorescence spectroscopy over fluorescence microscopy and flow cytometry to *in vivo* fluorescence imaging, include the comparatively simple measurement of a number of unique experimental parameters (excitation wavelength, emission wavelength, intensity/quantum yield, fluorescence lifetime, and emission anisotropy) with nanometer scale resolution and possible sensitivity down to the single molecule level [4]. The potential of these methods, e.g., the achievable sensitivity (detection limit), the dynamic range, and the number of emissive species to be distinguished or detected simultaneously (multiplexing capability), is controlled by the physico-chemical properties of the fluorescent reporter(s) employed. Generally, a suitable label or reporter must be (1) conveniently excitable, without excitation of the (biological) matrix, and detectable with conventional instrumentation; (2) bright, i.e., possess a high molar absorption coefficient at the excitation wavelength and a high fluorescence quantum yield; (3) soluble in application-relevant media such as buffers, cell culture media, or body fluids; and (4) thermally and photochemically stable under relevant conditions. (5) For site-specific labeling, functional groups, often in conjunction with spacers, are beneficial. Depending on

the desired application, additional important considerations should include (6) the luminescence lifetime of the label, e.g., for suitability for time-gated emission, lifetime sensing or fluorescence lifetime multiplexing [5] (7) steric and size-related effects, (8) the sensitivity of the chromophore's optical properties to its microenvironment including the interplay between the chromophore and the biological unit, (9) the possibility of delivering the fluorophore into cells, and (10) potential toxicity and biocompatibility. Similarly relevant are (11) the suitability for multiplexing and (12) compatibility with signal amplification strategies such as Förster resonance energy transfer (FRET) [6] in antennae-type systems or controlled aggregation approaches [7]. Crucial for the eventually desired application for routine analysis is (13) the reproducibility of the reporter's synthesis and chemical modification (binding to biomolecules, surface functionalization in the case of particles, etc.) in conjunction with the availability of simple and evaluated characterization procedures [1]. In this respect, reported photophysics of the chromophore can also be beneficial.

There is an ever increasing toolbox of fluorescent labels and reporters to choose from: (1) molecular systems with a defined, yet versatility tunable chemical structure like small organic dyes [1, 2], metal–ligand complexes (MLC) such as $[\text{Ru}(\text{bpy})_3]^{2+}$ [8, 9], and lanthanide chelates [10–12] as well as fluorophores of biological origin like phycobiliproteins and genetically encoded fluorescent proteins [3, 13], (2) nanocrystal labels with size-dependent optical and physico-chemical properties which includes quantum dots (QDs) made from II/VI and III/V semiconductors [1, 14], carbon [15] and silicon nanoparticles [16] as well as luminescent metal particles and clusters [17], self-luminescent organic nanoparticles [18], and (3) nanometer-sized upconversion phosphors as a new class of evolving inorganic nanocrystal labels with promising, partly size-dependent spectroscopic features composed of a crystalline host doped with emissive lanthanide ions (localized luminescent centers) [19]. (4) All these chromophores can be incorporated into nanometer- to micrometer-sized inorganic and organic polymeric particles, yielding multichromophoric particulate labels [20, 21].

In this chapter, we compare and evaluate the differences in physico-chemical properties and application-relevant features of organic dyes as the most versatile molecular labels and nanocrystal labels, thereby focusing on QDs made from II/VI and III/V semiconductors, which are the most frequently-used nanocrystal labels in bioanalytics or medical diagnostics. The discussion of many of the properties of organic dyes, such as their photophysics, is similarly relevant for fluorescent proteins. The spectroscopic properties of metal–ligand and lanthanide complexes, that are commonly employed only for specific applications, e.g., in fluoroimmunoassays or certain sensor systems as well as phosphorescence emitters and components in bio- and chemoluminescent systems, are only briefly reviewed, thereby providing the basis for judging their advantages and limitations in comparison to organic dyes and semiconductor QDs. Their applications are not further detailed here. This is similarly true for carbon and silicon nanoparticles, metal nanoparticles, and clusters, as well as for nanometer-sized upconverting phosphors, that are only currently becoming more prominent in the field of biological assays as well as

medical diagnosis and imaging. Increasingly used chromophore-doped particle labels (4) and materials based on conjugated polymers [22] are beyond the scope of this review. The optical properties of such chromophore-doped particles are controlled by the parent chromophores or dopants, and the surface modification and labeling strategies presented here for the QDs labels can also be typically applied to these systems.

2 Properties of Molecular and Nanoparticulate Labels and Reporters

2.1 Spectroscopic Properties

The relevant spectroscopic features of a chromophore include the spectral position, width (FWHM: full width at half height of the maximum), and shape of its absorption and emission bands, the Stokes shift, the molar absorption coefficient (ϵ_M), and the photoluminescence efficiency or fluorescence quantum yield (Φ_F). The Stokes shift equals the (energetic) difference (in frequency units) between the spectral position of the maximum of the lowest energy absorption band (or the first excitonic absorption peak in the case of QDs) and the highest energy maximum of the luminescence band. This quantity determines the ease of separation of excitation from emission and the efficiency of emission signal collection. It can also affect the degree of spectral crosstalk in two- or multi-chromophore applications such as FRET or spectral multiplexing and the amount of homo-FRET (excitation energy transfer between chemically identical chromophores) occurring, e.g., in chromophore-labeled (bio)macromolecules that can result in fluorescence quenching at higher labeling densities [23, 24]. The product of ϵ_M at the excitation wavelength (λ_{ex}) and Φ_F , that is termed brightness (B), presents a frequently used measure for the intensity of the fluorescence signal obtainable upon excitation at a specific wavelength or wavelength interval and is thus often used for the comparison of different chromophores. A value of B below $5,000 \text{ M}^{-1} \text{ cm}^{-1}$ renders a label practically useless for most applications [25]. Further exploitable chromophore properties include the luminescence or fluorescence lifetime (τ_F), that determines, e.g., the suitability of a label for time-gated emission [4], time-resolved fluorescence immunoassays [26–28], and lifetime multiplexing [5], and the emission anisotropy or fluorescence polarization. The latter quantity, that presents a measure for the polarization of the emitted light, reflects the rotational freedom or mobility of a chromophore in the excited state and provides information on the orientation distributions of fluorescent moieties or on the size of molecules (hydrodynamic radius) via the measurement of the rotational correlation time [4]. This can be exploited, e.g., for the study of enzyme activity, protein–peptide and protein–DNA interactions, and ligand–receptor binding studies in homogeneous solution.

2.1.1 Luminescent Nanocrystals and Nanoparticles

The most prominent nanomaterials for bioanalysis at present are semiconductor QDs. Rare-earth doped upconverting nanocrystals and precious metal nanoparticles are becoming increasingly popular, yet they are still far from reaching the level of use of QDs. Other luminescent nanoparticles like carbon-based nanoparticles start to appear, but the synthesis and application of these materials are still in their infancy and not significant for practitioners in the field of bioanalysis.

The photoluminescence of these nanoparticles has very different causes, depending on the type of nanomaterial: semiconductor QDs luminescence by recombination of excitons, rare-earth doped nanoparticles photoluminescence by atom orbital (AO) transitions within the rare-earth ions acting as luminescent centers, and metallic nanoparticles emit light by various mechanisms. Consequently, the optical properties of luminescent nanoparticles can be very different, depending on the material they consist of.

The optical properties of semiconductor QDs (Fig. 1a–c, Tables 1 and 2) are controlled by the particle size, size distribution (dispersity), constituent material, shape, and surface chemistry. Accordingly, their physico-chemical properties depend to a considerable degree on particle synthesis and surface modification. Typical diameters of QDs range between 1 and 6 nm. The most prominent optical features of QDs are an absorption that gradually increases toward shorter

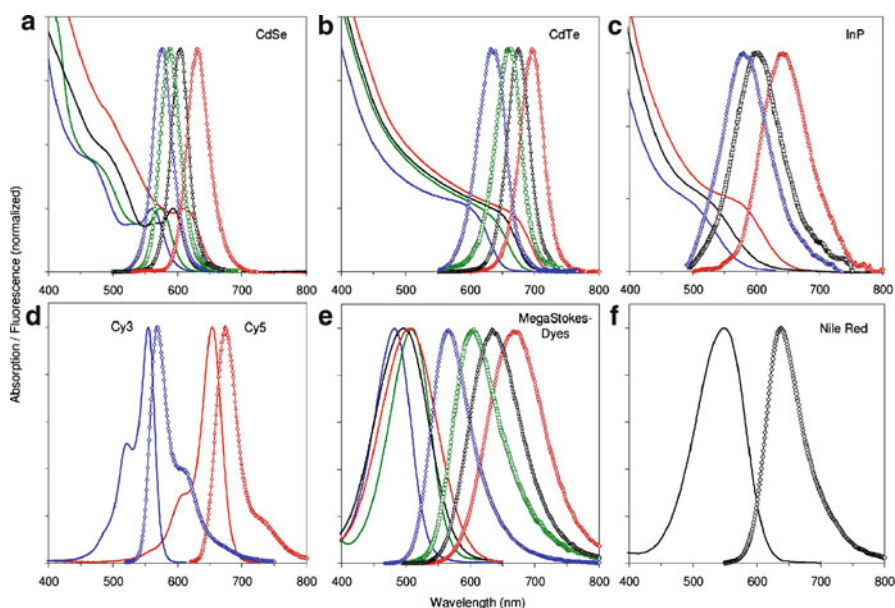


Fig. 1 Spectra of QDs and organic dyes. Absorption (*lines*) and emission (*symbols*) spectra of representative QDs (a–c) and organic dyes (d–f). Reprinted by permission from Macmillan Publishers Ltd: Nature Methods [1], copyright (2008)

Table 1 Spectroscopic properties of labels and reporters

	Organic dye	Semiconductor quantum dot
Absorption spectra	Discrete bands, FWHM ^a 35 nm ^b to 80–100 nm ^c <i>Examples</i> ^d (λ_{abs} /FWHM) <i>Nile Red</i> : 552 nm/90 nm (MeOH) <i>Cy3</i> : 550 nm/33 nm (phosphate buffer) <i>Alexa750</i> : 749 nm/55 nm (phosphate buffer) <i>IR125</i> : 782 nm/62 nm (MeOH)	Steady increase toward UV starting from absorption onset, enables free selection of excitation wavelength <i>CdSe</i> : 450–640 nm/- <i>CdTe</i> : 500–700 nm/- <i>PbSe</i> : 900–4000 nm/- <i>CuInS₂</i> : 400–900 nm/-
Molar absorption coefficient	2.5×10^4 – 2.5×10^5 M ⁻¹ cm ⁻¹ (at long wavelength absorption maximum) <i>Examples</i> <i>Nile Red</i> : 4.5×10^4 M ⁻¹ cm ⁻¹ (MeOH) <i>Cy3</i> : 1.5×10^5 M ⁻¹ cm ⁻¹ (phosphate buffer) <i>Alexa750</i> : 2.4×10^5 M ⁻¹ cm ⁻¹ (phosphate buffer) <i>IR125</i> : 2.1×10^5 M ⁻¹ cm ⁻¹ (MeOH)	10^5 – 10^6 M ⁻¹ cm ⁻¹ at first excitonic absorption peak, increasing toward UV, larger (longer wavelength) QDs generally have higher absorption <i>CdSe</i> : 1.0×10^5 (500 nm)– 7.0×10^5 (630 nm) M ⁻¹ cm ⁻¹ <i>CdTe</i> : 1.3×10^5 (570 nm)– 6.0×10^5 (700 nm) M ⁻¹ cm ⁻¹ <i>PbSe</i> : 1.23×10^5 M ⁻¹ cm ⁻¹ (chloroform) <i>CuInS₂</i> : <i>n. d.</i>
Emission spectra	Asymmetric, often tailing to long-wavelength side, FWHM 35 nm ^b to 70–100 nm ^c <i>Examples</i> (λ_{em} /FWHM) <i>Nile Red</i> : 636 nm/75 nm (MeOH) <i>Cy3</i> : 565 nm/34 nm (phosphate buffer) <i>Alexa750</i> : 775 nm/49 nm (phosphate buffer) <i>IR125</i> : 528 nm/58 nm (MeOH)	Symmetric, Gaussian-profile, FWHM 30–90 nm <i>CdSe</i> : 470–660 nm/~30 nm <i>CdTe</i> : 520–750 nm/35–45 nm <i>PbSe</i> : >1,000 nm/80–90 nm <i>CuInS₂</i> : 500–1,000 nm/70–150 nm
Stokes shift	Normally <50 nm ^b , up to >150 nm ^c <i>Examples</i> <i>Nile red</i> : 84 nm (MeOH) <i>Cy3</i> : 15 nm (phosphate buffer) <i>Alexa</i> : 26 nm (phosphate buffer) <i>IR125</i> : 44 nm (MeOH)	Typically <50 nm for vis-emitting QDs <i>CdSe</i> : 15–20 nm <i>CdTe</i> : 30–40 nm <i>PbSe</i> : 60–80 nm <i>CuInS₂</i> : ~100 nm
Quantum yield	0.5–1.0 (vis), 0.05–0.25 (NIR) <i>Examples</i> <i>Nile Red</i> : 0.7 (dioxane) <i>Cy3</i> : 0.04 (phosphate buffer) <i>Alexa</i> : 0.12 (phosphate buffer) <i>IR125</i> : 0.04 (MeOH)	0.1–0.8 (vis), 0.2–0.7 (NIR) <i>CdSe</i> : 0.65–0.85 <i>CdTe</i> : 0.3–0.75 <i>PbSe</i> : 0.12–0.81 <i>CuInS₂</i> : 0.2–0.3
Fluorescence lifetimes	1–10 ns, monoexponential decay	10–100 ns, typically multiexponential decay
Solubility/dispersibility	Control by substitution pattern	Control via surface chemistry (ligands)

(continued)

Table 1 (continued)

	Organic dye	Semiconductor quantum dot
Binding to biomolecules	Via functional groups following established protocols, often binding of several dyes to single biomolecule, labeling-induced effects on spectroscopic properties of reporter studied for many common dyes	Via ligand chemistry, only few protocols available, binding of several biomolecules to single QD, very little information on labeling-induced effects
Size	~0.5 nm	1–6 nm
Thermal stability	Dependent on dye class, can be critical for NIR-dyes	High, depends on shell/ligands
Photochemical stability	Sufficient for many applications (vis), but can be critical for high-light flux applications (e.g., fluorescence microscopy), often problematic for NIR dyes	High (vis and NIR), orders of magnitude that of organic dyes, can reveal photobrightening
Toxicity	From very low to high, dependent on dye	Little known yet (heavy metal leakage to be prevented, nanotoxicity)
Reproducibility of labels (optical, chemical properties)	Good, due to defined molecular structure and established methods of characterization, available from commercial sources	Limited by complex structure and surface chemistry, limited data available, few commercial systems available, often individual solutions
Single-molecule capability	Moderate, limited by photobleaching	Good, limited by blinking
FRET	Well described FRET pairs, mostly single donor–single acceptor configurations, enables optimization of reporter properties	Few examples, single donor–multiple acceptor configurations possible, limitation of FRET efficiency due to nanometer-size of QD-coating
Spectral multiplexing	Possible, 3 colors (MegaStokes dyes), 4 colors (energy-transfer cassettes)	Ideal for multicolor experiments, up to 5 colors demonstrated
Lifetime multiplexing	Possible	Possible
Signal amplification	Established techniques	Unsuitable for many enzyme-based techniques, other techniques remain to be adapted and/or established

^aFWHM: full width at half height of the maximum

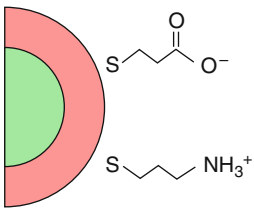
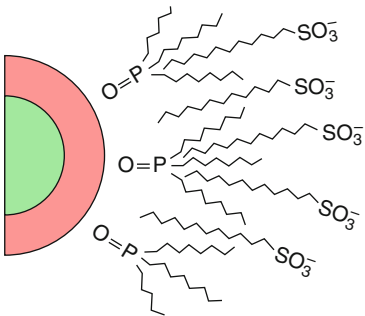
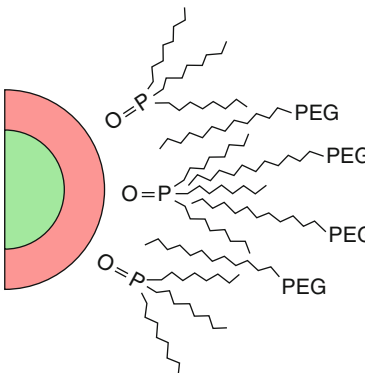
^bDyes with resonant emission like fluoresceins, rhodamines, cyanines (see section 3.3)

^cCT dyes (see section optical properties, organic dyes)

^dSpectroscopic data taken from [29–33]; data for Alexa750 provided by Invitrogen

wavelength below the first excitonic absorption band and a comparatively narrow luminescence band of typically Gaussian shape. Both the onset of absorption and the spectral position of the emission band shift to higher energies with decreasing particle size (Table 1 and Fig. 1a–c). This size dependence is caused by the alteration of the electronic properties of these materials (e.g., energetic position

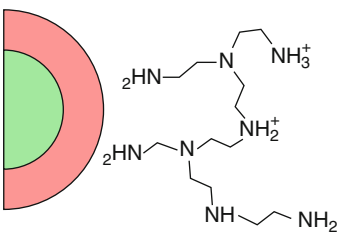
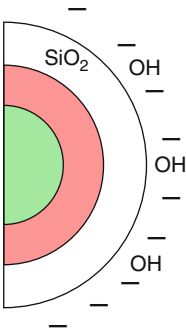
Table 2 Methods for water transfer

Method		Applications
Electrostatic stabilization	 <p>Ligand exchange with small charged adsorbants, e.g., 3-mercaptopropionic acid (MPA) [34]</p>	<ul style="list-style-type: none"> -Labeled with immunomolecules, QDs recognized specific antigens/antibodies -DNA immobilization to QDs surfaces and possibility of hybrid assemblies [35] -Coupled to transferrin, QDs underwent receptor-mediated endocytosis in cultured HeLa cells
	 <p>Intercalation with charged surfactants [36]</p>	
Steric stabilization	 <p>Intercalation with bulky, uncharged molecules, e.g., polyethyleneglycol [37]</p>	<ul style="list-style-type: none"> -In vivo cancer targeting and imaging -Conjugation with DNA and in vivo imaging (embryogenesis) [36] -Encoding of cells [38] -Noninvasive in vivo imaging with localization depending on surface coating [39]

(continued)

of the valence and conduction band etc.) if the dimensions of the relevant structural features interfere with the delocalized nature of the electronic states. For semiconductor QDs, such quantum-size effects occur typically for sizes in the range of a

Table 2 (continued)

Method	Applications
Hybrid methods	<ul style="list-style-type: none"> -Proteins can be directly coupled to PEI amine groups -Silica can be easily functionalized and then bioconjugated
	
Bulky, partially charged ligands (polyelectrolytes), e.g., polyethyleneimine (PEI) [40]	
	
Additional inorganic shells, e.g., silica [41, 42]	

few to 10 nm. The size of the photoluminescence quantum yield of QDs is primarily determined by the number of dangling bonds at the core particle's surface. Thus, the modification of the surfaces of bare QDs is very important for the realization of high fluorescence quantum yields. This can be achieved, e.g., by the deposition of a layer of inorganic, chemically inert material or by organic ligands. Accordingly, in the majority of cases, QDs present core-shell (e.g., CdSe core with a ZnS shell) or core-only (e.g., CdTe) structures capped with specific organic or polymeric ligand molecules. The most prominent materials for life science applications are currently CdSe and CdTe. III/V group or ternary semiconductors such as InP, InGaP, CuInS₂, and AgInS₂ – which lack cytotoxic cadmium ions – are possible alternatives that have been synthesized and used recently [43, 44]. At present, commercial products are available for CdSe (Sigma-Aldrich, Invitrogen, Evident, Plasmachem), CdTe (Plasmachem), and InP or InGaP (Evident).

Lanthanide (Ln) – or rare-earth-doped upconverting nanocrystals usually have similar optical properties as their bulk counterparts [45]. Upconversion is characterized by the successive absorption of two or more photons via intermediate

long-lived excited states followed by the emission of a photon of higher energy than each of the exciting photons. Accordingly, upconverting materials absorb light in the near infrared (NIR) part of the spectrum and emit comparatively sharp emission bands blue-shifted from the absorption in the visible region of the spectrum yielding large antiStokes shifts [46]. Nanoscale manipulation can lead to modifications of, e.g., the excited state dynamics, emission profiles, and upconversion efficiency [47]. For instance, the reduction in particle size can allow for the modification of the lifetime of intermediate states and the spatial confinement of the dopant ions can result in the enhancement of a particular emission. The most frequently used material for the design of upconverting nanocrystals is $\text{NaYF}_4:\text{Yb, Er}$. The attractiveness of upconverting nanocrystals lies in the fact that the NIR excitation light does not excite background fluorescence and can penetrate deep into tissue, in the large antiStokes shifted, narrow, and very characteristic emission, and in their long emission lifetimes. Despite their obvious potential as fluorescent reporters for the life sciences, upconverting nanoparticles are not commercially available yet. Moreover, in comparison to other longer existing fluorophores, many application-relevant properties have not been thoroughly investigated yet for nanometer-sized upconverting phosphors due to difficulties in preparing small particles (sub-50 nm), that exhibit high dispersibility and strong upconversion emission in aqueous solution.

Precious metal nanoparticles show strong absorption and scattering of visible (vis) light, which is due to collective oscillation of electrons (usually called localized surface plasmon resonance, LSPR) [48]. The cross section for light scattering scales with the sixth power of the particle diameter. Consequently, the amount of scattered light decreases significantly when the nanoparticles become very small. Fluorescence of metal nanoparticles was observed in the late 60s of the last century [49]. Even though this effect is often very small, it becomes increasingly interesting for small nanoparticles or clusters (the properties and applications of silver and gold nanoclusters are discussed in chapters of Diez and Ras [150] and of Muhammed and Pradeep [151] in this volume), since the absorption cross section scales only with the third power of the nanoparticle diameter. Quantum yields of Au_5 clusters as high as 0.7 have been reported [50]. At present, the major field of application of metal particles like gold involves Raman spectroscopy.

2.1.2 Organic Dyes

The optical properties of organic dyes (Fig. 1d–f, Table 1) are controlled by the nature of the electronic transition(s) involved [4]. The emission occurs either from an electronic state delocalized over the whole chromophore (the corresponding fluorophores are termed here as *resonant* or *mesomeric* dyes) or from a charge transfer (CT) state formed via intramolecular charge transfer (ICT) from the initially excited electronic state (the corresponding fluorophores are referred to as *CT dyes*) [4]. Bioanalytically relevant fluorophores like fluoresceins, rhodamines, most 4,4'-difluoro-4-bora-3a,4a-diaza-s-indacenes (BODIPY dyes), and cyanines (symmetric

cyanines in general and, depending on their substitution pattern, also asymmetric cyanines) present resonant dyes. Typical for these fluorophores are slightly structured, comparatively narrow absorption and emission bands, which often mirror each other, and a small, almost solvent polarity-insensitive Stokes shift (Fig. 1d) as well as high molar absorption coefficients. For example for the best cyanine dyes, ϵ_M values of $2\text{--}3 \times 10^5 \text{ M}^{-1} \text{ cm}^{-1}$ can be found. Commonly associated with a small Stokes shift are high fluorescence quantum yields for dyes with rigid structures emitting in the visible region (Φ_F values of 0.80–1, e.g., rhodamines, fluoresceins, and BODIPY dyes) and, in the case of near-infrared (NIR) chromophores, moderate Φ_F values of 0.1–0.2 (Table 1). The small Stokes shift of these chromophores results in a considerable spectral overlap between absorption and emission, that can be disadvantageous for certain applications (see, e.g., Sects. 3.4 and 3.5). CT dyes such as coumarins or dansyl fluorophores are characterized by well-separated, broader, and structureless absorption and emission bands at least in polar solvents and a larger Stokes shift (Fig. 1f). The molar absorption coefficients of CT dyes, and in most cases, also their fluorescence quantum yields, are generally smaller than those of dyes with a resonant emission. CT dyes show a strong polarity dependence of their spectroscopic properties (e.g., spectral position and shape of the absorption and emission bands, Stokes shift, and fluorescence quantum yield). Moreover, in the majority of cases, NIR absorbing and emitting CT dyes reveal only low fluorescence quantum yields, especially in polar and protic solvents. The spectroscopic properties of resonant and CT dyes can be fine-tuned by elaborate design strategies if the structure–property relationship is known for the respective dye class. Selection within large synthetic chromophore library becomes popular. The chapter of Kim and Park within these series [152] addresses the comparison of rational design and library selection approaches.

2.1.3 Metal Ligand Complexes

The most prominent metal ligand complexes used in bioanalytics and life sciences are ruthenium(II) complexes with ligands such as bipyridyl- or 1,10-phenanthroline derivatives [8, 9] followed by platinum(II) and palladium(II) porphyrins [51]. Ru(II) coordination compounds absorb energy in the visible region of the spectrum (typically excitable at, e.g., 488 nm) or in the NIR depending on the ligand [52] populating a metal-to-ligand charge transfer ($^1\text{MLCT}$) state. Subsequent intersystem crossing leads to quantitative population of the $^3\text{MLCT}$ state, which can be deactivated via luminescence, nonradiative decay, or via population of a nonemissive metal- or ligand-centered state. The most characteristic spectroscopic features of this class of fluorescent reporters are broad, well-separated absorption and emission bands, moderate luminescence quantum yields, and comparatively long emission lifetimes in the order of a few 10 ns up to several hundred nanoseconds due to the forbidden nature of the electronic transitions involved [53]. Platinum (II) and palladium(II) porphyrins, that present, e.g., viable oxygen sensors, as well as other coordination compounds such as iridium(II) complexes are not further detailed here. The spectral features of

these Ru(II) complexes (as well as other MLC), their luminescence quantum yields and their lifetimes can be elegantly tuned via the ligand [52].

Luminescent lanthanide complexes (Tb^{3+} , Eu^{3+} , etc.) are of growing interest, e.g., as fluorescent reporters for biological applications. Since the lanthanide f–f transitions have low absorption coefficients (symmetry-forbidden transitions), typically sensitized emission is used to rationalize more intense luminescence, thereby exploiting energy transfer (via intersystem crossing) from the triplet state of the initially excited sensitizer or antenna (ligand with an integral or appended chromophore like phenanthroline) to the emissive lanthanide ion. Accordingly, application-relevant compounds present multicomponent systems, in which the active components, the metal cation, the antenna, and the coordination site are organized in a supramolecular structure. The ligand is commonly also chosen to protect the rare earth ion (chelates in the case of DELFIA and cryptates for the compounds from CISBio International) from potential quenching by the environment (water molecules in the coordination sphere etc.) [54]. The optical properties of luminescent lanthanide complexes are thus determined by the absorption properties of the antenna ligand, the efficiencies of intersystem crossing in the ligand within the complex, triplet-mediated energy transfer from the excited state of the ligand to the lanthanide ion yielding the excited lanthanide, and the quantum yield of the lanthanide emission [55]. The most remarkable features of luminescent lanthanide complexes, that are typically only excitable in the short wavelength region (commonly at ca. 365 nm, sometimes at longer wavelength like 405 nm or even longer), are their narrow and characteristic emission bands in the visible (Tb^{3+} : 490, 545 nm; Eu^{3+} : 580, 613, 690 nm; Sm^{3+} : 598, 643 nm; Dy^{3+} : 575 nm), in the NIR region (Yb^{3+} : 980 nm; Nd^{3+} : 880, 1,065 nm; Er^{3+} : 1,522 nm) and their long luminescence lifetimes (e.g., Eu^{3+} : 300–1,500 μs , Tb^{3+} : 100–1,500 μs ; Sm^{3+} : 20–50 μs) [10, 56, 57]. Maximum luminescence quantum yields are in the order of 0.25 found for Eu^{3+} – and 0.15 for Tb^{3+} -complexes in aerated solution and decrease for all the other rare earth ions. Although criteria for the choice of the lanthanide ion and the antennae have been reviewed [11, 55, 58], the complicated mechanism of light generation renders the design of highly luminescent lanthanide reporters still a challenge.

2.1.4 Comparison of Chromophores

In comparison to organic dyes as well as metal–ligand and lanthanide complexes, nanocrystal labels offer a wide variety of spectroscopic properties which are often scalable, optically stable, and not achievable in these molecular fluorophores (e.g., size-controllable spectroscopic properties and continuous absorption below the first excitonic absorption band in the case of QDs, see Fig. 1a–c; upconversion luminescence). With values in the range of 100,000 to 1,000,000 $\text{M}^{-1} \text{cm}^{-1}$, the (size-dependent) molar absorption coefficients at the first excitonic absorption band of QDs are generally large as compared to organic fluorophores [33] (Table 1) and strongly exceeding the ϵ_{M} values obtained for MLC (in the order of a few 10,000 M^{-1}

cm^{-1}) and lanthanide complexes (ϵ_M determined by the organic ligand with typical values in the order of $20,000\text{--}70,000 \text{ M}^{-1} \text{ cm}^{-1}$) [58]. Fluorescence quantum yields of properly surface-passivated QDs are in the same order of magnitude that is found for vis-emitting organic dyes, [43, 59], thereby clearly exceeding the photoluminescence quantum yields of MLC and lanthanide complexes [58]. Moreover, QDs can have high quantum yields in the NIR above 700 nm in the range of about 0.3–0.8, found, e.g., for CdTe, HgCdTe, PbS, and PbSe [60, 61], whereas organic dyes are at maximum only moderately emissive above 750 nm, see Table 1. Compared to QDs and organic dyes emitting in the visible region, upconverting nanocrystals generally have a low absorption cross section and photoluminescence quantum yield, yet their narrow emission bands are rather characteristic and ideal for multiplexing. Other luminescent nanocrystals such as metal nanoclusters, silicon or carbon nanoparticles have comparatively low quantum yields and often broad emission bands.

Another favorable feature of QDs as compared to organic dyes are their typically very large two-photon (2P) action cross sections [62, 63] that are very attractive for two- (or multi) photon applications such as two- (or multi) photon microscopy and bioimaging [64]. The 2P action cross section equals the product of the two-photon absorption cross-section and the fluorescence quantum yield and describes the probability of simultaneous absorption of two photons and transition of the fluorophore to an excited state that differs energetically from the ground state by the energy of these two photons. The 2P action cross sections of organic fluorophores are commonly in the range of $1.0 \times 10^{-52}\text{--}4.7 \times 10^{-48} \text{ cm}^4 \text{ photon}^{-1}$ [65].

The fluorescence decay kinetics of exemplary chosen QDs and small organic dyes are compared in Fig. 2. The size of the fluorescence parameter luminescence lifetime is determined by the electronic nature of the transitions involved. As a rule

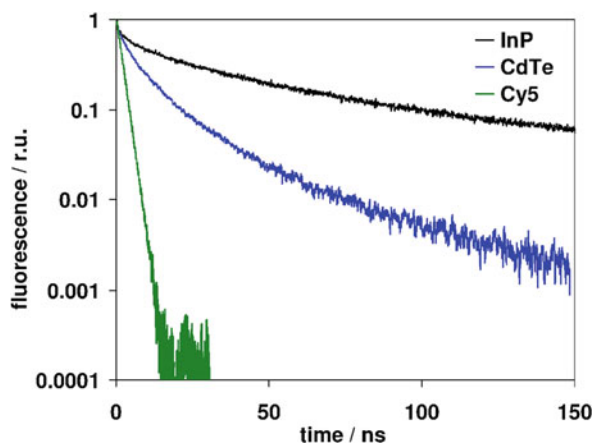


Fig. 2 Comparison of the luminescence decays of QDs and organic dyes. InP and CdTe QDs decay multiexponentially with a mean lifetime ($\tau_{1/e}$) of 17 and 6 ns, respectively. The organic dye Cy5 shows monoexponential decay with τ_F of 1.5 ns

of thumb, for molecular fluorophores, a high ϵ_M value does not allow obtaining a long emission lifetime. The fluorescence lifetimes of organic dyes, that typically display allowed transitions between singlet states, are in the order of about 5 ns for vis emitters and ≤ 1 ns for NIR fluorophores (Table 1). This is too short for efficient temporal discrimination of short-lived background fluorescence and scattered excitation light. The most prominent exceptions used for bioanalytical applications are the vis-emitting acridone dyes displaying fluorescence lifetimes in the order of 5–20 ns, that, however, require short-wavelength excitation (excitation, e.g., at 405 nm, emission at ca. 440–500 nm) [66] and the only recently reported UV-absorber and vis-emitter DBO (2,3-diazabicyclo[2.2.2]oct-2-ene) with a lifetime of ca. 300 ns in aerated water [67]. Due to the forbidden nature of the electronic transitions involved, in addition to its short wavelength absorption and emission (absorption and emission maximum at ca. 365 nm and ca. 430 nm, respectively, in water), DBO shows very low molar absorption coefficients which reduces the overall sensitivity. Nevertheless, advantageous for the vast majority of organic dyes can be their typically mono-exponential decay kinetics (in a homogeneous microenvironment), that can be exploited for the straightforward dye identification from measurements of fluorescence lifetimes [68].

In comparison to conventional organic dyes shown in Fig. 2, MLC like Ru(II) complexes and lanthanide complexes show attractive long emission lifetimes in conjunction with mono-exponential decay kinetics, that render them superior to organic chromophores in this respect [53]. This provides the basis for the straightforward temporal discrimination of shorter-lived autofluorescence and scattered excitation light from label emission with the aid of time-gated measurements, thereby enhancing the sensitivity [69], and enables lifetime-based sensing. Due to their long lifetimes in conjunction with the straightforward excitation and emission in the visible or rarely, even in the NIR, Ru(II) complexes are common probes and labels in lifetime-based assays and (bio)sensors and in fluorescence polarization assays [70]. As the emission lifetimes of Ru(II) complexes are typically oxygen-sensitive, these species present the most commonly used lifetime-based oxygen sensors [71, 72]. The exceptionally long luminescence lifetimes of the lanthanide chelates (typically monoexponential decay kinetics), detailed in the previous section, can, but must not necessarily be, oxygen-dependent [10, 58]. This, in combination with “shielding ligands” like certain chelates or cryptates and narrow emission bands makes these lanthanide fluorophores ideal candidates for all applications of time gated emission (e.g., DELFIA technology in fluoroimmunoassays) and as energy donors in homogeneous time-resolved fluorescence assays [10, 73]. Moreover, their distinct sharp emission bands can be exploited for spectral multiplexing applications [74].

Attractive for the use of QDs are their long lifetimes (typically 5 ns to hundreds of nanoseconds), compared to organic dyes, that are typically insensitive to the presence of oxygen. In conjunction with time-gated measurements, this provides the basis for enhanced sensitivity [69]. This property can be also favorable for time-resolved applications of FRET. The complicated size-, surface-, and wavelength-dependent, bi- or multi-exponential QD decay behavior (Fig. 2) can complicate

species identification from time-resolved fluorescence measurements. Nevertheless, for QD labels displaying a concentration-independent fluorescence decay behavior, the quantification of these multiexponentially decaying species could be recently demonstrated for mixtures of different chromophores [5]. The luminescence lifetimes of upconversion nanocrystals are in the long microsecond to millisecond time domain and are not sensitive to oxygen. Similarly as described for MLC and lanthanide chelates, this can be exploited, e.g., for time-gated emission and time-resolved FRET applications which have already been reported for micrometer-sized upconverting phosphors.

This comparison of the spectroscopic properties of the different types of fluorescent reporters underlines that semiconductor QDs and upconverting nanoparticles have no analogs in the field of organic dyes. Therefore, their unique features are unrivaled. The different molecular labels detailed here each display unique advantages that can compete with some of the favorable features of QDs and upconverting phosphors such as long lifetimes in the case of MLC systems and lanthanide chelates or very narrow emission bands for lanthanide chelates beneficial for spectral multiplexing.

2.2 Solubility and Aggregation

The solubility of a chromophore is one of the major factors governing its applicability. Suitable labels and probes should not aggregate or precipitate under application-relevant conditions. For bioanalysis and life sciences, this includes aqueous solutions, *in vitro* conditions (cell cultural media), on supports such as microarrays, in cells or *in vivo* conditions. Moreover, for many biological applications such as the specific labeling of cells and tissue, nonspecific binding to the cell surface and the extracellular matrix can also play a role. Organic molecules (dyes as well as ligands for MLC and lanthanide complexes) can be easily solubilized by derivatization with substituents such as sulfonic acid groups. Provided that the structure–property relationship is known for the respective dye class, the solubility can be tuned by substitution without considerably affecting the labels' optical properties and other application-relevant features. A whole range of organic dyes, that are soluble in relevant media, are commercially available.

Nanoparticle dispersibility is controlled by the chemical nature of the surface ligands (coating). Nanoparticles, which are prepared in aqueous solution, are inherently dispersible in water. However, with the exception of CdTe, high-quality nanocrystals with narrow size-distributions are typically synthesized in organic solvents and must be rendered water-dispersible (i.e., aggregation of nanoparticles in aqueous solution must be prevented). As summarized in Table 2, this can be accomplished electrostatically, by using small charged ligands such as mercaptopropionic acid [34], cystamine [75], or with charged surfactants that intercalate with the hydrophobic ligands present from synthesis [36]. Alternatively,

nanoparticle stabilization in aqueous solution can be accomplished by coating the particles with sterically demanding surface ligands such as polyethyleneglycol (PEG) [76].

Electrostatically stabilized nanoparticles are usually much smaller than sterically stabilized ones. Since this is favorable for most applications in the life sciences, electrostatic stabilization strategies are recommended if small nanoparticles in low ionic strength buffers are to be used. However, these particles tend to aggregate in solutions of high ionic strength such as biological matrices. Sterically stabilized nanoparticles are mostly too large to enter cells, but are less likely to aggregate. A compromise can be reached by using smaller, but nevertheless still bulky, charged polyelectrolytes such as polyethyleneimine (PEI) [40], or an additional amphiphilic inorganic shell like silica [41, 42] which can be further functionalized using standard silica chemistry.

It is difficult to predict the effect of surface functionalization on the optical properties of nanoparticles in general. Surface ligands have only minor influence on the spectroscopic properties of nanoparticles, the properties of which are primarily dominated by the crystal field of the host lattice (e.g., rare-earth doped nanocrystals) or by plasmon resonance (e.g., gold nanoparticles). In the case of QDs, the fluorescence quantum yield and decay behavior respond to surface functionalization and bioconjugation, whereas the spectral position and shape of the absorption and emission are barely affected.

2.3 Thermal and Photochemical Stability

Aside from spectroscopic considerations, one of the most important features of a fluorescent label or reporter is its stability under application-relevant conditions. This includes typically used solvents such as buffers, cell medium, or other supports, the presence of oxygen and typical reagents such as dithiothreitol (DTT), common temperatures as well as typical excitation wavelengths, and excitation light fluxes over routinely used detection times. The latter parameter is also linked to the detection method employed with certain fluorophores being suitable only for specific applications. In any case, chromophore stability is of crucial relevance for the achievable sensitivity and limit of detection, especially in single molecule experiments, and for contrast in fluorescence imaging. Blinking, that is the interruption of the photoluminescence of continuously illuminated QDs or organic dyes by dark periods, is relevant for single molecule applications and is briefly discussed in section 3.7.

Organic dyes like fluorescein and TRITC and the majority of NIR fluorophores suffer from poor photostability [77]. In addition, many NIR dyes, such as clinically approved indocyanine green (ICG) reveal poor thermal stability in aqueous solution [78]. Moreover, the presence of ozone can result in dye decomposition as observed for Cy5 [79]. In the last years, many organic dyes like the Alexa dyes have been

designed that display enhanced photostability in comparison to first generation fluorophores such as fluorescein. Simultaneously, due to technical improvements, readout times for many fluorescence techniques could be decreased. Despite these improvements, the nevertheless limited photostability of organic chromophores can still hamper microscopic applications requiring high excitation light intensities in the UV/vis region or long-term imaging. Thus, the search for brighter and especially more stable dyes is still going on. With respect to photochemical stability, lanthanide chelates can be superior to conventional organic chromophores.

In contrast, almost all types of luminescent nanoparticles display excellent thermal and photochemical stability. From the range of these nanocrystals, QDs are the ones most sensitive to photooxidation and photobleaching, but even these effects can be almost completely suppressed by epitaxial growth of a protective shell to shield the core material for relevant time intervals [80]. Moreover, the inorganic nature of the QDs makes them typically resistant to metabolic degradation in live cells and organism which is beneficial, e.g., for long-term imaging. This is a significant advantage over organic fluorophores for imaging applications, where excitation with intense lasers is employed for long periods of time [64]. A superior long-term stability compared to organic dyes has been demonstrated for example for CdSe/ZnS and rhodamine-labeled tubulin [42] CdSe and Texas Red [81] as well as for antibodies labeled with CdSe, FITC, R-phycoerythrin, and AlexaFluor 488 [77]. However, nanoparticles can show specific phenomena such as photobrightening [82] see also Sect. 3.7 on *Reproducibility, Quality Assurance, and Limitations*, and undesired aggregation of nanocrystals can contribute to reduced stability.

The thermal and photochemical stability of both organic dyes and nanocrystals are influenced by an extremely broad variety of conditions that need to be considered: excitation wavelength and intensity, matrix or microenvironment, label concentration, and, in the case of nanoparticles, surface chemistry. Therefore, the individual study of the stability of a chromophore under the conditions required can usually not be avoided.

2.4 *Cyto- and Nanotoxicity*

“All things are poison and nothing is without poison, only the dose permits something not to be poisonous (Paracelsus).” Although this property of molecular and nanoparticulate reporters is not relevant for *ex vivo* applications such as immunoassays, it is critical for imaging in cells or *in vivo*. In general, toxicity of organic dyes is not often reported as a significant problem, with the exception of DNA intercalators. Despite the ever increasing interest in *in vivo* imaging applications and the obvious importance of cytotoxicity data of fluorescent reporters for *in vivo* applications, there are only very few data available on the cytotoxicity of NIR fluorophores at present [78, 83].

The only organic fluorophores approved by the Food and Drug Administration (FDA) for use in humans are fluorescein (e.g., for ophthalmometry), Nile Blue, and

ICG, a symmetric cyanine [83]. It is common sense that the expression of green fluorescent protein (GFP) or fluorescent proteins in general can increase or at least sensitize cells to undergo apoptosis induced by the generation of reactive oxygen species (ROS) or due to aggregation of *GFP-fusions* [84]. Therefore, expression levels of fusion or reporter proteins have to be kept as low as possible. Organic dyes used as reporters in live cells can be loaded by incubation in their lipophilic acetoxymethyl-ester form, which achieves high intracellular dye concentrations, but can also result in toxic concentrations preferably in the mitochondria or other organelles with high esterase activity. Moreover, it has to be kept in mind that during continuous imaging, bleached dye species and/or ROS are formed, which can be toxic to live cells in contrast to the initially used fluorophore.

Toxicity of nanoparticles is a much more complicated issue as compared with organic fluorophores: Nanoparticles may be nanotoxic, they may contain cytotoxic elements or compounds, or their surface ligands/coating may contain toxic species. Nanotoxicity refers to the ability of a substance to be intrinsically cytotoxic due to its size (and independent of its constituent materials). The most prominent example of nanotoxicity is asbestos. Even though there are no systematic studies on the nanotoxicity of different nanocrystals available the results from several cytotoxicity studies suggest that nanotoxicity is not dominating for nanoparticulate reporters [85, 86].

The QD toxicity depends on multiple factors derived from both physico-chemical properties and environmental conditions like QD material, size, charge, concentration, and outer coating material (capping material and functional groups) as well as oxidative, photolytic, and mechanical stability [87]. Many of these factors also govern the cytotoxicity of other inorganic or organic fluorophore-doped nanoparticles [88]. The cytotoxicity of heavy metals or rare-earth elements, which are present in many nanocrystals as core and shell materials, is well known. Thus, it is critical to know whether these cytotoxic substances can leak out of the nanocrystals over time. This may happen upon illumination or oxidation [89]. Furthermore, toxic ligands or coatings might be released into solution [85]. Some groups found that CdSe-based QDs were cytotoxic to cells [90], other did not detect cytotoxic reactions [91]. In cases where cytotoxicity was observed, it was attributed to leaking of cytotoxic elements, cytotoxic surface ligands, and/or nanoparticle aggregation. Moreover, e.g., for unmodified cadmium telluride QDs, the induction of the formation of ROS formation leading to multiple organelle damage and cell death has been reported [92].

The preparation of both, the particles themselves and the protective surface layer, has direct influence on their cytotoxicity. It is common belief that in the case of core/shell nanoparticles, properly prepared, close shell or multiple shells such as ZnS/SiO₂-shells prevents the leakage of toxic elements and thus makes cytotoxicity unlikely. Naturally, a better solution is to avoid cytotoxic materials in the first place. QDs, for example, can be synthesized without utilization of any class A or B elements: InP/ZnS QDs have photophysical properties comparable to those of CdSe-based systems [43, 93]. Principally, whenever a new approach for QD synthesis or coating is used or if the QDs are applied in an extreme environment that could compromise their integrity, it is recommended to assess their cytotoxicity.

The work on the toxicity of nanoparticulate reporters is still in its infancy. The clear evaluation of cytotoxicity will require verified data using at least two or more independent test systems, standardization in the experimental set-up and exposure conditions in order to be reliable. In addition, the involvement of toxicologists in the systematic assessment of QD toxicity would be beneficial.

3 Application of Molecular and Nanoparticulate Fluorophores

The fast, sensitive, reliable, and reproducible detection of (bio)molecules including quantification as well as biomolecule localization, the measurement of their interplay with one another or with other species, and the assessment of biomolecule function in bioassays as well as *in vitro* and *in vivo* plays an ever increasing role in the life sciences. The vast majority of applications exploit extrinsic fluorophores like organic dyes, fluorescent proteins, and also increasingly QDs, as the number of bright intrinsic fluorophores emitting in the visible and NIR is limited. In the near future, the use of fluorophore-doped nanoparticles is also expected to constantly increase, with their applicability *in vivo* being closely linked to the intensively discussed issue of size-related nanotoxicity [88].

Suitable fluorescent labels and reporters must typically indicate the presence of a given target in the analyzed medium and must often also provide a quantitative measure for this species. Depending on the desired application, these chromophores can be chosen to retain their spectroscopic properties (dyes for labeling without real “reporting” function as, e.g., many dyes in fluorophore–biomolecule conjugates or so-called targeted optical probes for fluorescence *in vivo* imaging) or change their spectroscopic features on interacting with the target, typically in the broadest possible range of variation (i.e., affecting as many fluorescence parameters as possible). The latter type of chromophore is often termed dyes with reporting function or probe or sensor [24, 51]. In the following, we do not attempt to distinguish between both types of chromophores.

3.1 *Coupling Chromophores to Biomolecules*

In many cases, the application of fluorophores includes the covalent or noncovalent attachment of at least one fluorescent label to biomolecules like proteins, peptides, or oligonucleotides. Prerequisite for chromophore labeling of biomolecules are reactive or functional groups at the fluorophore. The great advantage of organic dyes in this respect is the commercial availability of a unique toolbox of functionalized chromophores, in conjunction with established labeling protocols, purification, and characterization techniques for dye-bioconjugates, as well as information on the site-specificity of the labeling procedure [1]. Also, many

metal ligand complexes and lanthanide chelates equipped with functional groups are commercially available. Furthermore, the small size of organic dyes minimizes possible steric hindrance, which can interfere with biomolecule function in the case of larger chromophores and allows attachment of several fluorophores to a single biomolecule to maximize the fluorescence signal [1]. Nevertheless, with regard to retaining biomolecule function, the dye-to-biomolecule ratio (D/P ratio) should not be too high and labeling of the biomolecule's binding sites is to be avoided. Moreover, high label densities can result in fluorescence quenching, with the D/P ratio where such effects become prominent being dependent on dye structure (e.g., planarity favoring π - π -interactions), charge (electrostatic repulsion of neighboring molecules), and hydrophilicity [30, 78, 94] as well as spectral overlap [24]. This is, e.g., an advantage of lanthanide labels where no fluorescence self-quenching as a function of label density is observed due to their strongly Stokes shifted emission. Also site-specificity can be problematic even for small organic dyes with the development of strategies for site-specific label attachment (often of a single label), that should be ideally generalizable and applicable to many different types of fluorophores - currently being an active area of research.

For nanoparticles, there is no consensus method for the labeling of biomolecules [95]. The most critical steps for labeling of biomolecules with QDs are ligand exchange to overcome the inherently hydrophilic nature of the QDs prior to bioconjugation, control of the number of linkers attached to a single QD (control of QD valency), and purification of the bioconjugated QDs. The general principle for biofunctionalization of nanoparticles is that, at first, the particles are made water-soluble and then bound to biomolecules (Table 2). This can be done electrostatically, by a biological immuno- or other key/lock reaction, by covalent linking (for example, carbodiimide-activated coupling between amine and carboxylic groups), or by nickel-based histidine tagging [96]. Biomolecules that bear surface active groups can replace ligands on nanoparticles directly [97]. Currently, only few standard protocols for labeling biomolecules with nanoparticles are available [64] and the choice of suitable coupling chemistries depends on the surface functionalization of the particles. It is difficult to define and employ general principles because nanoparticle surfaces may be very different, depending on their chemical nature and method used for their synthesis. Accordingly, for users of commercial nanoparticles, knowledge of surface functionalization is very important.

Most of the challenges in organic dye biofunctionalization also apply to nanoparticles, with the exception of fluorescence quenching at high label density. A problem which arises with nanoparticles is aggregation due to nonoptimal surface chemistry. Moreover, contrary to labeling with small organic fluorophores, several biomolecules are typically attached to a single nanocrystal due to the multivalency of QDs and control of biomolecule orientation is difficult. This can affect the spectroscopic properties and colloidal stability of the nanoparticles as well as biomolecule function. Similar drawbacks arise for all types of fluorophore-doped nanoparticles. Only recently, methods have been developed to optimize the 1:1 stoichiometry of QD-biomolecule conjugates [98].

3.2 *Extra- and Intracellular Targeting of Biomolecules*

The location and dynamics of biomolecules like proteins play an important role in cell signal transduction. Similarly relevant are issues like the assessment of molecular function of biomolecules, e.g., for cancer research and target quantification. A prerequisite, e.g., for monitoring molecular function *in vivo* is the ability to track biomolecules within their native environment, i.e., on the cell surface or inside cells, and needs to be met by any fluorescent label suitable for this purpose. The challenges here include intracellular delivery of the chromophore as well as selective labeling of the target biomolecule within its native setting without affecting its function. The latter is the prerequisite for assessing changes in the local environment or the distances between labeling sites using hetero-FRET (chemically different chromophores) or homo-FRET (chemically identical chromophores). Successful experiments require the selection of labels that are matched with the biological system, for instance, the location of the target (cell surface, intracellular, or vascular compartments), the expression level of the target, or whether the target is within a reducing versus an oxidizing environment.

The report of several established and recent methods for extracellular and intracellular labeling of biomolecules, in conjunction with some commercial tools for these applications [99] is mainly advantageous for organic fluorophores. This includes several strategies for site-specific covalent and noncovalent labeling of biomolecules, typically proteins, in living cells. Examples are enzyme-catalyzed labeling by posttranslational modification, as in biotin ligase-catalyzed introduction of biotin into biotin acceptor peptides, which may be used to label proteins at the cell surface. Both intracellular and surface labeling have also been achieved by specific chelation of membrane-permeant fluorescent ligands (biarsenical dyes such as FIASH or ReAsH bind to the tetracysteine motif, Ni-nitriloacetic acid (NTA) conjugates bind to the hexahistidine motif, and Zn conjugates), or by self-labeling, in which proteins fused to O6-alkylguanine-DNA alkyltransferase are combined with enzymatic substrate derivatives (O6-alkylguanine-DNA alkyltransferase (AGT) or SNAP-tags) [1, 99]. Other alternatives present the HaloTag technology, exploiting a modified haloalkane dehalogenase designed to covalently bind to synthetic ligands which can be used for the highly specific labeling of fusion proteins in living or chemically fixed cells and irreversible capture of these proteins onto solid supports [100] or the use of 2,4-diamino-5-(3,4,5-trimethoxybenzyl) pyrimidine (trimethoprim or TMP). For organic labels, also several methods are well established for fluorophore delivery into cells. This includes acetomethoxymethyl (AM) ester derivatization as well as simple microinjection, gene guns, cationic liposomes, controlled cell volume or cell membrane manipulation, and endocytosis [101] or electroporation [102]. In particular the first strategy which renders the dyes cell permeable, presents a huge advantage for this class of labels.

Meanwhile, extracellular targeting with QDs has been frequently reported [103]. Moreover, strategies have been described to reduce nonspecific QD binding and uptake as a prerequisite for applications, where specific cell-chromophore

interactions are to be investigated and the distinct, specific, and nonspecific pathways of QDs into cells as well as their intracellular fate have been studied [104]. Extracellular targeting is typically accomplished through QD functionalization with specific antibodies to image cell–surface receptors [39] or via biotin ligase-catalyzed biotinylation in conjunction with streptavidin-functionalized QDs [105]. The HaloTag method has just recently been combined with QDs allowing much simplified protocols for cell surface labeling [106]. Due to their larger size, the intracellular delivery of QDs is much more challenging compared to small organic dyes, and accordingly, the state-of-the-art of delivery of QDs into cells and internal labeling strategies are far behind. Although there exists no general protocol to achieve this so far, individual solutions have been reported, that, however, need to be empirically established in each case. Moreover, there are reports on successful cell labeling via microinjection [36], electroporation [107], nanoinjection [108], mechanochemical [109], or nonspecific or receptor-mediated endocytosis [1, 86]. As has been recently shown, the labeling specificity and efficiency can be improved with specifically functionalized QDs [98]. More sophisticated tools are needed for labeling of specific intracellular structures outside endocytosed vesicles or imaging of cellular reactions in the cytoplasm or the nucleus with QDs. Only a few successful studies have been published with QDs targeted to specific cellular locations so far [110]. More research is required in this respect to establish suitable strategies. Here, ligand design also plays a crucial role for the design of stable and small hydrophilic QDs, to minimize undesired nonspecific interactions, and to provide the basis for further functionalization [111]. Positively charged peptide transduction domains (PTDs) such as TAT (Tat peptide from the cationic domain HIV-1 Tat), polyarginine, polylysine, and other specifically designed cell penetrating peptides (CPPs), can be coated onto QDs to effect their delivery into cells [112]. It remains to be shown whether other recently developed cell penetrating agents like a synthetic ligand based on an *N*-alkyl derivative of 3 β -cholesterylamine termed streptaphage designed for efficient uptake of streptavidin conjugates by mammalian cells [113] or polyproline systems equipped with cationic and hydrophobic moieties [114] can be adapted for QD delivery.

3.3 Interactions Between Chromophores and their Microenvironment

One of the unique features of fluorophores is the general sensitivity of their spectroscopic properties to temperature and dye local environment, i.e., matrix polarity and proticity (hydrogen bonding ability), viscosity, pH, and ionic strength, and also to the presence of, e.g., surfactants or serum proteins in the case of *in vivo* studies as well as fluorescence quenchers such as oxygen or conjugated (bio) molecules. Such factors need to be considered for most applications of fluorescence ranging from analyte sensing to the characterization of cell function and behavior. Absolute quantification from measured fluorescence signals typically requires the

signal-relevant optical properties of fluorophores to be ideally insensitive to environmental factors [115]. This renders the assessment of the sensitivity of chromophores to their application-relevant environment increasingly important. In addition, the photochemical stability of fluorophores also responds to dye microenvironment.

The chromophore environment can affect the spectral position of the absorption and emission bands, the absorption and emission intensity (ϵ_M , Φ_f), and the fluorescence lifetime as well as the emission anisotropy, e.g., in the case of rigid matrices or hydrogen bonding. Changes in temperature typically result only in small spectral shifts, yet in considerable changes in the fluorescence quantum yield and lifetime. This sensitivity can be favorably exploited for the design of fluorescent sensors and probes [24, 51], though it can unfortunately also hamper quantification from simple measurements of fluorescence intensity [116]. The latter can be, e.g., circumvented by ratiometric measurements [24, 115].

The microenvironment dependence of the optical properties of organic fluorophores is controlled by dye class, nature of the emitting state(s), excited state redox potential, charge, and hydrophilicity. Dyes with resonant emission such as fluoresceins, rhodamines, and cyanines typically show only moderate changes in their spectral characteristics, yet can change considerably in fluorescence quantum yield and lifetime. Moreover, they are prone to aggregation-induced fluorescence quenching (due to, e.g., homo-FRET and static quenching [24, 117]). CT dyes with an emission from an excited state that has a considerable dipole moment like coumarins respond with notable spectral changes to changes in microenvironment polarity as well as with changes in absorption and emission intensity. These dyes can also be sensitive to solvent proticity. CT dyes, that are occasionally termed solvatochromic dyes, can be thus exploited for the design of fluorescence probes for microenvironment polarity [118].

In the case of QDs, the chromophore microenvironment mainly affects the fluorescence quantum yield and fluorescence decay behavior. These effects are governed by a whole range of factors: the nature of the nanocrystals, their ligands, shells, and the accessibility of the core surface [119]. Typically, properly shelled/ligated nanocrystals are minimally sensitive to microenvironment polarity provided that no ligand desorption occurs [5]. Also, the emission and absorption properties of most nanoparticles are barely responsive to viscosity, contrary to that of many organic dyes. All nanoparticles are colloids and thus susceptible to changes in ionic strength: electrostatically stabilized particles tend to aggregate upon increasing ionic strength. Some nanoparticles (e.g., gold nanoparticles) are prone to aggregation-induced optical changes that can be exploited as signal amplification strategy.

For both organic dyes and QDs, bioconjugation often leads to a decrease in fluorescence quantum yield and thus typically also in emission lifetime. Parameters that can affect label fluorescence are the chemical nature and the length of the spacer and, at least for organic dyes, the type of neighboring biomolecules like oligonucleotides or amino acids in the bioconjugated form.

Generally, the knowledge of microenvironment effects greatly simplifies label choice. This is an advantage of organic dyes as the spectroscopic properties of many

common labels have been investigated in a broad variety of environments including dye–biomolecule conjugates, whereas only few systematic studies have yet been performed on the microenvironment effect on QD spectroscopic properties. Moreover, the generalization of such effects is hampered by the broad variety of QD coatings used, matrix-dependent ligand adsorption–desorption equilibria, and the interplay between proper core shielding and microenvironment effects.

3.4 *Exploitation of Förster Resonance Energy Transfer*

FRET is an interaction between the electronic states of two chromophores, in which excitation energy is transferred from a donor fluorophore to an emissive or non-emissive acceptor chromophore. FRET is commonly exploited as a basis for tuning the Stokes shift (see also Sect. 3.5), to measure the distance between donor and acceptor chromophores (spectroscopic ruler, monitoring of conformational changes), for the design of ratiometric probes and sensors as well as signal amplification strategy [117, 120]. Typically, donor and acceptor chromophores are chemically different (hetero-FRET or donor–acceptor energy transfer (DAET)). More recently, chemically identical, yet photophysically different chromophores (homo-FRET or donor–donor energy migration (DDEM); measurement of the rate of energy migration) are also used for this purpose, e.g., to sense the protein aggregation state based on steady state and time-resolved measurements of the fluorescence anisotropy [117]. FRET applications thus require labeling of biomolecules or other targets with one donor and one acceptor group (hetero-FRET) or with a single class of chromophores (homo-FRET). Typically, challenging site-specific labeling is desired for hetero-FRET, whereas for homo-FRET, this can be circumvented by the performance of polarization-dependent measurements that, however, require sophisticated instrumentation. A measure of the efficiency and comparison of FRET pairs provides the Förster distance or radius (R_0) equaling the distance at which the energy transfer is 50% efficient.

There exists an ever increasing toolbox of commercial functionalized organic fluorophores with extensively described FRET properties [6]. For many FRET applications that do not need very small molecules, organic chromophores have been increasingly replaced by fluorescent proteins [121]. Numerous FRET probes based on fluorescent proteins for intracellular ion and second messenger measurements (calcium, pH, cAMP, cGMP, kinases) are established [122, 123]. For commonly used organic dyes, R_0 reaches values of 2–10 nm. Limitations of organic dyes and fluorescent proteins for FRET applications are related to crosstalk in excitation and emission. This can result from direct acceptor excitation due to the relatively broad absorption bands of these fluorophores. Moreover, the spectral discrimination of the fluorescence emission from the donor and acceptor can be difficult in the case of emissive acceptors, due to the relatively broad emission bands of organic fluorophores. In the case of dyes like fluoresceins, rhodamines, BODIPYS, and cyanines, that display a resonant emission (Fig. 1a), this is further complicated by the small

Stokes shifts and the “red” tails of the emission spectra of these chromophores. Thus, often tedious corrections of measured signals are mandatory.

Meanwhile, there are numerous examples for the successful use of QDs as FRET-donors in conjunction with organic dyes as acceptors, with the QD emission being size-tuned to match the absorption band of the acceptor dye [124]. There are also few examples of QD-only FRET pairs. In the case of QDs as donors and organic dyes as acceptors, excitation crosstalk can be easily circumvented due to the QD-inherent free choice of the excitation wavelength. Moreover, the longer lifetime of QDs can be exploited for time-resolved FRET. A QD-specific limitation for FRET applications presents both the bigger size of the QD itself and the size of the surface coating. This typically renders distance-dependent FRET with QD donors less efficient as compared to organic dyes. This limitation can be only partly overcome by using donor–acceptor ensembles where a single QD-donor is linked to several organic acceptor dyes. Due to the broad absorption bands of QDs favoring excitation crosstalk, use of QDs as FRET acceptors is not recommended [125]. Generally, FRET applications of QDs should only be considered if there is another QD-specific advantage for the system in question, such as the possibility of avoiding excitation crosstalk, their longer fluorescence lifetimes, their very large 2P action cross sections, or multiplexing FRET applications. In most cases, fluorescent proteins or organic dyes are to be favored for FRET. This is similarly true for metal ligand complexes and lanthanide chelates, the application of which in FRET pairs is not further detailed here. Despite their low molar absorption coefficients, lanthanide chelates are especially interesting FRET donors due to their strongly Stokes shifted narrow emission and long lifetime, that is often exploited for time-resolved FRET immunoassays (e.g., TR-FRET assays) [10, 54].

3.5 *Multiplexing Detection Schemes*

Current security and health concerns require robust, cost-effective, and efficient tools and strategies for the simultaneous analysis, detection, and often even quantification of multiple analytes or events in parallel. The ability to screen for and quantify multiple targets in a single assay or measurement is termed multiplexing.

3.5.1 *Spectral Multiplexing*

Spectral multiplexing or multicolor detection is typically performed at a single excitation wavelength, and relies on the discrimination between different fluorescent labels by their emission wavelength. Desirable optical properties of suitable fluorophores are a tunable Stokes shift and very narrow, preferably well-separated emission bands of simple shape.

The suitability of organic dyes for multicolor signaling at single wavelength excitation is limited due to their optical properties (Fig. 1d, f and Table 1). With

respect to small fluorescent labels and reporters, here, lanthanide chelates are to be favored, yet depending on the respective application, they may encounter problems with respect to accomplishable sensitivity. In the case of organic dyes, an increasingly common multiplexing approach implies the use of donor–acceptor dye combinations (so-called tandem dyes or energy-transfer cassettes) that exploit FRET to increase the spectral separation of absorption and emission and thus to tune the Stokes shift [6]. A typical example of a four color label system consists of a 5-carboxy-fluorescein (FAM) donor attached to four different fluorescein- and rhodamine-type acceptors (e.g., JOE, TAMRA, ROX) via a spacer such as an oligonucleotide. FRET dye-labeled primers and FRET-based multiplexing strategies are the backbone of modern DNA analysis enabling e.g. automated high speed and high throughput DNA sequencing and the development of robust multiplex diagnostic methods for the detection of polymerase chain reaction (PCR) products. With suitably designed systems, even intracellular dual FRET measurements using a single excitation wavelength were described [123]. Although broadly used, the limitations of organic dyes for FRET applications discussed in the previous section nevertheless also hamper the efficiency of these FRET-based multiplexing systems. This can be overcome by multiwavelength excitation using different lasers, which is becoming affordable due to progress in laser technology. This approach has been already successfully used in flow cytometry with the independent detection of 12 different analytes being reported using organic labels and state-of-the art cytometers [126].

The unique flexibility in excitation and the very narrow and symmetric emission bands simplifying color discrimination render QDs ideal candidates for spectral multiplexing at a single excitation wavelength. Accordingly, there are many reports of the use of QDs as labels in multiplexed assays or immunohistochemistry or imaging applications requiring multiplexing [6, 39]. Although rarely discussed, despite their very attractive spectroscopic features, the simultaneous detection and quantification of several different analytes with QD labels can also require spectral decomposition procedures of measured signals, as has been recently demonstrated for a multiplexed fluoroimmunoassay for four different toxins [127]. The importance of spectral unmixing for QD multiplexing was recently evaluated and demonstrated [128].

3.5.2 Lifetime Multiplexing

Multiplexing can also be performed by making use of the fluorophore-specific decay behavior, measured at a single excitation and single emission wavelength, to discriminate between different fluorophores. This approach requires sufficiently different lifetimes of the chromophores. With a single exception, lifetime multiplexing, as well as a combined spectral and lifetime discrimination have only been realized with organic chromophores [129]. This is most likely, related to the fact that the need for monoexponential decay kinetics was often assumed for this application. Meanwhile, successful lifetime multiplexing has been also reported both for a mixture of a QD and an organic dye and for a mixture of two different QDs [5] despite the multiexponential decay kinetics of the QDs. This may pave the road for future

applications of QDs for combined spectral and lifetime multiplexing, thereby further increasing the number of species to be discriminated.

3.6 Strategies for Signal Amplification

Signal enhancement is one of the major challenges not only in the improvement of luminescent sensors, but also for many luminescence-based methods used for the analysis of samples available only in very small quantities. This can help to improve the signal-to-noise ratio and to minimize the influence of background fluorescence or ambient light. Moreover, it paves the road for increasingly desired miniaturization and simple readout devices and helps to reduce costs. Fluorescence amplification strategies include enzymatic amplification, avidin–biotin or antibody–hapten secondary detection techniques, nucleic acid amplification, controlled aggregation, chromophore–metal interactions (metal-enhanced fluorescence or MEF, observed for the metals silver and gold), and multiple–fluorophore labels (e.g., phycobiliproteins or particle labels including systems with releasable fluorophores, dendrimeric systems, and FRET-based light harvesting systems). Such amplification strategies have been established for organic dyes and can often be used only for certain applications, such as fluoroimmunoassays. These approaches can be transferred to QDs only to certain degrees. For instance, methods involving the use of a fluorogenic enzyme substrate cannot be transferred to QD technology. However, enzymatic amplification has been combined with QDs in the past [130]. Approaches such as controlled aggregation or the construction of multichromophoric systems like chromophore-doped particle labels are similarly suited for both organic dyes and QDs. MEF, that exploits the coupling of the chromophore's transition dipole moment to metal plasmons, can provide emission enhancement factors of typically ca. 10 up to a few hundred for organic chromophores, depending on the fluorescence quantum yield of the respective dyes, in conjunction with reduction in fluorescence lifetime and increased photostability [131]. The enhancement factors, however, depend on the type, shape, and size of the metal, on the type of chromophore, and on geometrical parameters (metal–fluorophore distance, orientation) and thus require sophisticated dye–metal nanoparticle systems or (dye-doped) core/shell-nanostructures. In the case of QDs, only moderate amplification effects (e.g., fivefold fluorescence enhancement for a CdTe–Au-system) have been observed [132, 133]. The potential of this and other signal amplification approaches to optimize QD properties and to enable new sensor applications still needs to be thoroughly investigated.

3.7 Reproducibility, Quality Assurance and Limitations

Aside from instrument-specific contributions that can be corrected for, target quantification from measurements of fluorescence is affected to a nonnegligible

extent by both the sensitivity of the chromophore's spectroscopic properties to the environment and fluorophore photochemical and thermal stability [116]. Organic dyes have been successfully applied for quantification in a broad variety of *in vitro* fluorescence applications, but reports of analyte quantification with QD labels are still rare. In the case of organic dyes, dye stability can be critical for all fluorescence applications using intense light sources such as fluorescence microscopy or for methods like *in vivo* fluorescence imaging, where lasers are used as excitation light sources and measurements are performed over several days. This long term known stability issue has been partly overcome by the synthesis of more stable dyes, see section on thermal and photochemical stability [94, 134]. Nevertheless, there is still considerable interest in the development of brighter and more stable dyes. Of interest are also comparative stability studies of bioanalytically relevant dyes and labels under application-relevant conditions providing all the experimental parameters used including the excitation intensity or light flux reaching the sample as a prerequisite for data reliability and comparability. In the case of generally more photostable QDs, the recently reviewed problems still arise like photobrightening, blinking, bluing, and also bleaching [82]. QD photobrightening, i.e., the increase in emission efficiency with continuous illumination, can hamper direct quantification and may render the use of reference standards necessary [135]. This QD-specific effect is most likely related to light-induced surface passivation. The size of this phenomenon, that often reveals a dependence on excitation wavelength and is typically most pronounced for UV excitation [136], is expected to depend on the quality of the initial QD surface passivation (i.e., the saturation of surface defects by ligands or a passivating shell), and also on shell quality, thereby principally reflecting the accessibility of the QD core. This can be thus exploited as a screening test for QD quality [80]. In addition, the luminescence quantum yield of QDs can be concentration-dependent [5], thereby yielding concentration-dependent signal fluctuations, that hamper quantification. This effect depends on the bonding nature of organic ligands to the surface atoms of nanocrystals and the related ligand- and matrix-dependent adsorption-desorption equilibria which have been only marginally investigated [137–139]. This can be critical for all applications where the initially applied concentration of QD labels and probes changes during analysis, especially in the case of QDs capped and stabilized with weakly bound ligands such as many monodentate compounds. The latter processes can also result in concentration-dependent fluorescence quantum yields, especially for weakly bound ligands.

For single molecule spectroscopic applications, chromophore blinking (see Table 1) can be problematic. This phenomenon, that is often related exclusively with QDs, but also occurs for organic dyes, implies that a continuously illuminated chromophore emit detectable emission only for limited times, interrupted by dark periods during which no emission occurs. This can be a significant disadvantage of otherwise very attractive QDs as can be the blinking of organic dyes [140]. For example, QD blinking has been reported to affect the results from bioaffinity studies [141]. Another aspect that might influence the usability of QDs for quantification lies in the fact that not all QDs in a set of QDs luminesce [142]. For

ensembles of QDs, accurate quantification thus requires the ratio of emissive to nonemissive QDs to be constant.

Generally, reliable and comparable fluorescence measurements require fluorescent labels with reproducible physico-chemical properties and established tools to evaluate this. This is a unique advantage of organic dyes. These compounds can be synthesized on a large scale and characterized according to their structure and purity using well-established analytical techniques. This is more challenging for dye–biomolecule conjugates, such as fluorophore-labeled antibodies or proteins, due to batch-to-batch variations in label density and label density distribution and the lack of methods to reliably and accurately determine label density. Nevertheless, this is manageable in principle. In the case of QDs, the colloidal nature of these chromophores, in conjunction with the broad variety of synthetic strategies and surface functionalities, renders chromophore characterization more challenging compared to organic dyes. For commercial QDs, this is often further complicated by the fact that commercial distributors usually refrain from providing any information about the ligand(s). For instance, at present, there are no established methods available to determine the surface coverage and number of ligands attached to the surface of a QD. Even more challenging is the characterization of QD–biomolecule conjugates, e.g., the measurement of the QD-to-biomolecule ratio [143].

4 Applications of Nanoparticles: State-of-the-Art and Future Trends

Organic molecules are well established as fluorescent labels and reporters for *in vitro* assays and *in vivo* imaging, despite their nonoptimum spectroscopic features and photochemical instability. Due to their availability from many commercial sources, established functionalization protocols, and extensively studied properties organic dyes present a simple, safe, and comparatively inexpensive option. This holds similarly true for metal ligand complexes and lanthanide chelates. To further improve the reliability of the data obtained with these labels and reporters, e.g., the fluorescence quantum yields of typical chromophores under commonly used measurement conditions should be reevaluated and comparative photostability studies could be beneficial. With respect to the ever increasing number of *in vivo* applications of chromophores, reliable data on the cytotoxicity of these chromophores are also needed, preferably obtained under standardized measurement conditions. Generally, there is an increasing need for bright and stable NIR chromophores [144]. Whether this can be met with the rational design of organic dyes, metal ligand complexes, and lanthanide chelates or whether the use of established NIR chromophores encapsulated into organic or inorganic nanoparticles is a more straightforward approach to tune the spectroscopic properties and the stability of such NIR fluorophores [145] remains to be seen in the coming years. Here, particulate labels and reporters are expected to have a bright future if the

nanotoxicity issue is resolved. There also exist many different instances where QDs have been applied to biological systems. Although most of these studies are proof-of-principle, they underline the growing potential of these reagents. QDs are very attractive candidates for bioanalytical applications that can either exploit their potential for spectral multiplexing, do not require strong signal amplification or that rely on NIR fluorescence.

Apart from the advantageous properties discussed above, QDs could have a bright future especially in the field of near infrared fluorescence imaging (NIRF), because they show high fluorescence quantum yields in the 650–900 nm window, may have adequate stability, good water solubility as well as large 2P action cross sections as desired for deep tissue imaging. The only clinically approved organic NIR fluorophore ICG (Table 1) suffers from a very low fluorescence quantum yield [31, 78], limited stability, and binding to plasma proteins. Other organic fluorophores for the NIR range (with pending approval like, e.g., Cy5.5, $\Phi_F = 0.28$ in phosphate buffer solution) still possess small quantum yields compared to NIR-emitting QDs such as CdTe (Table 1). In addition, QDs are attractive candidates for the development of multifunctional composite reporters for the combination of two or more bioanalytical imaging techniques, such as NIRF/magnetic resonance imaging (MRI) [146].

Despite the promising possibilities offered by the different types of nanoparticles, their routine use is still strongly limited by the very small number of commercially available systems and the limited amount of data on their reproducibility (in preparation, spectroscopic properties, and application) and comparability (e.g., fluorescence quantum yields, stability) as well as on their potential for quantification. To date, no attempt has yet been published comparing differently functionalized nanoparticles from various sources (industrial and academic) in a Round Robin test, to evaluate achievable fluorescence quantum yields, and batch-to-batch variations for different materials and surface chemistries (including typical ligands and bioconjugates). Such data would be very helpful for practitioners and would present the first step to derive and establish quality criteria for these materials.

In addition to the practical questions linked to the application of nanoparticles, fundamental questions such as the elucidation of quantum dot lifetime characteristics, e.g., for lifetime multiplexing [147] and combined lifetime and spectral multiplexing in conjunction with the development of suitable algorithms for data analysis and for time resolved FRET have to be addressed. Other current limitations include the comparatively large size of nanoparticles. The ligand-controlled size of nanoparticles does not only affect their FRET efficiency but could also sterically hamper access to cellular targets and could affect the function of labeled biomolecules. So far, nanoparticles for bioanalytical applications can only be prepared on a very small scale. Commercialization of, e.g., NIR QDs requires more systematic studies of nanoparticle nucleation and growth. This involves the control of nanoparticle surface chemistry, and the establishment of functionalization protocols. A first useful step in this direction would be the design of a reliable and reproducible test for the quality of surface coatings, i.e., the degree of perfection of the surface ligand shell, as this is the most crucial parameter affecting the spectroscopic and

toxicity properties of nanoparticles [80]. Eventually, the cytotoxicity of differently functionalized nanoparticles (including typical ligands) should be systematically assessed using previously standardized procedures.

Even though nanoparticles have extremely promising and advantageous (optical) properties, at present, they cannot be recommended for routine applications, due to the problems discussed in this review. In very specific cases, such as single molecule/single particle imaging and tracking applications, QDs are superior to most luminescent dyes due to their photostability, in principle allowing single-particle tracking for a much longer time span compared with organic fluorophores. However, blinking that is observed for all QDs is a major drawback even for these specialized applications. Nevertheless, there is hope that quantum dot blinking can be overcome, making them eventually the ideal labels for all applications in need of exceptional photostability [148]. On the other hand, blinking, as well as other QD-specific features, may be even exploited for advanced techniques such as superresolution microscopy [82, 149]. Here, further exciting potential applications of QDs are expected to appear in the near future.

5 Conclusions

Nanocrystals have been exploited in several areas of biosensing and -imaging, including immunohistochemistry, microarray technologies as well as advanced fluorescence techniques such as FISH, and *in vivo* fluorescence imaging using conventional techniques and multiphoton microscopy. Despite many superior optical properties of these particles, such as tunable absorption and emission bands and extremely broad and intense absorption, high fluorescence quantum yields even in the NIR region, and large two-photon action cross sections as well as unique spectroscopic prerequisites for spectral multiplexing in the case of QDs, or sophisticated optical effects such as upconversion luminescence in the case of rare-earth doped nanocrystals, until now, nanocrystals failed to be routinely used on a large scale. The fact that these materials behave like colloids but not like molecules complicates their application in biological environments. Practitioners must consider the costs of finding a solution to the challenges of their particular experimental system against the benefits of their advanced spectroscopic features. However, it is anticipated that advances in nanosciences combined with the attractive features of many nanoparticle systems will render these particles increasingly attractive for bioanalytical applications in the future.

References

1. Resch-Genger U, Grabolle M, Cavaliere-Jaricot S, Nitschke R, Nann T (2008) Quantum dots versus organic dyes as fluorescent labels. *Nat Methods* 5:763–775
2. Lavis LD (2008) Bright ideas for chemical biology. *ACS Chem Biol* 3:142–155

3. Zhang J, Campbell RE, Ting AY, Tsien RY (2002) Creating new fluorescent probes for cell biology. *Nat Rev* 3:906–918
4. Lakowicz JR (2006) Principles of fluorescence spectroscopy, 3rd edn. Springer, New York
5. Grabolle M, Kapusta P, Nann T, Shu X, Ziegler J, Resch-Genger U (2009) Fluorescence lifetime multiplexing with nanocrystals and organic labels. *Anal Chem* 81:7807–7813
6. Sapsford KE, Berti L, Medintz IL (2006) Materials for fluorescence resonance energy transfer analysis: beyond traditional donor–acceptor combinations. *Angew Chem Int Ed* 45:4562–4588
7. Chan CP (2009) Ingenious nanopores in bioassays. *Bioanalysis* 1:115–133
8. Bissell RA, de Silva AP, Gunaratne HQN, Lynch PLM, Maguire GEM, Sandanayake KRAS (1992) Molecular fluorescent signalling with ‘Fluor-Spacer-Receptor’ systems: approaches to sensing and switching devices via supramolecular photophysics. *Chem Soc Rev* 21:187–195
9. Dixon IM, Lebon E, Sutra P, Igau A (2009) Luminescent ruthenium–polypyridine complexes & phosphorus ligands: anything but a simple story. *Chem Soc Rev* 38:1621–1634
10. Hemmila I, Laitala V (2005) Progress in lanthanides as luminescent probes. *J Fluoresc* 15:529–542
11. Parker D, Dickins RS, Puschmann H, Crossland C, Howard JAK (2002) Being excited by lanthanide coordination complexes: aqua species, chirality, excited-state chemistry, and exchange dynamics. *Chem Rev* 102:1977–2010
12. dos Santos CMG, Harte AJ, Quinn SJ, Gunnlaugsson T (2008) Recent developments in the field of supramolecular lanthanide luminescent sensors and self-assemblies. *Coord Chem Rev* 252:2512–2527
13. Shaner NC, Steinbach PA (2005) A guide to choosing fluorescent proteins. *Nat Methods* 2:905–909
14. Li JH, Zhang JZ (2009) Optical properties and applications of hybrid semiconductor nanomaterials. *Coord Chem Rev* 253:3015–3041
15. Sun YP et al (2006) Quantum-sized carbon dots for bright and colorful photoluminescence. *J Am Chem Soc* 128:7756–7757
16. Warner JH, Hoshino A (2005) Water-soluble photoluminescent silicon quantum dots. *Angew Chem Int Ed* 44:4550–4554
17. Prodi L, Battistini G, Dolci L, Montalti M, Zaccheroni N (2007) Luminescence of gold nanoparticles. In *frontiers in surface nanophotonics*, Springer series in optical sciences. Springer, Berlin, Heidelberg, pp 99–128 Available via http://dx.doi.org/10.1007/978-0-387-48951-3_5
18. Fu H, Yao JN (2001) Size effects on the optical properties of organic nanoparticles. *J Am Chem Soc* 123:1434–1439
19. Soukka T, Rantanen T, Kuningas K (2008) Photon upconversion in homogeneous fluorescence-based bioanalytical assays. *Ann N Y Acad Sci* 1130:188–200, *Fluorescence Methods and Applications: Spectroscopy, Imaging, and Probes*
20. Qian HS, Li ZQ, Zhang Y (2008) Multicolor polystyrene nanospheres tagged with up-conversion fluorescent nanocrystals. *Nanotechnology* 19(255601):4
21. Yan JL, Estevez MC, Smith JE, Wang KM, He XX, Wang L, Tan WH (2007) Dye-doped nanoparticles for bioanalysis. *Nano Today* 2:44–50
22. Swager TM (1998) The molecular wire approach to sensory signal amplification. *Acc Chem Res* 31:201–207
23. Luchowski R, Matveeva EG, Gryczynski I, Terpetschnig EA, Patsenker L, Laczko G, Borejdo J, Gryczynski Z (2008) Single molecule studies of multiple-fluorophore labeled antibodies. Effect of homo-FRET on the number of photons available before photobleaching. *Curr Pharm Biotechnol* 9:411–420
24. Demchenko AP (2005) Optimization of fluorescence response in the design of molecular biosensors. *Anal Biochem* 343:1–22
25. Nagl S, Schaeferling M, Wolfbeis OS (2005) Fluorescence analysis in microarray technology. *Microchim Acta* 151:1–21

26. Doering K, Meder G, Hinnenberger M, Woelcke J, Mayr LM, Hassiepen U (2009) A fluorescence lifetime-based assay for protease inhibitor profiling on human kallikrein 7. *J Biomol Screen* 14:1–9
27. Turconi S, Bingham RP, Haupts U, Pope AJ (2001) Developments in fluorescence for lifetime-based analysis for ultra-HTS. *Drug Discov Today* 6:27–39
28. Soukka T, Paukkunen J, Harma H, Lonnberg S, Lindroos H, Lovgren T (2001) Supersensitive time-resolved immunofluorometric assay of free prostate-specific antigen with nanoparticle label technology. *Clin Chem* 47:1269–1278
29. Sackett DL, Wolff J (1987) Nile red as a polarity-sensitive fluorescent probe of hydrophobic protein surfaces. *Anal Biochem* 167:228–234
30. Gruber HJ, Hahn CD (2000) Anomalous fluorescence enhancement of Cy3 and Cy3.5 versus anomalous fluorescence loss of Cy5 and Cy7 upon covalently linking to IgC and noncovalent binding to avidin. *Bioconjug Chem* 11:696–704
31. Soper SA, Mattingly QL (1994) Steady-state and picosecond laser fluorescence studies of nonradiative pathways in tricarboyanine dyes: implications to the design of near-IR fluorochromes with high fluorescence efficiencies. *J Am Chem Soc* 116:3744–3752
32. Dabbousi BO, Rodriguez-Viejo J, Mikulec FV, Heine JR, Mattoussi H, Ober R, Jensen KF, Bawendi MG (1997) (CdSe)ZnS core-shell quantum dots: synthesis and characterization of a size series of highly luminescent nanocrystallites. *J Phys Chem B* 101:9463–9475
33. Yu WW, Qu L, Guo W, Peng X (2003) Experimental determination of the extinction coefficient of CdTe, CdSe, and CdS nanocrystals. *Chem Mater* 15:2854–2860
34. Chan WC, Nie S (1998) Quantum dot bioconjugates for ultrasensitive nonisotopic detection. *Science* 281:2016–2018
35. Mitchell GP, Mirkin CA, Letsinger RL (1999) Programmed assembly of DNA functionalized quantum dots. *J Am Chem Soc* 121:8122–8123
36. Dubertret B, Skourides P, Norris DJ, Noireaux V, Brivanlou AH, Libchaber A (2002) In vivo imaging of quantum dots encapsulated in phospholipid micelles. *Science* 298:1759–1762
37. Gao XH, Yang LL, Petros JA, Marshal FF, Simons JW, Nie SM (2005) In vivo molecular and cellular imaging with quantum dots. *Curr Opin Biotechnol* 16:63–72
38. Wang Q, Xu Y, Zhao X, Chang Y, Liu Y, Jiang L, Sharma J, Seo DK, Yan H (2007) A facile one-step in situ functionalization of quantum dots with preserved photoluminescence for bioconjugation. *J Am Chem Soc* 129:6380–6381
39. Xing Y et al (2007) Bioconjugated quantum dots for multiplexed and quantitative immunohistochemistry. *Nat Protoc* 2:1152–1165
40. Nann T (2005) Phase-transfer of CdSe@ZnS quantum dots using amphiphilic hyperbranched polyethylenimine. *Chem Commun*:1735–1736
41. Nann T, Mulvaney P (2004) Single quantum dots in spherical silica particles. *Angew Chem Int Ed* 43:5393–5396
42. Riegler J, Nick P, Kielmann U, Nann T (2003) Visualizing the self-assembly of tubulin with luminescent nanorods. *J Nanosci Nanotechnol* 3:380–385
43. Xu S, Ziegler J, Nann T (2008) Rapid synthesis of highly luminescent InP and InP/ZnS nanocrystals. *J Mater Chem* 18:2653–2656
44. Xie R, Rutherford M, Peng X (2009) Formation of high-quality I–III–VI semiconductor nanocrystals by tuning relative reactivity of cationic precursors. *J Am Chem Soc* 131:5691–5697
45. Blasse G, Grabmaier BC (1994) Luminescent materials. Springer, Berlin
46. Auzel F (2004) Upconversion and anti-stokes processes with f and d Ions in solids. *Chem Rev* 104:139–174
47. Stouwdam JW, van Veggel F (2002) Near-infrared emission of redispersible Er³⁺, Nd³⁺, and Ho³⁺ doped LaF₃ nanoparticles. *Nano Lett* 2:733–737
48. Fort E, Gresillon S (2008) Surface enhanced fluorescence. *J Phys D Appl Phys* 41:013001
49. Mooradian A (1969) Photoluminescence of metals. *Phys Rev Lett* 22:185

50. Zheng J, Zhang C, Dickson RM (2004) Highly fluorescent, water-soluble, size-tunable gold quantum dots. *Phys Rev Lett* 93:077402
51. Borisov SM, Wolfbeis OS (2008) Optical biosensors. *Chem Rev* 108:423–461
52. Medlycott EA, Hanan GS (2005) Designing tridentate ligands for ruthenium(II) complexes with prolonged room temperature luminescence lifetimes. *Chem Soc Rev* 34:133–142
53. Montalti M, Credi A, Prodi L, Gandolfi MT (2006) Handbook of photochemistry, 3rd edn. CRC, Taylor & Francis Group, LLC, Boca Raton
54. Trinquet E, Mathis G (2006) Fluorescence technologies for the investigation of chemical libraries. *Mol BioSyst* 2:381–387
55. Leonard JP, Nolan CB, Stomeo F, Gunnlaugsson T (2007) Photochemistry and photophysics of coordination compounds. In: Balzani V, Campagna S (eds) *Topics in Current Chemistry Photochemistry and Photophysics of Coordination Compounds. Vol II, Lanthanides*, 281:1–43
56. Bünzli JG (2009) Lanthanide luminescent bioprobes (LLBs). *Chem Lett* 38:104–109
57. Deiters E, Song B, Chauvin AS, Vandevyver CDB, Gumy F, Bunzli JCG (2009) Luminescent bimetallic lanthanide bioprobes for cellular imaging with excitation in the visible-light range. *Chem Eur J* 15:885–900
58. Armelao L, Quici S, Barigelletti F, Accorsi G, Bottaro G, Cavazzini M, Tondello E (2010) Design of luminescent lanthanide complexes: from molecules to highly efficient photoemitting materials. *Coord Chem Rev* 254:487–505
59. McBride J, Treadway J, Feldman LC, Pennycook SJ, Rosenthal SJ (2006) Structural basis for near unity quantum yield core/shell nanostructures. *Nano Lett* 6:1496–1501
60. Fernee MJ, Thomsen E, Jensen P, Rubinsztein-Dunlop H (2006) Highly efficient luminescence from a hybrid state found in strongly quantum confined PbS nanocrystals. *Nanotechnology* 17:956–962
61. Lifshitz E et al (2006) Stable PbSe/PbS and PbSe/PbSexS1-x core-shell nanocrystal quantum dots and their applications. *J Phys Chem B* 110:25356–25365
62. He GS, Yong K, Zheng Q, Sahoo Y, Baev A, Rysanyanskiy AI, Prasad PN (2007) Multiphoton excitation properties of CdSe quantum dots solutions and optical limiting behavior in infrared range. *Opt Exp* 15:12818–12833
63. Clapp AR et al (2007) Two-Photon excitation of quantum-dot-based fluorescence resonance energy transfer and its applications. *Adv Mater* 19:1921–1926
64. Jaiswal JK, Simon SM (2004) Potentials and pitfalls of fluorescent quantum dots for biological imaging. *Trends Cell Biol* 14:497–504
65. Xu C, Zipfel W, Shera JB, Williams RM, Webb WW (1996) Multiphoton fluorescence excitation: new spectral window for biological nonlinear microscopy. *Proc Natl Acad Sci USA* 93:10763–10768
66. Mihindukulasuriya SH, Morcone TK, McGown LB (2003) Characterization of acridone dyes for use in four-decay detection in DNA sequencing. *Electrophoresis* 24:20–25
67. Hennig A, Florea M, Roth D, Enderle T, Nau WM (2007) Design of peptide substrates for nanosecond time-resolved fluorescence assays of proteases: 2,3-diazabicyclo[2.2.2]oct-2-ene as a noninvasive fluorophore. *Anal Biochem* 360:255–265
68. Zhu L, Stryjwesi WJ, Soper SA (2004) Multiplexed fluorescence detection with micro-fabricated devices with both time-resolved and spectral-discrimination capabilities using near-infrared fluorescence. *Anal Biochem* 330:206–218
69. Grecco HE, Lidke KA, Heintzmann R, Lidke DS, Spagnuolo C, Martinez OE, Jares-Erijman EA, Jovin TM (2004) Ensemble and single particle photophysical properties (two-photon excitation, anisotropy, FRET, lifetime, spectral conversion) of commercial quantum dots in solution and in live cells. *Microsc Res Tech* 65:169–179
70. Sakamoto T, Mahara A, Munaka T, Yamagata K, Iwase R, Yamaoka T, Murakami A (2004) Time-resolved luminescence anisotropy-based detection of immunoglobulin G using long-lifetime Ru(II) complex-labeled protein A. *Anal Biochem* 329:142–144

71. Morris KJ, Roach MS, Xu WY, Demas JN, DeGraff BA (2007) Luminescence lifetime standards for the nanosecond to microsecond range and oxygen quenching of ruthenium(II) complexes. *Anal Chem* 79:9310–9314
72. Wolfbeis OS, Klimant I, Werner T, Huber C, Kosch U, Krause C, Neurauder G, Dürkop A (1998) Set of luminescence decay time based chemical sensors for clinical applications. *Sens Actuators B* 51:17–24
73. Hemmilä I, Webb S (1997) Time-resolved fluorometry: an overview of the labels and core technologies for drug screening applications. *Drug Discov Today* 2:373–381
74. Samiotaki M, Kwiatkowski M, Ylitalo N, Landegren U (1997) Seven-color time-resolved fluorescence hybridization analysis of human papilloma virus types. *Anal Biochem* 253:156–161
75. Willner I, Patolsky F, Wasserman J (2001) Photoelectrochemistry with controlled DNA-cross-linked CdS nanoparticle arrays. *Angew Chem Int Ed* 40:1861–1864
76. Gao X, Yang L, Petros JA, Marshall FF, Simons JW, Nie S (2005) In vivo molecular and cellular imaging with quantum dots. *Curr Opin Biotechnol* 16:63–72
77. Sukhanova A et al (2004) Biocompatible fluorescent nanocrystals for immunolabeling of membrane proteins and cells. *Anal Biochem* 324:60–67
78. Pauli J, Vag T, Haag R, Spieles M, Wenzel M, Kaiser WA, Resch-Genger U, Hilger I (2009) An in vitro characterization study of new near infrared dyes for molecular imaging. *Eur J Med Chem* 44:3496–3503
79. Fare TL et al (2003) Effects of atmospheric ozone on microarray data quality. *Anal Chem* 75:4672–5
80. Ziegler J, Merkulov A, Grabolle M, Resch-Genger U, Nann T (2007) High-quality ZnS shells for CdSe nanoparticles: rapid microwave synthesis. *Langmuir* 23:7751–7759
81. Smith AM, Dave S, Nie S, True L, Gao X (2006) Multicolor quantum dots for molecular diagnostics of cancer. *Expert Rev Mol Diagn* 6:231–244
82. Lee SF, Osborne MA (2009) Brightening, blinking, bluing and bleaching in the life of a quantum dot: friend or foe? *Chemphyschem* 10:2174–2191
83. Achilefu S (2004) Lighting up tumors with receptor-specific optical molecular probes. *Technol Cancer Res Treat* 3:393–409
84. Greenbaum L, Rothmann C, Lavie R, Malik Z (2000) Green fluorescent protein photobleaching: a model for protein damage by endogenous and exogenous singlet oxygen. *Biol Chem* 381:1251–1258
85. Lewinski N, Colvin V, Drezek R (2008) Cytotoxicity of nanoparticles. *Small* 4:26–49
86. Parak WJ, Pellegrino T, Plank C (2005) Labelling of cells with quantum dots. *Nanotechnology* 16:R9–R25
87. Hardman R (2006) A toxicologic review of quantum dots: toxicity depends on physicochemical and environmental factors. *Environ Health Perspect* 114:165–172
88. Sun XK, Rossin R, Turner JL, Becker ML, Joralemon MJ, Welch MJ, Wooley KL (2005) An assessment of the effects of shell cross-linked nanoparticle size, core composition, and surface PEGylation on in vivo biodistribution. *Biomacromolecules* 6:2541–2554
89. Ma J, Chen J, Guo J, Wang CC, Yang WL, Xu L, Wang PN (2006) Photostability of thiol-capped CdTe quantum dots in living cells: the effect of photo-oxidation. *Nanotechnology* 17:2083–2089
90. Kirchner C, Liedl T, Kudera S, Pellegrino T, Munoz Javier A, Gaub HE, Stolzle S, Fertig N, Parak WJ (2005) Cytotoxicity of colloidal CdSe and CdSe/ZnS nanoparticles. *Nano Lett* 5:331–338
91. Selvan ST, Tan TT, Ying JY (2005) Robust, non-cytotoxic, silica-coated CdSe quantum dots with efficient photoluminescence. *Adv Mater* 17:1620–1625
92. Lovric J, Cho SJ, Winnik FM, Maysinger D (2005) Unmodified cadmium telluride quantum dots induce reactive oxygen species formation leading to multiple organelle damage and cell death. *Chem Biol* 12:1227–1234

93. Xu S, Kumar S, Nann T (2006) Rapid synthesis of high-quality InP nanocrystals. *J Am Chem Soc* 128:1054–1055
94. Berlier JE et al (2003) Quantitative comparison of long-wavelength Alexa Fluor dyes to Cy dyes: fluorescence of the dyes and their bioconjugates. *J Histochem Cytochem* 51: 1699–1712
95. Mazumder S, Dey R, Mitra MK, Mukherjee S, and Das GC (2009) Review: biofunctionalized quantum dots in biology and medicine. *J Nanomater* 2009:17
96. Michalet X et al (2005) Quantum dots for live cells, in vivo imaging, and diagnostics. *Science* 307:538–544
97. Mitchell GP, Mirkin CA, Letsinger RL (1999) Programmed assembly of DNA functionalized quantum dots. *J Am Chem Soc* 121:8122–8123
98. Howarth M, Liu WH, Puthenveetil S, Zheng Y, Marshall LF, Schmidt MM, Witttrup KD, Bawendi MG, Ting AY (2008) Monovalent, reduced-size quantum dots for imaging receptors on living cells. *Nat Methods* 5:397–399
99. Giepmans BNG, Adams SR, Ellisman MH, Tsien RY (2006) Review – the fluorescent toolbox for assessing protein location and function. *Science* 312:217–224
100. Los GV et al (2008) HaloTag: a novel protein labeling technology for cell imaging and protein analysis. *ACS Chem Biol* 3:373–382
101. Torchilin VP (2006) Recent approaches to intracellular delivery of drugs and DNA and organelle targeting. *Ann Rev Biomed Eng* 8:343–375
102. Nagayama S, Zeng SQ, Xiong WH, Fletcher ML, Masurkar AV, Davis DJ, Pieribone VA, Chen WR (2007) In vivo simultaneous tracing and Ca²⁺ imaging of local neuronal circuits. *Neuron* 53:789–803
103. Chang YP, Pinaud F, Antelman J, Weiss S (2008) Tracking bio-molecules in live cells using quantum dots. *J Biophotonics* 1:287–298
104. Hild WA, Breunig M, Goepferich A (2008) Quantum dots – nano-sized probes for the exploration of cellular and intracellular targeting. *Eur J Pharm Biopharm* 68:153–168
105. Howarth M, Takao K (2005) Targeting quantum dots to surface proteins in living cells with biotin ligase. *Proc Natl Acad Sci USA* 102:7583–7588
106. So MK, Yao HQ, Rao JH (2008) HaloTag protein-mediated specific labeling of living cells with quantum dots. *Biochem Biophys Res Commun* 374:419–423
107. Derfus AM, Chan WCW, Bhatia SN (2004) Intracellular delivery of quantum dots for live cell labeling and organelle tracking. *Adv Mater* 16:961–966
108. Chen X, Kis A, Zettl A, Bertozzi CR (2007) A cell nanoinjector based on carbon nanotubes. *Proc Natl Acad Sci USA* 104:8218–8222
109. Yum K, Na S, Xiang Y, Wang N, Yu MF (2009) Mechanochemical delivery and dynamic tracking of fluorescent quantum dots in the cytoplasm and nucleus of living cells. *Nano Lett* 9:2193–2198
110. Kim BYS, Jiang W, Oreopoulos J, Yip CM, Rutka JT, Chan WCW (2008) Biodegradable quantum dot nanocomposites enable live cell labeling and imaging of cytoplasmic targets. *Nano Lett* 8:3887–3892
111. Liu W et al (2010) Compact biocompatible quantum dots via RAFT-mediated synthesis of imidazole-based random copolymer ligand. *J Am Chem Soc* 132:472–83
112. Zhou M, Ghosh I (2006) Current trends in peptide science. Quantum dots and peptides: a bright future together. *Biopolymers (Peptide Science)* 88:325–339
113. Hussey SL (2002) Efficient delivery of streptavidin to mammalian cells: clathrin-mediated endocytosis regulated by a synthetic ligand. *J Am Chem Soc* 124:6265–6273
114. Fillon YA (2005) Cell penetrating agents based on a polyproline helix scaffold. *J Am Chem Soc* 127:11798–11803
115. Chen AK, Cheng ZL, Behlke MA, Tsourkas A (2008) Assessing the sensitivity of commercially available fluorophores to the intracellular environment. *Anal Chem* 80:7437–7444
116. Resch-Genger U, Hoffmann K, Nietfeld W, Engel A, Neukammer J, Nitschke R, Ebert B, Macdonald R (2005) How to improve quality assurance in fluorometry: fluorescence-inherent sources of error and suited fluorescence standards. *J Fluoresc* 15:337–362

117. Johansson MK, Cook RM (2003) Intramolecular dimers: a new design strategy for fluorescence-quenched probes. *Chem Eur J* 9:3466–3471
118. Grabowski ZR, Rotkiewicz K, Rettig W (2003) Structural changes accompanying intramolecular electron transfer: focus on twisted intramolecular charge transfer states and structures. *Chem Rev* 103:3899–4031
119. Ji X, Copenhaver D, Sichmeller C, Peng X (2008) Ligand bonding and dynamics on colloidal nanocrystals at room temperature: the case of alkylamines on CdSe nanocrystals. *J Am Chem Soc* 130:5726–5735
120. Kikuchi K, Takakusa H, Nagano T (2004) Recent advances in the design of small molecule-based FRET sensors for cell biology. *Trends Analyt Chem* 23:407–415
121. Shaner NC, Steinbach PA, Tsien RY (2005) A guide to choosing fluorescent proteins. *Nat Methods* 2:905–909
122. Mank M, Griesbeck O (2008) Genetically encoded calcium indicators. *Chem Rev* 108:1550–1564
123. Niino Y, Hotta K, OkA K (2009) Simultaneous live cell imaging using dual FRET sensors with a single excitation light. *PLoS One* 4:e6036
124. McGrath N, Barroso M (2008) Quantum dots as fluorescence resonance energy transfer donors in cells. *J Biomed Opt* 13(3):031210
125. Clapp AR, Medintz IL, Fisher BR, Anderson GP, Mattoussi H (2005) Can luminescent quantum dots be efficient energy acceptors with organic dye donors? *J Am Chem Soc* 127:1242–1250
126. Rosa SCD, Brenchley JM, Roederer M (2003) Beyond six colors: a new era in flow cytometry. *Nat Med* 9:112–117
127. Goldman ER, Clapp AR, Anderson GP, Uyeda HT, Mauro JM, Medintz IL, Mattoussi H (2004) Multiplexed toxin analysis using four colors of quantum dot fluororeagents. *Anal Chem* 76:684–688
128. Huang D, Peng X, Su L, Wang D, Khuri FR, Shin DM, Chen Z (2010) Comparison and optimization of multiplexed quantum dot-based immunohistochemistry. *Nano Res* 3:61–68
129. Snyder TM, McGown LB (2005) Multiplex single strand conformation polymorphism analysis by capillary electrophoresis with on-the-fly fluorescence lifetime detection. *Appl Spectrosc* 59:335–339
130. Ness JM, Akhtar RS, Latham CB, Roth KA (2003) Combined tyramide signal amplification and quantum dots for sensitive and photostable immunofluorescence detection. *J Histochem Cytochem* 51:981–987
131. Aslan K, Gryczynski I, Malicka J, Matveeva E, Lakowicz JR, Geddes CD (2005) Metal-enhanced fluorescence: an emerging tool in biotechnology. *Curr Opin Biotechnol* 16:55–62
132. Lee J, Javed T, Skeini T, Govorov AO, Bryant GW, Kotov NA (2006) Bioconjugated Ag nanoparticles and CdTe nanowires: metamaterials with field-enhanced light absorption. *Angew Chem Int Ed* 45:4819–4823
133. Govoroch AO, Bryant GW, Zhang W, Skeini T, Lee J, Kotov NA, Slocik JM, Naik RR (2006) Exciton–plasmon interaction and hybrid excitons in semiconductor–metal nanoparticle assemblies. *Nano Lett* 6:984–994
134. Panchuk-Voloshina N, Haugland RP, Bishop-Stewart J, Bhalgat MK, Millard PJ, Mao F, Leung WY, Haugland RP (1999) Alexa dyes, a series of new fluorescent dyes that yield exceptionally bright, photostable conjugates. *J Histochem Cytochem* 47:1179–1188
135. Parak WJ, Boudreau R, Le Gros M, Gerion D, Zanchet D, Micheel CM, Williams SC, Alivisatos AP, Larabell C (2002) Cell motility and metastatic potential studies based on quantum dot imaging of phagokinetic tracks. *Adv Mater* 14:882–885
136. Bentolila LA, Weiss S (2006) Single-step multicolor fluorescence in situ hybridization using semiconductor quantum dot–DNA conjugates. *Cell Biochem Biophys* 45:59–70
137. Ji X (2008) Ligand bonding and dynamics on colloidal nanocrystals at room temperature: the case of alkylamines on CdSe nanocrystals. *J Am Chem Soc* 130:5726–5735

138. Munro AM, Plante IJL, Ng MS, Ginger DS (2007) Quantitative study of the effects of surface ligand concentration on CdSe nanocrystal photoluminescence. *J Phys Chem C* 111:6220–6227
139. Kopping JT, Patten TE (2008) Identification of acidic phosphorus-containing ligands involved in the surface chemistry of CdSe nanoparticles prepared in tri-*n*-octylphosphine oxide solvents. *J Am Chem Soc* 130:5689–5698
140. Gomez DE (2006) Optical properties of single semiconductor nanocrystals. *Phys Chem Chem Phys* 8:4989–5011
141. Robelek R, Stefani FD, Knoll W (2006) Oligonucleotide hybridization monitored by surface plasmon enhanced fluorescence spectroscopy with bio-conjugated core/shell quantum dots. Influence of luminescence blinking. *Phys Status Solidi A-Appl Mater Sci* 203:3468–3475
142. Ebenstein Y, Mokari T, Banin U (2002) Fluorescence quantum yield of CdSe/ZnS nanocrystals investigated by correlated atomic-force and single-particle fluorescence microscopy. *Appl Phys Lett* 80:4033–4035
143. Casanova D, Giaume D, Moreau M, Martin JL, Gacoin T, Boilot JP, Alexandrou A (2007) Counting the number of proteins coupled to single nanoparticles. *J Am Chem Soc* 129:12592–12593
144. Kiyose K, Kojima H, Nagano T (2008) Functional near-infrared fluorescent probes. *Chem Asian J* 3:506–515
145. Altinoglu EI, Russin TJ, Kaiser JM, Barth BM, Eklund PC, Kester M, Adair JH (2008) Near-infrared emitting fluorophore-doped calcium phosphate nanoparticles for in vivo imaging of human breast cancer. *ACS Nano* 2:2075–2084
146. Wang S, Jarrett BR, Kauzlarich SM, Louie AY (2007) Core/Shell quantum dots with high relaxivity and photoluminescence for multimodality imaging. *J Am Chem Soc* 129:3848–3856
147. Grabolle M, Spieles M, Lesnyak V, Gaponik N, Eychmüller A, Resch-Genger U (2009) Determination of the fluorescence quantum yield of quantum dots: suitable procedures and achievable uncertainties. *Anal Chem* 81:6285–6294
148. Orrit M, Basché T (2009) Steady light from quantum dots, at last. But how? *ChemPhysChem* 10:2383–2385
149. Lidke K, Rieger B, Jovin T, Heintzmann R (2005) Superresolution by localization of quantum dots using blinking statistics. *Opt Express* 13:7052–7062
150. Diez I, Ras RHA (2010) Few atom silver clusters as fluorescence reporters. In: Demchenko AP (ed) *Advanced Fluorescence Reporters in Chemistry and Biology II*. Springer Ser Fluoresc 9:307–332
151. Muhammed MAH, Pradeep T (2010) Luminescent quantum clusters of gold as bio-labels. In: Demchenko AP (ed) *Advanced Fluorescence Reporters in Chemistry and Biology II*. Springer Ser Fluoresc 9:333–353
152. Kim E, Park SB (2010) Discovery of New Fluorescent Dyes: Targeted Synthesis or Combinatorial Approach? In: Demchenko AP (ed.), *Advanced Fluorescence Reporters in Chemistry and Biology I*. Springer Ser Fluoresc 8:149–186

Optimization of the Coupling of Target Recognition and Signal Generation

Ana B. Descalzo, Shengchao Zhu, Tobias Fischer, and Knut Rurack

Abstract Fluorescent reporters that literally “light up” upon binding of a target species are particularly interesting from an analytical point of view. This contribution introduces the main signaling concepts in fluorescent probe research, discusses strategies toward their optimization in terms of signal output, and highlights the wealth of alternative protocols that has been realized in the past two decades to create signaling systems with luminescence amplification features.

Keywords Dyes · Fluorescence · FRET · Molecular Recognition · Nanoparticles

Contents

1	Introduction	42
2	Channels of Communication between Binding Site and Fluorophore	44
2.1	π -Conjugated Binding Site and Fluorophore	46
2.2	Spacer-Separated Binding Site and Fluorophore	50
3	Strategies of Signal Optimization in Fluorescent Probes	56
3.1	Combinatorial Synthesis of Functional Fluorophores	57
3.2	Design of Communication Channels for “Light-Up” Probes	57
4	Strategies of Signal Amplification	65
4.1	Chemical Reactions	65
4.2	Displacement of Fluorophores from Binding Sites	74
4.3	Increasing the Number of Fluorophores per Binding Site	77
4.4	Involving Fluorophore Communication	81
4.5	Resonance Energy Transfer	86
5	Conclusion	92
6	Further Reading	95
	References	96

A.B. Descalzo, S. Zhu, T. Fischer, and K. Rurack (✉)

Div. I.5 Bioanalytics, BAM Bundesanstalt für Materialforschung und -prüfung, Richard-Willstätter-Str. 11, D-12489 Berlin, Germany

e-mail: knut.rurack@bam.de

1 Introduction

There are many techniques among the portfolio of analytical methods that allow the sensitive determination of a variety of different substances after clean-up and separation in one experimental run or that permit the identification of compounds unequivocally by their intrinsic fingerprint. Gas and liquid chromatography, mass spectrometry, and NMR spectroscopy as well as a number of other methods – ranging from more traditional electroanalytical techniques to miniaturized renditions of established methods or hyphenated methodological combinations – all are powerful tools to tackle today’s analytical problems. Why then bother with the often tedious development of a dye molecule that has to be inherently (and at best highly) fluorescent and that has to show a specific change in its fluorescence signal upon interaction with a designated target molecule? The answer is twofold. First, in contrast to all the methods mentioned above, analyte-responsive fluorophores and fluorescence measurements as such do not necessarily require a laboratory setting. Fluorophores simply need light to be excited and a detector (if not the naked eye) for the signal to be registered, whether addressed and accessed directly or remotely, through space or through tissue, with fiber optics or with a microscope objective. Chemi- and bioluminescent protocols in addition can even dispense with a light source. Second, fluorescence or more general luminescence is a very sensitive detection technique allowing the counting of single photons and tracking or observation of single molecules and, if required, at a rather high spatial resolution. Fluorescent reporters thus unfold their truly unique advantages as analytical tools *on site* – whether as a squad of individual indicator molecules hunting for a certain target analyte in a live cell or as a crowd of indicators immobilized in a solid porous matrix at the tip of a fiber, waiting for a certain target analyte to pass by the sensor head, in *real time* – whether for continuous monitoring of a specific parameter in a bioreactor or as a quick dip stick test for qualitative analysis in the hands of a food inspector, and in many diverse *imaging* applications, ranging from TIRF and FISH to FRAP and FLIM¹ and providing distinct spatial information on the object of interest [1–3].

Besides instrumental features such as the wavelength range of excitation and emission and the decay time of the luminescence signal, two quantities are especially important in the design of functional fluorophores, i.e., the molar absorption coefficient at the excitation wavelength (ϵ_λ) and the fluorescence quantum yield (Φ_f). A high molar absorption coefficient is a prerequisite for efficient transformation of a molecular emitter from the ground into its excited state and a high fluorescence quantum yield means that the absorbed photons are efficiently converted into emitted photons. For a fluorophore as a label² for a biomolecule, the

¹Total internal reflection fluorescence (TIRF) microscopy, fluorescence *in situ* hybridization (FISH), fluorescence recovery after photobleaching (FRAP), fluorescence lifetime imaging microscopy (FLIM).

²In this chapter, terms often used inconsistently in the literature for various types of functional fluorophores or fluorescent reporters are defined as follows: (1) *probe* = fluorophore, whether

intrinsic values of ε_λ and Φ_f are the essential determinants. The same holds for fluorescent stains, e.g., for cell compartments. Indicators on the other hand have to express another essential feature, i.e., a change in fluorescence signal upon binding to the designated analyte that is as pronounced as possible to guarantee optimum exploitation for sensitive and at best unequivocal detection. The most obvious key to success for the latter is to choose (a) potentially highly fluorescent dye(s) and to integrate (a) receptor unit(s) to the chromophore(s) in such a way that the signal is weak in the absence of the analyte and that only the arrival of the target species modulates a photophysical process that results in a strong output signal. Important parameters here are the chemical nature of the analyte, the type of interactions the binding or recognition event should be accomplished with, and the type of photophysical processes that can be installed in a certain (family of) dye(s). In other words, the primary task is to couple sensitive and selective target recognition with efficient signal generation. The present chapter will thus not dwell on the best fluorometric method for signal assessment [4] or the optimum chromophore [5–7] or luminescent (bio)macromolecule [8–12] or object [13–17] in terms of achievable quantum yield, wavelength range of operation, or intrinsic photophysical properties nor on the details of basic photophysical and photochemical processes such as excited-state proton, charge and electron transfer (ET) or aggregate formation [18–24] or versatility in dye synthesis, biochemical coupling, and conjugation [25–27]. Instead, it will introduce and highlight basic concepts and features that have been established in the last ca. 20 years for the achievement of strong analyte-induced signal modulations, covering a broad range of diverse system architectures, types of analytes, and physical processes.

Before embarking on the description and discussion of actual examples, a few additional comments are necessary. Because of the limited space available in a book article and the large variety of different approaches having been published to date, we will mainly focus on examples that show strong signal changes connected with an increase in luminescence. Amplified quenching, though frequently leading to dramatic signal modulations, will only be discussed for selected systems in Sect. 4. The advantage of realizing enhanced fluorescence signals upon analyte binding is perhaps most obvious from the following two considerations. First, the measurement of strong signals against a weak background harbors the physical

designed or not, that responds (often nonspecifically) to a change in a local environmental parameter (including solvatochromic and solvatokinetic responses); (1a) *indicator* = specific (often designed) *probe* that responds (often selectively) to a certain parameter (e.g., pH or Ca^{2+} indicator); (1b) *chemosensor* = synonym for *indicator*; (2) *stain* = fluorophore that provides a constant output signal to visualize (a certain region within) a larger object after staining, i.e., physical enrichment/accumulation based on hydrophilicity/lipophilicity partitioning or electrostatic forces; (3) *label* = fluorophore that provides a constant output signal to allow the monitoring/tracking of an object after (often) selective (usually covalent) chemical attachment to the latter; (3a) *tag* = synonym for *label*. Whereas the specificity of the *label* is imparted by the coupling reaction, the specificity of the *probe* is basically imparted by the spectroscopic response, whether a simple solvatochromic dye is used or an indicator dye that binds only to a certain analyte.

benefits of higher signal-to-noise ratios, lower measurement uncertainties (e.g., due to better counting statistics in a given time interval), and/or faster accumulation times. Second, from the viewpoint of the analytical chemist, the generation of a specific, enhanced output signal is preferable compared to unspecific quenching in terms of species identification because it offers quantitative and qualitative information, e.g., through a species-specific fluorescence lifetime of a certain host–guest ensemble. Quenching analyses usually cannot distinguish between the desired, analyte-related quenching effect and unspecific interactions by notorious quenchers being present in a sample such as electron-rich, colored or heavy atom-containing (naturally occurring or anthropogenic) compounds. Finally, this article concerns probes for inorganic and organic small-molecule ionic or neutral analytes. Bio- or other macromolecules are only very marginally covered here for illustrative purposes in Sect. 4.

2 Channels of Communication between Binding Site and Fluorophore

Some of the best performing examples in terms of signal enhancement upon analyte binding are truly “dinosaurs” among the fluorescent reporters known today, fluorescent ligands such as 2,2′-bipyridyl (**1**) [28], 8-hydroxyquinoline (**2**) [29] or the oldest fluorescent reporter described, morin (**3**), a flavone derivative [30] (Fig. 1). These ligands usually consist of an aromatic or a heterocyclic ring system, the heteroatoms of which (mostly nitrogen and oxygen) are arranged in such a way that they can form a chelate with a metal ion. Chromophore and binding unit are identical. The major prerequisite for strong signal enhancement upon analyte binding, the absence of or a weak fluorescence of the reporter in the unbound state, is here usually accomplished through one (or more) structurally inherent, efficient nonradiative relaxation pathways of the excited state, i.e., energetically low-lying $n\pi^*$ states, excited-state intramolecular proton transfer (ESIPT)

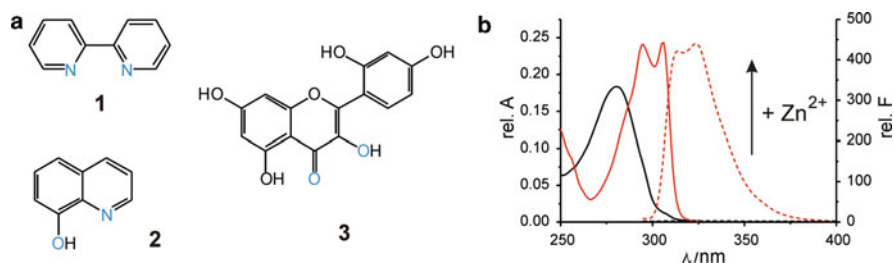


Fig. 1 (a) Chemical structures of fluorescent ligands; metal ion coordination sites are indicated in blue. (b) Absorption (*solid*) and fluorescence spectra (*dotted*) of **1** (*black*) and its Zn²⁺ complex (*red*) in water at pH 7; whereas uncomplexed **1** is virtually nonfluorescent ($\Phi_f < 10^{-5}$), the fluorescence quantum yield Φ_f of **1**-Zn²⁺ amounts to 0.34 [31]

reactions, or internal torsional motions around (a) flexible bond(s) [28, 32–34]. Metal ion coordination can then shift the $n\pi^*$ energy levels with respect to those of the ligand-centered $\pi\pi^*$ states, can shield the proton transfer sites or simply block rotational motion, leading to strong fluorescence enhancement (Fig. 1).

However, because of their simple architecture, the *metal ion* selectivity of such ligands is mostly rather poor and the binding affinity is basically dominated by the Irving–Williams order [35]. In addition, the possibilities of discriminating between different complexes of a certain ligand on the basis of absorption spectral shifts are also very limited, the bands of the single complexes generally showing strong overlap [36]. Moreover, although these compounds often undergo distinct changes in their absorption spectra upon interaction with a metal ion (see Fig. 1), dramatic fluorescence responses are restricted to “light” diamagnetic cations such as the upper row group-II and group-III metal ions and Zn^{2+} . Complexes with diamagnetic “heavy” ions such as Pb^{2+} and Hg^{2+} usually show only weak fluorescence due to enhanced spin–orbit coupling (heavy atom effect, [37])³ and complexes of paramagnetic ions with an open d shell like Cu^{2+} and Fe^{3+} are often essentially nonfluorescent due to efficient electronic energy transfer [39].

The main reason which is responsible for these restrictions is the concurrence of chromophore and chelator, i.e., they are identical (like in **1** or **2**) and any distinct and deliberately manipulable communication channel between these functional units simply does not exist. Any potentially quenching species interacting with the chromophore/chelator can thus unfold its activity unhindered. Such a behavior is not only found for metal ions, but also for *anions*, e.g., in the case of various fluorometric chloride indicators [40]. In fact, for these analytes, the situation is more complicated. Not only potential quenching interactions play a role (most of all for Cl^- , Br^- and I^-) but also the intrinsic feature that utmost anions possess a much lower charge density than metal cations, simply due to their polyatomic nature, larger size for equal net charge, and higher atomic similarity to most organic chromophores. Thus, already the spectral changes in absorption that have been reported for anions of low basicity and fluorescent ligands such as **4–6** are considerably weak and are only found in model environments like dichloromethane or other organic solvents (Fig. 2) [41, 42].⁴ Obviously, this situation is not improved for organic anions. Structurally, simple ligands that respond to anions with a lighting up of their fluorescence are thus virtually unknown.⁵ Taking the step from charged to neutral analytes, i.e., small organic molecules which are partly not even capable of forming electrostatic or hydrogen bonds with a receptor but have to rely on weaker forces such as π stacking, dipole–dipole, or van der Waals interactions, the picture remains unchanged. Apparently, the separation and

³The heavy atom effect offers certain possibilities for fluorescence lifetime-based analytical exploitation which will not be discussed here. The reader is referred to [38] for more details.

⁴The dramatic bathochromic shifts found for ligands such as **6** and various more elaborated probes in the presence of basic anions in organic solvents are mainly due to deprotonation effects [43, 44].

⁵Naturally, this holds for polyatomic (organic) cations as well. Simple fluorescent reporters for, e.g., ammonium, alkylammonium or guanidinium species have also not been reported.

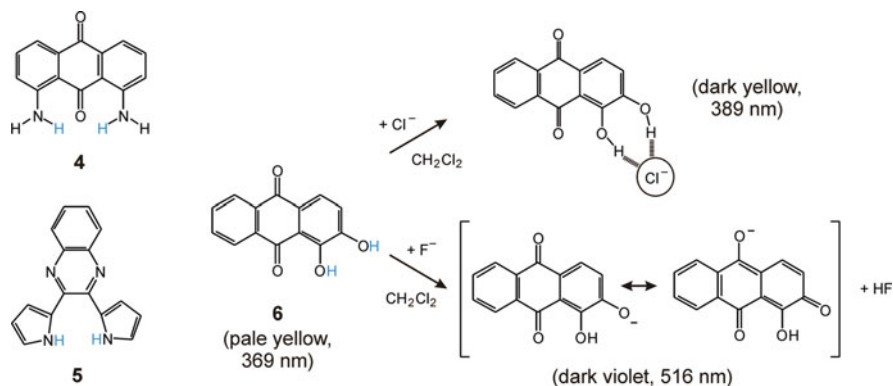


Fig. 2 Chemical structures of fluorescent ligands (anion coordination sites are indicated in blue) and tentative reaction schemes on interaction of **6** with chloride and fluoride in dichloromethane according to the color patterns observed in [41]. The wavelengths of absorption given in brackets have been calculated for the geometry optimized species **6**, **6-Cl⁻** and **6⁻** in the gas phase by semiempirical AM1 calculations (Ampac V6.55, Semichem)

individual design of binding and signaling site and the tailoring of the communication between them are essential for broader success.⁶

2.1 π -Conjugated Binding Site and Fluorophore

When individual units are combined in a modular fashion, perhaps the most obvious approach again relies on a direct integration of (part of) the receptor to the chromophore with only the electronic transitions in the resulting probe being of a more refined nature than in the ligands discussed above. In contrast to the latter where HOMO and LUMO are delocalized over the same parts of the molecule, i.e., usually over the entire ligand molecule, the reporters with π -conjugated binding site and fluorophore generally show different charge distributions in the molecular orbitals involved in the optical transitions. Absorption and emission processes thus have a (certain) charge transfer (CT) character, leading to a reversal of the charge densities upon photoexcitation. This feature is also responsible for the term commonly used for this class of reporters – intramolecular charge-transfer or ICT probes.⁷ In a simplified picture, the molecular entity that is electron-rich in the ground state becomes electron poor in the excited state and vice versa. Accordingly, integration of a binding site to the electron richest/poorest atom/molecular fragment should lead to the strongest modulation of its electron donating/accepting character

⁶A certain control of selectivity for simple ligands without altering their fluorescence features is possible when integrating them into more developed, often macrocyclic receptor units [45, 46].

⁷The term PCT probe for photoinduced charge transfer probe is also frequently used.

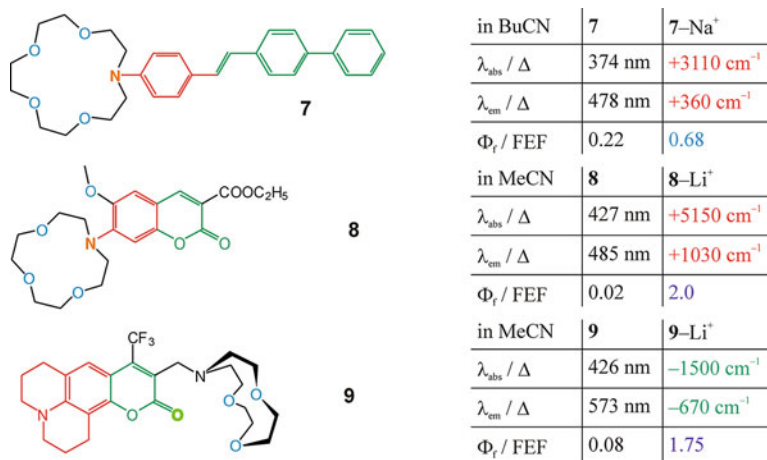


Fig. 3 Typical ICT probes (*left*) and representative spectroscopic responses toward selected metal ions (*right*). Color code: (*left*) coordinating atoms in *blue*, bridgehead atom of the fluorophore that takes part in complexation in *orange*, formal donor fragment in red, formal acceptor fragment in green; (*right*) hypsochromic shifts in *red*, bathochromic shifts in *green*, fluorescence enhancement in *violet*, fluorescence quenching in *blue*. Symbols in table: λ_{abs} , λ_{em} , Φ_f are absorption, fluorescence maxima, and quantum yield of ICT probe, Δ are the respective spectral shifts upon complexation, FEF is the fluorescence enhancement factor upon complexation

upon interaction with a target analyte and should thus entail the most pronounced optical response. Classic ICT probes are, for instance, donor–acceptor stilbenes (e.g., **7**) or coumarins (e.g., **8**) where the nitrogen atom of the donor unit is at the same time integrated into the receptor unit (Fig. 3, [47, 48]). Alternatively, acceptor group integration can be accomplished as in **9** (Fig. 3, [49]).

Without going too much into mechanistic details, the noncovalent interaction of an electron-poor analyte (e.g., a metal ion) with an electron donor or acceptor group of an ICT probe can be rationalized as follows. Interaction of the electron-deficient species with the donor monopolizes charge density and reduces the latter's strength, resulting in a weaker ICT character and hypsochromic spectral shifts (red entries in Fig. 3). Accordingly, binding at the acceptor group reinforces the ICT, yielding bathochromic shifts (green entries in Fig. 3).⁸ Whereas these features are straightforward in absorption, the noncovalent character of the interaction harbors an important implication for the fluorescence response. Upon excitation of such complexes, the ICT process is still triggered.⁹ This transfer of charge from the donor to

⁸The opposite effects are found for the interaction of an electron-rich species with these two molecular fragments.

⁹If covalent bond formation occurs like for protonation, the ICT is blocked. However, due to the fact that stilbenes, coumarins and related chromophores with a weak or absent ICT character are commonly only weakly or nonfluorescent, the analyte-bound form would show strongly blue-shifted absorption spectra and virtually no emission, both undesirable features in terms of sensing.

the acceptor fragment thus also leads to a formal positive charge on the donor in the excited complex, leading to electrostatic repulsion between the bridgehead atom and the cation. The net effect is the reduced influence of the guest in the S_1 state and on its deactivation, which is reflected by generally smaller shifts Δ in fluorescence than absorption, see Fig. 3.¹⁰ For further elaborations on the topic, the interested reader is referred to [53]. The important point in terms of this chapter, however, is the fact that, besides rather small shifts in fluorescence, the fluorescence intensity modulations expressed as the ratio of the fluorescence quantum yield of free (superscript fp) and bound probe (superscript bp) or the fluorescence enhancement factor FEF (1) typically found for ICT probes is also comparatively small, usually ranging between quenching and enhancement by a factor of 2, i.e., $0.5 < \text{FEF} < 2$ (the data in Fig. 3 are also representative in this respect). These moderate changes in conjunction with opposite signs are connected to the intrinsic complexity of the excited-state reaction mechanisms of donor–acceptor-substituted chromophores, especially when the fragments are connected by a series of single and double bonds such as in 7. A detailed discussion would go beyond the scope of this chapter so that [54, 55] are recommended for further reading. For rational design of fluorescence “light-up” ICT probes, however, a profound knowledge of the photo-physics of the parent chromophore is indispensable. If such data are not available, development can quickly result in success by serendipity or entail tedious preliminary mechanistic studies. A few rational approaches that led to success will be discussed in Sect. 3.

$$\text{FEF} = \frac{\Phi_f^{bp}}{\Phi_f^{fp}} \quad (1)$$

Although the aforementioned might suggest that ICT probes are generally not the best performers in terms of strong fluorescence output or high FEF, their architecture is ideally suited for the design of ratiometric probes. Ratiometric measurements rely on pronounced spectral separation of the absorption and/or the emission spectra of free and bound probe and can principally be realized in two ways, i.e., using two different excitation and a single observation wavelength or using a single excitation and two different observation wavelengths (see also Sect. 2.2.2). According to the mechanism of operation sketched above, i.e., usually strong shifts in absorption and weak shifts in fluorescence, ICT probes like 7–9 would mainly qualify for the former type. However, instrument operation with two different excitation settings and one emission channel is less favorable than the single excitation/double emission

ICT probes thus do not play a role as pH-indicators. However, this fact can be utilized for powerful sensing schemes in a different context, see Sect. 4.1.1.

¹⁰In principle, the trends should be exactly opposite for ICT probes carrying the receptor in the acceptor fragment. However, as can be seen for 9 in Fig. 3 and some other probes of this type (e.g., in [50–52]), the relationship is not straightforward. Moreover, since the literature on acceptor-type ICT probes is much less abundant than on their donor counterparts, the database for a comprehensive analysis and discussion is still rather weak and further conclusions will not be drawn here.

approach, which is for example the conventional setup realized in microscopes and cytometers. This is even more obvious when considering that the main advantage of ratiometric measurements is the insensitivity against photobleaching and light source fluctuations, because a loss in fluorophore or changes in lamp output would lead to reductions/modulations of both signals but would not affect their ratio, avoiding false results (Probe design for different technologies based on wavelength ratiometry is discussed in a recently published review [237]). Potent fluorescent probes for such applications should thus have rather high and not too different molar absorption coefficients and fluorescence quantum yields for both states, free and bound. If for instance ϵ_{λ} and Φ_f of the complex would be distinctly lower than those of the free probe, the less favorable signal-to-noise ratios on the weaker signal could introduce a higher uncertainty for low analyte concentrations. An example illustrating the approach is shown in Fig. 4 [56].

In contrast to the large number of fluorescent ICT probes reported for metal ions, such probes for anions and small organic molecules are very scarce, although

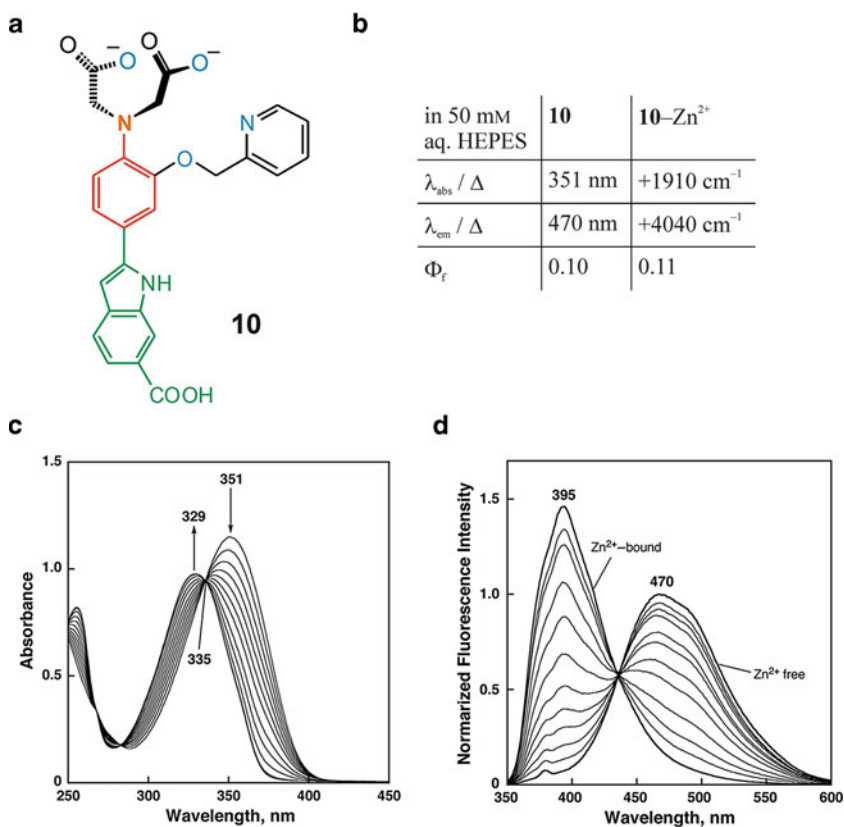


Fig. 4 Example of a ratiometric ICT probe (**a**) and representative spectroscopic responses toward Zn^{2+} (tabulated **b**), absorption (**c**), fluorescence (**d**). For color code and symbols, see Fig. 3. (Reprinted in part with permission from [56]. Copyright 2009 Elsevier)

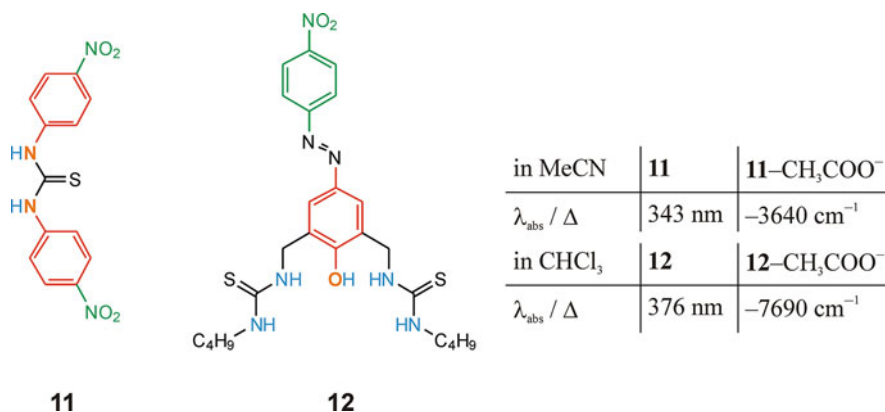


Fig. 5 Colorimetric ICT probes (*left*) and representative spectroscopic responses toward acetate (*right*). For color code and symbols, see Fig. 3

several colorimetric ICT probes for anions exist [57]. Without going too much into speculations, this lack is most likely connected to the same reasons as outlined in the previous section and is supported by findings that already the spectral shifts in absorption observed for many ICT probes and monovalent cations such as Na⁺ and K⁺ are rather weak and fluorescence modulations are often negligible. If one considers that most colorimetric ICT probes for anions carry the strongly electron accepting nitro group, which is known to quench many UV/vis fluorophores (see, e.g., **11** and **12** in Fig. 5 [58, 59]), the lack of fluorescent ICT anion probes is comprehensible. The few strategies for anion sensing that have been developed on the architectural basis of ICT probes but which operate through different mechanisms will be discussed in Sect. 3.

2.2 Spacer-Separated Binding Site and Fluorophore

The separation of binding site and fluorophore by a nonconjugating spacer opens the path to other mechanisms of communication, most prominently ET and excimer/exciple formation. In the first case, the electronic nature of both fluorophore and receptor unit and the steric nature of the spacer are the important parameters for signal generation. In the second case, for most systems the electronic nature of the fluorophores and the steric nature of the receptor as well as its change upon analyte binding determine the signal.

2.2.1 Single Binding Site-Single Fluorophore Architectures

Fluorescent reporter molecules consisting of a single receptor, a single fluorophore, and a spacer electronically separating these two are popular probes since the

seminal works of de Silva's and Czarnik's groups [60, 61]. In contrast to ICT probes, both functional units are not π -conjugated, i.e., they are both characterized by their own characteristic molecular orbitals, absorption, and emission bands. The absorption spectrum of the supramolecule is a linear combination of the individual fragments' bands. These molecules are designed in such a way that either the HOMO or the LUMO of the receptor (HOMO_R , LUMO_R) is energetically situated between the HOMO and LUMO of the fluorophore (HOMO_F , LUMO_F). In the first case, absorption of a photon by the fluorophore promotes an electron from HOMO_F to LUMO_F , making room for an electron to relax from the intermediately lying HOMO_R into HOMO_F . This ET is a nonradiative process and is then followed by a second nonradiative process, the decay of the electron from LUMO_F into HOMO_R upon return of the molecule to S_0 . For the second configuration, the sequence is as follows. Photoexcitation again transfers an electron from HOMO_F to LUMO_F . However, when now LUMO_R is situated between the fluorophore-centered MOs, the electron relaxes from LUMO_F into the empty LUMO_R and finally decays from there back to HOMO_F , again through two nonradiative processes. Because two ET processes are triggered in these probes by the absorption of a photon, these probes are commonly referred to as photoinduced ET or PET probes. The net effect in both cases is the quenching of the fluorescence of the fluorophore. The degree of quenching depends on the relative energetic positions of HOMO_F , LUMO_F and HOMO_R (or LUMO_R) and the distance between fluorophore and receptor. To provide these supramolecules with signaling capabilities, the receptor unit has to be chosen or designed in such a way that the binding of the analyte at the receptor dramatically alters the energy levels of the receptor-centered MOs, shifting them at best out of the HOMO_F – LUMO_F window and thus rendering PET energetically unfavorable. Since the fluorescence transition is only fluorophore-localized, the effect of target binding is an enhancement of the typical fluorophore emission, without any pronounced spectral shifts (cf. traces 2 and DMA in Fig. 6c). A detailed account on PET signaling can be found in [64] and earlier reviews cited therein.

With respect to signal enhancement, the PET mechanism harbors an enormous potential and already the very first PET probes reported set benchmarks comparatively high (Fig. 6). Fluorescence enhancement factor (FEF) of several hundred or higher are even today reached in only a few cases. Moreover, compared with the integrative ICT probes, system design is rather simple in the PET case. Knowledge of the redox potentials, absorption and emission data of common fluorophores, and receptor mimics, together with the knowledge of binding constants and coordination features for a certain host–guest pair (in a particular solvent),¹¹ allows to largely predict the achievable enhancement, employing the Rehm–Weller

¹¹The solvent has to be taken into account when comparing absolute FEF values (in particular of amine-containing probes such as **13** and **14**) because the quenched “off” state of a PET probe is often higher fluorescent in protic organic and especially aqueous solvents (or solvent mixtures) than in nonprotic solvents due to hydrogen bonding interactions between solvent and nitrogen atom. For example, **14** shows a 2,260-fold weaker fluorescence than its parent 9,10-dimethylantracene in nonrotic acetonitrile, the maximum FEF in water amounts to ca. 360.

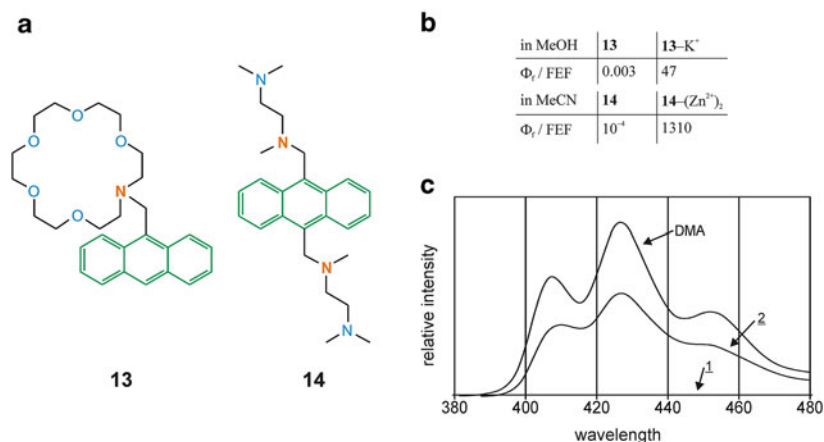


Fig. 6 Typical PET probes (**a**) and representative fluorescence light-up responses toward selected metal ions in tabulated (**b**) and graphical form (**c**; trace 1 = **14**, trace 2 = **14**-(Zn²⁺)₂, trace DMA = 9,10-dimethylantracene in MeCN). Color code: coordinating atoms in blue, atoms which take part in the complexation and show (main, in **14**) PET activity in orange, fluorophore in green. Lincoln and co-workers have demonstrated that the attachment of two dimethylamino groups through propylene spacers to the 9,10-positions of anthracene has a more than 100-fold weaker PET activity than the attachment through methylene spacers [62]. The blue N atoms in **14** are thus predominantly responsible for coordination. For symbols, see Fig. 3. Quantum yield of **14** in MeCN estimated from intensity readings published in [61] and quantum yield data of the parent compound without active PET, DMA, published in [63]. (Reprinted in part with permission from [61]. Copyright 1988 American Chemical Society)

formalism for the energetic consideration [65]. Due to these favorable signal amplification features, the basic architecture of PET probes did not change much over the past 20 years. Attempts were mainly made to increase the selectivity of the probes – as one can imagine, the polyaza crown analogs of **13** for instance do not discriminate satisfyingly between aminophilic heavy and transition metal ions such as Zn²⁺, Cu²⁺, and Hg²⁺ [66] – because all the complexes a single probe forms with various analytes show virtually identical spectral features [67, 68]. Moreover, since simple and flexible architectures such as **13** and **14** are also prone to quenching interactions by paramagnetic or heavy-atom species – for example, Cu²⁺ and Hg²⁺ even quench the “switched off” state of the azacrown analogs of **13** due to the mechanisms sketched in Sect. 2 [66] – research effort has also been directed toward achieving fluorescence enhancement upon binding to quenchers (see below). The third field of research activity has been the development of potent PET probes that rely on analytically more useful chromophores than anthracene and naphthalene, the traditional PET fluorophore “workhorses”, i.e., that emit well in the visible [69, 70] or the near-infrared region of the spectrum [71].

In contrast to the π -conjugated probe architecture utilizing an ICT process, the number of anion probes that rely on the fluorophore–spacer–receptor design and an active PET process is abundant [72]. Again, anthracene and naphthalene

fluorophores play outstanding roles and are combined mainly with short alkyl spacers (especially methylene) and the well-known neutral and charged anion recognition moieties such as (thio)ureas or imidazolium salts. In contrast to their cation analogs, fluorescence quenching is the predominant signaling mechanism for PET anion probes. Moreover, for those probes which show amplified fluorescence upon binding, the enhancement is often less dramatic than in the cation case and is often ascribed to a rigidification of the probe on anion coordination. PET probes that show comparatively strong responses (i.e., FEF > 5) such as **15–17** (Fig. 7) commonly involve the suppression of an oxidative PET process (e.g., **15,16**) or the inhibition of a reductive PET through coprotonation (e.g., **17**) [74–76]. As for cation reporters, issues of selectivity also play a significant role in anion probe design nowadays [77].

Besides inorganic anions, a lot of research effort is focussed on the development of indicator molecules for small organic molecules that possess an anionic and a cationic function such as, e.g., a carboxylate and an ammonium group as in the neurotransmitter γ -aminobutyric acid (**18**, Fig. 7) [78] or an anionic and a neutral

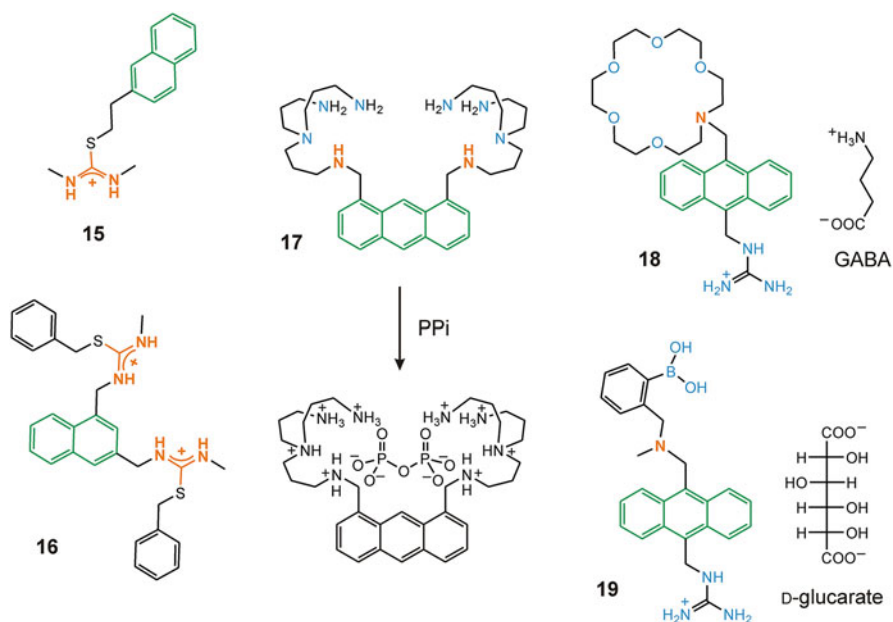


Fig. 7 PET probes for anions (**15–17**) and charged small molecules (**18,19**) showing enhanced fluorescence upon target binding. Typical FEF are ca. 4 for **15** and acetate in MeCN, ca. 5 for **16** and HPO_4^{2-} in $\text{H}_2\text{O}:\text{MeCN}$ (6:94, v/v), 2.5 for **17**/PPI in 50 mM aq. HEPES, 3.5 for **18**/GABA in $\text{H}_2\text{O}:\text{MeOH}$ (2:3, v/v) and ca. 5 for **19**/D-glucarate in $\text{MeOH}:\text{0.1 M aq. HEPES}$ (1:1, v/v). For color code, see Fig. 6; target analytes for **18,19** are shown as well; GABA = γ -aminobutyric acid. For **19** upon D-glucarate binding, the 9,10 substituents are presumably rearranged in such a way that the boron atom can interact strongly with the PET-active nitrogen atom (orange), hampering PET quenching [73]

function such as certain sugar acids (**19**, Fig. 7) [79]. The signaling mechanisms are very similar in these cases and will not be discussed in detail here. Besides the well-known receptor sites for anions and cations, boronic acid groups for example complement the functional entities when targeting sugar derivatives.

A special case of the single binding site-single fluorophore architectures are compounds like anthracene cryptands, i.e., anthracenes substituted through both their 9,10 positions with the two nitrogen atoms of a diaza-polyoxa macrocycle so that the fluorophore literally “sits” on top of the receptor and forms a macrobicyclus with it [80]. In such a case, the interaction between fluorophore and nitrogen atoms of the receptor does not proceed through PET, but through exciplex formation. Exciplex formation, i.e., the generation of an *excited complex* between excited fluorophore and for instance, an amino group in the ground state does not lead to unspecific quenching of the (isolated) fluorophore’s emission, but to the appearance of a red-shifted, broad, and structureless emission band – the so-called exciplex band. The reporter dyes are now designed in such a way that binding of the analyte either interacts with one of the partners (e.g., a metal ion with a crown nitrogen atom), rendering exciplex formation energetically unfavorable (related to the PET case) or the guest detaches both partners from each other, making the distance-dependent process less likely. The result of both effects is an increase of the fluorophore’s typical emission band at the expense of the exciplex band. Such an intrinsic two-band system again harbors all the advantages of ratiometric indication. However, because few fluorophores and few receptors constitute ideal exciplex partners (mainly anthracene and pyrene, paired with amino nitrogens) and the synthetic combination is challenging for more complex systems, these probes do not play a significant role in fluorescent reporter research today. The interested reader is referred to more specialized review literature [81].

2.2.2 Single Binding Site-Double or Multi Fluorophore Architectures

Closely related yet more important than exciplex systems are the so-called excimer probes. These probes also exhibit two distinct emission bands, very similar to the exciplex type. The short-wavelength band is again connected to emission from an excited (isolated) fluorophore whereas the red-shifted band stems from an *excited dimer*, involving a fluorophore in the ground and a second one in the excited state. Accordingly, the main characteristic of such probes is that they usually consist of one receptor site and two fluorophores. These two fluorophores usually do not form a ground-state dimer, and therefore the absorption spectrum of such bifluorophoric molecules very closely resembles that of an isolated (or monomeric) fluorophore. Thus, under conventional irradiation conditions, only one of the two fluorophores is excited. The entire probe molecule then has to be designed in such a way that nonexcited and excited fluorophore can encounter each other during the lifetime of the excited fluorophore, forming the excited dimer. Alignment of the chromophores is crucial, because the formation of an excimer relies on configurational mixing of exciton- and charge-resonance states [82]. In general, better alignment leads to

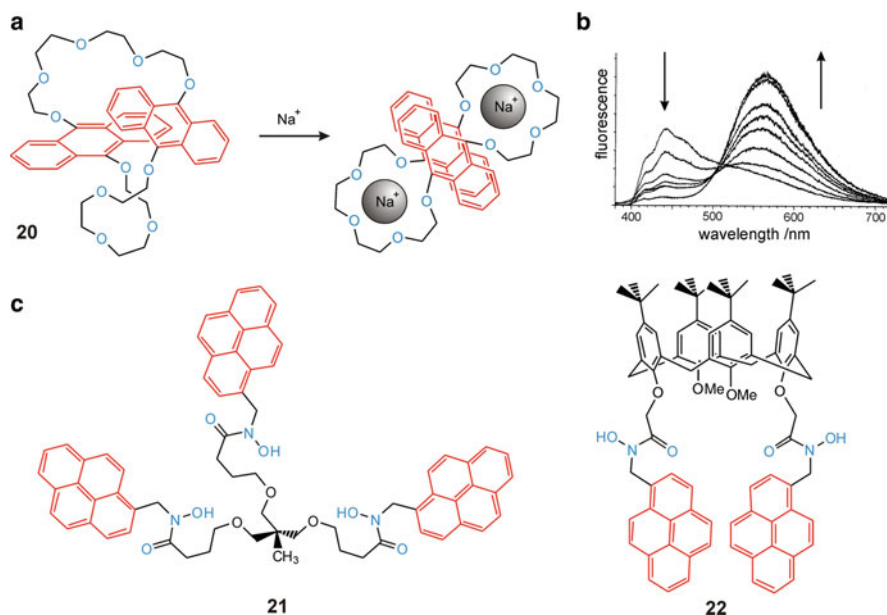


Fig. 8 Typical excimer probes utilizing two chelating sites and two fluorophores (**20**), a flexible central composite receptor site and three fluorophores (**21**) and a single receptor site with two pendant arms and two fluorophores (**22**). (a) Na^+ -induced excimer alignment in **20** and (b) respective spectroscopic response; (c) selective probes for Fe^{3+} (**21**) and Cu^{2+} and Ni^{2+} (**22**) that show quenching of monomer and excimer emission upon binding. Color code: fluorophores in red and atoms responsible for coordination in blue. (Reprinted in part with permission from [83]. Copyright 1995 American Chemical Society)

higher excimer yields and more pronounced quenching of the monomer emission, which can be utilized for signaling (**20**, Fig. 8) [83]. Many probes show residual excimer/monomer emission in both the free and the complexed state (e.g., Fig. 8b), which is predominantly due to the interplay of static and dynamic excimers [84]. As in the case of the exciplexes, the absorption spectrum is virtually identical to that of the parent fluorophore and binding of the target species leads to a change in monomer-to-excimer emission yield (Fig. 8). Since the possibilities of integrating a receptor site (or more than one site as in **20**, Fig. 8) and two (or more) fluorophores into a supramolecule are manifold, a considerable number of structures have been realized. However, one of the drawbacks of many excimer probe architectures is the fact that on binding of potential quenchers, these species are too close to the fluorophores and quench the emission nonspecifically, whether excimer or monomer (e.g., **21,22**, Fig. 8) [85, 86]. Attempts toward systems that are immune to quenching have been realized but are much less frequent [87].

While research in the area started with probes for cations, the last years have shown that the dual-fluorophore excimer concept seems especially promising for the development of anion probes. The benefit here is often twofold. On one hand, the observation of both emission bands provides a more stable differential or

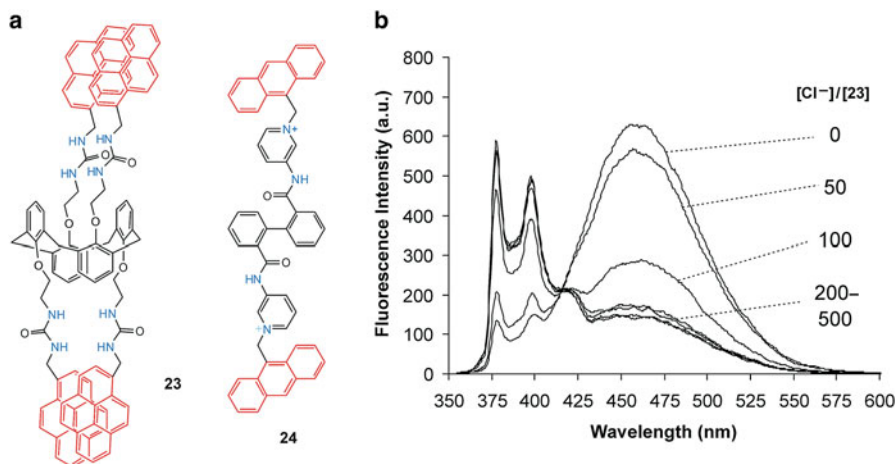


Fig. 9 (a) Two examples of excimer probes for anions and (b) response of **23** toward Cl^- in $\text{MeCN}:\text{CHCl}_3$ (95:5 v/v; excess of anion indicated). For color code, see Fig. 8. (Reprinted in part with permission from [88]. Copyright 2006 American Chemical Society)

ratiometric signal similar to the ratiometric ICT probes introduced above. On the other however, the excimer mechanism in cleverly designed systems especially allows obtaining FEF that are otherwise difficult to obtain for anions and probes that rely on a direct electronic perturbation of an intramolecular process by the analyte such as ICT or PET. Representative examples of excimer anion probes are shown in Fig. 9 [88, 89]. Here, for instance, chloride binding leads to the disruption of the perfectly aligned pyrene moieties in **23**, reducing excimer and enhancing monomer emission and H_2PO_4^- complexation entails a “switching on” of the excimer emission of **24** because of a reduction in PET interaction between the pyridinium and anthracene groups and alignment of the latter. Current research activities explore the use of other excimer forming fluorophores such as 1,4,5,8-naphthalenetetracarboxdiimide [90], target more complex anionic molecules such as ATP [91], or aim at enantioselective recognition [92].

3 Strategies of Signal Optimization in Fluorescent Probes

The optimization of a fluorescence signal upon target recognition can principally be accomplished along four different paths. Path #1 is a synthetic approach and utilizes combinatorial techniques to synthesize a larger library of functional fluorophores of a rather simple type with the aim of screening their performance. Path #2 follows mechanistic considerations and tries to rationally optimize the different photophysical process partly by taking into account as many data available on a certain class of fluorophores and receptor units as possible, including redox and spectroscopic

data, linear free energy relationships, and molecular modeling results. Path #3 inspects other fields of research more closely and tries to adapt strategies from those areas, e.g., from metallorganic catalysis, polymer chemistry or goes biometric. Path #4 finally is related to #3 yet is loosened from the format of the molecular indicator and integrates fluorophores and receptors into other materials or uses them in other, collective forms. Approaches taking the last two paths will be covered in Sect. 4. This section will briefly introduce some of the attempts that have been made along path #1 and detail more closely design concepts on path #2.

3.1 Combinatorial Synthesis of Functional Fluorophores

Combinatorial approaches to functional molecules in the areas of drug discovery and catalysis are not new. Commonly, a larger library of compounds is synthesized with the aid of solid-phase synthesis techniques and the outcome is screened with high-throughput monitoring techniques. In the field of fluorescent reporter development, combinatorial techniques can be used to screen for optimum receptors, optimum fluorophores, or optimum probe molecules. Because receptor chemistry is closer related to the chemistry of drugs and their interaction with biological receptors, attempts toward the screening for new receptor motifs has a longer history [93] compared to the combinatorial search for fluorophores or fluorescent reporters [94, 95]. The two latter saw first approaches in the late 1990s, for instance, the generation of a library of coumarin dyes [96] and dansyl-appended aza crowns with pendant chelators [97]. Although intriguing examples have been reported for several of the most important classes of dyes such as functionalized cyanines [98], xanthenes [99], and anthracenes, [100] or for the color tuning of organic dyes [101], the field is still in its infancy compared to the vast amount of literature on functional fluorophores (comparison of efficiencies of synthesis and of fluorescence properties for rational design and combinatorial library approaches can be found in the chapter of Kim and Park in Part I of these series [26]). The same is true for the combinatorial development of fluorescent probes, despite the fact that not only classic analytes like metal ions have been targeted [102, 103], but also charged organic small molecules [104]. However, considering the efforts that are made to design even (parts of) actual sensory devices according to combinatorial principles [105], we assume that this field will experience a boost in the nearer future.

3.2 Design of Communication Channels for “Light-Up” Probes

Aiming at strong signal changes for fluorescent reporter molecules, one has to think of ways of how to turn (conventional) probe architectures into switch architectures, i.e., into systems where the binding of the target of interest induces an effect which is similar to the switching on of a light bulb. Because inorganic cations on the one hand and anions and charged or neutral small organic molecules on the other

possess intrinsically different properties as detailed above, the following sections are divided into probes for cations and probes for anions and small molecules.

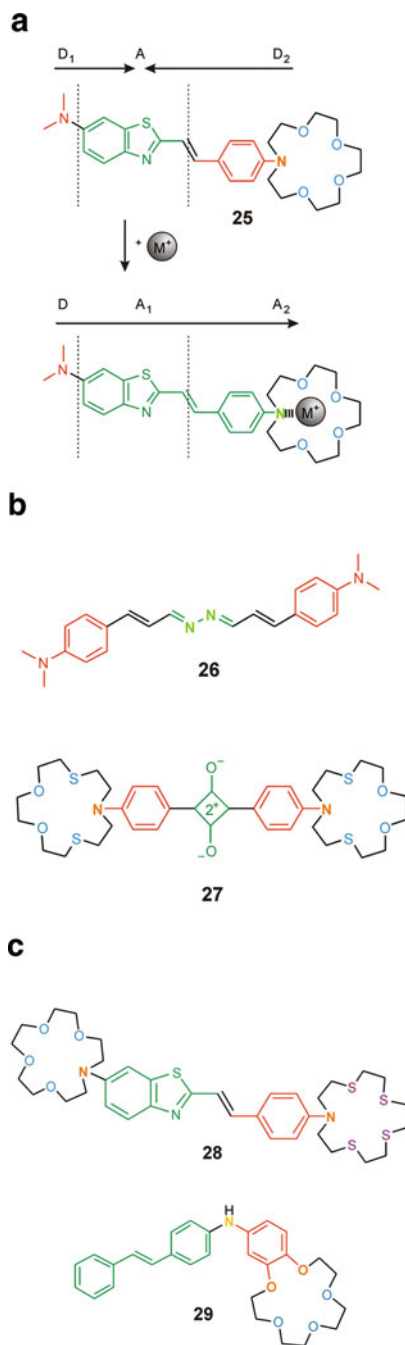
3.2.1 For Metal Cations

As we have discussed in Sect. 2, ICT and PET probe architectures are in principle well-suited concepts for the development of reporters that show pronounced spectroscopic responses upon metal ion binding. For ICT probes, the major challenge perhaps is how to design probe molecules which predictably show an analyte-induced increase in emission in a rational way. A key to success here is the installation of a second ICT process in the chemosensor molecule. Depending on the aspired architecture, the two ICT processes can be identical or different with intrinsically different emissivities. One such example of the latter type is asymmetric **25** in Fig. 10 [106]. For **25**, ICT₁ involving *D*₁ and *A* is highly emissive whereas ICT₂ involving *D*₂ and *A* is weakly emissive. The net effect is an intermediate fluorescence of the free probe ($\Phi_f = 0.03$). Accordingly, when a metal ion is bound at *D*₂, this donor is turned into an acceptor (*A*₂) and the ICTs in the molecule are reconfigured: ICT₁ is accelerated whereas ICT₂ is blocked. The net effect is a red-shift of the fluorescence spectrum and a strong 32-fold increase in quantum yield. Symmetric *D*–*A*–*D* probes operate in a related way, only that here both processes are convergent and the net effect is the amplification of a single ICT. Of course, both types are possible, i.e., reporters where cation binding takes place in the acceptor (e.g., **26** in Fig. 10) or in the two donor parts of the molecule (e.g., **27** in Fig. 10) [107, 108]. Although there are not too many reports on such type of dyes in the literature, other approaches relying on cruciform fluorophores [109] or utilizing the concept of colorimetric [110] and two-photon absorption [111] metal ion probes have also been published.

Before discussing a very powerful approach to signal enhancement that relies on the virtual decoupling of donor and acceptor moieties in fluorescent reporters, we will briefly highlight a strategy already introduced with **27** - the integration of more than one receptor site into such double ICT probes. Besides achieving an enhanced response as in **27** with its two identical binding sites, the integration of two different receptor units can be employed for the indication of more than one species or for the generation of cooperative signals. For instance, **28** expresses the same pattern as **25**, only the ICT from the tetraoxa monoaza crown can selectively be addressed with alkaline earth metal ions such as Ca²⁺ and the ICT from the tetrathia monoaza crown with thiophilic cations such as Ag⁺ [112]. **29** on the other hand utilizes a tandem donor configuration with H⁺ serving the nitrogen addressee and Mg²⁺ or Ca²⁺ the pentaoxa benzocrown moiety [113]. Accordingly, binding of one, the other, or both target species with **28** and **29** yields different spectral and intensity responses, allowing for various detection schemes.

Leaving the classic ICT architecture and moving toward electronically decoupled systems, a strategy for obtaining extraordinarily high fluorescence enhancement factors has been developed at the end of the 1990s - the concept of

Fig. 10 *D–A–D* probes for improved cation signaling. (a) Asymmetric approach; (b) symmetric approaches; (c) examples for probes containing two different receptors. For color code, see Fig. 3; *violet* atoms in **28** denote coordinating atoms of different analyte preference; *dark yellow* atom in **29** denotes second type of donor atom with different analyte preference



“virtual decoupling” [114]. Virtual decoupling means that the probes are formally π -conjugated molecules yet their donor and acceptor moieties are perpendicularly oriented (e.g., **30** in Fig. 11) [115]. This architecture reduces the distance between donor and acceptor to a minimum, i.e., to a shorter distance than in conventional PET probes, yet allows the subunits to interact during the lifetime of the excited state. The results are very weakly emissive free indicator dyes, sometimes showing a red-shifted, broad CT emission band of low intensity besides the fluorophore-localized or LE emission as **30** in Fig. 11, and dramatic analyte-induced fluorescence enhancement factors, reaching several hundreds up to several thousands and rivaling the most potent PET probes. Fine tuning of the redox potentials of the fluorophore further offers the possibility of optimally adjusting the signaling needs of a given receptor and was successfully introduced for comparatively PET-reluctant receptors like benzocrowns (e.g., **31** in Fig. 11) [116]. Today, the concept has been widely introduced to actual sensing applications and permits the actual imaging of toxic metal ion such as Pb^{2+} (with **32**) or Ni^{2+} (with **33**) in live cells [117, 118].

Besides direct virtual decoupling, another strategy for favorable signal generation relies on the employment of small, rigid, and geometrically oriented spacers such as Δ^2 -pyrazoline (**34**) (Fig. 12) [119], discussed already above in Sect. 2.2.1. The operative mechanism in these probes is a classic PET process. The advantage of using these architectures is that different signaling processes can be integrated into a single probe, allowing the tuning of the spectral ranges [68, 71, 119] or

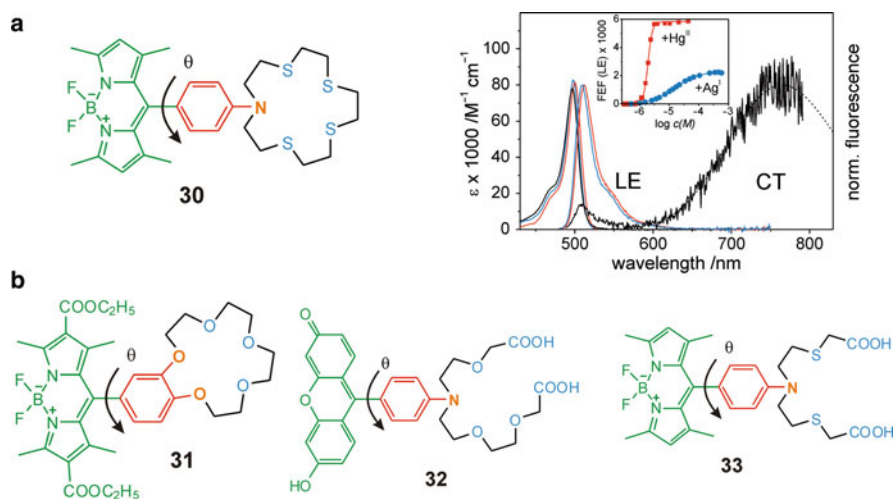


Fig. 11 (a) Chemical structure (left, $\theta \sim 90^\circ$) and cation response (right) of virtually decoupled probe **30** for Hg^{2+} and Ag^+ . Absorption and emission spectra of **30** in the absence (black, dotted line = fit of the CT emission; LE = fluorophore-localized emission band) and presence (at full complexation) of Hg^{2+} (red) and Ag^+ (blue) in MeCN; fluorometric titrations of **1** with Hg^{2+} and Ag^+ shown in the inset; FEF (LE) determined from the integrated fluorescence intensity of the LE band. (b) Chemical structures of other virtually decoupled probes for Na^+ (**31**), Pb^{2+} (**32**), and Ni^{2+} (**33**). For color code, see Fig. 3. (Adapted in part from [115]. Copyright 2000 American Chemical Society)

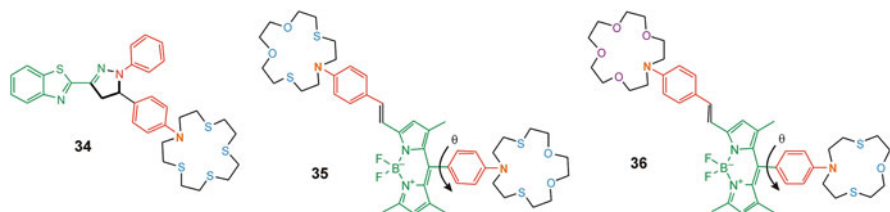


Fig. 12 *Left*: ICT-PET probe **34** with a small and rigid spacer (*thick black*), decoupling the PET active donor = receptor unit from the π -conjugated ICT fluorophore. *Middle and right*: probes **35** and **36** combining a conventional ICT and a virtually decoupled ICT process with two identical receptor units (**35**, for Hg^{2+}) and two different receptor units (**36**, tetraoxa monoaza crown for Na^+ and dithia monooxa monoaza crown for Ag^+). For color code, see Fig. 10

incorporation of a second binding site [120]. Potentially quenching species can be deliberately detected with “light up” responses. In accordance with the doubly receptor-substituted ICT dyes discussed before, the combination of a virtually decoupled and a $D-A-D$ configuration is also possible, giving rise to unique signaling protocols with high fluorescence output for a single (**35**) [121] or given combination of two analytes (**36**) [122].

The last approach for a designed cation signaling system with enhanced output utilizes the differences in fluorescence quantum yield of two tautomeric forms, the equilibrium of which is subject to analyte-induced changes (**37**, Fig. 13) [123].

3.2.2 For Anions

One of the main forces that can be utilized for the recognition of most inorganic and organic anions by fluorescent reporter molecules is hydrogen bonding. Whereas electrostatic forces are usually divergent and do not allow to selectively address a particular anion, hydrogen bonding is convergent and permits the specific tailoring of receptor sites and interaction processes; electrostatic forces can then support such binding interactions. Less strong and less hydrophilic forces such as π stacking, and van der Waals or hydrophobic interactions are usually much more difficult to realize in indicator molecules that are functional derivatives of organic dyes. Such effects can be utilized when the fluorescent reporter is incorporated into composite sensory systems such as porous organic or inorganic materials like molecularly imprinted polymers [124] or organic–inorganic hybrid materials [125] which try to mimic antibodies or the binding pockets of proteins. Due to space limitations, these composites will not be discussed here.

The use of hydrogen bonding assistance in fluorescent reporters is particularly attractive for ICT probes. Because of the charge redistribution taking place upon absorption of a photon and the ICT process, such anion-responsive probes can be designed in a way that hydrogen bonds formed in the ground state are strengthened in the excited state. These features can lead to enhanced rigidity, which would be reflected in enhanced fluorescence signals. The role of hydrogen bonds can be

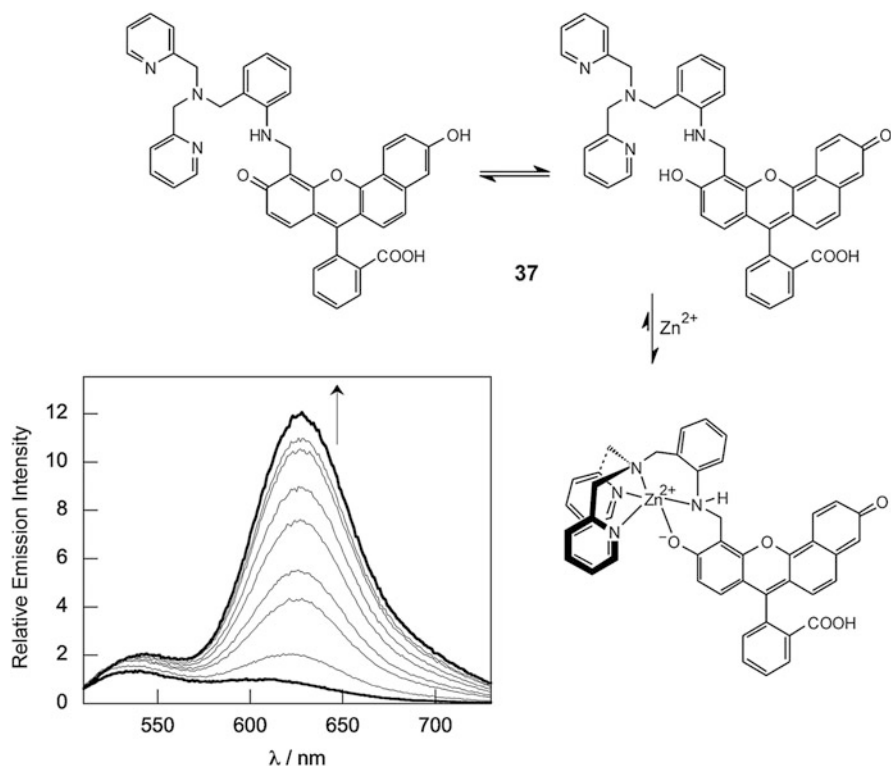


Fig. 13 Tautomeric indication protocol using the Zn^{2+} -modulated equilibrium between the naphthoxyquinone mesomer of **37** (top left), which has fluorescein-like optical properties, and the phenoxynaphthoquinone mesomer (top right), which possesses optical characteristics similar to naphthofluorescein, i.e., red-shifted bands. Titration spectra show the Zn^{2+} -induced fluorescence enhancement. (Reprinted in part with permission from [123]. Copyright 2004 National Academy of Sciences, USA)

twofold. On the one hand, probes such as **38** and **39** operate with reinforced rigidity, which leads to a change of the ratio of LE-to-CT emission in **38** (for a brief definition of LE and CT, see Fig. 11) and to enhanced fluorescence in **39** [126, 127]. The second type of impact of coordination-reinforced hydrogen bonds relates to the ESIPT process (see Sect. 2). Dyes that are able to form emissive ESIPT states usually show a favorably red-shifted emission band of moderate fluorescence quantum yield [31]. Anion coordination at an ESIPT site can thus promote ESIPT like in **40** (Fig. 14), leading to dramatically enhanced red-shifted fluorescence [128]. The drawback for most ESIPT systems, however, is that in aqueous solutions, water often competes favorably and hampers recognition.

A rather unique strategy which often works very well for anion signaling involves the recoordination that can take place in the ligating sphere of a metal ion in a stable complex with a fluorescent probe upon anion attack. The basic

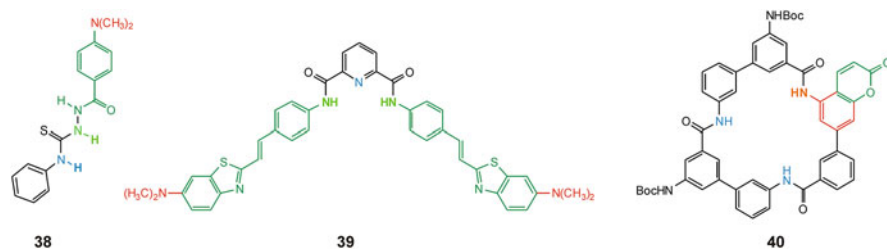
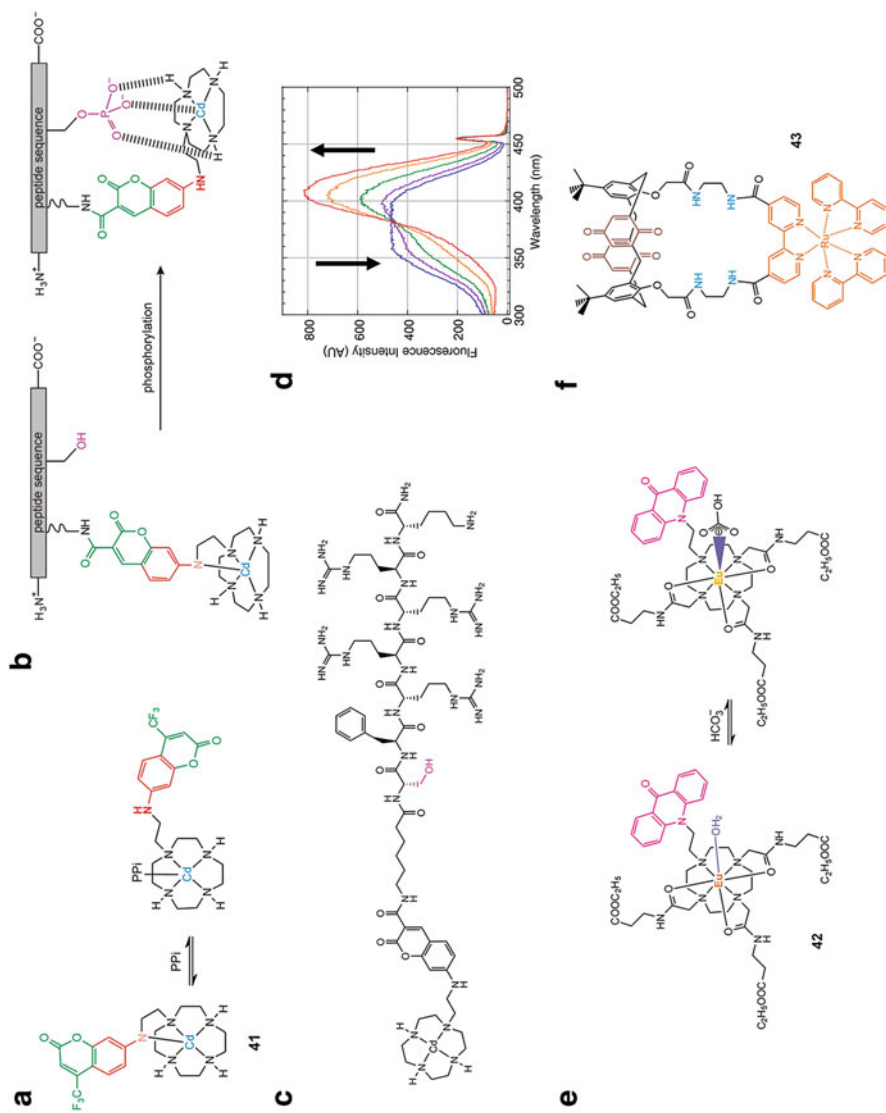


Fig. 14 Anion probes operating through the reinforcement of hydrogen bonds. For color code, see Fig. 3

mechanism is outlined in Fig. 15. In the absence of the analyte, the remaining coordination site of the metal ion is occupied by a donor atom of the probe. Anion addition then leads to the dissociation of the metal ion–fluorophore bond and formation of the coordinative bond between metal ion and anion, which has a pronounced electrostatic character [130]. Depending on the fluorescent probe chosen, strong shifts and intensity modulations can be encountered. As the peptide-appended derivative of **41** in Fig. 15b–d nicely shows, such a system can also be implemented in more advanced sensing schemes [129]. Moreover, this approach is not only suitable for stable metal ion complexes of ICT type but for PET type probes as well [131]. Recently, a metal ion–fluorescent probe complex has also been used in a redox-mediated fluorescence “light up” approach, in which a paramagnetic Cu^{2+} ion is bound close to the fluorophore and thus quenching the emission is turned into a diamagnetic noninterfering Cu^+ ion through reaction with iodide [132].

Related yet mechanistically different are two other types of metal complexes with organic (fluorescent) receptors using lanthanide ions or lower-row transition metal ions. The architecture of the lanthanide-based probes is very similar to the ICT complex probes (cf. **42** and **41** in Fig. 15) though the organic chromophore does not act as an emitter, but only as a light-harvesting antenna to efficiently sensitize the Eu^{3+} luminescence. Since the quantum yield of the latter is very sensitive toward the type of interaction at the remaining coordination site(s) of the metal ion, comparatively loosely coordinating species such as water molecules usually quench the emission to a considerable degree. Exchange of weakly by a strongly binding species such as an anion then reduces the probability of non-radiative decay and entails an increase in the typical line-shape Eu^{3+} luminescence [133]. Examples of the latter type of metal-based probes are for instance Ru^{II} -tris (bipyridine) chromophores exhibiting metal-to-ligand CT luminescence. These motifs are rather popular in anion probes though their luminescence effects are usually only modest and include quenching as well as enhancement features. However, if a deliberate quenching channel is introduced through remote redox sites as in **43**, anion binding in the receptor unit separating the Ru^{II} (bipy)₃ emitter and the quinine quenchers can revive luminescence and yield strong signal outputs [134].



4 Strategies of Signal Amplification

The examples discussed in the previous sections have shown how rational design of fluorescent reporters can yield strongly enhanced fluorescence signals upon target binding. In certain architectures, this enhancement can even reach factors of more than a thousand. However, all the examples rely on the stoichiometric interaction of reporter and analyte and generate a stoichiometric amount of photons, sometimes with a higher and sometimes with a lower probability, i.e., generate higher or lower fluorescence enhancement. The question is now if and how we can go beyond such traditional enhancement. One of the most obvious keys to success might lie in the consideration of signal amplification in natural systems, most of all enzymes. In a stimulated process, a single co-factor can induce the activation of an enzyme which then processes its substrates almost limitlessly or, more precisely, until inhibition occurs or it runs out of educts. These, in a general sense, catalytic approaches are very appealing and have also been realized in other areas of analytical chemistry, for instance, in the polymerase chain reaction (PCR) or in rolling circle amplification (RCA)-based techniques. However, many other strategies are possible. The following section will shed light on the most prominent concepts of fluorescence amplification for the indication of charged inorganic and small-molecule organic analytes.

4.1 Chemical Reactions

Perhaps the most obvious strategy for a chemist is to use an actual chemical reaction involving covalent bond formation rather than the interplay of supramolecular forces. The following section thus illustrates the use of chemical reactions in the context of luminescence signaling, concentrating on two different phenomena: (i) the production of a fluorophore in a chemical reaction, which still requires a conventional fluorescence measurement setup, and (ii) chemiluminescence (CL), where photons are produced by a chemical reaction, but which only needs a detector for registration of the emitted light.

← **Fig. 15** Metal complex-based anion probes. (a) Stable Cd^{2+} complex of ICT probe **41** undergoes recoordination of the metal ion in the presence of pyrophosphate, reinforcing ICT. (b) Elaboration of the concept shown in (a) to a peptide probe (see c) able to assess protein kinase activity; (d) time course of the corresponding bathochromic shift in fluorescence excitation spectra during enzyme activity according to (b). (e) Ligand exchange at the Eu^{3+} emitter in **42** leads to strong emission increase (sensitizer in magenta). (f) Ru^{II} -tris(bipyridine) probe quenched by the quinoid calix[4]arene subunits (*brown*); anion insertion into the binding site (*blue atoms*) leads to suppression of quenching. (Part d) adapted from [129]; graphical material kindly provided by the authors of the original publication)

4.1.1 Transformation of a Leuko¹² Dye into a Fluorophore (Chemodosimeter)

A rather new approach in selective fluorescence detection is the production of fluorophores in a chemical reaction. Compared to supramolecular reporters, for which the target is interacting via noncovalent interactions such as hydrogen bonding, π - π interactions, or electrostatic attraction with a binding site that is complementary to the analyte to modulate the fluorescence signal, the use of specific reactions is more straightforward. In a simplified picture, only a leuko dye is required which can be transformed into the respective fluorophore in a chemical reaction that should be specific for the analyte of interest. A prominent advantage of the reaction-based systems is that during the reaction, the site to which the analyte is attracted and at which it binds is removed (in most cases) from the fluorophore, enabling in a straightforward way the detection of notoriously quenching analytes (e.g., the heavy and transition metal ions mentioned above) by strong fluorescence signals. However, one disadvantage still resides with many reaction-based systems, i.e., they can only act as chemodosimeters. Most reactions that produce a fluorophore are essentially irreversible so that the indicator is consumed, prohibiting the continuous monitoring or reuse of the system; the chemosensing system is a disposable one and can only be applied in a single analysis.

For cations, various examples have been realized mostly concerned with the detection of the already mentioned heavy and transition metal ions. One of the first examples published involves the Cu^{2+} -induced hydrolysis of a rhodamine B hydrazide **44** to rhodamine B **45**, which can be employed in water to detect Cu^{2+} down to 10 nM with a linear response up to 2 μM (Fig. 16) [135].

A very popular target for reaction-based sensing is Hg^{2+} because of its outstanding thiophilicity and ability to cleave C-S bonds [136–139]. A remarkable example is the one shown in Fig. 17. Use of a squaraine dye as the target structure allows achieving intense absorption and emission bands in the far red region of the visible spectrum, facilitating “naked-eye” monitoring and fluorescence detection without the interference of autofluorescence and matrix absorption [140]. Moreover, due to

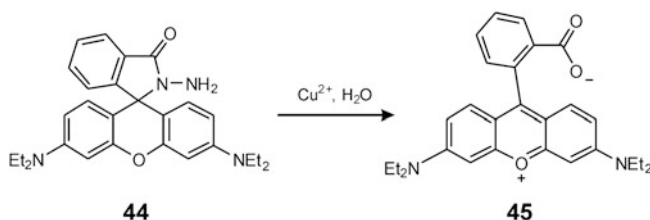


Fig. 16 Rhodamine-based Cu^{2+} chemodosimeter; **44** is colorless and nonfluorescent, **45** is pink and highly fluorescent

¹²“Leukos” (Greek) means “white, colorless”. The term “leuko dye” is commonly used for a colorless (or largely UV-absorbing) dye precursor.

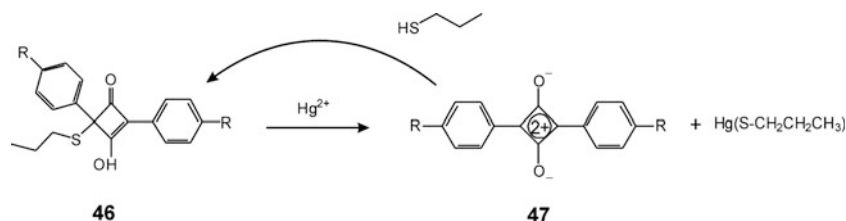


Fig. 17 Hg^{2+} -induced transformation and thiol-mediated regeneration of **46** and **47**; **46** is colorless and nonfluorescent, **47** is blue and highly fluorescent

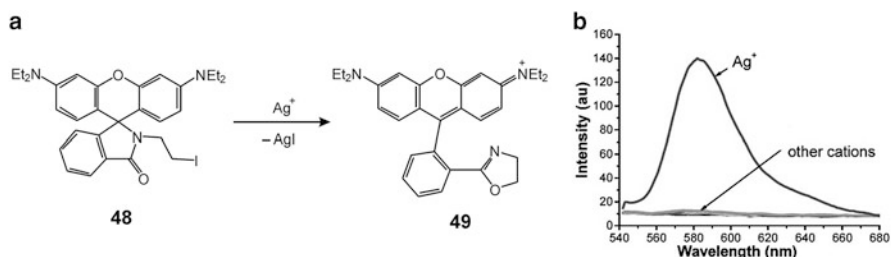


Fig. 18 (a) Rhodamine-based Ag^+ sensing system and (b) fluorescence response of **48** in the presence of Ag^+ and the other cations mentioned in the text. (Reprinted in part with permission from [141]. Copyright 2009 American Chemical Society)

the high electrophilicity of the squaraine's cyclobut-2-enone core, the leuko dye can be regenerated with propanethiol, circumventing the problem of irreversibility of the reaction. Sensing and regeneration of the system have been shown to work with a derivative of **46** in a poly(ethylene-terephthalate) based dip-stick assay.

A remaining issue when using sulfur-based leuco dyes is their sensitivity to oxidation, limiting long-term storage at ambient temperature. In addition, such indicator systems are commonly not able to detect mercury in sulfur-rich environments, where it is often present.

Cu^{2+} and Hg^{2+} are perhaps the most obvious targets for reaction-based signaling systems. However, this approach has also been realized for monovalent Ag^+ . Here, again a rhodamine derivative (rhodamine B spirolactam **48**, Fig. 18) allows the highly selective detection of Ag^+ with a detection limit of 14 ppb in water containing 20% ethanol. Silver nanoparticles, a topical analyte today, can also be detected, after oxidation of the particles with $\text{H}_2\text{O}_2/\text{H}_3\text{PO}_4$ [141]. The selectivity was tested with Ca^{2+} , Ba^{2+} , Mg^{2+} , Cr^{2+} , Mn^{2+} , Fe^{3+} , Co^{2+} , Ni^{2+} , Cu^+ , Cu^{2+} , Zn^{2+} , Pd^{2+} , Cd^{2+} , Hg^+ , and Hg^{2+} and no interference was found.

For the reaction-based sensing of anions, the most considerable success has been reached in cyanide sensing, basically due to the necessity for assessing this toxic species and because it can be easily addressed in water due to its high nucleophilicity. For instance, the coumarin derivative **50** shows a dramatic fluorescence increase after cyanide-induced cyanohydrin reaction (Fig. 19), no response to

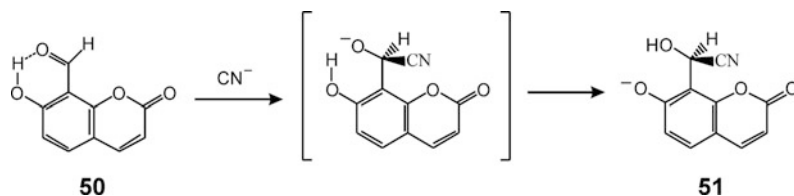


Fig. 19 Coumarin based cyanide chemodosimeter; **50** is nonfluorescent, **51** is highly fluorescent

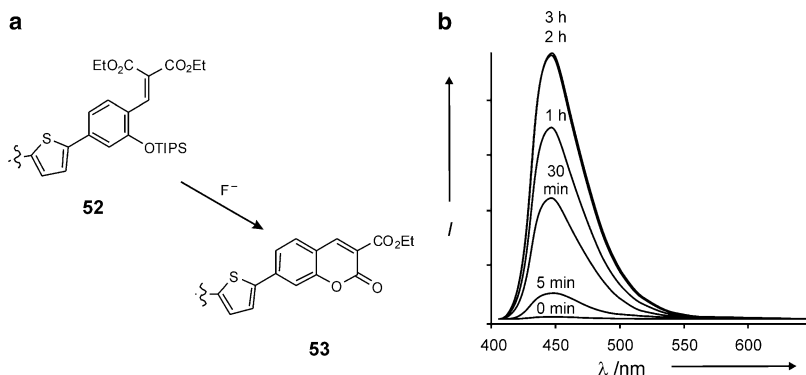


Fig. 20 (a) Fluoride sensing with coumarin leuko dye **52** and (b) time-dependent spectroscopic response of the reaction; TIPS = triisopropylsilyl group. (Reprinted in part with permission from [143]. Copyright 2003 Wiley-VCH)

other relevant small anions (F^- , AcO^- , ClO_4^- , $H_2PO_4^-$, Br^- , Cl^- , I^- , NO_3^- and N_3^-) and was positively tested for its applicability *in vivo* [142].

The sensing of fluoride with a reaction-based indicator can be based on its unique reactivity with silicon. As shown in Fig. 20, the O–Si bond cleavage with fluoride can be used to produce the coumarin dye **53**. For this system, a 100-fold sensitivity increase was seen after incorporation of the reaction scheme into a conjugated polymer [143].

Regarding neutral small-molecule analytes, reactive oxygen species (ROS) are a highly topical group. As the term ROS implies, these species should be particularly well-suited for the development of reaction-based protocols. However, this advantage is at the same time a disadvantage when the aim is the determination of a single species and not of “ROS” as a sum parameter. For instance, a well-established ROS probe like **54** responds only in a rather unselective way to oxidation especially by oxygen-based radicals (Fig. 21) [144]. A more sophisticated approach toward H_2O_2 sensing was realized with **56**. It invokes a hydroboration/oxidation approach and is based predominantly on the hydrolytic abilities of hydrogen peroxide rather than on its oxidation potential. Whereas the latter can be easily reached by other ROS, the basicity and nucleophilicity of the hydrogen peroxide anion is comparatively unique. Therefore, chemodosimeter **56** reaches a >500-fold selectivity over other anionic ROS and at least a 3-fold selectivity over radical ROS in water at pH 7 and was also shown to be applicable in living cells [145].

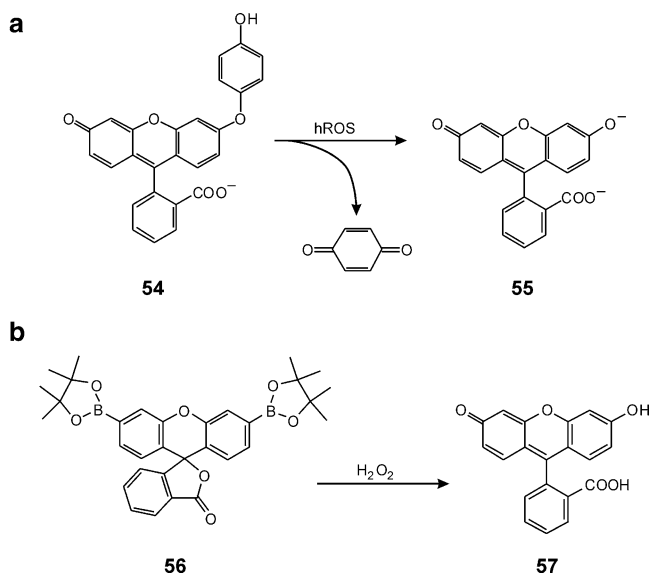


Fig. 21 Fluorescein-based chemodosimeter molecules for ROS. Whereas faintly colored and weakly fluorescent **54** reacts rather nonspecifically to green and highly fluorescent **55** (a; hROS = highly reactive oxygen species), colorless and nonfluorescent **56** is selectively converted into green and highly fluorescent **57** in the presence of H_2O_2

4.1.2 Catalytic Production of Fluorophores

Reaction-based indicators which are catalytically transformed by the analyte of interest are an attractive alternative due to the simple reason mentioned in the context of enzymes at the beginning of Sect. 4: one analyte molecule is qualified to produce a lot of fluorophores, increasing sensitivity dramatically. For an actual quantitative determination, however, the same conditional constraints are relevant like in enzyme-based methods, i.e., reproducible and defined incubation times, temperature, pH, etc. Up to now, transition metal cations have been mostly shown to be detectable by catalytic fluorophore production.

To circumvent some of the above-mentioned drawbacks of sulfur-based mercury chemodosimeters, a system based on the alkyne oxymercuration of **58** has been developed (Fig. 22) [146]. **58** shows high selectivity, a limit of detection of ca. 8 ppm, resistance against strong oxidants, and a positive reaction even in the presence of cysteine, which is known to form stable mercury complexes and is used for the extraction of mercury from tissue samples. Another metal that is well-known for its catalytic ability is palladium, catalyzing different reactions depending on its oxidation state. Since this metal is toxic, assessment of the maximum allowable concentration of Pd in consumer products such as pharmaceuticals requires highly sensitive and selective detection schemes. For this purpose, indicator **60** was conceived to undergo allylic oxidative insertion to the fluorescein

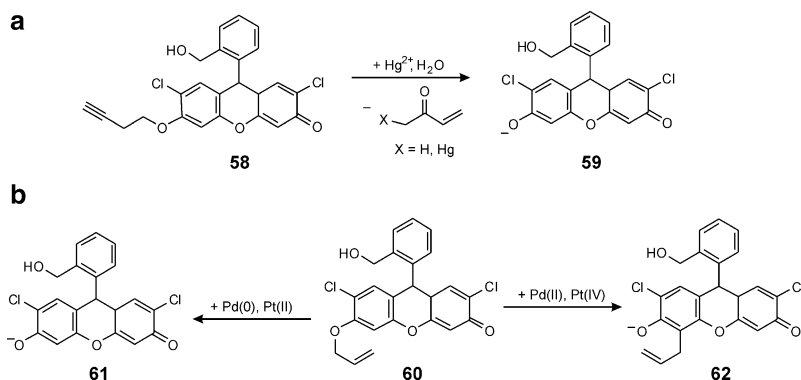


Fig. 22 (a) Oxymercuration reaction for Hg^{2+} sensing with **58**. (b) Oxidation state-selective Pd/Pt catalytic production of fluorophores **61** and **62** from **60**. Nonfluorescent **58** is selectively converted into strongly green fluorescent **59** and nonfluorescent **60** is either converted into strongly green fluorescent **61** or strongly greenish-yellow fluorescent **62**

derivative **61** by $\text{Pd}(0)$ and, to a lesser extent, Pt(II) and to the fluorescein dye **62** in a catalyzed Claisen rearrangement by Pd(II) and Pt(IV) , enabling not only Pd and (to a lesser extent) Pt detection at trace concentrations, but also a spectral distinction of the oxidation state [147, 148].

A rather new approach for detecting metal ions with very high sensitivity and selectivity utilizes DNAzymes. DNAzymes are a special class of enzymes formed from DNA nucleotides. Compared to proteins and ribozymes, they are more stable, structurally simpler, and therefore cheaper. As DNAzymes often require metal ion cofactors, they are interesting sensing platforms for these metal ions [149].

DNAzymes are usually composed of a substrate strand that forms a stable duplex with an enzyme strand. The substrate strand possesses a particular cleavage site at a defined position. The indication reaction then involves the cleavage of a certain substrate strand by the designated cofactor or metal ion, breaking the duplex and releasing the fragments. The cleavage sites are specific to certain metal ions, e.g., a ribo-adenosine (rA) for Pb^{2+} and UO^{2+} . Cu^{2+} on the other hand is capable of directly cleaving the strand at a guanidine position.

An example is displayed in Fig. 23. For sensory applications, the substrate strand is tagged with a fluorophore (e.g., 6-carboxyfluorescein, FAM) at the 3' end and the enzyme strand with a quencher (e.g., 4-(4'-dimethylaminophenylazo)benzoic acid, dabcyI) at the 5' end. As long as the duplex is formed, the emission of the fluorophore is quenched and no fluorescence is registered. Only after activation of the catalytic activity by the target ion, the substrate strand is cleaved and the fluorophore liberated, enabling the detection of the unquenched fluorescence. However, because of the bulged structure of the DNAzyme (Fig. 23), the melting temperature of the duplex is comparatively low. Thus, for optimum performance, i.e., for optimum suppression of background signals at relevant temperatures such as ambient or body temperature, a second internal quencher was attached to the

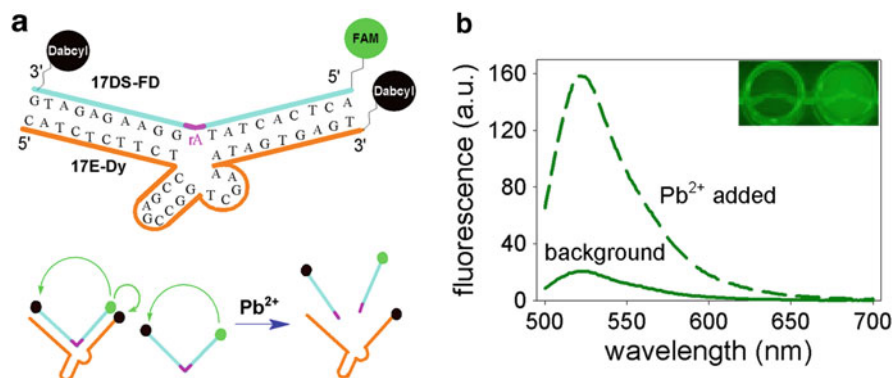


Fig. 23 (a) DNAzyme-based sensor design with two dabcyl quenchers and a FAM fluorophore (*top*) and mechanism of operation (*bottom*). (b) Fluorescence response before and after complete cleavage through Pb^{2+} ; inset contains the corresponding image of the DNAzyme probe in the absence (*left*) and presence of Pb^{2+} (after 2 min of reaction time, *right*). (Reprinted with permission from [150]. Copyright 2003 American Chemical Society)

5' end of the substrate strand, effectively reducing background fluorescence of the single strand [150].

The preparation of DNAzyme sensors is usually done in a combinatorial way by producing a random set of DNA strands and selecting the analyte-responsive strands on an affinity column followed by elimination of strands that are sensitive to a broader group of metal ions. In case of success, a DNAzyme with high selectivity and sensitivity is obtained after several iterative cycles. DNAzymes have been found by this process for Cu^{2+} , Pb^{2+} , and UO^{2+} [151–153].

4.1.3 Systems Based on Chemi- and Bioluminescence

The last systems discussed in this section dealing with the generation of luminescence signals through chemical reactions are based on chemiluminescence (CL). CL implies that electromagnetic radiation in the UV, visible, or NIR region is produced by a chemical reaction that yields electronically excited intermediates or products. System design is generally possible along two different strategies, i.e., involving (i) *direct* CL or (ii) *sensitized* CL. In the first approach, the reaction directly leads to the formation of a certain fraction of the products in an electronically excited state, emitting the photons that can be detected. Indirect or sensitized CL relies on the aid of a fluorophore. The chemical reaction here also produces an excited species which, however, does not emit to a sizable degree but relaxes mainly through nonradiative pathways. The aiding fluorophore added to the system is chosen in such a way that it can operate as an energy acceptor for the excited reaction product and, after energy transfer from product to fluorophore, decays by emission of a photon [154–156].

Although CL does not require a lamp as excitation source and thus allows measurements against a “zero” background, some basic requirements have to be

met. The production of an electronically excited state that emits in the visible region requires a strongly exothermic reaction (ca. 150–300 kJ mol⁻¹), which is usually only accomplished by redox reactions with strong oxidants like oxygen, hydrogen peroxide, or potassium permanganate. Furthermore, the quantum yield of P^* formation (P^* = excited reaction product) of the reaction must be favorable as well as the luminescence quantum yield of P^* . For sensitized CL, the efficiency of the energy transfer to the fluorophore and the fluorescence quantum yield of the latter are the crucial parameters.

$$\Phi_{\text{CL}} = \Phi_{\text{ex}} \Phi_f \quad (2)$$

The efficiency of CL (Φ_{CL}) is usually expressed as the product of the efficiency of the production of P^* (Φ_{ex}) and the luminescence efficiency (Φ_f) of the excited species (2). Efficiencies found in CL reactions are usually rather low with ca. 0.001–0.1; higher yields are only found in bioluminescence (BL). Although these values sound rather inefficient, it should be kept in mind that CL setups are very simple yet very sensitive. As mentioned above, no external light source is needed so that the experiment can be conducted in a light-tight cell. Furthermore, since background emission equals virtually zero, the reaction cell can be mounted directly in front of the detector with no dispersive elements or filters being required. Nonetheless, there are some important difficulties for CL analysis which have to be taken into account or circumvented. Because the reactions strongly depend on experimental parameters, these must be controlled meticulously for comparable results. Moreover, since CL reactions are usually performed with strong oxidants that show very low selectivity, today, most analytical CL applications are postseparation, i.e., CL is used as detection technique for HPLC and gel chromatography, involving for instance the injection of the reaction mixture into a flow-through cell [157].

A well known example of a CL reaction is the oxidation of luminol (**63**) with strong oxidants like permanganate, hypochlorite, and especially hydrogen peroxide in alkaline medium (Fig. 24). A representative example of sensitized CL is the oxidation of oxalates with hydrogen peroxide in the presence of a fluorophore [158].

A special case of CL is electrochemiluminescence (ECL) which will only be briefly mentioned here. In ECL, a redox reaction is conducted by switching the voltage of an electrode instead of mixing reactants like in CL, converting electrical energy into light [159]. The first compound that was found to show ECL is Ru^{II}-tris(bipyridine) [160] which is also the best studied and most applied ECL system (Fig. 25). It has an ECL efficiency of 0.05 [161] and is usually taken as a reference for ECL efficiency measurements [162]. With respect to ECL sensing, Ru^{II}-tris(bipyridine) can for instance be employed to indicate strong reductants such as oxalate [163]. The reaction scheme, however, is potentially more complicated since after oxidation of Ru^{II} to Ru^{III} at the electrode surface, reaction of the Ru^{III} species with oxalate can generate various highly reactive radical anion intermediates and proceed through various reaction sequences. Nonetheless, if conditions are properly controlled the ECL response is linear and allows for example the determination of oxalate in urine at relevant micromolar concentrations [163].

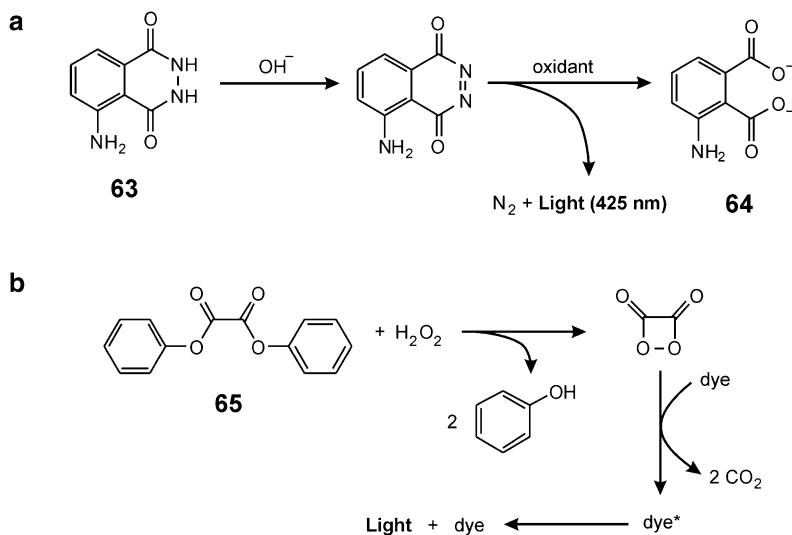


Fig. 24 (a) Chemiluminescence reaction of luminol (**63**) to 3-aminophthalic acid (**64**). (b) Oxidation of diphenyloxalate (**65**) to produce the high-energy dioxetandione as a sensitizer for an organic dye fluorophore

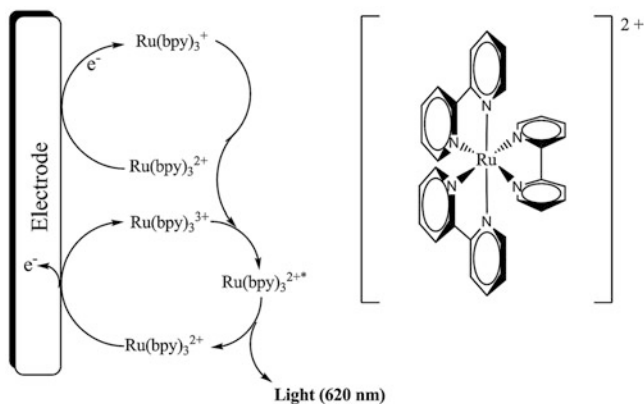


Fig. 25 Chemical structure of Ru^{II} -tris(bipyridine) (*right*) and proposed mechanism for ECL (*left*) (Adapted from [159])

The last type of CL discussed here is bioluminescence (BL). As the term suggests, BL is an enzyme-catalyzed process found in living organisms [164, 165]. In most BL reactions, luciferin is oxidized with molecular oxygen by luciferase with ATP as a cofactor. In addition, the luciferase activity depends on Ca^{2+} or Mg^{2+} . The analytically most often employed system is the firefly luciferase/ D -luciferin system shown in Fig. 26. Here, ATP is necessary to form the highly energetic AMP adduct required for further reaction sequence. Subsequent cleavage

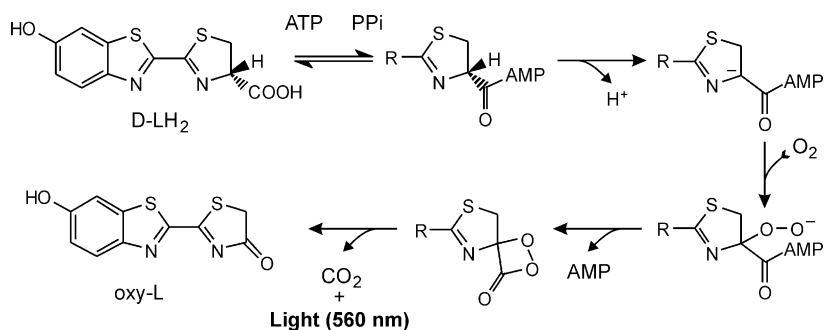


Fig. 26 Mechanism of the ATP- and Mg^{2+} -dependent firefly luciferase catalyzed bioluminescence oxidation reaction of D-luciferin (D-LH₂) to oxyluciferin (oxy-L)

leads to an intermediate with a four-membered dioxetane ring, which decomposes to CO_2 and the excited form of oxy-L that finally decays by emission. The efficiency of the reaction is $\Phi_{CL} = 0.41$ at pH 8.5 which is the highest known efficiency for a BL reaction. Being ATP-dependent, the firefly luciferase/D-luciferin system can be and has of course been used to detect and quantify ATP and even allows the monitoring of changes in ATP concentration in other ATP producing or consuming catalytic cycles.

4.2 Displacement of Fluorophores from Binding Sites

Indicator displacement assays (IDAs) – or, in the specific case of fluorescent indicators, F-IDAs – are based on the next alternative concept described here. A receptor with an affinity for a given analyte is loaded with an indicator, usually a fluorescent or colored dye, whose spectral properties undergo a change upon complexation with the receptor. Treatment of this indicator–receptor complex with the analyte results in the displacement of the indicator from the receptor and a restoration of the indicator’s original spectral properties, indirectly reporting analyte coordination (Fig. 27). For effective detection, two main requirements have to be fulfilled: (1) the receptor/indicator interaction must be reversible and weaker than the interaction of the receptor with the designated analyte and (2) the indicator must show significantly different optical properties when bound to the receptor and when freely dissolved in solution.

The use of synthetic receptors for such displacement assays was pioneered by Metzger and Anslyn in 1998, based on the concept of competitive immunoassays. The authors developed a method for the determination of citrate in beverages and chose receptor **66** as the host, consisting of three guanidinium groups for hydrogen bonding and electrostatic interaction with citrate, and 5-carboxyfluorescein (**67**) as the indicator, because it has one carboxylate group less available than the analyte for binding with **66** (Fig. 27). In this case, the fluorescence of **67** is increased when forming a complex with **66**. Upon citrate addition, **67** is displaced and a decrease in

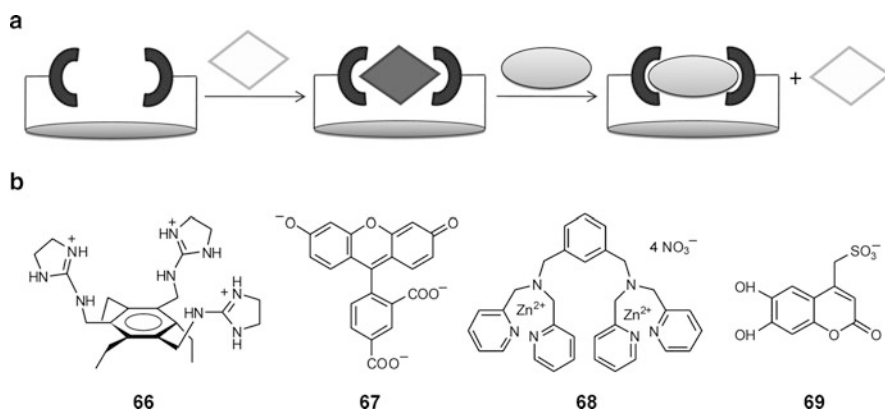


Fig. 27 (a) Representative scheme for a displacement assay protocol in which first a fluorescent indicator is coordinated to a host. As a consequence, its optical properties are altered. Second, upon analyte addition, the higher affinity of the analyte for the host leads to dissociation of the complex and displacement of the indicator. The original optical properties of the fluorophore are restored, signaling indirectly the presence of the analyte; (b) Some examples of receptors and fluorescent indicators reported in the literature for F-IDAs

the fluorescence is observed [166]. A similar approach was followed by the same authors for the determination of inositol-triphosphate (IP_3) [167].

In succession to this early example relying on a quenched signal, efforts have been made to achieve “light-up” F-IDAs. One example was described by Fabbrizzi et al. for the selective detection of carbonate in water, utilizing metal–ligand (coordinative) interactions for binding and displacement [168]. A dicopper(II) polyamino cage was chosen as the receptor and coumarin 343 as the fluorescent indicator, because it possesses a carboxylate function capable of bridging the two Cu^{2+} centers of the polyamino cage. Complete quenching of the coumarin emission at 487 nm was observed upon titration of the fluorophore with the polyamine- Cu^{2+} receptor. Addition of carbonate to the resulting chemosensing ensemble solution resulted in an almost complete recovery of the coumarin emission. Other anions tested like NCS^- , NO_3^- , SO_4^{2-} , HPO_4^{2-} , $HCOO^-$, and CH_3COO^- , whose association constants are well below that of coumarin 343, could not compete successfully with the indicator and could thus not be detected fluorometrically. In a similar fashion, Smith et al. described an F-IDA for the detection of pyrophosphate under physiological conditions [169]. Pyrophosphate was capable of displacing a fluorescent coumarin indicator (**69**) from a bis- Zn^{2+} -dipicolylamine host (**68**) with association constants of $10^7 M^{-1}$. The fluorescence of coumarin was quenched when bound to receptor **68**. When pyrophosphate displaced **69** from the complex, a strong enhancement of the emission at 480 nm was recorded. Remarkably, the chemosensing ensemble **68/69** was able to detect pyrophosphate almost 100-fold more sensitive than hydrogen phosphate. The same coumarin indicator **69** and a similar Zn^{2+} -dipicolylamine complex now integrating a phenylboronic acid group for the coordination of sugars was used recently by Horie and Kubo for the determination of phosphosugars in water at neutral pH [170].

Employing a supramolecular ON–OFF–ON fluorescence displacement assay, Ramaiah et al. were able to recognize guanine triphosphate (GTP). They combined the nonfluorescent and GTP-selective receptor **70**, incorporating two viologen units, and the highly fluorescent 8-hydroxy-1,3,6-pyrene trisulfonate indicator (*HPTS*, $\Phi_f = 0.7$). Addition of **70** to a solution of *HPTS* resulted in a gradual decrease of the absorbance and fluorescence intensity, yielding complete quenching of the fluorescence upon quantitative coordination through a PET process from the excited *HPTS* to the viologen moiety. In the competitive assay, the fluorescent indicator *HPTS* is displaced by GTP, entailing a signal enhancement with an FEF of ca. 150 (Fig. 28) [171].

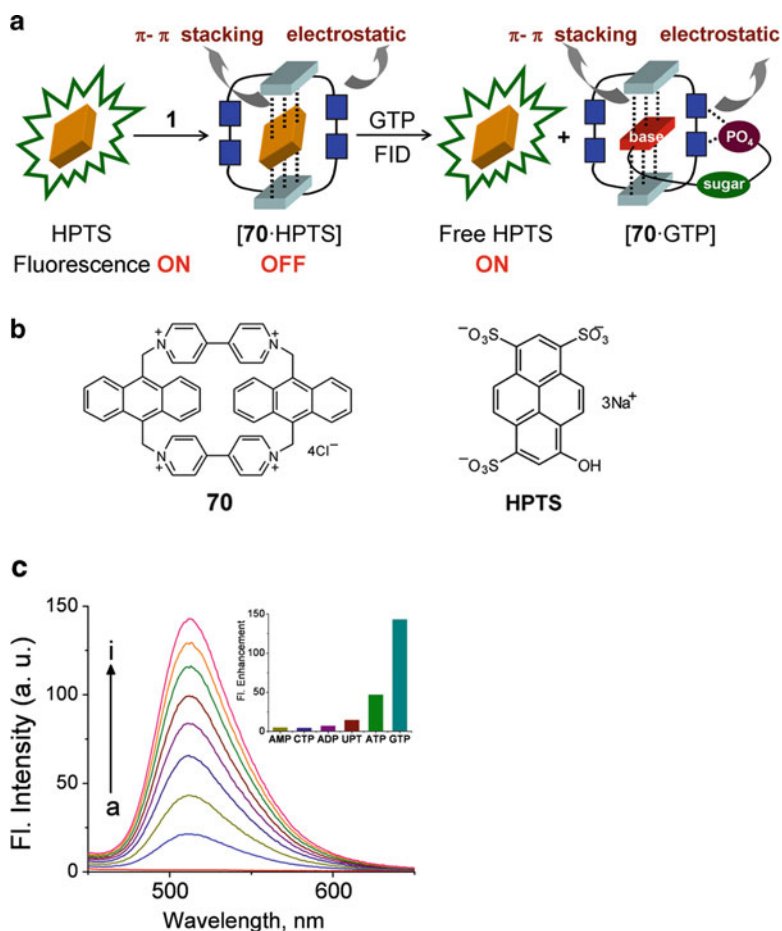


Fig. 28 (a) Scheme for the F-IDA protocol followed in [171] for GTP detection. (b) *HPTS* is the fluorescent indicator and **70** the viologen-based receptor. (c) Upon addition of GTP, *HPTS* is displaced from the complex with **70** and its fluorescence is restored. (Reprinted with permission from [171]. Copyright 2006 American Chemical Society)

F-IDAs have also been developed for the determination of neutral analytes. For instance, Waldvogel et al. used a fluorescent receptor with three urea groups as coordinating sites and a caffeine derivative labeled with a dye able to quench the fluorescence of the receptor for the detection of caffeine [172]. When the analyte, caffeine, is added, it competes with the labeled caffeine guest, displacing the latter from the receptor and yielding a fluorescent complex. Enantioselective recognition has also been accomplished with F-IDAs. For example, use of a fluorescent scandium 1,8-bis(3-*tert*-butyl-9-acridyl)naphthalene N,N' -dioxide ($\text{Sc}[(\pm)\text{-BTBAN}]_2$) complex allowed the sensing of chiral alaninol [173]. The fluorescence of the complex disappears upon addition of amino alcohols, indicating the replacement of *BTBAN*. Because the ligand exchange proceeds through diastereomeric Sc^{3+} complex intermediates, one enantiomer of alaninol was more effective in displacing enantiomeric (+)-*BTBAN* from the scandium complex than the other. Thus, the fluorescence signal of the N,N' -dioxide derived Sc^{3+} complex could be switched off enantioselectively by (*S*)-alaninol. Recently, F-IDAs have been proposed as “cheap” alternatives for continuous enzyme assays when substituting antibodies by synthetic macrocyclic hosts [174].

Interestingly, not only molecular systems perform well in IDAs but mesoporous solids functionalized with for instance anion-binding groups can also be used as suitable hosts in selective displacement assays. Martínez-Máñez et al. reported several examples of IDAs that use the pores of mesoporous silica hosts in the sense of “binding pockets” [175]. This approach involves (1) functionalization of the pores (ca. 3 nm in diameter) with adequate binding sites, (2) loading of the pores with a dye that will act as the indicator, and (3) indication of the target analyte, which forms a stronger complex with the binding groups than the dye. Following displacement, the dye diffuses into the bulk solution, enabling the optical detection of the guest *on-site* or remotely. Figure 29 sketches some examples which were successfully employed for the signaling of carboxylates and nucleosides, relying on receptor-functionalized mesoporous solids and 5-carboxyfluorescein as the indicator dye.

4.3 Increasing the Number of Fluorophores per Binding Site

Achieving very high sensitivity is a major goal for the detection of trace analytes and the modern analytical toolbox offers several strategies. Perhaps the most straightforward approach is to increase the association constant of the recognition (binding) event using receptors with high affinity for the analyte. The second strategy has already been mentioned at the beginning of this section – enzymatic amplification such as, e.g., ELISA techniques used in immunoassays or the PCR for sensitive DNA analysis. However, these amplification methods have some drawbacks. For example, the design of receptors with high binding constants for a specific analyte is usually synthetically demanding, enzymatic methods require the addition of enzymes, substrates, sometimes stopping or developing solutions,

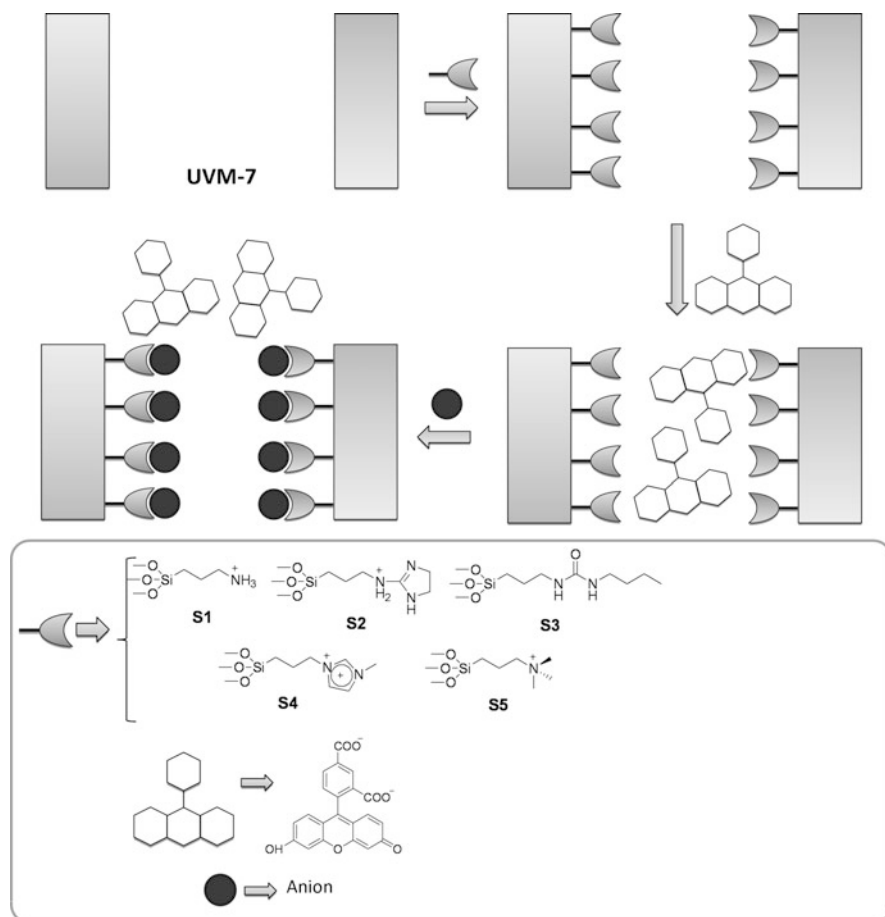


Fig. 29 Protocol for anion sensing using mesoporous MCM-41-like solids (UVM-7) containing nanoscopic binding pockets and suitable dyes

and often involve several steps which are time-consuming and error-prone so that meticulous control of the conditions is necessary.

An alternative method for increasing sensitivity to those mentioned above is to increase the number of fluorophores per binding site or biomolecule, i.e., the F/B ratio. In this way, every binding event can be signaled by several hundreds or thousands of fluorophores, realizing true fluorescence signal amplification (Fig. 30). However, the use of conventional fluorescent systems might involve self-quenching problems. For example, if more than 10–15 fluorophores are attached to one antibody, their distance is close to or within the Förster radius, resulting in significant loss of fluorescence emission intensity due to energy transfer. On the other hand, biomolecules labeled with many fluorophores may also exhibit reduced specificity and binding affinity [176]. To overcome these problems, the preparation

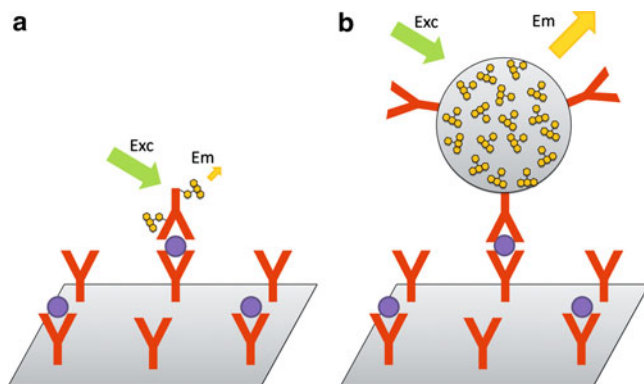


Fig. 30 Representative scheme for the signal amplification concept by increasing the number of fluorophores per binding site in an antigen–antibody sandwich assay. **(a)** Binding of a labeled antibody to the target analyte yields a moderate fluorescence signal because the antibody is labeled with only few fluorophores; **(b)** For the same binding event, the emission signal is dramatically amplified when using an antibody labeled with a nanoparticle that is doped with a large number of fluorophores

of new, highly emissive probes including fluorescently labeled nanoparticles, dendrimers, liposomes, or the use of nanocrystal labels has been considered in attempts to increase the F/B ratio while minimizing self-quenching and biomolecule perturbation.

The use of fluorescent *micro-* or *nanoparticles* (NPs) has allowed increasing the F/B ratio and, consequently, the sensitivity in different kind of bioassays. For example, in 1999, Hall et al. reported the use of fluorescent polystyrene microspheres as probes in sandwich immunoassays with mouse IgG as a model antigen and obtained tenfold signal amplification with respect to the corresponding molecular reporter [177]. In the case of DNA analysis, subfemtomolar detection limits (0.8 fm) have been achieved using NPs doped with a rhodamine fluorophore (*TMR*). Comparison experiments were carried out in which a probe DNA sequence was conjugated either with an NP or with a single *TMR* molecule. The resultant fluorescence signals showed that the NP provided approximately 10^4 times higher signal than *TMR* in the same assay [178]. The use of europium(III) NP labels is also very popular because the lanthanide(III) probe allows for time-gated measurements, further improving the limits of detection (LODs). For example, the application of fluorescent microspheres together with time-resolved fluorescence detection in a microtiter plate format could indicate prostate-specific antigen down to 60 zm (6×10^{-20} m) [179]. The use of such micro-/nanosphere probes with a 100–1,000-fold detection improvement compared to conventional time-resolved immunoassays was also successfully accomplished for nucleic acids [180] and adenovirus [181]. Viral nanoparticles could also serve as a structural base to anchor fluorescent probes. In a work from Soto et al., the attachment of >40 Cy5 reporter molecules at fixed locations on the viral capsid was shown. With organized spatial distribution of Cy5 reporter molecules on the capsid the problem of self-quenching is

circumvented and an enhancement of the fluorescence signal of the carbocyanine dye was achieved [182].

Another variation of the concept that can be employed when aiming to increase the F/B ratio relies on *dendrimers*. Dendrimers are highly branched, tree-like polymers that possess precise size and shape and defined surface groups. They are multifunctional macromolecules which can bear multiple dyes and biomolecules. Fluorescent dendrimers have been used for instance for signal amplification in DNA assays using flow cytometry techniques. With the dendrimer assay, the minimum detectable amount of analyte DNA was lowered from hundreds to tens of attomoles [183]. Dendrimers labeled with different families of organic dyes can also serve as strongly fluorescent probes for the detection of biomacromolecules [184].

The encapsulation of fluorescent molecules into *liposomes* is the third possibility in the series of multifluorophore objects. Liposomes are synthetic spherical structures composed of one or more phospholipid bilayers in which soluble markers of interest can be encapsulated. One of the first examples reporting its use as fluorescent labels for antibodies described the encapsulation of several hundreds of carboxyfluorescein and sulforhodamine fluorophores per liposome in their aqueous inner volume [185]. If the dyes possess a more hydrophobic character like, e.g., perylene dyes they can also be incorporated into the bilayer membrane [186]. The advantage of using dye-encapsulating liposomes over single fluorophore labels was demonstrated for the detection of specific DNA oligonucleotide sequences, yielding a 500-fold signal enhancement [187]. Liposomes can be detected either directly or by releasing their cargo with a detergent once the analyte has been traced. The signal is then generated by the fluorophores which are liberated into the solution upon liposome breakage [188]. Although this approach is attractive, the preparation of microcapsules with liposomes is rather elaborate and the stability of the systems is critical. Renneberg et al. reported a similar concept with liposomes as vehicles but used *fluorescent nanocrystals* instead of fluorescent dye molecules for signaling after liberation. They encapsulated microcrystalline fluorescein diacetate (FDA) with an average size of 500 nm in ultrathin polyelectrolyte layers of poly(allylamine hydrochloride) and poly(sodium 4-styrene sulphonate) via layer-by-layer (LbL) techniques. The polyelectrolyte coating was subsequently used as an interface for the attachment of antibodies through adsorption. The F/B ratio, ranging from 5×10^4 to 2×10^5 , yielded amplification rates of 70–2,000-fold for the microcrystal label-based assay compared with the corresponding immunoassay performed with conventional, directly fluorophore-labeled antibodies [189]. After the immunological reaction, the microcrystals are dissolved by a release reagent and the solubilized molecules are released into the surrounding medium (Fig. 31). In subsequent works, the authors simplified the performance of the assay by simplifying the preparation of the fluorescent conjugates. Assessing the analytical performance of the nanocrystal-based label system with a model sandwich immunoassay for the detection of mouse IgG, the authors could lower the LOD by a factor of 5–28 and increase the sensitivity 400–2,700-fold compared with conventional fluorescein isothiocyanate (FITC) conjugates [190]. The method was also employed for avidin–biotin protocols [191] and for the quantitative detection of a

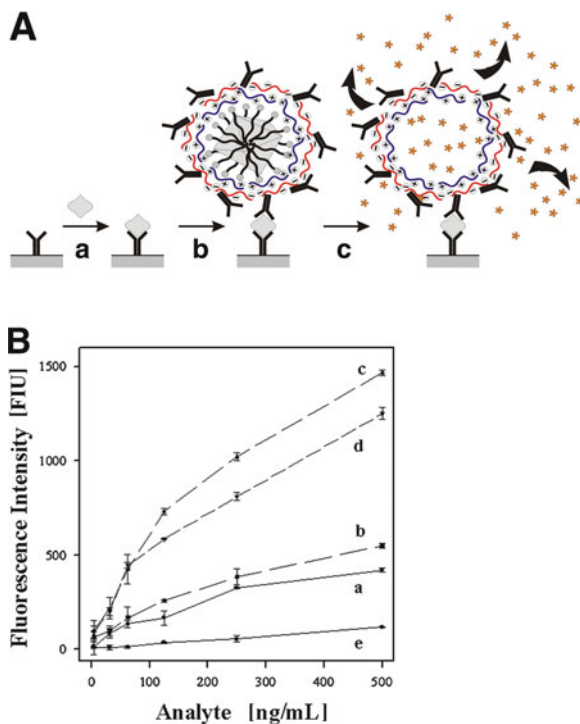


Fig. 31 (A) Principle of a sandwich immunoassay using FDA particulate labels. The analyte is first immobilized by the capture antibody preadsorbed on the solid phase (a) and then exposed to antibody-coated microparticle labels (b). Every microparticle contains $\sim 10^8$ FDA molecules. High signal amplification is achieved after solubilisation, release, and conversion of the precursor FDA into fluorescein molecules by the addition of DMSO and NaOH (c). (B) Calibration curves of IgG-FDA microcrystal labels with increasing surface coverage of detector antibody (a-d) compared with direct FITC-labeled detector antibody (e). The fluorescence signals increase with increasing IgG concentration. FDA microcrystals with a high IgG surface coverage (c,d) perform better than those with lower surface coverage (a,b). (Reprinted with permission from [189]. Copyright 2002 American Chemical Society)

PCR product [192]. The dye-doped polymer nanoparticles [13], silica nanoparticles [14] and nano-size all-dye aggregates [15] are overviewed in other chapters of this book.

4.4 Involving Fluorophore Communication

In addition to increasing the number of fluorophores per binding site, there are several other intriguing phenomena that can be utilized for fluorescence signal amplification. For instance, when a high local concentration of fluorophores is reached in a nanoscopic system, inter-fluorophore communication can occur.

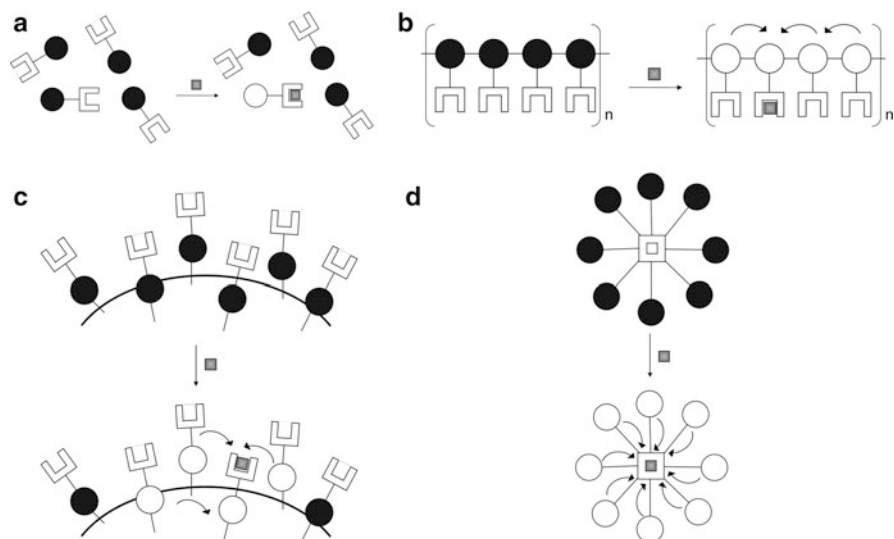


Fig. 32 Effect of analyte coordination in (a) a traditional molecular chemosensor system, (b) receptors wired in series in a conjugated polymer, (c) chemosensors grafted onto the surface of a nanoparticle, and (d) a fluorescent dendrimer. The *curved arrows* indicate the active processes, e.g., quenching

Contrary to what happens with conventional fluorescent chemosensors, for which the recognition of the target by the receptor unit affects only the fluorescence properties of a single covalently coupled fluorescent moiety, for the locally concentrated systems, a single binding event can modulate the fluorescence behavior of more than one fluorescent unit in the immediate neighborhood. The different types of systems realized along this strategy are illustrated in Fig. 32. The net effect is the transduction of a single binding event by an amplified response of several fluorophores. These collective effects will be discussed in the next chapter [23]. In the following, we will discuss the cases of conjugated fluorescent polymers, fluorescently doped dendrimers, and NPs.

4.4.1 In Conjugated Polymers

The dominant attribute that has driven interest in fluorescent conjugated polymers (CPs) sensory materials is their ability to produce signal gain in response to interactions with analytes. The increased sensitivity (amplification) is derived from the ability of a conjugated polymer to serve as a highly efficient transport medium of electronic excitation. Analyte specificity in CP-based sensors results from the covalent or physical integration of receptors, imprinting, and/or the CP's overall electrostatic and chemical characteristics. The observed amplification is a

result of the ability of the CP's delocalized electronic structure (i.e., energy bands) to facilitate efficient energy migration over large distances. To rationalize how energy migration can amplify fluorescence-based sensory events, consider a conjugated polymer with a receptor attached to every repeating unit. If energy migration is rapid with respect to the fluorescence lifetime, then the excited state can sample every receptor in the polymer, thereby allowing the occupation of a single binding site to dramatically change the entire emission. Once a single receptor site is occupied by a quenching agent, energy along the wire is funneled toward the sink resulting in enhanced deactivation (Fig. 32b).

A first proof-of-principle for the signaling amplification phenomena in CPs was reported by Zhou and Swager in 1995. They used poly(propylene ethylene) as CP with 34-crown-10 groups attached to the CP as receptors for the recognition of the well-known quencher paraquat (PQ^{2+}). The authors could observe how PQ^{2+} binding produced a trapping site for excitons, which were effectively deactivated by ET [193]. In several early works, Swager employed the concept of CPs for the amplified detection of explosives such as 2,4,6-trinitrotoluene (TNT) and 2,4-dinitrotoluene (DNT) by fluorescence quenching, using pentiptycene derived CPs [194]. As is obvious from this section so far, CPs are predestined for the amplification of quenched signals and thus most of the systems developed until today show these features. However, few examples reporting "turn-on" signal amplification have also been realized, e.g., a pH-sensitive fluorophore using energy harvested from a CP. System design includes a cationic poly(*p*-phenylene ethynylene) (PPE) polymer and an anionic polyacrylate polymer doped with fluoresceinamine dyes (PA-FA) which were deposited in an LbL type of fashion to form a pH sensor. PPE emission overlaps with the absorption band of the fluorescein moieties of the PA-FA, facilitating Förster resonance energy transfer (FRET; for an introduction to resonance energy transfer, see Sect. 4.5). At each pH, excitation in the absorption band of PPE produced an approximately tenfold higher PA-FA emission signal than direct excitation in the fluorescein absorption band of PA-FA. The authors thus attributed the amplification to an energy transfer from PPE to FA [195]. For this system, the overall fluorescence pH response depends on the pK_a of the pH-responsive FA fluorophore, of which the latter, however, is shifted to higher values because of the highly negatively charged environment in the PA-FA domains. A comprehensive overview of further examples and mechanistic descriptions of CP-based signaling systems can be found in [196].

4.4.2 In Nano- and Microparticles

One of the first examples describing the idea of fluorescence signal amplification in NPs was reported by Montalti et al. [197]. In an early work, silica NPs were covered with a layer of dansyl (Dns) moieties and were evaluated for their pH response. Photophysical studies indicated that protonation had a dramatic effect on the fluorescence of the NPs, leading to the quenching of both, the protonated Dns and

a number of unprotonated Dns units in the close vicinity, the amplified response arising from charge–transfer interactions. The signal modulation involved a number of units much larger than those effectively affected by the chemical modification so that the chemical input was translated into an amplified signal. Dansylated silica NPs were also employed for the detection of metal ions (Cu^{2+} , Ni^{2+} , Co^{2+}) by incorporation of a polyamine chain as receptor. Again, enhanced quenching of the fluorescence was observed and the authors estimated that each ion could quench up to 13 dansyl units [198]. Recalling the features of CPs, such hybrid NP design also seems much better suited for generating amplified quenching. However, also in this type of system, amplified “off–on” signals have been achieved. For instance, a 6-methoxy-8-*p*-toluene sulfonamidequinoline (TSQ) was used as ligand for Zn^{2+} ions (Fig. 33). The complexation process takes place in concert with the deprotonation of the sulfonamide group and leads to a red shift of the fluorescence band and a strong increase in its intensity (cf. the effects discussed for the very first ligand systems in Sect. 2). Due to the fact that the TSQ units are organized in a dense multichromophoric net on the particle surface, not only is the fluorescence of the moieties directly involved in the coordination of Zn^{2+} switched on, but the surrounding uncomplexed units also generate an intense fluorescence signal by transferring their excitation energy to the luminescent complexes [199].

4.4.3 In Dendrimers

Dendrimers containing photoactive components can exhibit particularly interesting properties [9] since cooperation among the photoactive units can allow the dendrimer to perform specific functions, e.g., light harvesting through antenna effects (see also the following chapter [23]). Properly designed dendritic materials can show efficient migration of energy from the dendrons or peripheral groups to the more conjugated units or core, leading to dramatically enhanced fluorescence intensity changes (Fig. 32d). One of the first works realizing the application of dendrimers in optical sensing and signal amplification was described by Vögtle, Balzani et al. [200]. A fourth generation (4D) poly(propylene amine) dendrimer decorated with 32 dansyl units at the periphery and containing 30 aliphatic amine units in the core was used for the detection of Co^{2+} . The fluorescence of all dansyl units was quenched when a single Co^{2+} ion was coordinated in the dendrimer’s core by the aliphatic amine units. In a further work, the authors described a polylysine dendrimer branched at the 1, 3, and 5 positions. Each branch carries eight fluorescent dansyl units in the periphery and six aliphatic amide units in the interior. The behavior of a monodansylated reference compound was also investigated for comparison. Addition of Ni^{2+} or Co^{2+} to a basic solution of the monodansyl compound did not cause any effect in the absorption or emission properties of the molecule. However, in the case of the dendrimer, a strong fluorescence quenching of the dansyl emission at 514 nm was observed. At low metal ion concentration, each metal quenches about nine dansyl units [201]. The effect of dendrimer size

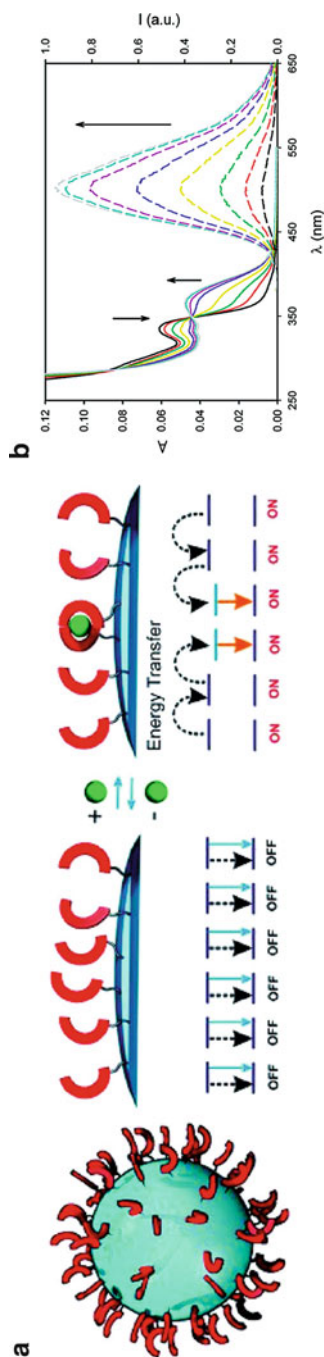


Fig. 33 (a) Schematic diagram of the excited state deactivation processes on the surface of the nanoparticle. In the absence of zinc ions (*left*), the excited states localized on the TSQ molecules deactivate mostly in a nonradiative way (*black dashed arrows*) because the radiative path (*blue arrows*) is inefficient. At low zinc concentrations (*right*), Zn^{2+} complexes are formed and the fluorescence of the complexed units is switched on (*orange arrows*). As a result of energy-transfer processes, the excitation energy absorbed by the surrounding free TSQ molecules is funneled toward the fluorescent excited states. (b) Absorption spectra (*left*, *solid lines*) and fluorescence spectra (*right*, *dashed lines*, $\lambda_{exc} = 370$ nm) recorded during the titration of NPs with Zn^{2+} ions up to equimolar concentration in DMSO (Reprinted with permission from [199]. Copyright 2008 American Chemical Society)

was also shown. Interestingly, a strong amplification of the fluorescence quenching signal was observed with increasing dendrimer generation, n . For the larger dendrimers ($n = 3, 4,$ and 5), 1:1 metal/dendrimer species were formed at very low metal ion concentration, in which the Co^{2+} guest quenches each of the dansyl units that is excited after light absorption. In the case of $n = 5$, one Co^{2+} is able to quench 64 dansyl units of the dendrimer [202].

Optically active dendrimers have also been described for fluorescence detection of chiral compounds, like those based on chiral 1,1'-bi-2-naphthol (*BINOL*) [203]. The light harvesting antennas of the dendrimer funnel energy to the central *BINOL* unit, whose hydroxyl groups lead to fluorescence quenching upon interaction with a chiral amino alcohol. This mechanism renders the dendrimers' fluorescence responses much more sensitive than those of the corresponding small-molecule sensors. For instance, the enantioselective fluorescence recognition of mandelic acid, a chiral α -hydroxycarboxylic acid, was also realized in such a way [204]. This last example is particularly interesting because, again in contrast to the majority of systems, the light-harvesting effect in this case entails fluorescence enhancement instead of quenching.

Mechanistically, exciton migration phenomena also seem to be responsible for the enhanced fluorescence quenching in dendrimers. For instance, Guo et al. studied the fluorescence quenching effects of an organic dendrimer in the presence of TNT by two- and three-photon absorption techniques. Their investigations showed that the quenching constant increased with the dendrimer generation number and that excitons can migrate over the dendrimer surface to the quenching site. The ability for exciton migration is thus the main contributor to the observed dynamic fluorescence quenching [205].

4.5 Resonance Energy Transfer

The last part of Sect. 4 deals with a concept that is in most cases not a true amplification strategy in the sense that one analyte as input generates an output from a larger number of fluorophores (for an exception, see the PPE/PA-FA example in Sect. 4.4.1). The advantageous effect here, however, comes from the unique signaling system, involving two chromophores and a distance-dependent process, and from the fact that the analytically relevant parameters excitation wavelength and emission spectrum are well separated, i.e., these systems show a very pronounced virtual Stokes shift. The concept is termed Resonance Energy Transfer (RET) and the mechanism can be basically described as follows. After photoexcitation, energy absorbed by a molecule (the RET donor, D_{RET}) can be transferred over a comparatively long distance to another molecule (the RET acceptor, A_{RET}) by resonance energy transfer. The latter then can emit with its characteristic spectrum. The pronounced virtual Stokes shift which is especially

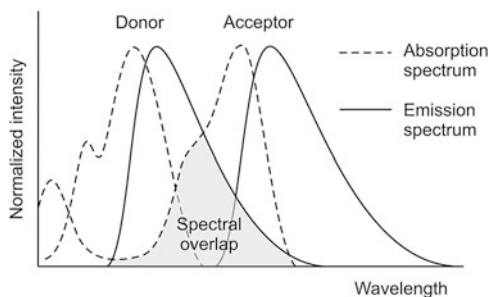
important for experimental reasons (e.g., suppression of scattering and background) arises from the fact that the experimentally relevant spectra are the absorption spectrum of the donor and the emission spectrum of the acceptor (3), in contrast to the mechanistically important spectra shown in Fig. 34 [206]. The RET process can take place when the emission spectrum of the donor overlaps with the absorption spectrum of the acceptor (Fig. 34). The optimum distance between the donor in the excited state and the acceptor in the ground state for RET to occur lies between 1 and 10 nm. Moreover, it is important to mention that the energy is transferred through a nonradiative pathway and no fluorescence (of the donor) is involved. Today, RET is very popular and widely used in various fields of analytical, life, and materials sciences.

$$\Delta\tilde{\nu}_{\text{Stokes}}^{\text{virtual}} = \tilde{\nu}_{\text{abs}}(D_{\text{RET}}) - \tilde{\nu}_{\text{em}}(A_{\text{RET}}) \approx \left| \frac{1}{\lambda_{\text{abs}}(D_{\text{RET}})} - \frac{1}{\lambda_{\text{em}}(A_{\text{RET}})} \right| \quad (3)$$

$$E_{\text{RET}} = \frac{R_0^6}{R_0^6 + r^6} \quad (4)$$

According to Förster's theory [207], the efficiency of the resonance energy transfer (E_{RET}) shows an inverse sixth-power dependence on the distance (r) between donor and acceptor (4), where R_0 is the so-called Förster distance at which the transfer efficiency is 50%. FRET is therefore a very sensitive process, well-suited for translating small conformational changes into large intensity modulations. R_0 represents a characteristic property for a given donor–acceptor pair. Other important molecular parameters that have to be considered in RET system design are the overlap integral between D_{RET} emission and A_{RET} absorption spectrum, the fluorescence quantum yield of D_{RET} , and the mutual orientation of the two partners. Details will not be discussed here but the reader is referred to [208] and relevant literature cited therein. Depending on the various D_{RET} that can principally be employed, RET can be divided into FRET (fluorescence resonance energy transfer), where the donor is a molecule intrinsically able to fluoresce and Bioluminescence Resonance Energy Transfer (BRET)

Fig. 34 Spectral representation of the RET process, highlighting the mechanistically important area of overlap between emission spectrum of the donor and absorption spectrum of the acceptor. (Reprinted with permission from [206]. Copyright 2009 Springer)



(bioluminescence RET), where the donor is an intrinsically bioluminescent molecule.¹³

4.5.1 Förster/Fluorescence Resonance Energy Transfer

Förster Resonance Energy Transfer (FRET) with a potentially fluorescent donor is unique in generating dramatically red-shifted fluorescence signals. Besides the mechanistic prerequisites as outlined before (high Φ_f of D_{RET} ; large overlap integral, the latter implying both, good spectral overlap between D_{RET} and A_{RET} , and a high molar absorption coefficient of A_{RET}), for strong fluorescence signals the RET acceptor also has to possess at best a high fluorescence quantum yield. In addition, if strong fluorescence modulations upon analyte binding are pursued, the FRET efficiencies between unbound and bound state of the signaling system have to be largely different. This means that analyte binding has to induce a distance change between D_{RET} and A_{RET} that is as pronounced as possible.

Among the chemical species discussed in this chapter, again metal ions and in particular notorious quenchers such as Cu^{2+} , Pb^{2+} , Hg^{2+} , or Cr^{3+} are primary targets for FRET signaling system development. One of the hopes here is that the FRET concept holds better promises for achieving “light-up” responses upon binding of these quenching species, simply because it operates over comparatively long distances. Related to the excimer probes introduced in Sect. 2.2.2, the traditional approach uses a metal chelating unit conjugated with two (different types of) fluorophores as the RET donor and acceptor units at the terminal ends of a linear receptor. Recognition and binding of the metal ion then leads to a folding of the receptor around the metal ion according to its preferred coordination geometry and the architecture of the ligand, bringing closer together D_{RET} and A_{RET} and producing an enhanced RET signal. However, it turned out that in line with the considerations mentioned for most of the concepts in Sect. 2, special care has also to be taken for FRET systems to avoid a direct interaction of quencher and FRET system. A typical example shows why. If a FRET system is constructed with a rather long yet flexible Cu^{2+} -chelating peptide sequence which is flanked by a tryptophan (donor) and a dansyl chloride (acceptor), FRET indeed occurs upon Cu^{2+} complexation though at the same time the overall fluorescence signal intensity is reduced because

¹³The correct and IUPAC-approved term for FRET is Förster RET [209], particularly motivated by a statement given under the entry ‘fluorescence resonance energy transfer’: *Term frequently and inappropriately applied to resonance energy transfer in the sense of Förster-resonance-energy transfer (FRET), which does not involve the emission of radiation* in [209]. The literature, on the other hand, uses both terms, Förster RET and fluorescence RET with the latter even prevailing in the biochemically and bioanalytically oriented communities. However, the dilemma becomes apparent when discussing FRET and BRET, both Förster-type processes which differ only in the properties of the donor. Interestingly, the IUPAC Photochemistry Commission does not mention BRET in their recommendations. To distinguish between the two different types of donors, however, it seems more adequate for us to use FRET for a RET involving a potentially fluorescent donor and BRET for a RET involving a potentially bioluminescent donor here.

the paramagnetic guest quenches both chromophores [210]. Steric or geometric control of the system is apparently also necessary. Figure 35 shows a second example of a considerably simple probe architecture which indeed yields enhanced acceptor emission. The key here is that the target, Cr^{3+} , is tightly bound by the chelating unit, that there exists almost no possibility for conformational flexibility in complexed **71**, and that the acceptor is virtually decoupled from the site of interaction [211].

Besides targeting single metal ions, the development of FRET systems for the highly sensitive and selective detection of more than a single analyte has also been reported. The system shown in Fig. 36 also serves as an example for a second strategy frequently employed for FRET signaling, i.e., the deliberate use of a

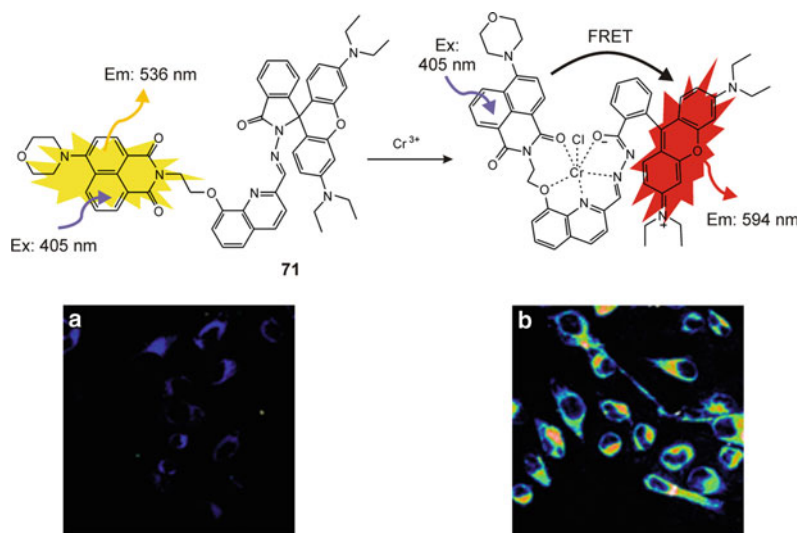


Fig. 35 Proposed mechanism of Cr^{3+} -selective FRET signaling system (top) and FRET images of HeLa cells incubated for 30 min with (a) 5 mM **71** and (b) 5 mM **71** and 50 mM Cr^{3+} (bottom). (Reprinted in part with permission from [211]. Copyright 2008 Royal Society of Chemistry)

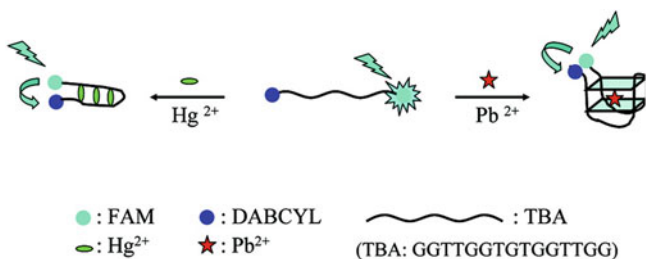


Fig. 36 Sensing mechanism of the TBA probe for the detection of Pb^{2+} and Hg^{2+} through enhanced RET-type quenching. (Reprinted with permission from [212]. Copyright 2009 American Chemical Society)

quencher dye as A_{RET} . This strategy does not generate specifically enhanced red emission and thus circumvents the task of finding an appropriate A_{RET} with a high fluorescence quantum yield in the visible/NIR wavelength range, but is aiming at large signal modulations, which are easier to realize with nonemissive but strongly absorbing NIR dyes. The system shown in Fig. 36 does not reach that far but adequately shows the first features, i.e., the metal ion-dependent formation of different foldamers by a thrombin-binding aptamer probe labeled with FAM (as donor) and dabcyI (as quencher; for dyes, refer to DNAzyme system shown in Fig. 23) at its 5' and 3' termini for selective detection of Pb^{2+} and Hg^{2+} , respectively [212]. When binding the metal ions, the DNA strand's conformation can change into two different folded structures, a G-quadruplex in the presence of Pb^{2+} and a hairpin-like structure in the case of Hg^{2+} , respectively, increasing RET-type quenching (Fig. 36). Because the distance between FAM and dabcyI is different in both complexes, the RET rates differ and fluorescence lifetime measurements permit discrimination unequivocally between the two complexes. Such dual-analyte detection has also been realized with conventional supramolecular chemistry receptors and two fluorophores (see also Sect. 3.2.1) [213].

FRET with enhanced red emission and FRET with quenching (Q-FRET) are both mechanisms intensively explored in connection with inorganic nanoparticles in recent years. Q-FRET applications here mainly rely on the use of gold NPs, because these quenchers are chemically very attractive for system design, their plasmon bands usually lie in a spectral range where a large number of organic dyes as possible D_{RET} are available, and because their extremely high absorption coefficients are ideal for efficient Q-FRET [214, 215]. On the other hand, the particular characteristics of semiconductor-type absorption bands with high absorption coefficients and usually narrow emission bands with moderate to high luminescence quantum yield render semiconductor nanocrystals or quantum dots (QD) attractive D_{RET} partners for sensitive FRET assays using organic dyes as A_{RET} . Alternatively, QDs can be combined with gold NPs or CPs, offering a wealth of possibilities for system design [216, 217].

With regard to target analytes, method development has not only focussed on metal ions, but the detection of gasses like CO_2 [218, 219] and organic compounds like cocaine [220] has also been pursued. For the latter analyte, an elegant example was realized in conjunction with an aptamer-based recognition motif, a QD as D_{RET} and an Atto 590 dye as A_{RET} , yielding enhanced red emission upon binding (Fig. 37). Figure 37 also contains a sketch of another popular QD-based FRET format, a competitive assay. Here, system design utilizes a QD (e.g., of CdSe/ZnS core-shell type) and a quencher dye (e.g., Black Hole Quencher-10, BHQ-10) as partners. The quencher is attached to a hapten, such as a TNT analog in Fig. 37c,d, and the QD carries analyte-responsive antibodies on its surface. In the absence of the analyte, the quencher-labeled hapten is bound at the receptors, efficiently deactivating the QD nonradiatively. Once a TNT molecule competes successfully for the binding site, the quenching conjugate is displaced and the full emission of the FRET donor is restored. Such competitive formats thus also rely on enhanced fluorescence signals, though now D_{RET} emission is enhanced. Highly luminescent D_{RET} thus perform best in such applications [221].

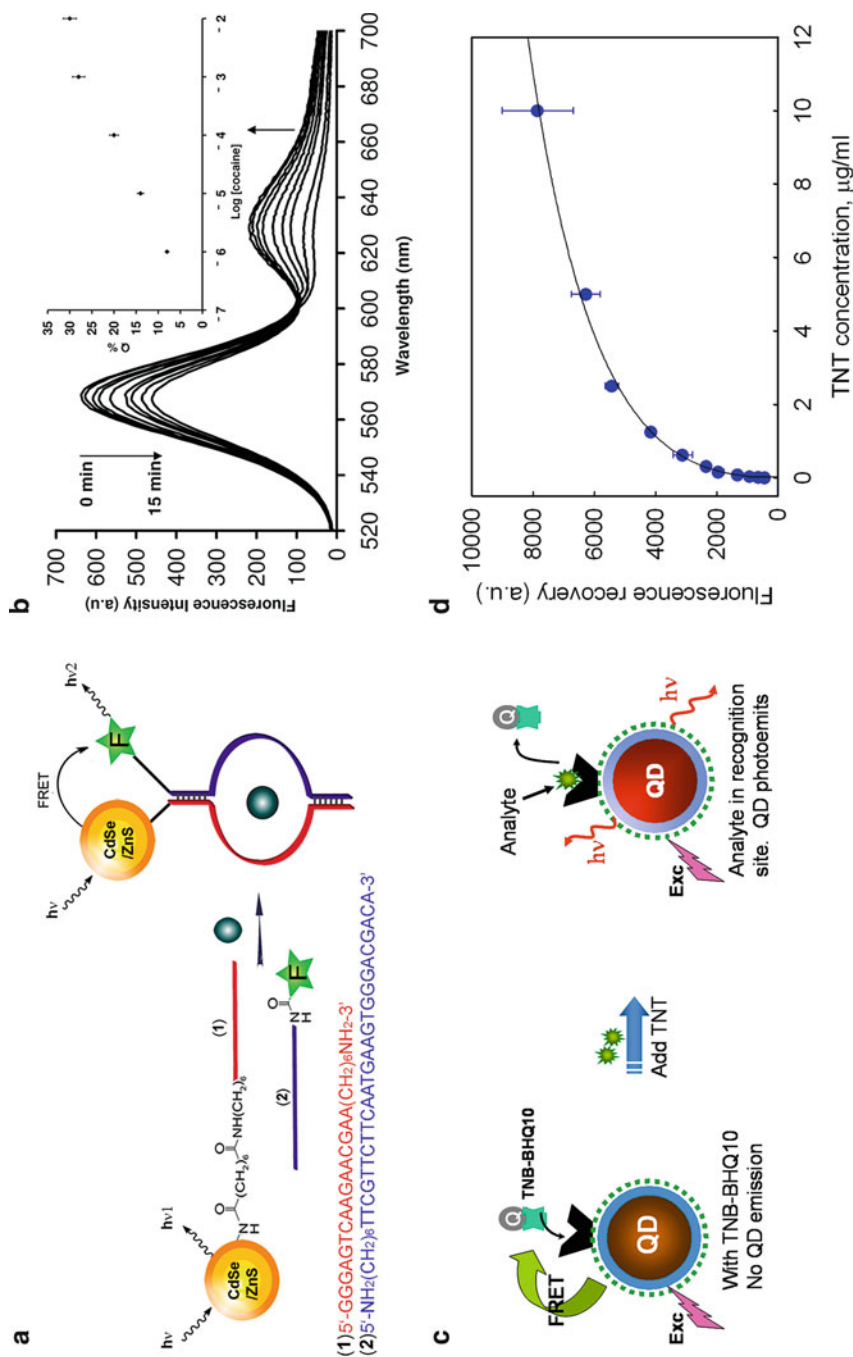


Fig. 37 (a) QD-based sensing of cocaine by the formation of a cocaine–aptamer supramolecular structure that triggers FRET and (b) time-dependent luminescence spectra of the system in the presence of cocaine. The inset shows a calibration curve for variable concentrations of cocaine and a fixed observation time of 15 min. (c) Schematic of the FRET-based TNT sensor and (d) increase of the QD luminescence upon addition of TNT in the competitive assay format. (Reprinted with permission from [220, 221]. Copyright 2009 Royal Society of Chemistry and 2005 American Chemical Society)

Besides these promising examples of systems for the indication of ions or small-molecules, FRET still finds more widespread application in bio(macro)molecule sensing because it operates over distances that are comparable with the size of biomolecules. In addition, common biomolecules do not affect FRET through less favorable quenching interactions and the large virtual Stokes shift allows the suppression of scattering and background signals effectively.

4.5.2 Bioluminescence Resonance Energy Transfer

BL resonance energy transfer is a nonradiative process of energy transfer from a bioluminescent donor (usually a biomolecule) to an acceptor. The most significant differences to fluorescence resonance energy transfer, i.e., FRET with a potentially fluorescent D_{RET} , are that there is no fluorescence background due to coexcitation of A_{RET} and that these systems can dispense with an external light source, which avoids photodamaging of biological samples, similar to what we have discussed in Sect. 4.1.3. Figure 38 summarizes the differences between BRET and FRET.

As a consequence of the virtual absence of fluorescence background, BRET-based QDs were developed by coupling carboxylate-functionalized QDs to a mutant of the bioluminescent protein *Renilla reniformis* luciferase (Luc8, Fig. 39a). On addition of the enzyme's substrate, coelenterazine, a weak luminescence at 480 nm, stemming from Luc8, and a strong signal at 655 nm, significant of BRET-sensitized QD luminescence, is registered (Fig. 39b). A unique feature of the system is shown in Fig. 39c. When monitored in serum, both emission bands are detectable. However, when employing the same system under identical conditions in blood, the residual Luc8 BL is absorbed by the matrix though the long-wavelength QD signal is virtually unquenched. This advantage distinguishes the BL–QD tandem as a very promising approach toward sensitive in vivo imaging in cells and deep tissues [222].

Like FRET, today BRET is predominantly used in biological sciences, especially in the monitoring of protein–protein interactions such as hormone–receptor interaction [223, 224] and protein–DNA interaction in living systems. However, BL resonance energy transfer can also be applied in immunoassays by using for instance a peptide-tagged luciferase and a fluorescein-labeled antipeptide antibody [225]. The development of more BRET assays for small-molecule analytes is thus awaited.

5 Conclusion

After Sousa [226] and Vögtle [227] rediscovered the potential of fluorescent and chromogenic complex forming reagents in the context of modern supramolecular photochemistry ca. 35 years ago, the field of the rational development of analyte-responsive fluorescent reporters saw a tremendous boost and naturally branched out

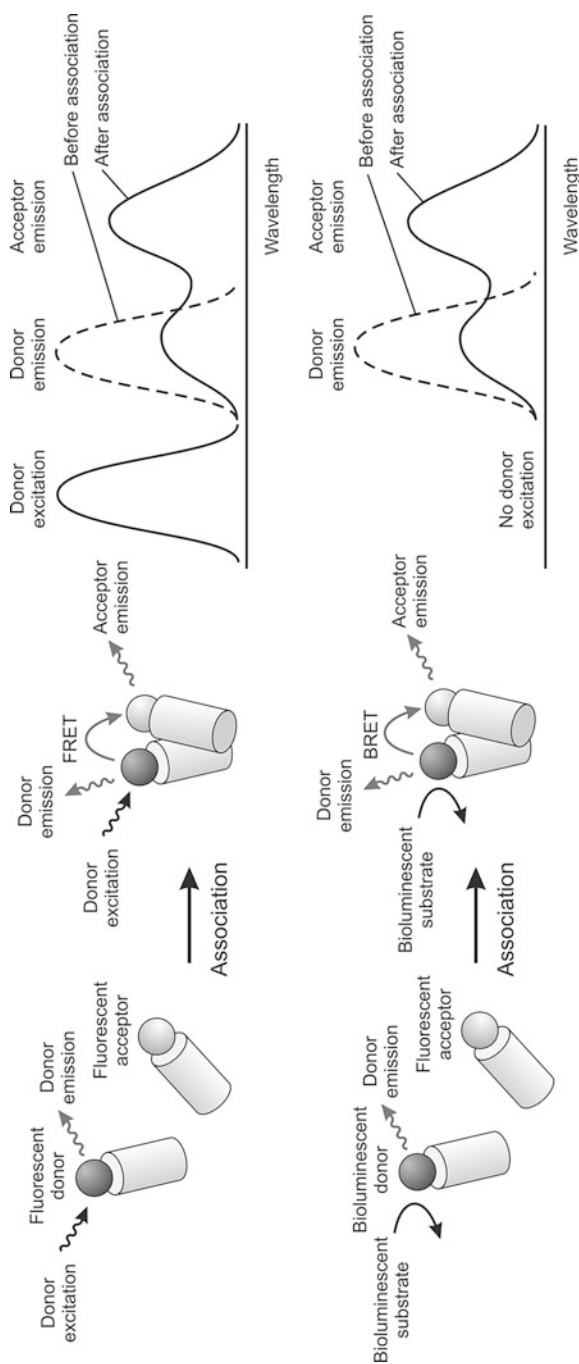


Fig. 38 Comparison of FRET (*top*) and BRET (*bottom*). (Reprinted with permission from [206]. Copyright 2009 Springer)

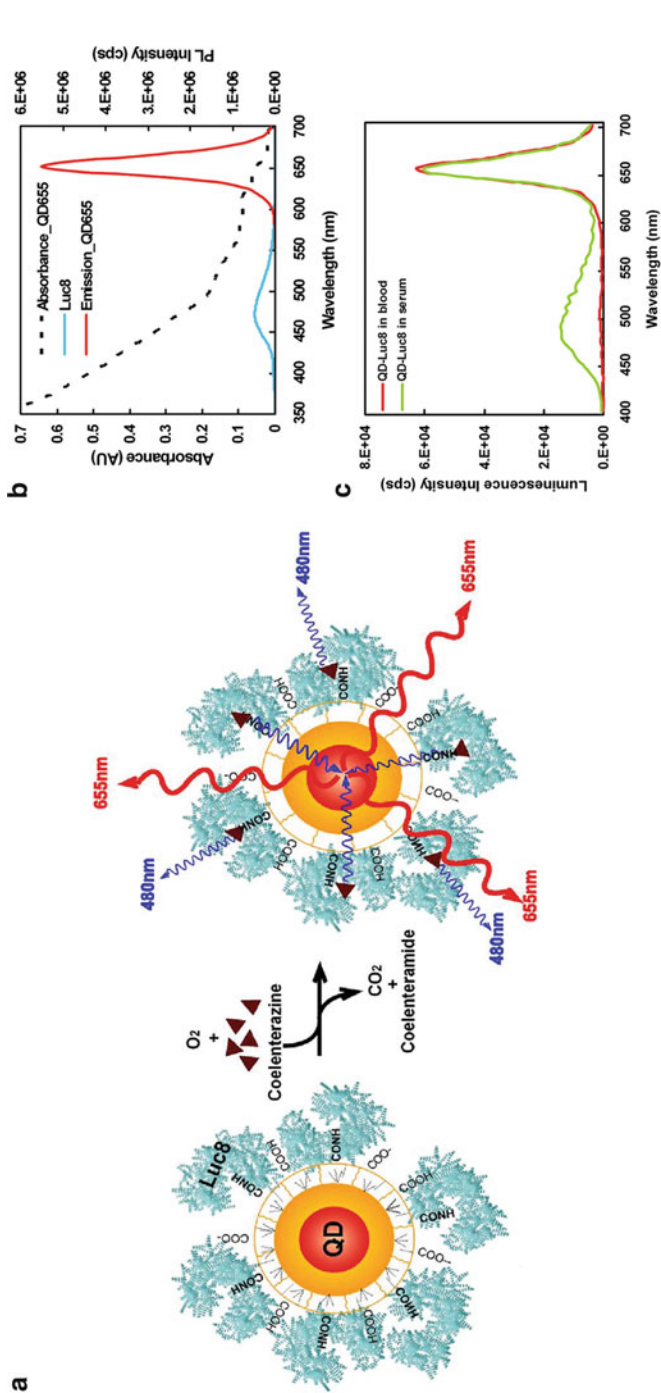


Fig. 39 (a) Design and principle of operation of the BL-QD system and (b) spectral manifestation of the assay. (c) Two assays performed under identical conditions in mouse serum (*green*) and mouse whole blood (*red*). (Reprinted with permission from [222]. Copyright 2006 Macmillan Publishers Ltd)

into numerous directions. At the heart of many of these attempts is the question of how molecular systems can be better designed to show ever more selective and sensitive responses to target analytes. One of the key issues is to couple the recognition event with strong signal modulation, at best in an amplifying manner. In the present contribution, we have illustrated the main concepts that have so far been developed for fluorescent reporters and reporting systems for ionic and small-molecule inorganic and organic species.

Naturally, such an overview can be anything but complete. In addition, it can only highlight the basis of the single concepts and discuss selected examples, but cannot raise too many details, evaluate the strategies in a comprehensive manner, or even give upfront recipes for the reader who is interested in the detection of a particular analyte. The attentive reader has noticed that we mentioned actual fluorescence enhancement/amplification factors only scarcely and might ask, why? The answer lies in the details. As anyone who sheds a glimpse into supramolecular chemistry knows well, noncovalent interactions depend tremendously on the solvent and/or buffer/ionic strength used in the study, the counterions (if applicable), and other experimental conditions. However, different researchers or different labs tend to use (if only slightly) different conditions. This makes a serious comparison of the data published on the many reported systems impossible without being unjust. Moreover, space also forbade the discussion of solvent or counterion effects in more detail; the reader has to revert to original literature. As a general advice it must be said that the majority of examples published until today in the fields presented in Sects. 2 and 3 still need a certain (sometimes still high) degree of organic (co-)solvent for operation. Although many of these approaches are intellectually very rewarding, it is exactly this drawback for actual applications which has stimulated much of the research in alternative directions that we have combined in Sect. 4. It is still a long and laborious road from the first idea or analytical question to a chemosensor that is applicable under realistic conditions.

So, what's next? Of course, research on all fronts will advance, with the approaches in Sect. 4 receiving perhaps the highest attention. The rapid development of nanoscopic and nanostructured materials has specially opened the path to sophisticated sensing ensembles Sousa and Vögtle would not even have dreamed about [228, 229]. However, for many applications, small molecules as reporters are indispensable, simply because of their size and the possibilities of interaction at the molecular level so that their future exploration is also essential. Finally, since technology will advance, new instrumental techniques and possibilities will appear and automatically fuel research on powerful fluorescent reporters.

6 Further Reading

Besides [1–27, 176] and the two seminal series on all aspects of fluorescence spectroscopy and fluorophores [230, 231], several monographs have appeared in the field of fluorescent reporter/functional fluorophore design and their application

among which we would like to specially recommend [232–236] to the interested reader.

References

1. Lakowicz JR (2006) Principles of fluorescence spectroscopy, 3rd edn. Springer, Berlin
2. Valeur B (2001) Molecular fluorescence. Wiley-VCH, Weinheim
3. Demchenko A (2009) Introduction to fluorescence sensing. Springer, Berlin
4. Demchenko AP (2010) Comparative analysis of fluorescence reporter signals based on intensity, anisotropy, time resolution and wavelength-ratiometry. In: Demchenko AP (ed) Advanced fluorescence reporters in chemistry and biology. I. Springer Ser Fluoresc 8:3–25
5. Patsenker LD, Tatarets AL, Terpetschnig EA (2010) Long-wavelength probes and labels based on cyanines and squaraines. In: Demchenko AP (ed) Advanced fluorescence reporters in chemistry and biology. I. Springer Ser Fluoresc 8:65–104
6. Przhonska OV, Webster S, Padilha LA et al (2010) Two-photon absorption in near-IR conjugated molecules: design strategy and structure–property relations. In: Demchenko AP (ed) Advanced fluorescence reporters in chemistry and biology. I. Springer Ser Fluoresc 8:105–147
7. Resch-Genger U, Grabolle M, Nitschke R et al (2010) Nanocrystals and nanoparticles vs. molecular fluorescent labels as reporters for bioanalysis and the life sciences. In: Demchenko AP (ed) Advanced fluorescence reporters in chemistry and biology. II. Springer Ser Fluoresc 9:3–40
8. Merola F, Levy B, Demachy I et al (2010) Photophysics and spectroscopy of fluorophores in the green fluorescent protein family. In: Demchenko AP (ed) Advanced fluorescence reporters in chemistry and biology. I. Springer Ser Fluoresc 8:347–383
9. Bergamini G, Marchi E, Ceroni P (2010) Luminescent dendrimers as ligands and sensors of metal ions. In: Demchenko AP (ed) Advanced fluorescence reporters in chemistry and biology. II. Springer Ser Fluoresc 8:253–284
10. Reppy MA (2010) Structure, emissive properties and reporting abilities of conjugated polymers. In: Demchenko AP (ed) Advanced fluorescence reporters in chemistry and biology. II. Springer Ser Fluoresc 9:357–388
11. Simon RA, Nilsson P (2010) Optical reporting by conjugated polymers via conformational changes. In: Demchenko AP (ed) Advanced fluorescence reporters in chemistry and biology. II. Springer Ser Fluoresc 9:389–416
12. Pu KY, Liu B (2010) Fluorescence reporting based on FRET between conjugated polyelectrolyte and organic dye for biosensor applications. In: Demchenko AP (ed) Advanced fluorescence reporters in chemistry and biology. II. Springer Ser Fluoresc 8:417–453
13. Borisov SM, Mayr T, Mistlberger G et al (2010) Dye-doped polymeric particles for sensing and imaging. In: Demchenko AP (ed) Advanced fluorescence reporters in chemistry and biology. II. Springer Ser Fluoresc 9:193–228
14. Liang S, John CL, Xu S et al (2010) Silica-based nanoparticles: design and properties. In: Demchenko AP (ed) Advanced fluorescence reporters in chemistry and biology. II. Springer Ser Fluoresc 9:229–251
15. Yao H (2010) Prospects for organic dye nanoparticles. In: Demchenko AP (ed) Advanced fluorescence reporters in chemistry and biology. II. Springer Ser Fluoresc 9:285–303
16. Díez I, Ras RHA (2010) Few-atom silver clusters as fluorescent reporters. In: Demchenko AP (ed) Advanced fluorescence reporters in chemistry and biology. II. Springer Ser Fluoresc 9:307–332
17. Muhammed MAH, Pradeep T (2010) Luminescent quantum clusters of gold as bio-labels. In: Demchenko AP (ed) Advanced fluorescence reporters in chemistry and biology. II. Springer Ser Fluoresc 9:333–353

18. Tomin VI (2010) Physical principles behind spectroscopic response of organic fluorophores to intermolecular interactions. In: Demchenko AP (ed) *Advanced fluorescence reporters in chemistry and biology. I.* Springer Ser Fluoresc 8:189–223
19. Hsieh CC, Ho ML, Chou PT (2010) Organic dyes with excited-state transformations (electron, charge and proton transfers). In: Demchenko AP (ed) *Advanced fluorescence reporters in chemistry and biology. I.* Springer Ser Fluoresc 8:225–266
20. Haidekker MA, Nipper M, Mustafic A et al (2010) Dyes with segmental mobility: molecular rotors. In: Demchenko AP (ed) *Advanced fluorescence reporters in chemistry and biology. I.* Springer Ser Fluoresc 8:267–307
21. Callis PR (2010) Electrochromism and solvatochromism in fluorescence response of organic dyes. A nanoscopic view. In: Demchenko AP (ed) *Advanced fluorescence reporters in chemistry and biology. I.* Springer Ser Fluoresc 8:309–330
22. Clarke RJ (2010) Electric field sensitive dyes. In: Demchenko AP (ed) *Advanced fluorescence reporters in chemistry and biology. I.* Springer Ser Fluoresc 8:331–344
23. Demchenko AP (2010) Collective effects influencing fluorescence emission. In: Demchenko AP (ed) *Advanced fluorescence reporters in chemistry and biology. II.* Springer Ser Fluoresc 9:107–132
24. Losytskyy MY, Yashchuk VM (2010) Fluorescent J-aggregates and their biological applications. In: Demchenko AP (ed) *Advanced fluorescence reporters in chemistry and biology. II.* Springer Ser Fluoresc 9:135–157
25. Sameiro M, Gonçalves T (2010) Optimized UV/visible markers. In: Demchenko AP (ed) *Advanced fluorescence reporters in chemistry and biology. I.* Springer Ser Fluoresc 8:27–64
26. Kim E, Park SB (2010) Discovery of new fluorescent dyes: targeted synthesis or combinatorial approach? In: Demchenko AP (ed) *Advanced fluorescence reporters in chemistry and biology. I.* Springer Ser Fluoresc 8:149–186
27. Patsenker LD, Tatarets AL, Klochko OP et al (2010) Conjugates, complexes and interlocked systems based on squaraines and cyanines. In: Demchenko AP (ed) *Advanced fluorescence reporters in chemistry and biology. II.* Springer Ser Fluoresc 9:159–190
28. Kotlicka J, Grabowski ZR (1979) The fluorescence of 2,2'-bipyridyl. *J Photochem* 11:413–418
29. Bishop JA (1963) Complex formation and fluorescence: complexes of 8-hydroxyquinoline-5-sulfonic acid. *Anal Chim Acta* 29:172–177
30. Goppelsröder F (1867) Ueber eine fluorescirende Substanz aus dem Kubaholze. *J Prakt Chem* 101:408–414
31. Rurack K, Radeaglia R (2000) Transition metal ion complexes of 2,2'-bipyridyl-3,3'-diol and 2,2'-bipyridyl-3-ol: spectroscopic properties and solvent-dependent binding modes. *Eur J Inorg Chem* 2271–2282
32. Popovych O, Rogers LB (1959) Fluorescence in the 8-quinolinol family and the $n-\pi$ transition. *Spectrochim Acta* 15:584–592
33. Bardez E, Devol I, Larrey B et al (1997) Excited-state processes in 8-hydroxyquinoline: photoinduced tautomerization and solvation effects. *J Phys Chem B* 101:7786–7793
34. Gutierrez AC, Gehlen MH (2002) Time resolved fluorescence spectroscopy of quercetin and morin complexes with Al^{3+} . *Spectrochim Acta Part A* 58:83–89
35. Irving H, Williams RJP (1948) Order of stability of metal complexes. *Nature* 162:746–747
36. Soroka K, Vithanage RS, Phillips DA et al (1987) Fluorescence properties of metal complexes of 8-hydroxyquinoline-5-sulfonic acid and chromatographic applications. *Anal Chem* 59:629–636
37. Masuhara H, Shioyama H, Saito T et al (1984) Fluorescence quenching mechanism of aromatic hydrocarbons by closed-shell heavy metal ions in aqueous and organic solutions. *J Phys Chem* 88:5868–5873
38. Rurack K, Resch-Genger U, Rettig W (1998) Global analysis of time-resolved emission – a powerful tool for the analytical discrimination of chemically similar Zn^{II} and Cd^{II} complexes. *J Photochem Photobiol A* 118:143–149

39. Varnes AW, Dodson RB, Wehry EL (1972) Interactions of transition-metal ions with photoexcited states of flavins. Fluorescence quenching studies. *J Am Chem Soc* 94: 946–950
40. Geddes CD, Apperson K, Karolin J et al (2001) Chloride-sensitive fluorescent indicators. *Anal Biochem* 293:60–66
41. Miyaji H, Sessler JL (2001) Off-the-shelf colorimetric anion sensors. *Angew Chem Int Ed* 40:154–157
42. Aldakov D, Anzenbacher P Jr (2003) Dipyrrolyl quinoxalines with extended chromophores are efficient fluorimetric sensors for pyrophosphate. *Chem Commun* 12:1394–1395
43. Amendola V, Esteban-Gomez D, Fabbrizzi L et al (2006) What anions do to N–H-containing receptors. *Acc Chem Res* 39:343–353
44. Ros-Lis JV, Martínez-Mañez R, Sancenón F et al (2007) Signalling mechanisms in anion-responsive push–pull chromophores: the hydrogen-bonding, deprotonation and anion exchange chemistry of functionalized azo dyes. *Eur J Org Chem* 2449–2458
45. Buhleier E, Wehner W, Vögtle F (1978) Ligandstruktur und Komplexierung, XIII: 2,2'-Bipyridin als Baustein für neue Aza-Kronenether und Cryptanden. *Chem Ber* 111:200–204
46. Mutai T, Abe Y, Araki K (1997) A novel bipyridine-based fluorescent host for diphenyl phosphate: affinity, photo-response and mechanism. *J Chem Soc Perkin Trans 2*: 1805–1809
47. Létard JF, Lapouyade R, Rettig W (1993) Synthesis and photophysical study of 4-(N-monoaza-15-crown-5) stilbenes forming TICT states and their complexation with cations. *Pure Appl Chem* 65:1705–1712
48. Blackburn C, Bai M, LeCompte KA et al (1994) Lithium responsive fluorophores derived from monoaza-12-crown-4 and coumarin. The influence of a methoxy side-arm on photophysical properties. *Tetrahedron Lett* 43:7915–7918
49. Bourson J, Pouget J, Valeur B (1993) Ion-responsive fluorescent compounds. 4. Effect of cation binding on the photochemical properties of a coumarin linked to monoaza- and diaza-crown ethers. *J Phys Chem* 97:4552–4557
50. Delmond S, Létard JF, Lapouyade R et al (1996) Cation-triggered photoinduced intramolecular charge transfer and fluorescence red-shift in fluorescence probes. *New J Chem* 20:861–869
51. Yang JS, Hwang CY, Hsieh CC et al (2004) Spectroscopic correlations between supermolecules and molecules. Anatomy of the ion-modulated electronic properties of the nitrogen donor in monoazacrown-derived intrinsic fluoroionophores. *J Org Chem* 69:719–726
52. Li YQ, Bricks JL, Resch-Genger U et al (2006) Bifunctional charge transfer operated fluorescent probes with acceptor and donor receptors. 2. Bifunctional cation coordination behavior of biphenyl-type sensor molecules incorporating 2, 2':6', 2''-terpyridine acceptors. *J Phys Chem A* 110:10972–10984
53. Valeur B, Leray I (2000) Design principles of fluorescent molecular sensors for cation recognition. *Coord Chem Rev* 205:3–40
54. Rettig W, Lapouyade R (1994) Fluorescence probes based upon twisted intramolecular charge transfer TICT states and other adiabatic photoreactions. In: Lakowicz JR (ed) *Topics in fluorescence spectroscopy: volume 4: probe design and chemical sensing*. Plenum, New York, pp 109–149
55. Rettig W, Rurack K, Szczepan M (2001) From cyanines to styryl bases – photophysical properties, photochemical mechanisms, and cation sensing abilities of charged and neutral polymethinic dyes. In: Valeur B, Brochon JC (eds) *New trends in fluorescence spectroscopy: applications to chemical and life sciences*. Springer, Berlin, pp 125–155
56. Taki M, Watanabe Y, Yamamoto Y (2009) Development of ratiometric fluorescent probe for zinc ion based on indole fluorophore. *Tetrahedron Lett* 50:1345–1347
57. Suksai C, Tuntulani T (2003) Chromogenic anion sensors. *Chem Soc Rev* 32:192–202
58. Kato R, Nishizawa S, Hayashita T et al (2001) A thiourea-based chromoionophore for selective binding and sensing of acetate. *Tetrahedron Lett* 42:5053–5056

59. Lee DH, Lee KH, Hong JI (2001) An azophenol-based chromogenic anion sensor. *Org Lett* 3:5–8
60. de Silva AP, de Silva SA (1986) Fluorescent signalling crown ethers; 'switching on' of fluorescence by alkali metal ion recognition and binding in situ. *J Chem Soc Chem Commun* 1709–1710
61. Huston ME, Haider KW, Czarnik AW (1988) Chelation-enhanced fluorescence in 9,10-bis (TMEDA)anthracene. *J Am Chem Soc* 110:4460–4462
62. Geue JP, Head NJ, Ward AD et al (2003) The formation of fluorescent alkaline earth complexes by 4-{2-[10-(2-morpholinoethyl)-9-anthryl]methyl}morpholine and its -ethyl}morpholine and -propyl}morpholine analogues in acetonitrile. *Aust J Chem* 56:301–307
63. Barnes RL, Birks JB (1966) Excimer fluorescence. X. Spectral studies of 9-methyl and 9,10-dimethyl anthracene. *Proc R Soc A Math Phys Eng Sci* 291:570–582
64. de Silva AP, Moody TS, Wright GD (2009) Fluorescent PET (Photoinduced Electron Transfer) sensors as potent analytical tools. *Analyst* 134:2385–2393
65. Rehm D, Weller A (1970) Kinetics of fluorescence quenching by electron and H-atom transfer. *Isr J Chem* 8:259–271
66. Akkaya EU, Huston ME, Czarnik AW (1990) Chelation-enhanced fluorescence of anthrylamacrocycle conjugate probes in aqueous-solution. *J Am Chem Soc* 112:3590–3593
67. Parkesh R, Lee TC, Gunnlaugsson T (2007) Highly selective 4-amino-1,8-naphthalimide based fluorescent photoinduced electron transfer (PET) chemosensors for Zn(II) under physiological pH conditions. *Org Biomol Chem* 5:310–317
68. Verma M, Chaudhry AF, Morgan MT et al (2010) Electronically tuned 1,3,5-triarylpyrazolines as Cu(I)-selective fluorescent probes. *Org Biomol Chem* 8:363–370
69. Ramachandram B, Samanta A (1998) Transition metal ion induced fluorescence enhancement of 4-(N,N-dimethylethylenediamino)-7-nitrobenz-2-oxa-1,3-diazole. *J Phys Chem A* 102:10579–10587
70. Chang CJ, Nolan EM, Jaworski J et al (2004) Bright fluorescent chemosensor platforms for imaging endogenous pools of neuronal zinc. *Chem Biol* 11:203–210
71. Rurack K, Resch-Genger U, Bricks JL et al (2000) Cation-triggered 'switching on' of the red/near infra-red (NIR) fluorescence of rigid fluorophore-spacer-receptor ionophores. *Chem Commun* 2103–2104
72. Martínez-Máñez R, Sancenón F (2005) New advances in fluorogenic anion chemosensors. *J Fluoresc* 15:267–285
73. James TD, Sandanayake KRAS, Iguchi R et al (1995) Novel saccharide-photoinduced electron-transfer sensors based on the interaction of boronic acid and amine. *J Am Chem Soc* 117:8982–8987
74. Kubo Y, Tsukahara M, Ishihara S et al (2000) A simple anion chemosensor based on a naphthalene-thiouronium dyad. *Chem Commun* 653–654
75. Kubo Y, Kato M, Misawa Y et al (2004) A fluorescence-active 1,3-bis(isothiouronium)-derived naphthalene exhibiting versatile binding modes toward oxoanions in aqueous MeCN solution: new methodology for sensing oxoanions. *Tetrahedron Lett* 45:3769–3773
76. Vance DH, Czarnik AW (1994) Real-time assay of inorganic pyrophosphatase using a high-affinity chelation-enhanced fluorescence chemosensor. *J Am Chem Soc* 116:9397–9398
77. Fang L, Chan WH, He YB et al (2005) Fluorescent anion sensor derived from cholic acid: the use of flexible side chain. *J Org Chem* 70:7640–7646
78. de Silva AP, Gunaratne HQN, McVeigh C et al (1996) Fluorescent signalling of the brain neurotransmitter γ -aminobutyric acid and related amino acid zwitterions. *Chem Commun* 2191–2192
79. Yang W, Yan J, Fang H et al (2003) The first fluorescent sensor for D-glucarate based on the cooperative action of boronic acid and guanidinium groups. *Chem Commun* 792–793
80. Fages F, Desvergne JP, Bouas-Laurent H et al (1989) Anthraceno-cryptands: a new class of cation-complexing macrobicyclic fluorophores. *J Am Chem Soc* 111:8672–8680

81. Bouas-Laurent H, Desvergne JP, Fages F et al (1993) Tunable fluorescence of some macrocyclic anthracenophanes. *ACS Symp Ser* 538:59–73
82. Birks JB (1975) Excimers. *Rep Prog Phys* 38:903–974
83. Marquis D, Desvergne JP, Bouas-Laurent H (1995) Photoresponsive supramolecular systems: synthesis and photophysical and photochemical study of bis-(9,10-anthracenediyl) coronands AAOnOn. *J Org Chem* 60:7984–7996
84. Kim SK, Bok JH, Bartsch RA et al (2005) A fluoride-selective PCT chemosensor based on formation of a static pyrene excimer. *Org Lett* 7:4839–4842
85. Bodenant B, Fages F, Delville MH (1998) Metal-induced self-assembly of a pyrene-tethered hydroxamate ligand for the generation of multichromophoric supramolecular systems. The pyrene excimer as switch for iron(III)-driven intramolecular fluorescence quenching. *J Am Chem Soc* 120:7511–7519
86. Bodenant B, Weil T, Businelli-Pourcel M et al (1999) Synthesis and solution structure analysis of a bispyrenyl bishydroxamate calix[4]arene-based receptor, a fluorescent chemosensor for Cu^{2+} and Ni^{2+} metal ions. *J Org Chem* 64:7034–7039
87. Yang JS, Lin CS, Hwang CY (2001) Cu^{2+} -induced blue shift of the pyrene excimer emission: a new signal transduction mode of pyrene probes. *Org Lett* 3:889–892
88. Schazmann B, Alhashimy N, Diamond D (2006) Chloride selective calix[4]arene optical sensor combining urea functionality with pyrene excimer transduction. *J Am Chem Soc* 128:8607–8614
89. Ghosh K, Sarkar AR, Patra A (2009) Pyridinium amide-based simple synthetic receptor for selective recognition of dihydrogenphosphate. *Tetrahedron Lett* 50:6557–6561
90. Lee HN, Xu Z, Kim SK et al (2007) Pyrophosphate-selective fluorescent chemosensor at physiological pH: formation of a unique excimer upon addition of pyrophosphate. *J Am Chem Soc* 129:3828–3829
91. Xu Z, Singh NJ, Lim J et al (2009) Unique sandwich stacking of pyrene-adenine-pyrene for selective and ratiometric fluorescent sensing of ATP at physiological pH. *J Am Chem Soc* 131:15528–15533
92. Qing G, He Y, Chen Z et al (2006) Sensitive fluorescent sensors for malate based on calix[4]arene bearing anthracene. *Tetrahedron Asymmetry* 17:3144–3151
93. Linton B, Hamilton AD (1999) Host–guest chemistry: combinatorial receptors. *Curr Opin Chem Biol* 3:307–312
94. Finney NS (2006) Combinatorial discovery of fluorophores and fluorescent probes. *Curr Opin Chem Biol* 10:238–245
95. Lee JS, Kim YK, Vendrell M et al (2009) Diversity-oriented fluorescence library approach for the discovery of sensors and probes. *Mol Biosyst* 5:411–421
96. Schiedel MS, Briehn CA, Bäuerle P (2001) Single-compound libraries of organic materials: parallel synthesis and screening of fluorescent dyes. *Angew Chem Int Ed* 40:4677–4680
97. Singh A, Yao QW, Tong L et al (2000) Combinatorial approach to the development of fluorescent sensors for nanomolar aqueous copper. *Tetrahedron Lett* 41:9601–9605
98. Isacson J, Westman G (2001) Solid-phase synthesis of asymmetric cyanine dyes. *Tetrahedron Lett* 42:3207–3210
99. Li JQ, Hu MY, Yao SQ (2009) Rapid synthesis, screening, and identification of xanthone- and xanthene-based fluorophores using click chemistry. *Org Lett* 11:3008–3011
100. Xie F, Sivakumar K, Zeng QB et al (2008) A fluorogenic ‘click’ reaction of azidoanthracene derivatives. *Tetrahedron* 64:2906–2914
101. Kim E, Koh M, Ryu J et al (2008) Combinatorial discovery of full-color-tunable emissive fluorescent probes using a single core skeleton, 1,2-dihydropyrrolo[3,4- β]indolizin-3-one. *J Am Chem Soc* 130:12206–12207
102. Mello JV, Finney NS (2005) Reversing the discovery paradigm: a new approach to the combinatorial discovery of fluorescent chemosensors. *J Am Chem Soc* 127:10124–10125
103. Rivero IA, Gonzalez T, Pina-Luis G et al (2005) Library preparation of derivatives of 1,4,10,13-tetraoxa-7,16-diaza-cyclooctadecane and their fluorescence behavior for signaling purposes. *J Comb Chem* 7:46–53

104. Wang SL, Chang YT (2006) Combinatorial synthesis of benzimidazolium dyes and its diversity directed application toward GTP-selective fluorescent chemosensors. *J Am Chem Soc* 128:10380–10381
105. Potyrailo RA, Mirsky VM (2008) Combinatorial and high-throughput development of sensing materials: the first 10 years. *Chem Rev* 108:770–813
106. Rurack K, Rettig W, Resch-Genger U (2000) Unusually high cation-induced fluorescence enhancement of a structurally simple intrinsic fluoroionophore with a donor–acceptor–donor constitution. *Chem Commun* 407–408
107. Ray D, Iyer ESS, Sadhu KK et al (2009) Ag(I) induced emission with azines having donor–acceptor–donor chromophore. *Dalton Trans* 5683–5687
108. Ros-Lis JV, Martínez-Máñez R, Rurack K et al (2004) Highly selective chromogenic signalling of Hg²⁺ in aqueous media at nanomolar levels employing a squaraine-based reporter. *Inorg Chem* 43:5183–5185
109. Tolosa J, Zuchero AJ, Bunz UHF (2008) Water-soluble cruciforms: response to protons and selected metal ions. *J Am Chem Soc* 130:6498–6506
110. Huang JH, Wen WH, Sun YY et al (2005) Two-stage sensing property via a conjugated donor–acceptor–donor constitution: application to the visual detection of mercuric ion. *J Org Chem* 70:5827–5832
111. Pond SJK, Tsutsumi O, Rumi M et al (2004) Metal–ion sensing fluorophores with large two-photon absorption cross sections: aza-crown ether substituted donor–acceptor–donor distyryl benzenes. *J Am Chem Soc* 126:9291–9306
112. Rurack K, Koval'chuck A, Bricks JL et al (2001) A simple bifunctional fluoroionophore signaling different metal ions either independently or cooperatively. *J Am Chem Soc* 123:6205–6206
113. Yang JS, Hwang CY, Chen MY (2007) Bimodal fluorescence signaling based on control of the excited-state conformational twisting and the ground-state protonation processes. *Tetrahedron Lett* 48:3097–3102
114. Rurack K, Resch-Genger U (2002) Rigidization, preorientation and electronic decoupling – the “magic triangle” for the design of highly efficient fluorescent sensors and switches. *Chem Soc Rev* 31:116–127
115. Rurack K, Kollmannsberger M, Resch-Genger U et al (2000) A selective and sensitive fluoroionophore for HgII, AgI, and CuII with virtually decoupled fluorophore and receptor units. *J Am Chem Soc* 122:968–969
116. Kollmannsberger M, Rurack K, Resch-Genger U et al (2000) Design of an efficient charge-transfer processing molecular system containing a weak electron donor: spectroscopic and redox properties and cation-induced fluorescence enhancement. *Chem Phys Lett* 329:363–369
117. He QW, Miller EW, Wong AP et al (2006) A selective fluorescent sensor for detecting lead in living cells. *J Am Chem Soc* 128:9316–9317
118. Dodani SC, He QW, Chang CJ (2009) A turn-on fluorescent sensor for detecting nickel in living cells. *J Am Chem Soc* 131:18020–18021
119. Rurack K, Bricks JL, Schulz B et al (2000) Substituted 1,5-diphenyl-3-benzothiazol-2-yl- Δ^2 -pyrazolines: synthesis, X-ray structure, photophysics, and cation complexation properties. *J Phys Chem A* 104:6171–6188
120. Rurack K, Bricks JL (2001) Towards simple and efficient molecular reporters: combining electron transfer and charge transfer in functional dyes of donor–acceptor–spacer–donor constitution. *Arkivoc* xi:31–40
121. Yuan MJ, Li YL, Li JB et al (2007) A colorimetric and fluorometric dual-modal assay for mercury ion by a molecule. *Org Lett* 9:2313–2316
122. Rurack K, Trieflinger C, Koval'chuck A et al (2007) An ionically driven molecular IMPLICATION gate operating in fluorescence mode. *Chem Eur J* 13:8998–9003
123. Chang CJ, Jaworski J, Nolan EM et al (2004) A tautomeric zinc sensor for ratiometric fluorescence imaging: application to nitric oxide-induced release of intracellular zinc. *Proc Natl Acad Sci USA* 101:1129–1134

124. Nguyen TH, Ansell RJ (2009) Fluorescent imprinted polymer sensors for chiral amines. *Org Biomol Chem* 7:1211–1220
125. Descalzo AB, Rurack K, Weisshoff H et al (2005) Rational design of a chromo- and fluorogenic hybrid chemosensor material for the detection of long-chain carboxylates. *J Am Chem Soc* 127:184–200
126. Wu FY, Li Z, Wen ZC et al (2002) A novel thiourea-based dual fluorescent anion receptor with a rigid hydrazine spacer. *Org Lett* 4:3203–3205
127. Kovalchuk A, Bricks JL, Reck G et al (2004) A charge transfer-type fluorescent molecular sensor that “lights up” in the visible upon hydrogen bond-assisted complexation of anions. *Chem Commun* 1946–1947
128. Choi K, Hamilton AD (2001) A dual channel fluorescence chemosensor for anions involving intermolecular excited state proton transfer. *Angew Chem Int Ed* 40:3912–3913
129. Kikuchi K, Hashimoto S, Mizukami S et al (2009) Anion sensor-based ratiometric peptide probe for protein kinase activity. *Org Lett* 11:2732–2735
130. Mizukami S, Nagano T, Urano Y et al (2002) A fluorescent anion sensor that works in neutral aqueous solution for bioanalytical application. *J Am Chem Soc* 124:3920–3925
131. Coskun A, Baytekin BT, Akkaya EU (2003) Novel fluorescent chemosensor for anions via modulation of oxidative PET: a remarkable 25-fold enhancement of emission. *Tetrahedron Lett* 44:5649–5651
132. Lin WY, Yuan L, Cao XW et al (2009) A fluorescence turn-on probe for iodide based on the redox reaction between cupric and iodide. *Sens Actuators B* 138:637–641
133. Bretonniere Y, Cann MJ, Parker D et al (2004) Design, synthesis and evaluation of ratiometric probes for hydrogencarbonate based on europium emission. *Org Biomol Chem* 2:1624–1632
134. Beer PD, Timoshenko V, Maestri M et al (1999) Anion recognition and luminescent sensing by new ruthenium(II) and rhenium(I) bipyridyl calix[4]diquinone receptors. *Chem Commun* 1755–1756
135. Dujols V, Ford F, Czarnik AW (1997) A long-wavelength fluorescent chemodosimeter selective for Cu(II) ion in water. *J Am Chem Soc* 119:12354–12355
136. Chae MY, Czarnik AW (1992) Fluorimetric chemodosimetry. Mercury(II) and silver(I) indication in water via enhanced fluorescence signaling. *J Am Chem Soc* 114:8704–8705
137. Zhang G, Zhang D, Yin S et al (2005) 1,3-Dithiole-2-thione derivatives featuring an anthracene unit: new selective chemodosimeters for Hg(II) ion. *Chem Commun* 2161–2163
138. Yang YK, Yook KJ, Tae J (2005) A rhodamine-based fluorescent and colorimetric chemodosimeter for the rapid detection of Hg²⁺ ions in aqueous media. *J Am Chem Soc* 127:16760–16761
139. Song KC, Kim JS, Park SM et al (2006) Fluorogenic Hg²⁺-selective chemodosimeter derived from 8-hydroxyquinoline. *Org Lett* 8:3413–3416
140. Ros-Lis JV, Marcos MD, Martínez-Máñez R et al (2005) A regenerative chemodosimeter based on metal-induced dye formation for the highly selective and sensitive optical determination of Hg²⁺. *Angew Chem Int Ed* 44:4405–4407
141. Chatterjee A, Santra M, Won N et al (2009) Selective fluorogenic and chromogenic probe for detection of silver ions and silver nanoparticles in aqueous media. *J Am Chem Soc* 131:2040–2041
142. Lee KS, Kim HJ, Kim GH et al (2008) Fluorescent chemodosimeter for selective detection of cyanide in water. *Org Lett* 10:49–51
143. Kim TH, Swager TM (2003) A fluorescent self-amplifying wavelength-responsive sensory polymer for fluoride ions. *Angew Chem Int Ed* 42:4803–4806
144. Setsukinai K, Urano Y, Kakinuma K et al (2003) Development of novel fluorescence probes that can reliably detect reactive oxygen species and distinguish specific species. *J Biol Chem* 278:3170–3175
145. Chang MCY, Pralle A, Isacoff EY et al (2004) A selective, cell-permeable optical probe for hydrogen peroxide in living cells. *J Am Chem Soc* 126:15392–15393

146. Song F, Watanabe S, Floreancig PE et al (2008) Oxidation-resistant fluorogenic probe for mercury based on alkyne oxymercuration. *J Am Chem Soc* 130:16460–16461
147. Song F, Garner AL, Koide K (2007) A highly sensitive fluorescent sensor for palladium based on the allylic oxidative insertion mechanism. *J Am Chem Soc* 129:12354–12355
148. Garner AL, Koide K (2008) Oxidation state-specific fluorescent method for palladium(II) and platinum(IV) based on the catalyzed aromatic Claisen rearrangement. *J Am Chem Soc* 130:16472–16473
149. Lu Y (2002) New transition-metal-dependent DNA-zymes as efficient endonucleases and as selective metal biosensors. *Chem Eur J* 8:4588–4596
150. Liu J, Lu Y (2003) Improving fluorescent DNAzyme biosensors by combining inter- and intramolecular quenchers. *Anal Chem* 75:6666–6672
151. Li J, Lu Y (2000) A highly sensitive and selective catalytic DNA biosensor for lead ions. *J Am Chem Soc* 122:10466–10467
152. Liu J, Lu Y (2007) A DNAzyme catalytic beacon sensor for paramagnetic Cu²⁺ ions in aqueous solution with high sensitivity and selectivity. *J Am Chem Soc* 129:9838–9839
153. Liu J, Brown AK, Meng X et al (2007) A catalytic beacon sensor for uranium with parts-per-trillion sensitivity and millionfold selectivity. *Proc Natl Acad Sci USA* 104:2056–2061
154. García-Campaña AM, Baeyens WRG (2000) Principles and recent analytical applications of chemiluminescence. *Analysis* 28:686–698
155. Zhang Z, Zhang S, Zhang X (2005) Recent developments and applications of chemiluminescence sensors. *Anal Chim Acta* 541:37–47
156. Su Y, Chen H, Wang Z et al (2007) Recent advances in chemiluminescence. *Appl Spectrosc Rev* 42:139–176
157. Francis PS, Adcock JL, Costin JW et al (2008) Chemiluminescence detection of opium poppy (*Papaver somniferum*) alkaloids. *J Pharm Biomed Anal* 48:508–518
158. Rauhut MM, Bollyky LJ, Roberts BG et al (1967) Chemiluminescence from reactions of electronegatively substituted aryl oxalates with hydrogen peroxide and fluorescent compounds. *J Am Chem Soc* 89:6515–6522
159. Richter MM (2004) Electrochemiluminescence (ECL). *Chem Rev* 104:3003–3036
160. Tokel NE, Bard AJ (1972) Electrogenerated chemiluminescence. IX. Electrochemistry and emission from systems containing tris(2,2'-bipyridine)ruthenium(II) dichloride. *J Am Chem Soc* 94:2862–2863
161. Wallace WL, Bard AJ (1979) Electrogenerated chemi-luminescence. 35. Temperature-dependence of the ECL efficiency of Ru(bpy)₃²⁺ in acetonitrile and evidence for very high excited-state yields from electron-transfer reactions. *J Phys Chem* 83:1350–1357
162. McCord P, Bard AJ (1991) Electrogenerated chemiluminescence: Part 54. Electrogenerated chemiluminescence of ruthenium(II) 4,4'-diphenyl-2,2'-bipyridine and ruthenium(II) 4,7-diphenyl-1,10-phenanthroline systems in aqueous and acetonitrile solutions. *J Electroanal Chem* 318:91–99
163. Rubinstein I, Martin CR, Bard AJ (1983) Electrogenerated chemiluminescent determination of oxalate. *Anal Chem* 55:1580–1582
164. Billard P, DuBow MS (1998) Bioluminescence-based assays for detection and characterization of bacteria and chemicals in clinical laboratories. *Clin Biochem* 31:1–14
165. Marques SM, Esteves da Silva JC (2009) Firefly bioluminescence: a mechanistic approach of luciferase catalyzed reactions. *IUBMB Life* 61:6–17
166. Metzger A, Anslyn EV (1998) A chemosensor for citrate in beverages. *Angew Chem Int Ed* 37:649–652
167. Niikura K, Metzger A, Anslyn EV (1998) Chemosensor ensemble with selectivity for inositol-trisphosphate. *J Am Chem Soc* 120:8533–8534
168. Fabbriizzi L, Leone A, Taglietti A (2001) A chemosensing ensemble for selective carbonate detection in water based on metal–ligand interactions. *Angew Chem Int Ed* 40:3066–3069

169. Hanshaw RG, Hilkert SM, Hua J et al (2004) An indicator displacement system for fluorescent detection of phosphate oxyanions under physiological conditions. *Tetrahedron Lett* 45:8721–8724
170. Horie S, Kubo Y (2009) Fluorescence-based indicator displacement assay for phospho-sugar detection using zinc(II) dipicolylamine-appended phenylboronic acid. *Chem Lett* 38:616–617
171. Neelakandan PP, Hariharan M, Ramaiah D (2006) A supramolecular ON–OFF–ON fluorescence assay for selective recognition of GTP. *J Am Chem Soc* 128:11334–11335
172. Siering C, Kerschbaumer H, Nieger M et al (2006) A supramolecular fluorescence probe for caffeine. *Org Lett* 8:1471–1474
173. Liu S, Pestano JPC, Wolf C (2008) Enantioselective fluorescence sensing of chiral alpha-amino alcohols. *J Org Chem* 73:4267–4270
174. Nau WM, Ghale G, Hennig A et al (2009) Substrate-selective supramolecular tandem assays: monitoring enzyme inhibition of arginase and diamine oxidase by fluorescent dye displacement from calixarene and cucurbituril macrocycles. *J Am Chem Soc* 131:11558–11570
175. Comes M, Aznar E, Moragues M et al (2009) Mesoporous hybrid materials containing nanoscopic “binding pockets” for colorimetric anion signaling in water by using displacement assays. *Chem Eur J* 15:9024–9033
176. Haugland RP (2005) *Invitrogen: a guide to fluorescent probes and labeling technologies*, 10th edn. Molecular Probes Inc, Eugene
177. Hall M, Kazakova I, Yao YM (1999) High sensitivity immunoassays using particulate fluorescent labels. *Anal Biochem* 272:165–170
178. Zhao X, Tapeç-Dytioco R, Tan W (2003) Ultrasensitive DNA detection using highly fluorescent bioconjugated nanoparticles. *J Am Chem Soc* 125:11474–11475
179. Härmä H, Soukka T, Lövgren T (2001) Europium nanoparticles and time-resolved fluorescence for ultrasensitive detection of prostate-specific antigen. *Clin Chem* 47:561–568
180. Huhtinen P, Vaarno J, Soukka T et al (2004) Europium(III) nanoparticle-label-based assay for the detection of nucleic acids. *Nanotechnology* 15:1708–1715
181. Valanne A, Huopalahti S, Soukka T et al (2005) A sensitive adenovirus immunoassay as a model for using nanoparticle label technology in virus diagnostics. *J Clin Virol* 33:217–223
182. Soto CM, Blum AS, Vora GJ et al (2006) Fluorescent signal amplification of carbocyanine dyes using engineered viral nanoparticles. *J Am Chem Soc* 128:5184–5189
183. Lowe M, Spiro A, Zhang YZ et al (2004) Multiplexed, particle-based detection of DNA using flow cytometry with 3DNA dendrimers for signal amplification. *Cytometry Part A* 60A:135–144
184. Wängler C, Moldenhauer G, Saffrich R et al (2008) PAMAM structure-based multifunctional fluorescent conjugates for improved fluorescent labelling of biomacromolecules. *Chem Eur J* 14:8116–8130
185. Truneh A, Machy P, Horan PK (1987) Antibody-bearing liposomes as multicolor immuno-fluorescence markers for flow cytometry and imaging. *J Immunol Methods* 100:59–71
186. Schott H, Von Cunow D, Langhals H (1992) Labeling of liposomes with intercalating perylene fluorescent dyes. *Biochim Biophys Acta* 1110:151–157
187. Edwards KA, Baemner AJ (2006) Optimization of DNA-tagged liposomes for use in microtiter plate analyses. *Anal Bioanal Chem* 386:1613–1623
188. Rongen HAH, Bult A, van Bennekom WP (1997) Liposomes and immunoassays. *J Immunol Methods* 204:105–133
189. Trau D, Yang W, Seydack M et al (2002) Nanoencapsulated microcrystalline particles for superamplified biochemical assays. *Anal Chem* 74:5480–5486
190. Chan CP, Bruemmel Y, Seydack M et al (2004) Nanocrystal biolabels with releasable fluorophores for immunoassays. *Anal Chem* 76:3638–3645
191. Sin KK, Chan CPY, Pang TH et al (2006) A highly sensitive fluorescent immunoassay based on avidin-labeled nanocrystals. *Anal Bioanal Chem* 384:638–644

192. Chan CP, Tzang LC, Sin K et al (2007) Biofunctional organic nanocrystals for quantitative detection of pathogen deoxyribonucleic acid. *Anal Chim Acta* 584:7–11
193. Zhou Q, Swager TM (1995) Fluorescent chemosensors based on energy migration in conjugated polymers: the molecular wire approach to increased sensitivity. *J Am Chem Soc* 117:12593–12602
194. Yang JS, Swager TM (1998) Fluorescent porous polymer films as TNT chemosensors: electronic and structural effects. *J Am Chem Soc* 120:11864–11873
195. McQuade DT, Hegedus AH, Swager TM (2000) Signal amplification of a “turn-on” sensor: harvesting the light captured by a conjugated polymer. *J Am Chem Soc* 122:12389–12390
196. Thomas SW III, Joly GD, Swager TM (2007) Chemical sensors based on amplifying fluorescent conjugated polymers. *Chem Rev* 107:1339–1386
197. Montalti M, Prodi L, Zaccheroni N et al (2002) Solvent-induced modulation of collective photophysical processes in fluorescent silica nanoparticles. *J Am Chem Soc* 124:13540–13546
198. Montalti M, Prodi L, Zaccheroni N (2005) Fluorescence quenching amplification in silica nanosensors for metal ions. *J Mater Chem* 15:2810–2814
199. Bonacchi S, Rampazzo E, Montalti M et al (2008) Amplified fluorescence response of chemosensors grafted onto silica nanoparticles. *Langmuir* 24:8387–8392
200. Balzani V, Ceroni P, Gestermann S et al (2000) Dendrimers as fluorescent sensors with signal amplification. *Chem Commun* 10:853–854
201. Balzani V, Ceroni P, Gestermann S et al (2000) Effect of protons and metal ions on the fluorescence properties of a polylysine dendrimer containing twenty four dansyl units. *J Chem Soc Dalton Trans* 3765–3771
202. Vögtle F, Gestermann S, Kauffmann C et al (2000) Coordination of CO^{2+} ions in the interior of poly(propylene amine) dendrimers containing fluorescent dansyl units in the periphery. *J Am Chem Soc* 122:10389–10404
203. Pugh VJ, Hu QS, Zuo X et al (2001) Optically active BINOL core-based phenyleneethynylene dendrimers for the enantioselective fluorescent recognition of amino alcohols. *J Org Chem* 66:6136–6140
204. Xu MH, Lin J, Hu QS et al (2002) Fluorescent sensors for the enantioselective recognition of mandelic acid: signal amplification by dendritic branching. *J Am Chem Soc* 124:14239–14246
205. Guo M, Varnavski O, Narayanan A et al (2009) Investigations of energy migration in an organic dendrimer macromolecule for sensory signal amplification. *J Phys Chem A* 113:4763–4771
206. Roda A, Guardigli M, Michelini E et al (2009) Nanobioanalytical luminescence: Förster-type energy transfer methods. *Anal Bioanal Chem* 393:109–123
207. Förster T (1948) Intermolecular energy migration and fluorescence. *Ann Phys* 2:55–75
208. Sapsford KE, Berti L, Medintz IL (2006) Materials for fluorescence resonance energy transfer analysis: beyond traditional donor–acceptor combinations. *Angew Chem Int Ed* 45:4562–4588
209. Braslavsky SE (2007) Glossary of terms used in photochemistry. 3rd Edition (IUPAC Recommendations 2006). *Pure Appl Chem* 79:293–465
210. White BR, Holcombe JA (2007) Fluorescent peptide sensor for the selective detection of Cu^{2+} . *Talanta* 71:2015–2020
211. Zhou Z, Yu M, Yang H et al (2008) FRET-based sensor for imaging chromium(III) in living cells. *Chem Commun* 3387–3389
212. Liu CW, Huang CC, Chang HT et al (2009) Highly selective DNA-based sensor for lead(II) and mercury(II) ions. *Anal Chem* 81:2383–2387
213. Yuan M, Zhou W, Liu X et al (2008) A multianalyte chemosensor on a single molecule: promising structure for an integrated logic gate. *J Org Chem* 73:5008–5014
214. Huang CC, Chang HT (2006) Selective gold-nanoparticle-based “turn-on” fluorescent sensors for detection of mercury(II) in aqueous solution. *Anal Chem* 78:8332–8338

215. Zheng AF, Chen JL, Wu GN et al (2009) Optimization of a sensitive method for the “switch-on” determination of mercury(II) in waters using rhodamine B capped gold nanoparticles as a fluorescence sensor. *Microchim Acta* 164:17–27
216. Wang X, Guo X (2009) Ultrasensitive Pb^{2+} detection based on fluorescence resonance energy transfer (FRET) between quantum dots and gold nanoparticles. *Analyst* 134:1348–1354
217. Jiang G, Susha AS, Lutich AA et al (2009) Cascaded FRET in conjugated polymer/quantum dot/dye-labeled DNA complexes for DNA hybridization detection. *ACS Nano* 3:4127–4131
218. Neurauter G, Klimant I, Wolfbeis OS (1999) Microsecond lifetime-based optical carbon dioxide sensor using luminescence resonance energy transfer. *Anal Chim Acta* 382:67–75
219. von Bültzingslöwen C, McEvoy AK, McDonagh C et al (2003) Lifetime-based optical sensor for high-level pCO_2 detection employing fluorescence resonance energy transfer. *Anal Chim Acta* 480:275–283
220. Freeman R, Li Y, Tel-Vered R et al (2009) Self-assembly of supramolecular aptamer structures for optical or electrochemical sensing. *Analyst* 134:653–656
221. Goldman ER, Medintz IL, Whitley JL et al (2005) A hybrid quantum dot-antibody fragment fluorescence resonance energy transfer-based TNT sensor. *J Am Chem Soc* 127:6744–6751
222. So MK, Xu CJ, Loening AM et al (2006) Self-illuminating quantum dot conjugates for in vivo imaging. *Nat Biotechnol* 24:339–343
223. Angers S, Salahpour A, Joly E et al (2000) Detection of β_2 -adrenergic receptor dimerization in living cells using bioluminescence resonance energy transfer (BRET). *Proc Natl Acad Sci USA* 97:3684–3689
224. Kroeger KM, Hanyaloglu AC, Seeber RM et al (2001) Constitutive and agonist-dependent homo-oligomerization of the thyrotropin-releasing hormone receptor. Detection in living cells using bioluminescence resonance energy transfer. *J Biol Chem* 276:12736–12743
225. Yamakawa Y, Ueda H, Kitayama A et al (2002) Rapid homogeneous immunoassay of peptides based on bioluminescence resonance energy transfer from firefly luciferase. *J Biosci Bioeng* 93:537–542
226. Sousa LR, Larson JM (1977) Crown ether model systems for the study of photoexcited state response to geometrically oriented perturbers. The effect of alkali metal ions on emission from naphthalene derivatives. *J Am Chem Soc* 99:307–310
227. Dix JP, Vögtle F (1978) Ion-selective crown ether dyes. *Angew Chem Int Ed Engl* 17:857–859
228. Basabe-Desmouts L, Reinhoudt DN, Crego-Calama M (2007) Design of fluorescent materials for chemical sensing. *Chem Soc Rev* 36:993–1017
229. Martínez-Máñez R, Sancenón F, Descalzo AB et al (2009) Supramolecular hybrid materials – integrating functionality with sensing. In: Abd-El-Aziz AS, Carraher CE Jr, Pittman CU Jr et al (eds) *Macromolecules containing metal and metal-like elements*, vol. 9, inorganic supramolecules. Wiley, Chichester
230. Lakowicz JR (1992–2006) *Topics in fluorescence spectroscopy series*, vol 1–11. Plenum, New York and Springer, Berlin
231. Wolfbeis OS (2001–2008) *Springer series on fluorescence*, vol 1–6. Springer, Berlin
232. Mason WT (ed) (1999) *Fluorescent and luminescent probes*, 2nd edn. London, Academic
233. Thompson RB (ed) (2005) *Fluorescence sensors and biosensors*. CRC, Boca Raton
234. Pawley JB (ed) (2006) *Handbook of biological confocal microscopy*, 3rd edn. New York, Springer
235. Kim SH (ed) (2006) *Functional dyes*. Elsevier, Amsterdam
236. Miller LW (ed) (2008) *Probes and tags to study biomolecular function*. Wiley-VCH, Weinheim
237. Demchenko AP (2010) The concept of lambda-ratiometry in fluorescence sensing and imaging. *J Fluoresc* DOI 10.1007/s10895-010-0644-y

Collective Effects Influencing Fluorescence Emission

Alexander P. Demchenko

Abstract Dramatic improvement of fluorescence sensing technologies can be achieved by combining molecular emitters into clusters, nanoparticles, and aggregates. This chapter addresses the new effects that appear on incorporation of dyes into these supramolecular structures. We consider different types of intermolecular interactions that influence the emission spectra, focusing on spectral changes that are observed on concentrating organic dyes in confined media. The mechanisms of energy transfer between fluorescence emitters are discussed. They provide possibilities for increasing the dynamic range of sensing response by extending the variation of intensity (light-harvesting, superquenching), and wavelength range (directed transfer, wavelength-shifting).

Keywords Excimers · Intermolecular interactions · Light-harvesting · Red-edge effects · Resonance energy transfer · Superquenching · Wavelength-shifting

Contents

1	Introduction	108
2	Spectroscopy of Intermolecular Interactions	109
2.1	Universal Intermolecular Interactions	109
2.2	Hydrogen Bonding in the Ground and Excited States	111
2.3	Excimers and Exciplexes	112
3	Resonance Interactions between Fluorophores	113
3.1	Electron Exchange Interactions	113
3.2	Förster Resonance Energy Transfer	113
4	Site-Selective Red-Edge Effects	114

A.P. Demchenko (✉)

Palladin Institute of Biochemistry, National Academy of Sciences of Ukraine, Kyiv 01601, Ukraine

e-mail: alexdem@ukr.net

5	Collective Effects Observed with Organic Dyes	116
5.1	Superquenching, Concentrational Quenching, and Directed Homo-FRET	117
5.2	Wavelength Converting	118
5.3	Light-Harvesting (Antenna) Effects	120
5.4	Red-Edge Effects in Energy Transfer	121
6	Collective Effects in Nanocomposites	122
6.1	FRET Modulation of Reporter Lifetime	122
6.2	Plasmonic Enhancement	123
7	Realization of Collective Effects in Sensing and Imaging Technologies	124
7.1	Collective Effects in Sensing	124
7.2	Collective Effects in Imaging	125
8	Concluding Remarks	126
	References	127

1 Introduction

Fluorescence is a well-observed phenomenon characteristic of many materials and the different forms of their aggregation. Meantime the vast majority of studies on fluorescence have been on small organic molecules in liquid solutions. Parameters of their emission (intensity, lifetime, anisotropy, and positions of excitation and emission spectra) were found to be extremely sensitive to intermolecular interactions [1], which justifies their extensive application in various sensing technologies [2]. The disadvantages of organic dyes (low photostability, insufficient brightness, short lifetimes, etc.) have resulted in competition from luminescent metal–ligand complexes, semiconductor nanoparticles (Quantum Dots), and conjugated polymers. These new materials show advanced performance in a variety of applications [3]. However, the development of organic fluorophores is ongoing, and they demonstrate remarkable improvement in many important properties [4–6]. In addition, technologies were developed for incorporation of organic dyes into organic [7] and inorganic [8] polymer nanoparticles and for making nanoparticles from aggregated forms of the dyes [9], which allow increasing their photostability and brightness comparable with that of Quantum Dots. The fact that the basic properties of organic dyes that are very attractive for applications can be retained and improved in these aggregates is important. Since all types of fluorescence reporters (molecules or nanoparticles) can be combined in nanocomposites, new routes to the perfection of fluorescence reporters by designing such composites have emerged.

Based on the specific requirements for the operation of fluorescence reporters, we have divided them into two broad categories [2]. One category comprises reporters that serve as *labels* and *tags*. Their only response is based on their presence in a particular medium or at a particular site, and the major parameters that have to be optimized are their brightness and photostability. Brightness and durability can be increased dramatically if, instead of single molecules, we use nanoscale structures containing hundreds or thousands of them, and if we incorporate

a matrix that can protect them against chemical destruction, photodestruction, and quenching. The second category comprises reporters serving as *probes* or those involved in *molecular sensors*. As probes, they should respond to changes in their molecular environment and as essential parts of the sensors, they should be coupled to recognition units and respond to the target binding through change in their fluorescence parameters. Here, improvement of response can be provided in several dimensions, particularly, at achieving the broadest range of the change of intensity and the strongest shifts on the wavelength scale.

These aims can be achieved by incorporating dyes into nanostructures and nanocomposites, but the routes to follow have to be different. If we wish to obtain the highest degree of brightness, the dyes should not interact, but their local environment (e.g., polymer matrix) should provide optimal protection against various quenching and bleaching effects. Alternatively, if we wish to attain the highest dynamic range of response in terms of variations of intensity or wavelength of emission together with high brightness, we need to induce dyes incorporated into the nanostructures to interact. These interactions exhibit new phenomena, the proper knowledge of which could lead to new dimensions for optimization of fluorescence response. This chapter describes these possibilities.

2 Spectroscopy of Intermolecular Interactions

A short excursion into the physics and spectroscopy of intermolecular interactions is intended to illustrate the effects of fluorescence spectra change on the transition of dye molecules from liquid solvents to solid environments, on the change of polarity and hydration in these environments, and on the formation of excited-state complexes (excimers and exciplexes).

2.1 *Universal Intermolecular Interactions*

Interactions that exist between molecules in any media are universal. Their physical modeling can be made on a mesoscopic level of description on which the solute can be represented by a point dipole with dipole moment, μ , and its environment, by its averaged macroscopic parameters, such as refractive index, n , and dielectric constant, ϵ . On this level, the theory explaining the shifts of light absorption and fluorescence bands is well developed [10–12], see also [13]. The concept of “solvation” or “stabilization” energy, which determines the position of an electronic state with the variation of intermolecular interactions is important. Since the position of the absorption or emission spectrum depends on the difference in the energies of the corresponding states, the higher solvation energy of the ground state (compared to that of the excited state) increases this energy gap and the spectra move to higher energies (shorter wavelengths). Meanwhile, the shift of spectra to

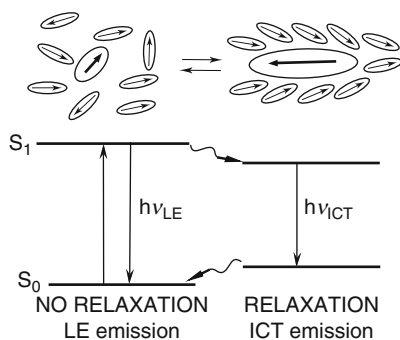
longer wavelengths is more common because in these cases the stronger electronic charge distribution in the excited state results in its stronger interaction with the environment.

The most efficient factor in stabilizing the electronic state is the dipole–dipole interaction. This creates a local electric field (reactive field) around the excited dye interacting with its dipole [14]. If the charges are present in its vicinity, they create an electric field that interacts with the dye dipole and induces electrochromic shifts of absorption and fluorescence spectra. The direction of these shifts depends on the relative orientation of the electric field vector and the dye dipole. These effects of electrochromism are overviewed in [15].

The act of light absorption is so fast that only the electronic subsystem in the dye environment can respond to it. In contrast, the finite values of the fluorescence lifetime, τ_F , allow for different reactions in the excited state that involve the motions of atoms and molecules before the emission. They provide additional stabilization for the excited state and the shift of fluorescence bands to longer wavelengths. The most common is the dielectric relaxation, which is the rotation of dipoles surrounding the excited fluorophore. This process is dynamic [16], so the dielectric relaxation time, τ_R , can vary in very broad ranges. In solid environments (vitrified solvent glasses, and polymers), the relaxation is slower than the emission ($\tau_R > \tau_F$) and the fluorescence spectrum occupies the short wavelength position, whereas in liquid solvents, the relaxation is much faster than the emission ($\tau_R < \tau_F$). There can be cases when $\tau_R \approx \tau_F$ (viscous solvents, and flexible polymers), where the motion of fluorescence spectra to longer wavelengths can be observed as a function of time. In common steady-state observation, the spectra in this case are sensitive to variations of temperature influencing τ_R and to the dynamic quenchers influencing τ_F .

In the excited state, the redistribution of electrons can lead to localized states with distinct fluorescence spectra that are known as intramolecular charge transfer (ICT) states. This process is dynamic and coupled with dielectric relaxations in the environment [16]. This and other solvent-controlled adiabatic excited-state reactions are discussed in [17]. As shown in Fig. 1, the locally excited (LE) state is populated initially upon excitation, and the ICT state appears with time in a process coupled with the reorientation of surrounding dipoles.

Fig. 1 Simplified energy diagram showing the influence of molecular relaxations (with lifetime τ_R) on the energies of LE and ICT states. The ICT states can be strongly stabilized in polar media by orientation of surrounding dipoles resulting in substantial shifts of fluorescence spectra to lower energies (longer wavelengths)



To summarize, it is essential to note that the polarity and rigidity of the dye environments can dramatically influence the fluorescence spectra. These effects should be taken into account; they may be beneficial in the incorporation of dyes into nanoparticles and in the design of nanocomposites.

2.2 *Hydrogen Bonding in the Ground and Excited States*

In addition to universal interactions, there are specific noncovalent intermolecular interactions – the most common and important of which is the hydrogen bond. The presence of H-bond donor and acceptor groups in the dye molecule coupled to aromatic structures possessing π -electrons allows forming these bonds with molecular partners in their environment. In excitation spectra, one can observe the shift to longer wavelengths in interactions with the H-bond donor at the acceptor site, and the shift to shorter wavelengths in interactions with the proton acceptor at the donor site [18]. The electronic excitation can dramatically change the H-bond reactivity. The H-bond proton-acceptor group (e.g., carbonyl C=O group forming the bonds of $>C=O \cdots H-O-$ type) included in the aromatic ring – being an acceptor for π -electrons – increases its electron acceptor power, which leads to bond strengthening [19]. Accordingly, the interaction of aromatic proton acceptors with different external proton donors produces the opposite effect on π -electronic system, which in this case is usually small or even unnoticed in spectra [20]. It is important to note that the shifts in π -electronic density on electronic excitation may result in reorganizations of H-bonds and to the new bond formation.

The H-bonds formed with proton acceptors by carbonyls incorporated into aromatic heterocycles can be of two types: strong and weak. Both of them can dramatically change the spectra and the latter are observed when the strong bonds are already at saturation [21]. In the presence of strong intramolecular bonds, the intermolecular bonds (such as in 3-hydroxychromone derivatives) are only weak, and they do not reorganize in the excited state. In this way, a fluorescent dye can serve as the H-bonding sensor [22].

The shift of fluorescence spectra to longer wavelengths in highly polar media is characteristic of many “polarity-sensitive” dyes [1, 10]. This effect is increased by the inclusion of electron donor and acceptor groups into the aromatic ring in opposite positions for creating the large excited-state dipole moment. Since these groups are also the H-bond formers, the bond formation produces shifts in fluorescence spectra that are comparable or even stronger in magnitude than the effects of polarity and in the same direction [23–25]. When the dye is exposed to water, this change can be the measure of hydration. At the same time, there are dyes in which the H-bonding to proton acceptor and the charge transfer produce shifts in opposite directions, and this effect can be used to identify protic targets from aprotic environments [26]. When incorporated into nanostructures, the dyes incorporated into the core and those exposed to the surface may exhibit different abilities to

form the H-bonds. This may lead to differences in their spectra and influence the resonance energy transfer between them.

2.3 *Excimers and Exciplexes*

When excited, the molecules of organic dyes tend to form complexes with unexcited molecules like themselves. These excited dimeric complexes are called the excimers. The excimer emission spectrum is easy to observe because it is very different from that of a monomer. It is usually broad and strongly shifted to longer wavelengths, and it does not contain vibrational structure. If the excimer is not formed, we observe emission of the monomer in the fluorescence spectra, and upon its formation there appears a characteristic emission of the excimer.

Selection of excimer formers is limited to aromatic hydrocarbons. Pyrene derivatives are more frequently used because of the unique property of these fluorophores to form stable excimers with long fluorescence lifetimes. The structured band of a pyrene monomer is observed at about 400 nm, whereas that of the excimer is located at 485 nm. Long lifetimes (~ 300 ns for monomer and ~ 40 ns for excimer) allow for easy rejection of background emission and application of lifetime sensing [27]. Different fluorescence sensor technologies are based on the target-induced shifts between monomer and excimer emissions. They use conformational changes in the sensor unit that brings the pyrene groups together [28]. It is not easy to provide this response at the level of nanoparticles.

The formation of excimers requires close location and proper orientation between the partners – specifically, the formation of a cofacial sandwich between two heterocycles rich in π -electrons. Weak ground-state complexes can be formed between proximate monomers that become excimers upon excitation. It has been observed that when pyrene groups are appended to a flexible polymer in solution, fluorescence shows the presence of a significant number of excimers [29]. When pyrene is incorporated into nanoparticles formed by miniemulsion polymerization, it shows noneven distribution indicated by an increased number of excimers, which means that some complexes between monomers are formed prior to excitation [30]. Depending on the polymer matrix, for some derivatives the excimers are not formed [31]. At the same time, it has been reported that highly emissive conjugated polymer excimers can be formed in the condensed states of these polymers [32]. These examples suggest many possibilities to explore monomer–excimer transitions in the sensor design. The excimers are also attractive because they successfully combine such properties as high degrees of brightness, long lifetimes, and dramatic Stokes shifts.

Exciplexes are the excited-state complexes that can be formed by partners of different origin [33]. Their formation on intermolecular interaction can provide a fluorescence reporting signal [28, 34]. The advantage of their formation in high-concentration matrices is the large Stokes shift that, as we will see below, can prohibit the homo-FRET.

3 Resonance Interactions between Fluorophores

When located at short distances, the dye molecules or nanoparticles can lose the properties of independent emitters. They may not interact in the ground state, but when excited they can not only interact but also transfer their interaction energies. By assembling a large number of dye molecules in a small unit and using the mechanisms of energy transfer, we can not only increase their brightness but also modulate their spectroscopic properties in extremely broad ranges.

3.1 *Electron Exchange Interactions*

Classical models of the fundamental mechanisms of excitation energy transfer distinguish three limiting cases of such transfer: Davydov free excitons (Simpson and Peterson strong coupling), localized excitons (weak coupling), and the Förster mechanism of vibrational–relaxation energy transfer [35]. The short-range transfer involves the coupling of electronic wave functions mediated by the bridging ligand orbitals (superexchange). Dexter was the first to take account of this factor generalizing the Förster theory, and therefore this mechanism is often called the Dexter-type energy transfer [36]. In this mechanism, close proximity of the two partners is required for their electronic orbital overlap, and the probability of transfer decays exponentially with the distance on a scale up to 1.5–1.8 nm. Therefore, it is frequently observed in covalently linked dye dimers. When the dyes form associates, both Förster-type Coulomb coupling and Dexter-type short-range electronic coupling mechanisms are involved in the transfer so that the two mechanisms operate in the same direction. The developed theory allows their unified description [37].

3.2 *Förster Resonance Energy Transfer*

The excited-state dyes can interact with unexcited dyes through space at larger distances, 5–8 nm. The elegant theory developed by Förster considering the resonant interaction between two point dipoles explains this interaction, which depends on the resonant frequencies of the partners and their distance and orientation. This theory describes the case when two or more dye molecules or light absorbing particles with similar excited-state energies exchange these energies due to Coulombic long-range dipole–dipole resonance interaction. One molecule, the *donor*, absorbs light and the other, the *acceptor*, accepts this energy and then relaxes to the ground state with or without emission. Förster resonance energy transfer (FRET) can take place if the emission spectrum of the donor overlaps, at least partially, with the absorption spectrum of the acceptor (Fig. 2).

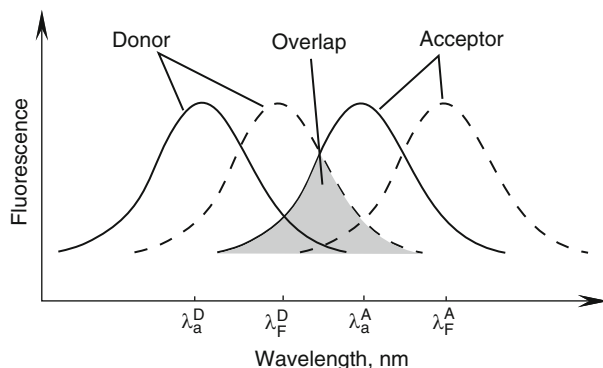


Fig. 2 Absorption (*solid lines*) and fluorescence (*dashed lines*) spectra of two fluorophores exhibiting FRET. The light-absorbing and emitting at shorter wavelengths fluorophore (donor) can transfer its excitation energy to another fluorophore (acceptor) absorbing and emitting at longer wavelengths. For efficient transfer, the absorption spectrum of the acceptor should overlap the emission spectrum of the donor (*shaded area*). At close donor–acceptor distance, the excitation of the donor results in emission of the acceptor, and if the distance is large, the donor itself will emit. This produces distance-dependent switching between two emission bands

The theory predicts a $1/R^6$ dependence of energy transfer rate on their separation distance, R , which is very steep. Deviation from this dependence is frequently observed for extended conjugated dye molecules, metal [38], and semiconductor [39] nanoparticles, the sizes of which are comparable with R , but the validity of this theory and $1/R^6$ dependence are confirmed in the studies of small dye molecules interacting at significant distances.

It is important that FRET is mechanistically reversible and that dyes with similar excitation and emission spectra may exchange their excited-state energies. At high local dye concentrations, energy can travel within the population of these dyes and be directed to the dyes with longer wavelengths of absorption and emission. Kinetically, FRET competes with other pathways of deactivation of the donor excited state, and the acceptor acquires the property to emit light with the lifetime of the donor. This is because the energy transfer is a stochastic process that develops during the donor fluorescence lifetime. These properties will be discussed in more detail in the following sections of this chapter.

4 Site-Selective Red-Edge Effects

Light of definite energy and polarization has a selective power to exclusively excite dye molecules whose electronic transition energy and orientation match these parameters. Thus, if a dye is excited by polarized light, its emission will also be highly polarized. Depolarization occurs only when the time correlation of these selectively excited species is lost due to their rotation or participation in some

photophysical process, such as FRET. Similarly, photoselection can be provided by variation of excitation energy. The dye molecule can absorb only the light quanta that correspond to its electronic transition energy.

These basic considerations permit the explanation of a group of phenomena that refer to fluorescence spectroscopy and have a common name “Red-Edge effects” [40–45]. It has been found that in solid or viscous polar environments, the fluorescence spectroscopic properties do not conform to classical rules. Thus, when fluorescence is excited at the red (long wavelength) edge of the absorption spectrum, the emission spectra start to depend on the excitation wavelength [40] (Fig. 3), and FRET, if present, fails at the “red” excitation edge. The Red-Edge excitation can profoundly influence not only FRET but also other excited-state reactions, such as electron and proton transfers if they occur in rigid or highly viscous environments [41].

The best tool for observation of these phenomena is time-resolved spectroscopy [42, 43] that makes it possible to observe the excitation-wavelength-dependent evolution of the spectra in time. The steady-state observations can be complicated by the existence of ground-state heterogeneity [44] that originates not only from the presence of different dyes but also from the same dyes participating in different (e.g., H-bonding) interactions.

The role of the conditions in which these phenomena are observed is now well understood [40, 45]. The chromophore should be solvatofluorochromic, that is, its fluorescence spectra should respond to changes in interaction energy with its environment by significant shifts. This environment should be relatively polar, but rigid or highly viscous, so that the relaxation times of its dipoles, τ_R , are comparable or longer than the fluorescence lifetime τ_F (in the case of recording the steady-state spectra) or on the time scale of observation (in time-resolved spectroscopy). Thus, these effects are coupled with molecular dynamics in condensed media.

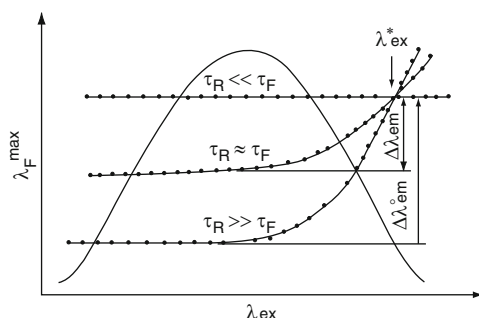


Fig. 3 Dependencies of positions of fluorescence band maxima, λ_F^{\max} , on excitation wavelength, λ_{ex} , for different correlations between the dipole relaxation time, τ_R , and fluorescence lifetime, τ_F . When relaxations are slow, the fluorescence band occupies extreme short wavelength position and the Red-Edge effect is the most significant, and when they are faster than the emissions, the spectrum is at long wavelengths and the Red-Edge effect is absent. The excitation spectrum, $F(\lambda_{ex})$, is also presented schematically. $\Delta\lambda_{em}^*$ and $\Delta\lambda_{em}$ are the magnitudes of Red-Edge effect, and $\Delta\lambda_{ex}^*$ is the isorelaxation point (the excitation wavelength at which the position of fluorescence band does not depend on relaxations) [32]

The major factor that produces broadening of the spectra is the so-called inhomogeneous broadening [13, 40]. It originates from the nonequivalence of chromophore environments in an ensemble of otherwise identical molecules resulting in the distribution of solute–solvent interaction energies. Therefore, the electronic transition energies for every species become distributed on the scale of energy, and their superposition forms an inhomogeneously broadened contour. Excitation at the band edge selects a part of this distribution, the spectroscopic properties of which are different from that of the mean. At the long wavelength edge of the emission band, the species for which the excitation energy with the environment is the strongest are excited, and for them the emission spectrum becomes shifted correspondingly.

Due to molecular motions, the excitation energies fluctuate in time causing redistribution within this ensemble, “mixing” different environments. When the dye is incorporated into a solid (polymers, low-temperature solvent glasses) under the condition $\tau_R > \tau_F$, the distribution persists during the time of emission, and the broadening is static. The broadening is dynamic if the motions in the chromophore environment occur simultaneously ($\tau_R \approx \tau_F$) or faster than the emission ($\tau_R < \tau_F$). Thus, the inhomogeneous broadening effects contain information about the dynamic properties of condensed systems, and the rate of fluorescence emission provides the necessary time scale for these observations [45].

The Red-Edge effects are popular tools to study the dynamics and interactions in nano-scale objects, such as proteins and biomembranes [45] or reverse micelles [46]. In this case, organic dyes are introduced into the system or, like tryptophan in proteins [47] or intrinsic fluorophore in green fluorescent protein [48], they are a part of it. Studies on polymer films with incorporated dyes [49] are quite frequent, suggesting the broader use of this tool in the studies of dye-doped nanoparticles. These effects were detected in conjugated polymers, particularly in polyfluorene copolymers [50], and more detailed studies on them are expected to be made in future. Regarding metal nanoclusters and Quantum Dots, the selective excitation may reveal a different property – their size distribution, though inhomogeneous broadening effects can also be detected [51].

5 Collective Effects Observed with Organic Dyes

Incorporation of organic dyes into nanoparticles in concentrations that allow efficient FRET to proceed between them due to short interchromophore distances can dramatically increase the range of variation of their spectroscopic properties. Due to the long-range but steep distance dependence of the effect, one can either activate or eliminate the exchange of their excited-state energies by a variation in dye concentration. Thus, in addition to variations in the spectroscopic properties of donor and acceptor, the collective effects in energy transfer can be efficiently explored. Based on effects in FRET, such as directed transfer and antenna effect, powerful tools can be developed for the design of advanced sensors.

5.1 Superquenching, Concentrational Quenching, and Directed Homo-FRET

Collective effects in multiple transfers can be seen when the donor and acceptor are the same molecules and display the so-called *homo-transfer*. The homo-transfer is reversible, so the excitation energy can travel within the ensemble of closely located dyes until the act of emission. Commonly, since the dyes are oriented randomly in space, the emission of such an ensemble becomes totally depolarized. This case is depicted in Fig. 4a.

Let's imagine then that there is a nonfluorescent molecule that works as the FRET acceptor. Directly from the neighboring donor or through the chain of other donor molecules, this acceptor gets the excitation energy and then relaxes without emission. Because of the significant number of dyes in an ensemble, their total brightness can be very high, and a single quencher molecule can quench the emission of the whole ensemble. This is the case of *superquenching* schematically depicted in Fig. 4b.

Nonfluorescent dimers of organic dyes are typical fluorescence quenchers [52]. Dimerization is commonly reversible, so the monomers and dimers exist in equilibrium, and this equilibrium is shifted to dimers at high concentrations leading to *concentrational quenching* (or "self-quenching"). It is known that when the protein or nucleic acid molecule is modified by attaching an increasing number of fluorescent dyes, very often, instead of a linear increase, its fluorescence passes through

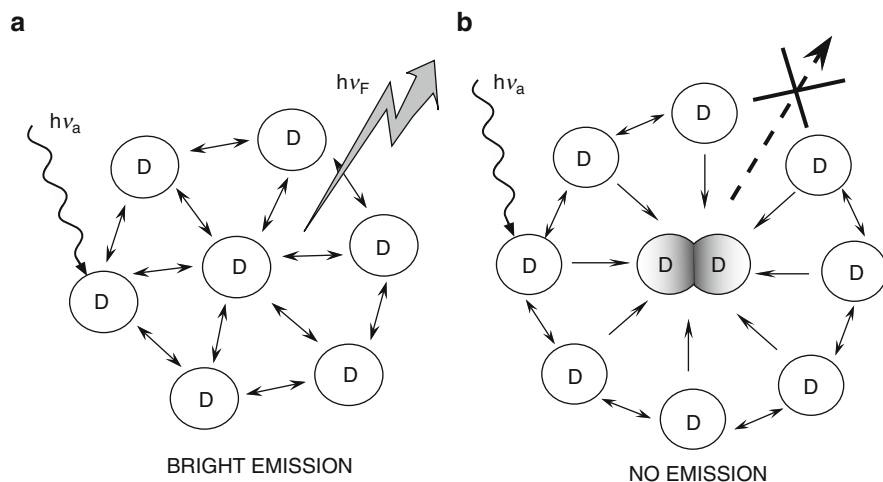


Fig. 4 Illustration of homo-FRET and self-quenching by dimers. (a) The dyes (D) exchange their excitation energies and are bright emitters. (b) The presence of nonfluorescent dye dimer (DD) acting as the trap for excitation energy results in quenching of all the dyes located within FRET distance to it

the maximum and falls down. For some dyes, self-quenching is a limiting factor in the design of dye-doped nanoparticles with high dye density. This happens due to FRET to nonfluorescent traps.

Since the same dye molecules can serve as both donors and acceptors and the transfer efficiency depends on the spectral overlap between the emission spectrum of the donor and the absorption spectrum of the acceptor, this efficiency also depends on the Stokes shift [53]. Involvement of these effects depends strongly on the properties of the dye. Fluoresceins and rhodamines exhibit high homo-FRET efficiency and self-quenching; pyrene and perylene derivatives, high homo-FRET but little self-quenching; and luminescent metal complexes may not exhibit homo-FRET at all because of their very strong Stokes shifts.

It has been frequently observed that in concentrated dye solutions in solid matrices (polymers, organic, and inorganic glasses) when conditions for concentrational quenching are avoided, fluorescence spectra are shifted to longer wavelengths compared to those recorded at low concentrations. This phenomenon is also related to homo-FRET. It acquired the name “*directed energy transfer*,” and its explanation is based on the concept of inhomogeneous broadening of spectra [40] (see Sect. 4). To provide a simple explanation, imagine an ensemble of identical molecules such that each of them interacts somewhat differently with the others and possesses its own excitation and emission spectrum, which contributes to the spectrum of the ensemble. In the case of homo-FRET, because of the interplay of FRET overlap integrals, the exchange of energies between individual emitters will occur in such a way that the dye with long wavelength-shifted emission spectrum is less efficient as the donor and more efficient as the acceptor. The results of steady-state and time-resolved spectroscopy are in accord with this explanation [40, 43].

We have to take into account these effects when the dyes are located in structurally inhomogeneous environments, for instance, in the core and on the surface of a nanoparticle. If their core is low-polar and the surface is exposed to an aqueous solvent, we will observe that the energy flow is directed to the dyes located at the surface. It is because their absorption and emission spectra are shifted to the red due to the fact that they are more efficient as FRET acceptors.

Thus, there are many possibilities to avoid homo-FRET or to use it efficiently in the design of fluorescence sensors. The excited-state energy can flow to the dyes in particular environments, and by manipulating with a single trigger dye, one can provide efficient collective sensor response by switching on and off the whole ensemble of fluorescence emitters.

5.2 Wavelength Converting

The collective effects of directed energy flow can be strongly enhanced when the dyes playing the role of donors and acceptors are different and optimally selected. The *hetero-FRET* (described in Sect. 3.2) occurring within an ensemble of dissimilar molecules allows many possibilities for this. The transfer and the quenching

efficiencies are determined by the interplay of the rate constants of all transformations of the excited states, starting from that of the initially excited donor [54]. The overlap integral J for the transfer is larger if the donor emission is at shorter and acceptor absorption is at longer wavelengths than in the opposite case (see Fig. 2), which makes the transfer strongly directional. By selecting dyes with optimal spectral overlap, one can excite fluorescence at short wavelengths and in a transfer process, obtain emission at much longer wavelengths. Such a system can operate as an efficient “*wavelength converter*”.

Wavelength converting can be very useful. FRET can occur in a cascade manner in a sequence of dyes, in which an energy acceptor can serve as the donor to another dye with lower excitation and emission energy. One can select the primary donor with the excitation spectrum that ideally fits the used light source and the final acceptor with the position of the emission maximum at the desired optimal wavelength for the assay. This wavelength can be chosen throughout the visible range, down to the near-infrared region. Moreover, a two-photonic excitation can be used. If this is not achievable with a single donor–acceptor pair, the “intermediate” dyes serving as both donors and acceptors may be needed to fill the gap in the energy transfer chain. Thus, by exciting a single donor at a single wavelength, one can achieve the broadest range of emission colors.

A transfer, in which several different dyes provide the chain of transfer events for achieving a very significant shift in emission wavelength, is called a “*cascade energy transfer*” [55], as depicted in Fig. 5.

Recent literature contains many examples of the construction of “*casca*des” [56]. Usually they are made by the covalent linking of monomer dyes, which allows strict control of their stoichiometry. The pyrene-Bodipy molecular dyads and triads are examples [57]. Efficient energy flow was reported in a purpose-built cascade molecule bearing three distinct chromophores attached to the terminal acceptor [58]. A combinatorial approach with the selection of the best hits can be applied using the assembly of fluorescent oligonucleotide analogs [59].

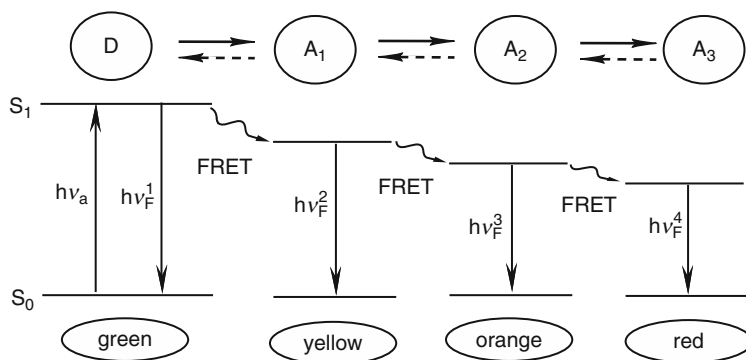


Fig. 5 Cascade systems with directed excited-state energy transfer. On each step, the emission spectrum shifts to longer wavelengths

In the studies on blended conjugated polymer nanoparticles [60], it was shown that about 90% of conversion of blue light into green, yellow, and red emissions can be achieved by the addition of less than 1% of polymer emitting at these wavelengths. It was stated that because of such a composition, the fluorescence brightness of the blended polymer nanoparticles can be much higher than that of inorganic quantum dots and dye-loaded silica particles of similar dimensions.

Direct application of such wavelength converters is found in *multiplex assays* (simultaneous analysis of many targets). In homogeneous-type assays, the possibility of distinguishing several types of sensor–target interactions can be realized if we are able to label every type of sensor molecule with a certain “barcode” that could be recognizable in chromatography or flow cytometry. Dyes (and nanoparticles) emitting at different wavelengths may serve as these barcodes. The requirement for their excitation with the same light source can be easily satisfied with the same dye as the FRET donor but with a different cascade of acceptors [61].

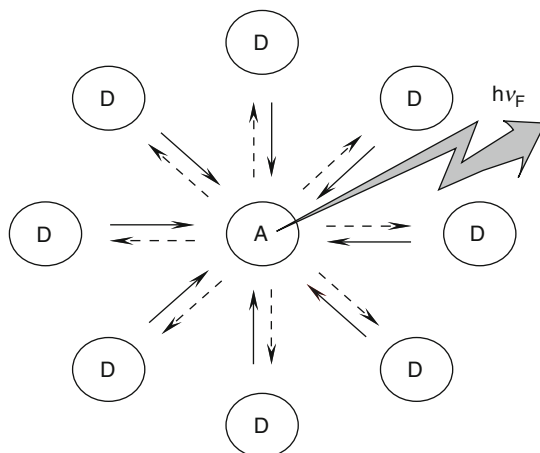
It is easy to intervene into a cascade system by removing and then adding the intermediates in the FRET process. When the donor and the acceptor are in proximity but their spectral overlap is insufficiently small for the transfer, the introduction of a third partner that can serve as an acceptor to the primary donor and as a donor to the terminal acceptor results in an efficient transfer. Such “*FRET-gating*” can be used in generating the fluorescence response, as it was shown in the DNA assay, in which fluorescein-labeled testing DNA was used as a “gate” in the cascade transfer between conjugated polymer and ethidium bromide intercalated into a double-helical structure [62]. New versions of this technology have been reported [63].

5.3 *Light-Harvesting (Antenna) Effects*

The FRET can be directed in such a way that a large number of strong light-absorbing donors, when excited, transfer their energy to a much smaller number of acceptors. Because they are excited via efficient energy transfer from many donors, the fluorescence of acceptors can be increased dramatically. This principle of *light-harvesting* is used in the natural systems of photosynthesis that collect an enormous amount of solar energy by exciting the so-called antenna pigments and redirecting it to reaction centers. The donors serve as “antennas” to provide the most efficient collection and transfer of energy to an acceptor. By providing amplification of acceptor emission, such “*antenna effects*” can be used for optimizing the fluorescence properties of many molecular and supramolecular systems, from dimers of organic dyes to complex nano-composites [64, 65].

The antenna effect is illustrated in Fig. 6. The necessary conditions for its efficient implementation are the high molar absorbance of antenna dyes, efficient energy transfer to acceptor dye, and high quantum yield of emission of the latter. At the same time, while evaluating the highly increased apparent brightness of the

Fig. 6 Illustration of antenna effect. Great number of donors (D) absorb light and transfer the excitation energy to a small number of acceptors (A). Excitation of acceptors via FRET increases their emission intensity and, often, lifetime in comparison with direct excitation. Homo-FRET between the donors is not shown



acceptor, one should not disregard the fact that its photodegradation also occurs at a much faster rate, in accordance with the frequency of the acts of excitation [66].

The theory describing the light-harvesting effects suggests going beyond the dipole–dipole approximation of Förster theory [67, 68]. Its development for modeling the natural systems of photosynthesis is beneficial for the design of fluorescence reporters.

The light-harvesting and cascade-transfer wavelength shifting are quite compatible. Moreover, the generation of “superquenching” effects can be easily produced in cascades and under the action of light harvesters. So, if the transfer is efficient, the quenching of the final acceptor quenches the whole ensemble. This opens up enormous possibilities in sensor design.

5.4 Red-Edge Effects in Energy Transfer

The easiest way to observe homo-FRET is to detect its influence on emission anisotropy in rigid environments, where the anisotropy in diluted systems is high [69]. If one dye molecule absorbs light and some others being in different orientations emit, the emission in the case of efficient FRET becomes totally depolarized. Surprisingly, this effect decreases or even disappears when fluorescence is excited at the long wavelength edge of the emission band (the Red-Edge effect in FRET). Its present interpretation is based on the inhomogeneous broadening of spectra [13] and on the idea that the species selected at the Red-Edge are unable to serve as FRET donors [40, 45].

To understand this effect, one can imagine an overlap integral (see Fig. 2) as a composition of overlap integrals formed by individual donor–acceptor pairs in an inhomogeneous ensemble of dye molecules. As explained in Sect. 5.1, at

the main-band excitation we have the “directed transfer” resulting in the shift of fluorescence spectra to longer wavelengths. The dyes excited in the Red-Edge conditions possess an excitation energy lower than the mean in this ensemble and the probability of their serving as donors is low.

Finally, it should be noted that homo-FRET, which is just the exchange of energies between the same dyes, is undetected by common spectroscopic or lifetime measurements and needs the “hetero-FRET probing” for its detection. The Red-Edge effect allows the easy distinguishing of the decrease of anisotropy due to FRET (static effect) from that occurring due to rotational freedom of fluorophores (dynamic effect), which does not depend on excitation wavelength.

6 Collective Effects in Nanocomposites

The design of fluorescent nanocomposites is a broad area of research and development. Different combinations of materials, including semiconductor nanocrystals, luminescent complexes of lanthanoids, and conjugated polymers can be chosen for the development of advanced reporters. The combination of organic dyes with other luminescent materials allows providing many improvements in sensing technologies, especially because organic dyes are much more “responsive”, but they are often behind these emitters in photostability, lifetime, and brightness. Two illustrations of these new possibilities are presented below.

6.1 FRET Modulation of Reporter Lifetime

In a donor–acceptor system connected by FRET, the donor lifetime determines the lifetime of the acceptor [70], which follows from the kinetic scheme of this reaction [71]. This fact has serious practical implications. Since the energy transfer occurs during the lifetime of the donor, its proper choice (e.g., as luminescent lanthanide complexes) allows increasing dramatically in the acceptor lifetime compared to the lifetime observed on direct excitation. The long lifetimes allows extending in the time window for the observation of decays and application of simple instruments for their recording. This provides a simple approach to discriminating the directly excited short-lived emission of the acceptor and the background fluorescence in the time domain [72].

With the choice of Quantum Dots as FRET donors [73, 74], the efficiency of the fluorescence response can be optimized in different directions. These emitters exhibit a very high degree of brightness that produces a strong antenna effect, the ability to modulate the emission wavelength within the same material by variation of particle sizes (for wavelength converting), and the lifetimes of $\sim 10^{-8}$ s, which are typically longer than those of organic dyes. They display excellent

photostability. Conjugated polymers [75] being used as FRET donors also offer advanced properties, such as high brightness and superquenching ability.

In the designed nanocomposites, the organic dyes are expected to maintain their role as FRET acceptors. This is due to their small size and the well developed chemistry of their covalent attachment to any molecular unit [76]. In this role, they keep their strong advantage over other emitters, offering a variety of possibilities of providing fluorescence reporting in intensity, lifetime, anisotropy and, especially, spectroscopic changes.

6.2 Plasmonic Enhancement

The spectral properties of fluorophores can be dramatically altered by the near-field (subwavelength distance) interactions with the free electrons present in metals. The presence of electron clouds in a metallic structure can alter the optical properties of a molecule by increasing the excitation field and by modifying the radiative and nonradiative decay mechanisms [77, 78]. It can be seen that on this interaction the emission lifetime, τ_R , decreases, whereas the quantum yield, Φ , increases, contrary to the commonly expected decrease [78]. This increase, by 1–2 orders of magnitude, is significant, so it can convert weak fluorescence emitters into good ones. This fact can be of great practical significance.

The generality of this phenomenon observed on metallic nanoparticles (especially those composed of silver, gold, and copper) is also important. The interaction with metal nanoparticles produces emission enhancement of not only organic dyes but also Quantum Dots [79, 80], conjugated polymers [81], and metal-chelator luminophores [82]. It is characteristic of not only fluorescence but also phosphorescence and chemiluminescence. In organic dyes, photostability is increased by decreasing the lifetime. It dramatically influences the FRET efficiency in a donor–acceptor system made of organic dyes adsorbed on silver or gold nano-island films [83].

Much effort has been made to establish the optimum distance between the dye and the surface of the metal particle. If fluorescence from a molecule or nanoparticle is directly adsorbed onto the surface of a metallic particle, it is strongly quenched due to electron transfer, and if the distance is too large, the enhancement effect has again to vanish; there should, therefore, be an optimal distance for the observation of the enhancement effect. Based on experiments with organic dyes [84, 85] and Quantum Dots [80], this distance should be 5–10 nm.

The optimal enhancement effect is observed when the localized surface plasmon resonance is tuned to the emission wavelength of a locally situated fluorophore [86]. This is consistent with the model suggesting a greatly increased efficiency for energy transfer from fluorophores to surface plasmons [78]. Since resonance energy transfer is involved, the important factors affecting the intensity of fluorescence emission must also be the orientation of the dye dipole moments relative to the

normal metal surface and the overlap of the absorption and emission bands of the dye with the plasmon band of the metal.

An immense variety of potentially useful nanocomposites can be constructed exhibiting enhanced emission.

7 Realization of Collective Effects in Sensing and Imaging Technologies

In conventional fluorescence sensor techniques, single dye molecules are used as reporters. The introduction of supramolecular structures containing multiple dyes can increase the output signal and thus achieve lower limits of detection. A convenient technique to create these structures is to produce nanoparticles of inorganic [8] and organic [7] polymer origin that are “soaked” with dyes. There may be different additional benefits of such incorporation, such as the isolation of the dyes from molecular contact with the test medium and protection against perturbation of their properties. The possibility that the degradation of dyes in aggressive media and in living cells may be avoided is also important. The dyes usually exhibit much higher fluorescence intensity, quantum yield, and lifetime in solid environments than in liquid media. This is due to the stronger restrictions imposed by a solid matrix on the rotation of dye segments, intermolecular collisions, and dielectric relaxations – all the factors that quench fluorescence. Porosity of nanoparticles is another property that can be modulated and optimized. The larger surface of nanoparticles may allow the attachment of several functional units – instead of one – that can allow facile bioconjugation, immobilization, and incorporation into various assays. Additional benefits can be gained with the exploration of the collective effects described above. They can include:

- Shifting of wavelength by engineering the local environment of dye molecules, their complexation, and directed homo-FRET.
- Selection of the most convenient excitation wavelength and shifting of wavelength in a broader range using cascade hetero-FRET.
- Engineering the rigidity of the dye environment and switching off the homo-FRET by variation of the excitation wavelength due to Red-Edge effect.
- Superenhancement due to light harvesting in FRET and plasmonic effects and superquenching due to homo-FRET with the participation of a quencher.

7.1 *Collective Effects in Sensing*

To determine many analytes simultaneously in solutions, the nanoparticles or larger microspheres carrying particular sensors should be recognizable in their mixtures by distinct spectroscopic properties [87]. This allows the mixing of the uniquely

optically encoded particles and the detection of the binding of specific analytes to each of their diverse types. Such *suspension arrays* may contain several thousand types of sensor particles. Dyes (and nanoparticles) emitting at different wavelengths may serve for constructing these barcodes. The composing dyes can emit individually forming the composite spectrum, but additional possibilities emerge when they are incorporated in different proportions into silica particles and coupled by FRET cascade reaction [88].

The particles with incorporated dye compositions allow excitation at a single wavelength (of the donor), and their recognition by different colors of fluorescence emission is provided by the acceptors. In theory, six colors at six different intensities should provide nearly 40,000 unique codes [87]. In practice, it is hard to achieve such values in view of spectral overlaps between the dyes and variability of fluorescence intensities introduced both on the production and reading steps. In this respect, Quantum Dots have much better prospects than organic dyes because they possess much narrower spectra covering the whole visible range, they can be excited by a single wavelength, and in addition, they exhibit higher photostability [89]. Employing them as FRET donors and organic dyes as acceptors allows realizing many new possibilities [90].

7.2 *Collective Effects in Imaging*

In cellular research, fluorescence microscopy is the technique that is the most frequently used in three cases: (1) analysis of the proximity and interaction of macromolecules and structural elements [91, 92], (2) quantitative detection and analysis of the distribution of analyzed metabolites and exogenic compounds [93], and (3) spatiotemporal recording of the dynamics of metabolites, including cellular signaling [92, 94, 95]. The studies in all three directions were stimulated by the introduction of new powerful tools, green fluorescent protein (GFP) and its relatives, which produce different colors of emission [96, 97] and also the means for specific intracellular labeling with organic dyes [97–99]. In this endeavor, the designed nanocomposites have found their own role. With the selection of materials and their composition, all means of spectral-resolution [100], time-resolved [101] and polarization [102] microscopy, and combinations of these methods [103–105] can be used.

Homo-FRET is a useful tool to study the interactions in living cells that can be detected by the decrease in anisotropy [106, 107]. Since commonly the donor and acceptor dipoles are not perfectly aligned in space, the energy transfer results in depolarization of acceptor emission. Imaging in polarized light can be provided both in confocal and time-resolved microscopies. However, a decrease of steady-state anisotropy can be observed not only due to homo-FRET, but also due to rotation of the fluorescence emitter. The only possibility of discriminating them in an unknown system is to use the variation of excitation wavelength and apply the

analysis of the Red-Edge effects [45]. Such a possibility was demonstrated in a designed version of polarization microscopy that uses a combination of the main-band and red-edge excitation in the construction of cell images for enhanced green fluorescent protein [108].

An example of the development of intracellular pH-sensors shows the prospects of coupling their response with different sensing events by using bichromophoric and similar constructions [109]. The necessary signal can be provided by different dyes that display pH-dependent changes in absorption spectra due to their transition between protonated and deprotonated forms [110, 111]. The large spectral separation and high emission intensities in the visible of these forms allow modulating the overlap integral [112]. The pair of Quantum Dot (donor) and organic dye (acceptor) are optimal in this application [113]. The application of dye-concentrated organically modified silica nanoparticles using the effect of homo-FRET makes it possible to achieve a strongly amplified collective response [114].

8 Concluding Remarks

Fluorescence is the basic reporting technique in many chemical sensors and biosensors. We observe that the properties of reporters and the range of their applications can be dramatically enhanced with the introduction of new materials of different composition. They can be organic dyes incorporated into nanoscale particles and more sophisticated supramolecular structures containing these dyes together with lanthanide chelates, Quantum Dots, metal nanoclusters, etc. [2]. Different intermolecular interactions contribute to new properties of these species. Among them are the effects observed with organic dyes trapped in confined media (e.g., polymer nanoparticles) at high concentrations. In addition to the effects of polarity, H-bonding, and excited-state reactions that are observed in free monomeric forms, there appear the effects of multiple excited-state energy transfer between the emitters. These collective properties go beyond the simple distance-dependent interactions between two dyes as described in textbooks – they lead to new spectroscopic effects. Monitoring some of them is possible by variation of the excitation wavelength (the Red-Edge effects). Regarding the sensor design, these collective effects can be both negative (e.g., formation of nonfluorescent dimers and concentrational quenching) and strongly positive (superquenching, wavelength-shifting, and light-harvesting). Their knowledge and the ability to apply them provides the researcher very powerful tools for further development of sensing and imaging technologies that are very necessary in clinical diagnostics [115], environment monitoring [116], agriculture and food safety control [117], detection of biological warfare agents [118], and in different industries.

References

1. Valeur B (2002) *Molecular fluorescence*. Wiley VCH, Weinheim
2. Demchenko AP (2009) *Introduction to fluorescence sensing*. Springer, Amsterdam
3. Resch-Genger U, Grabolle M, Nitschke R, Nann T, Resch-Genger U, Grabolle M, Nitschke R, Nann T (2010) Nanocrystals and nanoparticles vs. molecular fluorescent labels as reporters for bioanalysis and the life sciences. A critical comparison. In: Demchenko AP (ed) *Advanced fluorescence reporters in chemistry and biology*. II. Springer Ser Fluoresc 9:3–40
4. Patsenker LD, Tatarts AL, Terpetschnig EA (2010) Long-wavelength probes and labels based on cyanines and squaraines. In: Demchenko AP (ed) *Advanced fluorescence reporters in chemistry and biology*. I. Springer Ser Fluoresc 8:65–104
5. Przhonska OV, Scott Webster S, Padilha LA, Hu H, Kachkovski AD, Hagan DJ, Stryland EW V (2010) Two-photon absorption in near-IR conjugated molecules: design strategy and structure–property relations. In: Demchenko AP (ed) *Advanced fluorescence reporters in chemistry and biology*. I. Springer Ser Fluoresc 8:105–147
6. Kim E, Park SB (2010) Discovery of New Fluorescent Dyes: targeted Syn-thesis or combinatorial approach? In: Demchenko AP (ed) *Advanced fluorescence reporters in chemistry and biology*. I. Springer Ser Fluoresc 8:149–186
7. Borisov SM, Mayr T, Mistlberger G, Klimant I (2010) Dye-doped polymeric particles for sensing and imaging. In: Demchenko AP (ed) *Advanced fluorescence reporters in chemistry and biology*. II. Springer Ser Fluoresc 9:193–228
8. Liang S, John CL, Xu S, Chen J, Jin Y, Yuan Q, Tan W, Zhao JX (2010) Silica-based nanoparticles: design and properties. In: Demchenko AP (ed) *Advanced fluorescence reporters in chemistry and biology*. II. Springer Ser Fluoresc 9:229–251
9. Yao H (2010) Prospects for organic dye nanoparticles. In: Demchenko AP (ed) *Advanced fluorescence reporters in chemistry and biology*. II. Springer Ser Fluoresc 9:285–303
10. Suppan P, Ghoneim N (1997) *Solvatochromism*. Royal Society of Chemistry, Cambridge
11. Bakhshiev NG (1972) *Spectroscopy of intermolecular interactions*. Nauka, Leningrad
12. Mataga N, Kubota T (1970) *Molecular interactions and electronic spectra*. Marcel Dekker, New York
13. Tomin VI (2010) Physical principles behind spectroscopic response of organic fluorophores to intermolecular interactions. In: Demchenko AP (ed) *Advanced fluorescence reporters in chemistry and biology*. I. Springer Ser Fluoresc 8:189–223
14. Liptay W (1969) Electrochromism and solvatochromism. *Angew Chem Int Ed* 8:177–188
15. Callis PR (2010) Electrochromism and solvatochromism in fluorescence response of organic dyes. A nanoscopic view. In: Demchenko AP (ed) *Advanced fluorescence reporters in chemistry and biology*. I. Springer Ser Fluoresc 8:309–330
16. Maroncelli M, Macinnis J, Fleming GR (1989) Polar solvent dynamics and electron-transfer reactions. *Science* 243:1674–1681
17. Hsieh C-C, Ho M-L, Chou P-T (2010) Organic dyes with excited-state transformations (electron, charge and proton transfers). In: Demchenko AP (ed) *Advanced fluorescence reporters in chemistry and biology*. I. Springer Ser Fluoresc 8:225–266
18. Wang S-L, Lee T-C, Ho T-I (2002) Excited state proton transfer and steric effect on the hydrogen bonding interaction of the styrylquinoline system. *J Photochem Photobiol A Chem* 151:21–26
19. Druzhinin SI, Kovalenko SA, Senyushkina TA, Demeter A, Januskevicius R, Mayer P, Stalke D, Machinek R, Zachariasse KA (2009) Intramolecular charge transfer with 4-fluorofluorazene and the flexible 4-fluoro-N-phenylpyrrole. *J Phys Chem A* 113:9304–20
20. Jozefowicz M, Heldt JR (2003) Preferential solvation of fluorenone and 4-hydroxyfluorenone in binary solvent mixtures. *Chem Phys* 294:105–116

21. Pivovarenko VG, Klueva AV, Doroshenko AO, Demchenko AP (2000) Bands separation in fluorescence spectra of ketocyanine dyes: evidence for their complex formation with monohydric alcohols. *Chem Phys Lett* 325:389–398
22. Shynkar VV, Klymchenko AS, Piemont E, Demchenko AP, Mely Y (2004) Dynamics of intermolecular hydrogen bonds in the excited states of 4'-dialkylamino-3-hydroxyflavones. On the pathway to an ideal fluorescent hydrogen bonding sensor. *J Phys Chem A* 108:8151–8159
23. Balter A, Nowak W, Pawelkiewicz W, Kowalczyk A (1988) Some remarks on the interpretation of the spectral properties of prodan. *Chem Phys Lett* 143:565–570
24. Catalan J, Perez P, Laynez J, Garcia-Blanco F (1991) Analysis of the solvent effect on the photophysics properties of 6-propionyl-2-(dimethylamino)naphthalene (PRODAN). *J Fluoresc* 4:215–223
25. Moyano F, Biasutti MA, Silber JJ, Correa NM (2006) New insights on the behavior of PRODAN in homogeneous media and in large unilamellar vesicles. *J Phys Chem B* 110:11838–11846
26. Yuan MS, Liu ZQ, Fang Q (2007) Donor-and-acceptor substituted truxenes as multifunctional fluorescent probes. *J Org Chem* 72:7915–22
27. Yang CJ, Jockusch S, Vicens M, Turro NJ, Tan W (2005) Light-switching excimer probes for rapid protein monitoring in complex biological fluids. *Proc Natl Acad Sci USA* 102:17278–83
28. Kadirvel M, Arsic B, Freeman S, Bichenkova EV (2008) Exciplex and excimer molecular probes: detection of conformational flip in a myo-inositol chair. *Org Biomol Chem* 6:1966–72
29. Deepak VD, Asha SK (2009) Photophysical investigation into the self-organization in pyrene-based urethane methacrylate comb polymer. *J Phys Chem B* 113:11887–97
30. Taniguchi T, Takeuchi N, Kobaru S, Nakahira T (2008) Preparation of highly monodisperse fluorescent polymer particles by miniemulsion polymerization of styrene with a polymerizable surfactant. *J Colloid Interface Sci* 327:58–62
31. Búcsiová L, Hrdlovič P, Chmela S (2001) Spectral characteristics of fluorescence probes based on pyrene in solution and in polymer matrix. *J Photochem Photobiol A Chem* 143:59–68
32. Kim Y, Bouffard J, Kooi SE, Swager TM (2005) Highly emissive conjugated polymer excimers. *J Am Chem Soc* 127:13726–31
33. Bhattacharyya K, Chowdhury M (1993) Environmental and magnetic field effects on exciplex and twisted charge transfer emission. *Chem Rev* 93:507–535
34. Bichenkova EV, Gbaj A, Walsh L, Savage HE, Rogert C, Sardarian AR, Etchells LL, Douglas KT (2007) Detection of nucleic acids in situ: novel oligonucleotide analogues for target-assembled DNA-mounted exciplexes. *Org Biomol Chem* 5:1039–51
35. Kasha M, Kasha M (1991) Energy transfer, charge transfer, and proton transfer in molecular composite systems. *Basic Life Sci* 58:231–251, discussion 251–255
36. Madjet Mel A, Muh F, Renger T (2009) Deciphering the influence of short-range electronic couplings on optical properties of molecular dimers: application to “special pairs” in photosynthesis. *J Phys Chem B* 113:12603–14
37. Ishizaki A, Fleming GR (2009) Unified treatment of quantum coherent and incoherent hopping dynamics in electronic energy transfer: reduced hierarchy equation approach. *J Chem Phys* 130:234111
38. Saini S, Srinivas G, Bagchi B (2009) Distance and orientation dependence of excitation energy transfer: from molecular systems to metal nanoparticles. *J Phys Chem B* 113:1817–32
39. Clapp AR, Medintz IL, Mattoussi H (2006) Forster resonance energy transfer investigations using quantum-dot fluorophores. *Chemphyschem* 7:47–57

40. Nemkovich NA, Rubinov AN, Tomin VI (1991) Inhomogeneous broadening of electronic spectra of dye molecules in solutions. In: Lakowicz JR (ed) *Topics in fluorescence spectroscopy*. Plenum, New York, pp 367–428
41. Demchenko AP, Sytnik AI (1991) Site-selectivity in excited-state reactions in solutions. *J Phys Chem* 95:10518–10524
42. Vincent M, Gallay J, Demchenko AP (1995) Solvent relaxation around the excited-state of indole – analysis of fluorescence lifetime distributions and time-dependence spectral shifts. *J Phys Chem* 99:14931–14941
43. Nemkovich NA, Rubinov AN, Tomin VI (1981) Kinetics of luminescence spectra of rigid dye solutions due to directed electronic-energy transfer. *J Lumin* 23:349–361
44. Demchenko AP (2008) Site-selective red-edge effects. Chapter 4. *Methods in enzymology*. Academic, New York, pp 59–78
45. Demchenko AP (2002) The red-edge effects: 30 years of exploration. *Luminescence* 17:19–42
46. Chattopadhyay A, Mukherjee S, Raghuraman H (2002) Reverse micellar organization and dynamics: a wavelength-selective fluorescence approach. *J Phys Chem B* 106:13002–13009
47. Demchenko AP (1986) *Ultraviolet spectroscopy of proteins*. Springer Verlag, Berlin, Heidelberg, New York
48. Haldar S, Chattopadhyay A (2007) Dipolar relaxation within the protein matrix of the green fluorescent protein: a red-edge excitation shift study. *J Phys Chem B* 111:14436–9
49. Barja BC, Chesta C, Atvars TD, Aramendia PF (2005) Relaxations in poly(vinyl alcohol) and in poly(vinyl acetate) detected by fluorescence emission of 4-aminophthalimide and prodan. *J Phys Chem B* 109:16180–7
50. Dias FB, King S, Monkman AP, Perepichka II, Kryuchkov MA, Perepichka IF, Bryce MR (2008) Dipolar stabilization of emissive singlet charge transfer excited states in polyfluorene copolymers. *J Phys Chem B* 112:6557–66
51. Irimpan L, Krishnan B, Deepthy A, Nampoorei VPN, Radhakrishnan P (2007) Excitation wavelength dependent fluorescence behaviour of nano colloids of ZnO. *J Phys D Appl Phys* 40:5670–5674
52. Johansson MK, Cook RM (2003) Intramolecular dimers: a new design strategy for fluorescence-quenched probes. *Chemistry* 9:3466–3471
53. Runnels LW, Scarlata SF (1995) Theory and application of fluorescence homotransfer to melittin oligomerization. *Biophys J* 69:1569–83
54. Varnavski OP, Ostrowski JC, Sukhomlinova L, Twieg RJ, Bazan GC, Goodson T (2002) Coherent effects in energy transport in model dendritic structures investigated by ultrafast fluorescence anisotropy spectroscopy. *J Am Chem Soc* 124:1736–1743
55. Serin JM, Brousmiche DW, Frechet JMJ (2002) Cascade energy transfer in a conformationally mobile multichromophoric dendrimer. *Chem Commun* 21:2605–2607
56. Haustein E, Jahnz M, Schwillle P (2003) Triple FRET: a tool for studying long-range molecular interactions. *Chemphyschem* 4:745–8
57. Ziessel R, Goze C, Ulrich G, Cesario M, Retailleau P, Harriman A, Rostron JP (2005) Intramolecular energy transfer in pyrene-bodipy molecular dyads and triads. *Chemistry* 11:7366–78
58. Harriman A, Mallon L, Ziessel R (2008) Energy flow in a purpose-built cascade molecule bearing three distinct chromophores attached to the terminal acceptor. *Chemistry* 14:11461–73
59. Gao J, Strassler C, Tahmassebi D, Kool ET (2002) Libraries of composite polyfluors built from fluorescent deoxyribosides. *J Am Chem Soc* 124:11590–1
60. Huang B, Wu HK, Bhaya D, Grossman A, Granier S, Kobilka BK, Zare RN (2007) Counting low-copy number proteins in a single cell. *Science* 315:81–84

61. Szollosi J, Damjanovich S, Matyus L (1998) Application of fluorescence resonance energy transfer in the clinical laboratory: routine and research. *Cytometry* 34:159–79
62. Wang S, Gaylord BS, Bazan GC (2004) Fluorescein provides a resonance gate for FRET from conjugated polymers to DNA intercalated dyes. *J Am Chem Soc* 126:5446–51
63. Aneja A, Mathur N, Bhatnagar PK, Mathur PC (2008) Triple-FRET technique for energy transfer between conjugated polymer and TAMRA dye with possible applications in medical diagnostics. *J Biol Phys* 34:487–93
64. Chen CH, Liu KY, Sudhakar S, Lim TS, Fann W, Hsu CP, Luh TY (2005) Efficient light harvesting and energy transfer in organic–inorganic hybrid multichromophoric materials. *J Phys Chem B* 109:17887–91
65. Frigoli M, Ouadahi K, Larpent C (2009) A cascade FRET-mediated ratiometric sensor for Cu²⁺ ions based on dual fluorescent ligand-coated polymer nanoparticles. *Chemistry* 15:8319–30
66. Forde TS, Hanley QS (2005) Following FRET through five energy transfer steps: spectroscopic photobleaching, recovery of spectra, and a sequential mechanism of FRET. *Photochem Photobiol Sci* 4:609–616
67. May V (2009) Beyond the Forster theory of excitation energy transfer: importance of higher-order processes in supramolecular antenna systems. *Dalton Trans* 45:10086–105
68. Beljonne D, Curutchet C, Scholes GD, Silbey RJ (2009) Beyond Forster resonance energy transfer in biological and nanoscale systems. *J Phys Chem B* 113:6583–99
69. Jameson DM, Croney JC (2003) Fluorescence polarization: past, present and future. *Comb Chem High Throughput Screen* 6:167–73
70. Hildebrandt N, Charbonniere LJ, Lohmannsroben HG (2007) Time-resolved analysis of a highly sensitive Forster resonance energy transfer immunoassay using terbium complexes as donors and quantum dots as acceptors. *J Biomed Biotechnol* 2007:79169
71. Charbonniere LJ, Hildebrandt N, Ziessel RF, Lohmannsroben HG (2006) Lanthanides to quantum dots resonance energy transfer in time-resolved fluoro-immunoassays and luminescence microscopy. *J Am Chem Soc* 128:12800–9
72. Morrison LE (1988) Time-resolved detection of energy transfer: theory and application to immunoassays. *Anal Biochem* 174:101–20
73. Algar WR, Krull UJ (2008) Quantum dots as donors in fluorescence resonance energy transfer for the bioanalysis of nucleic acids, proteins, and other biological molecules. *Anal Bioanal Chem* 391:1609–18
74. Medintz IL, Mattoussi H (2009) Quantum dot-based resonance energy transfer and its growing application in biology. *Phys Chem Chem Phys* 11:17–45
75. Thomas SW 3rd, Joly GD, Swager TM (2007) Chemical sensors based on amplifying fluorescent conjugated polymers. *Chem Rev* 107:1339–86
76. Kikuchi K, Takakusa H, Nagano T (2004) Recent advances in the design of small molecule-based FRET sensors for cell biology. *Trends Analyt Chem* 23:407–415
77. Lakowicz JR (2005) Radiative decay engineering 5: metal-enhanced fluorescence and plasmon emission. *Anal Biochem* 337:171–94
78. Aslan K, Gryczynski I, Malicka J, Matveeva E, Lakowicz JR, Geddes CD (2005) Metal-enhanced fluorescence: an emerging tool in biotechnology. *Curr Opin Biotechnol* 16:55–62
79. Gryczynski I, Malicka J, Jiang W, Fischer H, Chan WCW, Gryczynski Z, Grudzinski W, Lakowicz JR (2005) Surface-plasmon-coupled emission of quantum dots. *J Phys Chem B* 109:1088–1093
80. Lee SY, Nakaya K, Hayashi T, Hara M (2009) Quantitative study of the gold-enhanced fluorescence of CdSe/ZnS nanocrystals as a function of distance using an AFM probe. *Phys Chem Chem Phys* 11:4403–9
81. Park HJ, Vak D, Noh YY, Lim B, Kim DY (2007) Surface plasmon enhanced photoluminescence of conjugated polymers. *Appl Phys Lett* 90:161107

82. Zhang YX, Aslan K, Prevote MJR, Malyn SN, Geddes CD (2006) Metal-enhanced phosphorescence: Interpretation in terms of triplet-coupled radiating plasmons. *J Phys Chem B* 110:25108–25114
83. Giorgetti E, Cicchi S, Muniz-Miranda M, Margheri G, Del Rosso T, Giusti A, Rindi A, Ghini G, Sottini S, Marcelli A, Foggi P (2009) Forster resonance energy transfer (FRET) with a donor–acceptor system adsorbed on silver or gold nanoisland films. *Phys Chem Chem Phys* 11:9798–803
84. Tovmachenko OG, Graf C, van den Heuvel DJ, van Blaaderen A, Gerritsen HC (2006) Fluorescence enhancement by metal-core/silica-shell nanoparticles. *Adv Mater* 18:91–95
85. Malicka J, Gryczynski I, Gryczynski Z, Lakowicz JR (2003) Effects of fluorophore-to-silver distance on the emission of cyanine-dye-labeled oligonucleotides. *Anal Biochem* 315:57–66
86. Cade NI, Ritman-Meer T, Kwaka K, Richards D (2009) The plasmonic engineering of metal nanoparticles for enhanced fluorescence and Raman scattering. *Nanotechnology* 20:285201
87. Wilson R, Cossins AR, Spiller DG (2006) Encoded microcarriers for high-throughput multiplexed detection. *Angew Chem Int Ed Engl* 45:6104–17
88. Ma Q, Wang XY, Li YB, Shi YH, Su XG (2007) Multicolor quantum dot-encoded microspheres for the detection of biomolecules. *Talanta* 72:1446–1452
89. Eastman PS, Ruan WM, Doctolero M, Nuttall R, De Feo G, Park JS, Chu JSF, Cooke P, Gray JW, Li S, Chen FQF (2006) Qdot nanobarcode for multiplexed gene expression analysis. *Nano Lett* 6:1059–1064
90. Clapp AR, Medintz IL, Uyeda HT, Fisher BR, Goldman ER, Bawendi MG, Mattoussi H (2005) Quantum dot-based multiplexed fluorescence resonance energy transfer. *J Am Chem Soc* 127:18212–18221
91. Sekar RB, Periasamy A (2003) Fluorescence resonance energy transfer (FRET) microscopy imaging of live cell protein localizations. *J Cell Biol* 160:629–33
92. Umezawa Y (2005) Genetically encoded optical probes for imaging cellular signaling pathways. *Biosens Bioelectron* 20:2504–11
93. Miyawaki A (2003) Fluorescence imaging of physiological activity in complex systems using GFP-based probes. *Curr Opin Neurobiol* 13:591–6
94. Xu X, Brzostowski JA, Jin T (2006) Using quantitative fluorescence microscopy and FRET imaging to measure spatiotemporal signaling events in single living cells. *Methods Mol Biol* 346:281–96
95. Miyawaki A (2003) Visualization of the spatial and temporal dynamics of intracellular signaling. *Dev Cell* 4:295–305
96. Miyawaki A, Nagai T, Mizuno H (2005) Engineering fluorescent proteins. *Adv Biochem Eng Biotechnol* 95:1–15
97. Giepmans BNG, Adams SR, Ellisman MH, Tsien RY (2006) Review – The fluorescent toolbox for assessing protein location and function. *Science* 312:217–224
98. Adams SR, Campbell RE, Gross LA, Martin BR, Walkup GK, Yao Y, Llopis J, Tsien RY (2002) New biarsenical ligands and tetracysteine motifs for protein labeling in vitro and in vivo: synthesis and biological applications. *J Am Chem Soc* 124:6063–6076
99. Guignat EG, Hovius R, Vogel H (2004) Reversible site-selective labeling of membrane proteins in live cells. *Nat Biotechnol* 22:440–444
100. Zimmermann T, Rietdorf J, Pepperkok R (2003) Spectral imaging and its applications in live cell microscopy. *FEBS Lett* 546:87–92
101. van Munster EB, Gadella TW (2005) Fluorescence lifetime imaging microscopy (FLIM). *Adv Biochem Eng Biotechnol* 95:143–75
102. Piston DW, Rizzo MA (2008) FRET by fluorescence polarization microscopy. *Methods Cell Biol* 85:415–30
103. Yan L, Rueden CT, White JG, Eliceiri KW (2006) Applications of combined spectral lifetime microscopy for biology. *Biotechniques* 41:249, 251, 253 passim

104. Bird DK, Eliceiri KW, Fan CH, White JG (2004) Simultaneous two-photon spectral and lifetime fluorescence microscopy. *Appl Opt* 43:5173–82
105. Fisz JJ (2009) Another treatment of fluorescence polarization microspectroscopy and imaging. *J Phys Chem A* 113:3505–16
106. Tramier M, Coppey-Moisan M (2008) Fluorescence anisotropy imaging microscopy for homo-FRET in living cells. *Methods Cell Biol* 85:395–414
107. Bader AN, Hofman EG, Voortman J, en Henegouwen PM, Gerritsen HC (2009) Homo-FRET imaging enables quantification of protein cluster sizes with subcellular resolution. *Biophys J* 97:2613–22
108. Squire A, Verveer PJ, Rocks O, Bastiaens PI (2004) Red-edge anisotropy microscopy enables dynamic imaging of homo-FRET between green fluorescent proteins in cells. *J Struct Biol* 147:62–9
109. Alamiry MAH, Harriman A, Mallon LJ, Ulrich G, Ziessel R (2008) Energy- and charge-transfer processes in a perylene–BODIPY–pyridine tripartite array. *Eur J Org: Chem* 16:2774–2782
110. Yao S, Schafer-Hales KJ, Belfield KD (2007) A new water-soluble near-neutral ratiometric fluorescent pH indicator. *Org Lett* 9:5645–8
111. Povrozin YA, Markova LI, Tatarets AL, Sidorov VI, Terpetschnig EA, Patsenker LD (2009) Near-infrared, dual-ratiometric fluorescent label for measurement of pH. *Anal Biochem* 390:136–40
112. Takakusa H, Kikuchi K, Urano Y, Kojima H, Nagano T (2003) A novel design method of ratiometric fluorescent probes based on fluorescence resonance energy transfer switching by spectral overlap integral. *Chemistry* 9:1479–85
113. Snee PT, Somers RC, Nair G, Zimmer JP, Bawendi MG, Nocera DG (2006) A ratiometric CdSe/ZnS nanocrystal pH sensor. *J Am Chem Soc* 128:13320–1
114. Kim S, Pudavar HE, Prasad PN (2006) Dye-concentrated organically modified silica nanoparticles as a ratiometric fluorescent pH probe by one- and two-photon excitation. *Chem Commun (Camb)* 19:2071–2073
115. Andreescu S, Sadik OA (2004) Trends and challenges in biochemical sensors for clinical and environmental monitoring. *Pure Appl Chem* 76:861–878
116. Riu J, Maroto A, Rius FX (2006) Nanosensors in environmental analysis. *Talanta* 69:288–301
117. Patel PD (2002) (Bio)sensors for measurement of analytes implicated in food safety: a review. *Trac-Trends Analyt Chem* 21:96–115
118. Gooding JJ (2006) Biosensor technology for detecting biological warfare agents: Recent progress and future trends. *Anal Chim Acta* 559:137–151

Part II
Encapsulated Dyes and
Supramolecular Constructions

Fluorescent J-Aggregates and Their Biological Applications

Mykhaylo Yu. Losytskyy and Valeriy M. Yashchuk

Abstract J-aggregates are stable fluorescent structures formed by a number of small molecules noncovalently. These structures can be formed not only in solution but also on biological objects that act as templates. As association of these small molecules leads to drastic changes in their spectral properties, this phenomenon can in principle be used for the detection of biological structures that induce the aggregation. Here, the photophysical properties of J-aggregates formed in different media and, particularly on attachment to the objects of biological origin, such as nucleic acids, proteins, and biomembranes, are discussed.

Keywords Biomembrane · DNA · Fluorescent detection · J-aggregate · Protein

Contents

1	Introduction	136
2	Molecular Aggregates and Their Spectroscopic Properties	136
3	Aggregation in Water Solutions	139
4	Biomembrane-Induced Dye Aggregation	143
5	J-Aggregates Formed on DNA	146
6	Proteins as the Templates for Aggregate Formation	151
7	Membrane Potential-Sensitive Aggregates of the Dyes JC-1 and JC-9 for Mitochondria Imaging	154
8	Possibilities of Application of J-Aggregates in Fluorescent Detection and Testing of the Objects of Biological Origin	155
	References	155

M.Y. Losytskyy and V.M. Yashchuk (✉)

Department of Physics, r.258, Kyiv Taras Shevchenko National University, Volodymyrs'ka St. 64, 01601 Kyiv, Ukraine
e-mail: valeriyya@yahoo.com

1 Introduction

The dyes exhibiting response manifested in change in one or several parameters of their fluorescence spectrum (quantum yield, maximum wavelength, excited state lifetime, etc.) are widely used in sensing. This response can be caused by various reasons. Here, one kind of dye response will be discussed, i.e., the formation of their associates or aggregates that often leads to drastic changes in the spectroscopic properties.

2 Molecular Aggregates and Their Spectroscopic Properties

Molecular aggregates are the stable structures formed by a number of molecules noncovalently, i.e., by van der Waals, hydrophobic, and Coulombic interactions. The effect of such assembling of several identical molecules into an associate strongly depends on several factors, first of all on the interaction energy. This dependence could be understood in the terms of the exciton theory, developed by Frenkel [1, 2] and then by Davydov [3], that describes the structure of energy levels of the infinite crystal based on one molecule in an elementary cell. If we consider the energy of intermolecular interaction in an aggregate to be much smaller than that of the intramolecular one, we could regard the wave function of the aggregate to be equal to the product of wave functions of the molecules, and the intermolecular interaction energy as the small perturbation of the internal energy of the molecules. Then, the Schrödinger equation applied for the ground and excited states of an aggregate gives the energy of these states, the difference of which equals to

$$\Delta E_f(\vec{k}) = \Delta \varepsilon_f + D_f + L_f(\vec{k}).$$

$\Delta \varepsilon_f$ being the difference between the energies of ground and excited states of a monomer molecule, D_f accounts for the change in the energy of the molecule's interaction with its neighbors upon excitation, and

$$L_f(\vec{k}) = \sum_{m,m \neq n} M_{nm}^f \times e^{i\vec{k}(\vec{n}-\vec{m})}.$$

\vec{n} and \vec{m} determine the positions of n -th and m -th molecules, and M_{nm}^f is the matrix element describing the excitation transfer from the n -th molecule to the m -th one:

$$M_{nm}^f = \int \phi_n^{*o} \phi_m^{*f} V_{nm} \phi_m^o \phi_n^f d\tau$$

where ϕ_n^o , ϕ_m^o , ϕ_n^f and ϕ_m^f are the wave functions of n -th and m -th molecules in the ground and excited states, respectively, V_{nm} is the operator of n -th and m -th molecules interaction energy, and $d\tau$ is the elementary volume. If the one-dimensional

aggregate with the infinite number of molecules is regarded, and the interaction is restricted to the neighbor molecules, i.e., m equals to either $n - 1$ or $n + 1$, then

$$L_f(k) = 2M^f \cos(ka)$$

where $M^f = M^f_{n,n+1} = M^f_{n-1,n}$, a is the lattice distance, and k is the wavenumber. Thus, the level of the aggregate electronic excitation becomes split for N levels, N being the number of the molecules in an aggregate. The energy of the aggregate excitation $\Delta E_f(k)$ is thus varied between $\Delta \epsilon_f + D_f - 2M^f$ and $\Delta \epsilon_f + D_f + 2M^f$ (Fig. 1). Consider the case when $2M^f \gg \Delta E_v$, where ΔE_v is the vibronic bandwidth of the single molecule absorption transition; it nearly equals to the half-width of the molecule absorption spectrum (“strong-coupling” in the Simpson and Peterson classification [4, 5]). In this case, the time of excitation transfer is much smaller than the time of the excitation relaxation to the lower vibrational levels. On such condition, the phase correlation of the transferred excitation does not disappear, and the aggregate could be regarded as a number of cooperatively “oscillating” molecules. In other words, the excitation could be considered as belonging to an aggregate as a whole, and the excitation (as well as the corresponding energy level) can be now characterized with the wavenumber k , and the definite excited molecule cannot be already determined. This collective excitation was called by Frenkel an *exciton*.

Here, the selection rules for absorption transitions in an aggregate should be mentioned. Because of the impulse conservation law, absorption transitions only to either the lowest or the highest level are possible (i.e., at $\cos(ka) = 1$), depending on the sign of the M^f matrix element. The first case corresponds to the *J-aggregates*, characterized by a long-wavelength shift of the absorption spectrum as compared to that for the monomer dye, a small Stokes shift, and a strong fluorescence (Fig. 2). The packing of molecules in the J-aggregate is in the “head-to-tail” manner, and more precisely, the angle α between the dipole moment of the molecule absorption transition (generally corresponding to its long axis) and the aggregate axis does not exceed 54.7° (Fig. 1) [5]. In the second case of allowed transitions to the highest aggregate level, the *H-aggregates* are formed. These structures are characterized by the short-wavelength shift of the absorption spectrum as compared to that of the monomer dye,

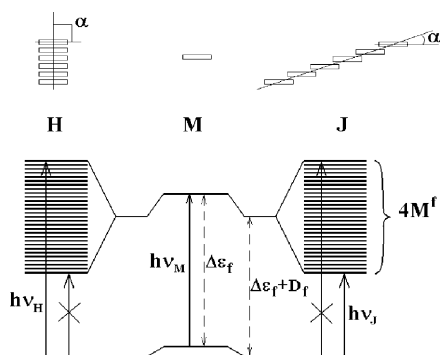


Fig. 1 Schematic representation of the molecule packing structure (top) and energy level structure (bottom) of H- and J-aggregates as compared to those of the monomer molecule (M)

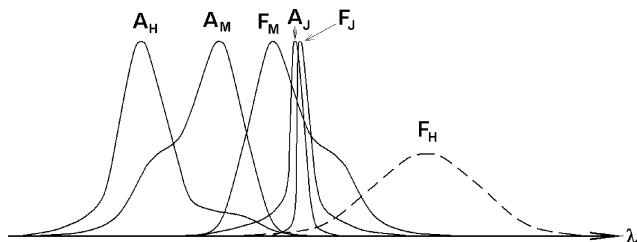


Fig. 2 Schematic representation of characteristic absorption (A) and fluorescence (F) spectra of H- and J-aggregates (marked as H and J, respectively) as compared to those of the monomer molecule (M). The dashed spectrum F_H means that H-aggregates could be nonfluorescent

and are either nonfluorescent or emit a weak fluorescence with broad spectrum and large Stokes shift (Fig. 2) [6, 7]. The dye molecules in an H-aggregate form the so called “card-pack” or “sandwich” structure, in which the angle α exceeds 54.7° (Fig. 1) [5].

The theory of the aggregate formation that accounts for the van der Waals attraction and Coulomb repulsion (as the majority of the dyes molecules are charged in water solution) was proposed [8]. It was shown that, within the frames of the assumptions made (large number of molecules, the point Coulomb charges, and uniform distribution of the electron density over the dye molecule surface) the aggregate energy has its minima at two values of the angle α between the molecule transition dipole moment and the aggregate axis. One of these values is equal to 90° , which corresponds to H-aggregates. Another one appearing at higher values of the number N is below 54.7° (and becomes the absolute minimum at the angle α lower than 38.2°); it can be attributed to the J-aggregate geometry. Though the theory concerned only the high N values, experimental results also show that the aggregate of the H-geometry could be formed by a small number of molecules, and dimers of a “sandwich” structure are often observed. At the same time, for the J-aggregate formation, a higher number of dye molecules are necessary.

The already mentioned Davydov theory regarded an infinite aggregate, the excitation being delocalized over the very large number of molecules N . But these ideal conditions cannot be met in reality. In the experimentally observed J-aggregates, the excitation is believed to be delocalized over a limited number of molecules $N_d < N$. The parameter N_d is called the *exciton delocalization length*. It depends on both the resonance dipole–dipole interaction and diagonal (or energy) disorder (i.e., some small difference in the excitation energy of separate molecules) in the J-aggregate [9].

It was already mentioned that the J-aggregates are highly fluorescent. This phenomenon is connected with the change in the aggregate radiative lifetime τ_{rad}^J as compared to that of the monomer dye τ_{rad}^m . (Radiative lifetime $\tau_{\text{rad}} = 1/k_{\text{rad}}$, k_{rad} being the rate constant of the fluorescent deactivation of the excitation. At the same time, fluorescence decay time $\tau = 1/(k_{\text{rad}} + k_{\text{nr}})$, k_{nr} being the total rate constant of the nonfluorescent deactivation pathways. Thus, the ratio τ/τ_{rad}

equals to the fluorescence quantum yield). That is, the ratio of the radiative lifetimes of the monomer dye to its J-aggregate is proportional to the exciton delocalization length N_d [10]:

$$\frac{\tau_{\text{rad}}^m}{\tau_{\text{rad}}^J} \approx \frac{8}{\pi^2} N_d.$$

One more peculiarity of the J-aggregates is the narrowing of their absorption and fluorescence spectra as compared to those of the monomer dyes. The ratio of the half-width values of the monomer ($\Delta v_{0.5}^m$) and J-aggregate ($\Delta v_{0.5}^J$) absorption bands could be connected under certain assumptions [11] with the square root of the N_d value:

$$\frac{\Delta v_{0.5}^m}{\Delta v_{0.5}^J} \approx \sqrt{\frac{2N_d}{3}}.$$

Measurement of the aggregate radiative lifetime and that of its absorption spectrum half-width are the two experimental ways to estimate the value of the delocalization length.

Up to this moment, we have regarded the case of the aggregate with the single molecule in an elementary cell. But this is not always the case. Davydov [3] regarded the crystal with m molecules in an elementary cell and found that the excitation levels of such a crystal form m exciton zones. It should be noted that the selection rules permit only one absorption transition to each zone. Thus, for an aggregate with m molecules in an elementary cell, up to m bands could be observed in an absorption spectrum. Such spectrum splitting is called the *Davydov splitting*. One of the examples of an aggregate with such a splitting is the helical one [12].

3 Aggregation in Water Solutions

The study of H- and J-aggregates spectra in the solutions began already in the first works dealing with J-aggregates [13–16]. Till now, wide amount of information has been collected concerning the aggregation conditions, as well as the spectral and physical properties of aggregates formed by various compounds [17, 18].

First of all, it should be noted that the cationic dyes form aggregates most efficiently either in water or in strongly nonpolar solvents (e.g., hexane) [19]. Besides, aggregation is enhanced by the addition of salts, and surfactants above the critical micelle concentration, and decreased upon increasing temperature [17]. The last mentioned dependence is clear; to understand the others, the interactions participating in the dye aggregation should be considered. These interactions are (1) van der Waals attraction of the π -electron systems of the dyes, (2) Coulombic interactions of the dyes' charges, and (3) hydrophobic force in the case of water. Hence, the effect of solvent on the aggregation is believed to be explained by the

dependence of the Coulombic interaction energy on the solvent dielectric constant. In highly polar solvents when the charged dye molecule and its counter ion are surrounded by the solvate shells and separated one from another, the counter ions do not participate in an aggregation process. Consequently the Coulombic repulsion between the dye molecules hinders the aggregate formation. Thus, the higher the dielectric constant, the weaker this repulsion, and hence, the stronger are the aggregation processes. As the value of the dielectric constant of water is extremely high ($\epsilon = 81$), the dye aggregation in water is the most intensive. Besides, the hydrophobic interactions also occur in this solvent enhancing the aggregation process. Addition of other organic solvents to the dye aqueous solution destroys aggregates, this destruction being stronger for the solvents with lower dielectric constant. On the other hand, increasing of the solvent ionic strength (i.e., addition of salts which would dissociate into ions) results in the screening of the Coulombic repulsion forces and thus promotes aggregation. At the same time, in a nonpolar solvent (e.g., hexane), the charged dye molecules as well as their counter ions cannot be solvated and separated from one another, and thus can be located closely. As a result, the total charge of the dye molecule is zero, but an additional dipole moment appears to be formed by the charged dye and its counter ion. As the dielectric constant of the nonpolar solvent is low and thus electrostatic forces are not weakened, the aggregates are formed by the dye – counter ion pairs because of dipole–dipole and van der Waals interactions [19].

One of the most interesting points to be elucidated upon the study of an aggregate is its geometry, i.e., the structure of the dye molecule packing within an aggregate. First of all, if the absorption spectrum of an aggregate contains only one band, then its either short-wavelength or long-wavelength shift as compared to that of the monomer dye permits to decide about “card-pack” or “head-to-tail” structure, respectively. In the case where several bands are present in the aggregate absorption spectrum, the elementary cell of an aggregate contains several molecules. Here, polarization measurements are useful. Particularly, linear dichroism (LD) and fluorescence polarization study could reveal the angles between the different permitted absorption transitions in an aggregate [20], while circular dichroism (CD) measurements point to the chirality of the aggregate structure [21]. At the same time, nonzero LD and birefringence of the sample could also cause contribution to the CD spectrum measured with the polarization-modulation method [22]. As both LD and birefringence values could be nonzero even in solution in the case of large aggregates (the ones observed in [22] were 1–2 μm wide and several tens of micrometer long), this possibility should be taken into account [22].

To study the size of the formed aggregate, several approaches could be used. First of all, large aggregates could be observed directly in a microscope. For example, an electron-microscope investigation of 12.5×10^{-3} M (that is rather high concentration) aqueous solution of pseudoisocyanine (Fig. 3) allowed observing the cylindrical aggregate structure with the length near 350 nm and width about 2.3 nm, that corresponds to about 3,000 molecules [23]. Besides, aggregate size could be estimated by the indirect methods, such as light scattering or centrifugation [17].

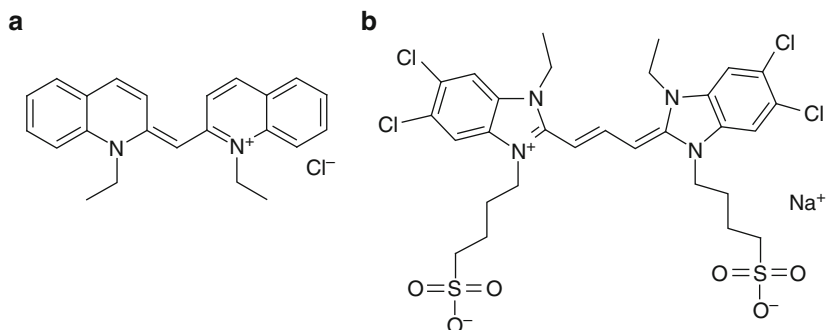
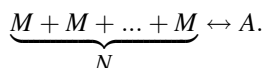


Fig. 3 Structures of the dyes: (a) pseudoisocyanine, (b) benzimidazolocarbo-cyanine

In addition, the excitation delocalization length of an aggregate could be estimated on the basis of the measurement of the aggregate radiative lifetime and its absorption spectrum half-width as described above [10, 11]. Such estimation, being interesting as itself, could also be regarded as the lower limit of physical dimension of the aggregate.

One more approach to determine the *aggregate dimension* that could be applied for small aggregates is as follows [16, 17]. Let us suppose that a dynamic equilibrium exists in solution between the monomer (M) and aggregate (A) forms of the dye, the aggregates being of the same dimension and geometry, and consisting of N molecules. Thus, the only processes occurring in solution are the aggregate formation and destruction, and in the case of equilibrium, their rates being equal



For such processes based on the law of mass action, one can write down that

$$\frac{C_A}{C_M^N} = K \times N$$

where C_A and C_M are the concentrations of dye molecules in aggregated form and in monomer, respectively, and K is the aggregation equilibrium constant. Taking the logarithm of the above equation gives

$$\ln(C_A) = N \times \ln(C_M) + \ln(K \times N).$$

Hence, if we are able to establish the dye concentrations in monomer and aggregated forms, C_M and C_A , for several different values of total dye concentration (e.g., dividing the total absorption spectrum into its aggregate and monomer components as it was done, e.g., in [24]), the slope of the $\ln(C_A)$ dependence on

$\ln(C_M)$ equals to N . With the help of this procedure, dimeric nature of the trimethine cyanine dye H-band was demonstrated in [24]; for the J-aggregates of benzimidazolocarboyanine (Fig. 3) $N = 4$ was found [17]. It is worth noting that according to the light scattering results, the mentioned J-aggregates had to be much larger; it was thus supposed that N calculated on the basis of the mass action law reflects delocalization length, and not the physical dimensions of an aggregate [17]. But the mass action law accounts for the kinetics of the aggregate formation, that is, it is on the basis of the statement that the aggregation rate is determined by the probability of simultaneous contact of N dye molecules. Thus, the possible way to explain both light scattering and mass action law results could be to suppose that the large aggregate could only grow upon addition of four dye molecules simultaneously.

As we succeeded in establishing C_M and C_A values and applying the mass action law to the aggregation process, the value of aggregation equilibrium constant K could be obtained. Its value characterizes the affinity of a certain dye to form aggregates in certain conditions (including both solvent and all the admixtures, e.g., ions and surfactants) at a certain temperature. Thus, K is an important characteristic of the aggregation (as well as of any other binding process). And once K is known, it is possible to obtain the change in the standard Gibbs energy upon aggregation ΔG_0 according to the expression

$$\Delta G_0 = -RT \times \ln(K),$$

where R and T are the gas constant and absolute temperature, respectively. But this is not all. If the aggregation occurs at constant temperature, then $\Delta G_0 = \Delta H_0 - T\Delta S_0$, ΔH_0 and ΔS_0 being the changes in standard enthalpy and standard entropy upon aggregation. At the same time, both K and ΔG_0 values depend on temperature. Thus, if one determines the K values for different temperatures and assumes ΔH_0 and ΔS_0 to be temperature independent, one could obtain

$$\ln(K) = -\frac{\Delta G_0}{RT} = \frac{\Delta S_0}{R} - \frac{\Delta H_0}{RT}.$$

Thus, approximation of the $\ln(K)$ dependence on $1/RT$ by the linear function provides both ΔH_0 and ΔS_0 values. And once these values are determined, some conclusions about the interactions causing the aggregation could be made. Particularly, $\Delta H_0 < 0$ means that the total of van der Waals and Coulombic forces promotes aggregation (i.e., roughly, van der Waals attraction is stronger than Coulombic repulsion); otherwise, the sum of these forces tends to destroy the aggregate structure. On the other hand, $\Delta S_0 > 0$ means that upon aggregation, the entropy is increased despite the fact that dye molecules become more structured in an aggregate than in the free state. Such results point to the hydrophobic forces as one of the factors causing aggregation, as hydrophobic interaction is known to be the entropy-driven effect. Of course it depends on the dye nature and solvent

conditions, whether the aggregation process would be enthalpy- or entropy-controlled, or both [17].

Concerning the influence of the dye aggregation in solution on the efficiency of fluorescent *detection of the objects of biological origin* with this dye, two points should be mentioned. First of all, if the dye besides binding with the target biomacromolecule is also able to form aggregates in solution, then a part of the dye molecules become aggregated. That shifts the equilibrium in solution and decreases the percent of the dye molecules bound to the target that consequently lowers the fluorescent response. On the other hand, if the aggregates of dye molecules in solution are non- or weak- fluorescent, which is the case for H-aggregates, this results in decreasing of the nonbound dye fluorescence intensity and thus in the increase of the signal-to-noise ratio of detection [6]. As the H-aggregate fluorescence (if it could be observed) is generally shifted to the long-wavelength region as compared to monomer one (Fig. 2), the signal-to-noise ratio could be additionally increased when measuring the fluorescence intensity on the monomer emission wavelength [6, 7]. Thus the influence of dye aggregation in solution on the detection efficiency is positive in the cases when the dye molecules are significantly fluorescent in nonbound monomer form, but are almost completely aggregated in water solution. In this case the fluorescence intensity enhancement upon addition of biological macromolecules occurs not only because of the dye molecule fixation upon binding (and thus increasing of the fluorescence quantum yield of the bound monomer as compared to the free one), but also because of the destruction of nonfluorescent aggregate formed in solution and of consequent binding to macromolecule of fluorescent monomer.

4 Biomembrane-Induced Dye Aggregation

Biological membranes are formed by the molecules of lipids which contain a polar (either charged or zwitterionic) “head” and two long aliphatic “tails.” In water environments, they form a bilayer as a result of the hydrophobic forces, the two layers having their heads solvated by water and the tails hidden from it. Membranes are known to be able to exist in two major phases, namely the gel phase at lower temperatures and fluid phase at higher ones. The gel phase is characterized by more ordered packing of the lipids that is explained by the all-*trans* conformations of their aliphatic tails, while for the fluid-phase the chaotic conformation of the lipid tails causes less tight lipid packing. Staining of the membranes with fluorescent probes is important, e.g., for the cells visualization in fluorescent microscopy [25]. It should be noted that the *vesicles* (spherical lipid formations with bilayer structures) and micelles (monolayer spherical formations, formed by surfactants containing only one “tail”) could be the modeling systems with the properties close to those of the membranes.

The dyes that bind to biomembranes are often designed to contain the polar “head” (that is often a chromophore) and long aliphatic “tails.” Being thus similar to that of the membrane-forming lipids, this structure favors their insertion into the membrane. At the same time, such dyes could form J-aggregates when available in the membrane at sufficient dye to lipid concentration ratios (Fig. 4).

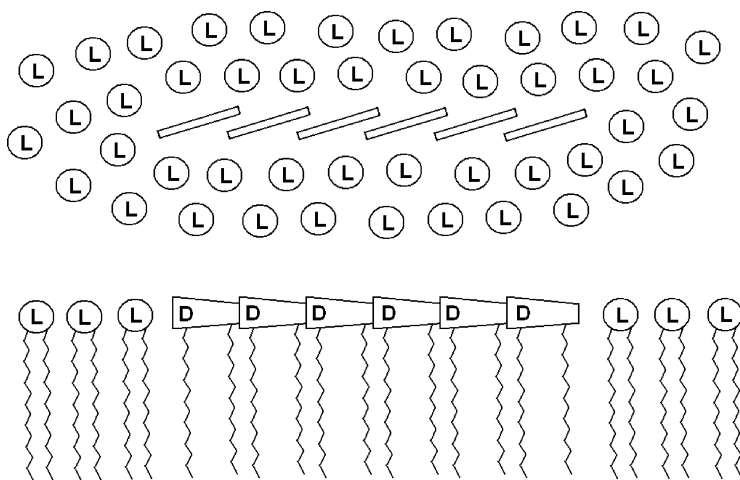


Fig. 4 Schematic representation of possible packing of dye (D, bars) molecules containing long aliphatic groups into the J-aggregates in lipid (L, circles) layer; presented as seen perpendicular (top) and along (bottom) the lipid layer surface

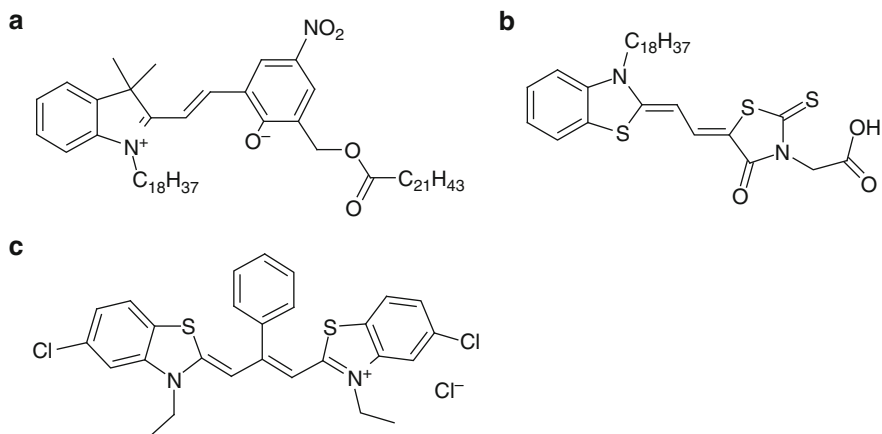


Fig. 5 Structure of dyes forming aggregates in membranes: (a) 2-[(E)-2-[2-hydroxy-5-nitro-3-[(1-oxodocosyl)oxy]methyl]phenyl]ethenyl]-3,3-dimethyl-1-octadecyl-3H-indolium (PMC), (b) 3-carboxymethyl-5-[2-(3-octadecyl-benzothiazolin-2-ylidene)-ethylidene]rhodanine (MD), (c) 5,5'-dichloro-3,3'-diethyl-9-phenylthiacarbocyanine chloride

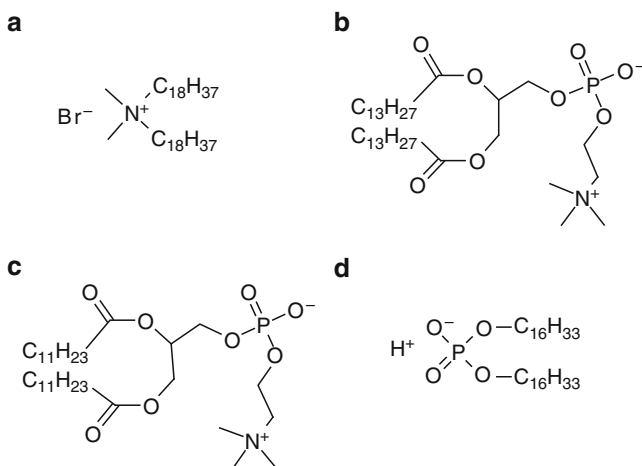


Fig. 6 Structure of membrane components: (a) dioctadecyldimethylammonium bromide, (b) 1,2-dimyristoyl-*sn*-glycero-3-phosphocholine (DMPC), (c) 1,2-dilauroyl-*sn*-glycero-3-phosphocholine (DLPC), (d) dicetyl phosphate (DCP)

Thus, it was shown that the merocyanine dye PMC containing two long alkyl chains (Fig. 5) when binding with the dioctadecyldimethylammonium (Fig. 6) membrane behaves as monomer at the dye to lipid concentrations ratio below 0.006, and forms J-aggregates in the same membrane when added in concentration ratio above 0.01 [26]. At the same time, merocyanine dye MD (Fig. 5) was shown to form fluorescent J-aggregates in the DMPC (Fig. 6) vesicles at dye to DMPC concentration ratios higher than 0.04 [27]. Moreover, depending on the metal ions present in water solution containing vesicles, J-aggregates of two different types were observed. For example, in the presence of Mg²⁺ and Co²⁺ the type I aggregates (absorption maximum near 635 nm) were formed, while the type II aggregates (absorption maximum near 600 nm) were induced by addition of Ca²⁺, Cu²⁺, Sr²⁺, Cd²⁺, Ba²⁺, and Co²⁺ (the last ion induces both types of J-aggregates). At the same time, in the presence of both Mg²⁺ and Cd²⁺, the transition from type I to type II was observed upon increasing the temperature. These results led the authors to an assumption about the metal ions participation in the J-aggregate structure. It should be noted that in the vesicles formed by DLPC (Fig. 6), the MD molecules form J-aggregates of the type II in the presence of all the metal ions studied including Mg²⁺ [27].

Aggregation of pseudoisocyanine (dye I, Fig. 3) and 5,5'-dichloro-3,3'-diethyl-9-phenylthiocarbocyanine chloride (dye II, Fig. 5) induced by the vesicles consisting of zwitterionic DMPC and anionic DCP (Fig. 6) lipids was studied in [28]. Both dyes were shown to form fluorescent J-aggregates upon addition of the vesicles formed of the mixture of DMPC and DCP with relative content equal to 1:1. At the same time, for both dyes pure DMPC vesicles did not induce the J-aggregation. Upon addition of the vesicles containing DMPC and DCP in the 4:1 ratio, as well as

of pure DCP, the J-aggregates formation was observed to be less efficient than in the case of 1:1 concentrations ratio. The complete absence of J-aggregates for the pure DMPC vesicles was explained by zwitterionic nature of this lipid. Thus, the negative charge of the vesicle (brought in by DCP) is important for the cationic (i.e., positively charged in water solution) dye J-aggregate formation. It should be noted that upon addition of the dye II to the aqueous solution of the vesicles in which the dye I J-aggregates were already formed, dye II formed J-aggregates in the vesicles as well, and resonance excitation energy transfer from dye I J-aggregates to the dye II J-aggregates was observed.

Aggregation of pseudoisocyanine molecules in the supported lipid bilayers formed by different lipid molecules was studied in [29]. In contrast to the results described in [28], pseudoisocyanine J-aggregates were shown to be present in zwitterionic lipid bilayers, while the charged (both positively and negatively) ones did not induce aggregation [29]. It should be also noted that depending on the lipid of which the bilayer consists, J-aggregates of two types were observed, the I-type J-aggregates having the spectra close to those of pseudoisocyanine J-aggregate in solution, and those of the II-type being shifted as compared to that of I-type. Preferentially, J-aggregates of both types were formed in the gel-phase regions of the bilayers. Moreover, J-aggregate formation was shown to occur at the center of the gel-phase domain, and to depend substantially on the area per lipid “head” (i.e., on the distance between the neighbor lipids).

The pseudoisocyanine J-aggregate formation in the lipid bilayer was suggested to occur as follows. First the dye molecules bind to the bilayer because of electrostatic attraction and because of cation– π interaction (i.e., interaction between the dye π -electron cloud and the lipid “head” cation); then reorientation of the lipids bound to the dyes occurs so that the dye J-aggregate structures are formed. This is supposed to be due to the energy gain upon dyes stacking, while the reorientation of lipid molecules does not require energy [29].

5 J-Aggregates Formed on DNA

Many of organic dyes, e.g., the cyanine ones, are widely used for DNA fluorescent detection [25]. Such dyes bind to the DNA, either intercalating between the nucleotide base pairs, or *via* the groove-binding. They can strongly increase the fluorescence intensity as a result of fixation of their structure. The dye molecules often bind to DNA close one to another, forming thus an aggregate. It was mentioned above that for the cationic dyes in aqueous solution, Coulombic repulsion between the dye charges hinders aggregation, while the addition of ions results in screening of the dye electric charge and thereby promotes aggregation. Hence, as the DNA sugar–phosphate backbone in aqueous solution is charged negatively, the aggregation of positively charged dye molecules on negatively charged DNA (as well as on other charged surfaces [17]) is accompanied by screening of the dye

positive charges that promotes the aggregate formation. Thus, if the dye molecule has the structure appropriate for its aggregate to fit to the DNA molecule, the aggregate can be formed. The above described role of the Coulombic interaction in the aggregation on DNA explains the fact that unlike aggregation in solution, increasing of ionic strength leads to the destruction of aggregates formed on DNA.

Unlike the aggregation in solution, there are very few works dealing with the dye aggregation on DNA, and only in few reports these aggregates are found fluorescent. In most of the cases, the aggregates formed on DNA are the non- or weakly fluorescent H-aggregates, and these aggregates are often supposed to be the dimers. Particularly, the monomethine cyanine dye thiazole orange (TO, Fig. 7) was shown to form dimer aggregates bound to single-stranded synthetic polynucleotides poly(dC), poly(dT), and poly(dG), while in the presence of dsDNA and poly(dA) no aggregates were observed [30]. The fluorescence of the dimers was not revealed because of its very low intensity as compared to that of the monomeric TO bound to polynucleotide. The authors explain the low fluorescence intensity of the bound aggregate by the peculiarities of the dimer structure, supposing that one of the dye

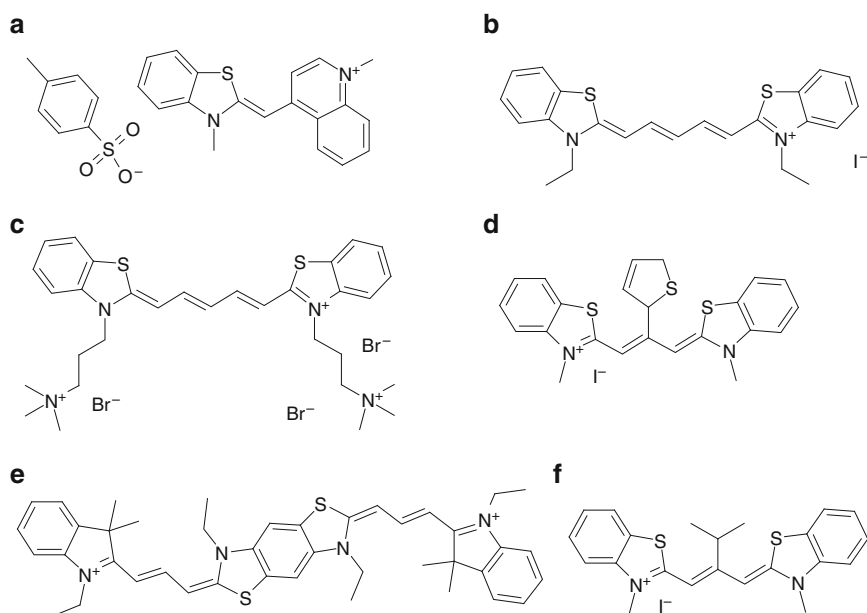


Fig. 7 Structures of the dyes forming aggregates on DNA: (a) 1-methyl-4-[[3-methyl-2(3*H*)-benzothiazolylidene]methyl]-quinolinium (Thiazole Orange, TO), (b) 3,3'-diethylthiadicarbocyanine (DiSC₂(5)), (c) 3,3'-trimethylammoniopropylthiadicarbocyanine (DiSC₃₊(5)), (d) 2-[(*Z*)-2-(2,5-dihydro-2-thienyl)-3-[3-methyl-2(3*H*)-benzothiazolylidene]-1-propenyl]-3-methylbenzothiazol-3-ium (L-21), (e) 2-[(*E*)-3-[3,7-diethyl-6-[(*E,2E*)-3-(1-ethyl-3,3-dimethyl-3*H*-indolium-2-yl)-2-propenylidene]-6,7-dihydrothiazolo[5,4-*f*]benzothiazol-2(3*H*)-ylidene]-1-propenyl]-1-ethyl-3,3-dimethyl-3*H*-indolium (BCD), (f) 3-methyl-2-[(*E*)-3-methyl-2-[[3-methyl-2(3*H*)-benzothiazolylidene]methyl]-1-butenyl]-benzothiazol-3-ium (Cyan βPr)

molecules forming the dimer is not fixed by DNA and is thereby able to dissipate the excitation energy by internal rotation around the methine bond. It should be mentioned here that another explanation exists for the very weak fluorescence intensity of an H-aggregate. That is, it is supposed that after the absorption transition to the higher of the split levels, excitation dissipates nonradiatively to the lower one, from where the radiative transition is forbidden [5].

The H-aggregates of the dyes formed on DNA that were supposed to be the dimers and aggregates of higher order, were studied in [6, 7]. For such aggregates the fluorescence spectrum was registered, which turned out to be of low intensity, broad, and shifted to the long-wavelength region as compared to that of a monomer. The mentioned aggregate formation decreases the DNA fluorescent detection sensitivity as aggregation is accompanied with the quenching of the intensive fluorescence of the monomer dyes bound to DNA. To explain this quenching, the aggregate is supposed to be formed by interaction of the free dye to another one already bound to DNA.

Interaction of the pentamethine cyanine dye DiSC₂(5) (Fig. 7) with different polynucleotides was studied in [31]. It was shown that in the presence of [poly(dA-dT)]₂ and [poly(dI-dC)]₂ the H-aggregates of the dye are formed, while in [poly(dG-dC)]₂ presence no spectral manifestations of aggregates were observed. As [poly(dA-dT)]₂ and [poly(dI-dC)]₂ have the same structures of the minor groove, while the major groove is similar for [poly(dG-dC)]₂ and [poly(dI-dC)]₂, the conclusion about formation of the dye dimers of H-type in the polynucleotide minor groove was made. The groove binding was supported by the viscosity measurements. It is interesting that in the DiSC₂(5) aggregates formed in the [poly(dI-dC)]₂ minor groove the splitting of the H-band was observed that was connected with the interaction of the neighboring dimers formed in the groove. As it is quite expected for the H-type aggregates, no fluorescence of the aggregates was observed, the aggregation produces quenching of the bound dye.

The dye DiSC₃₊(5) (Fig. 7) possessing similar structure to that of DiSC₂(5) but containing two additional charges in substituents was studied [32]. This dye also forms H-aggregates on the [poly(dI-dC)]₂ polynucleotide, though the percent of DiSC₃₊(5) molecules involved in such aggregation is far lower than that of DiSC₂(5). This is explained by the Coulombic repulsion of the dye molecules occurring because of the increase of the dye charge. At the same time, the narrow long-wavelength J-aggregate band appeared in the absorption spectrum of DiSC₃₊(5) in the presence of [poly(dI-dC)]₂. This band becomes more intense upon decreasing temperature and dominates in the spectrum below 15°C, while the H-aggregate band decreases when decreasing the temperature below 30°C. Besides, additional band manifested as a shoulder on the long-wavelength side of the monomer band was observed. It was connected with another permitted absorption transition of the aggregate. Addition of NaCl that increases the ionic strength of the solution leads to a decrease of the temperature of J-aggregate formation. Both H- and J-aggregates were clearly revealed in CD spectra indicating their chiral structure. Moreover, CD study demonstrates the presence of two separate bands not only for J-aggregates (that was also revealed in absorption), but for H-aggregates as well. The authors

explain their results as follows. At high temperatures (e.g., above 35°C) the DiSC₃₊₍₅₎ dye molecules form the face-to-face, i.e., sandwich-type, dimers in the minor groove of [poly(dI-dC)]₂, as it was supposed to be the case for DiSC₂₍₅₎ in [31]. As the temperature is high enough, the charged substituents of the opposite dye molecules are held away one from another due to *gauche*-conformations of the (CH₂)₃ groups. The decrease in the solution temperature results in all-*trans* conformations of the above mentioned groups that brings the charged N⁺(CH₃)₃ groups close to one to another. The latter condition causes an increase of electrostatic repulsion and a decrease in H-aggregate stability. This leads to the relative shift of the opposite dye molecules in dimers, which leads to the change in molecule packing geometry and hence to the transformation of H-aggregate to J-aggregate. At the same time, increase in the ionic strength of the solution leads to the screening of the dye electrostatic charges. This requires smaller distances between the charged N⁺(CH₃)₃ groups for the H-aggregates to become unstable, and thus leads to the decrease in the temperature of H- to J-aggregate transition. It should be noted that the authors regard the H- and J-aggregates of DiSC₃₊₍₅₎ on [poly(dI-dC)]₂ as a series of respective H- and J-dimers interacting one with another. This interaction is believed to lead to the appearance of another permitted J-aggregate absorption transition. At the same time, in our opinion, while for H-dimers the splitting of the spectrum could be explained as the perturbation, in the case of J-aggregates it would be more correct to regard the series of J-dimers as a single J-aggregate with several molecules in an elementary cell. Such J-aggregate structure should lead to the Davydov splitting and thus to the appearance of several separate bands in absorption spectrum. It should be noted that the aggregates of DiSC₃₊₍₅₎ on [poly(dI-dC)]₂ were also studied in more detail in [33] experimentally and in [34] *via* computer simulations.

Formation of an aggregate packed as a series of neighboring face-to-face dimers in DNA groove was suggested for the trimethine cyanine dye L-21 (Fig. 7) studied in [35]. Absorption spectrum of the above mentioned aggregate consisted of H- and J- bands, shifted to short- and long-wavelength regions respectively as compared to the monomer one. The aggregate revealed intensive narrow fluorescence band situated close to the absorption J-band. One more absorption band of L-21, called the D-band, was attributed to separate J-dimers formed in DNA groove.

The study of pseudoisocyanine absorption, LD and CD, in the presence of DNA revealed the appearance of new bands in addition to the monomer one in CD and LD spectra [36]. Increase in dye to DNA concentration ratio results in the generation of primary short-wavelength, and then long-wavelength CD and LD bands. The first one was attributed by authors to the dimer between the partly intercalated pseudoisocyanine molecule and another one bound to it, while the second corresponded to the J-aggregates of pseudoisocyanine molecules formed in the presence of DNA.

The J-aggregates of bichromophoric dye BCD (Fig. 7) formed on DNA were studied in [37]. While this dye was shown to be able to form J-aggregates with a rather broad absorption spectrum in water solution in the presence of NaCl, an addition of DNA also caused fluorescent J-aggregate formation with the appearance of narrow absorption band. Besides the fact of formation in the presence of DNA,

the above mentioned aggregates demonstrated strong CD band and thus were considered to be formed on DNA. The fluorescence quantum yield of the J-aggregates formed on DNA was equal to 0.05, while for the dye monomers in aqueous solution this value was 0.018, and for the DNA-bound dye monomer 0.44. Upon DNA addition, the maximum J-aggregate absorption was observed for DNA to dye concentrations ratio 7.0 ± 4.0 . A further increase of DNA concentration leads to destruction of aggregates and to binding of dye monomers to DNA.

The studies of carbocyanine dye Cyan β iPr (Fig. 7) in the presence of DNA [38] showed that in absorption spectrum, together with the band corresponding to the dye monomer bound to DNA, the long-wavelength band connected with the dye J-aggregates was present. As this band was not manifested in the absence of DNA, the aggregates were supposed to be formed on DNA. Moreover, the studies of the dye in the presence of double-stranded synthetic polynucleotides revealed that the GC-containing polynucleotides do not induce aggregate formation. At the same time, the addition of AT-containing species resulted in the appearance of pure J-aggregate spectrum that contained two bands, both shifted to the long-wavelength region as compared to the monomer one (Fig. 8). The studied aggregate demonstrated rather intense fluorescence (Fig. 8) with quantum yield of about 0.05 that is 50 times higher than that of free dye and close to that of the dye monomer bound to AT-containing polynucleotide [39]. The fluorescence excitation anisotropy study revealed the presence of significant angle between the dipole moments of the two allowed J-aggregate absorption transitions, pointing on Davydov splitting in the structure of excited energy levels of J-aggregate [20]. It was supposed that the aggregate is formed in DNA minor groove (Fig. 9), and the dipole moments of its

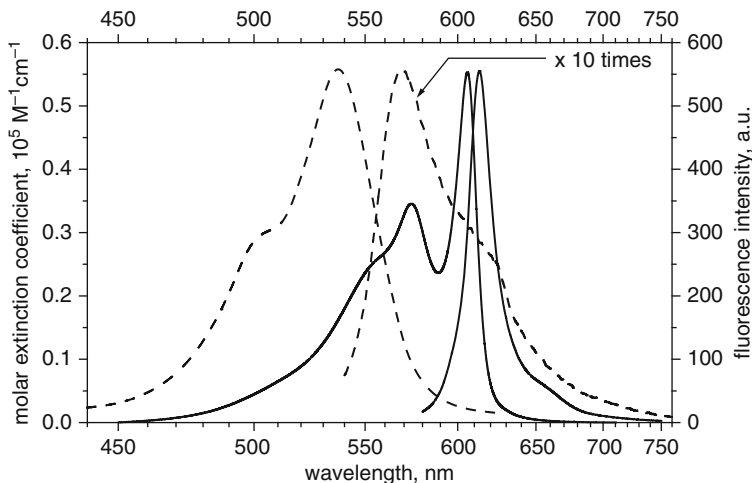


Fig. 8 Absorption (*left*) and fluorescence (*right*) spectra of 10^{-5} M Cyan β iPr in buffer (*dashed*) and of 3×10^{-5} M Cyan β iPr in presence of 3.5×10^{-5} M b.p. poly(dA)–poly(dT) (*solid lines*). Free dye fluorescence spectrum intensity is multiplied ten times [40]

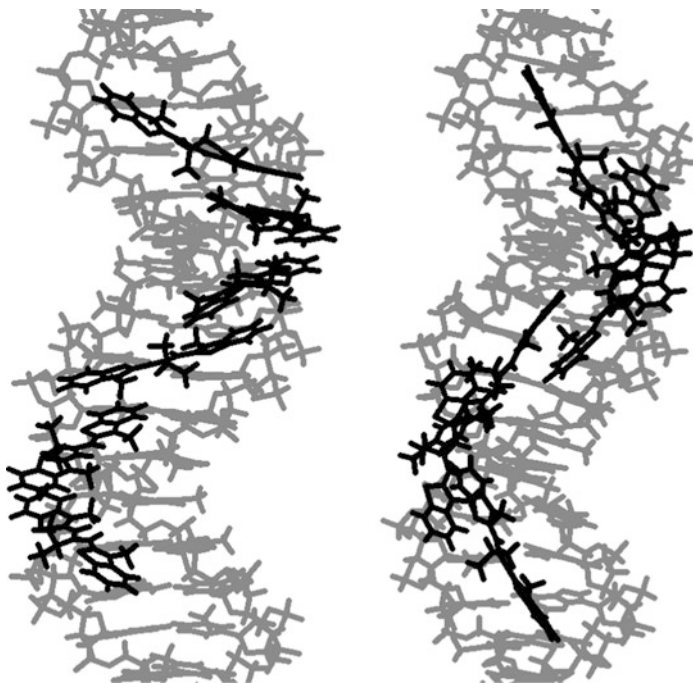


Fig. 9 Possible monomer packing structures in Cyan β iPr J-aggregate formed in the poly(dA)-poly(dT) groove, built in HyperChem 6.03

absorption transitions are directed along the DNA axis and perpendicular to it [20], according to Kasha prediction [12].

Summarizing, some of the organic dyes, particularly cyanines, are able to form fluorescent aggregates on DNA. Comparing with the dye monomers bound to DNA, the J-aggregates are more sensitive to the concentrations ratio and to DNA nucleotides content. Though these structures can hardly be applied for the routine DNA detection assays, they are rather interesting systems for special studies.

6 Proteins as the Templates for Aggregate Formation

Proteins in their native form are the globules, the structures of which (the so called tertiary structure) strongly differ for different proteins. At the same time, on the level of secondary structure only three major forms are realized, namely α -helix, β -sheet, and random coil. As the two first mentioned forms are periodical, they could possibly serve as the templates for the J-aggregate formation. Nevertheless, there are only a few reports about the dye aggregates formed on proteins.

Among the series of dyes, in which the effect of binding to human serum albumin (HSA) was studied [41], the dye 8 (Fig. 10) exhibited J-aggregate absorption and fluorescence bands, while these bands were not observed for the free dye. This led to the conclusion about the J-aggregation of the dye 8 in the HSA binding site.

A rather interesting observation was made for the trimethine cyanine dye phenyl-thiacarbocyanine (PTC) (Fig. 10) [42]. In aqueous solution, this dye exists in J-aggregate form, while the addition of HSA leads to partial destruction of these aggregates and to the dye binding to protein in monomeric form. At the same time, the addition of HSA induces the apparent CD signal of the absorption band corresponding to the rest of the J-aggregates. As no CD signal was observed for the J-aggregate band in the absence of HSA, the assumption about the interaction between the PTC J-aggregates and HSA was made. Moreover, increasing of HSA

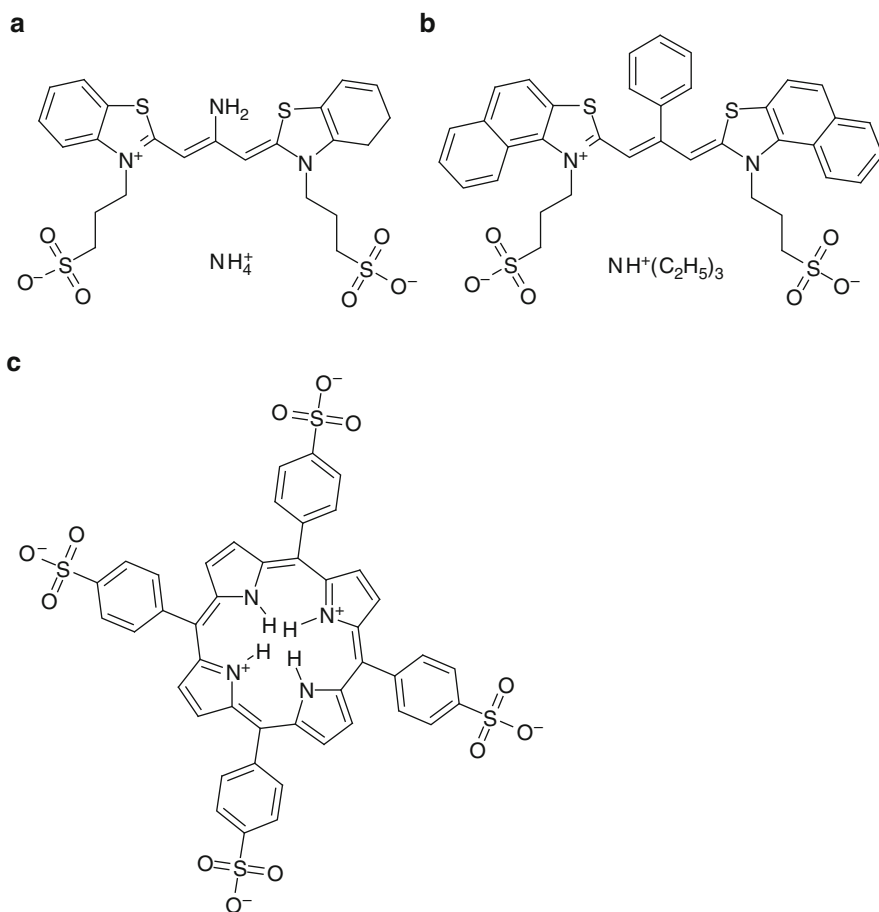


Fig. 10 Structures of dyes: (a) 3,3'-di(3-sulfopropyl)-9-amino-thiacarbocyanine (dye 8), (b) 3,3'-di(3-sulfopropyl)-4,5,4',5'-dibenzo-9-phenyl-thiacarbocyanine (PTC), (c) *meso*-tetrakis(*p*-sulfonatophenyl) porphine (TSPP, at pH lower than 4.8)

concentration led to the reversion of the CD spectrum i.e., to the reversion of the induced chirality of an aggregate. This was explained by the PTC J-aggregates binding to HSA regions of different secondary structure, namely α -helix and random-coil. The authors demonstrated the same chirality reversion to take place for PTC in the presence of poly-L-glutamate at pH values 2.92 and 8.08 that was explained by the poly-L-glutamate existence in α -helix and random-coil conformations respectively. Thus, it was concluded that increasing the HSA concentration led to increase of the relative content of PTC J-aggregates interacting with the random coil HSA regions. It was thus concluded that the interaction of J-aggregates with the α -helix regions of HSA was less stable as compared to that with the random-coil one. It should be noted that the CD spectrum of the J-aggregate induced by HSA addition was also observed for MTC and ETC dyes differing from PTC by the meso-substitution group (methyl and ethyl respectively instead of phenyl one) [43]. But in the case of MTC and ETC, no chirality reversion was observed indicating that these dyes form J-aggregates only with the random-coil regions of HSA.

The porphyrin *meso*-tetrakis(*p*-sulfonatophenyl) porphine (TSPP) (Fig. 10) was shown to demonstrate J-aggregates at acidic pH values lower than the pK_a of the porphyrin protonation ($pK_a = 4.8$). Such protonation gives to TSPP molecules two positive charges in addition to already existing four negative ones. Such strongly zwitterionic nature of the porphyrin is believed to cause its aggregation in aqueous solution upon increasing its concentration because of the electrostatic interactions between negative and positive charges of the molecules, when the positively charged nitrogen of one molecule is adjacent to the negatively charged sulphonate group of another one [44]. At the same time, addition of HSA and β -lactoglobulin (BLG) proteins to the aqueous solution of nonaggregated TSPP at pH = 2 also causes the appearance of the J-aggregate spectra, the Soret band being shifted from 434 to 490 nm, and the longest wavelength Q-band from about 650 to 704 nm. The J-aggregate bands were most intense at the porphyrin to protein concentration ratios 40 for HSA and 2 for BLG, while for the same ratios near 4 and 1 respectively the J-aggregate bands disappear, being transformed to monomer emission. Therefore, the observed J-aggregates were formed on the protein structure.

It is interesting that TSPP J-aggregates formed on both proteins revealed strong CD signal in the region of Soret band (490 nm), but the shapes of these CD bands significantly differed in the cases of HSA and BLG, pointing to the difference in J-aggregate packing on these two proteins [44]. The exciton delocalization length for TSPP J-aggregate formed on HSA was estimated to be about 6–8 porphyrin molecules [45]. The study of the influence of the ionic strength on the J-aggregate formation reveals the electrostatic nature of aggregation [44, 45]. That is, the TSPP molecules bearing two positive and four negative charges each, attract to each other and to the protein that is positively charged at acidic pH [45]. J-aggregates of TSPP were also shown to be formed on bovine serum albumin (BSA) and lysozyme at pH = 1.3 [46]. The model for TSPP J-aggregate formation on BSA was proposed in [47], though no assumptions about the site of their formation (e.g., α -helix, β -sheet, or random coil region) were made.

7 Membrane Potential-Sensitive Aggregates of the Dyes JC-1 and JC-9 for Mitochondria Imaging

Presently, the only commercially available dyes that are applied because of their ability to form fluorescent aggregates are trimethine cyanines JC-1 and JC-9 (Fig. 11) [25], the first one being studied much more extensively than the second one. The dye JC-1 is known to form red-fluorescent (emission maximum at 590 nm) J-aggregates in mitochondria possessing strong intramitochondrial negative potential, while upon depolarization of the mitochondrial membrane, the dye monomer green emission (maximum at 527 nm) is observed [25]. JC-9 demonstrates similar properties [25]. Such properties permit the application of these dyes for, e.g., detection of apoptotic electrical depolarization of mitochondria [25].

Mitochondria are the intracellular organelles in which ATP is synthesized. These organelles are about 0.3–5 μm long, surrounded by the double membrane. For the intact mitochondria, their inner medium known as the matrix bears a high value of negative potential $\Delta\Psi$ (about 150 mV [25]) as compared to the extra-mitochondrial cell cytoplasm, while upon apoptosis the $\Delta\Psi$ value is decreased. As the dye JC-1 is positively charged and is able to penetrate the membrane, the negative intramitochondrial potential induces the JC-1 uptake into the mitochondria [48]. The larger the $\Delta\Psi$ value, the stronger is the uptake and the higher is the concentration of JC-1 inside mitochondria, and upon increasing the dye concentration the J-aggregates are formed.

The concentration of J-aggregates is reported to increase linearly upon the $\Delta\Psi$ increase in the range 30–180 mV [49]. It is not clear whether the aggregate formation inside mitochondria occurs in aqueous phase or on the surface of some intramitochondrial substructures. In each case, the ability of JC-1 to form fluorescent aggregates in aqueous solution was shown [50]. The structure of these aggregates was studied and the assumption about the dye molecule packing in an aggregate was made [50]. At lower $\Delta\Psi$ values, when the dye concentration inside mitochondria is not enough to form the aggregates, the green fluorescence of dye monomers is observed. On the basis of this dependence of the fluorescence color on the mitochondrial membrane potential, regions of different electric potential were observed on a single long mitochondrion with fluorescent microscopy [48].

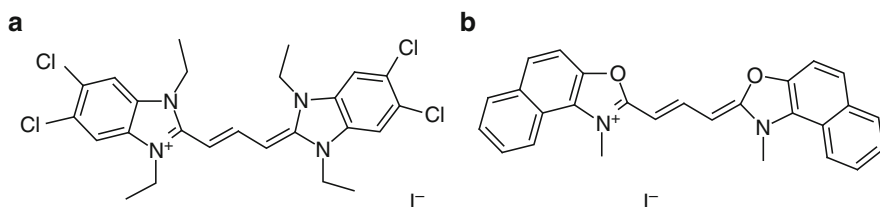


Fig. 11 Structures of dyes (a) 5,5',6,6'-tetrachloro-1,1',3,3'-tetraethylbenzimidazolylcarbocyanine iodide (JC-1), and (b) 3,3'-dimethyl- α -naphthoxycarbocyanine iodide (JC-9) sensitive to the membrane potential

8 Possibilities of Application of J-Aggregates in Fluorescent Detection and Testing of the Objects of Biological Origin

Thus, the fluorescent J-aggregates of the dyes could be formed on a wide range of biological structures, including nucleic acids, protein, and membranes. The absorption and fluorescence spectra of the aggregates strongly differ from those of the monomer, which is a positive fact for the detection of aggregates and of the structures to which they are absorbed. On the other hand, the negative aspect of the J-aggregate application in routine fluorescent detection is the fact that the aggregate formation on certain biological structure is much more sensitive to the experimental conditions (i.e., biological molecule conformation, membrane phase, biological object and dye concentrations, ionic strength, etc.) than the dye monomer binding to the same species. That is why the only dyes that are applied because of their property to aggregate are the membrane-sensitive JC-1 and JC-9, as their response in mitochondria is on the basis of the concentration increase due to electrostatic attraction and the concentration increase in aqueous medium finally results in aggregation. At the same time, because of the specificity of their formation, the J-aggregates could be used for some special studies requiring detection of specific structures of biological objects (e.g., AT-regions of dsDNA, gel-phase of lipid bilayer, etc.).

References

1. Frenkel J (1931) On the transformation of light into heat in solids. I. *Phys Rev* 37:17–44
2. Frenkel J (1931) On the transformation of light into heat in solids. II. *Phys Rev* 37:1276–1294
3. Davydov AS (1968) Theory of molecular excitons. Nauka, Moscow
4. Simpson WT, Peterson DL (1957) Coupling strength for resonance force transfer of electronic energy in Van der Waals solids. *J Chem Phys* 26:588–593
5. Kasha M (1976) Molecular excitons in small aggregates. In: Di Bartolo B (ed) *Spectroscopy of the excited state*. Plenum, New York, pp 337–363
6. Ogul'chansky TYu, Yashchuk VM, Losytskyy MYu, Kocheshev IO, Yarmoluk SM (2000) Interaction of cyanine dyes with nucleic acids. XVII. Towards an aggregation of cyanine dyes in solutions as a factor facilitating nucleic acid detection. *Spectrochim Acta A* 56:805–814
7. Ogul'chansky TYu, Losytskyy MYu, Kovalska VB, Yashchuk VM, Yarmoluk SM (2001) Interactions of cyanine dyes with nucleic acids. XXIV. Aggregation of monomethine cyanine dyes in presence of DNA and its manifestation in absorption and fluorescence spectra. *Spectrochim Acta A Mol Biomol Spectrosc* 57:1525–1532
8. Rosenbaum VM, Dekhtyar ML (1993) A simple model for formation of aggregate of polymethine dye molecules. *Ukr J Phys* 38:1296–1299
9. Malyukin YV, Kemnitz K (1998) Peculiarities of excitons relaxation in molecular chains (J-aggregates) of limited length. *Funct Mater* 5:345–348
10. Knapp EW (1984) Lineshapes of molecular aggregates, exchange narrowing and intersite correlation. *Chem Phys* 85:73–82
11. Bakalis LD, Knoester J (2000) Linear absorption as a tool to measure the exciton delocalization length in molecular assemblies. *J Lumin* 87–89:66–70

12. Kasha M (1963) Energy transfer mechanisms and the molecular exciton model for molecular aggregates. *Radiat Res* 20:55–71
13. Jelley EE (1936) Spectral absorption and fluorescence of dyes in the molecular state. *Nature* 138:1009–1010
14. Jelley EE (1937) Molecular, nematic and crystal states of 1:1-diethyl- Ψ -cyanine chloride. *Nature* 139:631–632
15. Scheibe G, Maries A, Ecker H (1937) Über reversible Polymerisation als Ursache neuartiger Arbsorptionsbanden (III). *Naturwissenschaften* 29:474–475
16. Scheibe G (1938) Reversible Polymerisation als Ursache neuartiger Arbsorptionsbanden von Farbstoffen. *Kolloid-Zeitschrift* 82:1–14
17. Herz AH (1974) Dye–dye interactions of cyanines in solution and at AgBr surfaces. *Photogr Sci Eng* 18:323–335
18. Mishra A, Behera RK, Behera PK, Mishra BK, Behera GB (2000) Cyanines during the 1990s: a review. *Chem Rev* 100:1973–2011
19. Ishchenko (1994) Structure and spectral-luminescent properties of polymethine dyes. *Naukova Dumka, Kyiv*
20. Losytskyy MYu, Yashchuk VM, Lukashov SS, Yarmoluk SM (2002) Davydov splitting in spectra of cyanine dye J-aggregates, formed on the polynucleotide. *J Fluoresc* 12:109–112
21. Pawlik A, Kirstein S, De Rossi U, Daehne S (1997) Structural conditions for spontaneous generation of optical activity in J-aggregates. *J Phys Chem B* 101:5646–5651
22. Yao H, Isohashi T, Kimura K (2006) Detection of spectral inhomogeneities of mesoscopic thiocyanine J aggregates in solution by the apparent CD spectral measurement. *Chem Phys Lett* 419:21–27
23. Von Berlepsch H, Boettcher C, Daehne L (2000) Structure of J-aggregates of pseudoisocyanine dye in aqueous solution. *J Phys Chem B* 104:8792–8799
24. West W, Pearce S (1965) The dimeric state of cyanine dyes. *J Phys Chem* 69:1894–1903
25. Haugland RP (2002) *Handbook of fluorescent probes and research products*, 9th edn. Molecular Probes Inc, Eugene
26. Seki T, Ichimura K, Ando E (1988) Stable J-aggregate formation of photoinduced merocyanine in bilayer membrane. *Langmuir* 4:1068–1069
27. Kato N, Prime J, Katagiri K, Caruso F (2004) Preparation of J-aggregate liposome dispersions and their chromic transformation. *Langmuir* 20:5718–5723
28. Sato T, Yonezawa Y, Hada H (1989) Preparation and luminescence properties of the J-aggregate of cyanine dyes at the phospholipid vesicle surface. *J Phys Chem* 93:14–16
29. Mo GCH, Yip CM (2009) Supported lipid bilayer templated J-aggregate growth: role of stabilizing cation- π interactions and headgroup packing. *Langmuir* 25:10719–10729
30. Nygren J, Svanvik N, Kubista M (1998) The interactions between the fluorescent dye thiazole orange and DNA. *Biopolymers* 46:39–51
31. Seifert JL, Connor RE, Kushon SA, Wang M, Armitage B (1999) Spontaneous assembly of helical cyanine dye aggregates on DNA nanotemplates. *J Am Chem Soc* 121:2987–2995
32. Wang M, Silva GL, Armitage B (2000) DNA-templated formation of a helical cyanine dye J-aggregate. *J Am Chem Soc* 122:9977–9986
33. Chowdhury A, Wachsmann-Hogiu S, Bangal PR, Raheem I, Peteanu LA (2001) Characterization of chiral H and J aggregates of cyanine dyes formed by DNA templating using stark and fluorescence spectroscopies. *J Phys Chem B* 105:12196–12201
34. Tomlinson A, Frezza B, Kofke M, Wang M, Armitage BA, Yaron D (2006) A structural model for cyanine dyes templated into the minor groove of DNA. *Chem Phys* 325:36–47
35. GYa G, Sorokin AV, Katrunov IK, Yefimova SL, Lebedenko AN, Malyukin YuV, Yarmoluk SM (2007) Specificity of cyanine dye L-21 aggregation in solutions with nucleic acids. *J Fluoresc* 17:370–376
36. Nordén B, Tjerneld F (1977) Optical studies of complexes between DNA and pseudoisocyanine. *Biophys Chem* 6:31–45

37. Schaberle FA, Kuz'min VA, Borissevitch IE (2003) Spectroscopic studies of the interaction of bichromophoric cyanine dyes with DNA. Effect of ionic strength. *Biochim Biophys Acta* 1621:183–191
38. Ogul'chansky TYu, Losytskyy MYu, Kovalska VB, Lukashov SS, Yashchuk VM, Yarmoluk SM (2001) Interaction of cyanine dyes with nucleic acids. XVIII. Formation of the carbocyanine dye J-aggregates in nucleic acid grooves. *Spectrochim Acta A Mol Biomol Spectrosc* 57:2705–2715
39. Losytskyy MYu, Yashchuk VM, Yarmoluk SM (2002) The electronic transitions in the cyanine dye J-aggregates, formed on the poly(dA)–poly(dT) polynucleotide. *Mol Cryst Liq Cryst* 385:27–32
40. Yarmoluk SM, Kovalska VB, Losytskyy MY (2008) Symmetric cyanine dyes for detecting nucleic acids. *Biotech Histochem* 83:131–145
41. Tatikolov AS, Costa SMB (2004) Complexation of polymethine dyes with human serum albumin: a spectroscopic study. *Biophys Chem* 107:33–49
42. Zhang Y, Xiang J, Tang Y, Xu G, Yan W (2007) Chiral transformation of achiral J-aggregates of a cyanine dye templated by human serum albumin. *ChemPhysChem* 8:224–226
43. Zhang Y, Du H, Tang Y, Xu G, Yan W (2007) Spectroscopic investigation on the interaction of J-aggregate with human serum albumin. *Biophys Chem* 128:197–203
44. Andrade SM, Costa SMB (2002) Spectroscopic studies on the interaction of a water soluble porphyrin and two drug carrier proteins. *Biophys J* 82:1607–1619
45. Andrade SM, Costa SMB (2002) Aggregation kinetics of meso-tetrakis(4-sulfonatophenyl) porphine in the presence of proteins: temperature and ionic strength effects. *J Fluoresc* 12:77–82
46. Valanciunaite J, Poderys V, Bagdonas S, Rotomskis R, Selskis A (2007) Protein induced formation of porphyrin (TPPS4) nanostructures. *J Phys Confer Ser* 61:1207–1211
47. Valanciunaite J, Bagdonas S, Streckyte G, Rotomskis R (2006) Spectroscopic study of TPPS4 nanostructures in the presence of bovine serum albumin. *Photochem Photobiol Sci* 5:381–388
48. Smiley ST, Reers M, Mottola-Hartshorn C, Lin M, Chen A, Smith TW, Steele GD Jr, Chen LB (1991) Intracellular heterogeneity in mitochondrial membrane potentials revealed by a J-aggregate-forming lipophilic cation JC-1. *Proc Natl Acad Sci USA* 88:3671–3675
49. Reers M, Smith TW, Chen LB (1991) J-aggregate formation of a carbocyanine as a quantitative fluorescent indicator of membrane potential. *Biochemistry* 30:4480–4486
50. Sorokin AV (2008) Optical properties and structure of JC-1 J-aggregates in solutions. *Biophys Bull* 21:115–121

Conjugates, Complexes, and Interlocked Systems Based on Squaraines and Cyanines

Leonid D. Patsenker, Anatoliy L. Tatarets, Oleksii P. Klochko,
and Ewald A. Terpetschnig

Abstract This chapter summarizes recent developments of red and near infrared fluorescent probes and labels based on cyanine and squaraine dyes encapsulated in macrocycles, and embedded in or bound to proteins, aptamers, dendrimers, and micro- or nano-particles. Combining these dyes with another macromolecular carrier- or host-molecule may have a positive impact on one or more of the following spectral and photophysical properties: water-solubility, brightness, fluorescence lifetimes, as well as chemo- and photostability, which promises great potential for fluorescence-based biomedical applications, pharmaceutical research, and clinical diagnostics. In general, the resulting properties of these compositions are strongly dependent on the type of dye molecule as well as the nature of the host or carrier macromolecule.

Keywords Cyanines · Encapsulation · Labels · Probes · Squaraines

Contents

1	Introduction	160
2	Dye–Cyclodextrins	161
3	Dye–Cucurbiturils	167
4	Squaraine Rotaxanes	169
5	Dye–Macromolecule Complexes	180
6	Microporous Solid-Phase Encapsulated Dyes	182
7	Fluorophore – Metallic Nanoparticle Compositions	183
8	Concluding Remarks	185
	References	186

L.D. Patsenker (✉), A.L. Tatarets, and O.P. Klochko
State Scientific Institution “Institute for Single Crystals”, National Academy of Sciences of
Ukraine, 60 Lenin Ave., Kharkiv 61001, Ukraine

L.D. Patsenker, E.A. Terpetschnig
SETA BioMedicals, LLC, 2014 Silver Ct East, Urbana, IL 61801, USA

1 Introduction

Because of their advantageous spectral and photophysical properties, cyanines and squaraines are favored for the design of fluorescent probes and labels for biomedical applications, pharmaceutical research, high-throughput screening, and clinical diagnostics [1]. Most of the well-known and widely used long-wavelength fluorescent tracers of dye series such as **Cy** (GE Healthcare), **Alexa Fluor** and **BODIPY** (Life Technologies), **DY** (Dyomics GmbH), **Seta** and **SeTau** (SETA BioMedicals, LLC), **HiLight** (Anaspec Inc.), and **IRDye** (Li-Cor Biosciences) are based on cyanine and squaraine chromophores. Nevertheless long-wavelength fluorescent dyes display shortcomings: lack of photo- and chemo-stability, high tendency of aggregation, and/or reduced quantum yields and fluorescence lifetimes in aqueous environments, which are important factors that limit the use of these dyes for biomedical applications. In particular, dye-aggregates have a strong influence on the above factors as they are known to photobleach faster, and to display lower quantum yields and shorter lifetimes compared to the monomers [2]. A promising way to improve dye performance is molecular encapsulation of the dye inside a host molecule such as a macrocycle to form a *rotaxane* [3–7] or binding to a *macromolecule*, by forming a dye–protein or dye–aptamer complex [8]. Encapsulation in a macromolecule or in a *micro-* or *nano-particle* prevents dye molecules from undesirable environmental impact and aggregation, and therefore helps to improve the photophysical properties of dyes.

Dye–rotaxanes are a mechanically-interlocked molecular architecture consisting of a dumbbell-shaped dye molecule (stem) which is threaded through a macrocycle (Fig. 1). Typical examples of the macrocycles are cyclodextrins (CDs), cucurbiturils (CBs), crown-ethers, and calixarenes. The three most common strategies to synthesize rotaxane are “capping”, “clipping”, and “slipping” [9–13], though others do exist [14, 15].

Capping. The synthesis *via* the capping method is based on the thermodynamically driven template effect, wherein the guest molecule is held within the “macrocycle” by noncovalent interactions. This *pseudorotaxane* is then converted to the rotaxane by reacting the ends of the threaded guest with large groups preventing disassociation.

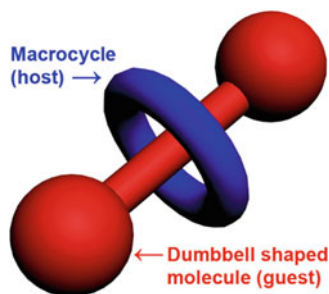


Fig. 1 Graphical representation of a rotaxane

Fig. 2 Graphical representation of a dye–aptamer system



Clipping. The clipping method relies on the synthesis of the rotaxane by formation of the macrocycle (host) in the presence of a dumbbell shaped molecule. The partial macrocycle undergoes a ring closing reaction around the dumbbell shaped molecule, thereby forming the rotaxane.

Slipping. The slipping method exploits the kinetic stability of the rotaxane. Provided the end groups of the dumbbell are of appropriate size, they are able to reversibly thread through the macrocycle at higher temperatures, but by lowering the temperature the dynamic complex becomes kinetically trapped as a rotaxane.

“Active template” methodology. In this method, recently explored by Leigh et al. [16, 17], the rotaxane is formed *via* synthesis of the guest molecule in the presence of the macrocyclic host, where the guest ions or organic molecules play an active template role in promoting rotaxane formation.

Aptamers are oligonucleic acids or peptide molecules that bind to a specific target biomolecule (Fig. 2). A dye molecule can be noncovalently or covalently bound to an aptamer.

This chapter describes the synthesis, properties, and biomedical applications of cyanine and squaraine dyes encapsulated in CDs, CBs, Leigh-type tetralactam macrocycles, aptamers, and micro- or nano-particles. The optical and photochemical properties of supramolecular “guest–host” nanostructures that are based on intra- and intermolecular complexes of crown-containing styryl dyes with metal cations, and aggregates of carbocyanine dyes are discussed in a separate review [18].

2 Dye–Cyclodextrins

There are three main types of CDs: α -cyclodextrin (α -CD), β -cyclodextrin (β -CD), and γ -cyclodextrin (γ -CD), which are macrocycles formed by six, seven, and eight sugar ring molecules, respectively. The spatial structure of β -CD is shown on Fig. 3. Review [19] generalizes data on the synthesis, modification, physicochemical and theoretical investigations of CDs, and certain applications particularly for enantio-separation and pharmaceutical applications. CDs are able to form host–guest complexes (pseudorotaxanes) with hydrophobic molecules such as aza-dyes

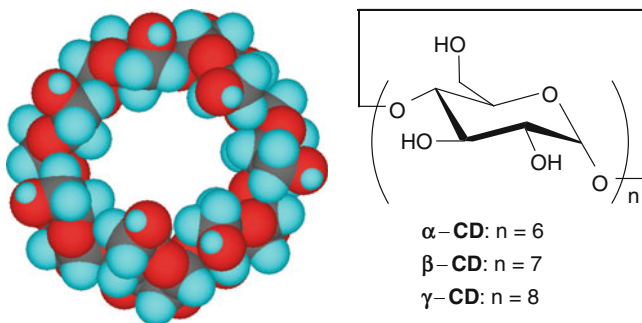


Fig. 3 Spatial structure of β -cyclodextrin (β -CD)

[20] or acetylene dyes [21] given the unique nature imparted by their structure. As a result, these molecules have found a number of applications in different fields. The formation of guest–host complexes between dye molecules and CD macrocycles leads to certain improvements of the dyes' physicochemical properties.

Cyanine dye–CD complexes were first reported by Kasatani et al. in 1984 using 3,3'-diethyloxadicyanin iodide (**DODC**) [22]. It was found that this dye formed complexes with β - and γ -CDs but not with α -CD. Later, they demonstrated the same tendency with cyanines **1** and **2** [23]. It was shown that inclusion of cyanine dyes in β -CD and Me- β -CD helps to inhibit dimer formation as well as to enhance the photostability of these cyanines, thereby enhancing the dyes' utility as a fluorescent probe [7, 24].

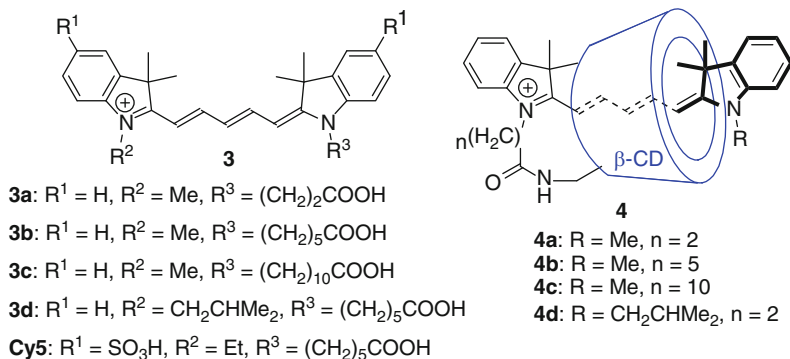
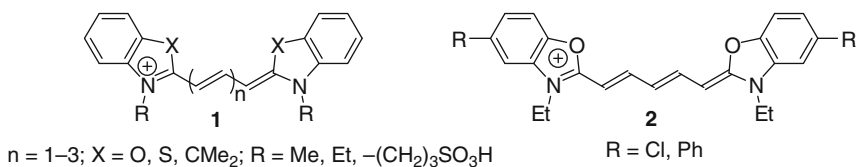


Table 1 Relative photostabilities (F/F_0) and quantum yields (Φ_F) in water [2]

Dye	F/F_0	Φ_F	$\Phi_F \times F/F_0$
Cy5	1.0	0.20	0.20
3a-dextran	0.95	0.14	0.13
3a	0.53	0.12	0.06
3b	0.41	0.11	0.05
3c	0.13	0.07	0.01
3d	0.53	0.13	0.06
4a	9.1	0.06	0.55
4b	1.6	0.10	0.16
4c	0.44	0.14	0.06
4d	20	0.07	1.40

In general, the aggregates of cyanine dyes photobleach faster than the monomeric (nonaggregated) dyes and they also display lower fluorescence quantum yields (Φ_F) [2]. In the series **3a–3d** shown in Table 1, the dye hydrophobicity increases as the side chain is lengthened causing increased dye aggregation in aqueous solution. Importantly, the photostability and quantum yields decrease in the same order: **3a** \approx **3d** > **3b** > **3c**. The water soluble **3a**–dextran (not CD) conjugate exhibits a similar photostability as **Cy5** (GE Healthcare) suggesting that the electronic differences between the sulfonated (**Cy5**) and nonsulfonated (**3a**) chromophores do not have a significant effect on their relative rates of photobleaching [2]. Coupling of dyes **3a–d** with 6-amino-6-deoxy- β -CD yields the water-soluble conjugates **4a–d** which are more photostable than their parent dyes (Table 1). The increase in photostability can be attributed to the reduced tendency to form aggregates and the protective effect of the CD. Conjugates **4a** and **4d** are able to emit approximately 2.7- and 7-fold, respectively, more photons than **Cy5**, before they are decomposed. When injected into live *Swiss 3T3* cells, conjugates **4a** and **4d** were found to be about 7- and 8-times more photostable than **3a**–dextran, which exhibited a similar photostability to **Cy5** conjugated to a non-specific antibody. Cyanine- β -CD conjugates therefore can be considered a viable approach to the preparation of fluorescent markers having improved photostability.

The complexation with CDs also results in spectral shifts of the absorption and emission maxima of cyanine dyes. The complexation of cyanine dyes **1** ($X = S$, $R = Et$, $n = 1-3$) with β -CD red-shifts the emission bands [25].

Importantly, α -CD, which has a smaller cave compared to β -CD, does not form complexes (pseudorotaxanes) with indocyanines. However, a heptamethine indocyanine dye rotaxane **5** \subset α -CD·PF₆⁻, consisting of the symmetrical cyanine **5**, threaded through an α -CD can easily be synthesized on a gram scale in one step from readily available starting materials – reacting glutacetaldehyde acetate with a tetramethyl indolium salt in the presence of a α -CD in aqueous potassium acetate (Fig. 4) [26]. The indolenine terminal groups of the cyanine dye were found to be sufficiently bulky to lock the α -CD permanently over the center of the chromophore, without the need for any additional bulky stopper groups.

Compared to the absorption and emission spectra of the free dye, the spectra of the rotaxane **5** \subset α -CD·PF₆⁻ are sharper and red-shifted. The absorption maximum

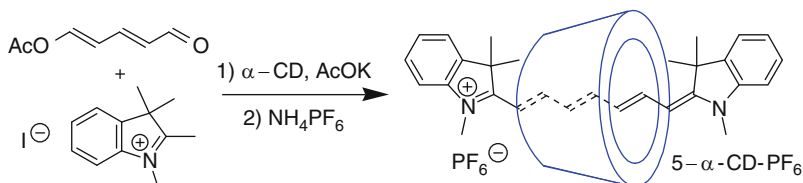


Fig. 4 Synthesis of cyanine dye rotaxane **5** \subset α -CD \cdot PF₆

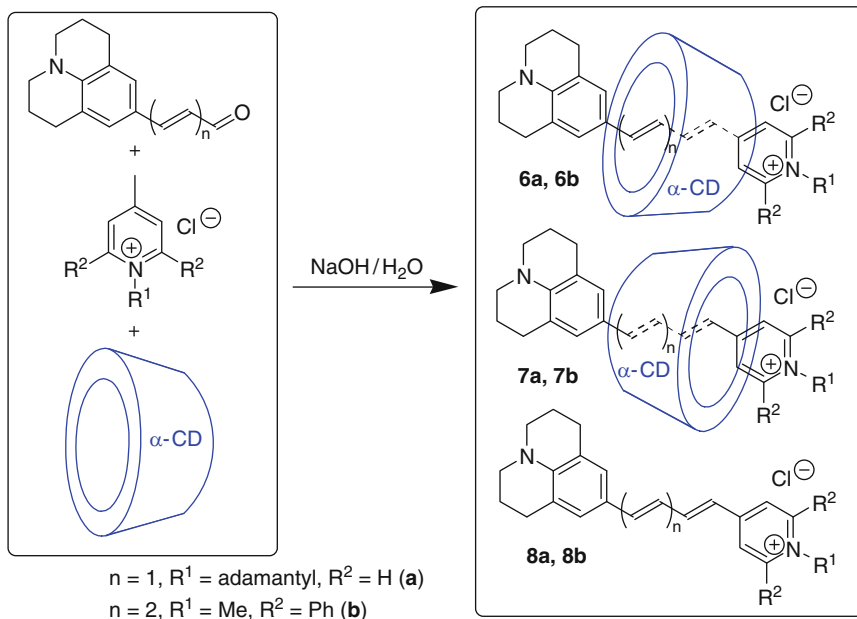


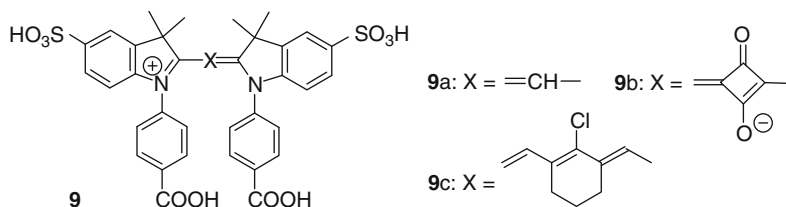
Fig. 5 Synthesis of α -CD-based styryl-rotaxanes **6a, b** and **7a, b** [4, 27]

of **5** \subset α -CD \cdot PF₆ in methanol is 770 nm ($\epsilon_M = 2.8 \times 10^5 \text{ M}^{-1} \text{ cm}^{-1}$) and the emission maximum is 796 nm ($\Phi_F = 0.23$), whereas the free dye **5** absorbs at 741 nm ($\epsilon_M = 2.3 \times 10^5 \text{ M}^{-1} \text{ cm}^{-1}$) and emits at 778 nm ($\Phi_F = 0.37$) [26]. Encapsulation of the cyanine dye **5** reduces the fluorescence quantum yield but increases its photostability (3.9-fold), and chemical stability.

Reaction of 3-(9-julolidinyl)prop-2-en-1-al with *N*-(1-adamantyl)-4-methyl-pyridinium chloride and α -CD in aqueous sodium hydroxide yielded *styryl* dye rotaxanes **6a** and **7a** as well as the free dye **8a** (Fig. 5) [4, 27]. Analogously, the two rotaxane isomers **6b** and **7b**, and the free dye **8b** were obtained from julolidine aldehyde and 4-methyl-2,6-diphenylpyridinium chloride. As compared to the hydrophobic dyes **8a, 8b**, the rotaxanes **6a, 6b** and **7a, 7b** are highly soluble in water. The absorption/emission maxima of the rotaxanes **6a** (525/710 nm) and **7a** (535/718 nm) in DMSO are red-shifted compared to free styryl dye **8a**

(477/678 nm). In water, the fluorescence quantum yields of rotaxanes **6a** and **7a** are lower than that of the free dye, whereas in other solvents such as acetone, DMSO, alcohols, and especially dioxane, the rotaxanes are more fluorescent. The rotaxane **7a** exhibits higher photostability as compared to the free dye **8a** (40-fold in water and twofold in dioxane) in air-saturated aqueous solutions under visible light exposure while the photostability of **6a** has not been reported. The absorption maxima of rotaxanes **6b** (590 nm) and **7b** (579 nm) are also red-shifted compared to the free styryl dye **8b** (571 nm). Inclusion of dyes **8a**, **8b** in the α -CD rotaxane system increases its photostability and the relative fading rates for **6b**, **7b**, and **8b** are 0.031, 0.044, and 1.00, respectively.

The absorption and emission maxima of trimethinecyanine **9a** (551 nm and 565 nm), squaraine **9b** (631 nm and 641 nm), and cyanine **9c** (784 nm and 805 nm) hardly change after complexation with α -CD and β -CD in water, but the fluorescence quantum yields increase noticeably [28]. CD complexes of these water-soluble dyes containing reactive carboxylic functionalities have potential use as fluorescent labels.



β -CD complexation can be used for the development of *fluorescence resonance energy transfer (FRET) based assays*. A FRET system based on the *Escherichia coli* maltose binding protein (MBP) modified with cyanine dye **Cy3** or **Cy3.5** as the donor and β -CD modified with either **Cy5** or the dark quencher **QSY9** as the acceptor was synthesized and used as a sensing system for maltose [29]. Binding of the modified β -CD to dye-conjugated MBP resulted in assembly of the FRET complex. Added maltose displaced the β -CD – dye adduct and disrupted the FRET complex, resulting in a change in fluorescence intensity of the donor moiety. Based on the use of these FRET pairs, the MBP dissociation values for maltose were estimated (0.14–2.90 μM). The FRET complexes allow a measurement range between 50 nM and 50 μM maltose.

The synthesis of a hetero-[3]rotaxane with one stilbene and one cyanine dye threaded through the γ -cyclodextrin macrocycle, which exhibits quantitative *energy transfer* between the two encapsulated guests was demonstrated by Klotz et al. [30]. The synthesis of a [3]rotaxane with two dumbbells threaded through the same macrocycle requires the use of a large macrocycle, which in turn requires the use of very bulky stopper groups to prevent unthreading. Suzuki coupling of iodoterphenylenedicarboxylic acid as the stopper with trimethine diboronic acid (**10**) or stilbene diboronic acid (**11**) in the presence of excess aqueous γ -CD yielded the [2]rotaxane **10** \subset γ -CD or **11** \subset γ -CD, respectively. The high affinities of

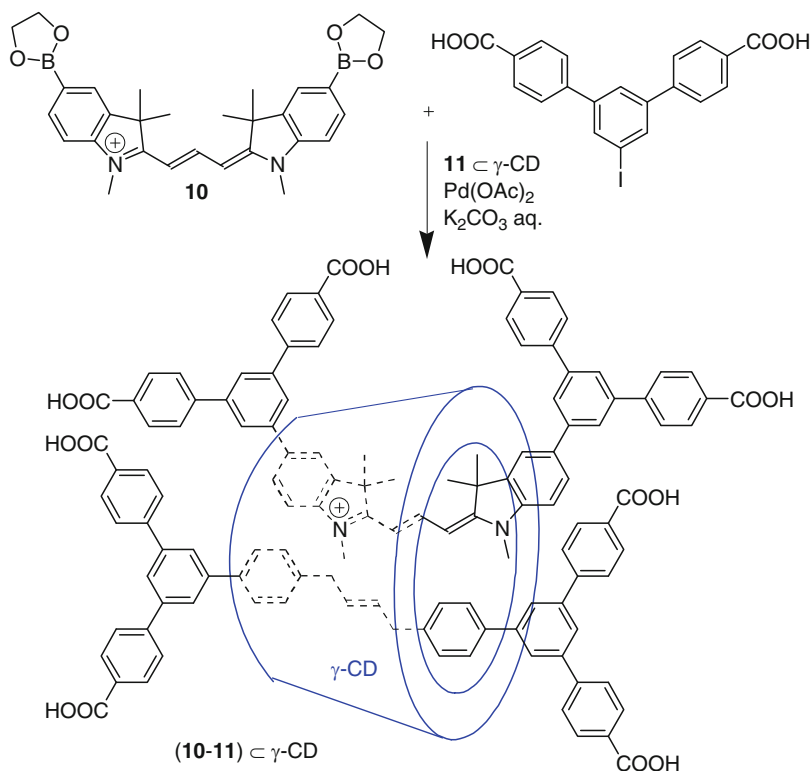


Fig. 6 Synthesis of (10-11) \subset γ -CD

[2]rotaxanes 10 \subset γ -CD and 11 \subset γ -CD for a second threaded guest provide an efficient route to [3]rotaxanes (10-11) \subset γ -CD (Fig. 6).

The absorption and emission spectrum of [3]rotaxane (10-11) \subset γ -CD were compared to those of the two analogous [2]rotaxanes 10 \subset γ -CD and 11 \subset γ -CD. The ground-state interaction between the two chromophores in (10-11) \subset γ -CD appears to be weak; the shapes of the absorption and emission bands are almost identical, although all the bands are red-shifted by about 10 nm in the [3]rotaxane. However, excitation of the stilbene component of (10-11) \subset γ -CD results in quantitative energy transfer to the cyanine dye and emission from the cyanine. Quantitative energy transfer is also demonstrated by the lack of stilbene-type emission at 430 nm when (10-11) \subset γ -CD is excited at 350 nm and by the fact that the excitation spectrum of (10-11) \subset γ -CD is superimposable over its absorption spectrum. The fluorescence quantum yield of the [3]rotaxane (10-11) \subset γ -CD ($\Phi_F = 0.56$) is substantially higher than that of the [2]rotaxane 11 \subset γ -CD ($\Phi_F = 0.12$) presumably because of restricted conformational freedom. The binding behavior of 10 \subset γ -CD and 11 \subset γ -CD suggests that they may be useful in *sensors*.

Analysis of the available literature data on host–guest complexes based on cyanine and styryl dyes with CDs shows that rotaxane formation in general

increases the water-solubility and photostability of the dyes, both important factors for biomedical applications. Nevertheless, sometimes rotaxane formation is accompanied by a reduction of the fluorescence quantum yields. The modification of the physicochemical properties of cyanine dyes by cyclodextrin complexation is a highly selective, structure dependent phenomenon, which is dependent upon the structure of the dye as well as the size of the host cavity.

3 Dye–Cucurbiturils

CBs are macrocyclic molecules that consist of 5–10 glycoluril repeat units joined by pairs of methylene bridges (Fig. 7). Because CBs are capable of binding or hosting positively charged or neutral molecules within their hydrophobic cavities, they are useful rotaxane macrocycles to protect dye molecules against aggregation [31–33] and environmental impact [20, 34]. CBs are also important for many applications such as drug delivery [35], molecular recognition [36, 37], and supramolecular catalysis [38, 39]. Numerous articles and reviews on the synthesis, chemical modifications [40–42], spectral, photophysical, and recognition properties [43], and applications of CBs and dye–CB complexes were published [44–46].

Importantly, CBs with an *odd* number of glycoluril units are highly *hydrophilic*. Cucurbit[5]uril (**CB5**) has very small inner volume which greatly limits its use in hosting dyes. The cavity dimensions of cucurbit[6]uril (**CB6**) allow accommodation of up to seven heavy atoms, but it is poorly water-soluble, which limits its biomedical applications. **CB8–CB10** have much larger cavities that can encapsulate more than one guest dye molecule, which does not prevent aggregation. **CB8** has a similar cavity volume as γ -cyclodextrin but displays very low water solubility. **CB7** seems to be the most attractive macrocycle for development of advanced biomedical markers because it combines sufficient water solubility and appropriate cavity size for hosting organic dyes with at least 12 heavy atoms.

Encapsulation in a cucurbit[7]uril (**CB7**) macrocycle was suggested to help improve solubility, prevent undesirable aggregation, and thereby increase the quantum yields and fluorescence lifetimes of fluorescent dyes [46].

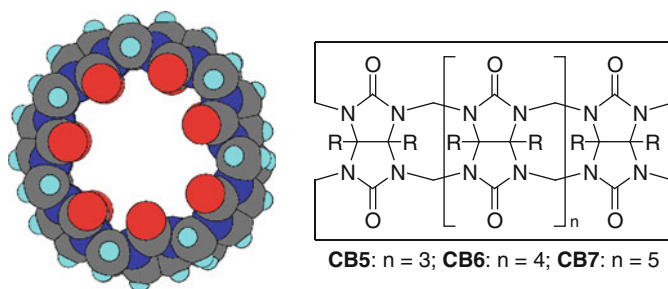
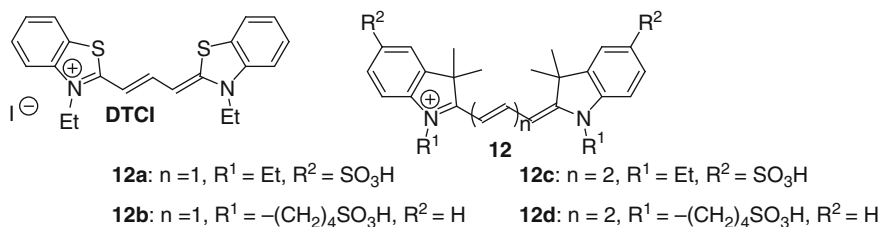


Fig. 7 Spatial structure of cucurbit[7]uril (**CB7**)

Encapsulation of 3,3'-diethyl-thiacarbocyanine iodide (**DTCI**) with **CB7** resulted in a fivefold increase of its quantum yield. The encapsulation decreases the 550 nm peak in the absorption spectrum and increases the shoulder at 510 nm [47]. The fluorescence lifetime for **DTCI** in aqueous solution is 0.12 ns, but in the presence of **CB7** it increased to 1.07 ns. The association constant of 1:1 complexes of **DTCI** with **CB7** was determined to be $K = (2.8 \pm 0.2) \times 10^4 \text{ M}^{-1}$.



While the encapsulation of the trimethine dyes **12a** and **12b** (**Cy3** analogs) leads to *red-shifted* absorption and emission spectra, the maxima of the pentamethines **12c** and **12d** (**Cy5** analogs) remain almost unchanged upon encapsulation (Table 2). The fluorescence quantum yield and relative brightness of dyes **12c** and **12d** substantially increase (~ 1.7 -fold) upon encapsulation in the **CB7** macrocycle, while the encapsulation of dye **12a** is accompanied by a 1.3–1.5-fold decrease in brightness [48]. The fluorescence lifetimes of **12b** and **12d** in water (0.46 and 0.63 ns) increase to 0.58 and 1.59 ns, respectively, after embedding in the **CB7** macrocycle. The **CB7** macrocycle was also suggested to protect dye molecules from photobleaching: indeed the photostability of the **12a**–**CB7** and **12c**–**CB7** complexes increases slightly compared to that of the free dyes, but the reported increases are small.

In summary, the encapsulation of cyanine dyes in **CB7** causes either an increase or a decrease in quantum yields and brightness but in general increases photostability. Enhancements in fluorescence intensity by about one order of magnitude or more were observed [46]. These fluorescence property changes are utilized for the development of *sensors*, where the fluorescent dye may serve as a probe to signal the binding of an analyte. No reports were found on the encapsulation of squaraines in CBs.

Table 2 Effect of the addition of **CB7** on the spectral characteristics and photostability of cyanine dyes in water [46, 48]

Dye	Without CB7			With 1 mM CB7			
	λ_{max} Ab (nm)	λ_{max} Em (nm)	Φ_{F}	λ_{max} Ab (nm)	λ_{max} Em (nm)	Φ_{F}	Stabilization factor
12a	545	560	0.15	559	571	0.108	1.4
12b	545	560	0.04	559	571	0.03	–
12c	642	660	0.27	642	657	0.456	1.3
12d	642	660	0.17	642	657	0.30	–

4 Squaraine Rotaxanes

Squaraines are one of the most promising classes of dyes for use as long-wavelength fluorescent probes and labels [49–51]. The limitations of some squaraine dyes are their insufficient photostability, lack of chemical stability to oxidizing agents such as hydrogen peroxide and ozone, and their inherent reactivity with nucleophiles, which leads to loss of the chromophoric system thereby rendering the molecule non-fluorescent. Another drawback is their tendency to form nonfluorescent aggregates in water. Smith and co-workers demonstrated that these problems can be overcome by encapsulation of bis-aniline-type squaraine dyes **13a–13f** in a tetralactam macrocycle and formation of squaraine rotaxanes such as **14a–14g** [52–54]. These squaraine rotaxanes were synthesized using a Leigh-type clipping reaction with a templated macrocyclization around the squaraine dye (Fig. 8). Encapsulation of squaraine dyes by *phenylene*-based macrocycles was achieved by treatment of *para*-xylylenediamine with 1,3-benzenedicarbonyl chloride to yield rotaxanes **14a** and **14g** or with 2,6-pyridinedicarbonyl chloride to give rotaxanes **14b–14f**.

The encapsulation of aniline-squaraine dyes inside Leigh-type tetralactam macrocycles causes slightly red-shifted absorption and emission spectra and substantially increased chemical and photochemical stabilities. The hydrophobic rotaxanes **14a** and **14c** have similar absorption (630–650 nm) and emission (650–680 nm) maxima as the squaraine precursor **13a**, but in THF–water (4:1) the quantum yield and fluorescence lifetime for rotaxane **14a** are significantly decreased as compared to those of **13a**, whereas rotaxane **14c** with a pyridyl-containing macrocycle shows a slightly higher quantum yield and a noticeably increased fluorescence lifetime (Table 3). As the water content in the solvent mixtures is increased (THF–water, 1:4), squaraine **13a** starts to form nonfluorescent aggregates, which severely quench fluorescence ($\Phi_F \sim 10^{-4}$), while the water-soluble squaraine **13b** and the related rotaxane **14b**, both containing four

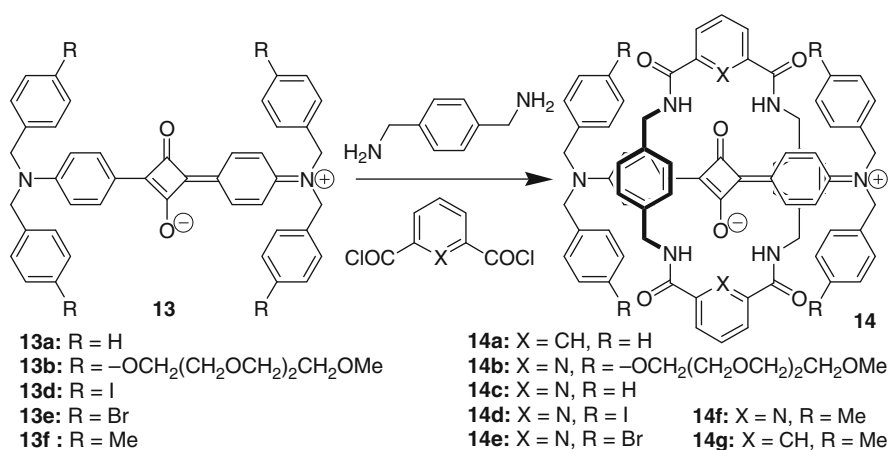


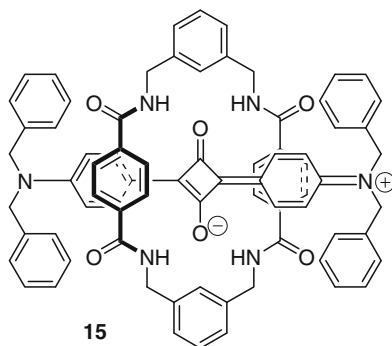
Fig. 8 Synthesis of squaraine-rotaxanes **14a–14g**

Table 3 Absorption and emission of squaraine and rotaxanes in THF–water (4:1) [52]

Dye	λ_{\max} Ab (nm)	$\log \epsilon_M$	λ_{\max} Em (nm)	Φ_F	τ_F (ns)
13a	637	5.41	660	0.45	2.14
14a	650	5.17	676	0.15	1.24
14c	643	5.14	667	0.58	2.16 ^a

^aOwn data

tri-(ethyleneoxy) chains, exhibit higher quantum yields (0.27 and 0.38, respectively) in this medium [53]. Rotaxane **14b** containing four tri(ethyleneoxy) chains exhibits improved solubility and reduced aggregation in aqueous media compared to **14a** and **14c**, which allowed its use in biological media; nevertheless, this rotaxane still cannot be considered highly water-soluble.



The stability of these compounds towards nucleophilic attack by agents like cysteine increases in the order: **13a** < **14a** < **14c**. The pyridyl-containing macrocycle in the rotaxane **14c** seems to protect the squaraine center slightly better than the isophthalamide-containing macrocycle in **14a**. Furthermore, because of better sterical protection of the squaraine dye by the macrocycle, rotaxane **14a** has a higher stability compared to **15**, the isomer with transposed carbonyl groups [53]. Rotaxane **14b** is quite resistant to biological quenchers such as tryptophan (30 mM). The chromophores of squaraines **13a–13f** and rotaxane **15** were readily decomposed in basic solutions but were moderately stable under acidic conditions, while solutions of the water-soluble rotaxane **14b** were completely stable for days when exposed to buffers, irrelevant of pH. Temperature, serum, and photobleaching studies produced essentially the same stability trend.

References [52–54] do not include any data directly comparing squaraine rotaxanes with common cyanine dyes such as **Cy5** (GE Healthcare) and **Alexa 647** (Life Technologies). Nevertheless, from the available data it can be concluded that squaraine rotaxanes are remarkably resistant to chemical and photochemical degradation, and likely to be very useful as a versatile fluorescent scaffold for constructing various types of highly stable, red and near infrared (NIR) *imaging* probes and labels.

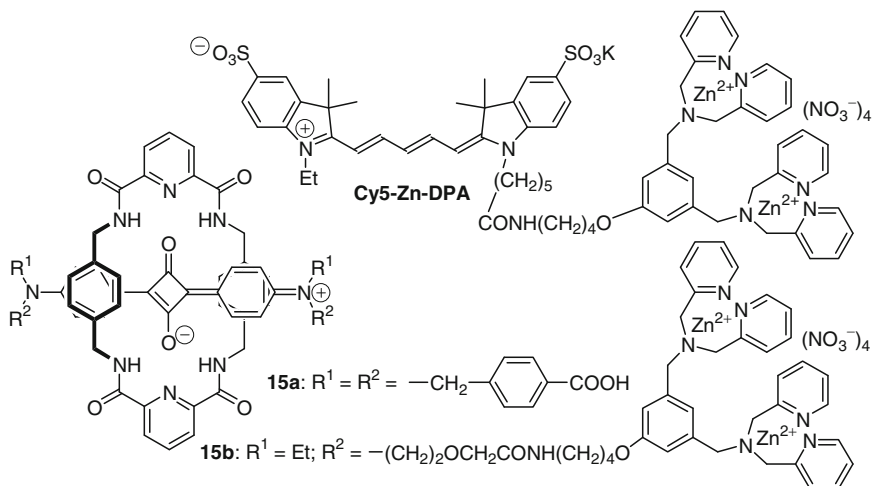
Squaraine rotaxane dyes also were utilized as extremely bright and highly stable NIR fluorescent probes for *in vitro* and *in vivo* optical imaging of live and fixed cells [55]. These probes were modified for targeting of different cellular locations, namely,

the *membranes* of organelles, the *internal* aqueous phase, and the *exterior* cell surface. Probes **14c**, **15a**, and **15b** have absorption and emission profiles that closely match the **Cy5** chromophore in control compound **Cy5-Zn-DPA** and therefore, they can be imaged using a standard **Cy5** filter set.

The relatively nonpolar squaraine rotaxane **14c** was found to interact with cells in a very similar way to the well-known lipophilic dye Nile Red: this probe rapidly accumulates at lipophilic sites inside a living cell, such as the endoplasmic reticulum and intracellular lipid droplets [55]. The red emission band for probe **14c** is quite narrow and permits the acquisition of *multicolor images*. It displayed *high chemical stability* and *low toxicity*.

The squaraine rotaxane tetracarboxylic acid **15a** is soluble in aqueous solution at physiological pH and acts as an excellent fluorescent marker with extremely high photostability, which allows trafficking processes in cells to be monitored in real-time, with constant sample illumination, over many minutes. This type of *real-time monitoring* cannot be done with other available NIR fluorescent probes, such as the amphiphilic styryl dye **FM4-64** and water-soluble dextran–**Alexa 647** conjugate, because they are rapidly photobleached.

With the example of stained *E. coli* cells, the squaraine rotaxane **15b** containing a zinc(II)–dipicolylamine (Zn–DPA) ligand, which is known to selectively associate with the anionic surfaces of bacterial cells, was found to be almost 100 times more photostable as compared to **Cy5-Zn-DPA** [55]. This can be attributed to stronger cell-surface affinity of **15b**, leading to a slower off rate for the probe. The remarkable stability of **15b** permits fluorescence imaging experiments that are impossible with probes based on conventional NIR cyanine dyes such as **Cy5**. Squaraine rotaxanes are likely to be superior substitutes for conventional cyanine dyes for biomedical imaging applications that require NIR fluorescent probes.



The *anthracene*-containing tetralactam macrocycles **16a** and **16b** were found to have an extremely high affinity for aniline-based squaraine dyes in chloroform [56].

Table 4 Spectral characteristics of squaraines and squaraine rotaxanes in chloroform [56, 58]

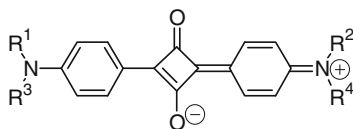
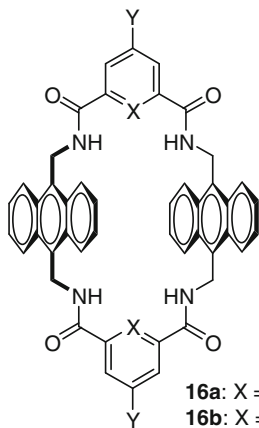
Dye	λ_{\max} Ab (nm)	$\log \epsilon_M$	λ_{\max} Em (nm)	Φ_F
17b	631	5.65	651	0.68
16a \supset 17b	648	5.45	699	0.45
16b \supset 17b	658	5.44	695	0.45
19a	635	4.91	649	0.65
18 \supset 19a	645	5.23	656	0.24
16b \supset 19b	661	5.24	704	0.47

Squaraines **17a–17c** were encapsulated in these macrocycles to form the corresponding pseudorotaxanes. Squaraine rotaxanes **14** and **15** with a *phenylene* tetralactam macrocycle have absorption/emission profiles (Table 3) that closely match those of **Cy5**, whereas squaraine rotaxanes **16** \supset **17** with an *anthrylene* macrocycle have a red-shifted absorption/emission that matches that of the homologous cyanine **Cy5.5** (Table 4). These rotaxanes should be useful for fluorescence microscopy *imaging* applications.

The impact of self-assembly on the geometry and visible absorption spectrum of a rotaxane formed by squaraine **17a** and anthracene-based tetralactam macrocycle **16a** was assessed using quantum-chemical DFT, TD-DFT, and QM/MM approaches [57].

Squaraines **17b** and **17c** have terminal acetylene residues, which allowed to convert the squaraine dyes and tetralactam macrocycles into permanently interlocked rotaxane structures using copper-catalyzed and copper-free cycloaddition reactions with bulky stopper groups [58].

Capping strategies to synthesize rotaxanes with phenylene-based tetralactam macrocycles are not effective because of very poor macrocycle solubility. To circumvent this problem, other macrocycles that have a similar isophthalamide tetralactam motif but exhibit higher solubility in organic solvents were investigated by Smith et al. [58]. The macrocycle **18**, which is soluble in methylene chloride, was used to encapsulate squaraine dye **17b**. Then, the protruding alkyne ends of the pseudorotaxane complex were covalently capped by conducting a copper mediated alkyne azide cycloaddition reaction. Mixing macrocycle **18** with excess dye **17b** and stopper **S1** followed by treatment with $\text{Cu}(\text{Ph}_3\text{P})_3\text{Br}$ catalyst generates the “clicked rotaxane” **18** \supset **T1** [58].

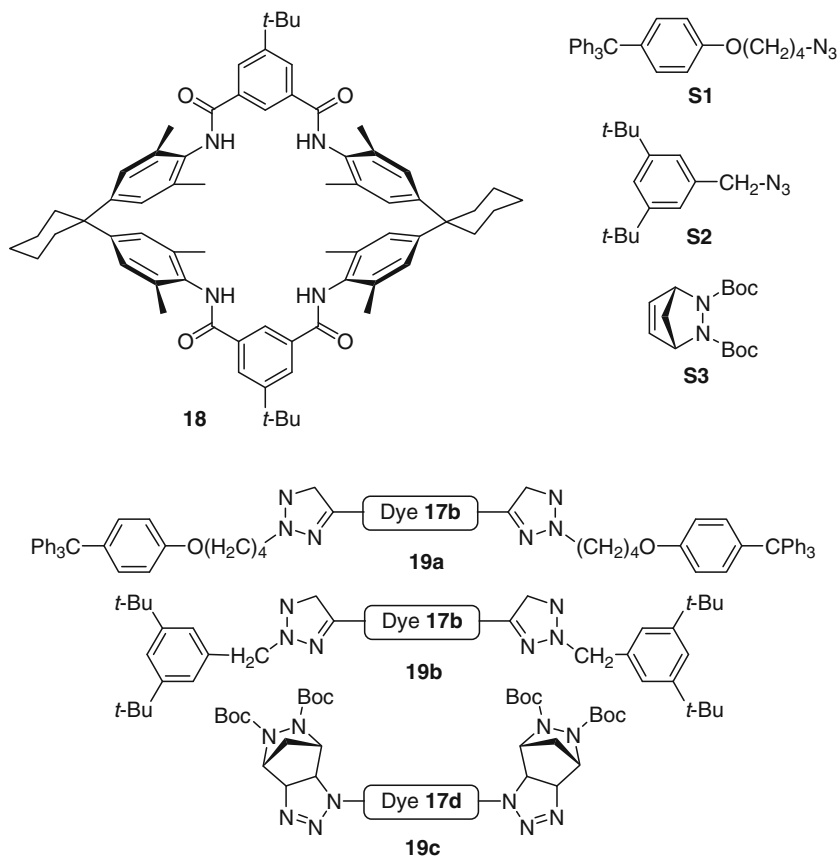


17a: $R^1 = R^2 = R^3 = R^4 = \text{Me}$

17b: $R^1 = R^2 = \text{Et}$, $R^3 = R^4 = -(\text{CH}_2)_2\text{OCH}_2\text{-C}\equiv\text{CH}$

17c: $R^1 = R^3 = \text{Ph}$, $R^2 = \text{Et}$, $R^4 = -(\text{CH}_2)_2\text{OCH}_2\text{-C}\equiv\text{CH}$

17d: $R^1 = R^2 = \text{Et}$, $R^3 = R^4 = -(\text{CH}_2)_2(\text{OCH}_2\text{CH}_2)_2\text{-N}_3$



The conversion of squaraine **19a** to the rotaxane **18** \supset **19a** causes a modest red-shift only in both absorption (10 nm) and emission (7 nm) but an approximately threefold decrease in quantum yield. The addition of two triazole rings (dye **19b**) did not significantly alter the quantum yield of **17b** (Table 4). A macrocycle-induced quenching effect was verified by fluorescence titration experiments adding aliquots of **18** to a solution of squaraine **17b** in methylene chloride [58]. Treatment of the **18** \supset **17b** pseudorotaxane system with the tetrabutylammonium salts of chloride, acetate, or benzoate leads to the displacement of squaraine **17b** from the macrocyclic cavity and the nearly complete restoration of its fluorescence intensity. The **18**-induced quenching of **17b** does not support the utility of this system as a bioimaging probe; however, the pseudorotaxane system **18** \supset **17b** acts as an effective and selective *anion sensor* with NIR fluorescence.

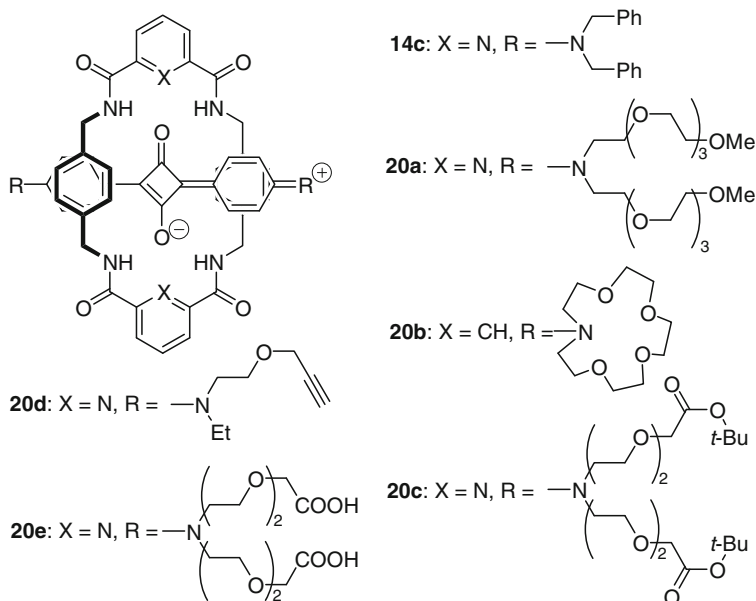
Compared to **18**, the anthrylene macrocycle **16b** is a more promising building block for squaraine rotaxane fabrication and fluorescent probe development.

An admixture of **16b** and **17b** self-assembles quantitatively at millimolar concentration in chloroform solution to produce an inclusion complex whose absorption and emission maxima are red-shifted by 40 nm [56]. “Clicking” both ends of this pseudorotaxane with two molar equivalents of stopper **S2** produces the squaraine rotaxane **16b** \supset **19b** in near-quantitative yield [58]. Pseudorotaxane **16b** \supset **17b** partially dissociates at micromolar concentrations in chloroform and produces two emission peaks, one at 638 nm which corresponds to free squaraine **17b** and one at 694 nm, corresponding to the pseudorotaxane. In contrast, the squaraine rotaxane **16b** \supset **19b** does not dissociate under these conditions or in more polar solvents such as pure methanol.

The squaraine rotaxane **16b** \supset **19c** was also produced in near-quantitative yield by heating of a mixture of bis-azide squaraine dye **17d**, macrocycle **16b**, and stopper **S3** [58]. The compound is stable enough for immediate characterization but slowly decomposes upon exposure to light.

The squaraine rotaxanes based on the macrocycle **16b** exhibit intense NIR absorption and emission maxima, and it should be possible to develop them into molecular probes for many types of photonic and *bioimaging* applications. In contrast, the squaraine fluorescence intensity is greatly diminished when the dye is encapsulated with macrocycle **18**. The fluorescence is restored when a suitable anionic guest is used to displace the squaraine dye from a pseudorotaxane complex, which indicates that the multicomponent system might be applicable as a fluorescent *anion sensor*.

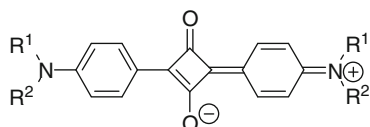
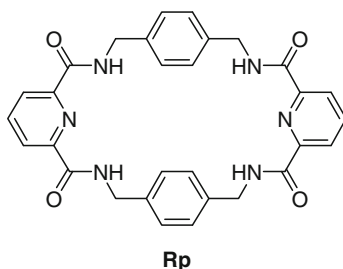
Also, the effects of the stopper size was thoroughly investigated in the example of a series of squaraine rotaxanes **14c** and **20a–20e** and were found *NOT* to be a main factor for rotaxane stability. In general, the host–guest complementarity between squaraine dyes and the encapsulating tetralactam macrocycle provides excellent mechanical stability and little propensity for unthreading [59]. In a less-polar organic solvent such as chloroform, rotaxanes are stabilized by strong hydrogen bonds (between squaraine and macrocycle molecules) and in water by hydrophobic, aromatic stacking interactions. The water-soluble, tetracarboxylic acid derivative **20e** was found to be highly stable in aqueous solutions. Only in highly polar aprotic solvents such as DMSO, there is evidence for rotaxane unthreading (because of weakening of the noncovalent association of host–guest complexes), which can be reduced by employing sterically large stopper groups. The high rotaxane stability in aqueous solution means that the size of the stopper group is *NOT* a major design constraint, and it should be possible to attach a wide range of targeting groups to these dyes and produce a diverse portfolio of *bioimaging* agents.



A variety of hydrophobic and hydrophilic squaraine rotaxane *probes* and *labels* such as **21a–21e** \subset **Rp** and **22a–22e** \subset **Rp**, containing reactive carboxylic functionalities and hydrophilic sulfo groups, are disclosed in a recent patent application [60]. It was shown that not only *aniline*-based squaraines **21a–21e** but also *heterocyclic* squaraines **22a–22e** can form stable pseudorotaxane complexes. The indolenine-based squaraine **22a** forms rotaxane **22a** \subset **Rp**. Importantly, also the sulfonated squaraine **22b** could be successfully encapsulated in a Leigh-type, phenylene-based, tetralactam macrocycle to yield the water-soluble rotaxane **22b** \subset **Rp**. Quaternized, indolenine-based squaraines do not form pseudorotaxanes probably because of sterical hindrance caused by *N*-alkyl and 3,3'-dimethyl groups. On the other hand, quaternized benzothiazole (**22c**) and benzoselenazole (**22d**) squaraines could be embedded in a Leigh-type macrocycle to yield rotaxanes **22c** \subset **Rp** and **22d** \subset **Rp**, respectively. The hydrophilic, mono-reactive rotaxane **22e-NHS** \subset **Rp** based on *asymmetric* squaraine, synthesized by a cross-reaction of squaric acid with the two different indolenines, was also obtained.

Some of the spectral properties of squaraine rotaxanes are given in Table 5. It can be seen that encapsulation of squaraines **22a–22d** with heterocyclic end-groups in a tetralactam macrocycle results in a small blue-shift of the absorption and emission maxima while the encapsulation of squaraines **22e** and **21a** leads to red-shifted rotaxanes [60]. Importantly, encapsulation in a tetralactam macrocycle has a positive effect not only on the photostability (Figs. 9 and 10) of these dyes but also on the *quantum yields* (Φ_F) and *fluorescence lifetimes* (τ_{mean}). Embedding of any type squaraines in tetralactam rotaxane system increases Φ_F and τ_{mean} (Table 5).

Lifetimes increase up to 18-fold and quantum yields up to $\Phi_F = 0.7$ have been measured for some of these dyes in aqueous media.



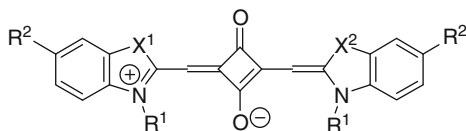
21a: $R^1 = \text{CH}_2\text{Ph}$, $R^2 = (\text{CH}_2)_5\text{COOH}$

21b: $R^1, R^2 = (\text{CH}_2)_3\text{COOH}$

21c: $R^1 = (\text{CH}_2)_3\text{SO}_3\text{H}$, $R^2 = (\text{CH}_2)_3\text{COOH}$

21d: $R^1 = (\text{CH}_2)_3\text{SO}_3\text{H}$, $R^2 = (\text{CH}_2)_3\text{COOEt}$

21e: $R^1 = (\text{CH}_2)_3\text{SO}_3\text{H}$, $R^2 = (\text{CH}_2)_3\text{COO-NHS}$



22a: $X^1 = X^2 = \text{CMe}_2$, $R^1 = R^2 = \text{H}$

22b: $X^1 = X^2 = \text{CMe}_2$, $R^1 = \text{H}$, $R^2 = \text{SO}_3\text{H}$

22c: $X^1 = X^2 = \text{S}$, $R^1 = \text{Me}$, $R^2 = \text{H}$

22d: $X^1 = X^2 = \text{Se}$, $R^1 = \text{Me}$, $R^2 = \text{H}$

22e: $X^1 = \text{CMe}_2$, $X^2 = \text{C}(\text{Me})(\text{CH}_2)_5\text{COOH}$, $R^1 = \text{H}$, $R^2 = \text{SO}_3\text{H}$

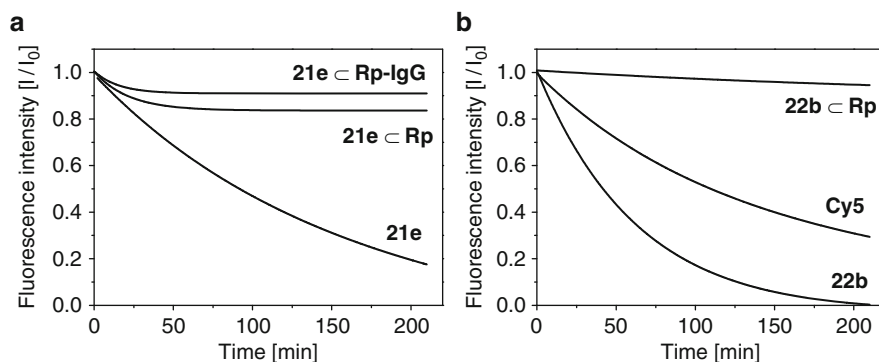
22e-NHS: $X^1 = \text{CMe}_2$, $X^2 = \text{C}(\text{Me})(\text{CH}_2)_5\text{COO-NHS}$, $R^1 = \text{H}$, $R^2 = \text{SO}_3\text{H}$

Conjugation of the squaraine-rotaxane–NHS ester **21e** to protein (IgG) results in a large increase in its fluorescence lifetime. In addition, the encapsulation of the squaraine dyes in a Leigh-type rotaxane increases the chemical stability towards hydrogen peroxide and alkaline agents (Fig. 10). Rotaxane **21e** can be considered a highly-stable, fluorescent label for fluorescence *imaging*, fluorescence *lifetime*, and *single molecule* applications.

Encapsulation of squaraine **23a** in diastereomeric *tritycene*-based tetralactam macrocycles **24a** and **24b** was described in [61]. The synthesis of the macrocyclic hosts was done by the reaction of pyridine-2,6-dicarbonyl dichloride and 2,7-diaminotriptycene in dry THF with Et_3N . Macrocycles **24a** and **24b** readily form

Table 5 Photophysical characteristics of squaraine dyes, squaraine rotaxanes, and IgG conjugates [60]

Dye	Solvent	λ_{\max} Ab (nm)	λ_{\max} Em (nm)	Φ_F	τ_{mean} (ns)
21a	Chloroform	634	652	–	–
21a \subset Rp	Chloroform	645	660	0.70	2.45
21e	Water	644	670	0.03	0.05
21e \subset Rp	Water	655	673	0.25	0.90
21e \subset Rp-IgG ($D/P = 1$)	Water	657	675	0.31	1.83
22a	DMF–water (1:2)	645	664	0.29	2.60 ^a
22a \subset Rp	DMF–water (1:2)	642	659	0.35	2.79 ^a
22b	Water	638	654	0.25	1.56
22b \subset Rp	Water	640	656	0.40	2.40
22c	Chloroform	681	697	0.58	–
22c \subset Rp	Chloroform	676	690	0.59	–
22d	Chloroform	681	698	0.57	3.36
22d \subset Rp	Chloroform	661	674	0.66	3.52
22e	Water	638	655	0.31	1.73
22e \subset Rp	Water	642	658	–	2.45

^aChloroform**Fig. 9** Comparison of the photostability (decrease of fluorescence intensity upon exposure to light of a 200 W Xenon lamp) of **21e**, **21e** \subset **Rp**, and **21e** \subset **Rp-IgG** conjugate (a) and **22b**, **22b** \subset **Rp**, and **Cy5** (b) in aqueous buffer [60]

pseudorotaxanes **24a** \supset **23a** and **24b** \supset **23a**. Relevant spectral data of **24a** \supset **23a** and **24b** \supset **23a** are shown in Table 6 in comparison to squaraine **23a**. Both the absorption and emission show red shifts, which are similar to those of the aniline–squaraine rotaxanes with phenylene- and anthrylene-based macrocycles [52, 53, 55, 56, 58]. Compared to the free squaraine **23a**, the fluorescence quantum yields of the pseudorotaxanes are reduced. Rotaxane **24b** \supset **23a** shows a higher quantum yield than rotaxane **24a** \supset **23a**. The association constants between the hosts and the guest in chloroform were determined to be $6.8 \pm 0.3 \times 10^5 \text{ M}^{-1}$ for **24a** \supset **23a** and $1.3 \pm 0.3 \times 10^6 \text{ M}^{-1}$ for **24b** \supset **23a**, respectively, which indicates that the macrocycles **24a** and **24b** are excellent hosts for the squaraine dye in a weakly polar solvent.

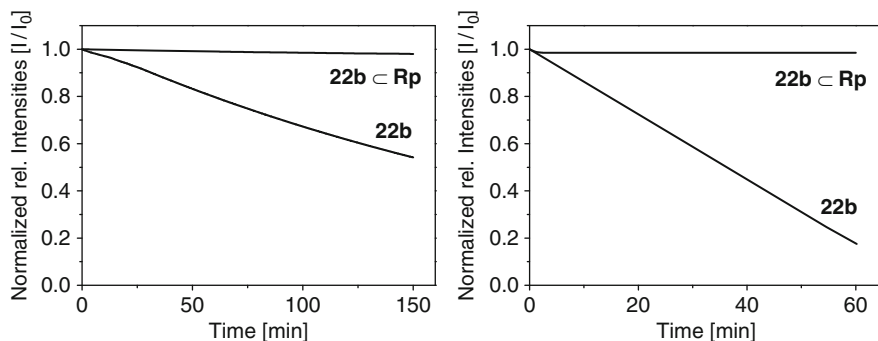
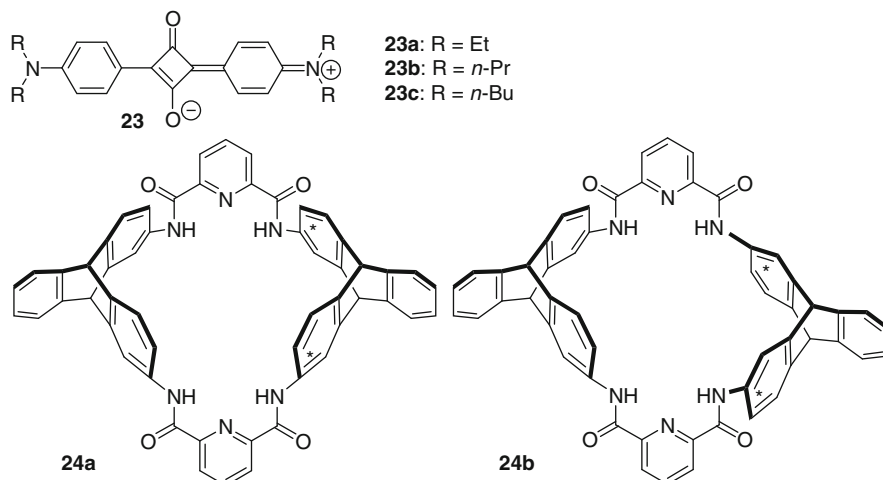


Fig. 10 Comparison of relative intensity changes of **22b** and **22b ⊂ Rp** upon exposure to a 0.5% hydrogen peroxide solution (a) and in presence of NaOH solution pH 13 (b) [60]



The clipping reaction used in [52, 53, 55] to synthesize tetralactam-based squaraine rotaxanes such as **14** and **15** afforded only moderate yields (ca. 28–35%) of the rotaxanes, possibly because of the unavoidable presence of nucleophiles that react with the chemically unstable squaraines during the reaction. The *slippage* approach [62] minimizes the squaraine dye's contact with nucleophiles during the rotaxane formation process and therefore can be used to efficiently encapsulate a squaraine dye such as **23** in a macrocycle such as **25** [63].

Formation of squaraine–pseudorotaxanes can be used to develop selective *chemosensors*: Na⁺ ions behave as highly selective templates, relative to other

Table 6 Spectral characteristics of squaraines and squaraine rotaxanes in chloroform

Dye	λ_{\max} Ab (nm)	$\log \epsilon_M$	λ_{\max} Em (nm)	Φ_F
23a	633	5.52	658	0.72
24a ⊃ 23a	637	5.44	666	0.22
24b ⊃ 23a	642	5.43	667	0.49

physiologically important metal ions such as Li^+ , K^+ , Mg^{2+} , and Ca^{2+} , for the formation of pseudorotaxanes from the molecular cage **25** and squaraines **23a–23c** (Fig. 11) [63, 64]. The complexation and decomplexation of the pseudorotaxane complexes in solution are observable with the naked eye. The encircling molecular cage protects the squaraine moiety from polar solvents, thereby substantially enhancing its quantum yield, and increasing its stability toward chemical attack.

Table 7 lists the photophysical properties of the squaraine **23a** and the rotaxane $[\mathbf{23a} \subset \mathbf{25} \supset \text{Na}_2][\text{2ClO}_4]$ in acetonitrile. Although both the absorption and emission maxima of the rotaxane are shifted to slightly shorter wavelengths relative to those of squaraine **23a**, the quantum yield is increased substantially. The authors explained this effect by the fact that the relatively nonpolar molecular cage partially protected the squaraine dye from solvation by polar CH_3CN molecules, thereby reducing the degree of nonradiative relaxation of the squaraine counterpart. This hypothesis is supported by observation that increasing the amount of CH_3CN in a solution of rotaxane $[\mathbf{23a} \subset \mathbf{25} \supset \text{Na}_2][\text{2ClO}_4]$ in $\text{CHCl}_3/\text{CH}_3\text{CN}$ decreases the emission intensity noticeably.

A substantial increase of the stability of squaraine dye **23a** toward nucleophilic attack after embedding it in a rotaxane system was demonstrated in the example of the reaction with octanethiol in acetonitrile. At the same time, the rotaxane $[\mathbf{23a} \subset \mathbf{25} \supset \text{Na}_2][\text{2ClO}_4]$ was destroyed rapidly in a solution of $\text{CH}_3\text{CN}/\text{H}_2\text{O}$ (9:1) after addition of a large excess of cysteine. Addition of Na^+ ions significantly increases stability of the rotaxane towards cysteine. Other important metal ions such as Li^+ , K^+ , Mg^{2+} , and Ca^{2+} do not affect instability of the rotaxane system, which is in good agreement with the observation [64–66] that the formation of the rotaxane is templated by Na^+ ions in a highly selective manner.

Rotaxane $[\mathbf{23a} \subset \mathbf{25} \supset \text{Na}_2][\text{2ClO}_4]$ was not investigated as a fluorescent probe for biological species and fluorescent imaging. Apparently, it can be used to

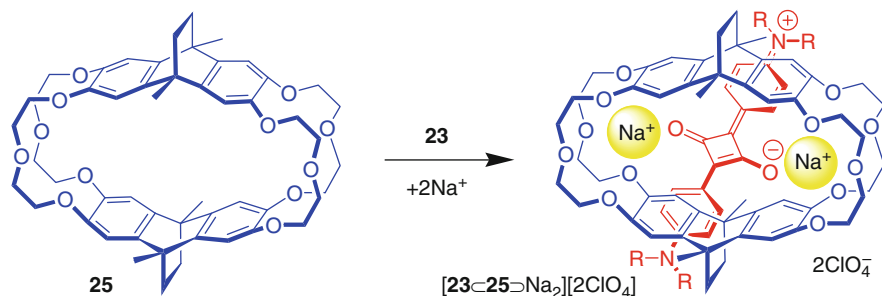


Fig. 11 Synthesis of squaraine rotaxane $[\mathbf{23a} \subset \mathbf{25} \supset \text{Na}_2][\text{2ClO}_4]$ [63, 64]

Table 7 Spectral characteristics of squaraine **23a** and rotaxane $[\mathbf{23a} \subset \mathbf{25} \supset \text{Na}_2][\text{2ClO}_4]$ in acetonitrile [63]

Dye	λ_{max} Abs (nm)	$\log \epsilon_{\text{M}}$	λ_{max} Em (nm)	Φ_{F}
23a	640	5.57	656	0.13
$[\mathbf{23a} \subset \mathbf{25} \supset \text{Na}_2][\text{2ClO}_4]$	634	5.04	643	0.38

develop a highly selective Na^+ indicator. However, applicability of this rotaxane to design highly stable, water-soluble labels is ambiguous because its stability is strongly dependent upon presence on Na^+ ions.

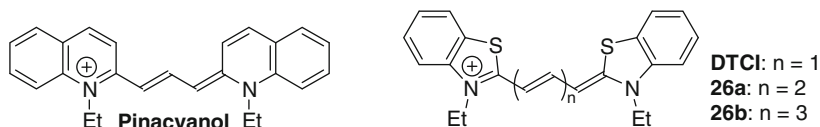
An overview of the synthesis, structure, photophysical properties, and applications of squaraine rotaxanes as fluorescent imaging probes and chemosensors is provided in a recent review [67]. Although a variety of squaraine dyes form rotaxanes with the molecular cage **25** or with a tetralactam macrocyclic system introduced by Leigh and co-workers [16, 17], there is no evidence in the literature that conventional *cyanine* dyes can be embedded in these macrocycles.

5 Dye–Macromolecule Complexes

Embedding of cyanine and squaraine dyes in macromolecules such as *proteins*, *dendrimers*, or *aptamers* also allows fine-tuning of the photophysical properties and the selectivity of these fluorescent probes and labels.

While the covalent attachment of *cyanine* dyes such as **Cy5** or **Alexa 647** to *proteins* does not result in noticeable changes in their spectral properties, *squaraine* dyes (oxo-squaraines and squaraines with substituted squaraine oxygens) behave quite the opposite: the absorption and emission maxima of squaraines are in general red-shifted after binding to proteins and the quantum yields and fluorescence lifetimes are manifold increased [68–70]. In general hydrophobic squaraines exhibit more pronounced increases compared to hydrophilic dyes. These effects are even stronger in noncovalent dye–protein complexes. Importantly, the photostability of squaraines also increases after binding to proteins.

Embedding of pinacyanol in a three-dimensional *polyphenylene dendrimer* results in a red-shift of absorption (from 600 to 620 nm) and emission (from 625 to 648 nm) maxima and in an increase of the quantum yield from 9×10^{-4} for free dye in water to 1.4×10^{-2} after insertion in the dendrimeric architecture [71]. This dendrimer was used to develop two FRET systems utilizing cyanine dyes as the donor (**DTCI**) and the acceptor (pinacyanol and **26a**) molecules [72]. The FRET system allows the time-resolved detection, where energy transfer can be observed at the single-molecule level.



A dendrimeric system with **Cy3** and **Cy5** as the reporter dyes was applied to develop a microarray-based technology for high-throughput functional genomics research [73].

The cyanine dye dimethylindole red (**DIR**), with significantly reduced affinity for double-stranded DNA and nonspecific RNA, was used to generate a fluorescent complex (fluoromodule) with high affinity RNA aptamers (Fig. 12) [8]. **DIR** has

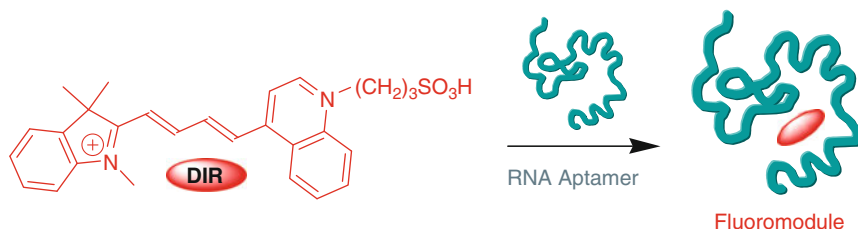
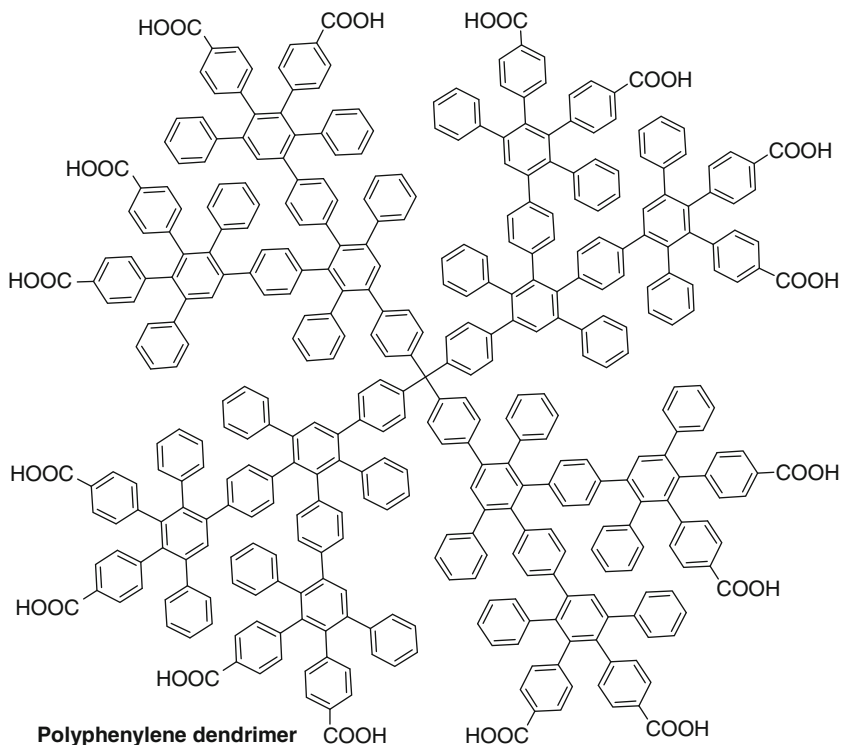


Fig. 12 Synthesis of the **DIR**–RNA-aptamer fluoromodule

intense absorbance in the red region of the visible spectrum with $\lambda_{\max} \text{ Ab} = 602 \text{ nm}$ and $\epsilon_{\text{M}} = 134,000 \text{ M}^{-1} \text{ cm}^{-1}$ in methanol. The dye fluorescence is very low in aqueous buffer but increases about 80-fold in a solution of 90% glycerol in water. In the presence of double-stranded DNA, the fluorescence of **DIR** increases only twofold. Binding to a specific RNA-aptamer strongly enhances **DIR** fluorescence, whereas nonspecific RNA has no effect on the dye fluorescence. The developed **DIR**–RNA-aptamer fluoromodule was proposed to have applications as a signaling component for sensors. This approach is suggested to be used to design new dye–aptamer complexes with improved properties.



Dye–aptamer complexes can be used also to develop high specific and selective colorimetric chemosensors. For example, the displacement of the heptamethine dye **26b**

from the anticocaine aptamer was used for selective measurement of cocaine in presence of other cocaine metabolites (benzoyl ecgonine and ecgonine methyl ester) [74].

6 Microporous Solid-Phase Encapsulated Dyes

The combination of dyes with *microporous* materials opens-up a way to develop selective chemosensors: microporous *zeolites* with an anchored squaraine **27** (Fig. 13) and some other types of dyes can be used as *chemosensors* for the chromogenic discrimination of amines [75]. These dye–zeolite hosts are expected to be promising sensor materials allowing the visible discrimination of selected target guests by size and/or polarity within families or closely related molecules. It was found that the response of the solid to amines was basically governed by the three-dimensional architecture of the solid material.

Encapsulation of organic dyes in *polymeric, silica, calcium phosphate*, and other types of *nanoparticles* allows to overcome some of the shortcomings of these dyes such as low fluorescent signal and insufficient chemical and photochemical stability. The size of nanoparticles varies in general between 2 and 400 nm. These nanoparticles contain a large number of dye molecules, yielding an intense fluorescence signal that is several thousand times higher than that of conventional dyes. Also, the matrix of a nanoparticle serves as a protective shell that protects the dye molecules against environmental impact and increases stability of the encapsulated dyes. Silica nanoparticles possess some advantages over other types of nanoparticles. They are easy to separate *via* centrifugation during particle preparation and processing because of the higher density of silica. Silica nanoparticles are hydrophilic and biocompatible, they are not subject to microbial attack, and no swelling or porosity change occurs with changes in pH. Because of these favorable properties, dye-doped silica nanoparticles show great potential in various biomedical applications (More detailed description of the properties of dye-doped nanoparticles can be found in chapter of Liang et al. [100]).

To overcome photobleaching and the low signal intensities of cyanine dyes **Cy3** and **Cy5**, these dyes were encapsulated in silica coreshell nanoparticles [76]. The obtained dye-doped nanoparticles were applied in the DNA microarray-based

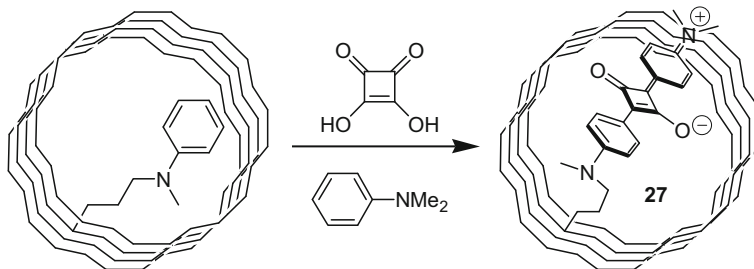
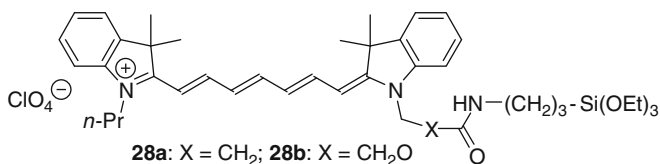


Fig. 13 Synthesis of squaraine–zeolite conjugate **27** [75]

bioanalysis with two-color detection. The use of these nanoparticles in a sandwich-type hybridization high-throughput microarray assay format revealed higher sensitivity with a detection limit of 1 pM for target DNA including more photostable signals as compared to the direct use of Cy3 and Cy5.

A series of silica nanoparticles doped with cyanine dye **DY-635** (Dyomics) were also prepared, characterized, and investigated in *flow cytometry* and fluorescence *imaging* applications [77]. Also these dye–nanoparticles demonstrate *high, stable*, and *tunable* fluorescence intensity and are useful for *multicolor detection*.

Heptamethine cyanine dyes **28a** and **28b** were encapsulated into silica nanoparticles providing a highly versatile and unique platform for *in vivo* diagnostics [78]. Utilizing this platform, multiple fluorophores can be loaded within a single particle allowing the light absorption and emission properties of the nanoparticle to be controlled independent of particle size. Furthermore, such dyed nanoparticles may have molar absorptivities (ϵ_M) as high as about $10^8 \text{ M}^{-1} \text{ cm}^{-1}$ in the NIR (on a per mole of particles basis), with quantum yields from about 8 to 10%. A simple synthetic method for varying particle size and dye-loading level was presented. The cyanine dyes are encapsulated in silica in a nonaggregated state and the fluorescence brightness is largely maintained to nominal dye concentrations approaching 50 μM . The ability to control light absorption and emission properties independent of particle size, and convenient access to particle sizes in the range of 20–100 nm, are important features for anatomical targeting in *in vivo* diagnostics and targeted therapeutic applications.



An overview on the synthesis and biomedical applications of dye-doped silica nanoparticles is given in recent review [79].

Bioresorbable *calcium phosphate nanoparticles* with the embedded NIR emitting dye indocyanine green were developed and applied for *diagnostic imaging* in the early detection of solid tumors. These 16-nm nanoparticles are stable in physiological solutions and exhibit significantly higher fluorescence intensity relative to the free dye: the quantum efficiency per molecule of the nanoparticle is 200% higher than that of the free dye in aqueous solution. The observed photostability of the encapsulated dye is 500% higher than that of the free dye.

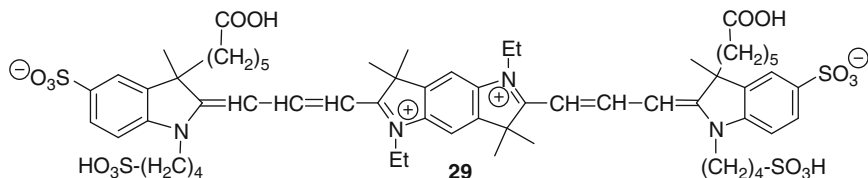
7 Fluorophore – Metallic Nanoparticle Compositions

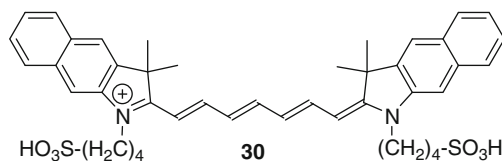
Novel, ultra-sensitive methods and techniques that enable measurements at low fluorophore concentrations are in high demand. The use of powerful excitation sources is not always an acceptable solution for increasing the sensitivity because

of increased photo-damage and background. *Metal-enhanced fluorescence* offers a way to increase the brightness and photostability at the same time [1]. Fluorophore–metallic nanoparticle interactions can cause diverse effects: at close proximity, below 4–5 nm from the nanoparticle, the fluorescence is strongly *quenched* [80, 81], and for a long time it was the only observed effect. Relatively recently, it has been shown experimentally that at a distance between 5 and 20 nm the fluorescence is *enhanced* [82, 83]. There are two possible contributions to this effect: firstly under the influence of incident light, the molecule goes into the excited state and interacts with the metal. Metal particles accelerate the fluorophore’s radiative decay rate and as a result enhance the emission. This effect is also known as *radiative decay engineering* (RDE) [84]. Under these conditions, the molecular mechanism of feedback de-excitation is activated, resulting in both increased photostability and quantum yield with a simultaneous decrease in lifetime. The second effect is the enhanced local field which acts simultaneously with the previous one. The impinging illumination on the metallic nanoparticles modifies the electric field around the metallic particles and induces free electron oscillations (localized plasmons) [84–86]. As it has been shown, the light intensity in the presence of metal particle can be increased about a 100-fold in comparison to that in the absence of a particle. The enhanced intensity provides locally a higher excitation rate. These effects also depend on the *size* and *shape* of the nanoparticle: the observed intensity is not equal on every location of the nanoparticle and therefore has the nature of a local field enhancement [87, 88]. The total fluorescence enhancement is the product of these two effects: RDE and enhanced local field.

A number of promising metal structures for fluorescence signal enhancement have been proposed: silver island films (SIFs) that provide about 5–15-fold enhancement [89], fractal-like structures that resulted in stronger enhancements at specific “hot spots” [90–92], and SIFs deposited on silver or gold films with about 50-fold enhancement [93, 94]. Recently, it was found that strong enhancement on a gold film based plasmonic platform may change even the shape of the emission spectrum [95].

A 2–4-fold increase in fluorescence intensity was demonstrated for the long-wavelength hydrophilic bis-trimethine label **29** (original $\Phi_F = 0.05$ in water) deposited on silver nanoparticles coated with a cryolite spacer [96]. A 20-fold increase of fluorescence intensity and a sixfold decrease of the mean decay time were obtained for heptamethine cyanine dye **30** on silver nanoparticles [97].





The fluorescent squaraine labels **Seta-670-mono-NHS** and **Seta-635-NH-mono-NHS** were covalently attached to antibodies and used in a *surface-enhanced immunoassay* [98]. In the fluorescence intensity and lifetime changes determined for a surface that had been coated with silver nanoparticles, both labeled compounds exhibited a 15–20-fold fluorescence enhancement on the silver-coated surface compared to that on the noncoated surface. In addition, the fluorescence lifetime decreased drastically for both labels on silver-coated surfaces. The fluorescence signal enhancement obtained for the two dyes exceeded those previously recorded for **rhodamine red-X** and **Alexa 647** labels.

The photophysical properties of the NIR fluorescent label **SeTau-665** (SETA BioMedicals) were investigated on a plasmonic platform of self-assembled colloidal structures of silver prepared on a semitransparent silver film [99]. A **SeTau-665**-based *immunoassay* was performed on this platform and a control glass slide. The fluorescence properties of this label substantially change because of plasmonic interactions. While the average brightness increase of **SeTau-665** in ensemble measurements was about 70-fold, fluorescence enhancements up to 400-times were observed on certain “hot spots” for single molecule measurements. The intensity increase is strongly correlated with a simultaneous decrease in fluorescence lifetime in these “hot spots”. The large increase in brightness allows the reduction of the excitation power resulting in a reduced background and increased photostability. The remarkable fluorescence enhancements observed for **SeTau-665** should allow to substantially improve single molecule detection and help to lower the detection limits in sensing devices.

8 Concluding Remarks

The process of combining cyanine and squaraine dyes by encapsulation, or covalent or noncovalent attachment with macrocyclic hosts, macromolecules, and micro- or nano-particles is a promising way to design novel probes and labels with substantially improved properties and for the development of advanced fluorescence-based assays. Nevertheless, the physicochemical properties of these dye-compositions are strongly dependent on the dye structure as well as the nature of the host macrocycle, macromolecule, or particle. Finally, development of new methods to synthesize these tracers can also be considered a challenging task.

References

1. Lakowicz JR (2006) Principles of fluorescence spectroscopy, 3rd edn. Springer, New York
2. Guether R, Reddington MV (1997) Photostable cyanine dye β -cyclodextrin conjugate. *Tetrahedron Lett* 38:6167–6170
3. Arunkumar E, Forbes CC, Smith BD (2005) Improving the properties of organic dyes by molecular encapsulation. *Eur J Org Chem* 2005:4051–4059
4. Buston JEH, Young JR, Anderson HL (2000) Rotaxane-encapsulated cyanine dyes: enhanced fluorescence efficiency and photostability. *Chem Commun* 11:905–906
5. Frampton MJ, Anderson HL (2007) Insulated molecular wires. *Angew Chem Int Ed* 46:1028–1064
6. Felder T (2007) Von Rotaxanen als potenziellen Enzym-Mimetika zu massenspektrometrischen Untersuchungen dendritischer Verbindungen in der hochverdünnten Gasphase. PhD thesis, Rheinischen Friedrich-Wilhelms-Universität, Bonn
7. Matsuzawa Y, Tamura SI, Matsuzawa N, Ata M (1994) Light stability of a β -cyclodextrin inclusion complex of a cyanine dye. *J Chem Soc Faraday Trans* 90:3517–3520
8. Constantin TP, Silva GL, Robertson KL, Hamilton TP, Fague K, Waggoner AS, Armitage BA (2008) Synthesis of new fluorogenic cyanine dyes and incorporation into RNA fluoromolecules. *Org Lett* 10:1561–1564
9. Aricó F, Badjic JD, Cantrill SJ, Flood AH, Leung KCF, Liu Y, Stoddart JF (2005) Templated synthesis of interlocked molecules. *Top Curr Chem* 249:203–259
10. Schalley CA, Weilandt T, Brüggemann J, Vögtle F (2004) Hydrogen-bond-mediated template synthesis of rotaxanes, catenanes, and knotanes. *Top Curr Chem* 248:141–200
11. Hübner GM, Reuter C, Seel C, Vögtle F (2000) Rotaxane synthesis via nucleophilic substitution reactions: the trapping of electrophilic threads by organic anion-wheel complexes. *Synthesis* 1:103–108
12. Dünnwald T, Jäger R, Vögtle F (1997) Synthesis of rotaxane assemblies. *Chem Eur J* 3:2043–2051
13. Leigh DA, Venturini A, Wilson AJ, Wong JKY, Zerbetto F (2004) The mechanism of formation of amide-based interlocked compounds: prediction of a new rotaxane-forming motif. *Chem Eur J* 10:4960–4969
14. Yoon I, Narita M, Shimizu T, Asakawa M (2004) Threading-followed-by-shrinking protocol for the synthesis of a [2]rotaxane incorporating a Pd(II)-salophen moiety. *J Am Chem Soc* 126:16740–16741
15. Kameta N, Hiratani K, Nagawa Y (2004) A novel synthesis of chiral rotaxanes via covalent bond formation. *Chem Commun* 4:466–467
16. Aucagne V, Berna J, Crowley JD, Goldup SM, Hänni KD, Leigh DA, Lusby PJ, Ronaldson VE, Slawin AMZ, Viterisi A, Walker DB (2007) Catalytic “active-metal” template synthesis of [2]rotaxanes, [3]rotaxanes, and molecular shuttles, and some observations on the mechanism of the Cu(I)-catalyzed azide-alkyne 1, 3-cycloaddition. *J Am Chem Soc* 129:11950–11963
17. Gatti FG, Leigh DA, Nepogodiev SA, Slawin AMZ, Teat SJ, Wong JKY (2001) Stiff, and sticky in the right places: the dramatic influence of preorganizing guest binding sites on the hydrogen bond-directed assembly of rotaxanes. *J Am Chem Soc* 123:5983–5989
18. Alfimov MV (2004) Photonics of supramolecular nanostructures. *Russ Chem Bull* 53:1357–1368
19. Dodziuk H (2006) Cyclodextrins and their complexes: chemistry, analytical methods, applications. Wiley-VCH Verlag GmbH & Co, Weinheim
20. Buschmann HJ, Schollmeyer E (1997) Cucurbituril and β -cyclodextrin as hosts for the complexation of organic dyes. *J Incl Phenom Macrocycl Chem* 29:167–174
21. Park JS, Wilson JN, Hardcastle KI, Bunz UHF, Srinivasarao M (2006) Reduced fluorescence quenching of cyclodextrin–acetylene dye rotaxanes. *J Am Chem Soc* 128:7714–7715

22. Kasatani K, Kawasaki M, Sato H (1984) Lifetime shortening of the photoisomer of a cyanine dye by inclusion in a cyclodextrin cavity as revealed by transient absorption spectroscopy. *J Phys Chem* 88:5451–5453
23. Kasatani K, Ohashi M, Kawasaki M, Sato H (1987) Cyanine dye–cyclodextrin system. Enhanced dimerization of the dye. *Chem Lett* 16:1633–1636
24. Rao TVS, Huff JB, Bieniarz C (1998) Supramolecular control of photophysical properties of cyanine dyes. *Tetrahedron* 54:10627–10634
25. Moritz ED, Sahyun MRV (2005) Spectroscopic studies of β -cyclodextrin-complexed cyanine dyes. *J Photochem Photobiol A Chem* 169:211–220
26. Yau CMS, Pascu SI, Odom SA, Warren JE, Klotz EJJ, Frampton MJ, Williams CC, Coropceanu V, Kuimova MK, Phillips D, Barlow S, Brédas JL, Marder SR, Millar V, Anderson HL (2008) Stabilisation of a heptamethine cyanine dye by rotaxane encapsulation. *Chem Commun* 25:2897–2899
27. Buston JEH, Marken F, Anderson HL (2001) Enhanced chemical reversibility of redox processes in cyanine dye rotaxanes. *Chem Commun* 11:1046–1047
28. Wang LQ, Zhao L, Nie WW, Zheng LH, Wang JD, Li QR, Zhai J, Liu ZW, Peng XJ (2008) Syntheses and properties of photostable near-infrared cyanines and their cyclodextrin conjugates. *Chin Chem Lett* 19:739–741
29. Medintz IL, Goldman ER, Lassman ME, Mauro JM (2003) A fluorescence resonance energy transfer sensor based on maltose binding protein. *Bioconjug Chem* 14:909–918
30. Klotz EJJ, Claridge TDW, Anderson HL (2006) Homo- and hetero-[3]rotaxanes with two π -systems clasped in a single macrocycle. *J Am Chem Soc* 128:15374–15375
31. Gadde S, Batchelor EK, Weiss JP, Ling Y, Kaifer AE (2008) Control of H- and J-aggregate formation via host–guest complexation using cucurbituril hosts. *J Am Chem Soc* 130:17114–17119
32. Batchelor EK, Gadde S, Kaifer AE (2010) Host–guest control on the formation of pinacyanol chloride H-aggregates in anionic polyelectrolyte solutions. *Supramol Chem* 22:40–45
33. Gadde S, Batchelor EK, Kaifer AE (2009) Controlling the formation of cyanine dye H- and J-aggregates with cucurbituril hosts in the presence of anionic polyelectrolytes. *Chem Eur J* 15:6025–6031
34. Mohanty J, Pal H, Ray AK (2007) Supramolecular dye laser with cucurbit[7]uril in water. *Chem Phys Chem* 8:54–56
35. Jeon YJ, Kim SY, Ko YH, Sakamoto S, Yamaguchi K, Kim K (2005) Novel molecular drug carrier: encapsulation of oxaliplatin in cucurbit[7]uril and its effects on stability and reactivity of the drug. *Org Biomol Chem* 3:2122–2125
36. Lehn JM (1995) Supramolecular chemistry: concepts and perspectives. VCH, Weinheim
37. Gellman SH (1997) Introduction: molecular recognition. *Chem Rev* 97:1231–1232
38. Jon SY, Ko YH, Park SH, Kim HJ, Kim K (2001) A facile, stereoselective [2 + 2] photoreaction mediated by cucurbit[8]uril. *Chem Commun* 19:1938–1939
39. Pattabiraman M, Natarajan A, Kaliappan R, Mague JT, Ramamurthy V (2005) Template directed photodimerization of *trans*-1,2-bis(*n*-pyridyl)ethylenes and stilbazoles in water. *Chem Commun* 36:4542–4544
40. Jon SY, Selvapalam N, Oh DH, Kang JK, Kim SY, Jeon YJ, Lee JW, Kim K (2003) Facile synthesis of cucurbit[*n*]uril derivatives via direct functionalization: expanding utilization of cucurbit[*n*]uril. *J Am Chem Soc* 125:10186–10187
41. Burnett CA, Lagona J, Wu A, Shaw JA, Coody D, Fettinger JC, Dayb AI, Isaacs L (2003) Preparation of glycoluril monomers for expanded cucurbit[*n*]uril synthesis. *Tetrahedron* 59:1961–1970
42. Kim K, Selvapalam N, Ko YH, Park KM, Kim D, Kim J (2007) Functionalized cucurbiturils and their applications. *Chem Soc Rev* 36:267–279
43. Isaacs L (2009) Cucurbit[*n*]urils: from mechanism to structure and function. *Chem Commun* 6:619–629

44. Lee JW, Samal S, Selvapalam N, Kim HJ, Kim K (2003) Cucurbituril homologues and derivatives: new opportunities in supramolecular chemistry. *Acc Chem Res* 36:621–630
45. Lagona J, Mukhopadhyay P, Chakrabarti S, Isaacs L (2005) The cucurbit[n]uril family. *Angew Chem Int Ed* 44:4844–4870
46. Koner AL, Nau WM (2007) Cucurbituril encapsulation of fluorescent dyes. *Supramol Chem* 19:55–66
47. Petrov NK, Ivanov DA, Golubkov DV, Gromov SP, Alfimov MV (2009) The effect of cucurbit[7]uril on photophysical properties of aqueous solution of 3,3'-diethylthiacarbocyanine iodide dye. *Chem Phys Lett* 480:96–99
48. Nau W, Mohanty J (2009) US Patent 7,511,284
49. Terpetschnig E, Wolfbeis OS (1998) Luminescent probes for NIR sensing applications. In: Daehne S, Resch-Genger U, Wolfbeis OS (eds) *Near-infrared dyes for high technology applications*, vol 53, NATO ASI Ser. 3. Kluwer Acad Publ, Dordrecht, pp 161–182
50. Patsenker L, Tatarets A, Kolosova O, Povrozin Y, Fedyunayeva I, Yermolenko I, Terpetschnig E (2008) Fluorescent probes and labels for biomedical applications. *Ann N Y Acad Sci* 1130:179–187
51. Gonçalves MST (2009) Fluorescent labeling of biomolecules with organic probes. *Chem Rev* 109:190–212
52. Arunkumar E, Forbes CC, Noll BC, Smith BD (2005) Squaraine-derived rotaxanes: sterically protected fluorescent near-IR dyes. *J Am Chem Soc* 127:3288–3289
53. Arunkumar E, Fu N, Smith BD (2006) Squaraine-derived rotaxanes: highly stable, fluorescent near-IR dyes. *Chem Eur J* 12:4684–4690
54. Fu N, Baumes JM, Arunkumar E, Noll BC, Smith BD (2009) Squaraine rotaxanes with boat conformation macrocycles. *J Org Chem* 74:6462–6468
55. Johnson JR, Fu N, Arunkumar E, Leevy WM, Gammon ST, Piwnica-Worms D, Smith BD (2007) Squaraine rotaxanes: superior substitutes for Cy-5 in molecular probes for near-infrared fluorescence cell imaging. *Angew Chem Int Ed* 46:5528–5531
56. Gassensmith JJ, Arunkumar E, Barr L, Baumes JM, DiVittorio KM, Johnson JR, Noll BC, Smith BD (2007) Self-assembly of fluorescent inclusion complexes in competitive media including the interior of living cells. *J Am Chem Soc* 129:15054–15059
57. Jacquemin D, Perpète EA, Laurent AD, Assfeld X, Adamo C (2009) Spectral properties of self-assembled squaraine–tetralactam: a theoretical assessment. *Phys Chem Chem Phys* 11:1258–1262
58. Gassensmith JJ, Barr L, Baumes JM, Paek A, Nguyen A, Smith BD (2008) Synthesis and photophysical investigation of squaraine rotaxanes by “clicked capping”. *Org Lett* 10:3343–3346
59. Fu N, Gassensmith JJ, Smith BD (2009) Effect of stopper size on squaraine rotaxane stability. *Supramol Chem* 21:118–124
60. Patsenker LD, Tatarets A, Povrozin Y, Klochko O, Terpetschnig EA, Kudryavtseva Y, Yermolenko I (2008) WO Patent 2,008,094,637
61. Xue M, Chen CF (2008) Triptycene-based tetralactam macrocycles: synthesis, structure and complexation with squaraine. *Chem Commun* 46:6128–6130
62. Asakawa M, Ashton PR, Ballardini R, Balzani V, Belohradsky M, Gandolfi MT, Kocian O, Prodi L, Raymo FM, Stoddart JF, Venturi M (1997) The slipping approach to self-assembling [n]rotaxanes. *J Am Chem Soc* 119:302–310
63. Hsueh SY, Lai CC, Liu YH, Wang Y, Peng SM, Chiu SH (2007) Protecting a squaraine near-IR dye through its incorporation in a slippage-derived [2]rotaxane. *Org Lett* 9:4523–4526
64. Hsueh SY, Lai CC, Liu YH, Peng SM, Chiu SH (2007) Highly selective Na⁺-templated formation of [2]pseudorotaxanes exhibiting significant optical outputs. *Angew Chem Int Ed* 46:2013–2017
65. Ashton PR, Baxter I, Fyfe MCT, Raymo FM, Spencer N, Stoddart JF, White AJP, Williams DJ (1998) Rotaxane or pseudorotaxane? That is the question! *J Am Chem Soc* 120:2297–2307

66. Chiu SH, Rowan SJ, Cantrill SJ, Glink PT, Garrell RL, Stoddart JF (2000) A rotaxane-like complex with controlled-release characteristics. *Org Lett* 2:3631–3634
67. Gassensmith JJ, Baumes JM, Smith BD (2009) Discovery and early development of squaraine rotaxanes. *Chem Commun* 42:6329–6338
68. Tatarski AL, Fedyunayeva IA, Dyubko TS, Povrozin YA, Doroshenko AO, Terpetschnig EA, Patsenker LD (2006) Ring-substituted squaraine dyes as probes and labels for fluorescence assays. *Anal Chim Acta* 570:214–223
69. Oswald B, Lehmann F, Simon L, Terpetschnig E, Wolfbeis OS (2000) Red laser-induced fluorescence energy transfer in an immunosystem. *Anal Biochem* 280:272–277
70. Oswald B, Gruber M, Böhmer M, Lehmann F, Probst M, Wolfbeis OS (2001) Novel diode laser-compatible fluorophores and their application to single molecule detection, protein labeling and fluorescence resonance energy transfer immunoassay. *Photochem Photobiol* 74:237–245
71. Köhn F, Hofkens J, Wiesler UM, Cotlet M, Van der Auweraer M, Müllen K, De Schryver FC (2001) Single-molecule spectroscopy of a dendrimer-based host–guest system. *Chem Eur J* 7:4126–4133
72. Köhn F, Hofkens J, Gronheid R, Cotlet M, Müllen K, Van der Auweraer M, De Schryver FC (2002) Excitation energy transfer in dendritic host–guest donor–acceptor systems. *Chem Phys Chem* 3:1005–1013
73. Stears RL, Getts RC, Gullans SR (2000) A novel, sensitive detection system for high-density microarrays using dendrimer technology. *Physiol Genomics* 3:93–99
74. Stojanovic MN, Landry DW (2002) Aptamer-based colorimetric probe for cocaine. *J Am Chem Soc* 124:9678–9679
75. Comes M, Marcos MD, Martínez-Mañez R, Millán MC, Ros-Lis JV, Sancenón F, Soto J, Villaescusa LA (2006) Anchoring dyes into multidimensional large-pore zeolites: a prospective use as chromogenic sensing materials. *Chem Eur J* 12:2162–2170
76. Zhou X, Zhou J (2004) Improving the signal sensitivity and photostability of DNA hybridizations on microarrays by using dye-doped core–shell silica nanoparticles. *Anal Chem* 76:5302–5312
77. Nakamura M, Shono M, Ishimura K (2007) Synthesis, characterization, and biological applications of multifluorescent silica nanoparticles. *Anal Chem* 79:6507–6514
78. Bringley JF, Penner TL, Wang R, Harder JF, Harrison WJ, Buonemani L (2008) Silica nanoparticles encapsulating near-infrared emissive cyanine dyes. *J Colloid Interface Sci* 320:132–139
79. Wang L, Wang K, Santra S, Zhao X, Hilliard LR, Smith JE, Wu Y, Tan W (2006) Watching silica nanoparticles glow in the biological world. *Anal Chem* 78:646–654
80. Axelrod D, Hellen EH, Fulbright RM (1992) Microparticle fluorescence. In: Lakowicz JR (ed) *Topics in fluorescence spectroscopy, vol 3, Biochemical applications*. Plenum, New York, pp 289–343
81. Barnes WL (1998) Fluorescence near interfaces: the role of photonic mode density. *J Mod Opt* 45:661–699
82. Malicka J, Gryczynski I, Gryczynski Z, Lakowicz JR (2003) Effects of fluorophore-to-silver distance on the emission of cyanine-dye-labeled oligonucleotides. *Anal Biochem* 315:57–66
83. Sokolov K, Chumanov G, Cotton TM (1998) Enhancement of molecular fluorescence near the surface of colloidal metal films. *Anal Chem* 70:3898–3905
84. Lakowicz JR (2001) Radiative decay engineering: biophysical and biomedical applications. *Anal Biochem* 298:1–24
85. Fu Y, Lakowicz JR (2009) Modification of single molecule fluorescence near metallic nanostructures. *Laser Photon Rev* 3:221–232
86. Lakowicz JR, Shen Y, D’Auria S, Malicka J, Fang J, Gryczynski Z, Gryczynski I (2002) Radiative decay engineering: 2. Effects of silver island films on fluorescence intensity, lifetimes, and resonance energy transfer. *Anal Biochem* 301:261–277

87. Hao E, Schatz GC (2004) Electromagnetic fields around silver nanoparticles and dimers. *J Chem Phys* 120:357–366
88. Kelly KL, Coronado E, Zhao LL, Schatz GC (2003) The optical properties of metal nanoparticles: the influence of size, shape, and dielectric environment. *J Phys Chem B* 107:668–677
89. Lukomska J, Malicka J, Gryczynski I, Lakowicz JR (2004) Fluorescence enhancements on silver colloid coated surfaces. *J Fluoresc* 14:417–423
90. Goldys EM, Drozdowicz-Tomsia K, Xie F, Shtoyko T, Matveeva E, Gryczynski I, Gryczynski Z (2007) Fluorescence amplification by electrochemically deposited silver nanowires with fractal architecture. *J Am Chem Soc* 129:12117–12122
91. Parfenov A, Gryczynski I, Malicka J (2003) Enhanced fluorescence from fluorophores on fractal silver surfaces. *J Phys Chem B* 107:8829–8833
92. Shtoyko T, Matveeva EG, Chang IF, Gryczynski Z, Goldys E, Gryczynski I (2008) Enhanced fluorescence immunoassays on silver fractal-like structures. *Anal Chem* 80:1962–1966
93. Barnett A, Matveeva EG, Gryczynski I, Gryczynski Z, Goldys EM (2007) Coupled plasmon effects for the enhancement of fluorescent immunoassays. *Phys B Condens Matter* 394:297–300
94. Matveeva EG, Gryczynski I, Barnett A, Leonenko Z, Lakowicz JR, Gryczynski Z (2007) Metal particle-enhanced fluorescent immunoassays on metal mirrors. *Anal Biochem* 363:239–245
95. Sørensen TJ, Laursen BW, Luchowski R, Shtoyko T, Akopova I, Gryczynski Z, Gryczynski I (2009) Enhanced fluorescence emission of Me-ADOTA⁺ by self-assembled silver nanoparticles on a gold film. *Chem Phys Lett* 476:46–50
96. Fedyunyayeva I, Patsenker L, Borovoy I, Terpetschnig E (2007) Photonics of polymethine dyes on silver and gold nanoparticles. 10th Conference on Methods and Applications of Fluorescence (MAF10). Book of Abstracts, p 222
97. Malicka J, Gryczynski I, Geddes CD, Lakowicz JR (2003) Metal-enhanced emission from indocyanine green: a new approach to in vivo imaging. *J Biomed Opt* 8:472–478
98. Matveeva EG, Terpetschnig EA, Stevens M, Patsenker L, Kolosova OS, Gryczynski Z, Gryczynski I (2009) Near-infrared squaraine dyes for fluorescence enhanced surface assay. *Dyes Pigm* 80:41–46
99. Luchowski R, Matveeva EG, Shtoyko T, Sarkar P, Patsenker LD, Klochko OP, Terpetschnig EA, Borejdo J, Akopova I, Gryczynski Z, Gryczynski I (2010) Single molecule immunoassay on plasmonic platforms. *Curr Pharm Biotechnol* 11:96–102
100. Liang S, John CL, Xu S et al (2010) Silica-based nanoparticles: design and properties. In: Demchenko AP (ed) *Advanced fluorescence reporters in chemistry and biology*. II. Springer Ser Fluoresc 9:229–251

Part III
Dye-Doped Nanoparticles and
Dendrimers

Dye-Doped Polymeric Particles for Sensing and Imaging

Sergey M. Borisov, Torsten Mayr, Günter Mistlberger, and Ingo Klimant

Abstract Dye-doped polymeric micro- and nanobeads represent smart analytical tools that have become very popular recently. They enable noninvasive contactless sensing and imaging of various analytical parameters on a nanoscale and are also widely employed in composite sensing materials, in suspension arrays, and as labels. This contribution gives an overview of materials and techniques used for preparation of dye-doped polymeric beads. It also provides examples of bead materials and their applications for optical sensing and imaging.

Keywords Bead · Dye · Imaging · Luminescence · Polymer · Sensor

Contents

1	Introduction	194
2	Materials Used for Preparation of the Dye-Doped Beads	194
2.1	Monomers and Polymers	194
2.2	Dyes	195
2.3	Functional Additives	200
3	Fabrication Techniques	201
3.1	Preparation of Stained Beads During Polymerization	201
3.2	Staining of the Beads via Surface Modification	202
3.3	Staining by Swelling	203
3.4	Preparation of Stained Beads via Precipitation	203
3.5	Techniques for Preparation of Dye-Doped Microbeads	204
3.6	Purification of the Beads	205
4	Optical Read-Out Schemes	205

S.M. Borisov (✉), T. Mayr, G. Mistlberger, and I. Klimant
Institute of Analytical Chemistry and Food Chemistry, Graz University of Technology,
Stremayrgasse 16, Graz 8010, Austria
e-mail: sergey.borisov@tugraz.at

5	Selected Examples of Dye-Doped Polymeric Bead Materials	206
5.1	Water-Dispersible Nanosensors	206
5.2	Dye-Doped Beads as Labels	212
5.3	Dye-Doped Beads in Composite Materials	214
5.4	Sensor Arrays Based on Dye-Doped Beads	215
5.5	Magnetic Dye-Doped Polymeric Beads	218
5.6	Dye-Doped Beads for Other Applications	221
6	Concluding Remarks	221
	References	222

1 Introduction

Optical chemical sensors mostly rely on advanced materials that reversibly respond to a chemical parameter in altering their optical properties [1]. A polymer serves not only as a host material for an indicator but also as a permeation-selective membrane. The sensor material is usually coated onto the tip of an optical fiber, a planar transparent support or any other surface of interest (such as a surface of an aircraft in case of pressure-sensitive paints). Dye-doped micro- and nanobeads represent yet another format of optical sensor materials that became widespread in the last decade [2–4]. These smart materials are self-contained analytical tools which can be either used on their own (“nanosensors”) to measure an analytical parameter in solution (extra- or intracellularly) or in combination with other beads in arrays and composite materials such as multianalyte sensors. Compared to planar optodes that sometimes make use of absorption-based indicators, the dye-doped beads almost exclusively rely on luminescent indicators. Although one can certainly distinguish between microbeads ($\varnothing > 1 \mu\text{m}$), submicrobeads ($100 \text{ nm} < \varnothing < 1 \mu\text{m}$) and nanobeads ($\varnothing < 100 \text{ nm}$), the borders are still rather vague. Some dendrimeric systems also perform very similarly to dyed polymeric beads. Moreover, the methods established for manufacturing of dye-doped micro- and nanobeads often are the same, and so are the sensing chemistries used. Often beads bear no indicator (that responds to the analyte of interest) but an inert luminescent dye, and act as labels or tracers in various assays. In the following sections, we will describe the materials and methods used for preparation of dyed beads, interrogation schemes and provide examples of the sensing materials.

2 Materials Used for Preparation of the Dye-Doped Beads

2.1 Monomers and Polymers

A variety of monomers and polymers have been used for preparation of sensing beads and many more may also be suitable. Many polymers are already commercially available as a dispersion of nano- or microbeads (such as e.g., carboxylated

polystyrene polybead[®] microspheres from Polysciences Inc., <http://www.polysciences.com>) and only need to be stained with an appropriate indicator. On the other hand, despite being time consuming, preparation of polymeric beads from monomers is much more flexible, since many parameters (size of the beads, amount of functional groups, tendency to swell in organic solvents, etc.) can be fine-tuned. Some common polymers are depicted in Fig. 1. Nonpolar polymers such as polystyrene are excellent matrices for immobilization of lipophilic indicators. Such beads can be successfully used if dispersed in other polymers but tend to aggregate in aqueous media. Therefore, they are often provided with charged groups which dramatically increase their stability in aqueous media. More polar polyacrylonitrile and polymethylmethacrylate are often polymers of choice as well. Their copolymers bearing carboxyl groups can be used for preparation of rather small beads ($\varnothing < 50$ nm). Notably, the surface of such beads is also available for further functionalization.

Although nonpolar polymers such as polystyrene are often the best choice for the preparation of oxygen-sensitive beads, optical temperature probes and labels cannot be employed to design particles for sensing pH, ions, basic and acidic gasses. For example, more polar ethylcellulose and cellulose acetate are polymers of choice for designing carbon dioxide and ammonia sensors, respectively. The pH sensing beads often rely on the use of hydrophilic water-swelling polymers such as cross-linked polyacrylamide, polyurethane hydrogels, etc. Alternatively, covalent attachment of a pH indicator to the surface of the bead can be used. Plasticized polyvinylchloride was found to be very suitable for preparation of ion-sensitive beads.

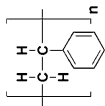
Block polymers that are able to form core-shell particles in aqueous media are also very promising. For example, lipophilic indicators can be embedded into the core of a block polymer of styrene and vinylpyrrolidone. The neutral lipophilic shell is responsible for the unique stability of the beads in water which do not aggregate even at very high ionic strength.

Finally, some hybrid inorganic-organic materials such as Ormosil (=Organically modified silica) are also very popular. The structure and properties of Ormosils resemble those of silica and organic polymers.

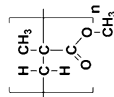
2.2 Dyes

Evidently, it is not possible to choose or design an “ideal” dye for an optical sensor. However, a potential candidate should fulfill as many of the following requirements as possible:

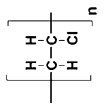
Be excitable in visible or NIR. Although the dyes excitable in UV can also be used, they are much less suitable for practical applications due to several reasons: (i) high level of background fluorescence originating from the optical components and biological substances present in the analyzed media; (ii) high scattering of the light; (iii) higher price and lower output of the light sources used for excitation (such as LEDs). Red-light excitable and NIR dyes are particularly promising since

neutral

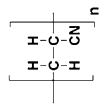
PS



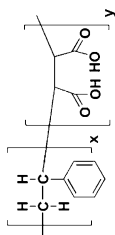
PMMA



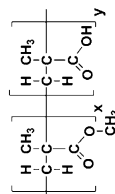
PVC



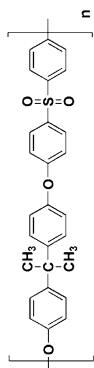
PAN

charged

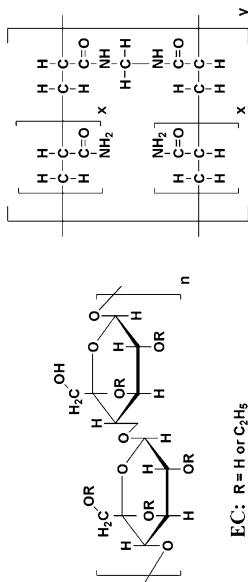
PS-MA



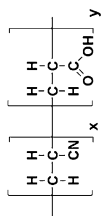
PMMA-MA



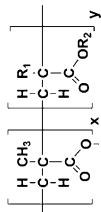
PSulf

EC: R = H or C₂H₅CAC: R = H or COCH₃

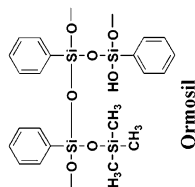
cross-linked PAAM



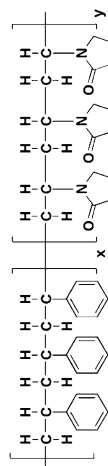
PAN-AA

R₁ = H, CH₃
R₂ = CH₃, C₂H₅

RL 100 and RS 100

hybrid materials

Ormosil

core-shell

PS-PVP

the interferences from autofluorescence and scattering are further minimized. Moreover, only such indicators can be made use of for subcutaneous monitoring of important analytes such as oxygen or glucose. Finally, dyes that are suitable for two-photon excitation with the NIR light have become increasingly popular (The chapter of Przhonska et al. [127] addresses this issue).

Have high brightness. Brightness is commonly defined as a product of a molar absorption coefficient ϵ and luminescence quantum yield QY. In other words, a dye having a QY approaching unity but ϵ in order of several thousands $\text{M}^{-1} \text{cm}^{-1}$ will be hardly of any practical use due to low brightness. For example, many cyclometallated complexes of iridium(III) and platinum(II) possess strong emission, but poorly absorb in visible. On the other hand, even a moderate emitter with $\text{QY} \sim 0.1$ but strong absorption $\epsilon > 100,000 \text{ M}^{-1} \text{cm}^{-1}$ is likely to be suitable.

Respond to the analyte of interest and preferably be inert to other species. That is not easy and often impossible to achieve in practice. For example, any metal–ligand luminescent complex employed for optical oxygen sensing will be liable to thermal quenching or any pH indicator will possess higher or lower cross-sensitivity to ionic strength. Some of these undesirable effects can be minimized by appropriate chemical modification of an indicator (e.g., by decreasing the charge of a pH-sensitive dye) or by making use of permeation-selective properties of a polymer. However, most of such effects should be compensated for in an independent measurement. Considering labels, a dye should be completely inert to any species in order to be suitable.

Have good photostability. Photostability is particularly critical if high light intensities are used for interrogation (such as in microscopy or fiber-optic micro-sensors) or if the measurements are performed over a long time. Photodegradation always affects luminescence intensity but is usually less critical in case of the decay time measurements since this parameter can remain unaffected by photobleaching.

Possess good solubility in the polymer or have functional groups for immobilization. It should be ensured that the dye remains in polymeric beads in the monomeric form and neither aggregates nor leaches out into the surrounding medium. In most cases a suitable dye is either lipophilic enough (such as e.g., many metalloporphyrins) or is rendered lipophilic. For example, this can be achieved by choosing a bulky counterion (e.g., BF_4^- , PF_6^- , dodecylsulfate used to lipophilize cationic ruthenium(II) complexes) or by providing a molecule with a lipophilic chain. It should be noted that hydrophilic dyes bearing reactive groups are also commonly used for staining beads. They are either copolymerized together with monomers or are covalently attached to the bead surface. These dyes are often applied to design pH sensors.

Fig. 1 Chemical structures of the polymers commonly used for preparation of beads: poly(styrene-*co*-maleic acid) (=PS-MA); poly(methyl methacrylate-*co*-methacrylic acid) (=PMMA-MA); poly(acrylonitrile-*co*-acrylic acid) (=PAN-AA); polyvinylchloride (=PVC); polysulfone (=PSulf); ethylcellulose (=EC); cellulose acetate (=CAc); polyacrylamide (=PAAm); poly(styrene-*block*-vinylpyrrolidone) (=PS-PVP) and Organically modified silica (=Ormosil). PS-MA is commercially available as an anhydride and negative charges on the bead surface are generated during preparation of the beads

Be nontoxic. Low cytotoxicity is desirable but not essential for the choice of dyes. Evidently, cytotoxicity is greatly reduced upon immobilization of dyes into polymeric beads. However, even individual dye molecules that leach out of the beads may undesirably affect biological systems. This also refers to other lumino-phores such as quantum dots which are known to be highly toxic.

Virtually all classes of luminescent dyes can be potentially used for staining polymeric beads. One can distinguish between fluorescent organic dyes and phosphorescent metal–ligand complexes. Such fluorescent dyes as coumarins, fluoresceins, rhodamines, seminaphthorhodafluors, phenoxazines, naphthalimides, polyaromatic hydrocarbons and their derivatives (pyrene, perylene, perylene-3,4,9,10-tetracarboxylic acid diimides, etc.), boradipyrroles, squaraines and cyanine dyes are very common (Fig. 2). The spectral properties of these fluorophores can be tuned over a wide range by choosing appropriate substituents and by varying the conjugation length. Most of these dyes possess good brightness exceeding 40,000. Modifications are done to increase photostability (e.g., by introducing fluorine and chlorine atoms or via sulfonation), to render the dyes lipophilic (usually by modification with an alkyl chain) or available for covalent coupling (e.g., via a carboxyl-group). Fluoresceins, seminaphthorhodafluors and 1-hydroxy-pyrene-3,6,8-trisulfonate (or its alkylsulfonamides) are well-known pH indicators and are used for preparation of pH-sensitive beads. Other dye classes are mostly used for preparation of fluorescent labels and tracers. They are also often contained together with an indicator to provide possibility of ratiometric referencing.

Luminescent metal–ligand complexes are mostly represented by metalloporphyrins and their derivatives (predominantly palladium(II) and platinum(II) complexes), ruthenium(II) polypyridyl complexes, cyclometallated platinum(II) and iridium(III) complexes and lanthanide chelates (mostly of terbium (III) and europium(III)), Fig. 3. Other luminescent complexes with rhodium(III), osmium(II), rhenium(I), etc. are used only sparsely. Platinum(II) and palladium(II) metalloporphyrins possess very strong absorption in the violet region but have much less efficient absorption in the green part of the spectrum ($\epsilon \sim 20,000 \text{ M}^{-1}\text{cm}^{-1}$). Although they can be used as labels, their relatively long phosphorescence decay times (tens to hundreds microseconds) make them particularly attractive as oxygen indicators. Most common are the complexes with octaethylporphyrin and much more photostable *meso*-tetra(pentafluorophenyl) porphyrin. Since the excitation in the red region is particularly attractive for many applications, porphyrin derivatives excitable at longer wavelength have become popular. These include the complexes with pophyrin-ketones and *meso*-porpholactones (absorbing at 570–600 nm) and with tetrabenzoporphyrins. The latter are seen as particularly strong NIR emitters ($\lambda_{\text{max}}(\text{abs}) = 610\text{--}630 \text{ nm}$, $\lambda_{\text{max}}(\text{em}) = 760\text{--}800 \text{ nm}$) and the brightnesses typically exceed 40,000. Tetranaphthoporphyrins extend the excitation window even further ($\lambda_{\text{max}}(\text{abs}) = 670\text{--}690 \text{ nm}$).

The ruthenium(II) polypyridyl complexes are also popular but the brightnesses do not exceed 15,000 and thermal quenching is rather significant. This property can be utilized to design temperature-sensitive probes providing that the dyes are effectively shielded from oxygen (e.g., in polyacrylonitrile beads). Despite often very high emission quantum yields the visible absorption of cyclometallated complexes of iridium(III) and platinum(II) is usually poor ($\epsilon < 10,000 \text{ M}^{-1}\text{cm}^{-1}$), thus,

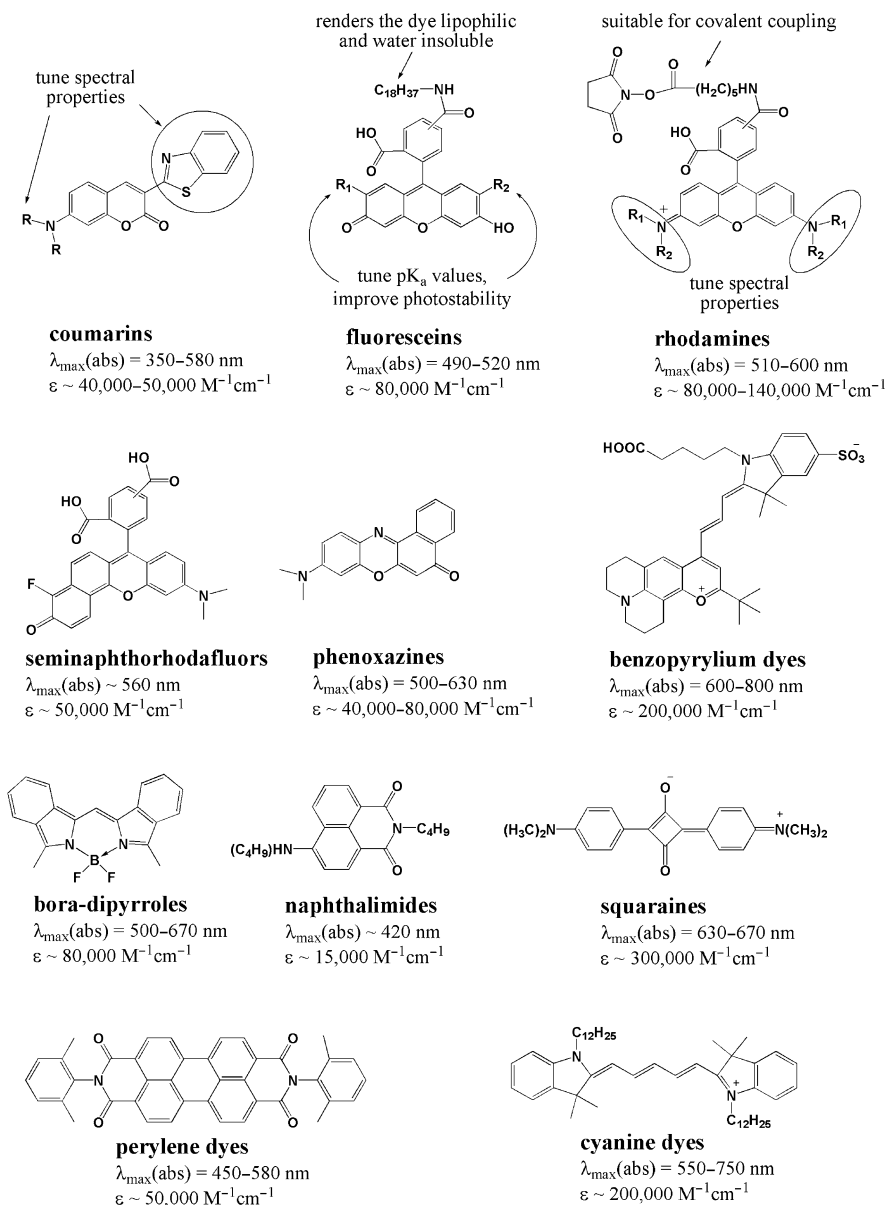


Fig. 2 Chemical structures and typical spectral properties of the common fluorophores that can be used for staining of the polymeric beads

they are not the best candidates for staining polymeric beads. Cyclometallated coumarin complexes represent the notable exception and are extremely bright ($BS > 50,000$). They can be successfully used for sensing and imaging but photostability can be an issue.

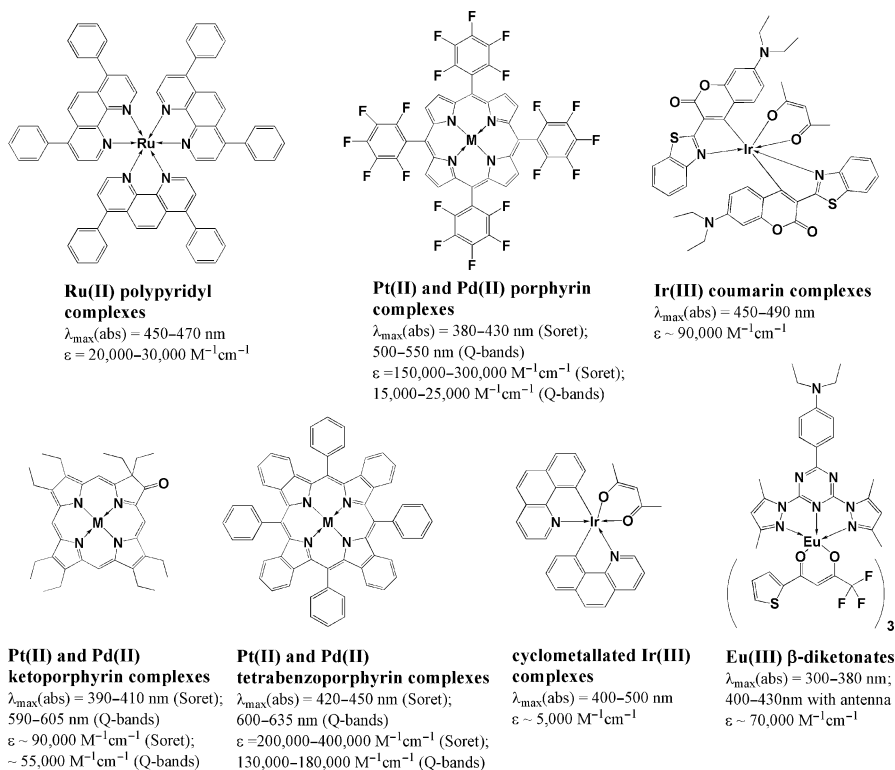


Fig. 3 Chemical structures and typical spectral properties of the common luminescent emitters used for staining of polymeric beads

Finally, luminescent europium(III) and terbium(III) chelates feature very narrow emission bands and large Stokes shifts. They possess long luminescence decay times of several hundred microseconds, but the emission is only minor quenched by oxygen. Thus, these chelates are primarily used for labeling purposes. The luminescence is also highly temperature-dependent which makes these dyes promising candidates for optical temperature sensing and imaging. Notably, most of these chelates are excitable in the UV region only, which may compromise their applicability. However, some of the europium(III) chelates reported recently possess bright blue light-excitable luminescence and were used for staining polymeric beads.

2.3 Functional Additives

Apart from polymers and indicators, the beads can contain a variety of other components that improve their properties or provide additional functionalities. For example, addition of titanium dioxide nanoparticles significantly increases the brightness of the beads due to light scattering [5]. The plasmonic enhancement

of fluorescence is a more elegant way and relies on the use of metal core covered with a polymeric or sol-gel shell that contains an indicator [6].

Micro- and nanobeads with magnetic properties have recently become popular since these tools can be manipulated, e.g., collected in the region of interest. Magnetite nanoparticles are introduced in order to render the polymeric beads magnetic. Preparation and application of magnetic beads will be discussed in more detail in Sect 5.5.

As in the case of bulk optodes, plasticizers can be added to modify the properties of polymers (e.g., gas permeability). Plasticizers are mainly used to design ion-sensitive nanobeads.

Certain biomolecules can be added into the bead or be attached to its surface. These mostly include such recognition elements as antibodies, oligonucleotides or other receptors such as concanavalin A. Enzymes can be used to design biosensors (e.g., for glucose) on a microscale but this research is still in its infancy. Finally, fluorescent proteins can be used as alternative to the dyes. The same refers to quantum dots which can also be used in principle.

3 Fabrication Techniques

Figure 4 schematically shows common strategies of making dye-doped beads. These are mostly suitable for preparation of both micro- and nanobeads. Some more specific methods such as grinding and spray-drying are mostly used for the preparation of microparticles. One can distinguish between the methods where dye-doped polymeric beads are produced in one step (entrapment during polymerization, precipitation, and spray-drying) and the methods where undoped polymeric beads are stained with an indicator (staining by swelling or covalent coupling to the surface). The details of these techniques will be discussed in the following section.

3.1 Preparation of Stained Beads During Polymerization

Many commercially important polymers are produced via emulsion polymerization. This is also one of the most common methods to produce dye-doped beads. A dye is added to the mixture of monomers prior to initiating the polymerization and is either noncovalently entrapped or is copolymerized. The second method ensures that no leaching will occur from the particle but requires modification of the dye (typically by providing it with a double bond). This method is most common for preparation of pH-sensitive beads where a pH indicator is entrapped inside cross-linked polyacrylamide particles. The size of the beads can be tuned over a wide range so that preparation of both nano- and microbeads is possible. Despite thorough washing the surfactants are rather difficult to remove completely and their traces can influence the performance of some biological systems.

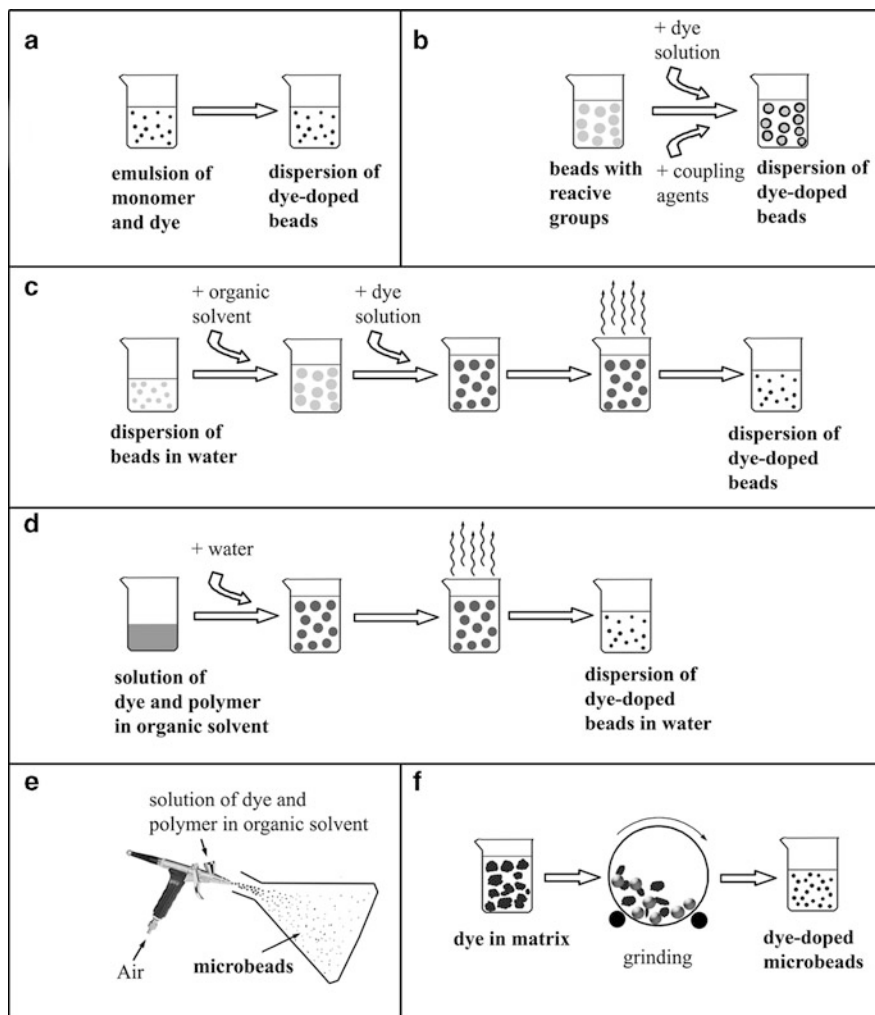


Fig. 4 Schematic representation of the techniques used for making stained beads: (a) staining during polymerization; (b) staining via covalent or electrostatic coupling of an indicator to the beads surface; (c) staining via swelling; (d) preparation of dye-doped beads via precipitation; (e) spray-drying; (f), grinding

3.2 Staining of the Beads via Surface Modification

Polymeric beads obtained via emulsion polymerization, precipitation, etc. can be stained with dyes providing that both have functional groups available [7]. Covalent coupling is mostly preferred but the attachment based on strong electrostatic interactions is also feasible. This method is mostly used to design pH- and ion-sensitive micro- and nanobeads. The dynamic response of such systems can be

rather fast since the sensing “chemistry” is localized on the surface of the beads. On the other hand, it is not always easy to obtain bright beads since indicators are only loaded on the surface. Higher dye loading may even result in decreased brightnesses due to self-quenching.

Some bead materials possess porous structure and, therefore, have very high surface to volume ratio. The examples include silica-gel, controlled pore glass, and zeolite beads. These inorganic materials are made use of to design gas sensors. Indicators are usually adsorbed on the surface and the beads are then dispersed in a permeation-selective membrane (usually silicone rubbers). Such sensors possess high sensitivity to oxygen and a fast response in the gas phase but can be rather slow in the aqueous phase since the gas contained in the pores needs to be exchanged. Porous polymeric materials are rarer and have not been used so far in optical nanosensors.

3.3 *Staining by Swelling*

Polystyrene and polymethylmethacrylate beads are commonly stained by swelling [8, 9]. The beads are suspended in a water/methanol mixture and swelled by the addition of a small amount of dichloromethane (where a dye is also dissolved). Unfortunately, not all indicators show sufficient solubilities in such mixtures so that dye loading is not very high. As was demonstrated [8], the incorporation of hydrophobic dyes into polymer particles can be facilitated by use of surfactants. However, these are often difficult to remove completely which may negatively affect biological systems. Charged groups on the surface of the beads provide additional stability toward aggregation and such materials can be usually stained more easily. For example, carboxylated polystyrene micro- and nanospheres (Polybead[®], Polysciences Inc.) can be stained from water/THF or water/acetone mixtures with a high content of organic solvent. In this case solubility of lipophilic dyes is usually not an issue. Core-shell poly(styrene-*block*-vinylpyrrolidone) beads were found to be excellently suitable for staining [10]. It was demonstrated that virtually any lipophilic oxygen indicators (such as Pt(II) and Pd(II) metalloporphyrins, Ru(II) polypyridyl complexes and Ir(III) coumarins) can be embedded into the core of the beads by swelling the particles in water/THF mixtures and by subsequently removing of THF at a reduced pressure [11]. Lipophilic pH indicators (fluoresceins and 1-hydroxypyrene-3,6,8-trisulfonamides) can be stained into the hydrophobic shell from ethanol/water mixtures [12]. Some ion sensors can also be prepared using this versatile material.

3.4 *Preparation of Stained Beads via Precipitation*

Precipitation is a rather widespread method of manufacturing polymeric beads [13, 14] but it has only been sparsely used for the preparation of dyed beads [15, 16]. However, this versatile method is very promising due to its simplicity. It was recently

demonstrated that a great variety of polymers can be used [17]. Typically, an indicator and a polymer are dissolved in an organic solvent and the stained beads are formed upon fast or slow addition of water. Many lipophilic indicators which are insoluble in water were found to be suitable. The size of the beads can be tuned in a broad range by varying the nature of the solvent, the speed of water addition and the concentration of the polymer. Diluted solutions favor the formation of smaller beads. Charged functional groups (e.g., carboxyl groups) usually and significantly increase the stability of the bead dispersions. On the other hand, beads based on apolar polymers (such as polystyrene) are very difficult to obtain upon precipitation with water and organic solvents should be used for precipitation. Such apolar polymeric beads show high tendency to aggregation upon addition of salts. It should also be mentioned that much smaller beads can be produced using highly charged polymers ($\varnothing < 50$ nm) compared to the less polar ones. The former can usually be freeze-dried and redispersed easily while the latter may show irreversible aggregation upon freeze-drying.

Precipitation was found to be a very useful method for preparation of nanobeads with magnetic properties [17] since not only indicators but also small lipophilic magnetite nanobeads (having diameter of a few nanometers) can be incorporated inside the polymeric beads. Such multifunctional magnetic beads can be guided to the region of interest, be collected and manipulated there.

3.5 Techniques for Preparation of Dye-Doped Microbeads

At first glance, dye-doped microbeads are not advantageous to the nanobeads since they are difficult to use for sensing and imaging in aqueous dispersions. In reality, microbeads are preferable in several applications. For example, they are easier to handle than the much smaller nanobeads especially if the particles are to be dispersed in a polymer matrix. In case of magnetic sensors, microbeads can be collected much faster and be manipulated more easily than the corresponding nanobeads. The microbeads are also less prone to some undesirable surface effects (e.g., leaching, nonspecific binding, quenching of luminescence by other species) since surface to volume ratio is much smaller than in the case of nanobeads.

The general methods described above are suitable for preparation of both nano- and microbeads. For example, dye-doped microbeads can be prepared via precipitation using a specially designed particle caster [18]. This device makes use of an oscillating piezoelectric transducer which disrupts a jet of a “cocktail” to form highly monodispersed micrometer-sized droplets. The droplets are guided into water where the organic solvent is removed. Several other techniques are useful for producing microbeads (Fig. 4). Spherical porous beads can easily be produced by spray-drying, using for example conventional air-brushes [19]. The size of the beads is determined by the concentration of the “cocktail” and by the dimensions of the nozzle. As was demonstrated, spray-drying enables preparation of multifunctional magnetic beads.

Finally, dye-doped microparticles of irregular form can be produced by grinding or ball milling of polymeric monoliths provided that the material is brittle enough to

be ground to fine particles (\sim several micrometer). Examples include poly(4-*tert*-butyl styrene) and Ormosils. Some less brittle materials can be ground at cryogenic temperatures although it is often problematic to obtain particles of the desired size.

3.6 Purification of the Beads

Purification is often required for the beads obtained by the techniques described above since undesired substances such as surfactants, coupling agents, etc. need to be removed. This is also valid for dye molecules noncovalently adsorbed on the surface of the beads since they usually have different properties (sensitivity, cross-talk to other analytes, leaching, etc.) compared to the molecules located in the core. The dye-doped beads can be purified by repeated precipitation which is achieved by adding salts (typically sodium chloride). In certain cases (typically for large beads) the addition of salts is not necessary so that the beads can be isolated by centrifugation. Washing with ethanol often helps remove lipophilic dye molecules adsorbed on the surface provided that the polymer is not swellable. Alternatively, dialysis can be useful especially if a hydrophilic water-soluble indicator is covalently coupled to the bead surface.

4 Optical Read-Out Schemes

Most dye-doped beads are interrogated using luminescent methods since they enable higher sensitivity compared to absorptiometry and reflectometry. Luminescence intensity is still the most popular analytical parameter due to the simplicity of the method. Obviously, luminescence intensity is not referenced if determined at a single wavelength and is affected by drifts of the opto-electronic system, light scattering, turbidity of the sample, etc. [20]. Therefore, ratiometric measurements at two different wavelengths are widely used [21]. Different techniques for wavelength-ratiometric sensing involving both single dyes and responsive-irresponsive dye pairs have been recently reviewed [128]. In one of the applied techniques an inert dye (insensitive to the analyte of interest and other species) is coembedded into the beads to be excited simultaneously with the indicator. Förster resonance energy transfer (FRET) is often employed to enable referenced measurements (where the intensities from a FRET donor and a FRET acceptor are collected at two different wavelengths). Fluorescein–rhodamine pairs are the most popular for designing FRET nanosensors for pH. As demonstrated recently for planar optodes [22], FRET can also be used to increase sensor brightness by means of light harvesting. This principle was also used to enhance the brightness of dye-doped polymeric beads [17].

Measurement of luminescence decay time represents another method of self-referencing. The method is widely used for the indicators that possess luminescence decay times in the microsecond and millisecond domain which can be interrogated

with simple and inexpensive instrumentation. Therefore, interrogation via decay time is usually applied for oxygen-sensitive and temperature-sensitive beads which rely on luminescent metal complexes. Autofluorescence from the sample can be easily discarded in time resolved measurements.

Dual lifetime referencing (DLR) is another powerful technique that enables referenced measurements in case of fluorescent indicators [23]. In this method, the analyte-dependent signal from an indicator is referenced against the signal from an inert luminophore. This can be realized in both the time domain [24] and in the frequency domain [25]. Often, a luminescent reference dye is embedded into gas blocking nanobeads to avoid oxygen quenching. Polymers with very low gas permeability such as poly(acrylonitrile) [24] or poly(vinylidene chloride-*co*-acrylonitrile) [26] are the best choice here.

Microscopic imaging of various parameters (oxygen, pH, etc.) with the help of dye-doped nanobeads has become more and more popular and is mostly realized with help of conventional fluorescent microscopes. Confocal and two-photon microscopies enable higher resolution and, therefore, are very popular. Since the light intensities are rather high, only highly photostable indicators can be used for microscopic applications in order to avoid drifts caused by photobleaching. Unfortunately, most conventional indicators are poorly suitable for the application in two-photon microscopy due to very low two-photon absorption cross-sections. Therefore, design of more efficient luminescent dyes is of extreme importance [27] for such applications and their application in nanobeads for sensing and imaging is yet to be realized.

5 Selected Examples of Dye-Doped Polymeric Bead Materials

Dye-doped polymeric beads are commonly employed in different formats (Fig. 5), namely as water-dispersible nanosensors, labels and in composite materials (DLR-referenced and multianalyte sensors, sensor arrays, magnetic materials, etc.). The sensing properties of the dye-doped beads are of little or no relevance in some more specific materials, e.g., the beads intended for photodynamic therapy (PDT). The different formats and applications of the beads will be discussed in more detail in the following section, and the relative examples of sensing materials will be given.

5.1 *Water-Dispersible Nanosensors*

These are introduced directly into the analyzed medium or even into the cells to measure analytical parameters there. Compared to dissolved indicators nanosensors are usually significantly less toxic and are less prone to interferences and quenching. On the other hand, similarly to the dissolved indicators, nanosensors

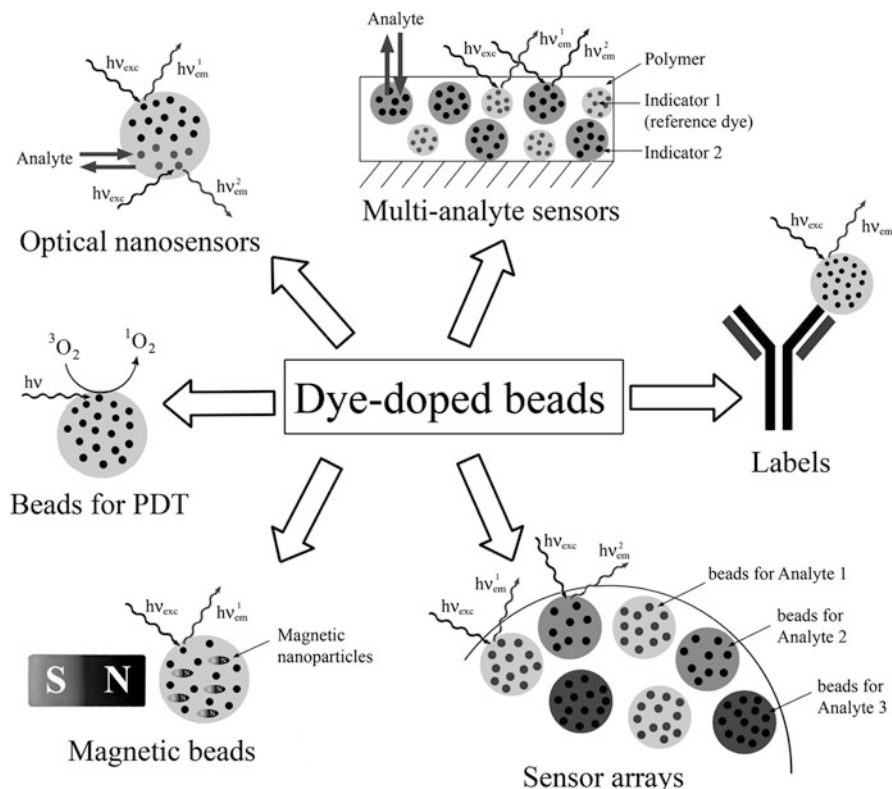


Fig. 5 Schematic representation of most common applications of dye-doped polymeric beads

respond to analytes virtually in real time. True nanosensors should fully and reversibly respond to the analyte of interest. Lübberts and co-workers were probably the first who reported nanosensors for oxygen and pH [28]. In this early work the indicators were incorporated into 150–200 nm large polyacrylamide beads. However, it was 20 years later that the potential of optical nanosensors was truly recognized. Since then the area of optical nanosensors has grown continuously. Nowadays, the principles of designing nanosensors for oxygen, protons, ions and some other species are well established. On the other hand, it is much more difficult to realize nanosensors for basic and acidic gasses, bioanalytes, etc. which is yet to be done. Below we summarize different approaches for designing of optical nanosensors.

5.1.1 Beads for Sensing and Imaging of Oxygen

Similarly to bulk oxygen sensors, optical nanosensors rely on dynamic quenching of luminescence. Numerous indicators and polymeric materials were found suitable

for designing oxygen nanosensors. For example, Kopelman and co-workers reported a ratiometric nanosensor for dissolved oxygen [29] based on platinum (II) octaethylporphyrin ketone entrapped into poly(decyl methacrylate) particles (150–250 nm) along with an oxygen-inert octaethylporphyrin that served as a reference. Remarkably, the Stern–Volmer plots were linear over the whole concentration range (0–100% oxygen saturation). The nanosensor proved to be rather sensitive to oxygen ($I_0/I_{\text{air sat}} = 10$), which, however, may be too sensitive for most applications (due to low S/N ratio at higher oxygen concentration). No leaching of the lipophilic dyes was detected within several days. The same dyes were incorporated into Ormosil beads to obtain oxygen nanosensors of 100–700 nm in diameter [30]. The sensitivity was found to be slightly lower than in poly(decyl methacrylate) beads ($I_0/I_{\text{air sat}} = 8$). Again, Stern–Volmer plots were found to be linear. Application of the nanobeads for intracellular imaging of oxygen tension was also demonstrated.

We discovered that poly(styrene-*block*-vinylpyrrolidone) is an excellent material for designing oxygen nanosensors [10]. The polymeric core–shell beads (\varnothing 220 nm) are commercially available at low price and can be stained by swelling using a simple protocol [10]. Virtually all lipophilic oxygen indicators including metalloporphyrins, ruthenium (II) polypyridyls and cyclometallated complexes can be immobilized into the core of the beads [11] and do not leach out even after several months' storage in an aqueous dispersion. The beads can be autoclaved and evidently show no cytotoxicity. The beads are suitable for monitoring of dissolved oxygen in bulk solution but cannot be used for intracellular measurements. Despite being uncharged the nanoparticles show unique stability toward aggregation which does not occur even at very high concentration of salts and in fermentation media. The sensitivity can be tuned by making use of an appropriate indicator.

We also recently demonstrated that a variety of polymers are suitable for preparation of optical nanosensors via precipitation [17]. The most promising nanobeads were obtained by immobilization of lipophilic oxygen indicators into poly(styrene-*co*-maleic anhydride) and poly(methyl methacrylate-*co*-methacrylic acid) bearing carboxyl-groups available for further covalent immobilization. Cationic Eudragit[®] RL 100 beads (polymethacrylates containing ~10% of quaternary ammonium groups) may be suitable for intracellular oxygen monitoring. The size of the beads can be tuned over a broad range by adjusting the concentration of polymer in initial solution and by varying the precipitation speed. We also developed the oxygen-sensitive nanobeads (\varnothing 55 nm) based on palladium(II) tetraphenyltetraenzoporphyrin incorporated into poly(methyl methacrylate-*co*-methacrylic acid). This promising material can be efficiently excited with the 632.8 nm line of He–Ne laser and 635 nm red laser diode and has a sensitivity optimal for physiological measurements ($\tau_0/\tau = 3.6$ at air saturation).

Wu et al. [31] have recently presented a novel concept of designing oxygen nanosensors. They used the precipitation method to obtain polyfluorene beads (\varnothing 25 nm) doped with the oxygen indicator platinum(II) octaethylporphyrin. Poly(9,9-dihexylfluorene) belongs to materials widely used in OLEDs and has a bright blue emission when excited in the UV region. In beads, FRET-mediated red emission

from the oxygen indicator is observed. Residual blue luminescence from polyfluorene enables ratiometric imaging of oxygen tension with optimal sensitivity ($I_0/I = 3.7$). Additionally, the nanobeads were found to be nicely suitable for oxygen imaging under two-photon excitation which is not surprising since polyfluorenes were previously found to have very high two photon absorption cross-sections [32]. The authors also demonstrated suitability of the nanobeads for intracellular imaging.

Pfister et al. [33] used difluoroboron dibenzoylmethane conjugate with poly(lactic acid) to prepare biocompatible oxygen-sensing nanoparticles (\varnothing 100 nm). The polymer-dye conjugate was found to possess both blue fluorescence and green phosphorescence. This unique property, in principle, enables ratiometric sensing of oxygen with one indicator only. However, the phosphorescence decay time was found to be too long (~ 200 ms) for optimal sensitivity in biological systems. The decay time for the iodine-substituted difluoroboron dibenzoylmethane-poly(lactic acid) conjugate was found to decrease by tenfold ($\tau_0 = 4.82$ ms) due to the heavy atom effect [34]. This modified material was demonstrated to be suitable for ratiometric imaging of tumor hypoxia ($pO_2 < 1$ kPa).

5.1.2 Beads for Sensing and Imaging of pH

Cross-linked polyacrylamide beads are often the material of choice for preparation of optical pH nanosensors [35]. A pH indicator (usually a fluorescein derivative) and a reference dye are introduced prior to polymerization and are physically entrapped into the beads. Such nanosensor operates fully reversibly and show acceptable photostability. However, leaching of the hydrophilic indicators often compromises the performance of such materials. For example, as much as 40% of the indicator leached out within the first 2 days [35]. Sun et al. [36] attempted to minimize leaching of an indicator (fluorescein) and a reference dye (rhodamine) by covalently immobilizing them into the polyacrylamide network. Although leaching was substantially reduced compared to the dyes simply dissolved in the polymer (6% vs. 70% in 6 h) the extent of leaching was still not negligible. Allard and Larpent [37] minimized leaching by covalently attaching fluorescein isothiocyanate to the surface of amino-functionalized crosslinked polystyrene nanobeads (\varnothing 20 nm). No detectable leaching was observed for at least 1 week. A highly hydrophobic reference dye 9,10-diphenylanthracene was also embedded into the beads by swelling. However, the reference dye required excitation in the UV region (375 nm) which is not very practical.

McNamara et al. [38] developed water-dispersible microbeads for ratiometric imaging of pH. The 1.6 μm polystyrene beads were covered with a phospholipid layer containing covalently coupled fluorescein and rhodamine. The material was suitable for sensing pH in bulk solution and in macrophages.

Funfak et al. [39] demonstrated recently that pH-sensitive microbeads based on 8-hydroxypyrene-1,3,6-trisulfonate covalently attached to amino-functionalized poly(hydroxyethylmethacrylate) (\varnothing 2.5 μm) can be successfully used to monitor

pH in microfluidic devices. Metabolic activity of *Escherichia coli* during cultivation was successfully monitored with help of the beads.

It was demonstrated that poly(styrene-*block*-vinylpyrrolidone) beads (\varnothing 220 nm) are suitable for preparation of pH nanosensors [12]. Various fluorescein derivatives were embedded and did not leach out of the beads due to functionalization with highly lipophilic octadecyl “anchor.” The pK_a of the indicators inside the nanobeads varied from 5.8 to 7.7 making them suitable for various biotechnological, biological and marine applications. The beads based on a lipophilic 1-hydroxypyrene-3,6,8-trisulfonate (pK_a 6.9) were also manufactured.

5.1.3 Beads for Sensing and Imaging of Ionic Species

One can distinguish between the two main types of nanosensors for ionic species: the beads relying on the indicators highly specific to a particular analyte and those employing ionophores as recognition elements. The nanosensors (\varnothing typically 20–200 nm) of the first type predominantly use cross-linked polyacrylamide as a matrix where a fluorescent indicator and a reference dye are entrapped. For example, Kopelman and co-workers reported nanosensors for Ca^{2+} [35], Mg^{2+} [40], Zn^{2+} [41] and Fe^{3+} [42]. Evidently, the extent of leaching is determined by the lipophilicity of the respective indicator and can vary from the very significant [35, 40] to the virtually negligible [41]. To prevent leaching, the reference dyes (such as Texas Red) are used as macromolecular conjugates with dextrane [41, 42]. Interestingly, such fluorescent dyes as coumarin C343 (a laser dye) and Alexa Fluor 488 (commonly used as a label) were found to be highly selective toward Mg^{2+} [40] and Fe^{3+} [42], respectively.

The second type of the nanosensors relies on ionophores which are entrapped into the polymeric bead along with a lipophilic pH-dependent chromionophore (usually a phenoxazine derivative). These nanosensors are designed similarly to the bulk optodes and ion-selective electrodes and usually possess very high selectivity. Poly(decyl methacrylate) [43, 44] and plasticized poly(vinyl chloride) [16, 45] are the polymers of choice for preparation of the nanobeads. For example, a nanosensor reported by Kopelman and co-workers [43] was suitable for determination of 0.63 mM–0.63 M of K^+ although showed very poor storage stability due to the leaching of the indicator. Chloride-selective neutral ionophores were used by Brasuel et al. [44] and Ceresa et al. [45] to prepare the sensing beads operating in similar dynamic ranges (0.4–190 mM and 0.3–300 mM, respectively) despite the fact that different polymers and ionophores were employed.

Bychkova and Shvarev [16] recently prepared nanosensors (0.2–20 μ m) for sodium, potassium and calcium using the precipitation method. Similarly to the previous works, the plasticized poly(vinyl chloride) included a phenoxazine chromionophore, a lipophilic ion exchanger and a cation-selective ionophore. The dynamic range of the very selective sensors was 5×10^{-4} –0.5 M for sodium, 1×10^{-5} –0.1 M for potassium and 2×10^{-4} –0.05 M for calcium. As was demonstrated by Bakker and co-workers [45] a particle caster can be used for preparation of much larger beads (\varnothing 11 μ m).

Similarly to dyes, some fluorescent proteins can be incorporated into polymeric beads to be used as an alternative for ion sensing. For example, a reporter protein (composed of a phosphate-binding protein, a FRET donor (cyan fluorescent protein) and a FRET acceptor (yellow fluorescent protein)) was incorporated into polyacrylamide nanobeads by Sun et al. [46]. FRET was inhibited upon binding of phosphate. Kopelman and co-workers [47] used a similar approach to design a nanosensor for copper ions. They have found that fluorescence of red fluorescent protein DsRed (commonly used as a label) is reversibly quenched by Cu^{2+} and Cu^+ . Both DsRed and Alexa Fluor 488 (used as a reference) were entrapped into polyacrylamide nanobeads. Typically, up to 2 ppb of copper ions can be reliably measured. It should be mentioned, that in contrast to much more robust dyes, mild conditions upon polymerization and purification are very important for immobilization of the biomolecule to avoid degradation.

Gouanve et al. [9] presented another approach to designing copper nanosensors. They prepared cross-linked polystyrene beads (\varnothing 14 nm) and functionalized the surface with 1,4,8,11-tetraazacyclotetradecane (Cyclam), which selectively bound copper ions. The core of the beads was stained with a lipophilic fluorescent dye 9,10-diphenylanthracene by swelling. Fluorescence of the dye was quenched in the presence of Cu^{2+} due to FRET. The particles were suitable for sensing Cu^{2+} in micromolar concentrations.

5.1.4 Beads for Sensing and Imaging of Metabolites

Kopelman and co-workers [48] attempted to design a nanobiosensor for glucose by immobilizing an oxygen indicator, ruthenium(II) tris(4,7-diphenyl-1,10-phenanthroline disulfonic acid) dichloride, glucose oxidase and a reference dye into polyacrylamide beads (\varnothing 45 nm). An increase of luminescence intensity of the oxygen indicator was observed in the presence of glucose due to the consumption of oxygen in the enzymatic reaction. The calibration plot remained linear between 0.3 and 5 mM of glucose. However, this is at variance with the results of Stein et al. [49] who found that even in case of much larger silica/alginate microbeads (\varnothing 14 μm) doped with an oxygen indicator (PtOEP) and glucose oxidase the diffusion of glucose is too fast for the sensor to operate in the physiologically relevant dynamic range (2–20 mM of glucose). The beads were found to respond linearly only from 0.1 to 5.5 mM of glucose. Additional polyelectrolyte bilayers poly(allylamine hydrochloride)/poly-(sodium 4-styrenesulfonate) were necessary to control the diffusion of the analyte and the linear dynamic range was extended to 11 mM of glucose [50]. Moreover, a rhodamine derivative was entrapped into the polyelectrolyte nanolayers to enable ratiometric referencing.

Zenkl et al. [51] presented another approach to design saccharide-sensitive nanobeads. They prepared particles (\varnothing 380 nm) based on poly(*N*-isopropylacrylamide) cross-linked with phenylboronic acid moieties. In the presence of a saccharide (glucose or fructose) the particles reversibly swell due to the formation of negative charges. A FRET-indicator couple (fluorescein/rhodamine) is used to monitor the

degree of swelling. In the presence of saccharide FRET is inhibited so that the ratio of emissions (fluorescein/rhodamine) is related to saccharide concentration. However, the beads showed pronounced cross-sensitivity to pH and the dynamic range was found to change from 0–150 mM at pH 8.5 to 0–30 mM at pH 9.0.

5.1.5 Beads for Detection of Reactive Oxygen Species

Reactive oxygen species (ROS) are known to be very important in cellular systems and particularly in pathological processes. Therefore, development of nanosensors for intracellular determination of ROS is of particular importance. It should be emphasized that it is extremely difficult (if not impossible) to realize a system capable of fully reversible detection of ROS. The systems developed so far are better referred to as “nanoprobes” due to their irreversible performance. For example, a nanoprobe for hydrogen peroxide was developed by Polsen et al. [52]. A fluorescein–dextran conjugate (a probe) and horseradish peroxidase (a biocatalyst) were entrapped into polyacrylamide beads. Hydrogen peroxide which irreversibly oxidized the dye could be determined in the concentration range from 0.5 to 10 μM . Henderson et al. [53] designed a nanoprobe for ROS by incorporating dihydrorhodamine 123 and Alexa Fluor 568–dextran conjugate (used as a reference) into polyacrylamide beads (\varnothing 18 nm). In the presence of ROS, dihydrorhodamine 123 is oxidized to give highly fluorescent rhodamine 123. The capability of the nanosensor for intracellular monitoring of ROS was demonstrated.

5.2 Dye-Doped Beads as Labels

Fluorescent dyes can be incorporated into the beads to be used as tracers for imaging applications. Such beads can also be used as labels providing that the polymer materials possess functional groups for covalent coupling. Dyes embedded in polymeric beads are protected from the surrounding environment and, therefore, are much less liable to quenching and nonspecific binding. Moreover, high local concentration of dyes enables superior luminescence brightness. Thus, functionalized dye-doped beads were successfully employed in fluorescent immunoassays [54]. It should be mentioned that dye-doped silica beads represent a promising alternative [55, 56] to the polymeric beads since preparation of much smaller beads ($\varnothing < 6$ nm) is feasible [57].

The dyes with long-lived luminescence are particularly attractive since background fluorescence can easily be discarded in time domain measurements. Cross-sensitivity to oxygen may be problematic but it can be minimized by utilizing gas-blocking polymers. For example, Kuerner et al. [15] used the precipitation technique to prepare polyacrylonitrile-based beads doped with a ruthenium(II) complex which showed virtually no cross-sensitivity to oxygen. Copolymers of polyacrylonitrile and polyacrylic acid were used to provide the beads with

functional groups to enable covalent coupling. Song et al. [58] used a similar method to encapsulate a phosphorescent platinum(II) porphyrin (PtTFPP) into a copolymer of vinyl chloride, ethyl acetate and maleic acid. The monodispersed beads ($40 < \varnothing < 300$ nm depending on solvent and precipitation speed) were found to be stable against aggregation and be redispersible after centrifugation, which was not the case for poly(vinyl chloride) beads used for comparison. Moreover, very high dye loading (up to 3.3% w/w) enabled preparation of brighter beads. Unfortunately, the degree of oxygen quenching in the beads remains unclear. The particles have been successfully used to covalently tag a C-reactive protein (CRP) monoclonal antibody and provide a very sensitive time-resolved phosphorescent assay for CRP. We recently reported nanobeads based on poly(methyl methacrylate-*co*-methacrylic acid) [17] with an average diameter of 55 nm. Luminescence of the iridium(III) coumarin complex incorporated into the beads was affected only in a minor way by oxygen. The beads may be suitable for labeling purposes due to the presence of reactive carboxyl groups on the surface.

Lanthanide complexes are particularly attractive in such applications since their luminescence is only minimally quenched by oxygen and, therefore, the choice is not limited by gas-blocking polymers. Thus, several highly sensitive lanthanide-based immunoassays were reported recently. For example, Huhtinen et al. [59] developed an assay for oligonucleotides where carboxyl-modified polystyrene nanoparticles (\varnothing 107 nm) were used as labels. The nanoparticle approach demonstrated a 100–1,000-fold improvement in the detection limit compared to the reference assay where biomolecules were labeled directly with the europium(III) chelates. The same group reported a competitive immunoassay for estradiol [60] which made use of polymeric beads stained with a luminescent europium(III) complex. The beads were used as labels for the antibodies which interacted with estradiol/Alexa Fluor 680 conjugates. Thus, FRET from the europium(III) complex to Alexa Fluor 680 was inhibited in the presence of estradiol. Performance of the immunoassays can be further improved by utilizing smaller beads based on the copolymer of polystyrene and acrylic acid (\varnothing 50 nm) [61]. As was demonstrated recently, the smaller beads are much more efficient in FRET applications since the amount of europium complex located far from the surface and not participating in FRET is significantly reduced [62]. Another group developed a fluorescent immunoassay for atrazine based on polystyrene beads stained with a europium(III) chelate [63]. Europium(III) complexes encapsulated into Ormosil beads were also shown to be promising for application in immunoassays [64]. Huhtinen et al. [65] have demonstrated that luminescent complexes of other lanthanides (samarium, terbium, dysprosium) can be used for staining polystyrene beads. Line type emission of the lanthanides can easily be separated which enables simultaneous determination of several analytes in immunoassays.

It should be mentioned that most of lanthanide chelates reported so far are excitable in the UV region. Although autofluorescence is eliminated in time-resolved measurements, high light scattering and absorption of light by biological substances can be sometimes inconvenient. Therefore, development of visible light-excitable probes is of much interest. Recently Wu et al. [66, 67] encapsulated

such a complex into silica beads which were used in immunoassay for the detection of bacteria. Thus, the excitation of the nanobeads with visible light (400–420 nm) became possible. The disadvantages include rather poor photostability of the complex and liability to thermal quenching [68].

5.3 *Dye-Doped Beads in Composite Materials*

Optical sensors for pH and ions almost exclusively rely on the use of fluorescent indicators. Sensors for carbon dioxide and ammonia also use fluorescent pH indicators as transducers. Since relatively bulky and expensive instrumentation is necessary for direct measurement of fluorescence lifetimes in the nanosecond time domain, different referencing schemes were developed. As was mentioned above, ratiometric dual wavelength measurements are very popular, particularly in case of nanosensors combining both an indicator and a reference dye in a single bead. On the other hand, DLR scheme is often used for planar optodes. A luminophore with relatively long decay time (microsecond–millisecond) serves as a reference and in order to be suitable should be inert to the analyte of interest and to other interfering species. Therefore, incorporation of reference dyes in gas-blocking polymers is essential, since virtually all luminescent dyes are liable to oxygen quenching. Polyacrylonitrile (PAN) and its copolymers possess very low gas permeability and represent an excellent choice here. Dye-doped PAN beads can be easily manufactured via precipitation and are embedded into the sensing layer along with a fluorescent indicator (Fig. 4). Ruthenium(II) tris(1,10-diphenylphenanthroline) in PAN was found to be spectrally compatible with many fluorescent indicators and was used as a reference in sensors for pH [24], chloride [25, 69], amines [70], copper [71], and carbon dioxide [72, 73]. Luminescent Ir(III) coumarin complexes are spectrally similar to the Ru(II) polypyridyls but possess much brighter luminescence and are less affected by thermal quenching [74]. Thus, they represent excellent candidates for DLR applications although their lower photostability should also be considered. We reported the DLR-referenced carbon dioxide [75] and ammonia sensors [26] which made use of micro- and nanobeads stained with Ir(III) coumarin complexes.

Composite materials allowing simultaneous optical detection of several analytes have recently become popular [76]. Immobilization of the individual indicators in permeation-selective beads is necessary to tune the sensitivity and to improve selectivity. Additionally, the bead-based sensors do not suffer from FRET issues between the indicators and usually have improved photostability (since the production of singlet oxygen can be avoided or is minimized). For example, several groups reported composite materials for simultaneous sensing and imaging of oxygen and temperature [77–79]. The temperature probe represented a luminescent Ru(II) polypyridyl complex which was embedded into gas blocking polyacrylonitrile nanobeads to avoid cross-sensitivity to oxygen. Alternatively, a temperature probe made use of a luminescent Eu(III) complex contained in poly(vinyl chloride)

particles [80]. Pt(II) and Pd(II) porphyrins used as oxygen indicators were embedded in various polymeric beads (such as poly(styrene-*co*-acrylonitrile)) to optimize the sensitivity. Luminescent microbeads also were used to design an optical sensor for simultaneous measurements of pH and oxygen [7, 81]. These materials relied on oxygen-sensitive microbeads based on a Pt(II) porphyrin and pH-sensitive microbeads with covalently immobilized 5(6)-carboxyfluorescein [7] or 8-hydroxypyrene-1,3,6-trisulfonate [81]. The beads were dispersed in a layer of polyurethane hydrogel D4 which is permeable to both oxygen and proton. Simultaneous sensing of three analytes (pH, oxygen and temperature) with the help of indicator-doped beads was also reported [82]. Due to the small size of the beads it was possible to manufacture fiber-optic microsensors (\varnothing 140 μm) for simultaneous sensing of pH and oxygen or oxygen and temperature [83]. Here, the tip of an optical fiber was covered with a “cocktail” containing the bead probes.

5.4 Sensor Arrays Based on Dye-Doped Beads

Stained polymeric particles have become a useful tool in multiplexed analysis in clinical diagnostics, drug discovery, gene-function analyzes, etc. In general, multiplexed analysis systems are divided into two classes: flat-surface and suspension arrays [84–86] (Fig. 6). Spotted microarrays also called biochips are the major representatives of the flat-surface type [87, 88]. Suspension arrays or liquid arrays consist of a multitude of particle carriers floating in solution. Each particle represents an array element that bears specific surface-bound receptor molecules. Suspension arrays offer advantages in handling and higher flexibility in array creation. Reaction rates of slide-bound assays are usually diffusion controlled, while bead-based analyte–receptor reactions are limited by binding kinetics that are faster than diffusion [89]. Additionally, bead arrays are intrinsically less prone to variations resulting from poor spot reproducibility for two reasons. First, the same batch of beads is split and used for calibration and sample analyzes. Thus, receptor immobilization is similar for all readouts. Second, several dozens or hundreds of beads are evaluated from one sample. Another type of array uses microspheres randomly absorbed at the distal end of a bundle or fixed in cavities of silicon chips [90]. In contrast to flat-surface arrays, where each type of assay is determined by its exact position, each bead family – representing one type of assay – has to carry a distinguishable code for identification. Various encoding methods including optical, chemical, graphical, electronic and physical are described in literature [85, 86].

5.4.1 Suspension Arrays

Fluorescent encoded beads represent the largest group in multiplexed suspension arrays (Fig. 6c). Luminescent dyes are commonly incorporated by swelling. The

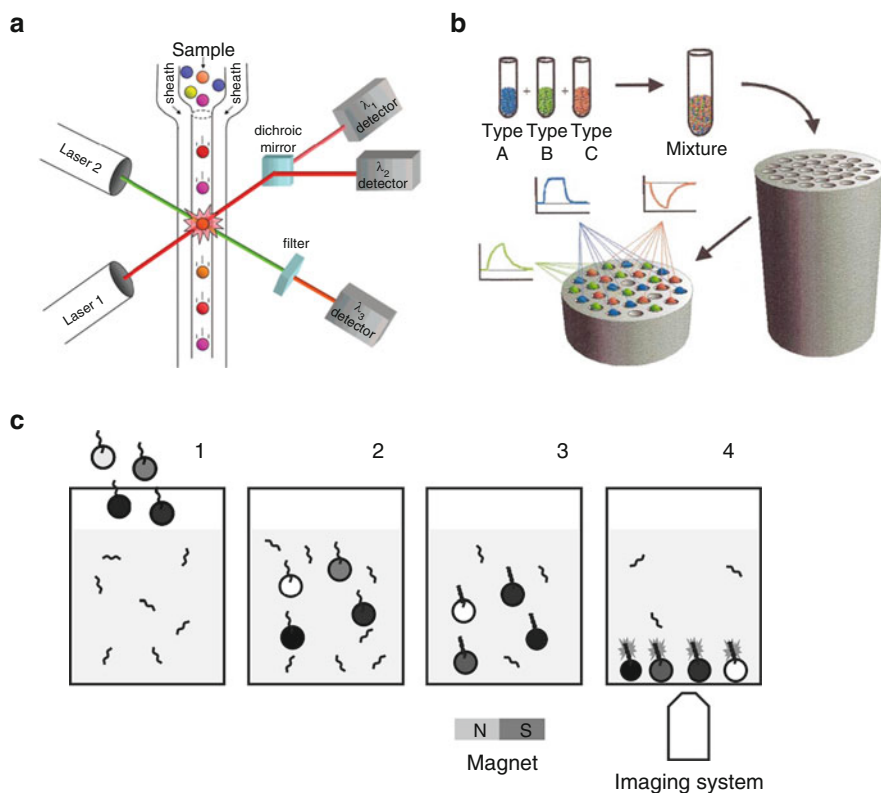


Fig. 6 (a) Schematic illustration of a flow cytometer used in a suspension array. The sample microspheres are hydrodynamically focused in a fluidic system and read-out by two laser beams. Laser 1 excites the encoding dyes and the fluorescence is detected at two wavelengths. Laser 2 is used to quantify the analyte. (b) Scheme of randomly ordered bead array concept. Beads are pooled and adsorbed into the etched wells of an optical fiber. (c) Scheme of randomly ordered sedimentation array. A set of encoded microspheres is added to the analyte solution. Subsequent to binding of the analyte, microparticles sediment and assemble at the transparent bottom of a sample tube generating a randomly ordered array. This array is evaluated by microscope optics and a CCD-camera. Reproduced with permission from Refs. [85] and [101]. Copyright 1999, 2008 American Chemical Society

number of codes depends on the number of different dyes and concentrations (=intensity level) according to the formula: $C=N^m$ (where C is the number of codes, N is the number of intensity levels and m is the number of colors). For example, fluorescently encoded microbeads (\varnothing 5.6 μm , available from Luminex Corporation, <http://www.luminexcorp.com>) doped with an orange and a red fluorescent dye at ten different concentrations yield in 100 different bead families and ~ 500 bead families are created by staining with three dyes. Fluorescence intensity is the standard parameter that is used for identification. The number of codes can be increased by measuring the luminescence lifetime as demonstrated by Keij and

Steinkamp [91] for the Luminex microspheres. Recently, Mayr et al. stained magnetic microspheres with luminescent ruthenium(II) metal ligand complexes [92] which were encoded by time resolved imaging in the microsecond domain.

It should be mentioned that semiconductor nanocrystals (quantum dots, QDs) represent a powerful alternative to organic dyes here. The QDs of many colors can be excited with a single light source and additionally benefit from size-tuneable emission and high photostability. Similarly to fluorescent dyes the hydrophobic QDs can be physically entrapped in polymeric beads (e.g., polystyrene) during polymerisation [93] or be incorporated by swelling [94] or using layer-by-layer deposition [95, 96]. The combination of several QDs can theoretically result in thousands of different codes [94], however, for many applications a few dozens of codes is usually more than adequate [84]. In practice, the large number of codes claimed is difficult to achieve because of the spectral overlap of the channels and the need of a certain spectral region for the detection of the fluorescent label.

The dominated read-out technique of suspension arrays is flow-cytometry (Fig. 6a). This technique was originally developed for cell counting and sorting and is ideally suited for the analysis of beads arrays. Particles are hydrodynamically focused from a sample into a narrow stream in the center of the column. The flowing stream of particles passes the beam of two lasers and the scattering light or fluorescent light is detected. One beam quantifies the reporter fluorescence intensity and the other is used to identify the beads. The most well known Luminex XMap instrument uses orange and red stained micro-beads and a green reporter dye (R-phycoerythrin). Particle analysis rates up to 10,000 per second can be obtained and the sampling time for a 100-plex array is theoretically only 2–5 s (200–500 replicas) [97]. Among other companies, Becton Dickinson offers various sets of beads to perform parallel assays on nonspecialised flow-cytometers with a multiplex capability of up to 30 (<http://wwwbdbiosciences.com>).

A new suspension array concept based on sedimentation and microscopic imaging was introduced by Moser et al. [98]. Magnetic microbeads settle to the bottom of a microplate well by magnetic forces and form randomly ordered arrays, which are examined by fluorescence microscopy and automated imaging analysis. Each bead carries specific capture molecules and can be identified by a defined luminescent code.

The number of multiplexed particles-based assays reported is manifold and summarized in several reviews [85, 86, 97, 99]. Bead sets for various nucleic acid or protein assays are commercially available that are fully optimized for clinical diagnostics and research purposes.

5.4.2 Randomly-Ordered Bead Arrays

In this type of arrays, microbeads carrying different indicator or receptor molecules are randomly loaded into the wells of chemically etched optical fiber or silicon chips [89, 90, 100] (Fig. 6b). The beads are encoded with single or multiple luminescent indicators or labels embedded into the polymeric core and/or bound

to the surface [90, 101, 102] and are loaded onto the fiber in a simple dipping and evaporation technique. A typical fiber bundle consists of 5,000–50,000 individual fibers which are read out with an imaging system based on microscope optics and a CCD camera. The system has separated color channels to identify each bead and detect the reporter fluorophores or indicator dyes. For example, in a highly efficient DNA assay [103] the individual beads are decoded by sequential hybridization of fluorescent complementary oligonucleotide sequences. However, reversible binding or sensing reaction is mandatory for this decoding method.

Randomly-ordered bead arrays can be divided into analyte-specific and cross-reactive sensor arrays. In the first, each element responds with high selectivity using specific receptors. In cross-reactive sensor arrays, the analytical information is gained by the pattern of the different sensing elements responding with a broad specificity. The scheme is based on the principles of the mammalian olfactory system. Analyte specific random bead arrays are applied according to the classic lock-and-key principles for nucleic acid detection and protein detection [85]. Systems for genotyping, sequencing and gene expression are commercially available from Illumina (<http://www.illumina.com>) and BeadArray Solutions (<http://www.immucor.com>). Fiber optic bead arrays for ions based on the extraction into the lipophilic phase by ion carriers were reported by Wygladacz et al. [104, 105].

Cross-reactive sensing arrays were developed to detect odors and vapors in an artificial nose manner. Solvatochromic dyes such as Nile Red are adsorbed on the surface or embedded into various polymeric or porous silica beads. The beads respond to analyte vapor by a change in fluorescence maxima or/and intensity due to changes of polarity inside the bead. A portable instrument and preliminary field test for the detection of petroleum products was recently described [106].

5.5 *Magnetic Dye-Doped Polymeric Beads*

Dye-doped polymeric beads with magnetic properties (either para- or ferromagnetic) became increasingly popular in the past decades. Compared to conventional micro- and nanobeads, these particles can be magnetically guided to a place of interest by an external magnetic field, or even rotated by an alternating field. On one hand, the magnetic separation from the medium can increase the signal strength, reduce the required amount of fluorescent dyes, speed up separation in sedimentation arrays, or localize an effect of the particle to a specific point of a biological material (e.g., targeted drug delivery). On the other hand, the modulated rotation of such particles can greatly extend the signal-to-noise ratio.

The magnetic beads usually consist of inorganic or metallic nanoparticles which are either homogeneously or inhomogeneously (e.g., core-shell) distributed in a dye-doped polymeric bead. Since the dye properties (e.g., luminescence brightness, solubility, etc.) are affected by the presence of magnetic additive the particle synthesis becomes more challenging and its optimization time consuming. Therefore, it is often the best to start with commercially available systems. Bangs

Laboratories, Inc. (<http://www.bangslabs.com>) and especially Spherotech, Inc. (<http://www.spherotech.com>) offer a variety of fluorescent, magnetically separable polymer particles (\varnothing 0.2–10 μm). The fluorescent dyes cover almost the whole visible range and the beads are ready for surface modification through amino-, epoxy or carboxyl groups. These particles cover already a wide range of applications such as immunoassays, cell labeling, imaging and purification, or represent at least a good basis for further modifications.

Whenever the commercially available particles do not match the operator's requirements, a variety of possibilities exist in order to modify the particles from company suppliers. Similarly to other doped beads the dyes [92] or quantum dots [107, 108] can be physically entrapped into magnetic beads by swelling or are covalently bound to the surface of the particles. If localization of the dye on the particle surface is desired or if the polarity of dye and/or matrix polymer does not allow the irreversible entrapment of the dye in the bulk polymer, a covalent attachment of the dye is preferable [109, 110]. Even the covalent binding of whole fluorescent nanoparticles to magnetic microparticles is possible, as shown by Kinoshita and co-workers who investigated the rotation of molecular motors [111].

5.5.1 Applications of Fluorescently Labeled Magnetic Beads

Magnetic fluorescent particles have some main advantages over their nonmagnetic counterparts. First of all, their separation is usually faster than plain sedimentation and does not require filtration or centrifugation steps. This greatly simplifies the handling in applications such as sedimentation arrays, multiplexed analysis and immunoassays [92, 98, 107]. A very interesting principle called "Magnetically-modulated nanoprobes" was introduced by Kopelman and co-workers [112]. They coated one hemisphere of ferromagnetic microspheres with a thin reflective layer (e.g., gold or aluminum), which prevents both emitted light from leaving and excitation light from entering the sphere. The ferromagnetic cores are then magnetized in order to achieve spheres with the north pole at the coated part and the south pole at the uncoated part (or vice versa) and these particles can be turned on and off by a varying magnetic field. In fact, a modulation of the luminescence intensity can be achieved as the response to a modulated external magnetic field. This increases the signal-to-noise ratio by several orders of magnitude and the authors were able to measure the fluorescent signal of single beads surrounded by a 1,000 times higher background signal. Applications of such a system are manifold and include nanoviscosimeters, nanothermometers, nanobarometers, and nanochemosensors [113]. Very recently, the same group correlated the slipping frequency (i.e., frequency, were the beads cannot follow the external field any more) with the growth of bacteria attached to the particles [114].

Another popular technique (particularly in medical applications) is the so called "dual- or multimodal imaging", i.e., combined magnetic resonance (MRI) and

fluorescence imaging. The magnetic properties of the beads can be utilized as contrast agent for MRI and the incorporated dyes are used as labels for affordable real-time tracking of particles in vivo [115]. A careful selection of both the surface groups and the dye is particularly important for designing multimodal probes. The surface property affects the cycle life time in vivo, the potential cellular uptake rate and also the contrasting efficiency in MRI [116]. NIR dyes are usually selected in order to ensure maximal penetration depth in human tissue. Besides the dual mode imaging of tumor tissue it is also possible to magnetically guide and deliver a drug there. For example, Deng et al. [117] incorporated doxorubicin, a common anti-cancer drug, in a stimuli responsive poly(*N*-isopropylacrylamide) shell, which was polymerized around a core of magnetic fluorescent nanobeads. It should be mentioned here that magnetic fluorescent silica beads [118] are used far more often for in vivo applications (such as multimodal imaging, magnetically guided drug delivery and stimuli mediated drug release [119]) than the polymeric beads, probably due to their excellent stability, simple modification chemistry and biocompatibility.

One particularly interesting report on polymeric beads with magnetic, luminescent and cell targeting properties was published by Kopelman et al. [120]. They constructed polyacrylamide beads with magnetic nanoparticles and a photosensitizer in the core. The surface was modified with an RGD peptide for specific cell targeting and polyethylene glycol for increasing the plasma residence time. These particles attached to the cell surface of tumor cells, enhanced the contrast in an MRI image and finally, produced ROS in the close vicinity of the tumor cells.

5.5.2 Magnetic Optical Sensor Particles

A more recent achievement in the field of magnetic, dye-doped polymer beads are magnetic optical sensor particles (MOSePs) [5, 19]. The first MOSePs were based on organically modified silica (Ormosil) and enabled the monitoring of oxygen [5] or pH [121]. As demonstrated by Klimant and co-workers [5], who monitored oxygenation in a shake flask during the growth of *E. coli* the results obtained with MOSePs matched the ones for a conventional, fixed sensor spot. Specially designed magnetic separators help collect MOSePs exactly in front of an optical fiber tip [122]. The concept of magnetically separable optical sensor beads is especially attractive for bioprocess monitoring since the advantages of dispersed sensor beads (easy handling) and fixed sensor spots (high signal intensity, no interference by the medium) are combined. MOSePs can be added to the medium prior to autoclavation and can be even separated from the medium after cultivation if contamination of the cell broth with polymeric particles is unacceptable. Moreover, compared to the water-dispersible nanosensors the amount of the sensor material is reduced tremendously [19]. The magnetic sensor beads are also attractive for microscopic applications where the location of such beads can be manipulated with magnetic tweezers [121].

As demonstrated by Mistlberger et al. [19] spray-drying is a very promising method for the production of MOSePs in the micrometer range. The obtained polymeric beads have a nano-porous structure and show excellent linearity from 0 to 100% oxygen saturation, a very rare phenomenon regarding optical sensors. Smaller MOSePs in the nanometer range can be produced using precipitation technique [17]. A completely different concept was proposed by Kreft et al. [123]. They synthesized mobile pH-sensitive microbeads that consisted of a seminaphthorhodafluor–dextrane conjugate incorporated in the magnetic polyelectrolyte shell. In these microbeads, the magnetic nanoparticles were incorporated by a layer-by-layer deposition together with positive and negative polyelectrolytes. Internalization of the beads by endocytosis into breast cancer cells was achieved, and the change in pH from the alkaline medium outside the cells to the acidic pH in the endo-/lysosome was followed in real time by fluorescence microscopy.

5.6 Dye-Doped Beads for Other Applications

As was demonstrated above, dye-doped polymeric particles are mostly designed for sensing and imaging. However, the range of potential applications is much broader. For example, Kopelman and co-workers demonstrated that ultra-fine polyacrylamide nanoparticles ($\varnothing \sim 2\text{--}3 \mu\text{m}$) stained with meta-tetra(hydroxyphenyl)chlorine can be successfully used for PDT [124]. Both dye aggregation within the water-dispersible nanoparticles and dye leaching were minimized. The nanobeads were shown to be as efficient in killing cancer cells as free photosensitizer molecules. The same group also showed the photodynamic effect for the 5,10,15,20-tetrakis(4-*N*-methylpyridinio) porphyrin-doped polyacrylamide beads under 2-photon excitation [125]. Rat C6 glioma cells incubated with the nanoparticles and irradiated with 780 nm pulsed light (1 min, 100 mW cm^{-2}) started to die 30 min after the exposure and were dead after 120 min. On the other hand, in the absence of nanoparticles all the cells were found to be still alive after 120 min. It was demonstrated that polymeric beads doped with phthalocyanines can also be used for PDT [126].

6 Concluding Remarks

As can be summarized from this survey dye-doped beads represent very versatile analytical tools which are applied in various fields of science and technology. The size of the particles is of the utmost importance here. The smallest beads are mostly designed for intracellular monitoring of analytes and much larger beads are often used in composite materials and sensor arrays. Sensing schemes for optical chemosensors are established and are similarly realized on nano- and microscale.

However, still a limited number of analytes can be sensed. It is very challenging to realize nanosensors for carbon dioxide, ammonia, saccharides, etc. but micrometer-sized particles can be prepared and used in composite materials. The nanosensors for neurotransmitters, nitrogen oxides and many other important species are yet to be established.

As was demonstrated, a variety of polymeric materials are used for preparation of dye-doped beads. Dye-doped silica beads are also extremely popular due to their chemical robustness, biocompatibility and simplicity in preparation and further functionalization of the surface [55]. Thus, polymeric, silica and Ormosil beads (which occupy intermediate position) are widely used as nanosensors and labels. On the other hand, quantum dots possess much higher cytotoxicity which often limits their application in biological systems.

The bead fabrication techniques are more or less established but can be improved further. Considering the material side, NIR dyes are clearly advantageous over UV–Vis ones and enable better S/N ratio due to lower levels of background fluorescence and light scattering. Unfortunately, only a few of them fulfill the requirements of chemical stability and brightness and even less respond to an analyte of interest and can be used as indicators in optical nanosensors. Dye-doped beads with magnetic properties are used increasingly often since they can be delivered, collected and manipulated easily. It can be concluded that many possibilities for further improvements exist and the most important part of the job is yet to be done. The dye-doped polymeric beads will be applied increasingly often also in some new application areas such as microfluidics, multiphoton microscopy, etc.

References

1. Wolfbeis OS (2005) Materials for fluorescence-based optical chemical sensors. *J Mater Chem* 15:2657–2669
2. Aylott JW (2003) Optical nanosensors—an enabling technology for intracellular measurements. *Analyst* 128:309–312
3. Bucka SM, Xua H, Brasuel M, Philbert MA, Kopelman R (2004) Nanoscale probes encapsulated by biologically localized embedding (PEBBLEs) for ion sensing and imaging in live cells. *Talanta* 63:41–59
4. Borisov SM, Klimant I (2008) Optical nanosensors – smart tools in bioanalytics. *Analyst* 133:1302–1307
5. Chojnacki P, Mistlberger G, Klimant I (2007) Separable magnetic sensors for the optical determination of oxygen. *Angew Chem Int Ed* 46:8850–8853
6. Aslan K, Wu M, Lakowicz JR, Geddes CD (2007) Fluorescent core–shell Ag@SiO₂ nanocomposites for metal-enhanced fluorescence and single nanoparticle sensing platforms. *J Am Chem Soc* 129:1524–1525
7. Vasilevska AS, Borisov SM, Krause Ch, Wolfbeis OS (2006) Indicator-loaded and permeation-selective microparticles for use in fiber optic simultaneous sensing of pH and dissolved oxygen. *Chem Mater* 18:4609–4616

8. Zhu H, McShane MJ (2005) Loading of hydrophobic materials into polymer particles: implications for fluorescent nanosensors and drug delivery. *J Am Chem Soc* 127:13448–13449
9. Gouanve F, Schuster T, Allard E, Meallet-Renault R, Larpent C (2007) Fluorescence quenching upon binding of copper ions in dye-doped and ligand-capped polymer nanoparticles: a simple way to probe the dye accessibility in nano-sized templates. *Adv Funct Mater* 17:2746–2756
10. Borisov SM, Mayr T, Klimant I (2008) Poly(styrene-block-vinylpyrrolidone) beads as a versatile material for simple fabrication of optical nanosensors. *Anal Chem* 80:573–582
11. Borisov SM, Klimant I (2009) Luminescent nanobeads for optical sensing and imaging of dissolved oxygen. *Microchim Acta* 164:7–15
12. Borisov SM, Herrod DL, Klimant I (2009) Fluorescent poly(styrene-block-vinylpyrrolidone) nanobeads for optical sensing of pH. *Sens Actuators B* 139:52–58
13. Yabu H, Higuchi T, Shimomura M (2005) Unique phase-separation structures of block-copolymer nanoparticles. *Adv Mater* 17:2062–2065
14. Higuchi T, Yabu H, Shimomura M (2006) Simple preparation of hemispherical polystyrene particles. *Colloids Surf A: Physicochem Eng Asp* 284–285:250–253
15. Kuerner JM, Klimant I, Krause Ch, Preu H, Kunz W, Wolfbeis OS (2001) Inert phosphorescent nanospheres as markers for optical assays. *Bioconjug Chem* 12:883–889
16. Bychkova V, Shvarev A (2009) Fabrication of micrometer and submicrometer-sized ion-selective optodes via a solvent displacement process. *Anal Chem* 81:2325–2331
17. Borisov SM, Mayr T, Mistlberger G, Waich K, Koren K, Chojnacki P, Klimant I (2009) Precipitation as a simple and versatile method for preparation of optical nanochemosensors. *Talanta* 79:1322–1330
18. Tsagakatakis I, Peperv S, Retter R, Bell M, Bakker E (2001) Monodisperse plasticized poly(vinyl chloride) fluorescent microspheres for selective ionophore-based sensing and extraction. *Anal Chem* 73:6083–6087
19. Mistlberger G, Borisov SM, Klimant I (2009) Enhancing performance in optical sensing with magnetic nanoparticles. *Sens Actuators B* 139:174–180
20. Demchenko AP (2010) Comparative analysis of fluorescence reporter signals based on intensity, anisotropy, time-resolution and wavelength-ratiometry. In: Demchenko AP (ed) *Advanced fluorescence reporters in chemistry and biology*. I. Springer Ser Fluoresc 8:3–25
21. Clark HA, Hoyer M, Philbert MA, Kopelman R (1999) Optical nanosensors for chemical analysis inside single living cells. 1. Fabrication, characterization, and methods for intracellular delivery of PEBBLE sensors. *Anal Chem* 71:4831–4836
22. Mayr T, Borisov SM, Abel T, Enko B, Waich K, Mistlberger G, Klimant I (2009) Light harvesting as a simple and versatile way to enhance brightness of luminescent sensors. *Anal Chem* 81:6541–6545
23. Klimant I, Huber C, Liebsch G, Neurauter G, Stangelmayer A, Wolfbeis OS (2001) Dual lifetime referencing (DLR) – a new scheme for converting fluorescence intensity into a frequency-domain or time-domain information. In: Valeur B, Brochon JC (eds) *Springer Ser Fluoresc* 1:257–274
24. Liebsch G, Klimant I, Krause C, Wolfbeis OS (2001) Fluorescent imaging of pH with optical sensors using time domain dual lifetime referencing. *Anal Chem* 73:4354–4363
25. Huber Ch, Klimant I, Krause Ch, Werner T, Mayr T, Wolfbeis OS (2000) Optical sensor for seawater salinity. *Fresenius J Anal Chem* 368:196–202
26. Waich K, Borisov SM, Mayr T, Klimant I (2009) Dual lifetime referenced trace ammonia sensors. *Sens Actuators B* 139:132–138
27. Kim HM, Cho BR (2009) Two-photon materials with large two-photon cross sections. Structure–property relationship. *Chem Commun* 2:153–164
28. Lübbers DW, Opitz N, Speiser PP, Bisson HJ (1977) Nanoencapsulated fluorescence indicator molecules measuring pH and pO₂ down to submicroscopical regions on the basis of the optode principle. *Z Naturforsch* 32:133–134

29. Cao Y, Koo YE, Kopelman R (2004) Poly(decyl methacrylate)-based fluorescent PEBBLE swarm nanosensors for measuring dissolved oxygen in biosamples. *Analyst* 129:745–750
30. Koo YE, Cao Y, Kopelman R, Koo SM, Brasuel M, Philbert MA (2004) Real-time measurements of dissolved oxygen inside live cells by organically modified silicate fluorescent nanosensors. *Anal Chem* 76:2498–2505
31. Wu C, Bull B, Christensen K, McNeill J (2009) Ratiometric single-nanoparticle oxygen sensors for biological imaging. *Angew Chem Int Ed* 48:2741–2745
32. Wu C, Bull B, Szymanski C, Christensen K, McNeill J (2008) Multicolor conjugated polymer dots for biological fluorescence imaging. *ACS Nano* 2:2415–2423
33. Pfister A, Zhang G, Zareno J, Horwitz AF, Fraser CL (2008) Boron polylactide nanoparticles exhibiting fluorescence and phosphorescence in aqueous medium. *ACS Nano* 2:1252–1258
34. Zhang G, Palmer GM, Dewhirst MW, Fraser CL (2009) A dual-emissive-materials design concept enables tumour hypoxia imaging. *Nat Mater* 8:747–751
35. Clark HA, Kopelman R, Tjalkens R, Philbert MA (1999) Optical nanosensors for chemical analysis inside single living cells. 1. Optical nanosensors for chemical analysis inside single living cells. 2. Sensors for pH and calcium and the intracellular application of PEBBLE sensors. *Anal Chem* 71:4837–4843
36. Sun H, Scharff-Poulsen AM, Gu H, Almdal K (2006) Synthesis and characterization of ratiometric pH sensing nanoparticles with covalently attached fluorescent dyes. *Chem Mater* 18:3381–3384
37. Allard E, Larpent C (2008) Core-shell type dually fluorescent polymer nanoparticles for ratiometric pH-Sensing. *J Polym Sci Part A Polym Chem* 46:6206–6213
38. McNamara KP, Nguyen T, Dumitrascu G, Ji J, Rosenzweig N, Rosenzweig Z (2001) Synthesis, characterization, and application of fluorescence sensing lipobeads for intracellular pH measurements. *Anal Chem* 73:3240–3246
39. Funfak A, Cao J, Wolfbeis OS, Martin K, Köhler JM (2009) Monitoring cell cultivation in microfluidic segments by optical pH sensing with a micro flow-through fluorometer using dye-doped polymer particles. *Microchim Acta* 164:279–286
40. Park EJ, Brasuel M, Behrend C, Philbert MA, Kopelman R (2003) Ratiometric optical PEBBLE nanosensors for real-time magnesium ion concentrations inside viable cells. *Anal Chem* 75:3784–3791
41. Sumner JP, Aylott JW, Monson E, Kopelman R (2002) A fluorescent PEBBLE nanosensor for intracellular free zinc. *Analyst* 127:11–16
42. Sumner JP, Kopelman R (2005) Alexa Fluor 488 as an iron sensing molecule and its application in PEBBLE nanosensors. *Analyst* 130:528–533
43. Brasuel M, Kopelman R, Miller TJ, Tjalkens R, Philbert MA (2001) Fluorescent nanosensors for intracellular chemical analysis: decyl methacrylate liquid polymer matrix and ion-exchange-based potassium PEBBLE sensors with real-time application to viable rat C6 glioma cells. *Anal Chem* 73:2221–2228
44. Brasuel MG, Miller TJ, Kopelman R, Philbert MA (2003) Liquid polymer nano-PEBBLES for Cl⁻ analysis and biological applications. *Analyst* 128:1262–1267
45. Ceresa A, Qin Y, Peper S, Bakker E (2003) Mechanistic insights into the development of optical chloride sensors based on the [9]mercuracarborand-3 ionophore. *Anal Chem* 75:133–140
46. Sun H, Scharff-Poulsen AM, Gu H, Jakobsen I, Kossmann JM, Frommer WB, Almdal K (2008) Phosphate sensing by fluorescent reporter proteins embedded in polyacrylamide nanoparticles. *ACS Nano* 2:19–24
47. Sumner JP, Westerberg NM, Stoddard AK, Fierke CA, Kopelman R (2006) *Sens Actuators B* 113:760–767
48. Xu H, Aylott JW, Kopelman R (2002) Fluorescent nano-PEBBLE sensors designed for intracellular glucose imaging. *Analyst* 127:1471–1477

49. Stein EW, Grant PS, Zhu H, McShane MJ (2007) Microscale enzymatic optical biosensors using mass transport limiting nanofilms. 1. Fabrication and characterization using glucose as a model analyte. *Anal Chem* 79:1339–1348
50. Stein EW, Singh S, McShane MJ (2008) Microscale enzymatic optical biosensors using mass transport limiting nanofilms. 2. Response modulation by varying analyte transport properties. *Anal Chem* 80:1408–1417
51. Zenkl G, Mayr T, Klimant I (2008) Sugar-responsive fluorescent nanospheres. *Macromol Biosci* 8:146–152
52. Poulsen AK, Scharff-Poulsen AM, Olsen LF (2007) Horseradish peroxidase embedded in polyacrylamide nanoparticles enables optical detection of reactive oxygen species. *Anal Biochem* 366:29–36
53. Henderson JR, Fulton DA, McNeil CJ, Manning P (2009) The development and *in vitro* characterisation of an intracellular nanosensor responsive to reactive oxygen species. *Biosens Bioelectron* 24:3608–3614
54. Hall M, Kazakova I, Yao YM (1999) High sensitivity immunoassays using particulate fluorescent labels. *Anal Biochem* 272:165–170
55. Liang S, John CL, Xu S, Chen J, Jin Y, Yuan Q, Tan W, Zhao JX (2010) Silica-based nanoparticles: design and properties. In: Demchenko AP (ed) *Advanced fluorescence reporters in chemistry and biology*. II. Springer Ser Fluoresc 9:229–251
56. Yang W, Zhang CG, Qu HY, Yang HH, Xua JG (2004) Novel fluorescent silica nanoparticle probe for ultrasensitive immunoassays. *Anal Chim Acta* 503:163–169
57. Burns AA, Vider J, Ow H, Herz E, Penate-Medina O, Baumgart M, Larson SM, Wiesner U, Bradbury M (2009) Fluorescent silica nanoparticles with efficient urinary excretion for nanomedicine. *Nano Lett* 9:442–448
58. Song X, Huang L, Wu B (2008) Bright and monodispersed phosphorescent particles and their applications for biological assays. *Anal Chem* 80:5501–5507
59. Huhtinen P, Vaarno J, Soukka T, Lövgren T, Härmä H (2004) Europium(III) nanoparticle-label-based assay for the detection of nucleic acids. *Nanotechnology* 15:1708–1715
60. Kokko L, Sandberg K, Lövgren T, Soukka T (2004) Europium(III) chelate-dyed nanoparticles as donors in a homogeneous proximity-based immunoassay for estradiol. *Anal Chim Acta* 503:155–162
61. Huhtinen P, Kivelä M, Soukka T, Tenhu H, Lövgren T, Härmä H (2008) Preparation, characterisation and application of europium(III) chelate-dyed polystyrene–acrylic acid nanoparticle labels. *Anal Chim Acta* 630:211–216
62. Valanne A, Suojanen J, Peltonen J, Soukka T, Hänninen P, Härmä H (2009) Multiple sized europium(III) chelate-dyed polystyrene particles as donors in FRET – an application for sensitive protein quantification utilizing competitive adsorption. *Analyst* 134:980–986
63. Cummins CM, Koivunen ME, Stephanian A, Gee SJ, Hammock BD, Kennedy IM (2006) Application of europium(III) chelate-dyed nanoparticle labels in a competitive atrazine fluoroimmunoassay on an ITO waveguide. *Biosens Bioelectron* 21:1077–1085
64. Tan M, Ye Z, Wang G, Yuan J (2004) Preparation and time-resolved fluorometric application of luminescent europium nanoparticles. *Chem Mater* 16:2494–2498
65. Huhtinen P, Kivela M, Kuronen O, Hagren V, Takalo H, Tenhu H, Lövgren T, Härmä H (2005) Synthesis, characterization, and application of Eu(III), Tb(III), Sm(III), and Dy(III) lanthanide chelate nanoparticle labels. *Anal Chem* 77:2643–2648
66. Wu J, Wang G, Jin D, Yuan J, Guan Y, Piper J (2008) Luminescent europium nanoparticles with a wide excitation range from UV to visible light for biolabeling and time-gated luminescence bioimaging. *Chem Commun* 3:365–367
67. Wu J, Ye Z, Wang G, Jin D, Yuan J, Guan Y, Piper J (2009) Visible-light-sensitized highly luminescent europium nanoparticles: preparation and application for time-gated luminescence bioimaging. *J Mater Chem* 19:1258–1264
68. Borisov SM, Klimant I (2008) Blue LED excitable temperature sensors based on a new europium(III) chelate. *J Fluoresc* 18:581–589

69. Huber C, Klimant I, Krause C, Wolfbeis OS (2001) Dual lifetime referencing as applied to a chloride optical sensor. *Anal Chem* 73:2097–2103
70. Mohr GJ, Klimant I, Spichiger-Keller UE, Wolfbeis OS (2001) Fluoro reactands and dual luminophore referencing: a technique to optically measure amines. *Anal Chem* 73:1053–1056
71. Mayr T, Klimant I, Wolfbeis OS, Werber T (2002) Dual lifetime referenced optical sensor membrane for the determination of copper(II) ions. *Anal Chim Acta* 462:1–10
72. von Bultzingslowen McEvoy, AK McDonagh C, MacCraith BD, Klimant I, Krause C, Wolfbeis OS (2002) Sol–gel based optical carbon dioxide sensor employing dual luminophore referencing for application in food packaging technology. *Analyst* 127:1478–1483
73. Cajlakovic M, Bizzarri A, Ribitsch V (2006) Luminescence lifetime-based carbon dioxide optical sensor for clinical applications. *Anal Chim Acta* 573–574:57–64
74. Borisov SM, Klimant I (2007) Ultrabright oxygen optodes based on cyclometalated Iridium (III) coumarin complexes. *Anal Chem* 79:7501–7509
75. Borisov SM, Krause C, Arain S, Wolfbeis OS (2006) Simultaneous and contactless luminescent sensing and imaging of oxygen and carbon dioxide. *Adv Mater* 18:1511–1516
76. Nagl S, Wolfbeis OS (2007) Optical multiple chemical sensing: status and current challenges. *Analyst* 132:507–511
77. Koese ME, Carroll BF, Schanze KS (2005) Preparation and spectroscopic properties of multiluminophore luminescent oxygen and temperature sensor films. *Langmuir* 21:9121–9129
78. Borisov SM, Vasylevska AS, Krause C, Wolfbeis OS (2006) Composite luminescent material for dual sensing of oxygen and temperature. *Adv Funct Mater* 16:1536–1542
79. Baleizao C, Nagl S, Schaeferling M, Berberan-Santos MN, Wolfbeis OS (2008) Dual fluorescence sensor for trace oxygen and temperature with unmatched range and sensitivity. *Anal Chem* 16:6449–6457
80. Stich MIJ, Nagl S, Wolfbeis OS, Henne U, Schaeferling M (2008) A dual luminescent sensor material for simultaneous imaging of pressure and temperature on surfaces. *Adv Funct Mater* 18:1399–1406
81. Kocincova AS, Nagl S, Arain S, Krause C, Borisov SM, Arnold M, Wolfbeis OS (2008) Multiplex bacterial growth monitoring in 24-well microplates using a dual optical sensor for dissolved oxygen and pH. *Biotechnol Bioeng* 100:430–438
82. Stich MIJ, Schaeferling M, Wolfbeis OS (2009) Multicolor fluorescent and permeation-selective microbeads enable simultaneous sensing of pH, oxygen, and temperature. *Adv Mater* 21:2216–2220
83. Kocincova AS, Borisov SM, Krause C, Wolfbeis OS (2007) Fiber-optic microsensors for simultaneous sensing of oxygen and pH, and of oxygen and temperature. *Anal Chem* 79:8486–8493
84. Nolan JP, Sklar LA (2002) Suspension array technology: evolution of the flat-array paradigm. *Trends Biotechnol* 20:9–12
85. LaFratta CN, Walt DR (2008) Very high density sensing arrays. *Chem Rev* 108:614–637
86. Wilson R, Cossins A, Spiller D (2006) Encoded microcarriers for high-throughput multiplexed detection. *Angew Chem Int Ed* 45:6104–6117
87. Schena M, Shalon D, Davis R, Brown P (1995) Quantitative monitoring of gene expression patterns with a complementary DNA microarray. *Science* 270:467–470
88. Wodicka L, Dong H, Mittmann M, Ho MH, Lockhart DJ (1997) Genome-wide expression monitoring in *Saccharomyces cerevisiae*. *Nat Biotechnol* 15:1359–1367
89. Henry MR, Wilkins Stevens P, Sun J, Kelso DM (1999) Real-time measurements of DNA hybridization on microparticles with fluorescence resonance energy transfer. *Anal Biochem* 276:204–214
90. Ferguson JA, Steemers FJ, Walt DR (2000) High-density fiber-optic DNA random microsphere array. *Anal Chem* 72:5618–5624
91. Keij J, Steinkamp J (1998) Flow cytometric characterization and classification of multiple dual-color fluorescent microspheres using fluorescence lifetime. *Cytometry* 33:318–323

92. Mayr T, Moser C, Klimant I (2007) Luminescence decay time encoding of magnetic microspheres for multiplexed analysis. *Anal Chim Acta* 597:137–144
93. Vaidya SV, Gilchrist ML, Maldarelli C, Couzis A (2007) Spectral bar coding of polystyrene microbeads using multicolored quantum dots. *Anal Chem* 79:8520–8530
94. Han M, Gao X, Su JZ, Nie S (2001) Quantum-dot-tagged microbeads for multiplexed optical coding of biomolecules. *Nat Biotechnol* 19:631–635
95. Ma Q, Wang X, Li Y, Shi Y, Su X (2007) Multicolor quantum dot-encoded microspheres for the detection of biomolecules. *Talanta* 72:1446–1452
96. Wang D, Rogach AL, Caruso F (2002) Semiconductor quantum dot-labeled microsphere bioconjugates prepared by stepwise self-assembly. *Nano Lett* 2:857–861
97. Salas VM, Edwards BS, Sklar LA (2008) Advances in multiple analyte profiling. *Adv Clin Chem* 45:47–74
98. Moser C, Mayr T, Klimant I (2006) Microsphere sedimentation arrays for multiplexed bioanalytics. *Anal Chim Acta* 558:102–109
99. Nolan J, Mandy F (2006) Multiplexed and microparticle-based analyses. Quantitative tools for the large-scale analysis of biological systems. *Cytometry A* 69:318–325
100. Walt DR (2000) Bead-based fiber-optic arrays. *Science* 287:451–452
101. Dickinson TA, Michael KL, Kauer JS, Walt DR (1999) Convergent, self-encoded bead sensor arrays in the design of an artificial nose. *Anal Chem* 71:2192–2198
102. Deiss F, LaFratta CN, Symer M, Blicharz TM, Sojic N, Walt DR (2009) Multiplexed sandwich immunoassays using electrochemiluminescence imaging resolved at the single bead level. *J Am Chem Soc* 131:6088–6089
103. Gunderson K, Kruglyak S, Graige M, Garcia F, Kermani B, Zhao C, Che D, Dickinson T, Wickham E, Bierle J, Doucet D, Milewski M, Yang R, Siegmund C, Haas J, Zhou L, Oliphant A, Fan J, Barnard S, Chee M (2004) Decoding randomly ordered DNA arrays. *Gen Res* 14:870–877
104. Wygladacz K, Radu A, Xu C, Qin Y, Bakker E (2005) Fiber-optic microsensor array based on fluorescent bulk optode microspheres for the trace analysis of silver ions. *Anal Chem* 77:4706–4712
105. Wygladacz K, Bakker E (2007) Fluorescent microsphere fiber optic microsensor array for direct iodide detection at low picomolar concentrations. *Analyst* 132:268–272
106. Aernecke MJ, Guo J, Sonkusale S, Walt DR (2009) Design, implementation, and field testing of a portable fluorescence-based vapor sensor. *Anal Chem* 81:5281–5290
107. Mulvaney SP, Mattoussi HM, Whitman LJ (2004) Incorporating fluorescent dyes and quantum dots into magnetic microbeads for immunoassays. *BioTechniques* 36:602–609
108. Zhang P, Dou H, Li W, Tao K, Xing B, Sun K (2007) Fabrication of fluorescent and magnetic multifunctional polystyrene microbeads with carboxyl ends. *Chem Lett* 36:1458–1459
109. Liu J, Zhang Y, Yang T, Ge Y, Zhang S, Chen Z, Gu N (2009) Synthesis, characterization, and application of composite alginate microspheres with magnetic and fluorescent functionalities. *J Appl Polym Sci* 113:4042–4051
110. Veisoh O, Sun C, Gunn J, Kohler N, Gabikian P, Lee D, Bhattarai N, Ellenbogen R, Sze R, Hallahan A, Olson J, Zhang M (2005) Optical and MRI multifunctional nanoprobe for targeting gliomas. *Nano Lett* 5:1003–1008
111. Harada Y, Ohara O, Takatsuki A, Itoh H, Shimamoto N, Kinoshita K (2001) Direct observation of DNA rotation during transcription by *Escherichia coli* RNA polymerase. *Nature* 409:113–115
112. Anker JN, Kopelman R (2003) Magnetically modulated optical nanoprobe. *Appl Phys Lett* 82:1102–1104
113. Anker JN, Behrend CJ, Huang H, Kopelman R (2005) Magnetically-modulated optical nanoprobe (MagMOONs) and systems. *J Magn Mater* 293:655–662

114. McNaughton BH, Kinnunen P, Smith RG, Pei SN, Torres-Isea R, Kopelman R, Clarke R (2009) Compact sensor for measuring nonlinear rotational dynamics of driven magnetic microspheres with biomedical applications. *J Magn Magn Mater* 321:1648–1652
115. Weissleder R, Pittet MJ (2008) Imaging in the era of molecular oncology. *Nature* 452:580–589
116. Fang C, Zhang M (2009) Multifunctional magnetic nanoparticles for medical imaging applications. *J Mater Chem* 19:6258–6266
117. Deng Y, Wang C, Shen X, Yang W, Jin L, Gao H, Fu S (2005) Preparation, characterization, and application of multistimuli-responsive microspheres with fluorescence-labeled magnetic cores and thermoresponsive shells. *Chem Eur J* 11:6006–6013
118. Lee J, Jun Y, Yeon S, Shin J, Cheon J (2006) Dual-mode nanoparticle probes for high-performance magnetic resonance and fluorescence imaging of neuroblastoma. *Angew Chem Int Ed* 45:8160–8162
119. Liang M, Angelos S, Choi E, Patel K, Stoddart JF, Zink JI (2009) Mesostructured multifunctional nanoparticles for imaging and drug delivery. *J Mater Chem* 19:6251–6257
120. Kopelman R, Lee Koo Y, Philbert M, Moffat BA, Ramachandra Reddy G, McConville P, Hall DE, Chenevert TL, Bhojani MS, Buck SM, Rehemtulla A, Ross BD (2005) Multifunctional nanoparticle platforms for in vivo MRI enhancement and photodynamic therapy of a rat brain cancer. *J Magn Magn Mater* 293:404–410
121. Anker JN, Koo Y, Kopelman R (2007) Magnetically controlled sensor swarms. *Sens Actuators B* 121:83–92
122. Mistlberger G, Chojnacki P, Klimant I (2008) Magnetic sensor particles: an optimized magnetic separator with an optical window. *J Phys D: Appl Phys* 41:085003(1)–085003(9)
123. Kreft O, Javier AM, Sukhorukov GB, Parak WJ (2007) Polymer microcapsules as mobile local pH-sensors. *J Mater Chem* 17:4471–4476
124. Gao D, Xu H, Philbert MA, Kopelman R (2007) Ultrafine hydrogel nanoparticles: synthetic approach and therapeutic application in living cells. *Angew Chem Int Ed* 46:2224–2227
125. Gao D, Agayan RR, Xu H, Philbert MA, Kopelman R (2006) Nanoparticles for two-photon photodynamic therapy in living cells. *Nano Lett* 6:2383–2386
126. Wang S, Gao R, Zhou F, Selke M (2004) Nanomaterials and singlet oxygen photosensitizers: potential applications in photo dynamic therapy. *J Mater Chem* 14:487–493
127. Przhonska OV, Webster S, Padilha LA et al (2010) Two-photon absorption in near-IR conjugated molecules: design strategy and structure–property relations. In: Demchenko AP (ed) *Advanced fluorescence reporters in chemistry and biology*. I. Springer Ser Fluoresc 8:105–147
128. Demchenko AP (2010) The concept of lambda-ratiometry in fluorescence sensing and imaging. *J Fluoresc* DOI 10.1007/s10895-010-0644-y

Silica-Based Nanoparticles: Design and Properties

Song Liang, Carrie L. John, Shuping Xu, Jiao Chen, Yuhui Jin, Quan Yuan, Weihong Tan, and Julia Xiaojun Zhao

Abstract A number of dye-doped silica nanoparticles (DDSNs) have been developed by encapsulating various fluorophores into silica nanomatrixes. These DDSNs have shown great potential as highly sensitive fluorescent labeling agents for biosensing and bioimaging. The silica nanomatrix affects the radiative properties and reactivity of doped fluorophores and endows the DDSN surface properties of silica. Compared with molecular fluorophores, the DDSNs exhibit advantageous properties such as high fluorescence intensity, good photostability, and biological compatibility. In this chapter, methods for silica nanoparticle synthesis and approaches for doping dye molecules within the silica nanomatrixes are over-viewed. Various advantageous properties of DDSNs are discussed including reaction kinetics, solubility, photostability, quantum yield, lifetime, and toxicity.

Keywords Fluorescence · Lifetime · Photostability · Quantum yield · Silica nanoparticle

Contents

1	Introduction	230
2	Design of Dye-Doped Silica Nanoparticles	231
2.1	Synthesis of Silica Nanoparticles	232
2.2	Methods of Doping Dye Molecules into Silica Nanoparticles	234
2.3	Configurations of DDSNs	236

S. Liang, C.L. John, J. Chen, Y. Jin, and J.X. Zhao (✉)

Department of Chemistry, University of North Dakota, Grand Forks, ND 58202, USA

e-mail: jzhao@chem.und.edu

S. Xu

State Key Laboratory of Supramolecular Structure and Materials, Jilin University, Changchun 130012, P. R. China

Q. Yuan and W. Tan

Department of Chemistry, University of Florida, Gainesville, FL 32611, USA

3	Properties of DDSNs	238
3.1	Fluorescence Intensity	239
3.2	Quantum Yield and Lifetime	240
3.3	Photostability of DDSNs	241
3.4	Fluorescence Enhancement	241
3.5	Solubility	244
3.6	Reaction Kinetics of Doped Molecules	245
3.7	Toxicity of DDSNs	246
4	Conclusions	248
	References	248

1 Introduction

Fluorescence imaging and sensing are powerful techniques in a wide variety of biological studies. The use of fluorophores as biomarkers or indicators, for *in vitro* and *in vivo* monitoring of biological processes and determinations of targets in biosamples has been achieved [1, 2]. However, two major limitations exist in molecular fluorophores, photobleaching and limited fluorescence intensity. When the amount of targets present is very low, these two limitations become significant. Additionally, poor water solubility of some organic fluorophores makes their applications in biosamples a challenge.

To overcome these limitations, dye molecules have been doped into a silica matrix to form a dye-doped silica nanoparticle (DDSN). According to an old story, firefly-lamps were made to light the night by collecting a large number of fireflies in a small glass bottle. Similarly, by encapsulating thousands of fluorophore molecules into a silica nanoparticle, DDSNs are produced to illuminate the dim views of biological samples [3, 4]. The first report on developing DDSNs was published in 1992 [5]. In this pioneering work, a fluorescein derivative was doped into a silica nanosphere. Since then, there has been a growing interest in DDSNs because of their unique optical properties. In contrast to free dye molecules, DDSNs exhibit two major features, dramatically improved photostability and high fluorescence intensity. Using DDSNs as fluorescence labeling agents, many biological processes, previously invisible, have now been observed.

In addition to the two features mentioned above, good biocompatibility of DDSNs is significant for their bioapplications. Their silica surface can be modified by various functional groups, through which they can be immobilized onto a wide variety of analytes. The hydrophilic surface of the silica matrix provides good water solubility. The low toxicity further favors the biological applications of the DDSNs. As a result, biolabeling and biosensing are the most important application areas of the DDSNs [3, 6, 7]. With recognizing groups on their surfaces such as antibodies and aptamers, the DDSNs can recognize and specifically bind to biotargets. The high signal intensity of the DDSNs greatly improves the detection limit. The silica nanomatrix protects the doped luminescent indicators from interference by the

environment [8–15]. Besides the biolabeling and biosensing, DDSNs can also be functionalized for drug delivery. The multifunctional DDSNs which carry photodynamic therapy agents or other anticancer drugs provide complete solutions from diagnosis and therapy [16–20].

There has been a rapid development of DDSNs in last 10 years or so. Tan's group reported a series of DDSNs using organic and inorganic fluorophores and applied them as biolabeling materials for both imaging and sensing [8, 10–12, 21–25]. The groups of Wiesner [6, 13, 14, 26], Montalti [27–29], and Lakowicz [30–34] among others [9, 15, 19, 35–43], have designed highly intense DDSNs with various structures and functions. These accomplishments have demonstrated the great potential of DDSNs to be revolutionary fluorescent labeling materials in bioanalysis.

In this chapter, the first section will focus on the designs of different structures of DDSNs. The basic synthesis methods of pure silica nanoparticles will be briefly summarized at the beginning. The general methods for doping dye molecules into a silica matrix will then be covered followed by the introduction of several DDSN designs. The second section will be a major focus of this chapter. Various advantageous properties of DDSNs will be discussed. These discussions will involve reaction kinetics, solubility, photostability, and fluorescence intensity including quantum yield and lifetime, as well as toxicity. With the rapid development of DDSNs, more features and functionalities of DDSNs are expected in the near future.

2 Design of Dye-Doped Silica Nanoparticles

Generally, two common methods, the Stöber method and the reverse microemulsion method are used for synthesis of silica nanoparticles. As derivatives of a sol–gel process, both methods involve hydrolysis of a silicon alkoxide precursor to form a hydroxysilicate followed by polycondensation of the hydroxysilicate to form a silica nanoparticle [44].

Both the Stöber method and the reverse microemulsion method can be used to prepare DDSNs. In the process of synthesizing of silica nanoparticles, dye molecules are added into the microemulsion either before or during the hydrolysis of the silicate precursor. However, some dye molecules cannot be doped within silica nanoparticles. An association between dye molecules and the silica matrix must exist to hold the dye molecules inside the silica matrix. A common linking force is covalent binding, which provides a more stable linkage but requires additional chemical reactions. Electrostatic interaction between the negatively charged silica and positively charged dye molecules is frequently employed as well. To design a DDSN, the first step is to select dyes with desired wavelength and corresponding dye doping methods. Second, a suitable synthesis method is to be chosen for the particle fabrication. Third, it is necessary to optimize particle size, pore structure, surface groups, and dye density. In addition

to fluorescence, DDSNs can also be designed with other functions. An amorphous silica matrix is a carrier of various materials. By encapsulating other materials into the DDSNs, fluorescent nanoparticles with multiple functionalities can be developed.

2.1 Synthesis of Silica Nanoparticles

2.1.1 Stöber Method

The Stöber method is also known as a sol–gel method [44, 45]. It was named after Stöber who first reported the sol–gel synthesis of colloid silica particles in 1968 [45]. In a typical Stöber method, silicon alkoxide precursors such as tetramethylorthosilicate (TMOS) and tetraethylorthosilicate (TEOS), are hydrolyzed in a mixture of water and ethanol. This hydrolysis can be catalyzed by either an acid or a base. In sol–gel processes, an acidic catalyst is preferred to prepare gel structure and a basic catalyst is widely used to synthesize discrete silica nanoparticles. Usually ammonium hydroxide is used as the catalyst in a Stöber synthesis. With vigorous stirring, condensation of hydrolyzed monomers is carried out for a certain reaction time period. The resultant silica particles have a nanometer to micrometer size range.

The Stöber method can be used to form core–shell silica nanoparticles when a presynthesized core is suspended in a water–alcohol mixture. The core can be a silica nanoparticle or other types of nanomaterials [46, 47]. If the core is a silica nanoparticle, before adding silicon alkoxide precursors, the hydroxysilicates hydrolyzed from precursors condense by the hydroxide groups on the surface of the silica cores to form additional layers. If the core is a colloid, surface modification of the core might be necessary. For example, a gold colloid core was modified by poly(vinylpyrrolidone) prior to a silica layer coating [46].

Besides the traditional Stöber method, a number of modified Stöber methods have been reported for preparation of various silica nanoparticles. An important example is the synthesis of mesoporous silica nanoparticles by modifying the Stöber method [41, 48–53]. Mesoporous silica nanomaterials have a wide variety of applications including drug delivery and developments of catalysts [50, 51]. The porosity of the silica nanoparticles produced by the traditional Stöber method is smaller than that of the mesoporous materials. To prepare mesoporous silica nanoparticles, cetyltrimethyl ammonium bromide (CTAB) [49, 50, 54], cetyltrimethyl ammonium chloride (CTAC) [40, 42, 48] or octadecyltrimethoxysilane was added to the synthetic solution as a template to support the “large” pores in the silica matrix. After the silica nanoparticles are made, the templates are removed by washing or heating the nanoparticles. Finally, the mesoporous silica nanoparticles can be obtained. The Stöber method is fast and simple. The major challenges of this method are how to improve the uniformity of the silica nanoparticles and how to efficiently dope dye molecules within the matrix.

2.1.2 Reverse Microemulsion Method

The reverse microemulsion method is another common method for synthesis of silica nanoparticles. This synthetic process takes more time than the Stöber method. However, the reverse microemulsion method can overcome the limitations of the Stöber method [25, 55–57] by producing silica nanoparticles with a uniform size distribution. Furthermore, this method can efficiently dope dye molecules into the silica nanoparticles. Reverse microemulsion is also known as water-in-oil microemulsion. In this system, oil (or a nonpolar organic solvent), water, surfactant and cosurfactant form an isotropic, transparent and thermodynamically stable single phase liquid mixture (Fig. 1). In a typical reverse microemulsion, micelles containing water droplets are stabilized by surfactant/cosurfactant molecules, which reduce the interfacial tension between water and the organic solvent. When doping dye molecules into the silica nanoparticles, the water soluble dye will be dissolved in the water droplet and eventually doped into the silica nanoparticles. Since water and the hydrolysis catalyst (mostly ammonium hydroxide) exist in the micelles, the added silicon alkoxide cannot be hydrolyzed until it diffuses into the micelles. Therefore, the polycondensation of the hydroxysilicates takes place within the micelles. The growth of silica nanoparticles is confined by the size of micelles. The resultant silica nanoparticles have narrow size distribution. However, the size of the nanoparticles is restricted by the size of micelles [25, 56]. It is difficult to produce large silica nanoparticles [25]. In addition, the surfactant used in a reverse microemulsion method cannot be completely removed from the silica nanoparticles.

2.1.3 Manipulation of the Size of Silica Nanoparticles

The size of silica nanoparticles affects their physical, chemical, electronic, and optical properties. Proper size of silica nanoparticles is crucial for design of silica-based nanomaterials. In Stöber methods, the size of silica nanoparticles is adjusted by changing the type of organic solvent, the amount of silicon alkoxide, and the

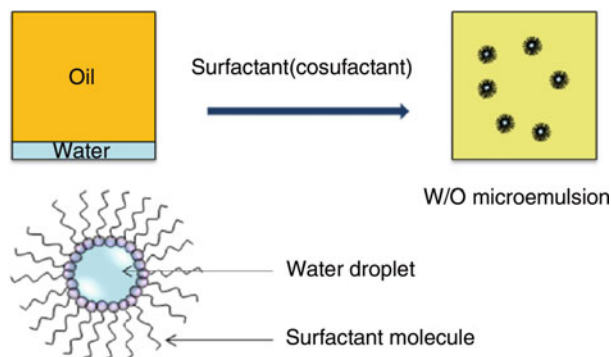


Fig. 1 Schematic diagram of water-in-oil microemulsion for synthesis of silica nanoparticles

hydrolytic reaction time [44, 45]. As mentioned above, the size of produced silica particles is distributed in a relatively broad range.

The reverse microemulsion method can be used to manipulate the size of silica nanoparticles [25]. It was found that the concentration of alkoxide (TEOS) slightly affects the size of silica nanoparticles. The majority of excess TEOS remained unhydrolyzed, and did not participate in the polycondensation. The amount of basic catalyst, ammonia, is an important factor for controlling the size of nanoparticles. When the concentration of ammonium hydroxide increased from 0.5 (wt%) to 2.0%, the size of silica nanoparticles decreased from 82 to 50 nm. Most importantly, in a reverse microemulsion, the formation of silica nanoparticles is limited by the size of micelles. The sizes of micelles are related to the water to surfactant molar ratio. Therefore, this ratio plays an important role for manipulation of the size of nanoparticles. In a Triton X-100/*n*-hexanol/cyclohexane/water microemulsion, the sizes of obtained silica nanoparticles increased from 69 to 178 nm, as the water to Triton X-100 molar ratio decreased from 15 to 5. The cosurfactant, *n*-hexanol, slightly influences the curvature of the radius of the water droplets in the micelles, and the molar ratio of the cosurfactant to surfactant faintly affects the size of nanoparticles as well.

The size of the silica nanoparticles can also be manipulated by changing organic solvents in the reverse microemulsion. A recent work systematically reported the correlation between the organic solvents and size of silica nanoparticles [56]. This investigation revealed that in a reverse microemulsion, as the length of the organic solvent alkane chain increased the size of the silica nanoparticles became larger (Fig. 2). A cyclohexane/*n*-hexadecane binary solvent mixture was used to prepare tunable silica nanoparticles. By reducing the percentage of *n*-hexadecane in the mixture, the size of nanoparticles continuously decreased from 100 to 50 nm. When a ternary solvent reverse microemulsion was used, the tunable size range could be extended down to 20 nm. A model explaining the effect of organic solvents on silica nanoparticles size was proposed. This size effect was attributed to the different micelle sizes and interdroplet percolation efficiency in various solvents.

2.2 Methods of Doping Dye Molecules into Silica Nanoparticles

2.2.1 Covalent Binding

The most reliable doping method is to chemically link dye molecules onto the silica matrix via covalent bonds [5, 58]. In this method, the dye molecules should be modified by linking a functional group of alkoxide. A common strategy to make an alkoxide modified dye derivative is to covalently attach a succinimide [12, 59] ester or isothiocyanate [5, 13] modified dye to a coupling reagent, 3-aminopropyltrimethoxysilane (APTS). The dye–APTS conjugate can hydrolyze and condense with the silicate during the formation of silica nanoparticles. As a result, dye molecules are covalently encapsulated into silica nanoparticles. Since the covalent bonds are stable at various conditions, this method prevents dye molecules from

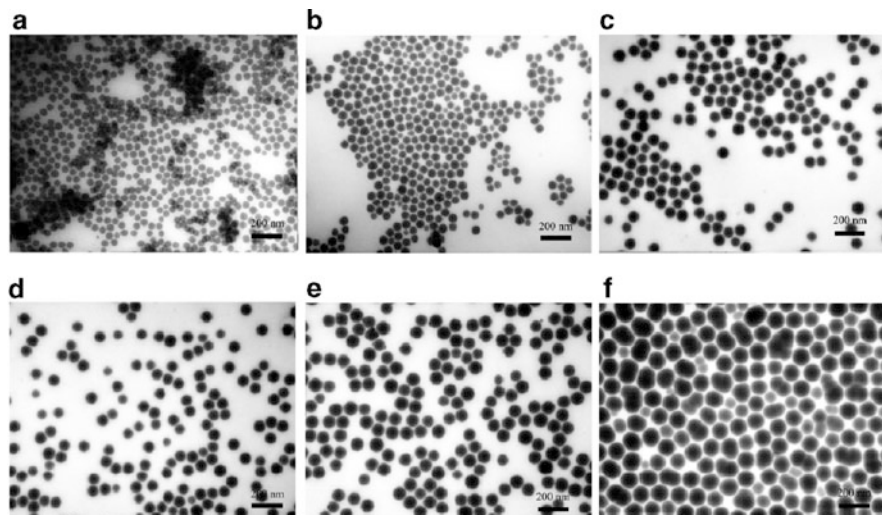


Fig. 2 TEM images of variable sizes of silica NPs obtained from a quaternary water-in-oil microemulsion using different organic solvents: (a) cyclohexane, (b) *n*-pentane, (c) *n*-hexane, (d) *n*-heptane, (e) *n*-decane, and (f) *n*-hexadecane. Reproduced with permission from Ref. [56]

leaking out of the silica matrix, which is a major challenge for making DDSNs. Due to this advantage, the covalent binding method has been widely used since the first report of DDSNs. Currently, various succinimide ester or isothiocyanate modified dyes are commercially available including most commonly used dyes, such as fluorescein [5, 13], tetramethylrhodamine [13, 60], rhodamine B [58], Cy5 [61], etc. With abundant dye molecule supplies, most of the reported DDSNs have been prepared using this doping method. However, covalent binding is not a universal method. The modification is difficult for some dye molecules, resulting in the impracticality of doping these dyes into silica based on the covalent bonds. Therefore, other doping methods are needed.

2.2.2 Electrostatic Interaction

Electrostatic interaction is a relatively weak association force compared to covalent bonds, but strong enough to keep dye molecules within a silica matrix [8, 21]. If a dye molecule is positively charged, it can be doped within a negatively charged silica matrix via the electrostatic interaction. The first example of employing electrostatic interactions to make DDSNs was reported in 2001 [8]. In this work, a positively charged tris(2,2'-bipyridyl)dichloro-ruthenium(II) hexahydrate ($\text{Ru}(\text{bpy})_3^{2+}$) was added to a reverse microemulsion, producing $\text{Ru}(\text{bpy})_3^{2+}$ doped silica nanoparticles. Electrostatic interactions are feasible doping forces only for the positively charged dye molecules, such as transition-metal–ligand complexes, quaternary ammonium organic compounds, etc.

2.2.3 Water Solubility

In a reverse microemulsion, the hydrolysis and polymerization of the silicate precursor occur in the water droplet, therefore, to dope dyes in the silica nanoparticles they must be water soluble. However, a number of organic dye molecules are hydrophobic, requiring modifications prior to doping. Several methods are available to link a hydrophobic dye molecule to a water soluble group. A simple and effective example is to link a hydrophilic dextran to the dye molecules [8]. This modification can greatly enhance the water solubility of hydrophobic dye molecules, but will increase the cost of resultant DDSNs.

In summary, a suitable association between dye molecules and the silica matrix is necessary for synthesis of DDSNs. Without the presence of chemical bonds or electronic interactions, the dye molecules will leak out from silica nanoparticles through the silica pores [22]. Such DDSNs will provide unstable fluorescence signals and cannot be used as a labeling agent in bioanalysis. Meanwhile, water solubility is critical for a dye molecule when using a reverse microemulsion method to make the DDSNs.

2.3 Configurations of DDSNs

Several different configurations of DDSNs have been reported. At the beginning, most DDSNs were designed with a single type of dye molecules homogeneously doped inside the silica nanoparticles [5, 8, 58]. These nanoparticles, as labeling materials, were successfully applied to bioanalysis and bioimaging. At the present, DDSNs contain multiple dye molecules [21, 60–62], have different configurations [6, 13, 14, 27, 28], and multiple functions [15, 19, 37, 43]. These new designs extend the range of DDSN applications.

2.3.1 Doping Multiple Dye Molecules

The purpose of doping multiple types of dye molecules in a silica nanoparticle is to simultaneously emit fluorescence signals at different wavelengths under a single excitation source. Different sizes of quantum dots made from the same materials can emit fluorescence at different wavelengths using a single excitation wavelength. Like quantum dots, DDSNs can also produce multiple-colored fluorescence if multiple dyes are doped into a silica nanoparticle. A series of dual-DDSNs were designed by doping tris(2,2'-bipyridyl)osmium(II)bis(hexafluoro-phosphate) ($\text{Os}(\text{bpy})_3^{2+}$) and $\text{Ru}(\text{bpy})_3^{2+}$ into silica nanoparticles with various dye molar ratios [21]. When excited at a single wavelength of 488 nm, the two emission spectra from $\text{Ru}(\text{bpy})_3^{2+}$ and $\text{Os}(\text{bpy})_3^{2+}$ have no overlap. Their emission peaks are at 610 nm ($\text{Ru}(\text{bpy})_3^{2+}$) and 710 nm ($\text{Os}(\text{bpy})_3^{2+}$), respectively. By changing their molar ratios of the two dye molecules, the resultant DDSNs displayed different colors. These

nanoparticles were applied to multiplexed immunoassays and the simultaneous detection of multiple samples. Further, the dual-DDSNs were extended to triple-DDSNs [12]. With the assistance of Förster resonance energy transfer (FRET) various distinct colors from green to dark red were obtained (Fig. 3).

Often, rather than emission of multiple wavelengths, the purpose of doping more than one type of dye molecules is to use one dye as an internal standard [6, 62], such as a real-time ratiometric oxygen nanosensor employing probes encapsulated by biologically localized embedding (PEBBELs) [63]. In this nanosensor, an oxygen-sensitive dye, Ru(II)-tris (4,7-diphenyl-1,10-phenanthroline) chloride ($\text{Ru}(\text{dpp})_3^{2+}$), was doped as the oxygen probe. Meanwhile, an oxygen-inert dye, Oregon Green 488-dextran, was doped as a reference. In the presence of oxygen, the fluorescence of $\text{Ru}(\text{dpp})_3^{2+}$ was quenched, while the fluorescence signal of the reference remained relatively stable. The results showed that the fluorescence intensity ratio of these two dyes was inversely proportional to the concentration of oxygen. Thus the oxygen could be quantitatively detected using the PEBBELs. The reference dye as an internal standard ensured the accuracy of the measurement.

2.3.2 Core-Shell Configurations

Recently, the design of multiple-layer DDSNs becomes popular [61]. These multiple-layer configurations can be categorized as a core-shell structure. Frequently, this core-shell structure involves metal enhancement. The dye-doped silica exists either as a fluorescent core coated with a silica shell or as a fluorescent shell on a metal core. These new designs have provided DDSNs with advanced fluorescence

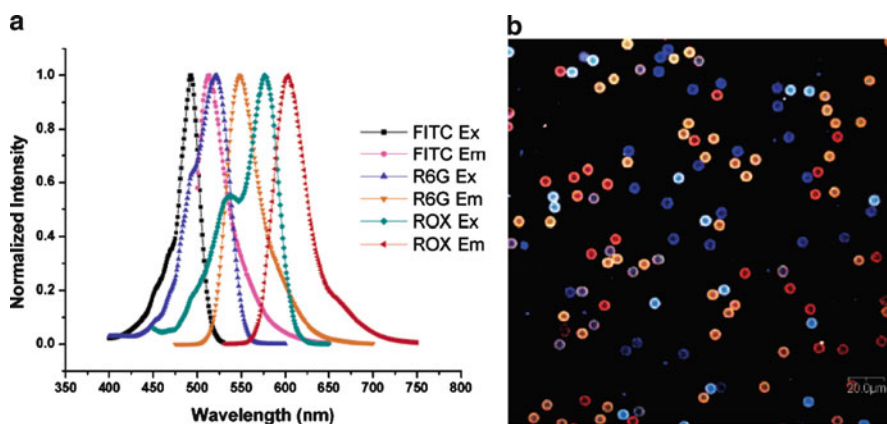


Fig. 3 (a) Normalized excitation and emission spectra of 5-(and-6)-carboxy-fluorescein, succinimidyl ester, rhodamine 6G (R6G), and 6-carboxy-X-rhodamine dyes in pH 7.4 phosphate buffer. (b) Confocal fluorescence image of a mixture of five types of microsphere-DDSN complexes under 488-nm Argon-ion laser excitation. Reproduced with permission from Ref. [12]

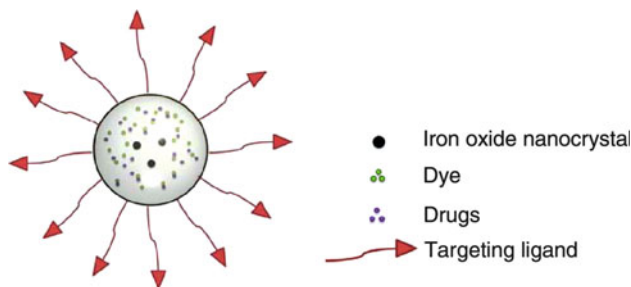


Fig. 4 Schematic illustration of magnetic mesoporous DDSN with targeting ligands

capability. Furthermore, some of the core-shell structures have different functions in addition to signaling analytes. A number of silica based multifunctional nanoparticles has been developed by encapsulating various components into silica nanomatrixes [15, 19, 37, 38, 41–43]. Some of these nanoparticles contain dye molecules and thus can be considered as DDSNs. The additional functions of these DDSNs include drug delivery, magnetic resonance imaging of targets, etc. A typical multifunctional DDSN encapsulates iron oxide nanocrystals, dye molecules, and drugs in a mesoporous silica nanomatrix. The surface of this DDSN was modified using targeting ligands (Fig. 4). In the application process, first, the targeting ligand brought the DDSNs specifically to the target cell in a sample. Then, the biologically compatible mesoporous silica matrixes delivered the drug to the target cell and released the drugs gradually. Afterwards, the iron oxide nanocrystals embedded in the DDSNs functioned as a contrast agent for magnetic resonance. Finally, the fluorescence images were taken to detect the amount of the target cells based on the covalently doped dye molecules. The multiple functions make DDSNs promising nanoparticles in biological and biomedical applications.

3 Properties of DDSNs

Nanomaterials have exhibited distinct optical, chemical, physical and mechanical properties, which are different from the bulk materials. Similarly, DDSNs offer several key performance advantages compared with individual molecular fluorophores. These include more intense fluorescence emission, greater photostability, good water solubility and low toxicity. While all four of these features offer great advantages for biological applications, it is important to note that some limitations may appear due to the environment of silica matrix. One noticeable limitation is the slow reaction rate of doped dye molecules with species outside the nanoparticles. In general, because a silica nanomatrix is distinctly different from either a bulk solution or a bulk silica matrix, after being encapsulated into a silica nanomatrix,

the dye molecules have less opportunity to react with other species. On the other hand, however, the slow reaction became an advantage when the reactant was a quencher, such as environmental oxygen. The photostability is greatly increased for DDSNs as compared to fluorophores in a bulk solution. In this section, a number of distinct properties of DDSNs will be discussed including major advantages and limitations.

3.1 *Fluorescence Intensity*

The optical properties of a DDSN are mainly determined by the properties of dye molecules. Since silica nanomaterials are effectively “transparent” they are unlikely to absorb light in the near-infrared, visible or ultraviolet regions, which allows the dye molecules inside the silica matrix to keep their original optical properties [64]. Meanwhile, the presence of the silica matrix provides a new environment for dye molecules and affects dye fluorescence properties.

By gathering thousands of dye molecules into a silica nanomatrix, a DDSN is much brighter than a single dye molecule. Although this comparison sounds unfair, considering limited binding sites in a biological sample, when one DDSN links to one binding site, the result appears to be thousands of dye molecules linked to one binding site. A direct comparison of a fluorophore with a DDSN showed that the fluorescence intensity of a 60 nm DDSN is about 10^4 times higher than that of a single fluorophore.

Moreover, an absolute increase of the brightness of fluorophores was indeed observed in DDSNs. For example [13], tetramethylrhodamine isothiocyanate molecules (TRITC) in the core–shell DDSNs were 20 times brighter than the constituent TRITC. Significantly, R6G doped DDSNs, are 230 times brighter than the same volume of the dye in a water solution at its maximum nondimerized concentration. One of the proposed mechanisms for the increased brightness was the reduction of the fluorophore aggregation. Most of the fluorescent compounds have planar conjugated π -structures, which cause their aggregations in either a solution or a bulk silica matrix. The higher the dye concentration is, the more severe their aggregation is. Moreover, when the dye concentration is over a certain limit, self quenching will occur and the fluorescence intensity will be decreased. In a DDSN, the dye molecules are immobilized inside the silica nanomatrixes where aggregation becomes difficult, allowing for more individual dye molecules to exist near one another than in a bulk dye solution. As a result, a DDSN suspension exhibits a higher fluorescence signal than the same amount of dye molecules in a solution. The physical barrier provided by the silica nanomatrix is a simple and direct explanation for the increase in fluorescence intensity of fluorophores. However, due to the complexity of fluorescence, systematic investigations on the fundamental characteristics of fluorophores in DDSNs are needed for a better understanding of the performance of the DDSNs.

3.2 Quantum Yield and Lifetime

Among several fluorescence properties, fluorescence quantum yield and lifetime are the two most important characteristics of a fluorophore. Studies of the effects of the silica nanomatrixes on these two characteristics reveal the mechanism of enhanced fluorescence intensity of DDSNs.

For a free space emission of dye molecules, the fluorescence quantum yield (Q) and the lifetime (τ) and are expressed by (1) and (2) [1].

$$Q = \frac{\Gamma}{\Gamma + k_{nr}} \quad (1)$$

$$\tau = \frac{1}{\Gamma + k_{nr}} \quad (2)$$

Herein, Γ is the radiative decay rate and k_{nr} is the nonradiative decay rate, which comes from quenching. It has been demonstrated that silica nanomatrixes can change the fluorescence quantum yield and lifetime of fluorophores. Several groups have reported that both quantum yield and lifetime of fluorophores increased in DDSNs [27, 28, 52, 65–67]. However, the mechanisms regarding this enhancement were reported differently.

Montalti and co-workers studied dansyl [27] and pyrene [28] derivatives and found the fluorescence quantum yields and excited-state lifetime of these two dyes increased in DDSNs. They attributed the enhancements to the shielding effect from the quenchers or polar solvent in the suspension. Their studies also demonstrated that the lifetime of the doped dye molecules was also dependent on the size of the DDSNs. Small DDSNs had a larger population of the short-living moieties that were more sensitive to the environment outside the DDSN. In contrast, the large DDSN had a larger population of the long-living moieties that were not sensitive to the environment.

Wiesner's group proposed an additional mechanism on quantum yield and lifetime enhancement [65, 66]. They observed a threefold enhancement in the fluorescence quantum yield per dye molecule. They believed that the effect of the inner architecture of the DDSN contributed to this result. The covalent bonds between dye molecules and the silica matrix restricted the mobility of the dye molecules and reduced their nonradiative decay rates, which correlated with the dye rotation. Their results also suggested that there was no energy transfer between neighboring dye molecules, indicating little self quenching among the doped dye molecules. The low self quenching also contributed to the reduction of nonradiative decay rate. As shown in (1) and (2), the decrease of the nonradiative decay increases the quantum yield and the lifetime.

The results regarding the effect of the silica matrix on the fluorescence quantum yield showed some disagreements. In contrast to the enhanced fluorescence quantum yield, the same [68] or decreased quantum yields [69] in DDSNs were reported

as well. These opposite phenomena may suggest the existence of dye aggregates within the DDSN. In the previous section, it was stated that the silica nanomatrix can prevent aggregation of dye molecules. However, if the dye concentration is too high, aggregation will occur. The aggregation can be identified by the shift of the emission spectrum. Usually in the bulk materials, the spectrum maxima shift could be an evidence of the presence of dye aggregates, which may cause quantum yield decrease. Without aggregation, the doped dye molecules have similar absorbance and fluorescence emission spectra as their free manners. However, slight shift of the spectrum maxima were observed in some DDSNs [8, 27, 28], which could be considered as the characters of the dye aggregations [69]. The research on quantum yield and lifetime on DDSNs is a relatively new area. More fundamental studies are needed to provide clear understanding about the effect of silica nanomatrix on the quantum yield and lifetime of fluorophores in the DDSNs.

3.3 *Photostability of DDSNs*

The high photostability and acute fluorescence intensity are two major features of DDSNs compared to dye molecules in a bulk solution. The early DDSN studies have focused on these two properties [8, 13]. For example, Santra et al. studied the photostability of the $\text{Ru}(\text{bpy})_3^{2+}$ doped silica nanoparticles. In aqueous suspensions, the $\text{Ru}(\text{bpy})_3^{2+}$ doped silica nanoparticles exhibited a very good photostability. Irradiated by a 150 W Xenon lamp for an hour, there was no noticeable decrease in the fluorescence intensity of suspended $\text{Ru}(\text{bpy})_3^{2+}$ doped silica nanoparticles, while obvious photobleaching was observed for the pure $\text{Ru}(\text{bpy})_3^{2+}$ and R6G molecules. To eliminate the effect from Brownian motion, the authors doped both pure $\text{Ru}(\text{bpy})_3^{2+}$ and $\text{Ru}(\text{bpy})_3^{2+}$ -doped silica nanoparticles into poly(methyl methacrylate). Under such conditions, both the pure $\text{Ru}(\text{bpy})_3^{2+}$ and $\text{Ru}(\text{bpy})_3^{2+}$ doped silica nanoparticles were bleached. However, the photobleaching of pure $\text{Ru}(\text{bpy})_3^{2+}$ was more severe than that of the $\text{Ru}(\text{bpy})_3^{2+}$ doped silica nanoparticles.

The high photostability of the nanoparticle originates from protection provided by the silica matrix for the embedded fluorophores. Environmental oxygen is a universal quencher for fluorophores in aqueous solution and the network structure of the silica matrix reduces diffusion of environmental oxygen to the fluorophores. Thus, the photostability of embedded fluorophores is greatly improved [3].

3.4 *Fluorescence Enhancement*

High photostability and intense fluorescence signals are always criteria for making better DDSNs. To obtain a better DDSN, various nanostructures for fluorescence enhancements have been developed. The coexistence of a noble metal nanostructure with fluorophores can enhance both the fluorescence intensity and photostability

of the fluorophores [70–77]. The interaction between the metal and the fluorophore is unique and complicated. A generally accepted mechanism is that the metal plasmon plays an important role in assisting energy transfer from the metal to the fluorophores. To investigate this effect, a core–shell structure composed of metal and a DDSN has been employed in some recent studies. This core–shell structure is a proper model for studying plasmon-controlled fluorescence enhancement.

Figure 5 shows two typical core–shell structures; (a) contains a metal core and a dye doped silica shell [30, 32, 33, 78–85] and (b) has a dye doped silica core and a metal shell [31, 34]. There is a spacer between the core and the shell to maintain the distance between the fluorophores and the metal to avoid fluorescence quenching [30, 32, 33, 78–80, 83]. Usually, the spacer is a silica layer in this type of nanostructures. Various Ag and Au nanomaterials in different shapes have been used for fluorescence enhancement. Occasionally, Pt and Au–Ag alloys are selected as the metal. A few fluorophores have been studied in these two core–shell structures including Cy3 [30], cascade yellow [78], carboxyfluorescein [78], Ru(bpy)₃²⁺ [31, 34], R6G [34], fluorescein isothiocyanate [79], Rhodamine 800 [32, 33], Alexa Fluor 647 [32], NIR 797 [82], dansylamide [84], oxazin 725 [85], and Eu³⁺ complexes [33, 83].

The geometry of the nanoscaled metals has an effect on the fluorescence enhancement. Theoretically, when the metal is introduced to the nanostructure, the total radiative decay rate will be written as $\Gamma + \Gamma_m$, where Γ_m corresponds to the radiative decay rate close to the metal surface. So, (1) and (2) should be modified and the quantum yield and lifetime are represented as:

$$Q = \frac{\Gamma + \Gamma_m}{\Gamma + \Gamma_m + k_{nr}} = \frac{\gamma_r \Gamma}{\gamma_r \Gamma + k_{nr}} \quad (3)$$

$$\tau = \frac{1}{\Gamma + \Gamma_m + k_{nr}} = \frac{1}{\gamma_r \Gamma + k_{nr}} \quad (4)$$

Here, γ_r is a factor of $(1 + \Gamma_m/\Gamma)$. In a fluorescence enhancement system, interactions between the metal and dye molecules result in shortening of the excited-state lifetime, thus improving the photostability of the dye.

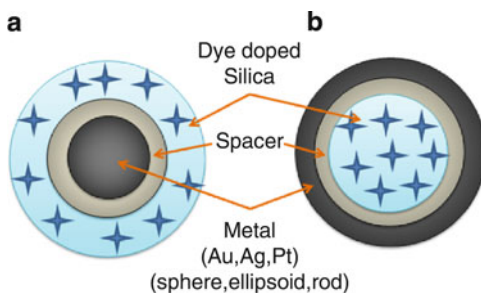


Fig. 5 Cores–shell structure of metal and DDSN complexes. (a) Metal core/silica shell, (b) silica core/metal shell

The mechanism of the metal enhanced fluorescence intensity of fluorophores has been proposed. In the core-shell nanostructures, the cross section between the metal and the dye molecules in silica is 10^5 larger than that of a dye molecule [77, 86, 87], which makes the radiation from the light source concentrate on the metal surface area. Thus, an enlarged localized electromagnetic field is manifested around the nanostructures, providing extra energy for signaling dye molecules present within this electromagnetic field (Fig. 6). In this case, the overlap between the excitation wavelength of fluorophores and the plasmon resonance band of the metal is recommended. This resonance interaction between the fluorophores and the metal is shown in Fig. 7a.

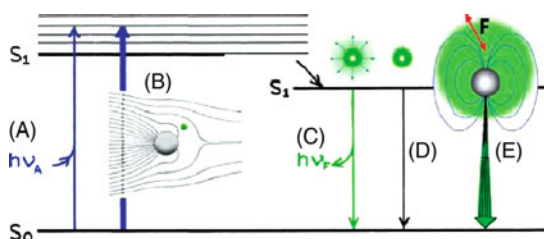


Fig. 6 Modified Jablonski diagram for illustrating metal-fluorophore interactions. (a) the transition of dye excited by the incident light, (b) the enhanced excitation according to enlarged electromagnetic field, (c) the fluorescent emission of dye molecule, (d) the nonradiative relaxation, (e) the enhanced emission of the fluorophores and metal coupling in far field. Reproduced with permission from Ref. [77]

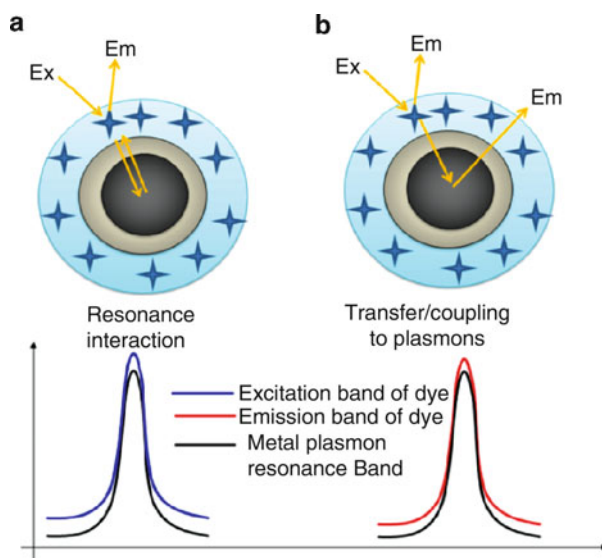


Fig. 7 The interaction and coupling modes of dye molecules and metal in a core-shell structure for fluorescence enhancement

An additional approach to enhance the fluorescence signal is to increase the coupling efficiency of the fluorescence emission to the far field (Fig. 6e). The excited dye molecules can transfer their energy to the metal, and then the metal starts emission of radiation. The overlap between the emission of dye molecules and the metal plasmon resonance band is more effective producing enhancement (Fig. 7b). In a recent review, it was discussed that the fluorophores–metal complex is the real emitting species and gave the complex the name “plasmonphore” or “fluoron” for distinguishing them from fluorophores and plasmonics [77].

The fluorescence quenching occurs when dye molecules are close to the metal. The energy from the first excited fluorophores can be consumed through a non-radiative path to the metal. A spacing layer is usually required to avoid this energy transfer process. In addition, the concentration of the dispersed dye molecules should be suitable to avoid self quenching [34, 81].

The plasmon decay time is adjusted by controlling the geometry of the metal nanoparticles. However, so far it is uncertain whether a longer or a shorter plasmon decay time is preferable for the fluorescence enhancement [77]. Shorter plasmon decay times can prevent energy conversion to thermal energy and thus produce more emission signals while longer decay time allows more time to radiate and thus enhance the emission. Currently, the effect of geometry of nanoscaled metal on the fluorescence enhancement is still under the study [77].

3.5 Solubility

The solubility of a DDSN is determined by its surface groups [24]. Without any surface modifications, the amorphous silica nanomatrix provides DDSNs good water solubility [3]. This water solubility can be further enhanced by surface modification of DDSNs with carboxyl groups. This surface can be obtained by adding 3-(trihydroxysilyl)propylmethylphosphonate or carboxyethylsilane-triol as a cocondensation agent with silicon alkoxide in a post coating process after the DDSNs have been synthesized [24]. The resultant carboxyl-group modified DDSNs have excellent water solubility, which can be stably suspended in aqueous solution for a long time period. The hydrophilic surface of the DDSNs may cause nonspecific binding to the biological samples, which challenges the applications of DDSNs in the biological area. A solution to this problem is to introduce some hydrophobic groups to the surface of the DDSNs. For example, the octadecyl groups can be integrated with carboxyl groups in the post coating process by adding octadecyltriethoxysilane in the reverse microemulsion [24]. The obtained octadecyl and carboxyl modified DDSNs exhibited minimal nonspecific binding to a DNA modified glass surface. Similarly, poly(lipid)-coated DDSNs avoided nonspecific adsorption in determination of analytes [88].

3.6 Reaction Kinetics of Doped Molecules

The amorphous silica matrixes are porous network structures that allow other species to penetrate [44]. Thus, the doped dye molecules have the ability to react with targets. However, the reaction kinetics is significantly different than the molecules in a bulk solution. In the synthesis of DDSNs, commonly used silicon alkoxides including TEOS and TMOS have tetrahedron structures, which allow compact polycondensation. As a result, the developed silica nanomatrix can be very dense. The small pore sizes provide limited and narrow pathways for other species to diffuse into the silica matrix.

In a bulk silica matrix that differs from the silica nanomatrix regarding only the matrix size but has a similar network structure of silica, several kinetic parameters have been studied and the results demonstrated a diffusion controlled mechanism for penetration of other species into the silica matrix [89–93]. When the silica is used as a catalyst matrix in the liquid phase, slow diffusion of reactants to the catalytic sites within the silica rendered the reaction diffusion controlled [90]. It was also reported that the reduction rate of encapsulated ferricytochrome by sodium dithionite decreased in a bulk silica matrix by an order of magnitude compared to its original reaction rate in a homogeneous solution [89]. In gas-phase reactions in the silica matrix, diffusion limitations were observed occasionally [93].

In the silica nanomatrix, the low diffusion was also reported in both liquid and gas phases. In the gas-phase reaction, it was found that the luminescence signal of $\text{Ru}(\text{bpy})_3^{2+}$ doped in DDSNs remained stable when the air pressure increased from 1 to 8 psi, showing no quenching by oxygen in the air. When the air pressure was further increased to above 8 psi, a decrease in fluorescence emission intensity was observed. The results suggested a slow diffusion of quencher oxygen in the silica nanomatrix.

The liquid-phase reaction kinetics of doped molecules in silica nanomatrixes was conducted using the metalation of *meso*-tetra (4-*N,N,N*-trimethylanilinium) porphyrin tetrachloride (TTMAPP) with Cu(II) as a model. To demonstrate the effect of the silica nanomatrix on the diffusion, pure silica shells with varied thickness were coated onto the same silica cores, which doped the same amount of TTMAPP molecules. The Cu(II) from the suspension could penetrate into the silica nanomatrixes and bind to the TTMAPP. The reaction rate of TTMAPP metalation with Cu(II) was significantly slower than that in a bulk solution. The increase in the thickness of the silica resulted in a consistent decrease of reaction rates (Fig. 8).

The diffusion limitations appeared to be the primary reason for the decreased reaction rate (Fig. 9).

The measurements of the reaction activation energies indicated that the reaction mechanism in the nanomatrix was different than in the bulk solution. Both adsorption-based diffusion and simple diffusion appeared to control the reaction rate in the nanomatrix. The adsorption-based diffusion corresponded to the relatively fast reaction of the doped TTMAPP, which were close to the particle surfaces. The simple diffusion correlated to the slow reaction of the deeply embedded TTMAPP.

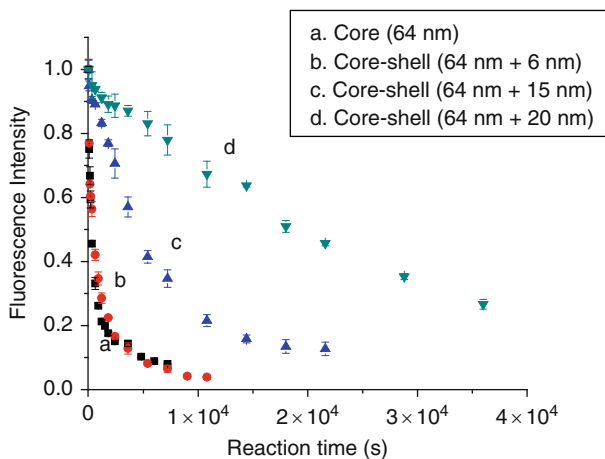


Fig. 8 Fluorescence intensities of doped TTMAPP versus metalation time. Reproduced with permission from Ref. [39]

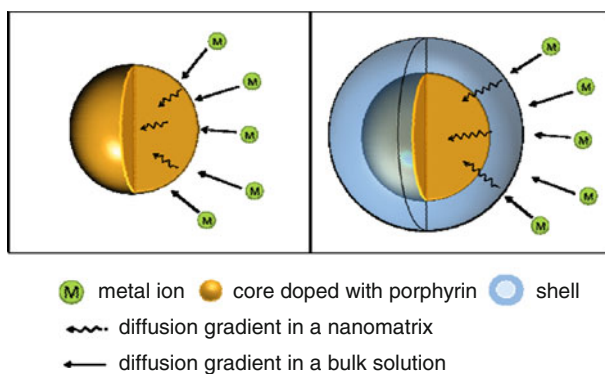


Fig. 9 A schematic diagram of the diffusion-controlled porphyrin metalation in a small nanomatrix (*left*) and a larger nanomatrix (*right*). Reproduced with permission from Ref. [39]

The reaction kinetic study suggested that dye molecules in DDSNs have limited reaction activity although they are accessible to outside species. If highly reactive dye molecules are desirable in DDSNs, less dense silica nanomatrixes should be considered, such as mesoporous nanostructures.

3.7 Toxicity of DDSNs

Toxicity of DDSNs is a critical concern for their applications in biological samples. The toxicity of DDSNs depends on size, surface modification, and dye molecule

properties [94–101]. Previous studies of particle toxicity have shown that size, shape and surface properties of the particles are key factors that determine whether or not the particles can eventually enter and remain inside living systems [99, 100, 102–105]. In general, foreign materials invade a living system through three pathways, namely the respiratory tract, the gastrointestinal tract, or by skin contact. The toxicity of airborne ultrafine particles and certain engineered nanomaterials have been well documented [98–100, 103, 106–108], with colloidal silica generally being accepted as either a nontoxic material or having low-toxicity [106, 109, 110]. When living systems come into direct contact with amorphous silica nanomaterials, a number of negative results may occur including chronic pulmonary changes during inflammation, generation of reactive oxygen species, and damage to intracellular DNA, RNA and proteins [110–117].

The size of the nanomaterial greatly influences its toxicity; particularly as the nanomaterial's size decreases, certain of its parameters changed [3, 11, 118, 119]. Many studies have shown that variations in the size of nanomaterials account for the different toxicity levels between nanosized and micrometer-sized materials [97, 99, 100, 103]. It is known that a reduction in size can increase the rate of uptake and translocation of silica nanomaterials *in vitro* and *in vivo*, thereby inducing a more severe and transient toxicity [56].

Currently available information suggests that the shape of nanomaterials can affect their toxicity in two ways. First, the shape has an effect on the rate of its cellular uptake; and second, it can affect the extent of nanomaterial aggregation, altering its cytotoxic properties. A recent *in vitro* toxicity study showed spherical nanomaterials to be more toxic than rods [120]. It was also shown to be more difficult for elliptical nanomaterials to penetrate the skin layer than spherical nanomaterials [121].

Based on well established silica chemistry, the surface of silica nanomaterials can be modified to introduce a variety of functionalizations [3, 11, 118]. The toxicity of surface-modified nanomaterials is largely determined by their surface functional groups. As an example, Kreuter reported that an apolipoprotein coating on silica nanoparticles aided their endocytosis in brain capillaries through the LDL-receptor [122–124]. Overall, silica nanomaterials are low-toxicity materials, although their toxicity can be altered by surface modifications.

Dose-dependent toxicity has frequently been observed in the study of nanomaterials [110–116], with increasing doses of silica nanomaterials invariably worsening their toxicity. Both, cell proliferation and viability were greatly hampered at higher doses in *in vitro* studies [111, 113, 116].

The toxicity is not only based on the amount or size of silica nanoparticles, but also on the cell line [95]. Cancer cell lines (A549, MKN-28) had a higher viability and resistance to silica nanoparticles than did normal cell lines (MRC-5, WS1 and CCD-966sk) [111]. Similarly, a previous study showed that A549 cells were more resistant to the treatment of silica nanoparticles than were macrophages [113].

The dopants, dye molecules, in general, have little effect on the toxicity of DDSNs because they are isolated from the environment [3, 11, 23, 118]. However, if the dopants are photosensitizers or some other specialized molecules, they can

have an effect on the toxicity of the DDSNs. For example, when a hydrophobic photosensitizer, PS HPPH [2-devinyl-2-(1-hexyloxyethyl)pyropheophorbide], was doped inside organically modified silica nanoparticles [125], and the nanoparticles were delivered into cells (under irradiation), ROS were produced by the doped photosensitizers and the cells were killed.

4 Conclusions

With a suitable doping method, DDSNs can be synthesized by adding the dye molecules into a Stöber or reverse microemulsion process. Compared with the molecular fluorophores, the DDSNs have advantages such as high fluorescence intensity, good photostability and water solubility, and low toxicity. It is evidenced that the silica nanoenvironment enhanced both the fluorescence quantum yield and lifetime of the doped fluorophores. The structure of a DDSN is designable. Various configurations endow the DDSNs with advantageous properties such as enhanced fluorescence and multiple functions. These special properties make the DDSNs promising fluorescent materials for biological sensing and labeling.

References

1. Lakowicz JR (2006) Principles of fluorescence spectroscopy. Springer, Singapore
2. Valeur B (2002) Molecular fluorescence: principles and applications. Wiley-VCH, Weinheim
3. Wang L, Wang K, Santra S, Zhao X, Hilliard LR, Smith JE, Wu Y, Tan W (2006) *Anal Chem* 78:646
4. Wang L, Zhao W, Tan W (2008) *Nano Res* 1:99
5. van Blaaderen A, Vrij A (1992) *Langmuir* 8:2921
6. Burns A, Sengupta P, Zedayko T, Baird B, Wiesner U (2006) *Small* 2:723
7. Bechet D, Couleaud P, Frochot C, Viriot M-L, Guillemin F, Barberi-Heyob M (2008) *Trends Biotechnol* 26:612
8. Santra S, Zhang P, Wang K, Tapeç R, Tan W (2001) *Anal Chem* 73:4988
9. He X, Wang K, Tan W, Liu B, Lin X, He C, Li D, Huang S, Li J (2003) *J Am Chem Soc* 125:7168
10. Zhao X, Tapeç-Dytioco R, Tan W (2003) *J Am Chem Soc* 125:11474
11. Zhao X, Hilliard LR, Wang K, Tan W (2004) In: Nalwa HS (ed) *Encyclopedia of nanoscience and nanotechnology*, American Scientific Publishers, Stevenson Ranch, CA, p 255
12. Wang L, Tan W (2005) *Nano Lett* 6:84
13. Ow H, Larson DR, Srivastava M, Baird BA, Webb WW, Wiesner U (2005) *Nano Lett* 5:113
14. Burns A, Ow H, Wiesner U (2007) *ChemInform*: 38
15. Kim J, Kim HS, Lee N, Kim T, Kim H, Yu T, Song IC, Moon WK, Hyeon T (2008) *Angew Chem Int Ed* 47:8438
16. Ohulchanskyy TY, Roy I, Goswami LN, Chen Y, Bergey EJ, Pandey RK, Oseroff AR, Prasad PN (2007) *Nano Lett* 7:2835

17. Lai C-W, Wang Y-H, Lai C-H, Yang M-J, Chen C-Y, Chou P-T, Chan C-S, Chi Y, Chen Y-C, Hsiao J-K (2008) *Small* 4:218
18. Kim S, Ohulchanskyy TY, Pudavar HE, Pandey RK, Prasad PN (2007) *J Am Chem Soc* 129:2669
19. Liong M, Lu J, Kovochich M, Xia T, Ruehm SG, Nel AE, Tamanoi F, Zink JI (2008) *ACS Nano* 2:889
20. Corr SA, O'Byrne A, Gun'ko YK, Ghosh S, Brougham DF, Mitchell S, Volkov Y, Prina-Mello A (2006) *Chem Commun*:4474
21. Wang L, Yang C, Tan W (2004) *Nano Lett* 5:37
22. Zhao X, Hilliard LR, Mechery SJ, Wang Y, Bagwe RP, Jin S, Tan W (2004) *Proc Natl Acad Sci USA* 101:15027
23. Zhao X, Bagwe RP, Tan W (2004) *Adv Mater* 16:173
24. Bagwe RP, Hilliard LR, Tan W (2006) *Langmuir* 22:4357
25. Bagwe RP, Yang C, Hilliard LR, Tan W (2004) *Langmuir* 20:8336
26. Burns AA, Vider J, Ow H, Herz E, Penate-Medina O, Baumgart M, Larson SM, Wiesner U, Bradbury M (2008) *Nano Lett* 9:442
27. Montalti M, Prodi L, Zaccheroni N, Battistini G, Marcuz S, Mancin F, Rampazzo E, Tonellato U (2006) *Langmuir* 22:5877
28. Rampazzo E, Bonacchi S, Montalti M, Prodi L, Zaccheroni N (2007) *J Am Chem Soc* 129:14251
29. Zanarini S, Rampazzo E, Ciana LD, Marcaccio M, Marzocchi E, Montalti M, Paolucci F, Prodi L (2009) *J Am Chem Soc* 131:2260
30. Aslan K, Lakowicz JR, Szmackinski H, Geddes CD (2004) *J Fluoresc* 14:677
31. Zhang J, Gryczynski I, Gryczynski Z, Lakowicz JR (2006) *J Phys Chem B* 110:8986
32. Aslan K, Wu M, Lakowicz J, Geddes C (2007) *J Fluoresc* 17:127
33. Aslan K, Wu M, Lakowicz JR, Geddes CD (2007) *J Am Chem Soc* 129:1524
34. Zhang J, Fu Y, Lakowicz JR (2007) *J Phys Chem C* 111:1955
35. Rossi LM, Shi L, Quina FH, Rosenzweig Z (2005) *Langmuir* 21:4277
36. Sokolov I, Naik S (2008) *Small* 4:934
37. Heitsch AT, Smith DK, Patel RN, Ress D, Korgel BA (2008) *J Solid State Chem* 181:1590
38. Wang L, Lei J, Zhang J (2009) *Chem Commun* 16:2195
39. Liang S, Hartvickson S, Kozliak E, Zhao JX (2009) *J Phys Chem C* 113:19046
40. Rosenholm JM, Meinander A, Peuhu E, Niemi R, Eriksson JE, Sahlgren C, Linden M (2009) *ACS Nano* 3:197
41. Liu H-M, Wu S-H, Lu C-W, Yao M, Hsiao J-K, Hung Y, Lin Y-S, Mou C-Y, Yang C-S, Huang D-M, Chen Y-C (2008) *Small* 4:619
42. Cauda V, Schlossbauer A, Kecht J, Zürmer A, Bein T (2009) *J Am Chem Soc* 131:11361
43. Lin Y-S, Haynes CL (2009) *Chem Mater* 21:3979
44. Hench LL, West JK (1990) *Chem Rev* 90:33
45. Stöber W, Fink A, Bohn EJ (1968) *Colloid Interface Sci* 26:62
46. Graf C, Vossen DLJ, Imhof A, van Blaaderen A (2003) *Langmuir* 19:6693
47. Graf C, Dembski S, Hofmann A, Ruhl E (2006) *Langmuir* 22:5604
48. Yang SM, Sokolov I, Coombs N, Kresge CT, Ozin GA (1999) *Adv Mater* 11:1427
49. Huh S, Wiench JW, Yoo J-C, Pruski M, Lin VSY (2003) *Chem Mater* 15:4247
50. Slowing II, Trewyn BG, Giri S, Lin S-Y (2007) *Adv Funct Mater* 17:1225
51. Slowing II, Vivero-Escoto JL, Wu C-W, Lin VSY (2008) *Adv Drug Deliv Rev* 60:1278
52. Lebreton V, Raehm L, Durand J-O, Smaïhi M, Gardin C, Nerambourg N, Werts MHV, Blanchard-Desce M (2008) *Chem Mater* 20:2174
53. Qian HS, Guo HC, Ho PC-L, Mahendran R, Zhang Y (2009) *Small* 5:2285
54. Trewyn BG, Slowing II, Giri S, Chen H-T, Lin VSY (2007) *Acc Chem Res* 40:846
55. Finnie KS, Bartlett JR, Barbé CJA, Kong L (2007) *Langmuir* 23:3017
56. Jin Y, Lohstreter S, Pierce DT, Parisien J, Wu M, Hall C, Zhao JX (2008) *Chem Mater* 20:4411

57. Arriagada FJ, Osseo-Asare KJ (1999) *Colloid Interface Sci* 211:210
58. Verhaegh NAM, van Blaaderen A (1994) *Langmuir* 10:1427
59. Nakamura M, Shono M, Ishimura K (2007) *Anal Chem* 79:6507
60. Wang L, Zhao W, O'Donoghue MB, Tan W (2007) *Bioconjug Chem* 18:297
61. Burns AA, Vider J, Ow H, Herz E, Penate-Medina O, Baumgart M, Larson SM, Wiesner U, Bradbury M (2009) *Nano Lett* 9:442
62. Koo Y-EL, Cao Y, Kopelman R, Koo SM, Brasuel M, Philbert MA (2004) *Anal Chem* 76:2498
63. Buck SM, Koo Y-EL, Park E, Xu H, Philbert MA, Brasuel MA, Kopelman R (2004) *Curr Opin Chem Biol* 8:540
64. Jin Y, Li A, Hazelton SG, Liang S, John CL, Selid PD, Pierce DT, Zhao JX (2009) *Coord Chem Rev* 253:2998
65. Larson DR, Ow H, Vishwasrao HD, Heikal AA, Wiesner U, Webb WW (2008) *Chem Mater* 20:2677
66. Herz E, Marchincin T, Connelly L, Bonner D, Burns A, Switalski S, Wiesner U (2009) *J Fluoresc* 20(1):1573–4994
67. Kim SH, Jeyakumar M, Katzenellenbogen JA (2007) *J Am Chem Soc* 129:13254
68. Fölling J, Polyakova S, Belov V, van Blaaderen A, Bossi ML, Hell SW (2008) *Small* 4:134
69. Nicolet O, Huber S, Lovey C, Chappellet S, Perrenoud J, Pauchard M, Ferrini R, Zuppiroli L (2009) *Adv Funct Mater* 19:1877
70. Geddes CD, Lakowicz JR (2002) *J Fluoresc* 12:121
71. Lakowicz J, Geddes C, Gryczynski I, Malicka J, Gryczynski Z, Aslan K, Lukomska J, Matveeva E, Zhang J, Badugu R, Huang J (2004) *J Fluoresc* 14:425
72. Stuart DA, Haes AJ, Yonzon C, Hicks EM, van Duyne RP (2005) *IEEE Proc Nanobiotechnol* 152:13
73. Haes AJ, Haynes CL, McFarland AD, Schatz GC, van Duyne RP, Zou S (2005) *MRS Bull* 30:368
74. Willets KA, van Duyne RP (2007) *Annu Rev Phys Chem* 58:267
75. Xia Y, Halas NJ (2005) *MRS Bull* 30:338
76. Lakowicz J (2006) *Plasmonics* 1:5
77. Lakowicz JR, Ray K, Chowdhury M, Szymanski H, Fu Y, Zhang J, Nowaczyk K (2008) *Analyst* 133:1308
78. Tovmachenko OG, Graf C, van den Heuvel DJ, van Blaaderen A, Gerritsen HC (2006) *Adv Mater* 18:91
79. Cheng D, Xu Q-H (2007) *Chem Comm*:248
80. Stranik O, Nooney R, McDonagh C, MacCraith B (2007) *Plasmonics* 2:15
81. Viger M, Live L, Therrien O, Boudreau D (2008) *Plasmonics* 3:33
82. Xu S, Hartvickson S, Zhao JX (2008) *Langmuir* 24:7492
83. Ma ZY, Dosev D, Kennedy IM (2009) *Nanotechnology* 20:085608
84. Liu S, Wong Y, Wang Y, Wang D, Han M-Y (2007) *Adv Funct Mater* 17:3147
85. Ming T, Zhao L, Yang Z, Chen H, Sun L, Wang J, Yan C (2009) *Nano Lett* 9(11):3896–3903
86. Yguerabide J, Yguerabide EE (1998) *Anal Biochem* 262:137
87. Yguerabide J, Yguerabide EE (1998) *Anal Biochem* 262:157
88. Senarath-Yapa MD, Phimphivong S, Coym JW, Wirth MJ, Aspinwall CA, Saavedra SS (2007) *Langmuir* 23:12624
89. Fiandaca G, Vitrano E, Cupane A (2004) *Biopolymers* 74:55
90. Frenkel-Muller H, Avnir D (2005) *J Am Chem Soc* 127:8077
91. Carlsson P-A, Zhdanov VP, Skoglundh M (2006) *Phys Chem Chem Phys* 8:270
92. Borgna A, Hensen EJM, Coulier L, de Croon MHJM, Schouten JC, van Veen JAR, Niemantsverdriet JW (2003) *Catal Lett* 90:117
93. Karatepe N, Ersoy-Meriçboyu A, Yavuz R, Küçükbayrak S (1999) *Thermochim Acta* 335:127

94. Kumar CSSR (2009) *Nanomaterials for the life sciences vol 2: nanostructured oxides*. Wiley-VCH, Weinheim
95. Thomassen LCJ, Aerts A, Rabolli V, Lison D, Gonzalez L, Kirsch-Volders, M, Napierska D, Hoet PH, Kirschhock CEA, Martens JA (2010) *Langmuir* 26(1):328–335
96. Di Pasqua AJ, Sharma KK, Shi Y-L, Toms BB, Ouellette W, Dabrowiak JC, Asefa TJ (2008) *Inorg Biochem* 102:1416
97. Napierska D, Thomassen LCJ, Rabolli V, Lison D, Gonzalez L, Kirsch-Volders M, Martens JA, Hoet PH (2009) *Small* 5:846
98. Lewinski N, Colvin V, Drezek R (2008) *Small* 4:26
99. Nel A, Xia T, Madler L, Li N (2006) *Science* 311:622
100. Oberdörster G, Oberdorster E, Oberdorster J (2005) *Environ Health Perspect* 113:823
101. Fujiwara K, Suematsu H, Kiyomiya E, Aoki M, Sato M, Moritoki N (2008) *J Environ Sci Health A Toxic Hazard Subst Environ Eng* 43:1167
102. Vega-Villa KR, Takemoto JK, Yanez JA, Remsberg CM, Forrest ML, Davies NM (2008) *Adv Drug Deliv Rev* 60:929
103. Gwinn MR, Vallyathan V (2006) *Environ Health Perspect* 114:1818
104. Baroli B, Ennas MG, Loffredo F, Isola M, Pinna R, Lopez-Quintela MA (2007) *J Invest Dermatol* 127:1701
105. Hagens WI, Oomen AG, de Jong WH, Cassee FR, Sips AJAM (2007) *Regul Toxicol Pharmacol* 49:217
106. Borm PJA, Schins RPF, Albrecht C (2004) *Int J Cancer* 110:3
107. Knaapen AM, Borm PJA, Albrecht C, Schins RPF (2004) *Int J Cancer* 109:799
108. Nel A (2005) *Science* 308:804
109. Nishimori H, Kondoh M, Isoda K, Tsunoda S, Tsutsumi Y, Yagi K (2009) *Pharmazie* 64:214–216
110. Johnston CJ, Driscoll KE, Finkelstein JN, Baggs R, O'Reilly MA, Carter J, Gelein R, Oberdorster G (2000) *Toxicol Sci* 56:405
111. Chang J-S, Chang KLB, Hwang D-F, Kong Z-L (2007) *Environ Sci Technol* 41:2064
112. Cho W-S, Choi M, Han BS, Cho M, Oh J, Park K, Kim SJ, Kim SH, Jeong J (2007) *Toxicol Lett* 175:24
113. Jin Y, Kannan S, Wu M, Zhao JX (2007) *Chem Res Toxicol* 20:1126
114. Kaewamatawong T, Kawamura N, Okajima M, Sawada M, Morita T, Shimada A (2005) *Toxicol Pathol* 33:745
115. Kaewamatawong T, Shimada A, Okajima M, Inoue H, Morita T, Inoue K, Takano H (2006) *Toxicol Pathol* 34:958
116. Lin W, Huang Y-W, Zhou X-D, Ma Y (2006) *Toxicol Appl Pharmacol* 217:252
117. Sayes CM, Reed KL, Warheit DB (2007) *Toxicol Sci* 97:163
118. Yao G, Wang L, Wu Y, Smith J, Xu J, Zhao W, Lee E, Tan W (2006) *Anal Bioanal Chem* 385:518
119. Rosi NL, Mirkin CA (2005) *Chem Rev* 105:1547
120. Brown SC, Kamal M, Nasreen N, Baumuratov A, Sharma P, Antony VB, Moudgil BM (2007) *Adv Powder Technol* 18:69
121. Ryman-Rasmussen JP, Riviere JE, Monteiro-Riviere NA (2006) *Toxicol Sci* 91:159
122. Kreuter J (2001) *Adv Drug Deliv Rev* 47:65
123. Kreuter J, Shamenkov D, Petrov V, Ramge P, Cychutek K, Koch-Brandt C, Alyautdin RJ (2008) *Drug Target* 10:317
124. Michaelis K, Hoffmann MM, Dreis S, Herbert E, Alyautdin RN, Michaelis M, Kreuter J, Langer KJ (2006) *Pharmacol Exp Ther* 317:1246
125. Smith JE, Medley CD, Tang Z, Shanguan D, Lofton C, Tan W (2007) *Anal Chem* 79:3075

Luminescent Dendrimers as Ligands and Sensors of Metal Ions

Giacomo Bergamini, Enrico Marchi, and Paola Ceroni

Abstract Suitably designed luminescent dendrimers can play the role of ligands for luminescent and nonluminescent metal ions. This combination leads to species capable of exhibiting interesting and unusual properties, including (1) shielding excited states from quenching processes, (2) light harvesting, (3) conversion of incident UV light into visible or infra red emission, and (4) metal ions sensing with signal amplification.

Keywords Dendrimers · Luminescent sensors · Metal complexes · Metal ions

Contents

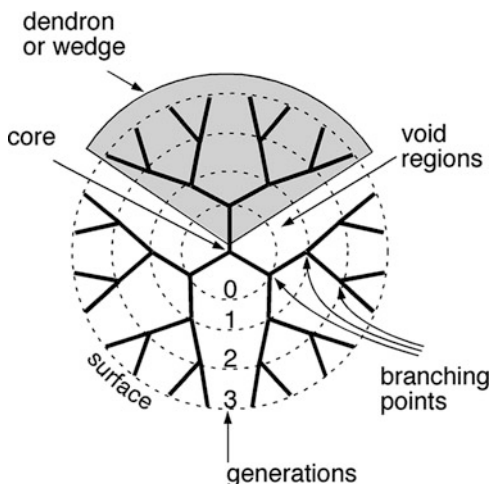
1	Introduction	253
2	Luminescent Dendrimers Hosting Nonluminescent Metal Ions	256
2.1	Luminescent Dendrimers Hosting Innocent Metal Ions	256
2.2	Luminescent Dendrimers Hosting Metal Ion Quenchers	263
3	Luminescent Dendrimers Hosting Luminescent Metal Ions	269
3.1	Dendrons with a Coordinating Focal Point	270
3.2	Dendrimers with Amide Coordinating Units	272
3.3	Dendrimers with a Cyclam Coordinating Core	275
4	Conclusions	278
	References	278

1 Introduction

Dendrimers [1] constitute a class of multibranched molecules that can – by design – exhibit not only a high degree of order but also a high degree of complexity. From a topological viewpoint, dendrimers contain three different regions: core, branches,

G. Bergamini, E. Marchi, and P. Ceroni (✉)
Department of Chemistry “G. Ciamician”, via Selmi 2, 40126 Bologna, Italy
e-mail: paola.ceroni@unibo.it

Fig. 1 Schematic representation of a dendrimer



and surface (Fig. 1). A most important feature of dendrimer chemistry is the possibility of inserting selected chemical units in predetermined sites of the dendritic architecture. Moreover, thanks to their three-dimensional structure, internal dynamic cavities are present, where ions or molecules can be hosted. It is thus possible to construct large nanoobjects capable of performing complex functionality that derives from the integration of the specific properties of the constituent moieties. Nowadays both chemistry and physics of dendritic molecules are rapidly expanding for fundamental research as well as for technological applications [2].

When the functional units incorporated into the dendrimers are luminescent, information on dendrimer structure and properties can be gained by luminescence studies. Indeed, a large number of chromophores can be arranged according to predetermined patterns in a restricted space. Therefore, coupling luminescence and dendrimer chemistry can lead to interesting photophysical properties [3], such as (1) interactions of the dendritic luminescent units in the ground and/or in the excited states (possible formation of excimers and/or exciplexes), (2) quenching of dendrimer luminescence by external species, and (3) sensitization of luminescent metal ions or dyes encapsulated by the dendrimer. Indeed, luminescent dendrimers have been extensively investigated in the last few years both from a fundamental viewpoint (e.g., theoretical studies on energy transfer processes [4], fluorescence at the single molecule level) [5] and a variety of applications, including (1) light harvesting [6], (2) changing the “color” of light [7], (3) sensing with signal amplification [8], and (4) quenching and sensitization processes [9].

If dendrimers contain both luminescent units and coordination sites, they can perform as luminescent ligands for metal ions [10]. Coupling luminescence with metal coordination can indeed be exploited for a variety of purposes that include investigation of dendrimer structures [11], encapsulated metal nanoparticles [12],

light harvesting [13], stepwise complexation [14], and reversible metal complex assembly [15].

In most cases, metal ion coordination by a dendrimer takes place by units that are present along the dendrimer branches (e.g., amine, imine, or amide groups) or appended at the dendrimer periphery (e.g., terpyridine, catecholamide ligands). When multiple identical coordinating units are present, dendrimers give rise to metal complexes of variable stoichiometry and unknown structures. Luminescent dendrimers with a well defined metal-coordinating site have been reported so far [16, 17], and the most used coordination site is 1,4,8,11-tetraazacyclotetradecane (cyclam).

A very interesting feature of luminescent dendritic ligands is the possibility of their performing as sensors of metal ions with signal amplification. The advantage of using a dendrimer for sensory applications is related to the fact that a single analyte can interact with a great number of units and change their properties, which results in signal amplification. In the case of luminescent dendrimers, *one* analyte can quench the luminescence of *all* the peripheral luminescent units appended at the dendrimer periphery (Fig. 2a). This is a significant advance compared to a conventional luminescent sensor, in which the ratio between quenched units and analyte is 1:1 (Fig. 2b). This behavior is made possible by the well-ordered and flexible dendritic structure in which any excited fluorophore can “feel” the presence of the coordinated metal ion. Signal amplification effects have already been obtained with polymeric chains of sensors [18], and nanoparticles [19]. Because of their well defined and fully programmable structures, dendrimers are the more promising

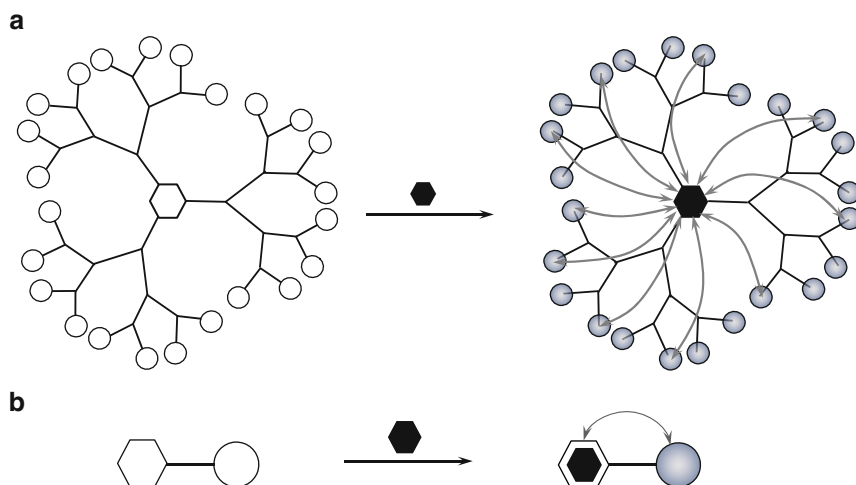


Fig. 2 Schematic representation of (a) a luminescent dendritic sensor with signal amplification and (b) a conventional luminescent sensor. The *curved arrows* represent interaction processes which changes the luminescence properties (from *empty to filled circles*). Analyte is represented by a *solid hexagon*, while the recognition site is by an *empty hexagon*

species for this kind of application [20]. The signal amplification that got the name ‘superquenching’ can be realized by different mechanisms. In dye-doped nanoparticles it can be homo-FRET with excitation energy transfer to nonfluorescent acceptor [47]. In conjugated polymers this effect can be due to a trap in exciton propagation [48]. Dendritic structures allow realizing both mechanisms.

The aim of this chapter is limited to reviewing some recent developments concerning luminescent dendrimers that can play the role of ligands and sensors for luminescent and nonluminescent metal ions, mainly investigated in our laboratories, with particular references to transition metal or lanthanide ions. We will not discuss dendrimers constituted by polypyridine metal complexes [21] and porphyrins [22] since it is outside the scope of the present paper.

2 Luminescent Dendrimers Hosting Nonluminescent Metal Ions

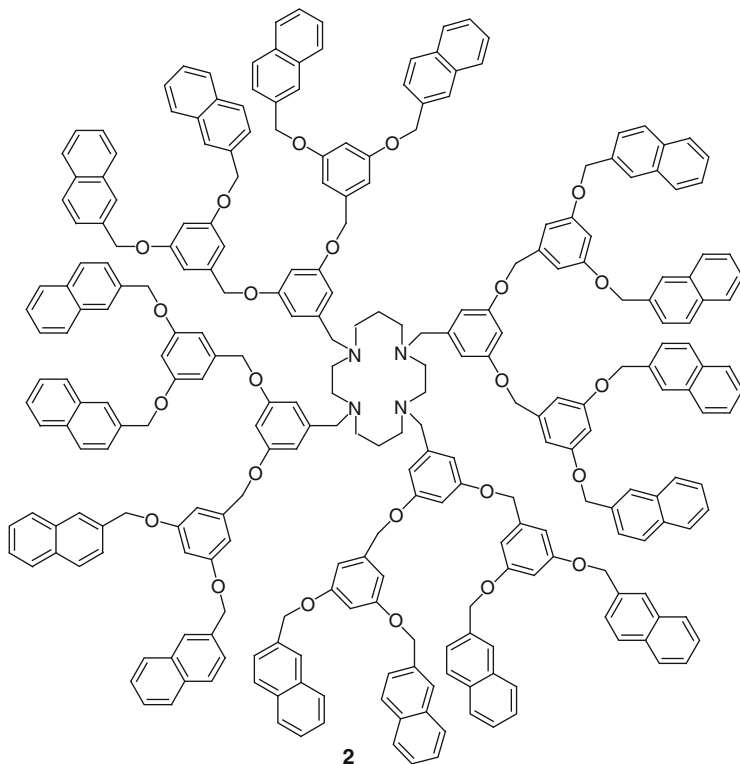
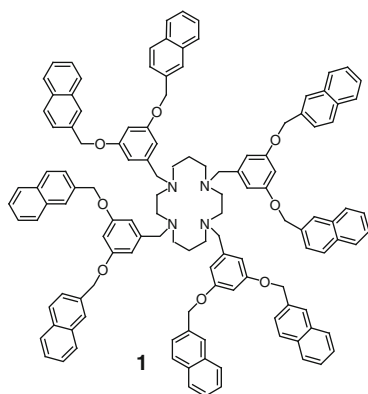
Among nonluminescent metal ions, we can distinguish two classes: metal ions that can quench dendrimer luminescence once they are coordinated inside the dendrimer and metal ions that cannot. The latter class is constituted by metal ions that do not possess low-lying excited states and do not show oxidation or reduction processes at easily accessible potentials so that they cannot be involved in photoinduced energy/electron transfer processes with the dendritic luminescent units. Also in the latter case, the presence of the metal ion inside the dendrimer can be revealed by changes in the luminescence spectra due to charge perturbation effect or to the shutting down of quenching processes, so that metal coordination cause the revival of dendrimer luminescence.

We will discuss in the following selected examples of the two cases.

2.1 Luminescent Dendrimers Hosting Innocent Metal Ions

2.1.1 Dendrimers with a Cyclam Coordinating Core

Cyclam is one of the most extensively investigated ligands in coordination chemistry [23]. Both cyclam and its 1,4,8,11-tetramethyl derivative in aqueous solution can be mono and diprotonated and can coordinate metal ions such as Co^{2+} , Ni^{2+} , Cu^{2+} , Zn^{2+} , Cd^{2+} , and Hg^{2+} with very large stability constants [24]. Furthermore, cyclam and its derivatives have been studied in medical applications [25], as carrier of metal ions in antitumor [26], imaging contrast agents [27], and as antiHIV agents [28].



Dendrimers **1** and **2** consist of a cyclam core appended with 4 dimethoxybenzene and 8 naphthyl units, and 12 dimethoxybenzene and 16 naphthyl units, respectively [29].

In acetonitrile–dichloromethane 1:1 v/v solution, their absorption spectra are dominated by naphthalene absorption bands and they exhibit three types of emission bands, assigned to naphthyl localized excited states ($\lambda_{\text{max}} = 337$ nm), naphthyl excimers (λ_{max} ca. 390 nm), and naphthyl-amine exciplexes ($\lambda_{\text{max}} = 480$ nm) (*solid lines* in Fig. 3). The tetraamine cyclam core undergoes only two protonation reactions, which not only prevent exciplex formation for electronic reasons but also cause strong nuclear rearrangements in the cyclam structure which affect excimer formation between the peripheral naphthyl units of the dendrimers.

Extensive investigation has been performed on the interaction of dendrimers **1** and **2** with metal ions [17a, e–h]. Complexation with Zn^{2+} engages the nitrogen lone pairs and thereby prevents exciplex formation, with a resulting intense naphthyl fluorescence (*dashed lines* in Fig. 3). This strong fluorescent signal is

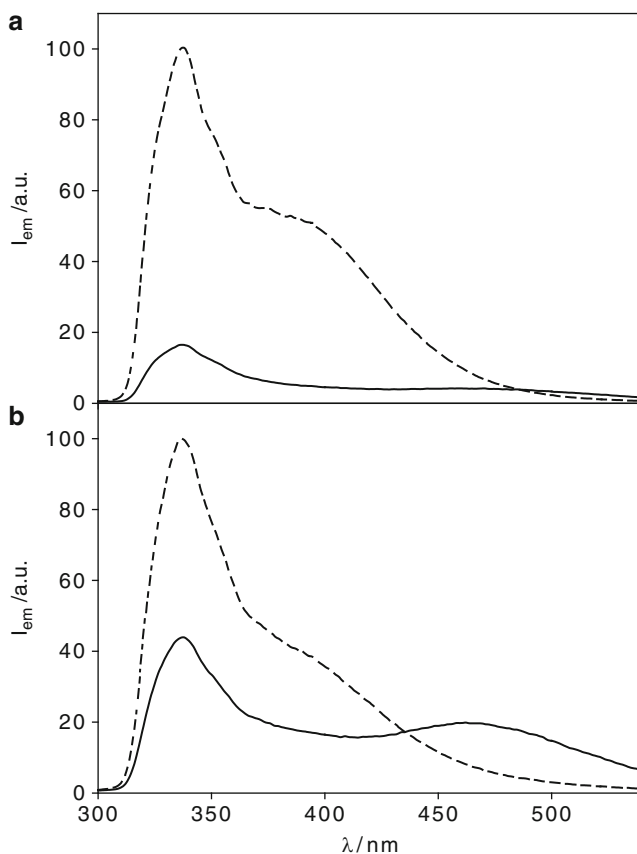


Fig. 3 Emission spectra of (a) **1** (1.3×10^{-5} M), and (b) **2** (6.7×10^{-6} M), before (*solid line*) and after (*dashed line*) addition of 1.1 equivalents of $\text{Zn}(\text{CF}_3\text{SO}_3)_2$ in $\text{CH}_3\text{CN}:\text{CH}_2\text{Cl}_2$ 1:1 v/v at 298 K with $\lambda_{\text{ex}} = 275$ nm

quite suitable for monitoring the formation of complexes in dendrimer/metal titration experiments (Fig. 4). Surprisingly, both dendrimer **1** and **2** give rise to complexes with 2:1 ligand to metal stoichiometry at low Zn^{2+} concentration, as evidenced by both fluorescence and ^1H NMR titrations. In particular, in the case of the largest dendrimer **2**, at low metal ion concentration, only the species $[\text{Zn}(\mathbf{2})_2]^{2+}$ is present with a high formation constant ($\log \beta_{2:1} > 13$). The unexpected $[\text{Zn}(\mathbf{2})_2]^{2+}$ species shows that the dendrimer branches not only do not hinder, but in fact favor coordination of cyclam to Zn^{2+} with respect to coordination of solvent molecules or counter ions. Two limiting structures can be proposed for the 2:1 complexes: (1) an “inward” structure, stabilized by the intermeshing of the branches of the two coordinated dendrimers; (2) an “outward” structure in which the branches of the two coordinated dendrimers do not interact but impose to the cyclam core a very specific coordination structure. Indeed, an “inward” structure for the 2:1 complex

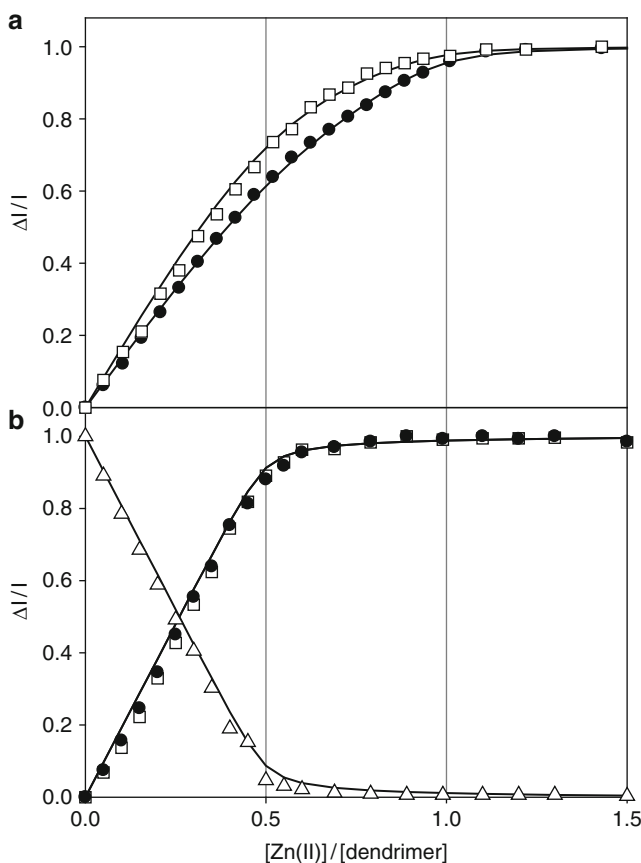


Fig. 4 Normalized emission intensity changes observed upon addition of $\text{Zn}(\text{CF}_3\text{SO}_3)_2$ to **1** (a), and **2** (b) at $\lambda_{\text{em}} = 337$ (solid circles), 390 (empty squares), and 480 nm (empty triangles). $\lambda_{\text{ex}} = 275$ nm

stabilized by branch intermeshing should increase the probability of excimer formation compared with the 1:1 species. In such a case, the intensity of the excimer band (λ_{\max} ca. 390 nm) should grow more rapidly at the beginning of the titration, when formation of a 2:1 species is favored. This seems to be the case for dendrimer **1**, but not for dendrimer **2**. Therefore, in the $[\text{Zn}(\mathbf{2})_2]^{2+}$ species the dendrimer branches are likely extending outward (Fig. 5). Furthermore, the two cyclam cores, to account for the coordination number (≤ 6) of Zn^{2+} , are likely forced to adopt a structure in which not all of the four N atoms are available for Zn^{2+} coordination, thereby favoring a 2:1 stoichiometry.

In the $[\text{Zn}(\mathbf{2})_2]^{2+}$ species, a single Zn^{2+} ion is able to revive the luminescence of all the 32 naphthyl units present in the two dendritic structures. This result shows that dendrimers can be profitably used as supramolecular fluorescent sensors for metal ions, as shown in Fig. 2. In this case, the sensor fluorescence is switched on upon metal ion coordination, and low Zn^{2+} concentrations (ca. 1 μM) can be easily detected.

The kinetics of complex formation with Zn^{2+} can be followed by monitoring the change in the fluorescence intensity [17g]. In the case of **1**, the change in the fluorescence intensity with time indicates a biphasic kinetics with the incorporation rate constants $k_1 = 4.9 \times 10^5 \text{ M}^{-1} \text{ s}^{-1}$ followed by a first order process

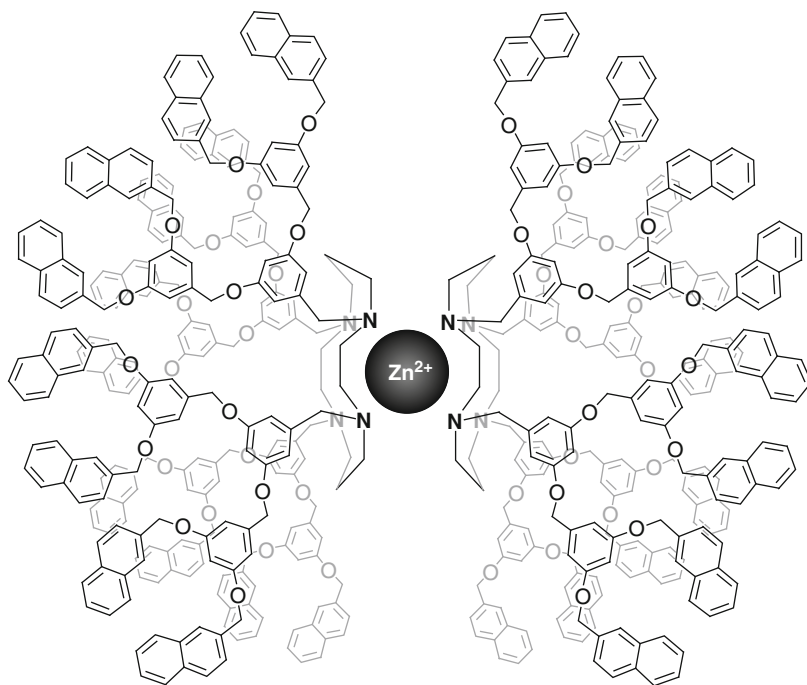
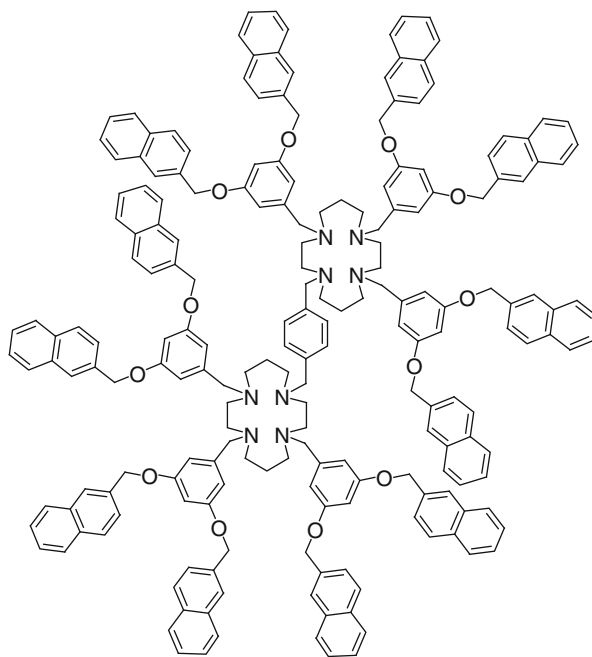


Fig. 5 Schematic representation of the $[\text{Zn}(\mathbf{2})_2]^{2+}$ species in which the dendrimer branches are extending outward

$k_2 = 0.40 \text{ s}^{-1}$. The second-order process contributes to 95% of the total change in fluorescence. For the reaction of Zn^{2+} with **2**, the observed changes in the fluorescence intensity can be accounted for by only a second order process alone, with $k_1 = 1.2 \times 10^5 \text{ M}^{-1} \text{ s}^{-1}$. The rate-limiting step does not correspond to the simple desolvation of Zn^{2+} . The observed decrease in the second order rate constant upon increasing dendrimer generation can be accounted for by a decrease, on increasing size of the branches, of either cyclam flexibility, or accessibility to the dendrimer core due to efficient hydrophobic shielding. Incorporation of Zn^{2+} into dendrimers of different generations could indeed involve structural changes resulting in slow kinetics. Conformational changes in the dendron subunits are necessary for the closure of the chelate ring and it is likely that the reorganization of the dendron subunits becomes slower on increasing dendrimer size because of steric congestions.

A step further in cyclam-based dendritic ligands for metal ions is constituted by dendrimer **3**, containing two covalently linked cyclam units as a core, appended to six branches, each one of them consisting of a dimethoxybenzene and two naphthyl units [17d]. Its photophysical properties are qualitatively similar to that observed for **1**. For example, the emission spectrum evidences the presence of naphthyl localized excited states ($\lambda_{\text{max}} = 337 \text{ nm}$), naphthyl excimers (λ_{max} ca. 390 nm), and naphthyl-amine exciplexes ($\lambda_{\text{max}} = 480 \text{ nm}$). Upon titration with trifluoroacetic acid, the two cyclams undergo protonation reactions, that, as previously discussed, not only prevent exciplex formation and, consequently, increase naphthyl localized emission, but also cause strong nuclear rearrangements in the cyclam structure which affect excimer formation between the peripheral naphthyl units of the dendrimers. At variance with dendrimer **1** and **2**, no further change in the emission spectrum was observed after addition of two equivalents of protons per dendrimer, i.e., after formation of a $\mathbf{3}(2\text{H}^+)$ species. These results suggest that the two cyclam units of **3** do not behave independently and that in the $\mathbf{3}(2\text{H}^+)$ species the two protons are likely shared by the two cyclam units in a sandwich-type structure.

Dendrimer **3** ability to coordinate Zn^{2+} in acetonitrile/dichloromethane 1:1 (v/v) solution has been carefully investigated [17d]. Upon titration with $\text{Zn}(\text{CF}_3\text{SO}_3)_2$ no change was observed in the absorption spectrum, whereas strong changes were observed in the emission spectrum. Such changes, qualitatively similar to those caused by protonation, indicate that a 1:1 complex, $[\text{Zn}(\mathbf{3})]^{2+}$, is first formed and then replaced by a 2:1 species, $[\text{Zn}_2(\mathbf{3})]^{4+}$ ($\log \beta_{1:1} = 9.7$ and $\log \beta_{2:1} = 16.1$ for these two species, respectively). In the 1:1 complex $[\text{Zn}(\mathbf{3})]^{2+}$, the metal ion is likely sandwiched between the two cyclam units. As previously observed in the case of dendritic ligands **1** and **2**, apparently, the dendrimer branches favor coordination of cyclam units to metal ions with respect to solvent molecules and counter ions. Furthermore, the experimental observation that in going from $[\text{Zn}(\mathbf{3})]^{2+}$ to $[\text{Zn}_2(\mathbf{3})]^{4+}$ the intensity of the excimer band does not change suggests that in these sandwich-type complexes the dendrimer branches extend outward and maintain the same structure in both species.

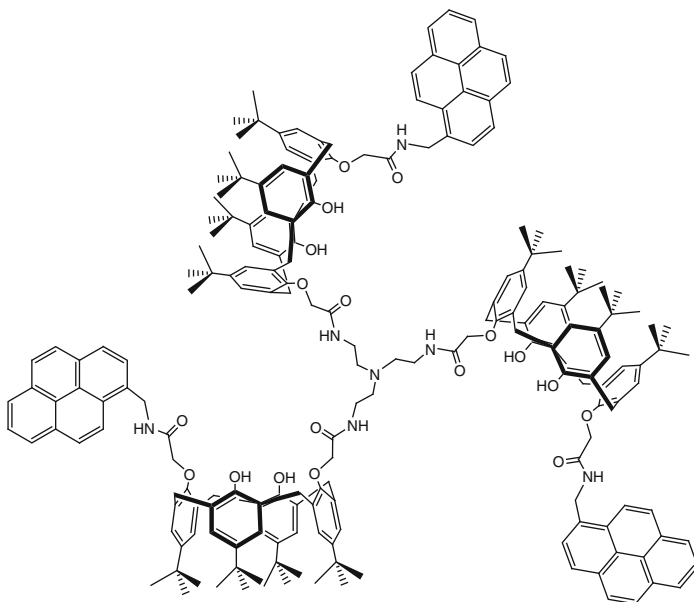


3

2.1.2 Dendrimers with Multiple Amide Coordinating Units

A first generation poly(amido amine) dendrimer has been functionalized with three calyx[4]arenes, each carrying a pyrene fluorophore (**4**) [30]. In acetonitrile solution the emission spectrum shows both the monomer and the excimer emission band, typical of the pyrene chromophore. Upon addition of Al^{3+} as perchlorate salt, a decrease in the excimer emission and a consequent revival of the monomer emission is observed. This can be interpreted as a change in the dendrimer structure and flexibility upon metal ion complexation that inhibits close proximity of pyrenyl units, thus decreasing the excimer formation probability. ^1H NMR studies of dendrimer **4** revealed marked differences upon Al^{3+} addition only in the chemical shifts of the CH_2 protons linked to the central amine group, demonstrating that the metal ion is coordinated by the dendrimer core. MALDI-TOF experiments gave evidence of a 1:1 complex. Similar results have been obtained for In^{3+} , while other cations such as Ag^+ , Cd^{2+} , and Zn^{2+} do not affect the luminescence properties of

dendrimer **4**. This example is very interesting, since the core of the dendrimer contains metal ion coordinating units, while the appended calix[4]arene can bind the counteranion with a synergic effect.

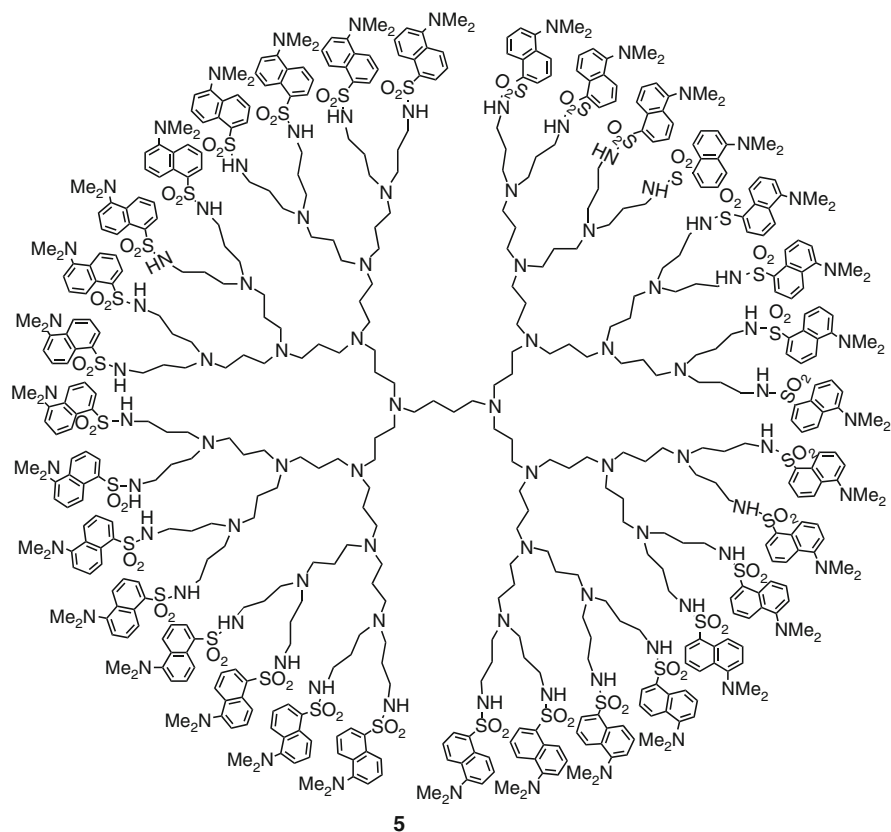


4

2.2 Luminescent Dendrimers Hosting Metal Ion Quenchers

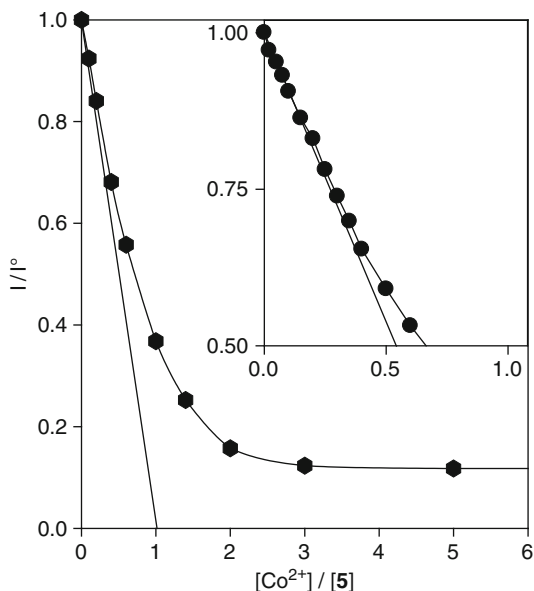
2.2.1 Dendrimers with Multiple Amine Coordinating Units

The dendrimers of the poly(propylene amine) family can be easily functionalized in the periphery with luminescent units. Each dendrimer nD , where the generation number n goes from 1 to 5, comprises $2^{(n+1)}$ dansyl functions in the periphery and $2^{(n+1)}-2$ tertiary amine units in the interior. Compound **5** represents the fourth generation dendrimer 4D containing 30 tertiary amine units and 32 dansyl functions. The dansyl units behave independently from one another so that the dendrimers display light absorption and emission properties characteristic of dansyl, i.e., intense absorption bands in the near UV spectral region ($\lambda_{\max} = 252$ and 339 nm; $\epsilon_{\max} \approx 12,000$ and $3,900 \text{ L mol}^{-1} \text{ cm}^{-1}$, respectively, for each dansyl unit) and a strong fluorescence band in the visible region ($\lambda_{\max} = 500$ nm; $\Phi_{\text{em}} = 0.46$, $\tau = 16$ ns) [31].



Because of the presence of the aliphatic amine in their interior these dendrimers can be used as ligands for transition metal ions. The interaction with Co^{2+} ions (as nitrate salt) has been carefully studied [32]. For comparison purposes, the behavior of a monodansyl reference compound has also been investigated. The results obtained have shown that: (1) the absorption and fluorescence spectra of a monodansyl reference compound are not affected by addition of Co^{2+} ions; (2) in the case of dendrimers, the absorption spectra are unaffected, but a strong quenching of the fluorescence of the peripheral dansyl units is observed; (3) the fluorescence quenching takes place by a static mechanism involving coordination of metal ions in the interior of the dendrimers; (4) metal ion coordination by the dendrimers is a fully reversible process; (5) a strong amplification of the fluorescence quenching signal is observed with increasing dendrimer generation. When a Co^{2+} ion enters dendrimer **5**, the fluorescence of all the 32 dansyl units is quenched, with a 32 time increase in sensitivity with respect to a normal dansyl sensor (Fig. 6). This concept is illustrated in Fig. 2.

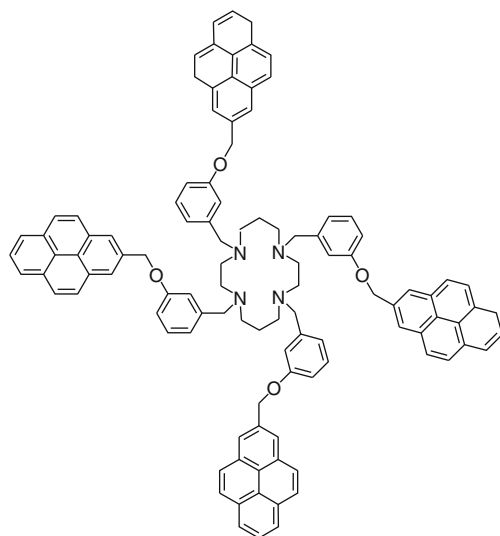
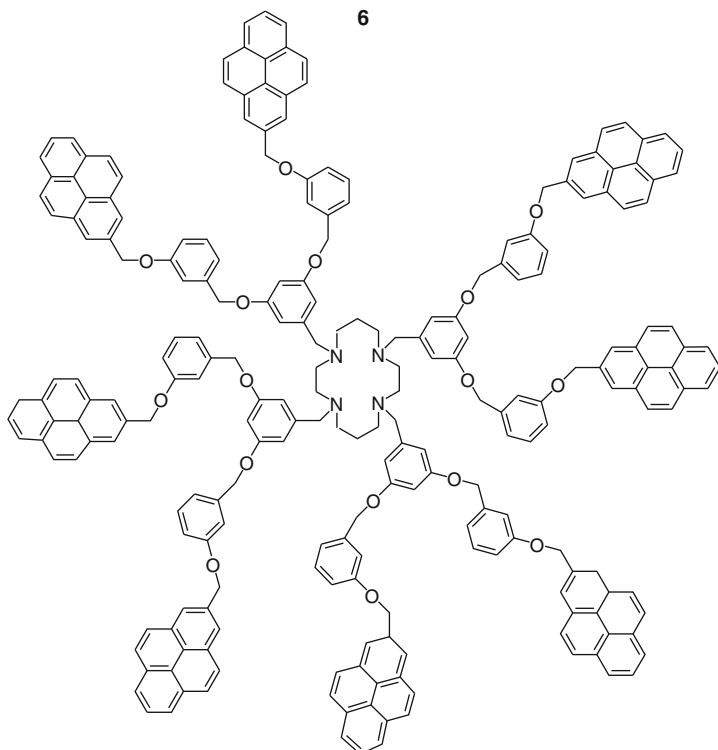
Fig. 6 Effect of addition of Co^{2+} ions on the fluorescence intensity of a solution of dendrimer **5** (4.6×10^{-6} M) in $\text{CH}_3\text{CN}/\text{CH}_2\text{Cl}_2$ 5:1 (v/v). *Inset* shows the results of a detailed investigation at low Co^{2+} concentration



2.2.2 Dendrimers with a Cyclam Coordinating Core

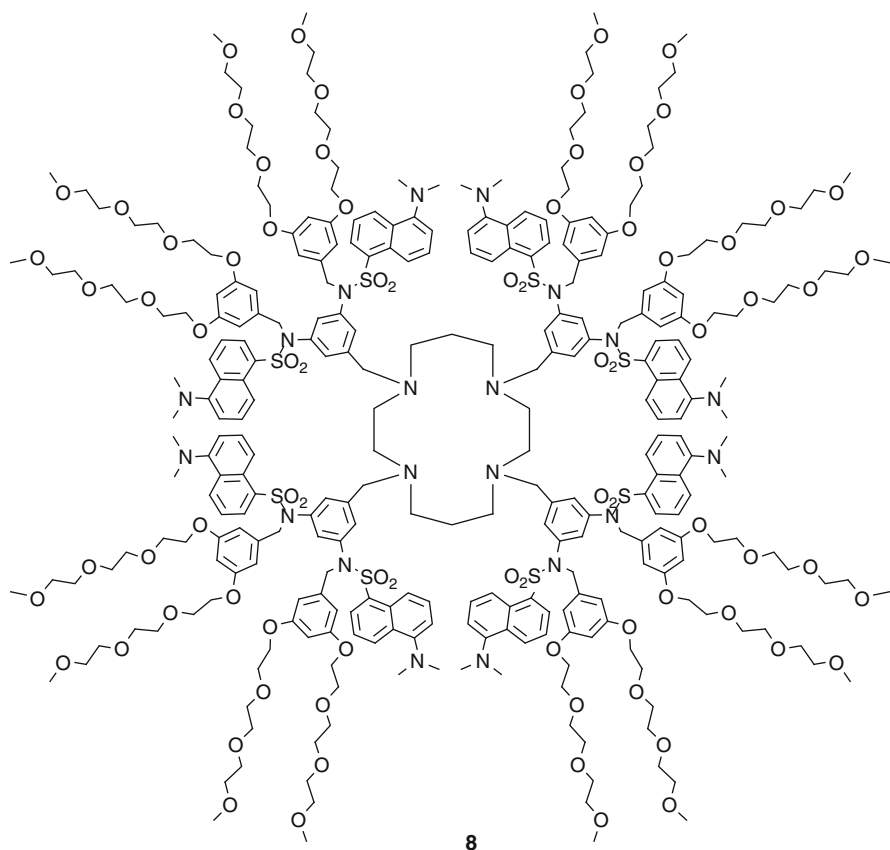
The above discussed dendrimers **1** and **2** containing a cyclam core and 8 or 16 naphthyl units at the periphery, respectively, can also efficiently bind metal ion quenchers, such as Ni^{2+} , Co^{2+} , and Cu^{2+} . However, changes in the luminescence properties are completely different from those reported before upon addition of Zn^{2+} because the dendritic naphthyl units can be involved in photoinduced energy and/or electron transfer processes with the presently investigated metal ions.

Upon titration of dendrimer **2** in acetonitrile/dichloromethane 1:1 solution with nitrate salts of Ni^{2+} , Co^{2+} , and Cu^{2+} , the intensity and shape of the naphthyl luminescence bands are strongly affected [17a]. Complexation with these metal ions, in contrast to the previously investigated Zn^{2+} complexes, has a double-faced effect: on the one hand, it can increase naphthyl localized emission and suppress exciplex emission, engaging nitrogen lone pairs of cyclam; on the other, it can quench this fluorescence by offering additional deactivation pathways to the naphthyl singlet excited state via energy or electron transfer processes. Complexation with Cu^{2+} causes not only changes in the relative intensities of the fluorescence bands but also the appearance in the absorption spectrum of a new and broad tail in the 300–400 nm region, assigned to ligand-to-metal charge-transfer (LMCT) transitions (a similar absorption band was also observed in the case of mere cyclam). Analysis of the titration curves showed clear evidence of formation not only of 1:1 species but also 1:2 metal to ligand species.

**6****7**

Dendrimers **6** and **7** contain a cyclam core and 4 or 8 pyrenyl units at the periphery [17c]. In dichloromethane solution they show the expected absorption spectra on the basis of their model compounds. As far as emission spectra are concerned, stronger excimer emission intensities are observed compared to the corresponding dendrons at similar concentrations. Upon addition of Cu^{2+} , as triflate salt, dramatic fluorescence changes are observed, indicative of the formation of a 1:1 complex with a binding constant much lower than that observed for the parent cyclam, indicating that a steric barrier is imposed by the dendrons. Along the same trend, a higher complexation constant is observed for Cu^{2+} complexed by **6** than by **7**. The strong pyrenyl fluorescence decrease observed upon addition of Cu^{2+} is explained in terms of photoinduced electron transfer. At variance with the previously reported examples, however, this process is not reversible and leads to decomposition products, so that the present dendrimers are not good candidates for ion sensing.

In the case of dendrimer **3** containing two cyclam units linked by a benzyl spacer as a core, titration with $\text{Cu}(\text{CF}_3\text{SO}_3)_2$ leads to dramatic changes both in absorption and emission spectra [17d]. The absorption spectrum showed the appearance of a broad tail in the 300–400 nm region assigned to LMCT transitions as for dendrimer **2**. The absorbance values increase almost linearly up to the addition of 2 equivalents of metal ion per dendrimer. Therefore, upon addition of $\text{Cu}(\text{CF}_3\text{SO}_3)_2$ to **3**, both the cyclam units of the dendrimer coordinate a Cu^{2+} ion ($\log \beta_{2:1} = 11.9$). More details were obtained from the changes observed in the emission spectrum, that can be summarized as follows: (1) the intensity of the naphthyl band is almost constant up to the addition of one equivalent of metal ion and then decreases slightly; (2) the intensity of the exciplex band decreases linearly and disappears after addition of two equivalents of metal ions; (3) the intensity of the excimer band increases at the beginning of the titration, and reaches a maximum value after addition of one equivalent of metal ion and then decreases. At variance with the case of H^+ or Zn^{2+} , the decrease in the intensity of the exciplex emission, caused by the engagement of the cyclam N atoms by protons or metal ions, is not accompanied by an increase in the intensity of the naphthyl localized emission. This result can be easily rationalized considering that coordination of Cu^{2+} , while preventing deactivation of the excited naphthyl units via exciplex formation, introduces another deactivation channel related to the presence of the low energy LMCT state. Furthermore, analysis of the emission spectral changes upon addition of Cu^{2+} evidences the formation of a 1:1 complex, $[\text{Cu}(\mathbf{3})]^{2+}$, then replaced by a 2:1 species, $[\text{Cu}_2(\mathbf{3})]^{4+}$.



Another example of this class is represented by dendrimer **8** in which the cyclam core is appended with four benzyl substituents that carry, in the 3 and 5 positions, a dansyl amide derivative in which the amide hydrogen is replaced by a benzyl unit that carries, in the 3 and 5 position, a oligoethylene glycol chain [17b]. All together, the dendrimer contains 16 potentially luminescent moieties (8 dansyl- and 8 dimethoxybenzene-type units) and three distinct types of multivalent sites that, in principle, can be protonated or coordinated to metal ions (the cyclam nitrogens, the amine moieties of the 8 dansyl units, and the 16 oligoethylene glycol chains). The absorption spectrum of dendrimer **8** in acetonitrile is that expected on the basis of the model compounds apart from a small red-shift of the lowest energy dansyl absorption band, indicating that in the dendrimer the dansyl unit indeed feels a less polar environment because of the oligoethylene glycol chains. As far as the emission spectra are concerned, the dansyl units maintain their strong fluorescence, slightly red shifted ($\lambda_{\max} = 532$ nm, $\Phi = 0.27$, and $\tau = 15$ ns, compared to the

dansyl model compound under the same experimental conditions: $\lambda_{\max} = 522$ nm, $\Phi = 0.30$, and $\tau = 13$ ns), and no dimethoxybenzene emission is present due to a quenching process by the nearby dansyl units. Double protonation of the cyclam ring takes place before protonation of the dansyl units, and the oligoethylene glycol chains do not interfere with protonation of the cyclam core and the dansyl units in the ground state, but affect the luminescence of the protonated dansyl units by reversible proton transfer.

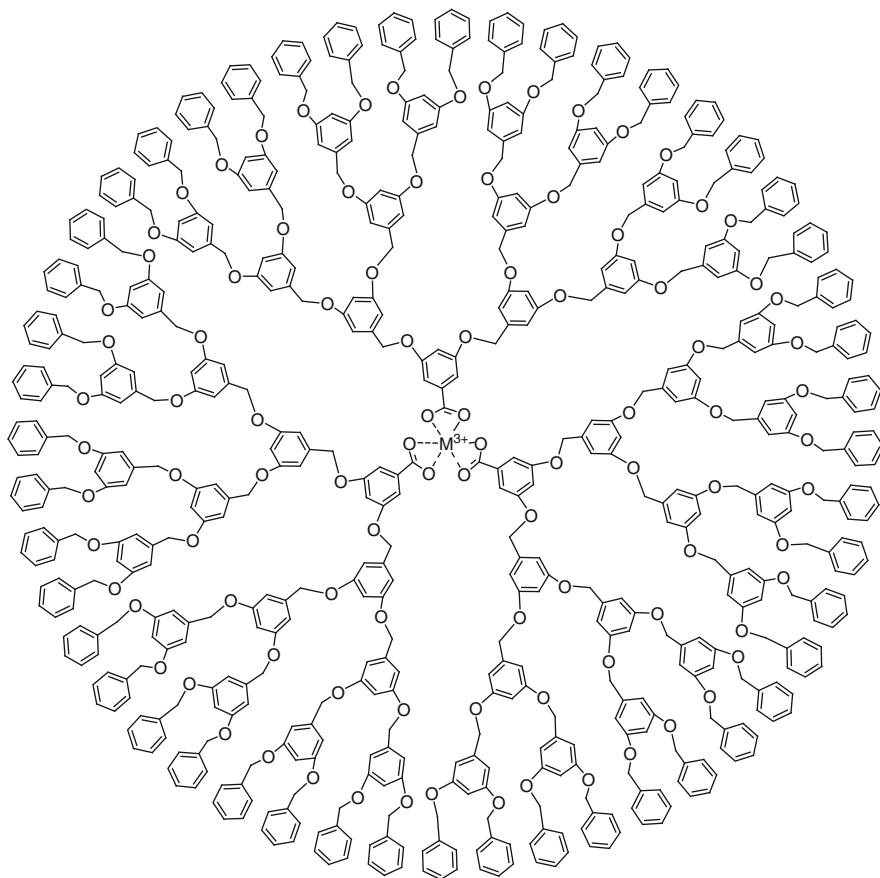
As to metal ion coordination, dendrimer **8** possesses three distinct types of multivalent, potentially coordinating sites, as previously observed: the cyclam core, the 16 oligoethylene glycol chains appended in the periphery, and the 8 amine moieties of the dansyl units. Upon complexation of Co^{2+} , Ni^{2+} , and Cu^{2+} , three quenching mechanisms are active, namely (1) an effect of the positive charge of the metal ion on the dansyl emission transition moment, (2) an energy transfer quenching since the investigated metal ions have low-lying excited states, and (3) an electron transfer quenching for metal ions that can be easily reduced, as in the case of Cu^{2+} . Changes in absorption and emission spectra are quite complex, but some general conclusions can be drawn: (1) the first equivalent of metal ion is coordinated by the cyclam core; (2) coordination of metal ions by the dansyl units follows at high metal ion concentrations. The interaction of the resulting cyclam complex with the appended dansyl units depends on the nature of the metal ion and the counter ion. For example, in the case of Cu^{2+} coordination, a strong quenching of the dansyl excited state takes place and it is related to the occurrence of an electron transfer process. This example demonstrates that dendrimers may exhibit complex functionality resulting from the integration of the specific properties of their component units. Therefore, such design is interesting for understanding relations between complex structure and multiple functionality.

3 Luminescent Dendrimers Hosting Luminescent Metal Ions

Lanthanide ions are known to show very long lived luminescence, which is quite a useful property for several applications (e.g., sensors [33], imaging [34], and photonics) [35]. Because of the forbidden nature of their electronic transitions, however, lanthanide ions exhibit very weak absorptions bands, which is a severe drawback for applications based on luminescence. In order to overcome this difficulty, lanthanide ions are usually coordinated to ligands containing organic chromophores whose excitation, followed by energy transfer, causes the sensitized luminescence of the metal ion (antenna effect) [36]. Such a process can involve either direct energy transfer from the singlet excited state of the chromophoric group with quenching of the chromophore fluorescence [37], or, most frequently, via $S_1 \rightarrow T_1$ intersystem crossing followed by energy transfer from the T_1 excited state of the chromophoric unit to the lanthanide ion [33].

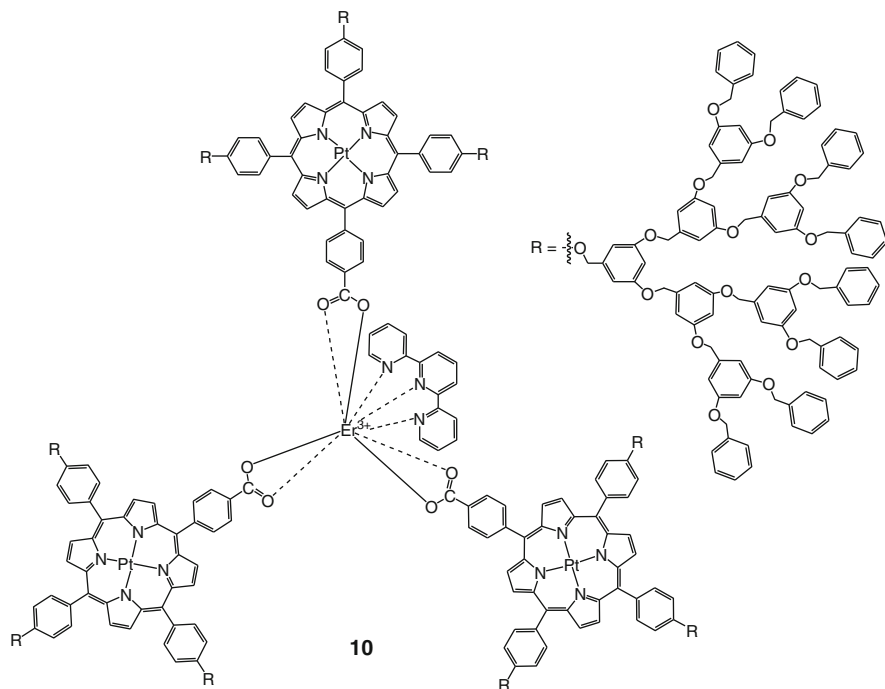
3.1 Dendrons with a Coordinating Focal Point

Many examples of this class of compounds have been reported [13a–c]. The first one was constituted by Fréchet-type dendrons bearing a 3,5-dioxybenzoate focal point. It can self-assemble around Er^{3+} , Tb^{3+} , or Eu^{3+} ions leading to the formation of dendrimer **9** [38]. Experiments carried out in toluene solution showed that UV excitation of the chromophoric groups contained in the branches caused the sensitized emission of the lanthanide ion, presumably by an energy-transfer Förster mechanism. The much lower sensitization effect found for Eu^{3+} compared with Tb^{3+} was ascribed to a weaker spectral overlap, but it could be related to the fact that Eu^{3+} can quench the donor excited state by electron transfer [39].

**9**

In a more recent paper, dendrons with a 3,4-dioxybenzoate focal point were used as ligands for Tb^{3+} , apparently with improved luminescence yield [40]. The discussion

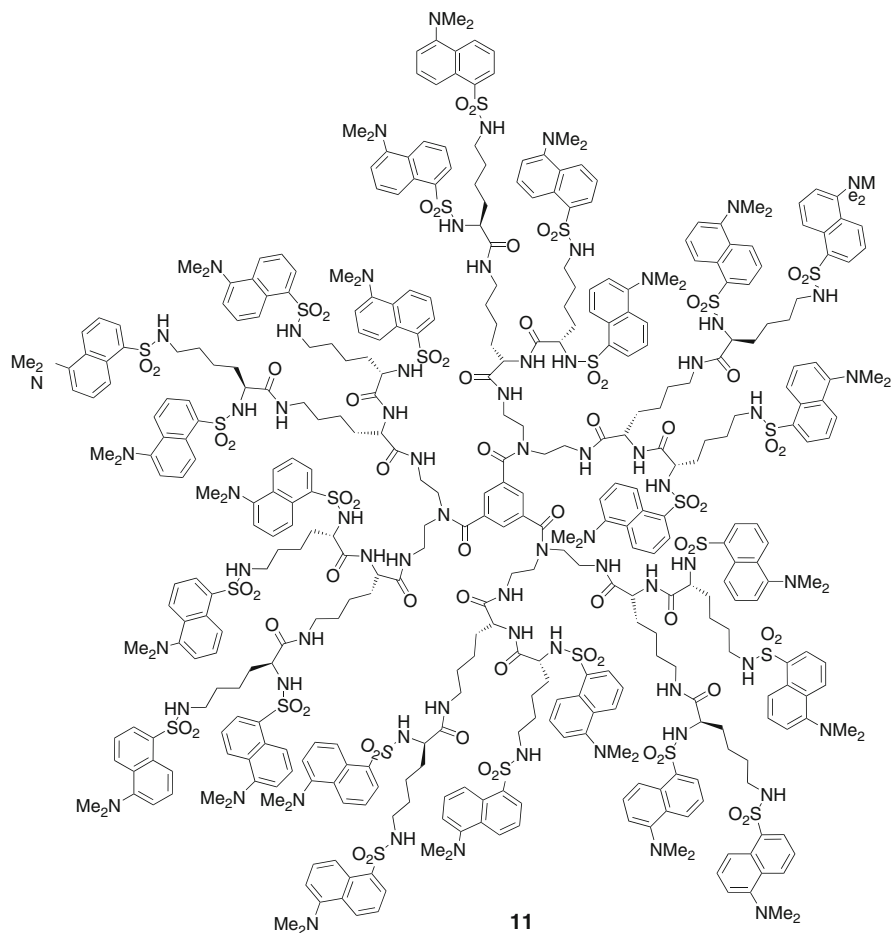
of the results obtained, however, is unclear. For example, comparison with the spectra of the component units is neglected and the reported relative intensities apparently refer to excitation at different wavelengths.



Another example of this class of compounds is constituted by a dendron with carboxylate focal point and a Pt porphyrin substituted with three Fréchet type dendrons of generations 1–3 (dendron **10** represents the third generation) [13a]. These dendrons are able to coordinate Er^{3+} ions and form a stable complex containing a lanthanide ion surrounded by three dendrons and one 2,2':6',2''-terpyridine (tpy) ligand. These complexes have been studied both in tetrahydrofuran (THF) solution and in thin film. The NIR emission of Er^{3+} at 1,530 nm is sensitized by the Pt porphyrin and not from the Fréchet dendrons. This result is in contrast to the fact that in the case of dendrons without the coordinated metal ion, an efficient energy transfer from the dimethoxybenzene units to the Pt porphyrin is reported by the authors. Coming back to the Er^{3+} complexes, the sensitized Er^{3+} emission intensity increases as a function of generation: this effect is much larger (ca. ten times from generation 1 to 3) in thin film than in THF solution (ca. four times from generation 1 to 3). This has been attributed to an increase in the site-isolation efficiency upon increasing dendron generation and is consistent with the observed increase in the lifetime of the luminescent excited state of the lanthanide ion in going from generation 1 to 3 ($\tau = 0.98, 1.64, \text{ and } 6.85 \mu\text{s}$ in going from generation 1 to 3).

3.2 Dendrimers with Amide Coordinating Units

Amide groups are known to be good ligands for lanthanide ions. Dendrimer **11**, which is based on a benzene core branched in the 1, 3, and 5 positions, contains 18 amide groups in its branches and 24 chromophoric dansyl units in the periphery. As we have seen above, the dansyl units show strong absorption bands in the near UV spectral region and an intense fluorescence band in the visible region. In acetonitrile/dichloromethane (5:1 v/v) solutions, the absorption spectrum and the fluorescence properties of the dendrimer are those expected for a species containing 24 noninteracting dansyl units [41].



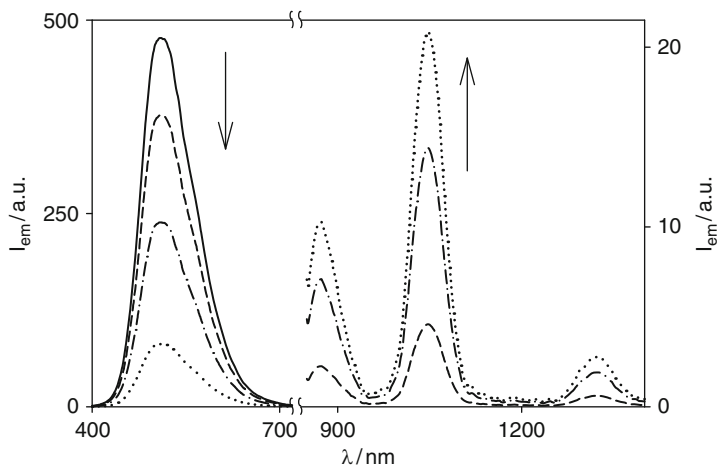


Fig. 7 Spectral changes observed upon titration of a 4.2×10^{-6} M solution of dendrimer **11** by $\text{Nd}(\text{CF}_3\text{SO}_3)_3$. *Left-hand side spectra* refer to the quenching of the fluorescence of the dansyl units in the visible region and *right-hand side spectra* to the sensitization of the NIR luminescence of Nd^{3+}

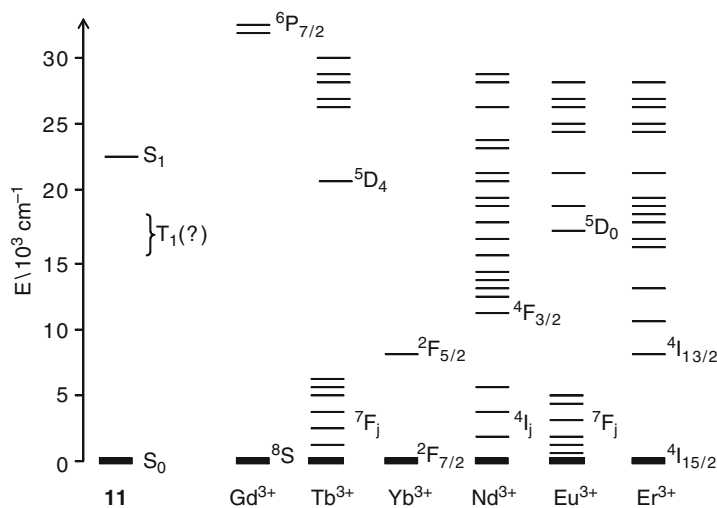
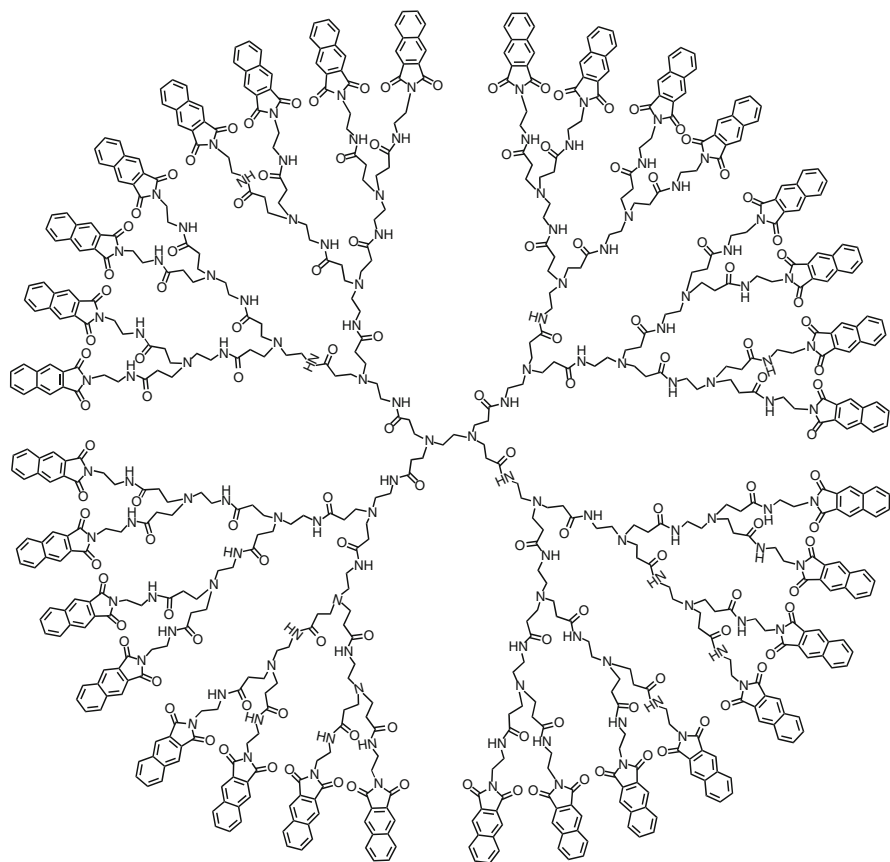


Fig. 8 Energy level diagrams for the dansyl units of dendrimer **11** and the investigated lanthanide ions. The position of the triplet excited state of **11** is uncertain because no phosphorescence can be observed

Addition of lanthanide ions to dendrimer solutions showed that: (a) the absorption spectrum of the dendrimer is almost unaffected, (b) the fluorescence of the dansyl units is quenched; (c) the quenching effect is very large for Nd^{3+} (Fig. 7) and Eu^{3+} , moderate for Er^{3+} and Yb^{3+} , small for Tb^{3+} , and very small for Gd^{3+} ; (d) in the case of Nd^{3+} (Fig. 7), Er^{3+} , and Yb^{3+} quenching of the dansyl fluorescence is accompanied by the sensitized near-infrared emission of the lanthanide ion [42].

Interpretation of the results obtained on the basis of energy levels (Fig. 8) and redox potentials of the dendrimer and of the metal ions have led to the following conclusions: (1) at low metal ion concentrations, each dendrimer hosts only one metal ion; (2) when the hosted metal ion is Nd^{3+} or Eu^{3+} , all the 24 dansyl unit of the dendrimer are quenched with unitary efficiency; (3) quenching by Nd^{3+} and Er^{3+} takes place by direct energy transfer from the fluorescent (S_1) excited state of dansyl to a manifold of Nd^{3+} energy levels, followed by sensitized near-infrared emission from the metal ion ($\lambda_{\text{max}} = 1,064$ nm for Nd^{3+} and $\lambda_{\text{max}} = 1,525$ for Er^{3+}); (4) quenching by Eu^{3+} does not lead to any sensitized emission since the lowest excited state of the system is an electron-transfer excited state; upon protonation of the dansyl units, however, the electron-transfer excited state moves to very high energy and at 77 K a sensitized Eu^{3+} emission is observed, which originates from the quenching of the T_1 excited state of the protonated dansyl units; (v) in the case of Yb^{3+} , the sensitization of the near-infrared metal-centered emission occurs via the intermediate formation of an electron-transfer excited state; at 77 K the electron-transfer excited state moves to higher energy, thus preventing the population of the Yb^{3+} emitting excited state; (vi) the small quenching effect observed for Tb^{3+} is partly caused by a direct energy transfer from the fluorescent (S_1) excited state of dansyl; on protonation of the dansyl units, a strong Tb^{3+} sensitized emission is observed at 77 K, originating from the T_1 excited state of the protonated dansyl units; (vii) the very small quenching effect observed for Gd^{3+} is assigned to either induced intersystem crossing or, more likely, to charge perturbation of the S_1 dansyl excited state.

Another interesting example of dendrimer containing multiple amide coordinating units for lanthanide ions is a third generation poly(amido amine) dendrimer (**12**) containing 60 amide units in its interior and 32 luminescent 2,3-naphthalimide groups at the periphery [43]. Upon titration of dendrimer **12** in dimethylsulfoxide (DMSO) solution with Eu^{3+} , slow changes in the emission spectra were obtained. No fragmentation of the naphthalimide groups or the aliphatic structure takes place, as demonstrated by ^1H NMR and ^{13}C NMR. Dendrimer **12** is able to coordinate up to 8 Eu^{3+} ions as an average, over a period of 7 days. The slow coordination process has been ascribed by the authors to the internal location of the amide binding units. A relatively low sensitized emission quantum yield of Eu^{3+} ($\Phi_{\text{em}} = 0.06\%$) was obtained, but this was compensated for by the high molar absorption coefficient of dendrimer **12**, so that Eu^{3+} red emission could be observed by naked eye under a conventional UV lamp for a 8.7×10^{-5} M dendrimer solution in DMSO containing 8 equivalents of lanthanide ions.



12

3.3 Dendrimers with a Cyclam Coordinating Core

Complexation of dendritic ligands **1** and **2** with lanthanide ions (Nd^{3+} , Eu^{3+} , Gd^{3+} , Tb^{3+} , Dy^{3+}) [17f] leads to results qualitatively similar to those obtained upon Zn^{2+} complexation (see above): an increase in the monomer naphthalene emission band at 337 nm and a complete disappearance of the exciplex band at 480 nm. However, the complex stoichiometry is different. Emission data were best fitted considering the formation of 1:3 and 1:2 (metal/ligand) complexes ($\log \beta_{1:2} = 14.1$ and $\log \beta_{1:3} = 20.0$) in the case of **1** and a 1:3 (metal/ligand) complex ($\log \beta_{1:3} = 20.3$) for compound **2**. Therefore, at low metal ion concentration, only the $[\text{M}(\mathbf{2})_3]^{3+}$ species is present, as also demonstrated by NMR titration. It is likely that in this complex

not all the 12 nitrogens of the three cyclam cores are engaged in metal ion coordination. However, upon metal coordination, the exciplex emission band completely disappears, as is observed upon acid titration. Clearly, as is also shown by NMR results, the presence of the 3+ ion is “felt” by all the nitrogens of the three cyclam moieties, thereby raising the energy of the exciplex excited state above that of the naphthyl-based one. For all the lanthanide complexes of **1** and **2**, no sensitized emission from the lanthanide ion was observed. Therefore, energy transfer from either the S_1 or T_1 excited state of the naphthyl units of **1** and **2** to the lanthanide ion is inefficient. By contrast, efficient energy transfer from naphthalene-like chromophores to Eu^{3+} has been reported in the case in which naphthalene is linked through an amide or carboxylate bond to the lanthanide [44]. Apparently, the nature of the coordination sphere plays an important role in energy transfer efficiency.

To overcome this problem a supramolecular approach has been followed [6a]. It was known that complexes of Ru^{2+} containing 2,2'-bipyridine (bpy) and cyanide ligands, i.e., $[\text{Ru}(\text{bpy})_2(\text{CN})_2]$ and $[\text{Ru}(\text{bpy})(\text{CN})_4]^{2-}$, are luminescent and can play the role of ligands giving rise to supercomplexes [45, 46]. Titration of an acetonitrile:dichloromethane 1:1 (v/v) solution of $[\text{Ru}(\text{bpy})_2(\text{CN})_2]$ with Nd^{3+} causes changes in the absorption spectrum and quenching of the Ru^{2+} complex emission, accompanied by sensitized Nd^{3+} emission, demonstrating the ability of $[\text{Ru}(\text{bpy})_2(\text{CN})_2]$ to complex the lanthanide metal ion. Titration of a 1:1 mixture of dendrimer **2** and $[\text{Ru}(\text{bpy})_2(\text{CN})_2]$ in acetonitrile:dichloromethane 1:1 (v/v) with $\text{Nd}(\text{CF}_3\text{SO}_3)_3$ brings about changes in the absorption and emission spectra. The lowest energy absorption band is blue-shifted, as observed for the titration of $[\text{Ru}(\text{bpy})_2(\text{CN})_2]$ in the absence of dendrimer. Upon excitation at 260 nm, where most of the light is absorbed by dendrimer **2**, the intensity of the naphthyl monomer emission at 337 nm does not show a monotonous increase, as observed in the absence of the $[\text{Ru}(\text{bpy})_2(\text{CN})_2]$ complex, reaches a maximum at 0.5 equivalents, and then decreases up to about 1.0 equivalent of Nd^{3+} to rise again for higher metal ion concentration. The emission intensity at 1.0 equivalent is lower than that observed in the absence of $[\text{Ru}(\text{bpy})_2(\text{CN})_2]$. These results show that a three-component system $\{\mathbf{2}\cdot\text{Nd}^{3+}\cdot[\text{Ru}(\text{bpy})_2(\text{CN})_2]\}$ (Fig. 9) is formed in which the dendrimer emission is quenched. The three-component system can be disassembled by addition of an excess of each component or cyclam. The main photophysical processes of the $\{\mathbf{2}\cdot\text{Nd}^{3+}\cdot[\text{Ru}(\text{bpy})_2(\text{CN})_2]\}$ adduct are summarized in Fig. 6, which shows the energy levels of the three components. In the two-component dendrimer- Nd^{3+} system, energy transfer from either the lowest singlet (S_1) or triplet (T_1) excited state of the naphthyl units of the dendrimer to the lanthanide ion does not occur. Sensitization of the Nd^{3+} emission upon dendrimer excitation in the three-component system is mediated by the $[\text{Ru}(\text{bpy})_2(\text{CN})_2]$ component. Comparison between the emission quantum yield of $[\text{Ru}(\text{bpy})_2(\text{CN})_2]$ upon excitation at 260 nm (dendrimer absorption) and 450 nm ($[\text{Ru}(\text{bpy})_2(\text{CN})_2]$ absorption) has allowed to estimate that the energy transfer efficiency from the S_1 excited state of the naphthyl groups to the $^1\text{MLCT}$ excited state of $[\text{Ru}(\text{bpy})_2(\text{CN})_2]$ is about 60% (Fig. 10). The energy transfer efficiency from the $^3\text{MLCT}$ excited state of

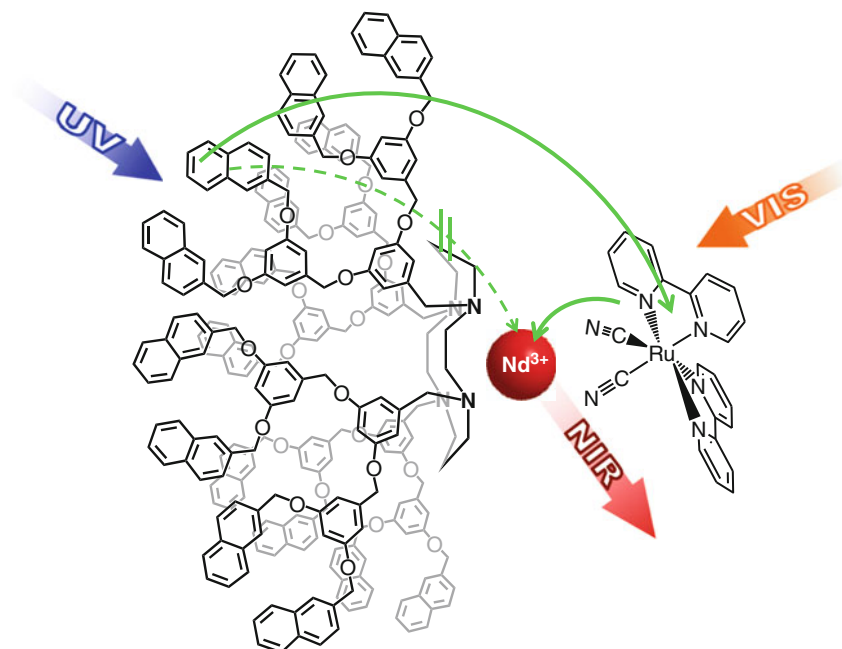


Fig. 9 Schematic representation of the self-assembled $\{2\bullet\text{Nd}^{3+}\bullet[\text{Ru}(\text{bpy})_2(\text{CN})_2]\}$. Curved arrows represent photoinduced energy transfer processes. For more details, see text

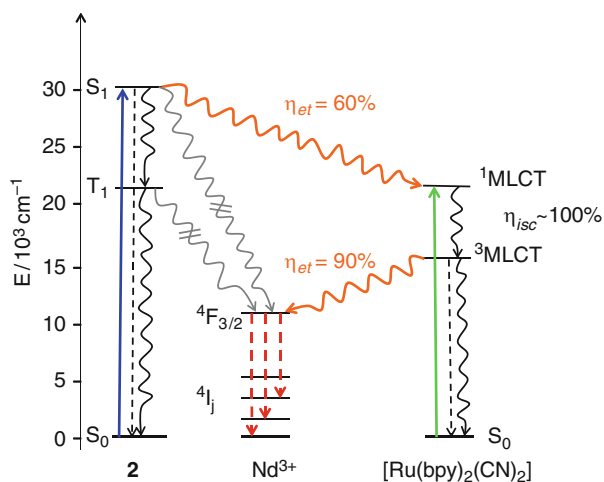


Fig. 10 Energy level diagram showing the excited states involved in the main photophysical processes (excitation: *solid lines*; radiative deactivation: *dashed lines*; nonradiative deactivation processes: *wavy lines*) of the $\{2\bullet\text{Nd}^{3+}\bullet[\text{Ru}(\text{bpy})_2(\text{CN})_2]\}$ three-component system. For the sake of clarity, naphthyl excimer energy level has been omitted

[Ru(bpy)₂(CN)₂] to Nd³⁺ can be assumed to be equal to the efficiency of the quenching of the [Ru(bpy)₂(CN)₂] emission (ca. 90%) because quenching by electron transfer can be ruled out in view of the Nd³⁺ redox properties. No evidence of energy transfer in the adduct from the naphthyl-localized *T*₁ excited state of the dendrimer to the lowest ³MLCT state of [Ru(bpy)₂(CN)₂] has been found since no change in the *T*₁ lifetime at 77 K has been observed.

The three components of the self-assembled structure have complementary properties, so that new functions emerge from their assembly. Dendrimer **2** has a very high molar absorption coefficient in the UV spectral region because of 12 dimethoxybenzene and 16 naphthyl units, but it is unable to sensitize the emission of a Nd³⁺ ion placed in its cyclam core. The [Ru(bpy)₂(CN)₂] complex can coordinate (by the cyanide ligands) and sensitize the emission of Nd³⁺ ions. Self-assembly of the three species leads to a quite unusual Nd³⁺ complex which exploits a dendrimer and a Ru²⁺ complex as ligands. Such a system behaves as an antenna that can harvest UV to VIS light absorbed by both the Ru²⁺ complex and the dendrimer and emit in the NIR region with line-like bands. In principle, the emission wavelength can be tuned by replacing Nd³⁺ with other lanthanide ions possessing low-lying excited states.

4 Conclusions

The above discussed examples show that the design of dendrimers capable of playing the role of ligands for metal ions can lead to novel classes of metal complexes where the properties of the dendrimer and metal ion moieties can be profitably combined to obtain interesting and useful light-related functions that reflect the occurrence of intercomponent energy and electron transfer processes. It is likely that improving the design of these types of dendrimers will lead to coordination compounds capable of performing even more sophisticated functions, such as energy up-conversion, electrochemiluminescence, and light emitting diodes (LED), besides those discussed in this paper.

References

1. (a) Vögtle F, Richardt G, Werner N (2009) Dendrimer chemistry. Wiley-VCH, Chichester
(b) Newkome GR, Vögtle F (2001) Dendrimers and dendrons. Wiley-VCH, Weinheim
(c) Fréchet MJM, Tomalia DA (2001) Dendrimers and other dendritic polymers. Wiley, Chichester
2. For some reviews, see: (a) Majoral J-P (2007) Influence of cationic phosphorus dendrimers on the surfactant-induced synthesis of mesostructured nanoporous silica. *New J Chem* 31:1259–1263 (b) Puntoriero F, Nastasi F, Cavazzini M et al (2007) Coupling synthetic antenna and electron donor species: a tetranuclear mixed-metal Os(II)–Ru(II) dendrimer containing six phenothiazine donor subunits at the periphery. *Coord Chem Rev*

- 251:536–545 (c) Méry D, Astruc D (2006) Dendritic catalysis: major concepts and recent progress. *Coord Chem Rev* 250:1965–1979 (d) Astruc D (2006) Dendrimers and nanoscience. *C R Chimie* 6(6–8) (e) Tomalia DA, Fréchet JMJ (eds) (2005) Special issue: dendrimers and dendritic polymers. In: *Prog Polym Sci* 30(3–4) (f) Scott RWJ, Wilson OM, Crooks RM (2005) Synthesis, characterization, and applications of dendrimer-encapsulated nanoparticles. *J Phys Chem B* 109:692–704 (g) Chase PA, Klein Gebbink RJM, van Koten G (2004). Where organometallics and dendrimers merge: the incorporation of organometallic species into dendritic molecules. *J Organomet Chem* 689:4016–4054 (h) Ong W, Gomez-Kaifer M, Kaifer AE (2004) Dendrimers as guests in molecular recognition phenomena. *Chem Commun* 15:1677–1683 (i) Ballauff M, Likos CN (2004) Dendrimers in solution: insight from theory and simulation. *Angew Chem Int Ed* 43:2998–3020 (l) Caminade A-M, Majoral J-P (2004) Nanomaterials based on phosphorus dendrimers. *Acc Chem Res* 37:341–348
3. (a) Hwang S-H, Shreiner CD, Moorefield CN et al (2007) Recent progress and applications for metal lodendrimers. *New J Chem* 31:1192–1217 (b) Ceroni P, Bergamini G, Marchioni F et al (2005) Luminescence as a tool to investigate dendrimer properties. *Prog Polym Sci* 30:453–473 (c) Balzani V, Ceroni P, Maestri M et al (2003) Luminescent dendrimers. Recent advances. *Top Curr Chem* 228:159–191 (d) Nierengarten JF, Armaroli N, Accorsiet G et al (2003) [60]Fullerene: a versatile photoactive core for dendrimer chemistry. *Chem Eur J* 9:36–41
 4. (a) Varnavski O, Yan X, Mongin O et al (2007) Strongly interacting organic conjugated dendrimers with enhanced two-photon absorption. *J Phys Chem C* 111:149–162 (b) Ahn TS, Thompson AL, Bharathi P et al (2006) Light-harvesting in carbonyl-terminated phenylacetylene dendrimers: the role of delocalized excited states and the scaling of light-harvesting efficiency with dendrimer size. *J Phys Chem B* 110:19810–19819 (c) Ortiz W, Krueger BP, Kleiman VD et al (2005) Energy transfer in the nanostar: the role of Coulombic coupling and dynamics. *J Phys Chem B* 109:11512–11519 (d) Thompson AL, Gaab KM, Xu J et al (2004) Variable electronic coupling in phenylacetylene dendrimers: the role of Förster, dexter, and charge–transfer interactions. *J Phys Chem A* 108:671–682
 5. (a) Wöll D, Uji-i H, Schnitzler T et al (2008) Radical polymerization tracked by single molecule spectroscopy. *Angew Chem Int Ed* 47:783–787 (b) Uji-i H, Melnikov SM, Deres A et al (2006) Visualizing spatial and temporal heterogeneity of single molecule rotational diffusion in a glassy polymer by defocused wide-field imaging. *Polymer* 47:2511–2518 (c) De Schryver FC, Vosch T, Cotlet M et al (2005) Energy dissipation in multichromophoric single dendrimers. *Acc Chem Res* 38:514–522 (d) Cotlet M, Masuo S, Luo G et al (2004) Probing conformational dynamics in single donor–acceptor synthetic molecules by means of photoinduced reversible electron transfer. *Proc Natl Acad Sci* 101:14343–14348
 6. For some recent examples see: (a) Giansante C, Ceroni P, Balzani V et al (2008) Self-assembly of a light-harvesting antenna formed by a dendrimer, a Ru^{II} complex, and a Nd^{III} ion. *Angew Chem Int Ed* 47:5422–5425 (b) Wang J-L, Yan J, Tang Z-M et al (2008) Gradient shape-persistent π -conjugated dendrimers for light-harvesting: synthesis, photophysical properties, and energy funneling. *J Am Chem Soc* 130:9952–9962 (c) Larsen J, Puntoriero F, Pascher T et al (2007) Extending the light-harvesting properties of transition-metal dendrimers. *ChemPhysChem* 8:2643–2651
 7. (a) Furuta P, Brooks J, Thompson ME et al (2003) Simultaneous light emission from a mixture of dendrimer encapsulated chromophores: a model for single-layer multichromophoric organic light-emitting diodes. *J Am Chem Soc* 125:13165–13172 (b) Hahn U, Gorka M, Vögtle F et al (2002) Light-harvesting dendrimers: efficient intra- and intermolecular energy-transfer processes in a species containing 65 chromophoric groups of four different types. *Angew Chem Int Ed* 41:3595–3598
 8. (a) Harpham MR, Suezer O, Ma C-Q et al (2009) Thiophene dendrimers as entangled photon sensor materials. *J Am Chem Soc* 131:973–979 (b) Xu M-H, Lin J, Hu Q-S et al (2002) Fluorescent sensors for the enantioselective recognition of mandelic acid: signal amplification by dendritic branching. *J Am Chem Soc* 124:14239–14246 (c) Pugh VJ, Hu QS, Zuo X et al

- (2001) Optically active BINOL core-based phenyleneethynylene dendrimers for the enantio-selective fluorescent recognition of amino alcohols. *J Org Chem* 66:6136–6140
9. For some recent examples, see: (a) Puntoriero F, Bergamini G, Ceroni P et al (2008) A fluorescent guest encapsulated by a photoreactive azobenzene dendrimer. *New J Chem* 32:401–406 (b) Ramakrishna G, Bhaskar A, Bauerle P et al (2008) Oligothiophene dendrimers as new building blocks for optical applications. *J Phys Chem A* 112:2018–2026 (c) Cao D, Dobis S, Gao C et al (2007) Optical switching and antenna effect of dendrimers with an anthracene core. *Chem Eur J* 13:9317–9323 (d) Li W-S, Kim KS, Jiang D-L et al (2006) Construction of segregated arrays of multiple donor and acceptor units using a dendritic scaffold: remarkable dendrimer effects on photoinduced charge separation. *J Am Chem Soc* 128:10527–10532 (e) Ahn T-S, Nantalaksakul A, Dasari RR et al (2006) Energy and charge transfer dynamics in fully decorated benzyl ether dendrimers and their disubstituted analogues. *J Phys Chem B* 110:24331–24339
 10. (a) Balzani V, Bergamini G, Marchioni F et al (2007) Electronic spectroscopy of metal complexes with dendritic ligands. *Coord Chem Rev* 251:525–535 (b) Ceroni P, Vicinelli V, Maestri M et al (2004) Luminescent dendrimers as ligands for metal ions. *J Organomet Chem* 689:4375–4383
 11. (a) Paulo PMR, Gronheid R, De Schryver FC et al (2003) Porphyrin–dendrimer assemblies studied by electronic absorption spectra and time-resolved fluorescence. *Macromolecules* 36:9135–9144 (b) Epperson JD, Ming LJ, Woosley BD et al (1999) NMR study of dendrimer structures using paramagnetic Cobalt(II) as a probe. *Inorg Chem* 38:4498–4502 (c) Ottaviani MF, Bossamann S, Turro NJ et al (1994) Characterization of starburst dendrimers by the EPR technique. 1. Copper complexes in water solution. *J Am Chem Soc* 116:661–671
 12. See e.g. (a) Yamamoto K, Imaoka T, Chun W-J et al (2009) Size-specific catalytic activity of platinum clusters enhances oxygen reduction reactions. *Nat Chem* 1:397–402 (b) Ornelas C, Aranzaes JR, Salmon L et al (2008) “Click” Dendrimers: synthesis, redox sensing of Pd (OAc)₂, and remarkable catalytic hydrogenation activity of precise Pd nanoparticles stabilized by 1,2,3-triazole-containing dendrimers. *Chem Eur J* 14:50–64 (c) Ye H, Crooks RM (2007) Effect of elemental composition of PtPd bimetallic nanoparticles containing an average of 180 atoms on the kinetics of the electrochemical oxygen reduction reaction. *J Am Chem Soc* 129:3627–3633 (d) Dend S, Locklin J, Patton D et al (2005) Thiophene dendron jacketed poly (amidoamine) dendrimers: nanoparticle synthesis and adsorption on graphite. *J Am Chem Soc* 127:1744–1751
 13. For some recent examples, see e.g.: (a) Oh JB, Nah M-K, Kim YH et al (2007) ErIII-cored complexes based on dendritic pti-porphyrin ligands: synthesis, near-IR emission enhancement, and photophysical studies. *Adv Funct Mater* 17:413–424 (b) Li B-L, Liu Z-T, Deng G-J et al (2007) The Synthesis of dendritic β -diketonato ligands and their europium complexes. *Eur J Org Chem* 508–516 (c) Baek NS, Kim YH, Roh S-G et al (2006) The first inert and photostable encapsulated lanthanide(III) complexes based on dendritic 9,10-diphenylanthracene ligands: synthesis, strong near-infrared emission enhancement, and photophysical studies. *Adv Funct Mater* 16:1873–1882 (d) Shen L, Shi M, Li F et al (2006) Polyarylether dendrimer with a 4-phenylacetyl-5-pyrazolone-based terbium(III) complex as core: synthesis and photophysical properties. *Inorg Chem* 45:6188–6197 (e) Cross J-P, Lauz M, Badger PD et al (2004) Polymetallic lanthanide complexes with PAMAM-naphthalimide dendritic ligands: luminescent lanthanide complexes formed in solution. *J Am Chem Soc* 126:16278–16279 (f) Larsen J, Puntoriero F, Pascher T et al (2007) Extending the light-harvesting properties of transition-metal dendrimers. *ChemPhysChem* 8:2643–2651
 14. (a) Imaoka T, Tanaka R, Arimoto S et al (2005) Probing stepwise complexation in phenylazomethine dendrimers by a metallo-porphyrin core. *J Am Chem Soc* 127:13896–13905 (b) Kimoto A, Cho J-S, Higuchi M et al (2004) Synthesis of asymmetrically arranged dendrimers with a carbazole dendron and a phenylazomethine dendron. *Macromolecules* 37:5531–5537 (c) Higuchi M, Tsuruta M, Chiba H et al (2003) Control of stepwise radial complexation in dendritic polyphenylazomethines. *J Am Chem Soc* 125:9988–9997

15. (a) Bergamini G, Saudan C, Ceroni P et al (2004) Proton-driven self-assembled systems based on cyclam-cored dendrimers and $[\text{Ru}(\text{bpy})(\text{CN})_4]^{2-}$. *J Am Chem Soc* 126:16466–16471 (b) van de Coevering R, Kuil M, Gebbink JMK et al (2002) A polycationic dendrimer as noncovalent support for anionic organometallic complexes. *Chem Commun* 15:1636–1637
16. (a) Puntoriero F, Bergamini G, Ceroni P et al (2008) Azacrown ethers with naphthyl branches. Fluorescence properties, protonation and metal coordination. *J Inorg Organomet Polym Mater* 18:189–194 (b) Antoni P, Malkoch M, Vamvounis G et al (2008) Europium confined cyclen dendrimers with photophysically active triazoles. *J Mater Chem* 18:2545–2554
17. (a) Bergamini G, Ceroni P, Maestri M et al (2007) Cyclam cored luminescent dendrimers as ligands for Co(II), Ni(II) and Cu(II) ions. *Inorg Chim Acta* 360:1043–1051 (b) Branchi B, Ceroni P, Bergamini G et al (2006) A cyclam core dendrimer containing dansyl and oligoethylene glycol chains in the branches: protonation and metal coordination. *Chem Eur J* 12:8926–8934 (c) Gu T, Whitesell JK, Fox MA (2006) Intramolecular charge transfer in 1:1 Cu(II)/pyrenylcyclam dendrimer complexes. *J Phys Chem B* 110:25149–25152 (d) Bergamini G, Ceroni P, Balzani V et al (2005) Dendrimers based on a bis-cyclam core as fluorescence sensors for metal ions. *J Mater Chem* 15:2959–2964 (e) Saudan C, Ceroni P, Vicinelli V et al (2004) Simple and dendritic cyclam derivatives. Photophysical properties, effect of protonation and Zn^{2+} coordination, preliminary screening as inhibitors of tumour cell growth. *Supramol Chem* 16:541–548 (f) Saudan C, Ceroni P, Vicinelli V et al (2004) Cyclam-based dendrimers as ligands for lanthanide ions. *Dalton Trans* 10:1597–1600 (g) Saudan C, Balzani V, Gorka M et al (2004) Dendrimers as ligands: an investigation into the stability and kinetics of Zn^{2+} complexation by dendrimers with 1,4,8,11-tetraazacyclotetradecane (Cyclam) cores. *Chem Eur J* 10:899–905 (h) Saudan C, Balzani V, Gorka M et al (2003) Dendrimers as ligands. Formation of a 2:1 luminescent complex between a dendrimer with a 1,4,8,11-tetraazacyclotetradecane (Cyclam) core and Zn^{2+} . *J Am Chem Soc* 125:4424–4425
18. Thomas SW, Joly GD, Swager TM (2007) Chemical sensors based on amplifying fluorescent conjugated polymers. *Chem Rev* 107:1339–1386
19. (a) Sarkar K, Dhara K, Nandi M et al (2009) Selective zinc(II)-ion fluorescence sensing by a functionalized mesoporous material covalently grafted with a fluorescent chromophore and consequent biological applications. *Adv Funct Mater* 19:223–234 (b) Gouanvé F, Schuster T, Allard E et al (2007) Fluorescence quenching upon binding of copper ions in dye-doped and ligand-capped polymer nanoparticles: a simple way to probe the dye accessibility in nano-sized templates. *Adv Funct Mater* 17:2746–2756 (c) Yan J, Estevez MC, Smith JE et al (2007) Dye-doped nanoparticles for bioanalysis. *Nano Today* 2:44–50
20. For some recent reviews, see: (a) Astruc D, Ornelas C, Ruiz J (2008) Metallophenyl dendrimers and their applications in molecular electronics, sensing, and catalysis. *Acc Chem Res* 41:841–856 (b) Kaifer AE (2007) Electron transfer and molecular recognition in metallo-cene-containing dendrimers. *Eur J Inorg Chem* 5015–5027
21. See for example: (a) Balzani V, Campagna S, Denti G et al (1998) Designing dendrimers based on transition-metal complexes. light-harvesting properties and predetermined redox patterns. *Acc Chem Res* 31:26–34 (b) Huisman B-H, Schönherr H, Huck WTS et al (1999) Surface-confined metallodendrimers: isolated nanosize molecules. *Angew Chem Int Ed* 38:2248–2251 (c) McClenaghan ND, Loiseau F, Puntoriero F et al (2001) Light-harvesting metal dendrimers appended with additional organic chromophores: a tetranuclear heterometallic first-generation dendrimer exhibiting unusual absorption features. *Chem Commun* 24:2634–2635
22. For some examples, see e.g.: (a) Hogan CF, Harris AR, Bond AM et al (2006) Electrochemical studies of porphyrin-appended dendrimers. *PhysChemChemPhys* 8:2058–2065 (b) Jang W-D, Nishiyama N, Zhang G-D et al (2005) Supramolecular nanocarrier of anionic dendrimer porphyrins with cationic block copolymers modified with polyethylene glycol to enhance intracellular photodynamic efficacy. *Angew Chem Int Ed* 44:419–423 (c) Loiseau F, Campagna S, Hameurlaine A et al (2005) Dendrimers made of porphyrin cores and carbazole chromophores as peripheral units. Absorption spectra, luminescence properties, and oxidation

- behavior. *J Am Chem Soc* 127:11352–11363 (d) Chavan SA, Maes W, Gevers LEM et al (2005) Porphyrin-functionalized dendrimers: synthesis and application as recyclable photocatalysts in a nanofiltration membrane reactor. *Chem Eur J* 11:6754–6762 (e) Brinas RP, Troxler T, Hochstrasser RM et al (2005) Phosphorescent oxygen sensor with dendritic protection and two-photon absorbing antenna. *J Am Chem Soc* 127:11851–11682
23. (a) Lukeš I, Kotek J, Vojtíšek P et al (2001) Complexes of tetraazacycles bearing methylphosphinic/phosphonic acid pendant arms with copper(II), zinc(II) and lanthanides(III). A comparison with their acetic acid analogues. *Coord Chem Rev* 216–217:287–312 (b) Hay BP, Hancock RD (2001) The role of donor group orientation as a factor in metal ion recognition by ligands. *Coord Chem Rev* 212:61–87
 24. (a) Bianchi A, Micheloni M, Paletti P (1991) Thermodynamic aspects of the polyazacycloalkane complexes with cations and anions. *Coord Chem Rev* 110:17–113 (b) Kimura E (1994) Macrocyclic polyamine zinc(II) complexes as advanced models for zinc(II) enzymes. *Prog Inorg Chem* 41:443–491 (c) Meyer M, Dahaoui-Gindrey V, Lecomte C et al (1998) Conformations and coordination schemes of carboxylate and carbamoyl derivatives of the tetraazamacrocycles cyclen and cyclam, and the relation to their protonation states. *Coord Chem Rev* 178:1313–1405 (d) Fabbri L, Licchelli M, Pallavicini P et al (2001) Supramolecular assemblies containing metalocyclam subunits. *Supramol Chem* 13 569–582
 25. Liang X, Sadler PJ (2004) Cyclam complexes and their applications in medicine. *Chem Soc Rev* 33:246–266
 26. Sibert JW, Cory AH, Cory JC (2002) Lipophilic derivatives of cyclam as new inhibitors of tumor cell growth. *Chem Commun* 2:154–155
 27. (a) Brucher E, Sherry AD (2001) Stability and toxicity of contrast agents. In: Merbach AE, Toth E (eds) *The chemistry of contrast agents in medical magnetic resonance imaging*. Wiley, New York (b) Caravan P, Ellison JJ, McMurry TJ et al (1999) Gadolinium(III) chelates as MRI contrast agents: structure, dynamics, and applications. *Chem Rev* 99:2293–2352
 28. (a) Paisey SJ, Sadler PJ (2004) Anti-viral cyclam macrocycles: rapid zinc uptake at physiological pH. *Chem Commun* 3:306–307 (b) Liang X, Weishäupl M, Parkinson JA et al (2003) Selective recognition of configurational substates of zinc cyclam by carboxylates: implications for the design and mechanism of action of anti-HIV agents. *Chem Eur J* 9:4709–4717 (c) Kimura E, Koike T, Inouye Y (1999) Macrocyclic polyamines and their metal complexes: a novel type of anti-HIV agent. In: Hay RW, Dilworth JR, Nolan KB (eds) *Perspective on bioinorganic chemistry*, vol 4. JAI Press Inc, Stamford
 29. Saudan C, Balzani V, Ceroni P et al (2003) Dendrimers with a cyclam core. Absorption spectra, multiple luminescence, and effect of protonation. *Tetrahedron* 59:3845–3852
 30. Ben Othman A, Lee JW, Abidi R (2007) A novel pyrenyl-appended tricalix[4]arene for fluorescence-sensing of Al(III). *Tetrahedron* 63:10793–10800
 31. Vögtle F, Gestermann S, Kauffmann C et al (1999) Poly(propylene amine) dendrimers with peripheral dansyl units: protonation, absorption spectra, photophysical properties, intradendrimer quenching, and sensitization processes. *J Am Chem Soc* 121:12161–12166
 32. (a) Balzani V, Ceroni P, Gestermann S et al (2000) Dendrimers as fluorescent sensors with signal amplification. *Chem Commun* 10:853–854 (b) Vögtle F, Gestermann S, Kauffmann C et al (2000) Coordination of Co²⁺ ions in the interior of poly(propylene amine) dendrimers containing fluorescent dansyl units in the periphery. *J Am Chem Soc* 122:10398–10404
 33. For some recent reviews, see: (a) Leonard JP, Nolan CB, Stomeo F et al (2007) Photochemistry and photophysics of coordination compounds: lanthanides. *Top Curr Chem* 281:1–43 (b) Bünzli J-CG, Piguet C (2005) Taking advantage of luminescent lanthanide ions. *Chem Soc Rev* 34:1048–1077 (c) Parker D (2000) Luminescent lanthanide sensors for pH, pO₂ and selected anions. *Coord Chem Rev* 205:109–130
 34. Escribano P, Julian-Lopez B, Planelles-Arago J et al (2008) Photonic and nanobiophotonic properties of luminescent lanthanide-doped hybrid organic–inorganic materials. *J Mater Chem* 18:23–40

35. (a) de Bettencourt-Dias A (2007) Lanthanide-based emitting materials in light-emitting diodes. *Dalton Trans* 22:2229–2241 (b) Kuriki K, Koike Y, Okamoto Y (2002) Plastic optical fiber lasers and amplifiers containing lanthanide complexes. *Chem Rev* 102:2347–2356
36. (a) Parker D, Dickins RS, Puschmann H et al (2002) Being excited by lanthanide coordination complexes: aqua species, chirality, excited-state chemistry, and exchange dynamics. *Chem Rev* 102:1977–2010 (b) Sabbatini N, Guardigli M, Lehn J-M (1993) Luminescent lanthanide complexes as photochemical supramolecular devices. *Coord Chem Rev* 123:201–228
37. See e.g.: Hebbink GA, Klink SI, Grave L et al (2002) Singlet energy transfer as the main pathway in the sensitization of near-infrared Nd³⁺ luminescence by dansyl and lissamine dyes. *ChemPhysChem* 3:1014–1018
38. Kawa M, Fréchet JMJ (1998) Self-Assembled lanthanide-cored dendrimer complexes: enhancement of the luminescence properties of lanthanide ions through site-isolation and antenna effects. *Chem Mater* 10:286–296
39. Sabbatini N, Dellonte S, Bonazzi A et al (1986) Photoinduced electron-transfer reactions of poly(pyridine)ruthenium(II) complexes with europium(III/II) cryptates. *Inorg Chem* 25:1738–1742
40. Kawa M, Takahagi T (2004) Improved antenna effect of terbium(III)-cored dendrimer complex and green-luminescent hydrogel by radical copolymerization. *Chem Mater* 16:2282–2286
41. Balzani V, Ceroni P, Gestermann S et al (2000) Effect of protons and metal ions on the fluorescence properties of a polylysine dendrimer containing twenty four dansyl units. *J Chem Soc Dalton Trans* 21:3765–3771
42. (a) Vicinelli V, Ceroni P, Maestri M et al (2002) Luminescent lanthanide ions hosted in a fluorescent polylysine dendrimer. Antenna-like sensitization of visible and near-infrared emission. *J Am Chem Soc* 124:6461–6468 (b) Vögtle F, Gorka M, Vicinelli V et al (2001) A Dendritic antenna for near-infrared emission of Nd³⁺ ions. *ChemPhysChem* 2:769–773
43. Cross J-P, Lauz M, Badger PD et al (2004) Polymetallic lanthanide complexes with PAMAM-naphthalimide dendritic ligands: luminescent lanthanide complexes formed in solution. *J Am Chem Soc* 126:16278–16279
44. (a) Beeby A, Parker D, Williams JAG (1996) Photochemical investigations of functionalised 1,4,7,10-tetraazacyclododecane ligands incorporating naphthyl chromophores. *J Chem Soc Perkin Trans 2* 1565–1579 (b) Tung C-H, Wu L-Z (1996) Enhancement of intramolecular excimer formation, photodimerization and energy transfer of naphthalene end-labelled poly(ethylene glycol) oligomers *via* complexation of alkali-metal and lanthanide cations. *J Chem Soc Faraday Trans* 92:1381–1385 (c) Parker D, Williams JAG (1995) Luminescence behaviour of cadmium, lead, zinc, copper, nickel and lanthanide complexes of octadentate macrocyclic ligands bearing naphthyl chromophores. *J Chem Soc Perkin Trans 2* 1305–1314
45. (a) Ward MD (2006) [Ru(bipy)(CN)₄]²⁻ and its derivatives: photophysical properties and its use in photoactive supramolecular assemblies. *Coord Chem Rev* 250:3128–3141 (b) Scandola F, Indelli MT (1988) Second sphere donor acceptor interactions in excited states of coordination compounds. Ruthenium(II) bipyridine cyano complexes. *Pure Appl Chem* 60:973–980 (c) Balzani V, Sabbatini N, Scandola F (1986) “Second-sphere” photochemistry and photophysics of coordination compounds. *Chem Rev* 86:319–337
46. For some recent papers, see: (a) Lazarides T, Easun TL, Veyne-Marti C et al (2007) Structural and photophysical properties of adducts of [Ru(bipy)(CN)₄]²⁻ with different metal cations: metallochromism and its use in switching photoinduced energy transfer. *J Am Chem Soc* 129:4014–4027 (b) Bernhardt PV, Bozoglian F, Font-Bardia M et al (2007) The influence of ligand substitution at the electron donor center in molecular cyano-bridged mixed-valent Co^{III}/Fe^{II} and Co^{III}/Ru^{II} complexes. *Eur J Inorg Chem* 2007:5270–5276 (c) Davies GM, Pope SJA, Adams H et al (2005) Structural and photophysical properties of coordination networks combining [Ru(bipy)(CN)₄]²⁻ Anions and lanthanide(III) cations: rates of photoinduced ru-to-lanthanide energy transfer and sensitized near-infrared luminescence. *Inorg Chem*

- 44:4656–4665 (d) Kovács M, Horváth A (2004) The effect of H/D-bond solute–solvent interaction on deactivation channels of MLCT excited state of $[\text{Ru}(\text{bpy})(\text{CN})_4]^{2-}$. *J Photochem Photobiol A Chem* 163:13–19 (e) Loiseau F, Marzanni G, Quici S et al (2003) An artificial antenna complex containing four $\text{Ru}(\text{bpy})_3^{2+}$ -type chromophores as light-harvesting components and a $\text{Ru}(\text{bpy})(\text{CN})_4^{2-}$ subunit as the energy trap. A structural motif which resembles the natural photosynthetic systems. *Chem Commun* 2:286–287
47. Demchenko AP (2010) Collective effects influencing fluorescence emission. In: Demchenko AP (ed) *Advanced fluorescence reporters in chemistry and biology. II*. Springer Ser Fluoresc 9:107–132
48. Reppy MA (2010) Structure, emissive properties and reporting abilities of conjugated polymers. In: Demchenko AP (ed) *Advanced fluorescence reporters in chemistry and biology. II*. Springer Ser Fluoresc 9:357–388

Prospects for Organic Dye Nanoparticles

Hiroshi Yao

Abstract A review of organic nanoparticles consisting of small functional dye molecules is presented in this chapter. The study of organic dye nanoparticles does not have a lengthy history, but there is growing scientific and technological interest owing to their special characteristics: physicochemical properties of organic dye nanoparticles considerably differ not only from those of individual molecules due to the presence of van der Waals type intermolecular interactions, but also from those of bulk crystals since the nanoparticles have a large proportion of surface molecules. Simple and versatile synthesis strategies that have been developed and widely applied for obtaining organic dye nanoparticles are first discussed – reprecipitation method and ion-association method. Next, their unique size-dependent optical properties are introduced. More attention is paid to their novel and interesting emission behavior – aggregation-induced enhanced emission (AIEE) that closely relates to the restriction of intramolecular twisting motion. Finally, concluding remarks and the future outlook of research in this area are provided.

Keywords Aggregation-induced enhanced emission (AIEE) · Fluorescent organic nanoparticles · Ion-association method · Organic dye nanoparticles · Reprecipitation method · Restriction of intramolecular rotation · Size-dependent optical properties

Contents

1	Introduction: Organic Dye Nanoparticles Exhibit Unique Physicochemical Properties	286
2	How to Synthesize Organic Dye Nanoparticles: Preparation Strategies	288
2.1	Reprecipitation Method	289
2.2	Ion-Association Method	290

H. Yao

Graduate School of Material Science, University of Hyogo, 3-2-1 Koto, Kamigori-cho, Ako-gun, Hyogo 678-1297, Japan

e-mail: yao@sci.u-hyogo.ac.jp

3	Optical Properties of Organic Dye Nanoparticles	291
3.1	Photocatalytic Properties	291
3.2	Size-Dependent Spectroscopic Properties	292
3.3	Why Can Organic Dye Nanoparticles Be Fluorescent?	295
4	Concluding Remarks and Outlook	300
	References	302

1 Introduction: Organic Dye Nanoparticles Exhibit Unique Physicochemical Properties

Physicochemical properties of organic nanoparticles with their size smaller than a hundred of nanometers generally differ from those of individual molecules due to intermolecular interactions such as van der Waals attractive forces and/or hydrogen-bonding in the solid state [1, 2]. In addition, they do not resemble those of bulk crystals because they are closely related to the large proportion of surface molecules that characterize nanoarchitectures. Therefore, organic nanoparticles can be seen as novel materials in an intermediate state, bridging the gap between single molecules and bulk materials, and are expected to give access to original applications in various cutting-edge fields of technology such as bioanalysis [3], photocatalysis [4], pharmacology [5], photonics, and microelectronics [6].

Constructing organic nanoparticles, chromophoric (or fluorophoric) molecular systems with a defined chemical structure are useful and promising potential [7–9]. Such systems involve “organic dyes” that possess absorption of electromagnetic radiation of varying energies. The optical properties of the organic dyes depend on their electronic transitions that reflect molecular geometries and can be tuned by elaborate molecular design strategies. In particular, fluorescence properties in dye molecules offer a wealth of information so that they can be a useful extrinsic reporter for the investigation of many fundamental processes in life and material sciences [10]. Fluorescence of organic dyes typically originates either from an optical transition delocalized over the whole chromophore (*resonant dyes*) or from intramolecular charge-transfer transitions (*CT dyes*) [11]. The majority of common fluorophores (for example, fluoresceins, rhodamines, and cyanines) are resonant dyes that are characterized by slightly structured, comparatively narrow absorption and emission bands with a small solvent polarity-insensitive Stokes shift, high molar absorption coefficients, and moderate-to-high fluorescence quantum yields. In contrast, CT dyes such as coumarin and styryl dyes have well-separated, broader, and structureless absorption and emission bands, with larger Stokes shift, which strongly depends on solvent or matrix polarity. Their molar absorption coefficients, and in most cases also their fluorescence quantum yields, are generally smaller than those of resonant dyes [11].

Fabrication of organic dye nanoparticles and the ability to tailor their photo-physical characteristics represent an important challenge, although they have been paid little attention principally due to the following two factors (1) Owing to their

lower thermal stability and poorer mechanical properties compared to inorganic materials, there were few routes for fabricating well-defined organic compounds into nanostructures, resulting in difficulties in applying the top-down strategy that is common in producing inorganic nanostructures. (2) Until recently, size-dependent optical and electronic properties have not been anticipated in organic nanomaterials because, unlike the case of Wannier excitons [12] in inorganic or semiconductor crystals, the spectroscopic properties of organic crystals are essentially determined by Frenkel excitons with a very smaller radius [13] or by monomer photochemistry. However, in the 1990s, Nakanishi and co-workers succeeded in preparing some kinds of organic dye nanoparticles systematically by adopting a “reprecipitation method” as a facile synthetic technique [14, 15]. After these epochal events, more strategies have been developed for constructing organic nanostructures with interesting morphologies and optical (absorption and fluorescence) properties. During the course of many investigations, it was noticed that many photophysical properties exhibit an obvious size effect via aggregation of organic molecules. Emergence of interesting fluorescent properties was also no exception. For example, perylene is used in demonstrating the size dependent fluorescent properties [15]. Subsequently, various types of organic dye compounds have been introduced to make fluorescent organic nanoparticles. Figure 1 shows representative dye molecules that have been used for producing organic nanoparticles with exciting fluorescence properties. As a consequence of the variety and designability of organic dye molecules to convert

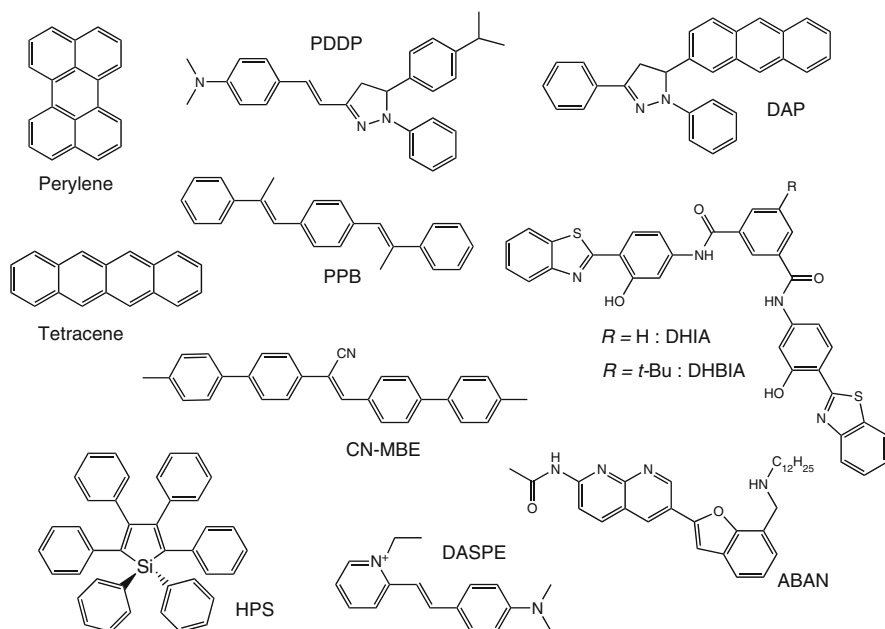


Fig. 1 Typical organic dye molecules that have been converted to fluorescent nanoparticles. The abbreviation for each dye molecule is also shown in the figure

nanoparticles, extensive work is being carried out to extend research on nanostructured materials of many organic compounds.

This chapter focuses on zero-dimensional nanomaterials of organic dye molecules, that is, organic dye nanoparticles. Note that nanoparticles of organic polymers or micelles are excluded because of their vast studies and fundamental differences. In Sect. 2, preparation strategies and protocols that have been developed for obtaining organic dye nanoparticles are reviewed in detail. The organic dye nanoparticles are composed mostly of neutral (that is, noncharged) molecules, but many ionic dyes are also available. Taking the diversity of ionic dye molecules into consideration, therefore, the present author has developed a simple and versatile method, called “ion-association method,” which can be applied for constructing ion-based organic dye nanoparticles in aqueous solution. By introducing some examples of organic dye nanoparticles, their unique optical properties that involve the size effect are described in Sect. 3. More attention is paid to the novel and interesting fluorescent behavior. In conclusion, my personal view of future prospect in this area is provided.

2 How to Synthesize Organic Dye Nanoparticles: Preparation Strategies

It is of fundamental and technological interest to understand how physicochemical properties of organic dye nanoparticles develop as a function of size. The first step to reach this goal is to synthesize well-defined organic dye nanoparticles in a controlled manner.

Typically, the organic dye nanoparticle system can be obtained in two ways (1) top-down approach by mechanical milling of the raw organic materials by wet or dry milling processes and (2) bottom-up approach by precipitation or condensation of the organic products in certain solvents [16]. In method (2), a mixed solvent system with changes in its composition is frequently used. A purely aqueous system has been developed by the present author for ion-based organic dye nanoparticles, which can be classified in category (2). In both cases, various stabilizers, such as surfactants or polymers, are added if necessary and the function of boundary layer of nanoparticles by adsorption is taken over. Milling processes (category (1)) are in principle unsuitable for the production of nanodispersed systems with narrow size distribution because with decrease in the particle size, it becomes increasingly more difficult to use applied mechanical energy in the form of shearing and cavitation forces for particle milling without simultaneously including particle agglomeration [16]. Note that a recent development in laser ablation technology may overcome such a mechanical energy problem in the milling process, although it needs an expensive short-pulse laser system [17]. For example, laser ablation of organic microcrystalline powders, such as red dye quinacridone, dispersed in a poor solvent is applied for the synthesis of the dye nanoparticles with tuning laser wavelength,

pulse width, laser fluence, and total shot number, and the powder is converted directly into a colloidal solution [17]. On the other hand, precipitation processes (category (2)) are rather controllable methods of nanoparticle production with simplicity; hence, this technique has been widely employed to prepare organic nanoparticles of a wide variety of dye compounds.

2.1 Reprecipitation Method

Starting from a molecularly dispersed solution of the target dye compound, the so-called “reprecipitation method” would be the most facile, size-controllable, and widely used one. As described before, this method was first reported by Nakanishi and co-workers [14, 15]. It involves a rapid mixing of a small amount of the concentrated dye solution (namely, the target dye compound dissolved in a “good” solvent) with an excess of a “poor” solvent. The great disparity between the solubilities of the target compound in the good and poor solvents and the good compatibility of the two solvents are essential for this method. The free molecules in the solution begin to aggregate following the mixing of a certain quantity of the poor solvent. A schematic representation of a typical reprecipitation method is shown in Fig. 2. One can control the size and its distribution by the level of adjustable supersaturation as well as by stabilizers, which possibly intercede specifically in the elementary steps of nucleation, growth, and agglomeration. In this framework, several parameters can be tuned with the aim of gaining control on the particle size. These parameters are, for example, the type of poor solvent,

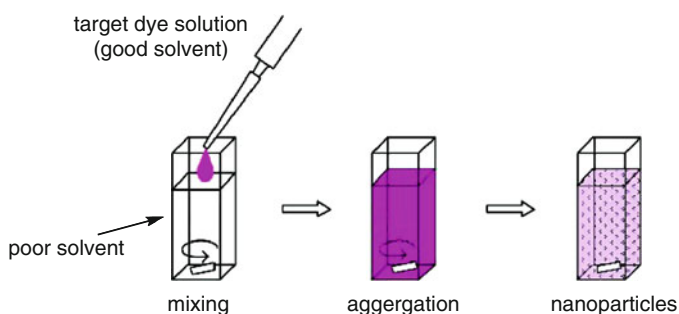


Fig. 2 Schematic representation of a typical “reprecipitation method.” The idea of this process is the delicate mixture of good and poor solvents for the target dye compound: A small volume of solution of the target dye (typically millimolar in concentration) is rapidly injected into a large amount of vigorously stirred poor solvent of the target. The good solvent of the dye is completely miscible with its poor solvent. Hence, the target dye molecules reprecipitated as nanoparticles via aggregation. In general, good solvents involve alcohol, acetone, acetonitrile, THF, etc. and poor solvent is normally water. Tuning of varieties of good solvent and poor solvent pairs along with different parameters, such as temperature, use of sonication, and the presence/absence of a stabilizer brings about controllable size of the nanoparticles

fraction of the injected solution, temperature [18], ultrasonication [19], time for aging [20], and stabilizer concentrations [21]. The reprecipitation method is also called the *Ouzo* effect [22]. The *Ouzo* effect is a phenomenon seen when water is added to ouzo (anise-flavored Greek liqueurs), a cloudy oil-in-water microemulsion form.

2.2 Ion-Association Method

Despite the simplicity in the operation of the reprecipitation method, it is fraught with some difficulties; for instance, some kinds of “organic” solvents are used for controlling precipitation processes. The search for ways of controlling size, shape, and the physical/chemical properties of organic dye nanoparticles in *pure* aqueous media without using specific organic cosolvents is still a challenge, and certainly provides an important aspect in the development of environmental nanoscience.

The present author has developed a novel method called “ion-association method.” This is also a simple and versatile method for the preparation of *ion-based* organic dye nanoparticles in pure aqueous solution by the ion association approach [23]. It utilizes the control of hydrophilicity/hydrophobicity of the ionic material itself via ion-pair formation; for example, addition of a cationic target dye solution into aqueous solution containing a certain kind of hydrophobic anions forms an electrically neutral ion-pair because of the strong electrostatic attraction, followed by aggregation of ion-pair species originated from van der Waals attractive interactions between them to produce nuclei and the subsequent nanoparticles (Fig. 3). In this case, hydrophobic but water-soluble anions, such as tetraphenylborate (TPB) or its derivatives (tetrakis(4-fluorophenyl)borate (TFPB), tetrakis[3,5-

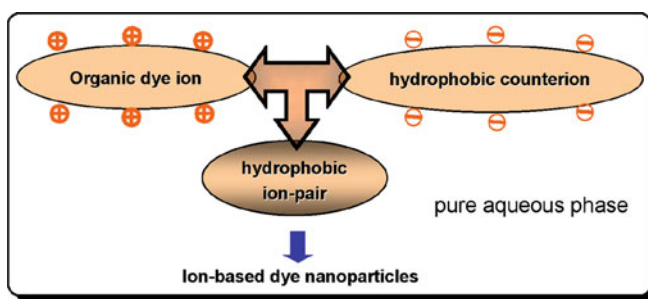


Fig. 3 Concept of the “ion-association method” for fabricating ion-based organic dye nanoparticles in pure aqueous media. The approach is based on ion-pair formation between the ionic dye (for example, cationic dye) and the hydrophobic counterion that is soluble in water [for example, tetraphenylborate (TPB) or its derivative anion], which gives rise to a hydrophobic phase in water. For preparation, organic cosolvent is unnecessary. The size of the dye nanoparticles can be controlled by adjusting the interionic interaction between the dye cation and the associative hydrophobic counteranion

bis(trifluoromethyl)phenyl]borate, etc.), are used to prepare the cationic dye nanoparticles in aqueous solution [23]. Since the particle size can be typically controlled by adjusting the molar ratio between the anion and the cation added, competition between aggregation of the ion-pairs and adsorption of excess anions onto nanoparticles, which influences the surface charge density and electrostatic screening, would determine the size of the nanoparticles. An opposite situation, anionic chromophore-based organic nanoparticles can also be synthesized by mixing a functional dye anion and a hydrophobic but water-soluble cation in aqueous solution¹. In any case, no specific organic solvents are needed.

3 Optical Properties of Organic Dye Nanoparticles

In addition to exploration of the preparation strategies, much effort has also been made to investigate the unique optical and electronic properties of organic dye nanoparticles. It is found that the optical/electronic properties of organic nanoparticles are fundamentally different from those of their inorganic counterparts, since the intermolecular interactions are basically of weak types, such as hydrogen-bonding, π - π stacking, and/or van der Waals interactions. In this section, representative examples of dye nanoparticles prepared by the “reprecipitation method” and “ion-association method” are shown. Their interesting photocatalytic and size-dependent optical properties are discussed, and more attention is paid to the unique fluorescence properties from a viewpoint of aggregation-induced enhanced emission (AIEE) that involves the conformational planarization or restriction of molecular twisting motion as well as *J*-type aggregation.

3.1 Photocatalytic Properties

Photosensitization reactions of a chromophore in the presence of oxygen are commonly classified as *type I* reactions, where the absorber reacts directly with the substrate via a charge-transfer mechanism; or *type II* reactions, where the absorber transfers energy to singlet oxygen, which then reacts with the substrate [4]. Tetracene (chemical structure is shown in Fig. 1) is a known photosensitizer of singlet oxygen, and the mechanism of the photocatalytic destruction of some other dye molecules does not depend on the presence of oxygen, implying a *type I* mechanism. This photocatalytic activity suggests that tetracene may be worth

¹Anion-based organic dye nanoparticles can be also synthesized on the basis of the ion-association method. In this case, hydrophobic “phosphazanium” cations such as tetrakis[tris(dimethylamino)phosphoranylideneamino]phosphonium cation are effective for ion-pair formation with anionic dyes. A neutral polymer stabilizer polyvinylpyrrolidone (PVP) that is soluble in water is sometimes added for preventing agglomeration

investigating as an alternative to inorganic semiconductors in applications such as photo-remediation of wastewater and solar energy conversion [24].

Tetracene nanoparticles (typically ~ 60 nm in diameter) with high stability made using a simple reprecipitation method possess interesting and useful properties [4]. Their optical properties are similar to what is observed for bulk polycrystalline films of tetracene, indicating substantial amount of crystallinity – absorption with a large red shift compared to that of the monomer due to its polarizable environment of the surrounding tetracene molecules and emission from the lowest exciton state in the aggregate. Due to the large surface area of the dye nanoparticles, they had significant photocatalytic activity (photo-oxidative destruction) toward other chemical species such as cyanine and rhodamine. The kinetics and oxygen dependence of the photocatalytic reactions indicated the involvement of adsorption onto the particle surface, followed by electron-transfer chemistry (*type I*). This study gave us two potential advantages for the use of organic dye nanoparticles relative to large band gap semiconductors – the ability to drive the reaction using visible wavelengths as opposed to near-UV and the possibility of low costs.

3.2 *Size-Dependent Spectroscopic Properties*

Size-dependent optical properties of organic dye nanoparticles, which cannot be explained by the so-called quantum size effect that were previously observed in inorganic semiconductor nanoparticles, were first observed in perylene nanoparticles [15]. With reducing the size of the perylene nanoparticles, the emission peak position from a free-exciton state was gradually shifted to a higher energy side, and this behavior could be attributed to change of a lattice or boundary state in the nanoparticles [15]. Recently, size-tunable optical properties of organic nanoparticles comprising a series of aromatically substituted pyrazoline dyes (PDDP and DAP, see Fig. 1), which were prepared by the reprecipitation method, have been investigated [2, 20]. A change in their optical properties essentially comes from the particle size-dependent intermolecular interactions between chromophores and/or the change of lattice state due to the surface area increase – *not* from the Mie scattering [20].

1. In PDDP nanoparticles with their size ranging 20–310 nm, when the size increased from tens to hundreds of nanometers, the three observed absorption bands, arising from the phenyl π – π^* (~ 260 nm) and the pyrazoline n – π^* (~ 315 nm) and π – π^* (~ 370 nm) transitions, were shifted to longer wavelength. Concomitantly, a new peak gradually appeared and also shifted to the lower energy side (~ 420 – 460 nm). The newly emerged absorption peak was ascribed to the transition from an extended charge-transfer (CT) (or CT exciton) state of the PDDP aggregates stacked in the nanoparticles. The bathochromic shift of n – π^* or π – π^* transition as a function of nanoparticle sizes would come from the increased overlap of the pyrazoline π -orbital and intermolecular interactions

between PDDP molecules in the nanoparticles, whereas the CT peak evolution was probably due to exciton confinement.

2. In DAP nanoparticles (40–160 nm), whose average diameter could be controlled by varying the aging time, the absorption at the lower-energy side experienced a bathochromic shift with an increase in the particle size as a result of a change in the intermolecular interactions, while the higher-energy bands of anthracene moiety split due to the electronic coupling between the pyrazoline ring of one molecule and the anthracene unit of the neighboring one. The nanoparticle emission in the blue region from the pyrazoline chromophore shifted to shorter wavelengths (from about 480 to 430 nm) with an increase in particle size, accompanied by a gradual dominance of the emission at about 540 nm from the exciplex (=heterodimeric molecule formed from two species at an electronic excited state) formed by the pyrazoline ring of one molecule and the anthracene moiety of the neighboring molecule.

The reprecipitation strategy lies in the conversion of the products dissolved in a suitable organic solvent into nanodispersed systems in a different medium by a precipitation/condensation procedure. On the other hand, the ion-association strategy can produce ion-based dye nanoparticles in pure aqueous media by utilizing a water-insoluble ion-pair formation reaction. The following example shows the size-dependent absorption properties for the cation-based pseudoisocyanine (PIC; see the chemical structure in Fig. 4) dye nanoparticles.

3. PIC nanoparticles with average diameters ranging from 64 to 125 nm were prepared in pure aqueous media using the ion-association method [23]. Figure 4 shows typical transmission electron microscopy (TEM) images and size distributions of the PIC nanoparticles. Rapid addition of aqueous PIC bromide solution into the ultrasonicated aqueous solution of sodium tetraphenylborate (NaTPB) produced the dye nanoparticle dispersion; that is, ion association between PIC^+ and TPB^- and subsequent nucleation and growth of the ion-pair species ($\text{PIC}^+\cdot\text{TPB}^-$) led to water-insoluble nanoparticle formation. The particle size could be controlled by changing the molar ratio (or, charge ratio) of the loaded TPB^- to PIC^+ ($=[\text{TPB}^-]/[\text{PIC}^+]$), and were correlated with the surface charge density of the nanoparticles. On the basis of Gibbs' adsorption equation, $\Gamma = -C/(RT)(d\gamma/dC)$, where Γ , C , γ , R , or T are the surface excess of adsorbate, solute concentration, surface tension, gas constant, or temperature, respectively, the increase in surface adsorption of ions (=the increase in Γ accompanied by an increase in C) brings about the reduction of surface tension of nanoparticles (that is, $d\gamma/dC < 0$), resulting in decrease in particle size. The spectroscopic features exhibit that (a) absorption of nanoparticles was quite similar to that of the dye monomer, indicating that the PIC chromophores did not aggregate themselves in the nanoparticle (Fig. 4) and (b) the absorption peak originated from the 0–0 band of PIC was red-shifted compared to that of monomer in water. Such a large red shift essentially comes from the “solvent (or matrix) effect” that is related to the matrix polarizability. This behavior is a characteristic feature of ion-based organic nanoparticles. (c) Most interestingly, as the average nanoparticle size

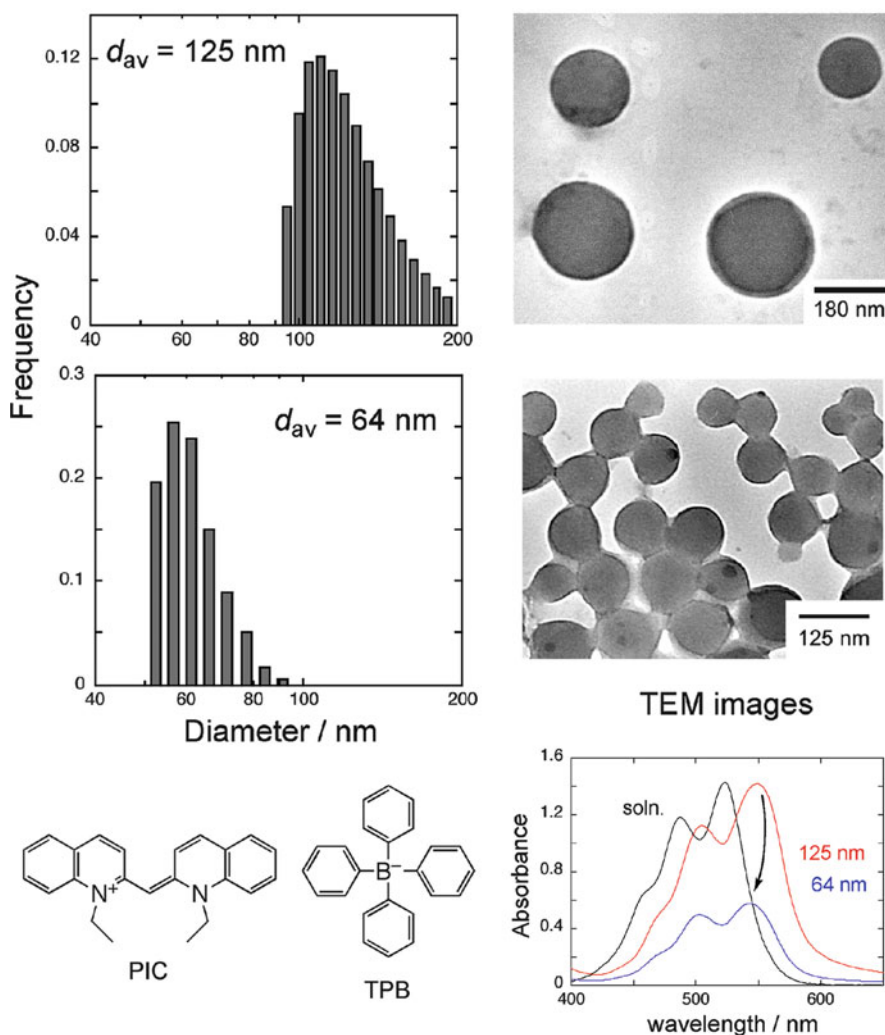


Fig. 4 PIC dye nanoparticles prepared by the ion-association method. (1) Particle size distributions (determined by the dynamic light scattering technique) and the corresponding electron micrographs of the dye nanoparticles. The average diameter can be controlled by tuning the molar ratio of TPB^- to PIC^+ ($=[\text{TPB}^-]/[\text{PIC}^+]$). With an increase in the molar ratio, the average diameter decreased. (2) Absorption spectra of PIC nanoparticles in aqueous solution with different sizes (125 and 64 nm in diameter), exhibiting size-dependent peak shift of the 0–0 band. The spectrum of the aqueous PIC–Br monomer solution is also shown

decreased, the 0–0 band slightly shifted to shorter wavelength. This size-dependent phenomenon might have originated from that of the surface-to-volume ratio of nanoparticles that can induce matrix softening due to surface distortion.

3.3 Why Can Organic Dye Nanoparticles Be Fluorescent?

In organic dye nanoparticles, unique fluorescence behaviors have been observed, which resulted from the special aggregation or interaction modes of the target dye molecules. In particular, molecular distortion, planarization, or conformational restriction in the nanoparticle induces such interaction modes for the chromophores. In this section, I first introduce interesting emission properties of the solid-state nanomaterials, that is, aggregation-induced emission (AIE) or AIEE. Next, some examples of the fluorescent organic dye nanoparticles synthesized by means of both the reprecipitation and ion-association methods are presented in detail. For organic dye nanoparticles prepared by the ion-association technique, matrix polarity (that is, counterion polarity) strongly influences their fluorescence properties, so that the counterions are able to bestow the highly fluorescent nature on the dye nanoparticles.

3.3.1 Aggregation-Induced Enhanced Emission

In most cases, chromophore (fluorophore) aggregation that is brought about by fabrication into solid-state materials quenches its emission (the phenomenon is often called “concentration quenching” or “aggregation-caused quenching”), even though the chromophores are highly emissive in their dilute solutions [13]. The close vicinity between the chromophores in the aggregates opens their nonradiative decay channels, resulting in self-quenching of fluorescence and a drastic reduction in the emission intensity. The concentration quenching in the solid-state materials has prevented many important fluorophores from finding applications in an engineering robust form. Recently, a very interesting phenomenon that molecular aggregation plays a constructive role in the light-emitting process, called AIE or AIEE, has been found; a series of nonemissive or weakly-emissive chromophores are induced to emit intensely by molecular aggregation [25–27].

The mechanistic understanding of AIEE has been mostly found in the restriction of intramolecular rotation of some substituents (for example, peripheral aromatic rings), which blocks the nonradiative channels and populates the radiative routes. This implies the significance of molecular geometry and flexibility (or intramolecular rotation) that affects the relaxation dynamics in the excited state. External controls of relaxation dynamics by cooling or pressurization sometimes boost the emission of AIEE molecules efficiently. In addition, aggregation-induced planarization of the chromophore with π -systems and subsequent *J*-type aggregation can also contribute to enhanced emission. In this case, bulky substituents play a significant role in preventing the parallel face-to-face molecular stacking (*H*-aggregation) and thus in inducing the head-to-tail stacking (*J*-aggregation). When *J*-aggregation proceeds, one can observe the rise of a new red-shifted, strongly narrowed absorption band in addition to a broad monomeric band. The excited states in *J*-aggregates are considered to be of excitonic nature (Frenkel excitons)

[28] (See also the chapter of Losytskyy and Yashchuk [48] addressing this subject). The exciton states are the delocalized electronic states that are caused by the strong long-range dipole–dipole interactions among the monomers within the aggregate, and the width of the exciton band is proportional to the coupling strength. In the simplest case of one molecule per unit cell and a negative coupling energy (namely, head-to-tail arrangements), only transitions to states at the bottom of the exciton band are optically allowed. The total oscillator strength of the coupled molecules is thus swept together in a few eigenstates, and as a consequence, the radiative rates of the bottom states are strongly enhanced as compared to the single molecule.

3.3.2 Highly Fluorescent Organic Dye Nanoparticles

Organic nanoparticles of AIEE molecules can be highly emissive and thus be a useful fluorescence probe. In what follows, some examples prepared by the reprecipitation and ion-association methods are presented.

1. The AIEE phenomena from organic CN-MBE nanoparticle systems prepared by a reprecipitation method have been observed (chemical structure of CN-MBE is shown in Fig. 1) [29]. Interestingly, although the emission from CN-MBE monomeric solution is very weak, the nanoparticles emitted very strong fluorescence with intensity almost 700 times that of the solution. The optimized geometry of free CN-MBE is nonplanar according to the DFT/B3LYP/6-31G* level calculation. The planarization accompanied by a twisting around a single bond of the CN-MBE molecules would be induced by aggregation in the nanoparticles (Fig. 5), which resulted in strong intermolecular interactions

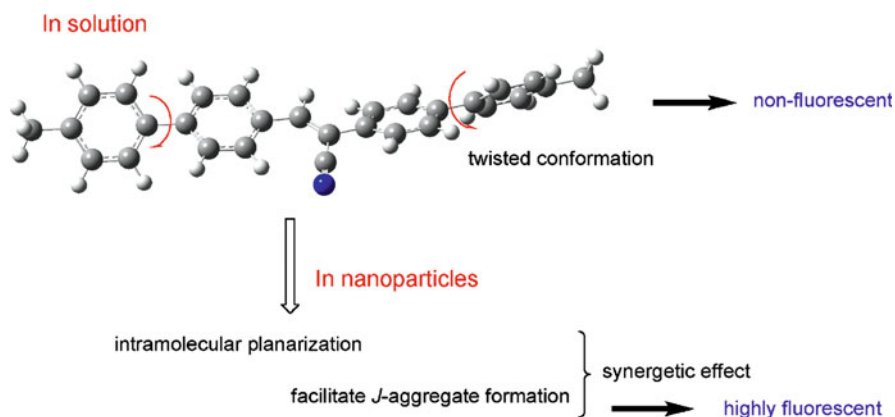


Fig. 5 A proposed mechanism for enhanced emission (or AIEE) in solid-state organic dye nanoparticles. The dye considered here is *trans*-biphenylethylene (CN-MBE) compound. The geometry is optimized by the density functional theory (DFT) calculation at the B3LYP/6-31G* level. Molecular distortion such as twisting and/or subsequent planarization causes prevention of radiationless processes along with specific aggregation such as the *J*-aggregate in the nanoparticles

causing a specific aggregate. In addition, the protruded cyano group restricted the parallel face-to-face intermolecular interactions, which favored the formation of *J*-aggregate instead of *H*-aggregate. Namely, the synergetic effect of intramolecular planarization and *J*-aggregation in the nanoparticles was considered to be responsible for the enhanced emission. Furthermore, a research work moved toward preparation of multifunctional fluorescent molecule for photo-switchable memory by replacing one of the end tolyl groups in CN-MBE with the photochromic 1,2-bisthiénylene moiety [30].

2. A silole molecule named hexaphenylsilole (HPS, see the chemical structure in Fig. 1) is nonluminescent when dissolved in its good solvent (acetonitrile) but becomes highly emissive when aggregated, which is induced by addition of water (poor solvent) [25], that is, AIEE active. The fluorescence quantum yield of HPS monomer was as low as 0.22%, but in the solvent mixture with 99% water, the value rose to ~56%, about 255-fold higher than that in pure acetonitrile. In all the solvent (acetonitrile/water) mixtures, their spectral profiles experienced little red shifts but those with high water content showed absorption tails extending well into the long wavelength region, implying molecular aggregation in the dye nanoparticles. Particle size analyses revealed the existence of relatively large nanoparticles with average diameters of 190 and 130 nm in the solvent mixtures with 80% and 90% water, respectively. The absence of bathochromic shift of absorption for the nanoparticles excludes the possibility that the conformational planarization is a major cause of the AIEE phenomenon. In HPS, six phenyl peripheries are attached to one silole core, so the former (rotors) can rotate against the scaffold (stator) via the single-bond axes. Hence, the intramolecular rotation is restricted due to the physical constraint in the aggregates, which blocks the nonradiative path and activates the radiative channel.
3. With a reprecipitation method using a solvent mixture of THF/water, fluorescent PPB nanoparticles, which feature very weak emission in solution but exhibit strong emission as aggregates, have been synthesized (see Fig. 1 for the chemical structure of PPB) [31]. The size of nanoparticles increased with an increase in the volume fraction of water (ranged in 50–1,000 nm). In contrast to the twisted structure of an isolated PPB molecule that is responsible for a nonfluorescent nature of the dye in solution, the enhanced emission of nanoparticles is primarily due to the combined effects of a rigid planar conformation (three benzene rings in a PPB unit being nearly planar and two methyl groups of the unit pointing along the same direction) and the formation of herringbone *J*-type aggregates with an edge-to-face feature that can be seen in the structure of PPB in a single crystal.
4. Organic dye nanoparticles of DHIA and DHBIA (the chemical structures are shown in Fig. 1) have been synthesized in THF/water mixed solvent by a reprecipitation method [32]. These dye molecules possess a 2-(2-hydroxyphenyl) benzothiazole (HBT) unit, which is known to be more stable as an enol imine form in the ground state and as a keto amine form in the excited state [32, 33] (Fig. 6). The nanoparticles exhibited the AIEE phenomenon mainly due to a restricted intramolecular motion, that is, impediment to free rotation of two end-substituted HBT units around single bonds. It is interesting to note that the

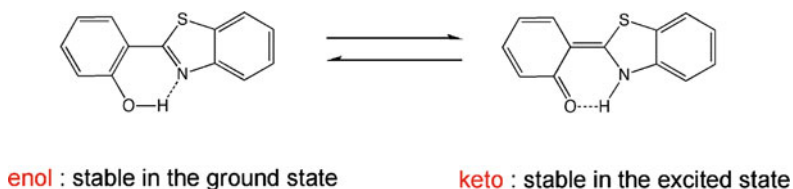


Fig. 6 The 2-(2-hydroxyphenyl)benzothiazole (HBT) unit that represents the keto–enol equilibrium (tautomerism). Normally, the enol (keto) form is rather stable in the ground state (in the excited state), respectively

emission of DHBIA nanoparticles increased more remarkably than that of DHIA nanoparticles, because an additional effect of fast excited-state intramolecular proton transfer in the solid state contributed to its enhancement. Different aggregation modes of these two organic compounds, due to the steric hindrance of a single *tert*-butyl group, could be responsible for the different degrees of fluorescence enhancement.

- The benzofuran–naphthyridine linked dye compound (ABAN, see Fig. 1) has been successfully converted to fluorescent organic nanoparticles [34], for which their photophysical properties such as spectral features and emission intensity are remarkably different from those at the molecular level (solution). The results are rationalized by coplanarization of the benzofuran–naphthyridine molecule in the nanoparticle to extend its effective conjugation length and hence increase the oscillator strength, as is similar to the cases described above.

The next example shows the fluorescent organic nanoparticle of a CT dye (styryl dye DASPE; see Fig. 1 for its chemical structure) synthesized by the ion-association method [35] in pure aqueous solution. DASPE exhibits negative absorption solvatochromism, and this behavior is interpreted in terms of a highly polar nature of this dye bearing electron-donor (dimethylamino group) and electron-acceptor (ethylpyridinium group) substituents at the opposite ends of the rod-shaped conjugated π -electron system [36]. Photoexcitation of DASPE induces the internal twisting motion of a single bond that leads to the twisted intramolecular charge transfer (TICT) states without emission [37, 38]. It is also known that the fluorescence yield of DASPE decreases as the solvent polarity increases due to the decrease in a polarity-dependent potential barrier against the rotation of the single bond responsible for the fast radiationless processes, resulting in very low fluorescence quantum yield in aqueous solution [38].

- The DASPE nanoparticles have been synthesized by the ion association reaction between the dye cation (note that the native compound is an iodide salt; DASPE-I) and the hydrophobic borate anion (TPB^- or TFPB^-) in the presence of neutral polymer stabilizer polyvinylpyrrolidone (PVP) in aqueous solution [38, 39]. In the *absence* of PVP, mixing of aqueous TPB^- (or TFPB^-) and DASPE^+ solutions at the same molar fraction yielded the orange opaque solid dispersion composed of the anion-exchanged dye species, DASPE–TPB (or

DASPE–TFPB), respectively. The obtained solid precipitates were brightly emissive whereas that of the native DASPE-I were almost nonemissive (Fig. 7a; the photo is taken under normal illumination and UV-light irradiation). This indicates that, in the solid of the ion-pair species between DASPE⁺ and TPB⁻ (or TFPB⁻), concentration quenching is effectively suppressed, and more importantly, these ion-pair complexes can generate fluorescent

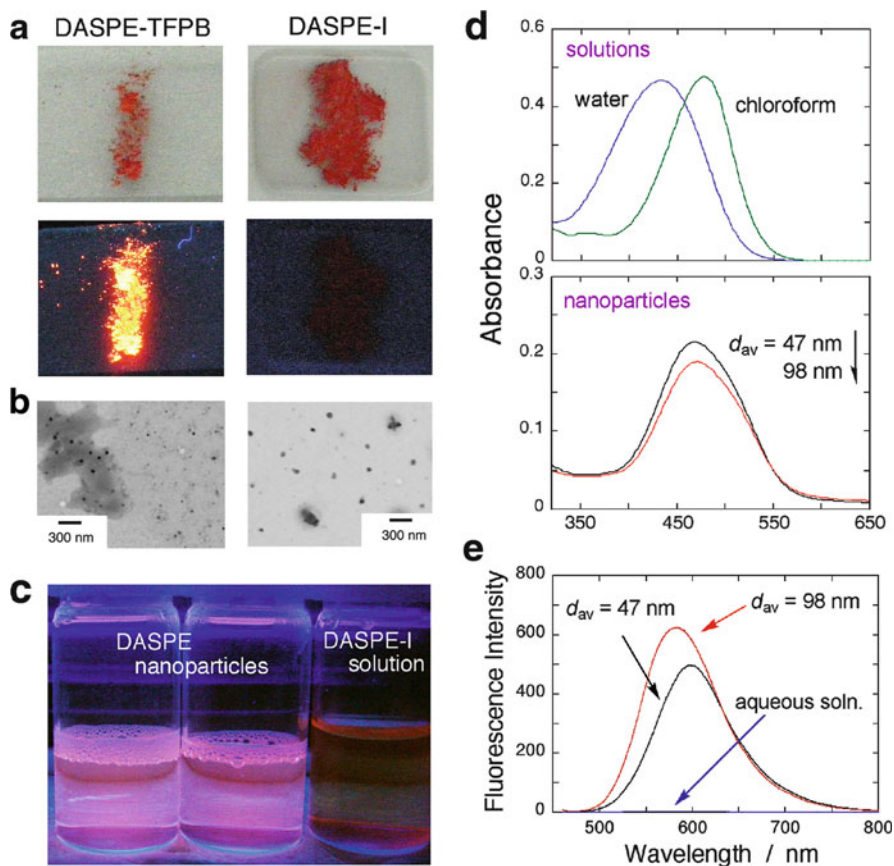


Fig. 7 (a) Photograph of the solid-state DASPE–TFPB and DASPE-I. The upper and lower images were obtained under normal-light and UV-light (365 nm) irradiation, respectively, showing an intense emission from the solid-state DASPE–TFPB with excitation at 365 nm. (b) Electron microscopy images of the prepared DASPE nanoparticle samples (average diameter = 47 and 98 nm, respectively). (c) Photograph (two *left-side* vials with different nanoparticle sizes) representing the highly emissive property of the DASPE nanoparticles. The aqueous solution of DASPE-I (*right-side* vial) showed almost no emission. (d) Absorption spectra of DASPE-I in water and chloroform along with those of DASPE nanoparticles ($d_{av} = 47$ and 98 nm) prepared using TFPB⁻. (e) Fluorescence spectra of DASPE nanoparticles of $d_{av} = 47$ and 98 nm. Emission of the dye monomer in water is also shown. The nanoparticle exhibited greater than 20-fold enhancement

organic nanoparticles. In the *presence* of PVP, on the other hand, well-dispersed DASPE nanoparticles ranged in about 30–100 nm in diameter were successfully synthesized (Fig. 7b). The nanoparticles were emissive in dispersion as expected and seen in Fig. 7c, whose photo was taken under UV-light irradiation. Absorption of the DASPE nanoparticles exhibited a large bathochromic shift in comparison with that of the dye monomer in water, and thus the local polarity of the counteranion matrix (TPB or TFPB) had a strong influence on the red shift of absorption (Fig. 7d). Moreover, formation of the DASPE nanoparticles resulted in enhanced fluorescence as compared to that of the monomeric dye molecule in water – >20-fold enhancement in the fluorescence quantum yield (Fig. 7e). The enhancement was dependent on the counteranion used (using TFPB is more fluorescent than that of TPB), and can be attributed to both the high frictional resistance of the internal single-bond twisting of the ethylpyridinium unit and the matrix polarity effect around DASPE, which can suppress the deactivation processes from the excited fluorescence states of the chromophore [35].

4 Concluding Remarks and Outlook

In this chapter, a review of organic dye nanoparticles consisting of small functional chromophores was presented. I first described their versatile preparation strategies; “reprecipitation method” and “ion-association method.” Then I presented unique spectroscopic properties of some representatives of the dye nanoparticles prepared to date. One of the most interesting features is the size-dependent optical properties, which are completely different from the so-called quantum size effect (or quantum confinement effect) widely observed in inorganic semiconductor nanomaterials or quantum dots. In addition, I placed emphasis on their fluorescence properties (namely, fluorescent organic nanoparticles). The highly emissive characteristics of the dye nanoparticles are generally based on the AIEE that is brought about by a control of molecular geometry, arrangement, and morphology as well as relevant molecular interaction and/or matrix polarity.

Currently, research on organic dye nanoparticles is still in its infancy, and much remains to be done for their future development. For example, developing methods for fabrication of organic dye nanoparticles with desired sizes, morphologies, and structures is still a key task. Indeed, the tiny organic dye nanoparticles whose size is comparable to the inorganic ones (less than about 10 nm in diameter) are still hard to synthesize. Next, the design and synthesis of molecules with unique spectroscopic properties and their controllable construction of nanostructures are a great challenge. In particular, chromophores having flexible conformations/configurations or CT characteristics may be interesting. With regard to fabrication of fluorescent organic dye nanoparticles and their utilization, the following properties should be also taken into account [11]; (1) they possess high fluorescence quantum yield, (2) they are dispersible (soluble) in relevant buffers, or in some cases, cell culture

media, (3) they are sufficiently stable and thus provide reproducible quality, (4) they have functional groups for site-specific labeling, and (5) they have suitable size for suitable interactions between the nanoparticle and the environment. Note that a different group of organic nanomaterials, such as vesicles and dendrimers, has been applied to in vivo fluorescence imaging; for instance, polyamidoamine dendrimer-based fluorogenic substrates are designed to image tumor-associated matrix metalloproteinase-7 (one of an extracellular matrix-degrading metalloproteinase) in vivo [40]. This enables us to anticipate the future practical use of organic dye nanoparticles as a new probe. For further broad utilization, novel performances such as optical waveguides, thin film, and pattern fabrications [41] on solid substrates are also important.

The uniqueness of organic dye nanoparticles can also make them the building blocks for many potential applications, such as light harvesting, drug delivery, chemical and biochemical sensors, and so forth. In particular, light harvesting, which is the trapping of energy via peripheral chromophores and funneling to a central point where it is converted back into visible light, is highly anticipated because of large amounts of absorbing chromophores on the surface periphery in the nanoparticle, providing a high probability for the capture of light. When the ideally designed syntheses of dye nanoparticles are successful, the relatively short distance from the periphery to the core would allow for highly efficient energy transfer as dendrimers do [42]. The mechanism for light harvesting in organic dye nanoparticles will begin with the periphery chromophore molecules capturing the energy of photons from light. Resonance energy transfer or migration between chromophores then occurs mostly by the Förster excitation transfer mechanism, where the energy is transferred through-space via dipole–dipole interactions. Through energy transfer in the nanoparticles, we can use the energy (for example, fluorescence enhancement) that is channeled to the nanoparticle core.

In relation to the resonance energy transfer phenomenon, doping technology may help to improve emission efficiency and tune emission colors, which have been widely used in electroluminescent (EL) devices [43]. In a doped system, the slight variation of the content of energy acceptor will result in significant emission color change. In addition, the energy transfer significantly increases the fluorescence quantum yield of the energy acceptor [44]. A pioneer work on doped organic dye nanoparticles with tunable emission has been reported for the DCM-doped 1,3,5-triphenyl-2-pyrazoline (TPP) nanoparticles prepared by a simple reprecipitation of the binary mixture, with DCM as the energy acceptor and TPP the donor [45]. DCM, 4-dicyanomethylene-2-methyl-6-(4-dimethylaminostyryl)-4*H*-pyran, is a well-known fluorescent dye with red emission widely used in EL devices. The emission colors of the doped dye nanoparticles evolved from blue to red with increasing DCM concentration. Other than tuning emission by size, the work provides an alternative method to control the emission of organic dye nanoparticles by employing the doping technique.

Finally, it should be noted that, as the concentration of the absorbing chromophores is increased to the point where efficient energy transfer takes place between them, the energy can be dissipated by an alternative route known as “concentration

quenching.” Concentration quenching is proposed to take place by successive energy transfer (Förster type) and trapping at a lower energy site that can be a nonradiative channel for the excited state [46]. The trap is often a special molecular nonemissive aggregate, in which the molecules are close enough to interact, resulting in quenching of emission [47]. The behavior of solid-state AIEE on the basis of conformational distortion, restriction, or immobilization in the nanoparticles shed light not only on a new light harvesting system but also on a new fluorescent probe in concentrated conditions. In any case, I anticipate that future improvements in organic dye nanoparticles will provide increased benefit to areas of life as well as material sciences.

References

1. Silinsh EA (1980) Organic molecular crystals: their electronic states. Springer, Berlin
2. Fu H-B, Yao JN (2001) Size effects on the optical properties of organic nanoparticles. *J Am Chem Soc* 123:1434–1439
3. Jinshui L, Lun W, Feng G, Yongxing L, Yun W (2003) Novel fluorescent colloids as a DNA fluorescence probe. *Anal Bioanal Chem* 377:346–349
4. Kim HY, Bjorklund TG, Lim S-H, Bardeen CJ (2003) Spectroscopic and photocatalytic properties of organic tetracene nanoparticles in aqueous solution. *Langmuir* 19:3941–3946
5. Shekunov BY, York P (2000) Crystallization processes in pharmaceutical technology and drug delivery design. *J Cryst Growth* 211:122–136
6. Masuhara H, Nakanishi H, Sasaki K (eds) (2003) Single organic nanoparticles. Springer, Berlin
7. Zhang J, Campbell RE, Ting AY, Tsien RY (2002) Creating new fluorescent probes for cell biology. *Nat Rev* 3:906–918
8. Waggoner A (2006) Fluorescent labels for proteomics and genomics. *Curr Opin Chem Biol* 10:62–66
9. Mason WT (1999) Fluorescent and luminescent probes for biological activity, 2nd edn. Academic, London
10. Tang CW, Van Slyke SA (1987) Organic electroluminescent diodes. *Appl Phys Lett* 51:913–915
11. Resch-Genger U, Grabolle M, Cavaliere-Jaricot S, Nitschke R, Nann T (2008) Quantum dots versus organic dyes as fluorescent label. *Nat Methods* 5:763–775
12. Shinozuka Y, Matsuura M (1983) Wannier exciton in quantum wells. *Phys Rev B* 28:4878–4881
13. Pope M, Swenberg CE (1999) Electronic processes in organic crystals and polymers, 2nd edn. Oxford University Press, Oxford
14. Kasai H, Kamatani H, Okada S, Oikawa H, Matsuda H, Nakanishi H (1996) Size-dependent colors and luminescences of organic microcrystals. *Jpn J Appl Phys* 35:L221–L223
15. Kasai H, Kamatani H, Yoshikawa Y, Okada S, Oikawa H, Watanabe A, Itoh O, Nakanishi H (1997) Crystal size dependence of emission from perylene microcrystals. *Chem Lett* 11:1181–1182
16. Horn D, Rieger J (2001) Organic nanoparticles in the aqueous phase: theory, experiment, and use. *Angew Chem Int Ed* 40:4330–4361
17. Asahi T, Sugiyama T, Masuhara H (2008) Laser fabrication and spectroscopy of organic nanoparticles. *Acc Chem Res* 41:1790–1798

18. Nakanishi H, Katagi H (1998) Microcrystals of polydiacetylene derivatives and their linear and nonlinear optical properties. *Supramol Sci* 5:289–295
19. Kang P, Chen C, Hao L, Zhu C, Hu Y, Chen Z (2004) A novel sonication route to prepare anthracene nanoparticles. *Mater Res Bull* 39:545–551
20. Xiao D, Xi L, Yang W, Fu H, Shuai Z, Fang Y, Yao J (2003) Size-tunable emission from 1,3-diphenyl-5-(2-anthryl)-2-pyrazoline nanoparticles. *J Am Chem Soc* 125:6740–6745
21. Onodera T, Oshikiri T, Katagi H, Kasai H, Okada S, Oikawa H, Terauchi M, Tanaka M, Nakanishi H (2001) Nanowire crystals of π -conjugated organic materials. *J Cryst Growth* 229:586–590
22. Vitale SA, Katz JL (2003) Liquid droplet dispersions formed by homogeneous liquid–liquid nucleation: “The Ouzo effect”. *Langmuir* 19:4105–4110
23. Yao H, Ou Z, Kimura K (2005) Ion-based organic nanoparticles: synthesis, characterization and optical properties of pseudoisocyanine dye nanoparticles. *Chem Lett* 34:1108–1109
24. Kamat PV, Vinodgopal K (1998) Environmental photochemistry with semiconductor nanoparticles. In: Ramamurthy J, Schanze K (eds) *Molecular and supramolecular photochemistry*. Dekker, New York, pp 307–350
25. Hong Y, Jacky WYL, Tang BZ (2009) Aggregation-induced emission: phenomenon, mechanism and applications. *Chem Commun*:4332–4353
26. Deans R, Kim J, Machacek MR, Swager TM (2000) A poly(*p*-phenyleneethynylene) with a highly emissive aggregated phase. *J Am Chem Soc* 122:8565–8566
27. Yin S, Peng Q, Shuai Z, Fang W, Wang Y-H, Luo Y (2006) Aggregation-enhanced luminescence and vibronic coupling of silole molecules from first principles. *Phys Rev B* 73:205409
28. Davydov AS (1971) *Theory of molecular excitons*. Plenum, New York
29. An B-K, Kwon S-K, Jung S-D, Park SY (2002) Enhanced emission and its switching in fluorescent organic nanoparticles. *J Am Chem Soc* 124:14410–14415
30. Lim S-J, An B-K, Jung S-D, Chung M-A, Park SY (2004) Photoswitchable organic nanoparticles and a polymer film employing multifunctional molecules with enhanced fluorescence emission and bistable photochromism. *Angew Chem Int Ed* 43:6346–6350
31. Bhongale CJ, Chang C-W, Lee C-S, Diao EW-G, Hsu C-S (2005) Relaxation dynamics and structural characterization of organic nanoparticles with enhanced emission. *J Phys Chem B* 109:13472–13482
32. Qian Y, Li S, Zhang G, Wang Q, Wang S, Xu H, Li C, Li Y, Yang G (2007) Aggregation-induced emission enhancement of 2-(2'-hydroxyphenyl)benzothiazole-based excited-state intramolecular proton-transfer compounds. *J Phys Chem B* 111:5861–5868
33. Nakagaki R, Kobayashi T, Nagakura S (1978) Luminescence properties and the primary process of photochromism of 2-(2-hydroxyphenyl)benzothiazole. *Bull Chem Soc Jpn* 51:1671–1675
34. Sun Y-Y, Liao J-H, Fang J-M, Chou P-T, Shen C-H, Hsu C-W, Chen L-C (2006) Fluorescent organic nanoparticles of benzofuran–naphthyridine linked molecules: formation and fluorescence enhancement in aqueous media. *Org Lett* 8:3713–3716
35. Yao H, Yamashita M, Kimura K (2009) Organic styryl dye nanoparticles: synthesis and unique spectroscopic properties. *Langmuir* 25:1131–1137
36. Mishra A, Behera RK, Behera PK, Mishra BK, Behera GB (2000) Cyanines during the 1990s: a review. *Chem Rev* 100:1973–2012
37. Strehmel B, Seifert H, Rettig W (1997) Photophysical properties of fluorescence probes 2: a model of multiple fluorescence for stilbazolium dyes studied by global analysis and quantum chemical calculations. *J Phys Chem B* 101:2232–2243
38. Sczegan M, Rettig W, Tolmachev AI, Kurdyukov VV (2001) The role of internal twisting in the photophysics of stilbazolium dyes. *Phys Chem Chem Phys* 3:3555–3561
39. Ou Z, Yao H, Kimura K (2007) Preparation and optical properties of organic nanoparticles of porphyrin without self-aggregation. *J Photochem Photobiol A Chem* 189:7–14

40. McIntyre JO, Fingleton B, Wells KS, Piston DW, Lynch CC, Gautam S, Matrisian LM (2004) Development of a novel fluorogenic proteolytic beacon for in vivo detection and imaging of tumor-associated matrix metalloproteinase-7 activity. *Biochem J* 377:617–628
41. An B-K, Kwon S-K, Park SY (2007) Photopatterned arrays of fluorescent organic nanoparticles. *Angew Chem Int Ed* 46:1978–1982
42. Moore JS, Bharathi P, Devadoss C (1996) Energy transfer in dendritic macromolecules: molecular size effects and the role of an energy gradient. *J Am Chem Soc* 118:9635–9644
43. Tang CW, VanSlyke SA, Chen CH (1989) Electroluminescence of doped organic thin films. *J Appl Phys* 65:3610–3616
44. Mattoussi H, Murata H, Merritt CD, Iizumi Y, Kido J, Kafafi ZH (1999) Photoluminescence quantum yield of pure and molecularly doped organic solid films. *J Appl Phys* 86:2642–2650
45. Peng AD, Xiao DB, Ma Y, Yang WS, Yao JN (2005) Tunable emission from doped 1,3,5-triphenyl-2-pyrazoline organic nanoparticles. *Adv Mater* 17:2070–2073
46. Porter G (1978) Pure and applied photochemistry. *Pure Appl Chem* 50:263–271
47. Demchenko AP (2010) Collective effects influencing fluorescence emission. In: Demchenko AP (ed) *Advanced fluorescence reporters in chemistry and biology. II*. Springer Ser Fluoresc 9:107–132
48. Losytskyy MY, Yashchuk VM (2010) Fluorescent J-aggregates and their biological applications. In: Demchenko AP (ed) *Advanced fluorescence reporters in chemistry and biology. II*. Springer Ser Fluoresc 9:135–157

Part IV
Luminescent Metal Nanoclusters

Few-Atom Silver Clusters as Fluorescent Reporters

Isabel Díez and Robin H.A. Ras

Abstract Silver clusters, composed of only a few silver atoms, have remarkable optical properties based on electronic transitions between quantized energy levels. They have large absorption coefficients and fluorescence quantum yields, in common with conventional fluorescent markers. But importantly, silver clusters have an attractive set of features, including subnanometer size, nontoxicity and photostability, which makes them competitive as fluorescent markers compared with organic dye molecules and semiconductor quantum dots. In this chapter, we review the synthesis and properties of fluorescent silver clusters, and their application as bio-labels and molecular sensors. Silver clusters may have a bright future as luminescent probes for labeling and sensing applications.

Keywords Fluorescent marker · Nanoclusters · Nanodots · Nanoscale metal · Quantum dots

Contents

1	Introduction	308
2	Metal Clusters: The Missing Link Between Single Atoms and Plasmonic Nanoparticles	309
3	Terminology	310
4	Synthesis of Fluorescent Silver Clusters in Various Scaffolds and Their Application as Bio-Labels	311
4.1	DNA Oligonucleotides	311
4.2	Proteins and Peptides	317
4.3	Polymers and Dendrimers	321
4.4	Transfer of Silver Clusters Between Scaffolds	323

I. Díez, and R.H.A. Ras (✉)

Department of Applied Physics, Aalto University (formerly Helsinki University of Technology),
Puumiehenkuja 2, FI-02150 Espoo, Finland

e-mail: robin.ras@tkk.fi

5	Silver Clusters as Fluorescent Probes for Molecular Sensors	325
5.1	Quenching	325
5.2	Analyte-Induced Synthesis of Fluorescent Silver Clusters	326
5.3	Wavelength-Shifting	327
6	Conclusion	328
	References	329

1 Introduction

Luminescence of silver by quantum confinement has been known for several decades e.g., silver clusters in zeolites [1–3], in cryogenic noble gas matrices [4, 5], in inorganic glasses [6–8] and in silver oxide films [9–11]. In the 1980s and 1990s, silver clusters could be prepared in aqueous solution, often using radiolysis, however they were rather unstable and their luminescence was not reported [12–14]. For example, Henglein wrote about “long-lived” silver clusters that live “for many hours” [14, 15]. Obviously, for many practical applications a lifetime of hours is not sufficient. Stable aqueous solutions containing small silver clusters and their luminescence were reported in 2002 in the pioneering work by Zheng and Dickson [16]. Meanwhile, silver clusters have gained importance [17], and basically two kinds of applications have been explored: (1) their use as fluorescent labels for microscopic imaging, and (2) their use as fluorescent probes in molecular sensing.

In general, silver clusters in solution are prepared by reduction of silver ions. Proper scaffolds, e.g., DNA, proteins, dendrimers and polymers, are essential to prevent the aggregation of clusters to larger nanoparticles. Although it is clear that the emission originates from few-atom silver clusters, many aspects of this exciting class of nanoscopic metals are not yet fully understood.

Current fluorescence applications mostly involve organic fluorophores (e.g., rhodamine dyes) or semiconductor quantum dots (e.g., CdSe), both have their own weaknesses and strengths (see Table 1). For example organic fluorophores exist in a wide range of chemical structures and spectral properties; however, their main weakness is that they are prone to photobleaching. On the other hand, semiconductor quantum dots are photostable; however, their large physical size may hinder their use as fluorescent reporters of binding events and, in addition, they are toxic, which may compromise their use for in-vivo applications. Silver clusters combine their positive properties. They are extremely bright, photostable, and nontoxic, have a subnanometer size, and do not blink at time scales relevant for biological applications (0.1 ms–1 s) [18, 19]. These properties allow their use even in single-molecule studies [19]. Recently, Ras et al. demonstrated that silver

Table 1 Comparison of silver clusters with conventional fluorophores [18]

	Silver clusters	Organic dyes	Semiconductor quantum dots
Size	<1 nm	~1 nm	10–20 nm
Photostability	Stable	Bleaches	Stable
Toxicity	Nontoxic	Toxic/nontoxic	Toxic
Blinking	No	Yes	Yes

clusters exhibit electrogenerated chemiluminescence (also called electrochemiluminescence) [20]. In summary, silver clusters have an appealing set of features that complements the conventional fluorophores.

In this chapter, we discuss first how the silver clusters relate to silver atoms and silver nanoparticles. Then we overview the formation of fluorescent silver clusters in aqueous solution, using silver salts as precursors and various scaffolds as stabilizers. Finally we discuss applications of silver clusters in fluorescent labeling of biological tissues, and their use as fluorescent probes for sensing of molecules.

2 Metal Clusters: The Missing Link Between Single Atoms and Plasmonic Nanoparticles

The behavior of metals goes through several noticeable transitions when their size is varied (Fig. 1). Metals of macroscopic dimensions, such as silver jewelry and copper wires, have a mirror-like luster and are good electrical conductors. This

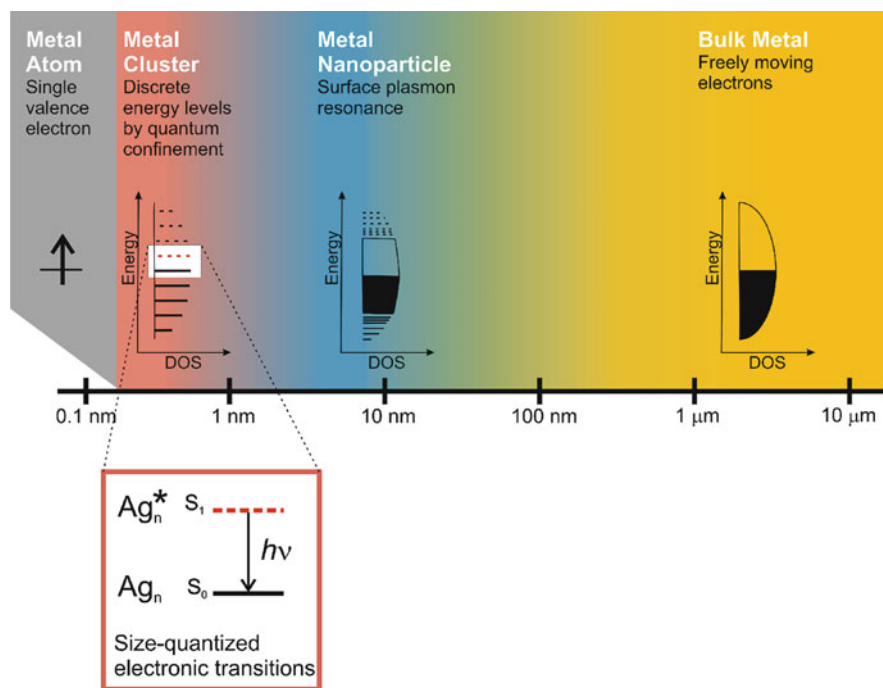


Fig. 1 The effect of size on metals. Whereas bulk metal and metal nanoparticles have a continuous band of energy levels, the limited number of atoms in metal clusters results in discrete energy levels, allowing interaction with light by electronic transitions between energy levels. Metal clusters bridge the gap between single atoms and nanoparticles. Even though in the figure the energy levels are denoted as singlets, we must remark that the spin state of the silver clusters is not yet firmly established

behavior finds its origin in that the atoms in bulk metal share their valence electrons into a homogeneously distributed sea of freely moving electrons. In bulk metal, the energy levels of the electrons are squeezed to such an extent that they appear as a continuum. As metals do not have a band gap between the valence band and the conduction band, electrons do not experience a barrier to populate the conduction band. In bulk, the scattering of the electrons is determined by the electron mean free path, which is 52 nm in the case of silver [21].

When the size of metals is comparable or smaller than the electron mean free path, for example in metal nanoparticles, then the motion of electrons becomes limited by the size of the nanoparticle and interactions are expected to be mostly with the surface. This gives rise to surface plasmon resonance effects, in which the optical properties are determined by the collective oscillation of conduction electrons resulting from the interaction with light. Plasmonic metal nanoparticles and nanostructures are known to absorb light strongly, but they typically are not or only weakly luminescent [22–24].

Further reduction of the particle size down to 1 nm or less leads to breaking up of the band structure into discrete energy levels because the number of atoms becomes limited. The metal at this small scale is called a metal cluster and is not a conductor any more, as the energy levels are too far separated. Therefore, the collective oscillation of electrons is also obstructed and the metal cluster is not plasmonic. Interaction with light is still possible though, via electronic transitions between the energy levels, similar as in organic dye molecules. The metal clusters have a molecule-like behavior. The physics behind few-atom metal clusters is well described in the review by Dickson and coworkers [25]. The nanoclusters of gold and their biolabeling applications are described in the chapter of Muhammed and Pradeep [78].

3 Terminology

The materials described in this chapter are denoted in the literature mostly as “metal clusters” or “metal nanoclusters”. However, the terminology “metal clusters” spans various scientific disciplines and has consequently multiple meanings, including plasmonic nanoparticles and various nanosized metallic structures. Therefore alternative names have been given, although they are at the moment supported only by a fraction of the scientific community: quantum clusters [26], nanodots [27], metal quantum dots [25] and superatoms [28].

A clear, commonly accepted terminology to describe few-atom subnanoscale metals exhibiting quantized energy levels is lacking. The lack of a coherent terminology leads to confusion and may hamper development. In this chapter, we restrict the term “*metal cluster*” to describe few-atom metals with discrete energy levels, and use “*metal nanoparticle*” for particles that have surface plasmon resonance effects (approximate size range between 1 and 100 nm).

The quantized silver clusters can be considered as “metal quantum dots”, because these are zero-dimensional materials where the band gap is formed by

quantum confinement. The silver clusters can also be considered as a “superatom”, since they may have a clear valence electron shell structure, similar as the electrons in ordinary atoms.

4 Synthesis of Fluorescent Silver Clusters in Various Scaffolds and Their Application as Bio-Labels

Silver clusters in solution are prepared by reduction of silver ions in the presence of proper scaffolds, including DNA, proteins, dendrimers and polymers. The scaffolds typically have multiple groups that allow strong interaction with silver ions, such as complexation with DNA bases or ionic interactions with acrylate polymers. The formation of clusters requires suitable conditions to avoid aggregation of the clusters into larger nanoparticles, such as the initial ratio silver:scaffold, the overall concentration, or the type of reductant. Even though many recipes exist for silver clusters in solution, it is not yet understood why the accumulation of silver atoms stops at the size of few-atom clusters. The reduction of silver ions to silver clusters is carried out mainly by two methods, by using a chemical reductant, for instance sodium borohydride, or by photoactivation, i.e., reduction initiated by ultraviolet light [29, 30] or visible light [9, 31]. Furthermore, recent developments and potential applications of fluorescent silver clusters as fluorophores in the field of bio-imaging will be described.

4.1 DNA Oligonucleotides

The strong attraction of silver ions for DNA bases allows the use of these as templates for the formation of silver clusters (Fig. 2a), but special care is needed to avoid the formation of larger nanoparticles [33–39]. It is known that silver ions bind preferentially the heterocyclic bases and not the phosphates [40–42] and prefer the single-stranded DNA (ssDNA) over the double-stranded DNA [43–45].

In this section, the complexity encountered in the design of a proper oligonucleotide as template for the formation of highly luminescent and very stable silver clusters will be shown. Some of the templates discussed in literature are summarized in Table 2.

The first silver clusters made using DNA as template were reported by Dickson et al. in 2004 [32]. The paper describes the time-dependent formation of silver clusters in a 12-base (5'-AGGTCGCCGCC-3'). The clusters have intense absorption in the region 400–550 nm (Fig. 2b) and emission at around 630 nm. The latter band could be decomposed as the emission bands of two distinct excitations at 540 and 580 nm, indicating the existence of two different emitters. As the clusters do not have inherent chirality, the induced circular dichroism associated with the silver cluster electronic transitions is evidence that the clusters are bound to DNA (Fig. 2c).

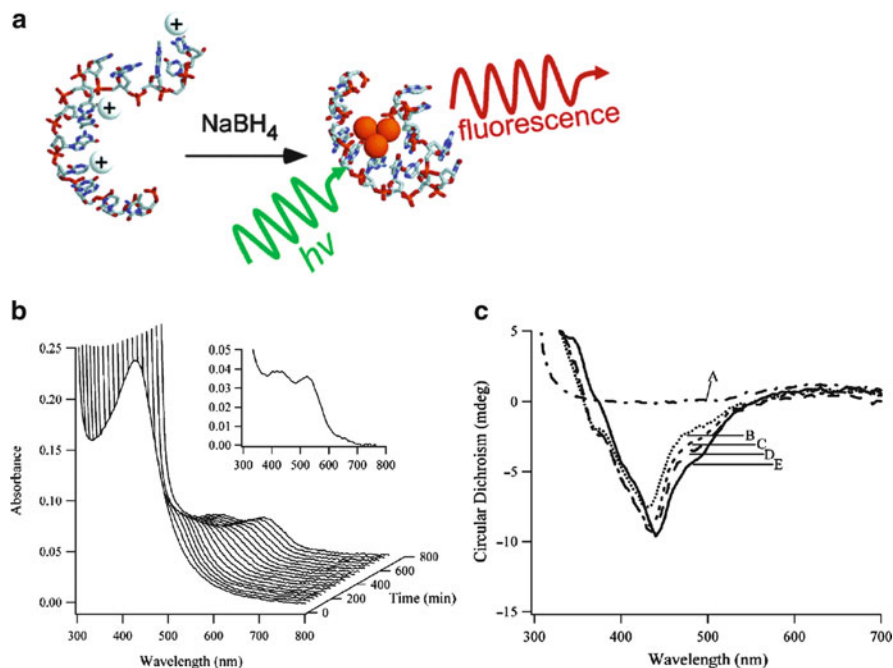
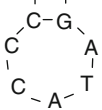
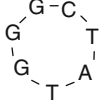


Fig. 2 (a) Schematic of the formation of silver clusters using DNA oligonucleotide as scaffold. After complexation of DNA with silver cations, the mixture is reduced with NaBH₄ and the fluorescent cluster is formed. (b) Absorption spectra of silver clusters acquired every 30 min using [5'-AGGTCGCCGCC-3'] = 10 μM, [Ag⁺] = 60 μM, and [BH₄⁻] = 60 μM. The foremost spectrum was acquired 9 min after adding the BH₄⁻, and it has λ_{max} at 426 nm. The inset spectrum shows the last spectrum in the series (692 min), with peaks at 424 and 520 nm. (c) Induced circular dichroism spectra. The cell path length was 5 cm. The spectra were collected 2 min (A, dashed-dotted line), 20 min (B, dotted line), 40 min (C, fine dashed line), 60 min (D, coarse dotted line), and 150 min (E, solid line) after adding the BH₄⁻ [32]

Although the final stoichiometry of the solution was 2:1:1 in bases:Ag⁺:BH₄⁻, the complexes formed have a maximum of 4 Ag⁺ or 4 Ag atoms per DNA strand, as demonstrated by electrospray ionization mass spectrometry. This stoichiometry was explained as an end-effect of the short oligonucleotide. Moreover, ¹H NMR indicates that silver interaction with cytosine base is stronger than with other bases.

This was the starting point of further studies on the formation of silver clusters in oligonucleotides, for example in a 12-mer cytosine (5'-CCCCCCCCCCCC-3'; also denoted as dC₁₂). Using the same stoichiometry, 2:1:1 in bases:Ag⁺:BH₄⁻, emission spectra recorded at various excitation wavelengths reveal the presence of multiple electronic transitions with emissions centered at 485 nm, 525 nm and 665 nm, this last one, from two different excitations (Fig. 3a). The evolution in time after addition of the reductant shows an isosbestic point with a decrease in the emission band at 665 nm and an increase of the bands at ~500 nm, suggesting a chemical transformation between the emitters, at least at pH lower than 10

Table 2 Oligonucleotide sequences used as templates for the formation of silver clusters

Template sequence	Emission max (nm)	Φ_F (%)	Ref.
5'-CCCTTTAACCCC-3'	485	–	[46]
5'-CCCTCTTAACCCC-3'	520	16.3	[46]
5'-CCCTTAATCCCC-3'	572	28.2	[46]
5'-CCTCCTTCCTCC-3'	620	32.4	[46]
5'-AGGTCGCCGCC-3'	630	–	[32]
5'-CCCATATCCCC-3'	660	18	[47]
5'-CCCTATAACCCC-3'	680	37	[47]
5'-CCCTAACTCCCC-3'	710	31	[47]
dC ₁₂	700, 665, 485, 525	17	[19, 48]
dC ₄ T ₄ C ₄	495	–	[49]
dT ₄ C ₄ T ₄	475	–	[49]
dT ₁₂	540	–	[49]
dC ₂₄	634	–	[50]
TATCCGTCC-GCA	648	–	[45]
			
ATAGGCAGG-CGT	574	–	[45]
			

Φ_F Fluorescence quantum yield, C cytosine, G guanine, A adenine, T thymine

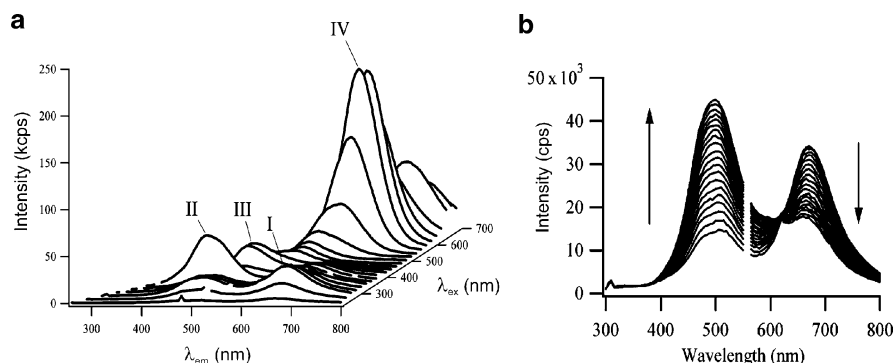


Fig. 3 (a) Fluorescence emission spectra (*bottom axis*) as a function of the excitation wavelengths (*right axis*), for silver clusters prepared with the molar ratio dC₁₂:Ag⁺:BH₄⁻ of 1:6:6. The spectra were acquired 4.5 h after adding the BH₄⁻. The dominant emission band occurs at (IV) $\lambda_{\text{ex}} = 580$ nm/ $\lambda_{\text{em}} = 665$ nm. Three other bands occur at (I) $\lambda_{\text{ex}} = 280$ nm/ $\lambda_{\text{em}} = 665$ nm, (II) $\lambda_{\text{ex}} = 340$ nm/ $\lambda_{\text{em}} = 485$ nm and (III) $\lambda_{\text{ex}} = 440$ nm/ $\lambda_{\text{em}} = 525$ nm. (b) Time evolution of the fluorescence emission spectrum using $\lambda_{\text{ex}} = 280$ nm, which excites both the red- and green-emitting species. The isosbestic point at 615 nm, results as the intensity at 495 nm increases, while the intensity at 670 nm decreases. Spectra collected every 30 min starting 3 h after adding the BH₄⁻ [48]

(Fig. 3b). The conversion of red emitters into green emitters with time was explained as an oxidation reaction confirmed by the addition of extra reductant, which leads to the transformation of green emitters into red ones [48].

There are several publications describing the role of DNA bases and base sequence on the formation of fluorescent silver clusters. The different bases have different affinity for silver and the different base-silver cluster interaction produces different emissions. For a given DNA strand, every particular base sequence creates a different environment for the clusters and consequently a different emission. For instance, Petty et al. have studied the influence of thymine (T) and cytosine (C) bases by playing with their combinations in oligonucleotides [49]. Fluorescent silver clusters formed in dT₁₂ and dT₄C₄T₄ have similar properties. The emission intensity increases with pH having a midpoint at pH 9.5, which is close to the pK_a of the N3 of thymine indicating that the deprotonated thymine forms a complex with the fluorescent silver clusters. In nitrogen atmosphere, nonfluorescent clusters are formed, whereas the presence of oxygen allows the formation of fluorescent species, which suggests in this case that nonfluorescent species are reduced while fluorescent ones are oxidized. A ratio bases:Ag⁺ of 2:1 leads to a maximum in the emission intensity when using both templates, dT₁₂ and dT₄C₄T₄, interpreted by the authors as the same cluster size is stabilized by both oligonucleotides. Silver clusters show similar excitation maxima, but different Stokes shifts, pointing out the role of the bases and their influence on the environment of the clusters and therefore on the optical properties of the clusters. In the case of more cytosine-rich oligonucleotides such as dC₄T₄C₄ similar properties were found but an additional emitter was formed here, a red emitter.

Dickson et al. carried out a high-throughput analysis of 12-mer DNA strands and found that the cluster properties are highly sequence-dependent, claiming that discrete sequences lead to well defined silver cluster sizes and hence to distinct emission properties ranging from visible to near-IR [46]. Three long-wavelength emitters, yellow, red and near-IR, were prepared in oligonucleotides and presented as good candidates for their use as single molecule biolabels (Fig. 4). The synthesis of each of the emitters in oligonucleotides does not follow a general procedure, since the optimal synthetic conditions differ for every case, for instance regarding the use of buffered or unbuffered solutions and pH closer to 5 or to 8. However, the efforts are rewarded since silver clusters protected by oligonucleotides present many advantages, especially those emitting in the near-IR. For instance, these clusters can be excited with low energy, which is beneficial for the photostability of the clusters and preserves the chemical stability of the scaffold. Moreover, biological samples have low background fluorescence signals in the near-IR, providing high signal-to-noise ratio. These silver clusters present large absorption coefficients and quantum yields exceeding 30% (Table 2). Compared to cyanine dyes, these emitters have higher emission intensities (1,500 and 2,500 counts/s for cyanine dyes and clusters respectively, Fig. 5) and longer lifetimes (decay to 1/*e* emitters in 9 and 580 s respectively) [46]. They do not blink in relevant timescales (0.1–1,000 ms) and the dark-state lifetime of 30 μs can be reduced to less than 10 μs by increasing the intensity of the excitation [19].

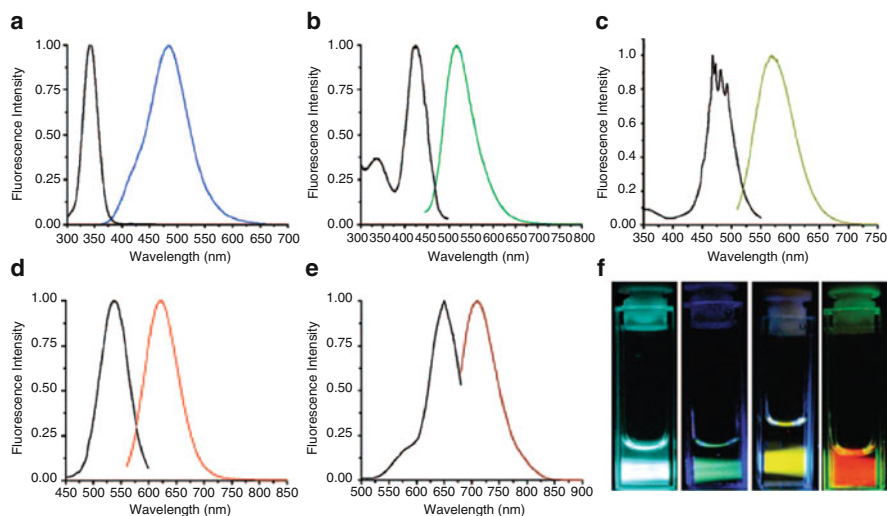


Fig. 4 Steady-state excitation and emission spectra for five distinct ssDNA encapsulated Ag clusters. (a) Blue emitters created in 5'-CCCTTTAACCC-3', (b) green emitters created in 5'-CCCTCTTAACCC-3', (c) yellow emitters created in 5'-CCCTTAATCCCC-3', (d) red emitters created in 5'-CCTCCTTCCTCC-3', and (e) near-IR emitters created in 5'-CCCTAACTCCCC-3'. (f) Pictures of emissive solutions in (a)–(d) [46]

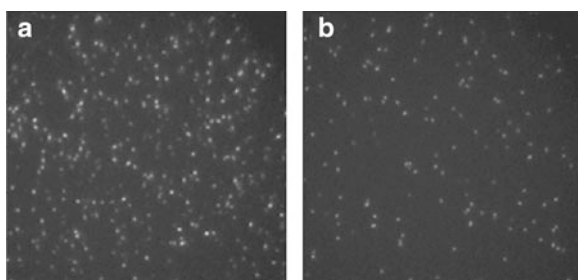


Fig. 5 (a) Image of single IR-emitting dC₁₂-Ag_n molecules in a poly(vinyl alcohol) (PVA) film. (b) Image of single Cy5.29 molecules in a PVA film. The image dimensions are 40 × 40 μm, and imaging conditions of (a) and (b) are identical [19]

Recently it was shown that optical modulation of the silver cluster fluorescence could allow extracting weak signals from extremely fluorescing backgrounds. The method consists in coillumination with an intensity-modulated secondary laser (excitation ~800 nm) and produces a photobrightening of higher energy cluster emissions by depopulation of the dark state without increasing the background (Fig. 6a, b) [27]. In this way, silver clusters with emission at ~710 nm (upon excitation at 633 nm) can be distinguished from background signals created by autofluorescence (Fig. 6c, d) or dyes (Cy5) (Fig. 6e, f) [27].

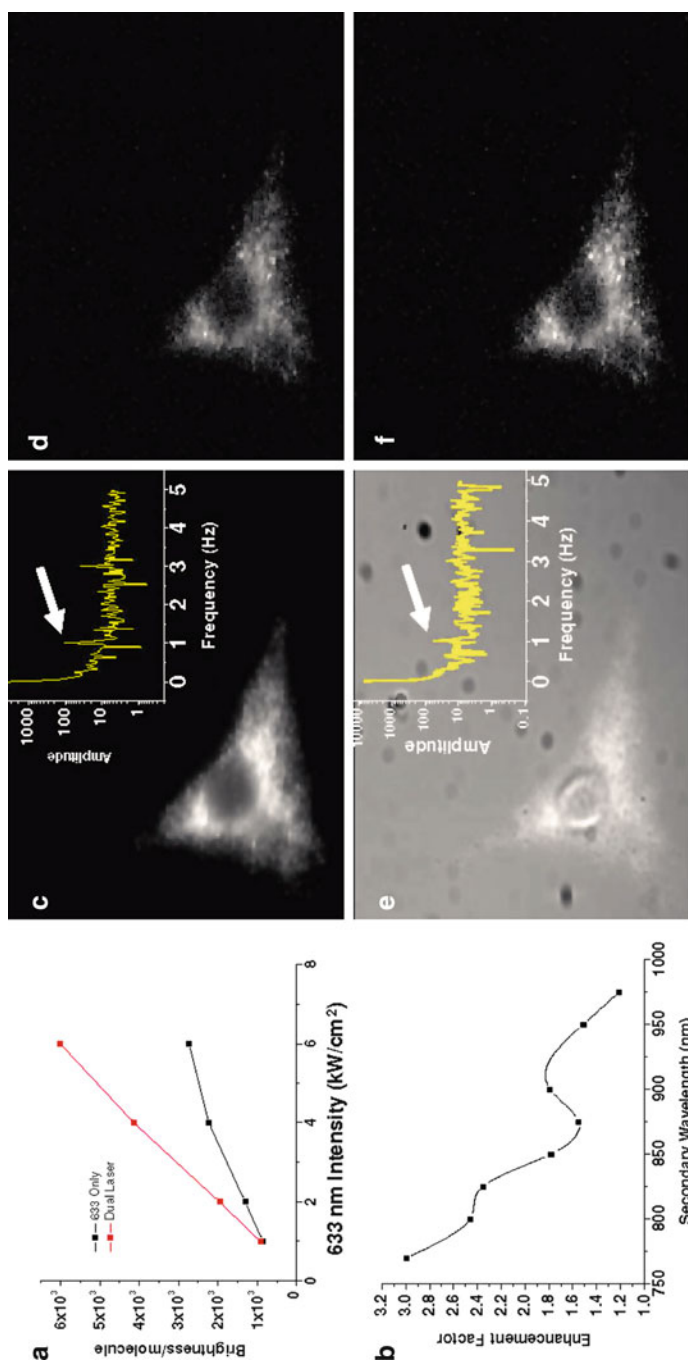


Fig. 6 (a) Brightness per Ag cluster under single-laser (633 nm, *black*) and dual-laser (633 nm + 805 nm, *red*) excitation, as determined by fluorescence correlation spectroscopy. Simultaneous 805 nm excitation (8 kW/cm²) recovers the linearity between excitation and 710 nm emission. (b) Excitation scan of the secondary laser-based enhancement (4 kW/cm²) relative to single laser excitation (633 nm, 1.2 kW/cm²). (c) Typical dual-laser ccd image of biotinylated NIH 3T3 cells surface-labeled with avidin and biotinylated Ag cluster. The secondary laser modulates the fluorescence at every pixel simultaneously. *Inset*: Fourier transform of a typical pixel intensity as a function of time. (d) Autofluorescence is removed from the recovered cell image after demodulation at the modulation frequency [indicated by the *arrow* in the *inset* of (c)]. (e) Image of the same cell with highly concentrated Cy5 solution added to simulate a very high autofluorescent background. *Inset*: the modulation frequency remains readily apparent in the Fourier transform of a typical pixel intensity vs. time. (f) Demodulated image showing the nearly complete elimination of the Cy5 and autofluorescent background signals, leaving only the distinct signal of Ag clusters [27]

Additional studies confirmed the sequence dependency on the generation of fluorescent silver clusters when using scaffolds of 19 bases, with a shape of a hairpin or containing two single-stranded (C or G rich) sequences bound by two base pairs (Table 2). In this case, the authors claim that based on mass spectra, silver binds with comparable affinities to chemically similar sites on C and G bases. The reason for the differences in the emission peaks might be the unique local environment offered by different base stacking between the two strands or by distinct of the strand, since the incorporation of silver in the loop of the hairpin is more difficult than in the open geometry. The discrepancy regarding the silver-oligonucleotide affinity described by various groups could be also explained considering the different relative concentrations used in the experiments. Authors claiming higher affinity of silver for cytosine have used 0.5 silver per nucleotide, whereas authors claiming similar affinities for cytosine and guanine have used 0.29 silver per nucleotide and the preferences of silver might be different at different ratios [43, 44, 51, 52].

The fluorescence properties and stability of silver cluster in hairpins were reported to be related to the number of cytosines in the loop (varying from 3 to 12 cytosines) [53]. However, as a general rule, red emitters were brighter than green emitters. Further specific studies on the 9C loop show that the red emitter corresponds to $\text{Ag}_{13}:\text{DNA}$ and the green emitter correlates with $\text{Ag}_{11}:\text{DNA}$. A great advantage of silver clusters encapsulated in hairpins is that they are bright enough to be imaged by using an epifluorescence microscope.

The high fluorescence quantum yield of DNA-encapsulated silver clusters ($\Phi_F > 30\%$) [46, 50] makes them good candidates as fluorophores in cell imaging. Aiming the application for cell imaging, the DNA-encapsulated silver clusters were prepared as described before but using a longer strand, a 24-mer oligocytosine (dC_{24}), linked to a protein, avidin. The presence of avidin does not affect the chemical or photophysical stability of the clusters (emission maximum at 634 nm, excitation at 580 nm, fluorescence lifetime of about 2.86 ns and remarkable brightness).

First results in this research showed that biotinylated fixed cells became fluorescent upon staining with avidin- dC_{24} -Ag clusters (Fig. 7a, b). However, in the case of living cells, loading with avidin- dC_{24} -Ag clusters produces bright spots, indicating endocytosis (Fig. 7c). The results were quite different when using an antibody, heparin sulfate (HS) instead of avidin. HS- dC_{24} -Ag clusters can penetrate the cells when incubated at 37°C showing fluorescent nuclei (Fig. 7d–f) [50].

4.2 Proteins and Peptides

A commonly used staining method for the cell nucleolus is based on silver nanoparticles [54]. The proteins of the nucleolus, such as nucleolin, are known to have high affinity to silver ions due to their amino-terminal domain. Subsequent reduction leads to the formation of the silver nanoparticles stain. In spite of all the efforts, a general and definitive conclusion regarding the attraction between silver

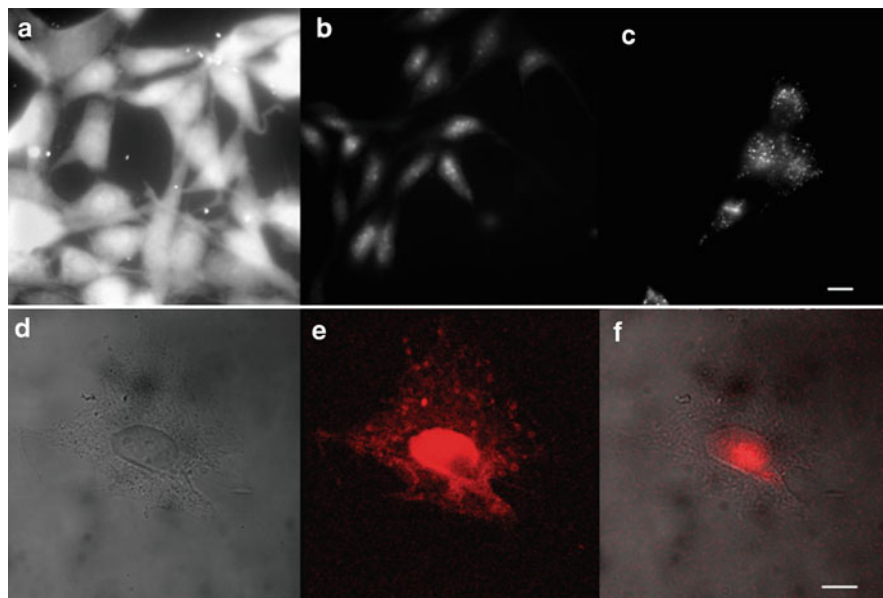


Fig. 7 (a)–(c) Fluorescence images of NIH 3T3 cells stained with Avidin-dC₂₄-Ag. (a) Fixed cells, biotinylated. (b) Fixed cells, nonbiotinylated. (c) Live cells, biotinylated. Images were recorded on a Zeiss Axiovert 200 microscope with a CoolSNAP CCD camera (Roper Scientific). Scale bar 30 μm . (d)–(f) Fluorescence images of live NIH 3T3 cells stained with anti-HS-dC₂₄-Ag. Live cells incubated with anti-HS-dC₂₄-Ag at 37°C for 6 min (d, bright field; e, silver clusters; f, merge). Images were recorded on Zeiss LSM 10 confocal microscope. The fluorescence images were taken at 543 nm excitation. Scale bar 25 μm [50]

ions and peptides cannot be easily extracted. In addition to the silver binding amino groups, some authors have demonstrated higher degree of silver binding in peptides rich in proline and hydroxyl residues [55], whereas others showed a preferential affinity of silver for methionine-containing peptides compared to their nonmethionine containing counterparts [56].

In 2007, Dickson et al. found that it is possible to stain fixed cells with fluorescent silver clusters instead of silver nanoparticles by tuning the staining conditions [57]. The new approach consists of staining fixed cells with a low concentrated silver nitrate solution 20–100 mM, within 20 h at ambient conditions, and reducing the silver by photoactivation, with the result of small silver clusters that present a broad emission band between 500 and 700 nm (Fig. 8a–d). The discovery that fluorescent silver clusters can be generated by photoactivation of cells fed with silver salt, opens up new paths for the application of silver clusters in biological systems.

Besides the formation of luminescent silver clusters in fixed cells, likely due to the presence of proteins, fluorescent silver clusters have been synthesized using proteins as templates. In 2008, Pal et al. reported on the use of an enzyme, bovine pancreatic α -chymotrypsin (CHT) as biotemplate during the chemical reduction of

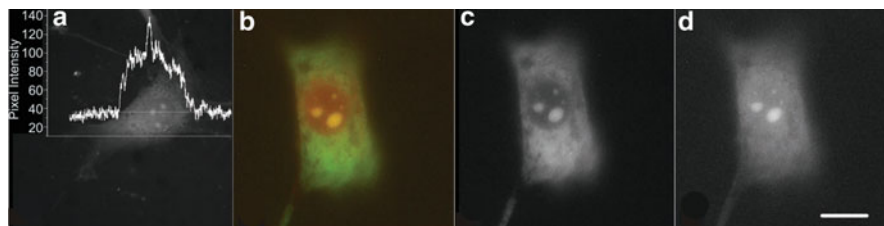


Fig. 8 Emission from formaldehyde-fixed NIH3T3 cells loaded with 100 mM silver nitrate for 20 h. (a) Fluorescence image; the *inset* is the intensity profile along the line drawn across the cell. (b) Merge of (c) and (d). (c) Emission from RNASelect fluorescence (*green channel*); (d) Emission from silver clusters (*red channel*); Scale bar 30 μm [57]

silver ions to produce well dispersed and stable solutions of protein-conjugated fluorescent silver clusters [58]. The protein-protected silver clusters show emission at 680 nm when excited at 500 nm. The molar ratio of $\text{CHT}:\text{Ag}^+:\text{BH}_4^-$ was 1:10:100, where the large excess of NaBH_4 provokes two adverse effects in the system. A first consequence of the excess of NaBH_4 , is that the reductant cleaves disulfide bonds inducing denaturation of the protein. Partial reconstitution of the protein was achieved with efficient oxidation, by dialyzing the sample against water of pH 8.0–8.5 for 24 h in aerated conditions. The functional integrity of the protein was confirmed by studying the enzymatic activity on a substrate Ala-Ala-Phe 7-amido-4-methyl coumarin. The enzymatic activity of CHT-Ag was retarded by 2.8 times compared to the activity of native CHT. The origin of the retard might be the reduction and oxidation processes since reconstituted CHT presents similar delays. This indicates that silver clusters are not located in the enzymatic active site of CHT. A second event caused by the excess of sodium borohydride is the increase in the pH and a subsequent aggregation of the protein. However, the aggregation might be reversible by lowering the pH with an exhaustive dialysis against pure water.

Prior to these findings, in 2005, fluorescent silver clusters in combination with a fluorophore, thioflavin T (ThT), were already used to image proteins [31]. Silver clusters were prepared by photoreduction at ~ 330 nm of solutions containing ThT and Ag^+ . The emission band centered at ~ 450 nm grew by fivefold when $\text{ThT}:\text{Ag}^+$ was 100:1 and by 50-fold when the ratio was 1:1 (Fig. 9a, b), suggesting the enormous effect of silver. The authors proposed that the emission observed is originated by both, intrinsic formation of fluorescent silver clusters (when the samples were irradiated at 500 W/cm^2) and by metal-enhanced fluorescence of ThT (with irradiation at 1 W/cm^2). Amyloid fibrils stained with ThT-Ag clusters present a time-dependent increase of fluorescence with no photobleaching after 24 h of illumination at 475 nm (500 W/cm^2) in contrast to ThT-stained fibrils, which have a rapid decay of fluorescence (Fig. 9c). With this method, the authors managed also to image a single fibril and claim that the luminescence produced by ThT-Ag clusters is at least 100-fold higher than the luminescence reported in photoreduced silver clusters formed in water solution with dendrimers [16] or in Ag_2O films [9].

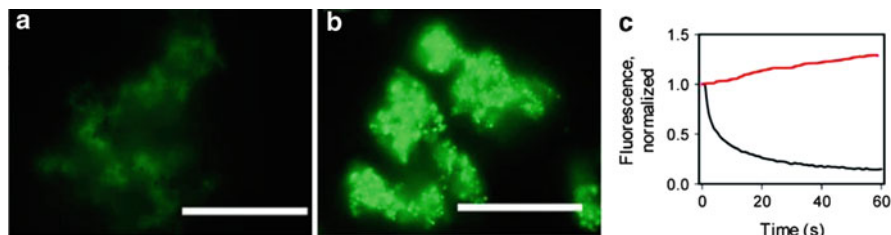


Fig. 9 Epifluorescence microscopy images of the amyloid fibrils of PrP 90–231 (1 μM), stained at room temperature with (a) ThT alone (10 μM) (exposure time 1.6 s), and (b) with preformed ThT-Ag clusters (exposure time 0.02 s). ThT-Ag clusters were preformed by irradiation of aqueous solutions of ThT (10 μM)/AgNO₃ (1 μM) at 312 nm for 3 min. Scale bars = 10 μm. (c) Photobleaching kinetics of the fibrils stained with ThT (*black line*) vs. photoactivation kinetics of the fibrils stained with ThT-Ag clusters (*red line*). Data collected from a 5 μm × 5 μm area and normalized to the intensity measured at zero time [31]

Taking advantage of the well-established affinity of silver cations for proteins as shown before in the case of nucleolin and due to the importance of nucleolin in actual investigations [59, 60], synthetic peptides derived from nucleolin were used as scaffolds for the formation and protection of fluorescent silver clusters [57]. The earliest peptide mentioned in literature as template for the formation of fluorescent silver clusters was the histidine-rich AHHAHHAAD, but synthesis and optical properties were only briefly described since that was not the main topic of the publication [61]. The first detailed study of peptides as scaffold [57] describes oligopeptides that contains 15–18 amino acids, including the most abundant amino acids in nucleolin, like glutamic acid (E), lysine (K), and aspartic acid (D) as well as cysteine (C), which is minor in nucleolin but it is known to bind silver [62]. The resulting peptide allows formation of silver clusters by reducing a silver solution (0.22 mM in peptide, 0.37 mM in AgNO₃) with sodium borohydride (18 mM). But this peptide was not very effective as a stabilizer since it offers to the clusters a chemical lifetime of only 3 days. To overcome this problem other peptides were created. The tested peptides contain 18 amino acids, including D, C and K but also histidine (H) and asparagine (N) or leucine (L). The peptide capable of stabilizing silver clusters during 5 weeks had the sequence “HDCNKDKHDCNKDKHDCN”, and the silver clusters produce fluorescence at 630 nm when excited at 400 nm. Giving a closer look to the composition of this peptide, one can notice that it is far from the composition of nucleolin, for instance, it contains three histidines (H) and three cysteines (C) which are minor constituents in nucleolin (~0.1% each) and also three asparagines (N) (~3% in nucleolin) [63]. Although this peptide and its use as scaffold in the synthesis of silver clusters represent a great advance in the field, the different composition compared to nucleolin, clearly points to the lack of understanding of the basics of cluster synthesis and calls for more exhaustive research to identify both, the mechanism of formation of silver clusters in peptides and the requirements for their stabilization.

A remarkable contribution regarding the use of peptide-protected fluorescent silver clusters in biological systems came with the insertion of fluorescent silver

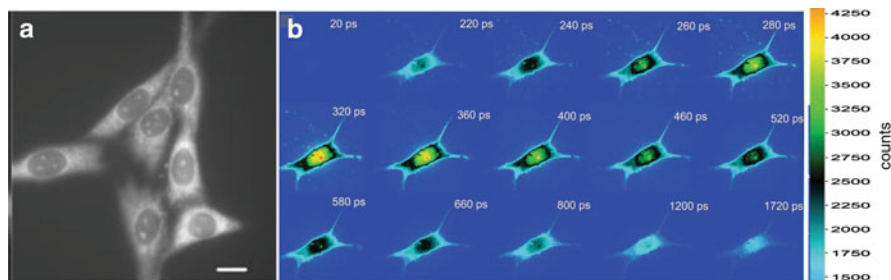


Fig. 10 (a) Fluorescence image of methanol-fixed NIH3T3 cells loaded with peptide encapsulated silver clusters for 1 h at room temperature. (b) Time profile of the time series images of cell stained with silver nitrate showing the fast silver cluster emission centered in the nucleus at short times with a maximum at 320 nm. Note that *black* indicates an intermediate intensity level in this color scheme [57]

clusters in living cells. Living cells can be loaded with peptide-encapsulated silver clusters even at low temperature, and the cells show evenly distributed silver clusters emission indicating that clusters do not penetrate in the cells by endocytosis. In fixed cells, there is an additional strong staining in the nuclear region (Fig. 10a). The lifetime of silver clusters protected by peptides is similar to the lifetime of fluorescent silver clusters formed in cells, and has two components, one fast of 220 ps (33%) and one slow of 1,760 ps (67%). The fast component allows high signal-to-noise ratio, minimizing contributions from autofluorescence or other added dyes when using picosecond-gated microscopy (Fig. 10b). As a disadvantage, the peptide-encapsulated silver clusters have still relatively low fluorescence quantum yield, about 3% [50].

4.3 Polymers and Dendrimers

The first reported water-soluble fluorescent silver clusters were prepared in dendrimers, by Dickson et al. The combination of second-generation OH-terminated poly(amidoamine) (PAMAM) dendrimer (16 OH per dendrimer) and irradiation with blue light (30 W/cm^2 , $\sim 6 \text{ s}$) transforms a 1:3 dendrimer: Ag^+ ($\text{OH}:\text{Ag}^+$ 1:0.19) solution into a highly luminescent solution containing silver clusters encapsulated in dendrimers [16]. The silver clusters after more than 30 min of continuous excitation ($\sim 500 \text{ nm}$, 300 W/cm^2) keep still about 80% of their fluorescence intensity providing a good photostability. Further studies showed that silver clusters prepared in dendrimers have the similar level of cytotoxicity than that of the corresponding dendrimers. For instance, the NH_2 -terminated PAMAM and its succinamic acid-derivative show cytotoxicity only at high concentrations ($1 \mu\text{M}$), and cells incubated with their silver nanocomposites show intracellular

fluorescence which could make these composites suitable for applications as biomarkers [64] although the composite size is quite large, between 3 and 7 nm. Goodson et al. reported on the fluorescent properties of gold clusters prepared using PAMAM dendrimers [65].

Microgel particles (220 nm) of poly(*N*-isopropylacrylamide-acrylic acid-2-hydroxyethyl acrylate) (poly(NIPAM-AA-HEA)) were used by Kumacheva et al. for the fabrication of fluorescent silver clusters from solutions with molar ratio COOH:Ag of 1:1 and with UV irradiation (365 nm) [66]. The silver clusters present an emission band at 610 nm at the excitation of 450 nm. With control reactions, the authors determined that the presence of PAA (COOH) was decisive for the formation of fluorescent silver clusters, whereas the importance of HEA (OH) was less obvious. Microgels respond to external stimuli like temperature, pH or ionic strength by undergoing noticeable volume changes that influence the optical properties of silver clusters. A high pH (~ 8) favors deprotonation of the COOH groups and swollen microgel particles, which lead to a higher emission intensity of the silver clusters. The irradiation conditions were a bit different from the conditions reported in PAMAM: weaker UV source (0.3 W/cm^2) and longer irradiation (minutes) were used here.

Similarly, fluorescent silver clusters could be prepared in so called molecular hydrogels, formed by polyglycerol-*block*-poly(acrylic acid) (PG-*b*-PAA), using a ratio COOH:Ag of 2:1 with UV irradiation (365 nm). The emission band centered at 590 nm reached a maximum after 200 min of irradiation. The authors claim improved photostability of the clusters since they are still luminescent even after 9 h of irradiation, but it has to be mentioned that the irradiation source was weak, only 0.5 mW/cm^2 . They claim that it is the number of arms in the star polymer rather than the length of the arms (thus the density of COOH) that plays a crucial role in the formation of silver clusters [30].

In a more simple and cheap way, silver clusters can be prepared in aqueous solutions of commercially available polyelectrolytes, such as poly(methacrylic acid) (PMAA) by photoactivation using visible light [20] or UV light [29]. Ras et al. found that photoactivation with visible light results in fluorescent silver cluster solutions without any noticeable silver nanoparticle impurities, as seen in electron microscopy and from the absence of plasmon absorption bands near 400 nm ($\Phi_F = 5\text{--}6\%$). It was seen that using PMAA in its acidic form, different ratios $\text{Ag}^+:\text{MAA}$ (0.15:1–3:1) lead to different emission bands, as discussed in the next section (Fig. 12) [20]. When solutions of PMAA in its sodium form and silver salt were reduced with UV light (365 nm, 8 W), silver nanoclusters were obtained with emission band centered at 620 nm and $\Phi_F = 18.6\%$.

As a last example on the fabrication of silver clusters, it is worth mentioning that they can also be prepared in microemulsions, where the small droplets of water act as nanoreactors. The surfactant used was AOT and the reducing agent was a very mild one, i.e. sodium hypophosphite. In this manner, fluorescent silver clusters with less than ten atoms are formed and showed planar shape when deposited onto gold substrates, as determined by scanning tunneling microscopy [67, 68].

4.4 Transfer of Silver Clusters Between Scaffolds

Although many individual biomolecular functions have already been studied by labeling bioactive molecules, proteins, antibodies and DNA strands with organic dyes and quantum dots, the extraordinary properties of silver clusters suggest that these species might be competitive alternatives (Table 1 and Fig. 11a). Nevertheless, silver clusters present some disadvantages in their application to biological systems.

The major issue is the formation of silver clusters in situ in the presence of the biomolecule to be labeled. On one hand, this problem is due to the fact that only a few scaffolds are suitable systems providing the proper environment for the formation of these very small species and preventing the formation of larger silver nanoparticles. On the other hand, the biomolecules might be harmfully

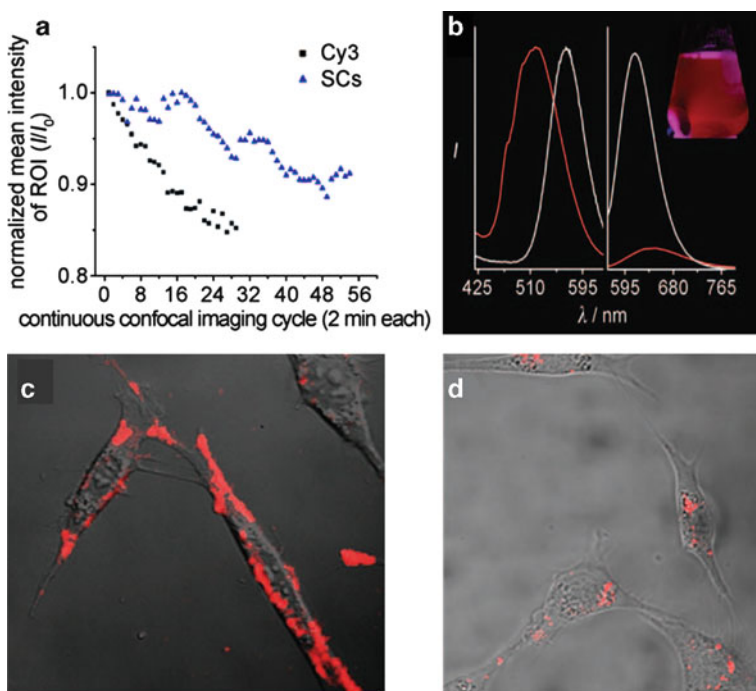


Fig. 11 (a) Photostability and comparison between Cy3-labeled and silver clusters-labeled cells under identical staining conditions. (b) Silver clusters transferred from PAA to dC₁₂. *Left panel*, normalized excitation spectra of reaction mixture detected at 640 nm before (red) and after (white) the addition of dC₁₂, which corresponds to individual excitation spectra of PAA-Ag clusters and dC₁₂-Ag clusters, respectively. *Right panel*, tenfold increase in the fluorescence intensity after the addition of dC₁₂ (white); excited at 545 nm. The *inset* shows PAA-Ag clusters (100 mL) prepared in a Pyrex conical flask, under 354 nm excitation. (c)–(d) Live NIH 3T3 cells stained with FSP-dC₂₄ with silver clusters transfer as the last step. Merge bright-field and silver clusters fluorescence (pseudo color red, excited at 543 nm) in cells incubated with FSP-dC₂₄ at (c) 4°C and (d) 37°C [69]

affected during the reduction of silver either by a chemical reductant or by an irradiation source. For example, silver salts can be easily reduced by sodium borohydride, but this reductant may also reduce other functional groups, including disulfide bonds to sulfhydryl groups and could destabilize the folding and function of proteins.

To overcome the difficulty of finding a proper scaffold, which provides the required environment for the formation of silver clusters being at the same time stable during reduction of silver, Dickson et al. proposed a new approach where silver clusters are first prepared using a polymer and then transferred, or shuttled, to the desired biomolecule [69]. These two steps for labeling of cellular components introduce additional advantages to those already mentioned. For instance, the production of silver clusters can be optimized in the first step by adding 3-(2-aminoethylamino)propyltrimethoxy silane (APTAMOS) to complex silver ions before stabilization with the proper organic polymer, in this case poly(acrylic acid) (PAA) [69]. The silver clusters prepared in this way have tenfold increased emission intensity (Fig. 11b) and the formation of nanoparticles, was eliminated. In the second step, the transfer efficiency of fluorescent clusters to high-affinity ssDNA sequences (oligocytosines) can be as well optimized for the specific sequence by adjusting the temperature, the pH and the buffer in the transfer step and by varying the ratio of Ag^+ /APTAMOS in the reduction step.

The shuttle of silver clusters from PAA to oligocytosine due to the stronger interaction of clusters with oligonucleotides was confirmed by a pronounced shift in the excitation spectra from 515 to 570 nm (Fig. 11b). The specific conditions required in each system for the successful shuttle of silver clusters represent an enhancement in the selectivity of the labeling process. Using the cluster transfer, it is possible to produce silver clusters in a polymer and then label ssDNA or oligopeptides [77]. In a similar manner, antibodies conjugated with ssDNA were labeled with fluorescent silver clusters and then the antibody-DNA-Ag clusters were applied to tag live cells. Incubation of live cells at 4°C results in cell-surface staining (Fig. 11c) whereas incubation at 37°C results in internalization of silver clusters and staining inside the cells (Fig. 11d).

The concept of dynamic silver clusters capable to transfer between molecules was also pointed out recently by Ras et al. for silver clusters prepared by photo-activation using PMAA as scaffold [20]. Every specific initial ratio of silver ions to methacrylate unit, $\text{Ag}^+:\text{MAA}$, results in distinct spectral bands (Fig. 12a, b). Thus, an initial ratio 0.5:1 gives an absorption band at ~ 503 nm, whereas a ratio 3:1 gives a band at ~ 530 nm. The shuttle effect was proven when for a given silver cluster solution with ratio 3:1 and absorption at 530 nm, a blue shift was achieved by the addition of pure PMAA. For instance if the added amount of polymer decreases the ratio $\text{Ag}^+:\text{MAA}$ from 3:1 to 0.5:1, the new optical band will match exactly with the band corresponding to a solution with initial ratio 0.5:1, that is 503 nm (Fig. 12c). The explanation given for this blue shift was the redistribution of the existent silver clusters in PMAA chains over the newly available PMAA chains, in other words that the clusters shuttle from partly clusters-filled chains to empty ones.

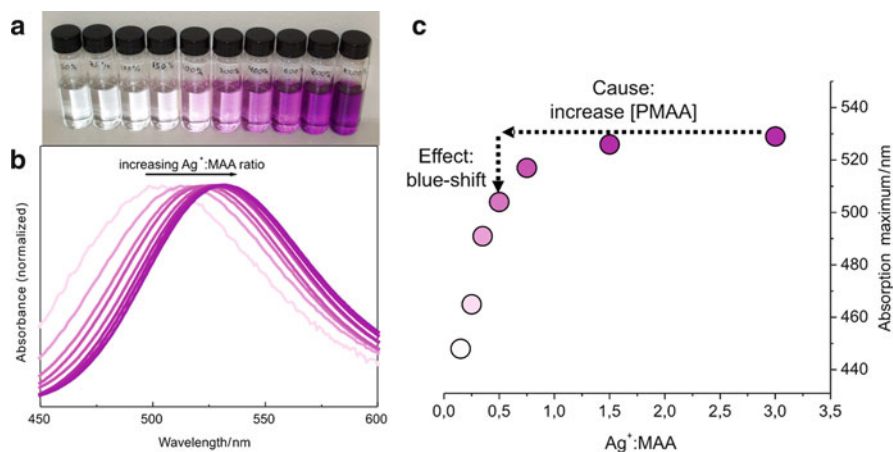


Fig. 12 (a) Image of PMAA-protected fluorescent silver clusters prepared with increasing initial ratio $\text{Ag}^+:\text{MAA}$ from 0.5:1 to 12:1 and equal irradiation time. (b) Absorption spectra of the same samples as in (a). (c) Variation of absorption maxima of some of the samples in (a) with molar ratio. *Black arrows* indicate how the absorption band shifts to the blue with the addition of extra polymer to a fluorescent cluster solution explaining the transfer effect of silver clusters among PMAA chains [20]

5 Silver Clusters as Fluorescent Probes for Molecular Sensors

The silver clusters can be applied as fluorescent probes to retrieve information about the chemical environment. There are reported three classes of sensors based on silver clusters. First, we discuss silver cluster sensors of which the fluorescence quenches in the presence of the analyte. Second, we discuss a sensor in which fluorescent clusters are formed only in presence of the analyte. Finally, we discuss the shift in the absorption and fluorescence bands of silver clusters while sensing the chemical environment.

5.1 Quenching

Quenching of silver cluster fluorescence is suitable to detect the presence of small analytes such as cysteine [70] and metal ions [71–73]. Sensing is possible with a low detection limit and high selectivity. Interestingly, Guo et al. show selectivity for Hg^{2+} , not for Cu^{2+} [72], whereas Lan et al. show the selectivity for Cu^{2+} , not for Hg^{2+} [73]. This may seem at first sight a discrepancy; however, both papers use a different DNA sequence leading to a different type of emitter. It shows that the properties of a specific type of silver cluster cannot always be generalized to all silver clusters. Figure 13 shows the case of cysteine detection, in which the silver

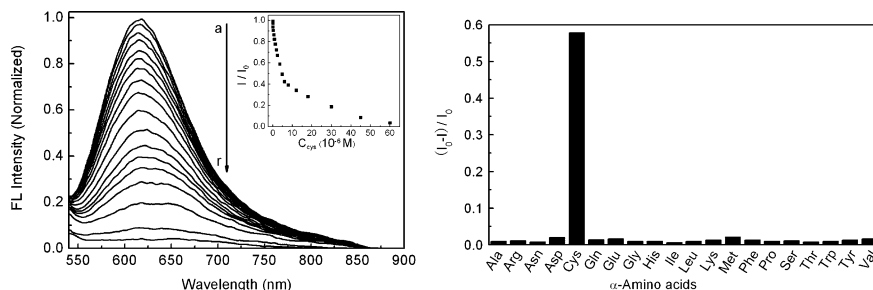


Fig. 13 (Left) Emission spectra of PMAA-Ag clusters in the presence of varying concentrations of cysteine from (a) 0 to (r) 60×10^{-6} M. The inset displays the relative fluorescence intensity of Ag clusters recorded at 615 nm vs. the concentration of cysteine. (Right) Fluorescence response of Ag clusters in the presence of various α -amino acids [70]

clusters were prepared using PMAA as the scaffold [70]. As shown in Fig. 13, the emission of silver clusters was strongly quenched by cysteine. The quenching exhibited a good linear relationship by Stern–Volmer analysis in the range of 25 nM–6 μ M. Other amino acids did not result in fluorescence quenching, demonstrating the excellent selectivity for cysteine detection. The quenching indicates that there is a strong interaction between the clusters and cysteine. Shang and Dong propose that the thiol group of cysteine forms an Ag–S bond followed by oxidation of silver by oxygen, resulting in the quenching of the fluorescence of silver clusters [70].

5.2 Analyte-Induced Synthesis of Fluorescent Silver Clusters

The formation of silver clusters is known to be very sensitive to the local environment of the scaffold. For example, we described earlier in this chapter that in case of DNA, the spectral properties depend strongly on the nucleotide sequence (see Table 2). Recently Guo et al. reported on the application of silver clusters to detect single nucleotide mutations in DNA [74]. In their paper they were able to identify the sickle cell anemia mutation in hemoglobin beta chain (HBB) gene. A single-nucleotide mutation (A instead of T) is responsible for the sickle cell disease. They first synthesized a DNA strand (Str-C) that forms a duplex with a normal HBB (Str-B) and has an additional six-base cytosine loop (C_6 loop) at two bases away from the mutation point (See Fig. 14). The C_6 loop is the site where the silver clusters form. When this probe DNA strand was hybridized with the normal HBB gene, it could be used to synthesize intensely fluorescing silver clusters. However, when the probe strand was hybridized with the mutated HBB gene (Str-A), no fluorescence could be detected, indicating that the formation of clusters is prohibited.

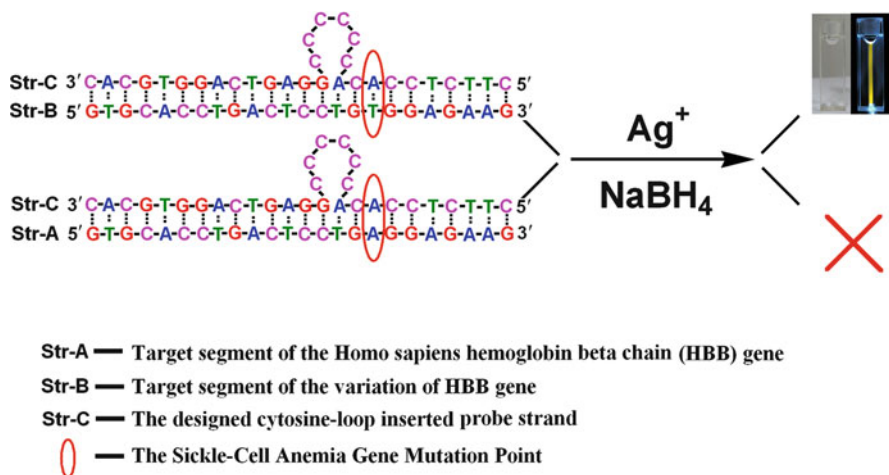


Fig. 14 Use of two different DNA duplexes with inserted cytosine loops working as synthetic scaffolds to generate fluorescent silver clusters for the identification of the sickle cell anemia gene mutation (*black dots* represent hydrogen bonds formed in base pairing and *black dashed lines* the sugar–phosphate backbone) [74]

The duplex with the normal HBB gene has one hydrogen-bonded base pair more than the duplex with the mutated HBB gene, and therefore the first duplex has more double-helical region. The single-nucleotide mismatch has a significant effect on the structure of the duplexes, which in turn strongly influences the local environment where the clusters could form.

5.3 Wavelength-Shifting

Silver clusters change color while sensing their surroundings [20, 75]. Ras et al. have demonstrated that the absorption and emission bands of silver clusters are tunable by changing the chemical environment, such as solvent (Fig. 15) or the relative amount of silver ions (Fig. 12) [20]. In Fig. 15b is shown a photograph of the clusters in a series of water–methanol mixtures. Figure 15c shows the fluorescence of the same samples under UV illumination. The absorption and emission spectra clearly demonstrate a large solvatochromic shift without significant broadening of the spectral bands (Fig. 15d, e). The principles behind the wavelength shift are not yet known. The wavelength-shifting of plasmonic metal nanoparticles forms the basis of localized surface plasmon resonance sensing, a technology which is useful in detecting single molecules of chemical and biological relevance [76]. Analogously, we expect that wavelength-shifting of the fluorescent silver clusters may lead to applications for molecular sensing.

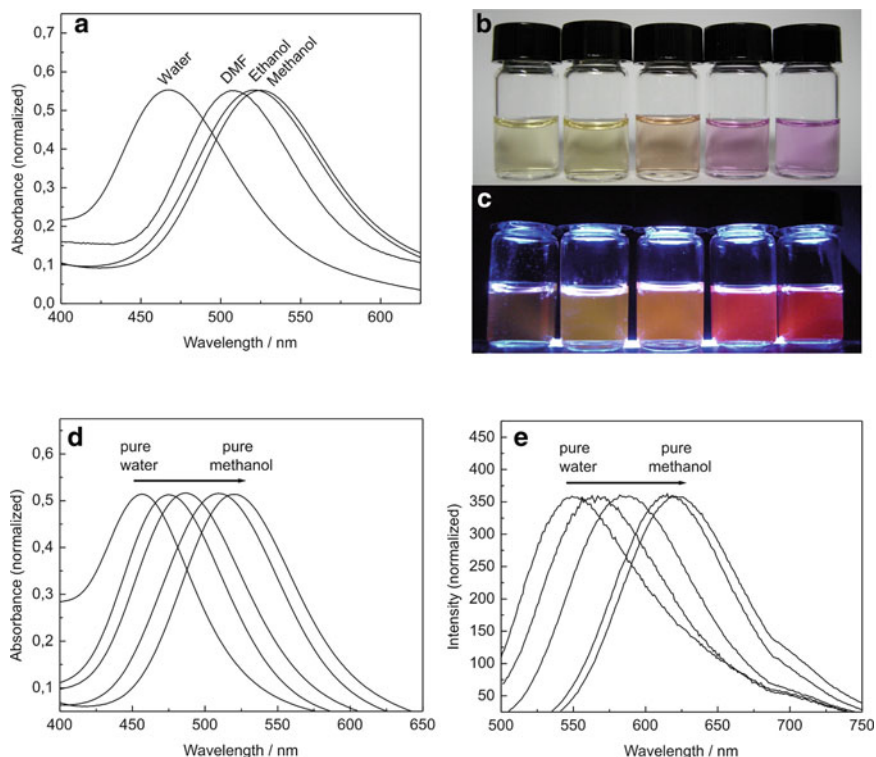


Fig. 15 Color tunability of silver clusters. (a) Absorption spectra in various solvents. (b) Photograph under visible light and (c) under UV light of Ag clusters in water/methanol mixtures, from pure water on the left to pure methanol on the right. (d) Absorption and (e) emission spectra of the samples imaged in (b) [20]

6 Conclusion

Fluorescent silver clusters that are stable in solution are a relatively new class of materials, first reported less than a decade ago. They have optical properties based on electronic transitions between quantized energy levels, resulting in excellent figures of merit including high absorption coefficients and high fluorescence quantum yields. In addition silver clusters have a subnanometer size, are nontoxic, photostable and electrochemiluminescent. Silver clusters are very sensitive to the local environment, which is put into advantage for sensing purposes. However, their sensitivity to local environment also implies that the recipes for silver cluster synthesis are suited only for a specific type of scaffold under specific synthesis conditions and would require optimization to extend the recipe for a different scaffold. In conclusion, fluorescent silver clusters have a unique set of properties making them suitable as fluorescent reporters in labeling and sensing applications, and in future may solve some issues related with organic fluorophores or semiconductor quantum dots.

References

1. Sun T, Seff K (1994) Silver clusters and chemistry in zeolites. *Chem Rev* 94:857–870
2. Ozin GA, Hugues F, Mattar SM, McIntosh DF (1983) Low nuclearity silver clusters in faujasite-type zeolites: optical spectroscopy, photochemistry and relationship to the photodimerization of alkanes. *J Phys Chem* 87:3445–3450
3. De Cremer G, Antoku Y, Roeffaers MJB, Sliwa M, Van Noyen J, Smout S, Hofkens J, De Vos DE, Sels BF, Vosch T (2008) Photoactivation of silver-exchanged zeolite A. *Angew Chem Int Ed* 47:2813–2816
4. Klotzbücher WE, Ozin GA (1980) Optical spectra of hafnium, tungsten, rhenium and ruthenium atoms and other heavy transition-metal atoms and small clusters (Zr1, 2, Pd1, 2, Au1, 2, 3) in noble-gas matrixes. *Inorg Chem* 19:3767–3776
5. König L, Rabin I, Schulze W, Ertl G (1996) Chemiluminescence in the agglomeration of metal clusters. *Science* 274:1353–1355
6. de Lamaestre RE, Bea H, Bernas H, Belloni J, Marignier JL (2007) Irradiation-induced Ag nanocluster nucleation in silicate glasses: analogy with photography. *Phys Rev B* 76:205431
7. Eichelbaum M, Rademann K, Hoell A, Tatchev DM, Weigel W, Stosser R, Pacchioni G (2008) Photoluminescence of atomic gold and silver particles in soda-lime silicate glasses. *Nanotechnology* 19:135701
8. Bilan ON, Tyul'nin VA, Cherenda NG, Shendrik AV, Yudin DM (1980) Radiation paramagnetic centers and luminescence centers in silver-doped quartz glasses. *J Appl Spectrosc* 33:717–720
9. Peyser LA, Vinson AE, Bartko AP, Dickson RM (2001) Photoactivated fluorescence from individual silver nanoclusters. *Science* 291:103–106
10. Lee T-H, Gonzalez JI, Dickson RM (2002) Strongly enhanced field-dependent single-molecule electroluminescence. *Proc Natl Acad Sci USA* 99:10272–10275
11. Peyser LA, Lee T-H, Dickson RM (2002) Mechanism of Ag_n nanocluster photoproduction from silver oxide films. *J Phys Chem B* 106:7725–7728
12. Henglein A, Tausch-Tremel R (1981) Optical absorption and catalytic activity of subcolloidal and colloidal silver in aqueous solution: a pulse radiolysis study. *J Colloid Interface Sci* 80:84–93
13. Ershov BG, Henglein A (1998) Time-resolved investigation of early processes in the reduction of Ag⁺ on polyacrylate in aqueous solution. *J Phys Chem B* 102:10667–10671
14. Linnert T, Mulvaney P, Henglein A, Weller H (1990) Long-lived nonmetallic silver clusters in aqueous-solution – preparation and photolysis. *J Am Chem Soc* 112:4657–4664
15. Henglein A (1989) Small-particle research – physicochemical properties of extremely small colloidal metal and semiconductor particles. *Chem Rev* 89:1861–1873
16. Zheng J, Dickson RM (2002) Individual water-soluble dendrimer-encapsulated silver nanodot fluorescence. *J Am Chem Soc* 124:13982–13983
17. Xu H, Suslick KS (2010) Water-soluble fluorescent silver nanoclusters. *Adv Mater* 22:1078–1082
18. de Souza N (2007) All that glitters but does not blink. *Nat Methods* 4:540–540
19. Vosch T, Antoku Y, Hsiang J-C, Richards CI, Gonzalez JI, Dickson RM (2007) Strongly emissive individual DNA-encapsulated Ag nanoclusters as single-molecule fluorophores. *Proc Natl Acad Sci* 104:12616–12621
20. Díez I, Pusa M, Kulmala S, Jiang H, Walther A, Goldmann AS, Müller AHE, Ikkala O, Ras RHA (2009) Color tunability and electrochemiluminescence of silver nanoclusters. *Angew Chem Int Ed* 48:2122–2125
21. Ashcroft NW, Mermin ND (1976) *Solid state physics*. Saunders College, Philadelphia
22. Mohamed MB, Volkov V, Link S, El-Sayed MA (2000) The 'lightning' gold nanorods: fluorescence enhancement of over a million compared to the gold metal. *Chem Phys Lett* 317:517–523

23. Boyd GT, Yu ZH, Shen YR (1986) Photoinduced luminescence from the noble metals and its enhancement on roughened surfaces. *Phys Rev B* 33:7923
24. Geddes CD, Parfenov A, Gryczynski I, Lakowicz JR (2003) Luminescent blinking from silver nanostructures. *J Phys Chem B* 107:9989–9993
25. Zheng J, Nicovich PR, Dickson RM (2007) Highly fluorescent noble-metal quantum dots. *Annu Rev Phys Chem* 58:409–431
26. Shibu ES, Muhammed MAH, Tsukuda T, Pradeep T (2008) Ligand exchange of Au₂₅SG₁₈ leading to functionalized gold clusters: spectroscopy, kinetics, and luminescence. *J Phys Chem C* 112:12168–12176
27. Richards CI, Hsiang J-C, Senapati D, Patel S, Yu J, Vosch T, Dickson RM (2009) Optically modulated fluorophores for selective fluorescence signal recovery. *J Am Chem Soc* 131:4619–4621
28. Walter M, Akola J, Lopez-Acevedo O, Jadzinsky PD, Calero G, Ackerson CJ, Whetten RL, Grönbeck H, Häkkinen H (2008) A unified view of ligand-protected gold clusters as superatom complexes. *Proc Natl Acad Sci USA* 105:9157–9162
29. Shang L, Dong S (2008) Facile preparation of water-soluble fluorescent silver nanoclusters using a polyelectrolyte template. *Chem Commun* 9:1088–1090
30. Shen Z, Duan H, Frey H (2007) Water-soluble fluorescent ag nanoclusters obtained from multiarm star poly(acrylic acid) as molecular hydrogel templates. *Adv Mater* 19:349–352
31. Makarava N, Parfenov A, Baskakov IV (2005) Water-soluble hybrid nanoclusters with extra bright and photostable emissions: a new tool for biological imaging. *Biophys J* 89:572–580
32. Petty JT, Zheng J, Hud NV, Dickson RM (2004) DNA-templated Ag nanocluster formation. *J Am Chem Soc* 126:5207–5212
33. Stoltenberg RM, Woolley AT (2004) DNA-templated nanowire fabrication. *Biomed Micro-devices* 6:105–111
34. Wei G, Wang L, Liu Z, Song Y, Sun L, Yang T, Li Z (2005) DNA-network-templated self-assembly of silver nanoparticles and their application in surface-enhanced raman scattering. *J Phys Chem B* 109:23941–23947
35. Kumar A, Ramakrishnan V, Gonnade R, Ganesh KN, Sastry M (2002) Electrostatically entrapped DNA molecules in lipid thin films as templates for the in situ growth of silver nanoparticles. *Nanotechnology* 13:597
36. Sun L, Wei G, Song Y, Liu Z, Wang L, Li Z (2006) Fabrication of silver nanoparticles ring templated by plasmid DNA. *Appl Surf Sci* 252:4969–4974
37. Wirges Christian T, Timper J, Fischler M, Sologubenko Alla S, Mayer J, Simon U, Carell T (2009) Controlled nucleation of DNA metallization. *Angew Chem Int Ed* 48:219–223
38. Yang W, Shen C, Ji Q, An H, Wang J, Liu Q, Zhang Z (2009) Food storage material silver nanoparticles interfere with DNA replication fidelity and bind with DNA. *Nanotechnology* 20:085102
39. Braun E, Eichen Y, Sivan U, Ben-Yoseph G (1998) DNA-templated assembly and electrode attachment of a conducting silver wire. *Nature* 391:775–778
40. Izatt RM, Christensen JJ, Rytting JH (1971) Sites and thermodynamic quantities associated with proton and metal ion interaction with ribonucleic acid, deoxyribonucleic acid, and their constituent bases, nucleosides and nucleotides. *Chem Rev* 71:439–481
41. Eichhorn GL (1973) *Inorganic biochemistry*. Elsevier Scientific Pub. Co., Amsterdam
42. Marzilli LG (1977) Metal-ion interactions with nucleic acids and nucleic acid derivatives. In: Stephen JL (ed) *Progress in inorganic chemistry*. Wiley, Hoboken, NJ
43. Yamane T, Davidson N (1962) On the complexing of deoxyribonucleic acid by silver(I). *Biochim Biophys Acta (BBA)* 55:609–621, Specialized section on nucleic acids and related subjects
44. Luk KFS, Maki AH, Hoover RJ (1975) Studies of heavy metal binding with polynucleotides using optical detection of magnetic resonance. Silver(I) binding. *J Am Chem Soc* 97:1241–1242
45. Gwinn EG, O'Neill P, Guerrero AJ, Bouwmeester D, Fygenson DK (2008) Sequence-dependent fluorescence of DNA-hosted silver nanoclusters. *Adv Mater* 20:279–283

46. Richards CI, Choi S, Hsiang J-C, Antoku Y, Vosch T, Bongiorno A, Tzeng Y-L, Dickson RM (2008) Oligonucleotide-stabilized Ag nanocluster fluorophores. *J Am Chem Soc* 130:5038–5039
47. Patel SA, Richards CI, Hsiang J-C, Dickson RM (2008) Water-soluble Ag nanoclusters exhibit strong two-photon-induced fluorescence. *J Am Chem Soc* 130:11602–11603
48. Ritchie CM, Johnsen KR, Kiser JR, Antoku Y, Dickson RM, Petty JT (2007) Ag nanocluster formation using a cytosine oligonucleotide template. *J Phys Chem C* 111:175–181
49. Sengupta B, Ritchie CM, Buckman JG, Johnsen KR, Goodwin PM, Petty JT (2008) Base-directed formation of fluorescent silver clusters. *J Phys Chem C* 112:18776–18782
50. Yu J, Choi S, Richards CI, Antoku Y, Dickson RM (2008) Live cell surface labeling with fluorescent Ag nanocluster conjugates. *Photochem Photobiol* 84:1435–1439
51. Dattagupta N, Crothers DM (1981) Solution structural studies of the Ag(I)–DNA complex. *Nucl Acids Res* 9:2971–2985
52. Arakawa H, Neault JF, Tajmir-Riahi HA (2001) Silver(I) complexes with DNA and RNA studied by Fourier transform infrared spectroscopy and capillary electrophoresis. *Biophys J* 81:1580–1587
53. O'Neill PR, Velazquez LR, Dunn DG, Gwinn EG, Fyngenson DK (2009) Hairpins with poly-C loops stabilize four types of fluorescent Ag_n:DNA. *J Phys Chem C* 113:4229–4233
54. Kerényi L, Gallyas F (1972) A highly sensitive method for demonstrating proteins in electrophoretic, immunoelectrophoretic and immunodiffusion preparations. *Clin Chim Acta* 38:465–467
55. Naik RR, Stringer SJ, Agarwal G, Jones SE, Stone MO (2002) Biomimetic synthesis and patterning of silver nanoparticles. *Nat Mater* 1:169–172
56. Li H, Michael Siu KW, Guevremont R, Le Blanc JCY (1997) Complexes of silver(I) with peptides and proteins as produced in electrospray mass spectrometry. *J Am Soc Mass Spectrom* 8:781–792
57. Yu J, Patel Sandeep A, Dickson RM (2007) In vitro and intracellular production of peptide-encapsulated fluorescent silver nanoclusters. *Angew Chem Int Ed* 46:2028–2030
58. Narayanan SS, Pal SK (2008) Structural and functional characterization of luminescent silver–protein nanobioconjugates. *J Phys Chem C* 112:4874–4879
59. Ayres JG, Crocker JG, Skilbeck NQ (1988) Differentiation of malignant from normal and reactive mesothelial cells by the argyrophil technique for nucleolar organiser region associated proteins. *Thorax* 43:366–370
60. Giuffrè G, Mormandi F, Barresi V, Bordi C, Tuccari G, Barresi G (2006) Quantity of AgNOR in gastric endocrine carcinoid tumours as a potential prognostic tool. *Eur J Histochem* 50:45–50
61. Peyser-Capadona L, Zheng J, González JI, Lee T-H, Patel SA, Dickson RM (2005) Nanoparticle-free single molecule anti-stokes Raman spectroscopy. *Phys Rev Lett* 94:058301
62. Andersson L-O (1972) Study of some silver-thiol complexes and polymers: stoichiometry and optical effects. *J Polym Sci Part A 1 Polym Chem* 10:1963–1973
63. Srivastava M, Fleming PJ, Pollard HB, Burns AL (1989) Cloning and sequencing of the human nucleolin cDNA. *FEBS Lett* 250:99–105
64. Lesniak W, Bielinska AU, Sun K, Janczak KW, Shi X, Baker JR, Balogh LP (2005) Silver/dendrimer nanocomposites as biomarkers: fabrication, characterization, in vitro toxicity, and intracellular detection. *Nano Lett* 5:2123–2130
65. Varnavski O, Ispasoiu RG, Balogh L, Tomalia D, Goodson T III (2001) Ultrafast time-resolved photoluminescence from novel metal–dendrimer nanocomposites. *J Chem Phys* 114:1962–1965
66. Zhang J, Xu S, Kumacheva E (2005) Photogeneration of fluorescent silver nanoclusters in polymer microgels. *Adv Mater* 17:2336–2340
67. Ledo A, Martínez F, López-Quintela MA, Rivas J (2007) Synthesis of Ag clusters in microemulsions: a time-resolved UV–vis and fluorescence spectroscopy study. *Phys B Condens Matter* 398:273–277

68. Ledo-Suárez A, Rivas J, Rodríguez-Abreu Carlos F, Rodríguez María J, Pastor E, Hernández-Creus A, Oseroff Saul B, López-Quintela MA (2007) Facile synthesis of stable subnanosized silver clusters in microemulsions. *Angew Chem Int Ed* 46:8823–8827
69. Yu J, Choi S, Dickson RM (2009) Shuttle-based fluorogenic silver-cluster biolabels. *Angew Chem Int Ed* 48:318–320
70. Shang L, Dong SJ (2009) Sensitive detection of cysteine based on fluorescent silver clusters. *Biosens Bioelectron* 24:1569–1573
71. Shang L, Dong SJ (2008) Silver nanocluster-based fluorescent sensors for sensitive detection of Cu(II). *J Mater Chem* 18:4636–4640
72. Guo W, Yuan J, Wang E (2009) Oligonucleotide-stabilized Ag nanoclusters as novel fluorescence probes for the highly selective and sensitive detection of the Hg²⁺ ion. *Chem Commun* 23:3395–3397
73. Lan G-Y, Huang C-C, Chang H-T (2010) Silver nanoclusters as fluorescent probes for selective and sensitive detection of copper ions. *Chem Commun* 46:1257–1259
74. Guo W, Yuan J, Dong Q, Wang E (2010) Highly sequence-dependent formation of fluorescent silver nanoclusters in hybridized DNA duplexes for single nucleotide mutation identification. *J Am Chem Soc* 132:932–934
75. Patel SA, Cozzuol M, Hales JM, Richards CI, Sartin M, Hsiang JC, Vosch T, Perry JW, Dickson RM (2009) Electron transfer-induced blinking in Ag nanodot fluorescence. *J Phys Chem C* 113:20264–20270
76. Willets KA, Van Duyne RP (2007) Localized surface plasmon resonance spectroscopy and sensing. *Annu Rev Phys Chem* 58:267–297
77. Díez I, Hahn H, Ikkala O, Börner HG, Ras RHA (2010) Controlled growth of silver nanoparticle arrays guided by a self-assembled polymer-peptide conjugate. *Soft Matter* 6:3160–3162
78. Muhammed MAH, Pradeep T (2010) Luminescent quantum clusters of gold as bio-labels. In: AP Demchenko (ed) *Advanced Fluorescence Reporters in Chemistry and Biology II*, Springer Ser Fluoresc 9:333–353

Luminescent Quantum Clusters of Gold as Bio-Labels

M.A. Habeeb Muhammed and Thalappil Pradeep

Abstract Quantum clusters of gold are materials with a core dimension in the subnanometer regime. They exhibit a totally different chemistry when compared with the metallic nanoparticles. In this chapter, we present this new family of materials. Various approaches used for the synthesis of both water and organic soluble clusters are described. After reviewing the various properties of these clusters with special reference to their luminescent properties, we look at their bio-labeling applications. We hope that this chapter initiates the reader into a new family of materials in the context of luminescence imaging and other purposes.

Keywords Biolabeling · Gold · Luminescence · Quantum clusters

Contents

1	Introduction	334
2	History of Clusters in the Condensed Phase	335
3	Synthetic Approaches	335
3.1	Synthesis From Au ³⁺ Ions	336
3.2	Formation of Quantum Clusters Inside the Cavities of Biologically Relevant Molecules as well as Biomolecules	337
3.3	Synthesis of Quantum Clusters by the Core Etching or Core Size Reduction of Metallic Nanoparticles	337
3.4	Synthesis of Cluster From Another Cluster	338
4	Characterization Techniques	339
5	Stability	341
6	Electronic Structure and Optical Properties	341
7	Photoluminescence	343
7.1	Photostability	344

M.A.H. Muhammed and T. Pradeep (✉)

DST Unit on Nanoscience (DST UNS), Department of Chemistry and Sophisticated Analytical Instrument Facility, Indian Institute of Technology Madras, Chennai 600 036, India
e-mail: pradeep@iitm.ac.in

7.2	Luminescence Enhancement During Aqueous to Organic Phase Transfer	345
7.3	Fluorescence Resonance Energy Transfer	346
7.4	Two-Photon Emission	347
7.5	Photon Antibunching	348
7.6	Photoreactivity at Single-Cluster Level	348
7.7	Quantum Clusters as Metal Ion Sensors	350
7.8	Quantum Clusters for In Vitro Imaging	350
8	Conclusion	352
	References	352

1 Introduction

Synthesis of novel materials with desired and tunable physical and chemical properties continues to draw wide interest. Nanomaterials with a variety of shapes and sizes have been synthesized as they offer numerous possibilities to study size and shape-dependent variations of electronic, optical, and chemical properties. Nanomaterials of a particular element show drastic differences in physical and chemical properties when compared with the bulk state. For example, bulk gold, a metal that is insoluble in water can be made dispersible when it is in the nanoparticle form. There are drastic changes in the optical properties as well. Bulk gold appears yellow in color, but when it is in the nanoparticle form with an average core diameter of 16 nm, it appears wine red. Likewise, the chemistry of gold, such as catalysis, also shows a drastic change when the constituent units are in the nanometer range.

When we study the variation in chemical and physical properties from atoms to nanoparticles consisting of hundreds to thousands of atoms, one wonders about the properties of materials composed of only a few tens of atoms. This question led to the discovery of a new class of nanomaterials called quantum clusters or subnanoclusters. Quantum clusters can be considered as the missing link between the nanoparticle and atomic behavior, and they are entirely different from these two size regimes [1]. They consist of only a few atoms with a core size in the subnanometer regime. This extremely small size changes the entire electronic structure of the particles and hence they show different physico-chemical properties. Quantum clusters are generally represented in terms of the number of core atoms and the protecting ligands, unlike the conventional metallic nanoparticles, which are represented by their core diameter. For example, $\text{Au}_{25}\text{SG}_{18}$, a well known water soluble quantum clusters of gold, consists of a core of 25 gold atoms protected with 18 glutathione ligands [2]. Having subnanometer size, these clusters cannot possess surface plasmon resonance as the density of states is insufficient to create metallicity. They show discrete energy levels and exhibit distinct, but different, optical absorption and emission features. In other words, quantum clusters show “molecule-like” optical transitions in absorption and emission and are termed also as molecular clusters. A range of names such as gold molecules, super atoms, molecular clusters and subnanoclusters can be used to describe these materials. However, we follow the term quantum clusters (QC) in this chapter.

The quantized nature of electronic energy levels due to size confinement is amplified in this term. They show characteristic absorption features and can be distinguished from each other from their absorption profiles [2]. Quantum clusters typically exhibit strong photoluminescence and their wavelength of emission can be tuned from the near infra red (NIR) to ultra violet (UV) [1].

In this chapter, we present this new family of materials. The chapter mainly focuses on the photoluminescence properties of gold clusters. Reference [3] describes the corresponding silver analogues. After describing the synthetic approaches used and after reviewing the various properties of these clusters with special reference to their luminescent properties, we look at their bio-labeling applications. Although many of their known properties, such as fluorescence resonance energy transfer, (FRET) are not used yet in imaging in the biological context, the exploitation of activities in this area suggests adaptation of several of their properties in diverse aspects of bio-labeling. We hope that this chapter initiates the reader into a new family of materials in the context of luminescence imaging and other purposes.

2 History of Clusters in the Condensed Phase

A very brief history of quantum clusters in the condensed state is presented below. This area of research started with the synthesis of water-soluble undecagold (Au_{11}) in 1978 [4]. Authors predicted the use of these gold clusters as high-resolution electron-dense labels for immunoelectron microscopy because of their extraordinary heavy atom density, as well as their use in biological studies. This was followed by the synthesis of triphenyl phosphine capped Au_{55} clusters [5]. Whetten et al. [6] prepared a 10.4 kDa gold/glutathione cluster compound, $\text{Au}_{28}\text{SG}_{16}$ (later reassigned as $\text{Au}_{25}\text{SG}_{18}$ by Tsukuda et al. [2]). Dickson et al. synthesized a series of clusters such as Au_5 , Au_8 , Au_{13} , Au_{23} , and Au_{31} , which are encapsulated in the poly(amidoamine) (PAMAM) cavity [7]. These clusters have very high quantum yields, as high as 70%, which is comparable with strongly emitting organic dyes. A series of glutathione thiolate (SG-thiolate) protected gold clusters with well-defined compositions were synthesized and separated utilizing polyacrylamide gel electrophoresis (PAGE) by Tsukuda et al. [2]. The molecular compositions of these clusters were characterized by electrospray ionization (ESI) mass spectrometry. Following these important studies, several groups have explored the research area of quantum clusters in detail. New clusters have been synthesized, crystal structures of a few well-known clusters have been determined, and their applications in different areas have been reported.

3 Synthetic Approaches

Quantum clusters of gold can be synthesized in different ways. All the synthetic methods reported so far can be broadly classified into four categories.

1. Synthesis from Au^{3+} ions: In this method, Au^{3+} ions are reduced in the presence of a suitable ligand to form the clusters.
2. Synthesis of clusters inside the cavities of biologically relevant molecules as well as biomolecules: in this method, gold ions are sequestered into the cavities of biomolecules and are subsequently reduced into gold clusters.
3. Core etching of metallic nanoparticles: Here, the bigger metallic nanoparticles are etched into smaller clusters by selected molecules.
4. Synthesis from another cluster: In this method, an already synthesized cluster is converted into another cluster.

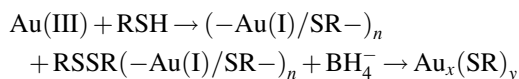
Before going into the details of the synthetic methods, it is good to have an understanding about the protecting molecules known as ligands. These ligands play a crucial role in determining some of the properties of the clusters since most of the atoms of the cluster are located at the surface and are subjected to covalent interactions with the ligands. The ligands influence the geometry of the cluster and cluster stabilization at a certain size and also block agglomeration. They potentially alter the electronic structure and hence significantly modify their properties. The common ligands used for the synthesis of clusters are water and organic soluble thiols, phosphines, amines, and carboxylic acids. Dendrimers and biomolecules such as DNA and proteins are also used as scaffolds or templates for the synthesis of quantum clusters. In the section below we discuss some of the methods in detail.

3.1 Synthesis From Au^{3+} Ions

The following methods of cluster synthesis come under this classification.

Two phase reduction (Brust synthesis): This method is usually employed to make organic soluble quantum clusters [8]. This method consists of two steps. The first is the transfer of AuCl_4^- from aqueous to the organic layer by a phase transfer reagent such as tetraoctyl ammonium bromide (TOABr). The next step is the subsequent reduction of AuCl_4^- in the presence of suitably selected ligands such as thiols, phosphines, etc.

Single phase reduction: Here, Au^{3+} ions are reduced to Au(I) by the addition of thiols followed by the complete reduction to Au(0) by adding reducing agents such as sodium borohydride (NaBH_4) [2]. The reaction can be represented as,



A group of water-soluble glutathione-protected clusters with defined chemical compositions have been synthesized by reducing Au^{3+} ions in the presence of glutathione. This produces a mixture of quantum clusters that are the kinetically

trapped intermediates of the growing Au cores. These clusters can be separated from each other by PAGE.

3.2 Formation of Quantum Clusters Inside the Cavities of Biologically Relevant Molecules as well as Biomolecules

Biologically important molecules also act as templates. For example, dendrimers assist in the synthesis of gold clusters. This method produces clusters of cores ranging from Au₅ to Au₃₃, by changing the Au³⁺/dendrimer ratio [7]. Assignment of these clusters to various cluster cores was largely based on fluorescence spectroscopy [1]. Limited mass spectral data have also been reported. G2-OH and G4-OH PAMAM dendrimers (second and fourth generation dendrimers with –OH functionality) are used for the synthesis. In this method, gold ions are sequestered into the cavities of dendrimers and can be reduced into gold clusters by slow reduction. Proteins are also used to make clusters. A simple, one-pot, green synthetic route was developed for the synthesis of gold clusters based on the reduction capability of the protein, bovine serum albumin (BSA) [9]. The cluster produced in this method is said to have a core of Au₂₅. This process is similar to the bio-mineralization behavior of organisms in nature. Upon addition of Au(III) ions to the aqueous BSA solution, the protein molecules sequestered Au ions and entrapped them. The reduction ability of BSA molecules was then activated by adjusting the reaction pH to 12 and the entrapped ions underwent progressive reduction to form gold clusters in-situ.

3.3 Synthesis of Quantum Clusters by the Core Etching or Core Size Reduction of Metallic Nanoparticles

In this method, a metallic nanoparticle is synthesized first. The metallic nanoparticles are then treated with large amounts of suitably selected molecules, resulting in the formation of quantum clusters.

The mechanism of formation of the clusters by this method is not well understood. We present below our tentative suggestions regarding the formation of clusters [10]. There are two possible routes for etching. In the first route, gold atoms are removed from the surface of the nanoparticles by excess ligands as a gold (I)–ligand complex. The gold(I) complex may undergo strong aurophilic interactions as there is a tendency for gold(I) compounds to form dimers, oligomers, chains, or layers via gold(I)–gold(I) interactions because of the hybridization of the empty 6s/6p and filled 5d orbitals to form quantum clusters. In the second possible route, ligands may etch the surface gold atoms of the nanoparticles leading to a

reduction in the size of the nanoparticles in steps, resulting in the formation of a thermodynamically stable cluster. The gold atoms removed from the nanoparticle surface by the ligands deposit as gold(I)–ligand complex. Some examples of the formation of quantum clusters are given below.

Etching with branched molecules (dendrimers): This method employed a ligand-induced etching process for preparing highly fluorescent and water-soluble metal nanoclusters by a multivalent coordinating polymer called polyethylenimine (PEI), which is able to etch metal nanoparticles [11]. Starting from dodecyl amine capped organic soluble metal nanoparticles of 8 nm diameter, a green fluorescent gold cluster consisting of only eight gold atoms, represented as Au₈ as indicated by ESI mass spectrometry, was synthesized.

Etching with simple molecules (glutathione): Two fluorescent quantum clusters of gold, namely Au₂₅ and Au₈, have been synthesized from mercaptosuccinic acid (MSA) protected gold nanoparticles of 4–5 nm core diameter by etching with excess glutathione [10]. Etching at pH ~3 yielded Au₂₅, while that at pH 7–8 yielded Au₈. This simple method makes it possible to synthesize well-defined clusters in gram quantities.

Etching with Au³⁺ ions: An organic soluble didodecyldimethylammonium bromide (DDAB) stabilized nanoparticle of diameter 5–6 nm was synthesized and was etched by the addition of Au precursors (HAuCl₄ or AuCl₃) to form smaller nanoclusters [12]. After size reduction, the product was brought to aqueous phase upon ligand exchange with dihydrolipoic acid (DHLA) resulting in the formation of brightly red emitting nanoclusters.

3.4 Synthesis of Cluster From Another Cluster

In this method, an already synthesized cluster is converted to another cluster. Some examples are presented below.

Synthesis of Au₂₅ from Au₁₁: A phosphine-stabilized Au₁₁ cluster, when treated with water soluble thiol glutathione, the cluster underwent aggregation and dissociation to form Au₂₅(SG)₁₈ selectively [13]. This method produced Au₂₅ clusters in large-scale. Cluster size increases during the ligand exchange reaction of Au₁₁ and the selective formation of Au₂₅ clusters confirms the extraordinary thermodynamic stability of the latter [14].

Synthesis of Au₂₃ from Au₂₅: A novel interfacial route has been developed for the synthesis of a bright-red-emitting new quantum clusters, Au₂₃, by the core etching of Au₂₅SG₁₈ [15]. An interface was created by making an immiscible biphasic mixture of toluene containing octanethiol (OT) and an aqueous solution of Au₂₅SG₁₈. The biphasic mixture was stirred at 25 and at 55°C, separately. A highly luminescent, water-soluble Au₂₃ cluster was obtained by etching at 25°C. In contrast, at 55°C, an organic soluble Au₃₃ cluster was formed.

Synthesis of Au₇₅ from Au₅₅: Phosphine-protected Au nanoclusters, Au₅₅(PPh₃)₁₂Cl₆, were reacted with hexanethiol and other thiols leading to the formation of Au₇₅

clusters [16]. Laser desorption/ionization mass spectrometry (LDI-MS) shows that the product contains a high proportion of a cluster of mass in the 14–15 kDa range, which was proposed to be Au₇₅.

4 Characterization Techniques

The main techniques employed for the characterization of clusters include UV/vis optical absorption, luminescence, mass spectrometry, X-ray photoelectron spectroscopy (XPS), transmission electron microscopy (TEM), and Fourier transform infrared (FT-IR). Single crystal X-ray diffraction (XRD) has been used to determine the structures of a few clusters [17–19].

UV/vis optical absorption spectroscopy: The first and important characterization is optical absorption. The synthesis of clusters can be monitored by the appearance of the optical absorption features. Each cluster has a characteristic absorption spectrum and can be distinguished from each other by their characteristic absorption features.

Luminescence spectroscopy: Clusters exhibit luminescence ranging from UV to NIR as a function of cluster core size. Quantum yield of the clusters ranges from 1×10^{-3} to 7×10^{-1} . While smaller clusters emit at shorter wavelengths with higher quantum yield, larger clusters emit at longer wavelength with relatively lower quantum yield.

Mass spectrometry: Quantum clusters are generally represented in terms of the number of core atoms and the corresponding ligands. Matrix assisted laser desorption ionization (MALDI) and ESI are the commonly used mass spectrometric techniques to determine the chemical composition of the clusters. Figure 1 is the ESI mass spectra of the nine fractionated (by PAGE) glutathione protected gold clusters [2]. Clusters are negatively charged in solution since most of the carboxyl groups of the glutathione ligands tend to be dissociated. The negative-ion ESI mass spectra of the clusters are comprised of a series of peaks associated with multiply charged anions $[\text{Au}_n(\text{SG})_{m-x}\text{H}]^{x-}$, where n , m , and x represent the numbers of gold atoms, GS ligands, and dissociated protons, respectively (left panels of Fig. 1). The right panels represent the $\text{Au}_n(\text{SG})_m$ spectra deconvoluted from the measured mass spectra. Theoretical spectra for $\text{Au}_n(\text{SG})_m$ are shown by the colored peaks with the corresponding n – m values. The chemical compositions assigned for these nine clusters from the mass spectral data are as follows: (1) Au₁₀SG₁₀, (2) Au₁₅SG₁₃, (3) Au₁₈SG₁₄, (4) Au₂₂SG₁₆, (5) Au₂₂SG₁₇, (6) Au₂₅SG₁₈, (7) Au₂₉SG₂₀, (8) Au₃₃SG₂₂, and (9) Au₃₉SG₂₄.

X-ray photoelectron spectroscopy: The Au(4f) peak positions of the subnanoclusters are located between those of the Au(I) thiolate complexes and Au(0) film. The Au(4f) peak widths of the Au clusters are appreciably broader than those of Au nanoparticles and Au(0) film.

Transmission electron microscopy: The subnanometer size of the clusters can be imaged using TEM, which will give faint spots due to the presence of clusters.

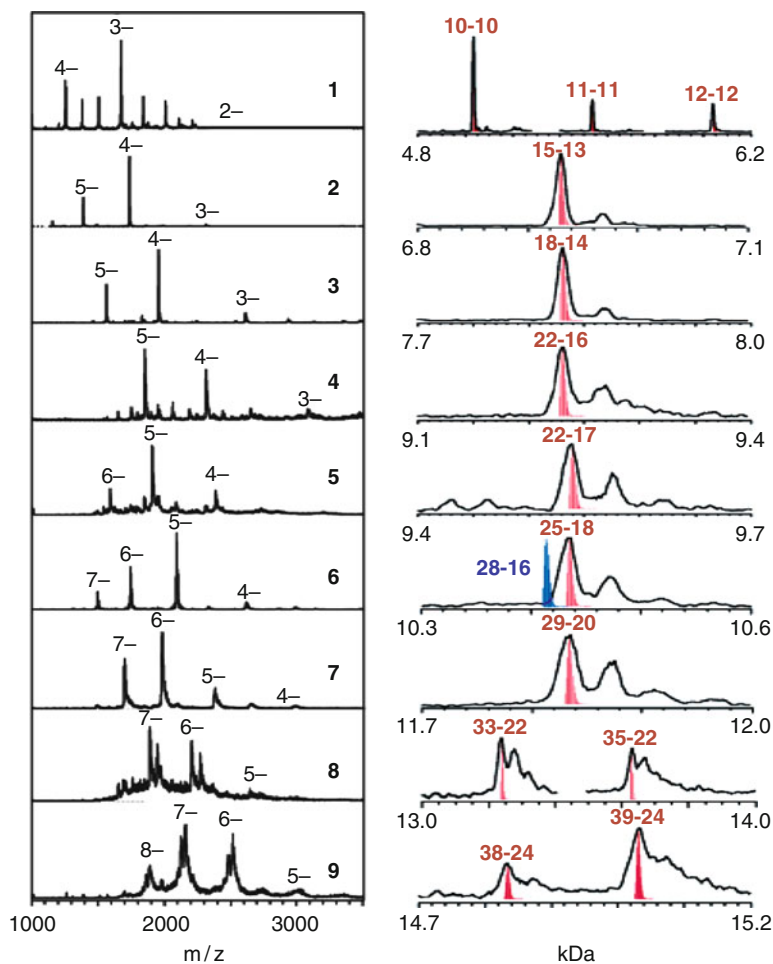


Fig. 1 Low-resolution ESI mass spectra of the nine fractionated gold clusters (*left*). The deconvoluted mass spectra (*right*). The calculated spectra for $Au_n(SG)_m$ are shown by the *colored peaks* with the corresponding $n-m$ values [2]

Fourier transform infrared spectroscopy: This analysis gives information about the nature of ligation on the cluster surface. For example, the FT-IR spectrum of $Au_{25}SG_{18}$ shows an absence of the absorption band at $2,526/cm$, which is due to $-SH$ stretching vibration of glutathione, when compared with free glutathione. This absence suggests a covalent linking of Au core with glutathione by Au-S bond formation [20].

X-ray Diffraction: Structures of several clusters such as Au_{13} , [17] Au_{55} , [18] Au_{25} , [19] and Au_{102} [21] have been determined. As an example, we describe below the crystal structure of phenylethanethiol capped Au_{25} clusters.[19] This cluster has an icosahedral Au_{13} core as shown in Fig. 2a. It is capped by an exterior shell

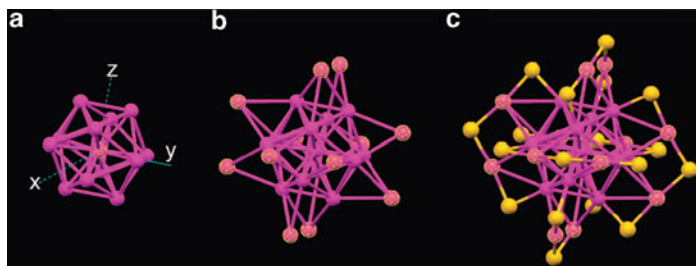


Fig. 2 Crystal structure of a $\text{Au}_{25}(\text{SR})_{18}$ cluster (R is phenylethyl group): (a) the icosahedral Au_{13} core; (b) the Au_{13} core covered by 12 Au atoms; (c) the whole Au_{25} cluster is protected by 18 thiolate ligands (for clarity, only S was shown, magenta, Au; yellow, S)[19]

composed of the remaining 12 Au atoms (Fig. 2b), and the whole cluster is covered by 18 phenylethane thiolate ligands (Fig. 2c). The 12 exterior Au atoms form an incomplete shell because out of the 20 triangular faces of the icosahedron, 8 are uncapped. The 18 ligands cap the gold core as follows (for clarity only sulfur atom of the ligand is shown in the figure): six ligands bridge the exterior Au–Au pairs (six in total) and the remaining 12 ligands bridge the exterior Au atoms and the icosahedral core.

5 Stability

Some clusters that are known as “magic number” clusters are “more stable compared with others. The stability of clusters can be classified into two [2]. First is the intrinsic stability of the core, which arises either due to the closing of the electronic shell as in Au_8 , Au_{18} , Au_{20} , Au_{34} or due to the closing of the geometric shell as in Au_{13} , Au_{55} . Second is the stability induced by ligands via charge transfer, which can stabilize clusters by the closing of the electronic shell or by the complete coverage of surface atoms, leading to inertness. For example, $\text{Au}_{25}\text{SG}_{18}$ is the most stable cluster among the various glutathione protected clusters because of the complete coverage of surface gold atoms by glutathione ligands.

6 Electronic Structure and Optical Properties

The electronic structure and hence optical properties of nanomaterials depend on the core size. For example, nanoparticles of core size ≥ 3 nm show surface plasmon resonance, which is due to the excitation of surface plasmons of nanoparticles by light. When the size of gold nanoparticles comes down to around 1 nm, which is equal to the de Broglie wavelength of the conduction electrons, the electronic bands

will resolve to discrete levels. Because of this, small nanoparticles or quantum clusters no longer support the plasmon excitation unlike the bigger, metallic nanoparticles. The electronic structure and the corresponding absorption features of quantum clusters can be explained by taking the example of $\text{Au}_{25}(\text{SH})_{18}^-$ [19].

On the one hand, the optical absorption spectrum of Au_{25} is molecule-like, in sharp contrast to that of metallic gold nanoparticles. It has several absorption features in the 400–1,000 nm range. On the other hand, spherical nanoparticles show one absorption peak (520 nm for a gold nanoparticle of ~ 15 nm core diameter). The optical absorption spectrum of Au_{25} is given in Fig. 3. Three prominent features, marked as “a,” “b,” and “c” are present in the absorption spectrum of Au_{25} . These absorption features can be explained with the help of Kohn–Sham orbital energy level diagram of $\text{Au}_{25}(\text{SH})_{18}^-$. In the electronic structure of $\text{Au}_{25}(\text{SH})_{18}^-$, the HOMO and the lowest three LUMOs are mainly composed of 6sp atomic orbitals of gold; thus, these orbitals constitute the *sp* band. The HOMO-1 through HOMO-5 are mainly constructed from the $5d^{10}$ atomic orbitals of gold and hence constitute the *d* band. The first absorption is at 1.52 eV (670 nm), denoted by peak “a” in the figure corresponding to a HOMO–LUMO transition, which is otherwise called an intraband (*sp* to *sp*) transition. The peak at 2.63 eV (marked as “b” in figure) arises from mixed intraband (*sp* to *sp*) and interband (*d* to *sp*) transitions. The peak at 2.91 eV (marked as “c” in figure) arises principally from an interband transition (*d* to *sp*). The absorption peak due to intraband transition shows a blue shift with decrease in core size. For example, glutathione protected Au_{39} clusters show absorption at 1.4 eV or 730 nm because of the intraband transition while Au_{18} shows the same feature at 570 nm [2].

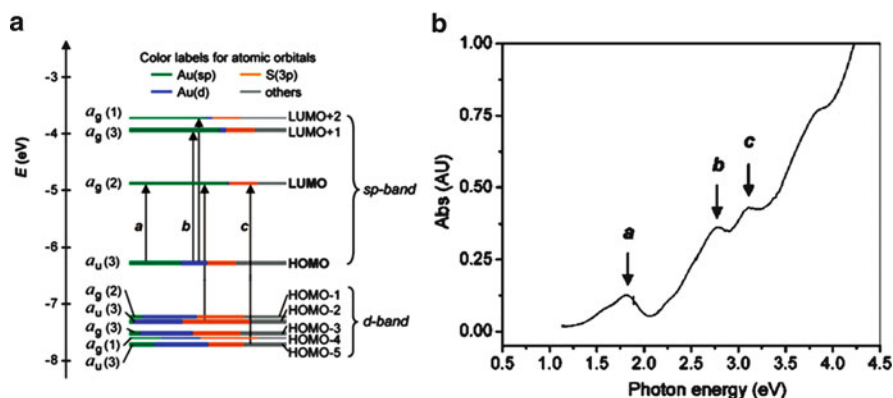


Fig. 3 (a) Kohn–Sham orbital energy level diagram for $\text{Au}_{25}(\text{SH})_{18}^-$. Each KS orbital is drawn to indicate the relative contributions (line length with color labels) of the atomic orbitals of Au (6sp) in green, Au (5d) in blue, S (3p) in yellow, and others in grey. The left column of the KS orbitals shows the orbital symmetry (g, u) and degeneracy (in parenthesis); the right column shows the HOMO and LUMO sets. (b) The absorption spectrum of $\text{Au}_{25}(\text{SH})_{18}^-$ [19]

7 Photoluminescence

Quantum clusters exhibit luminescence with quantum yields in the range of 10^{-1} – 10^{-3} . Quantum clusters of gold synthesized inside cavities of dendrimer exhibit very bright photoluminescence with quantum yields in the range of 10–70%. The wavelength of photoluminescence can be tuned by changing the core size. Smaller clusters emit at shorter wavelength with higher quantum yield and larger clusters emit at longer wavelength with comparatively low quantum yield. For example, clusters Au_5 , Au_8 , Au_{13} , Au_{23} , and Au_{31} , grown inside dendrimers, show emissions at 3.22, 2.72, 2.43, 1.65, and 1.41 eV with quantum yields of 70, 42, 25, 15, and 10%, respectively [1]. The excitation and emission spectra of these clusters are shown in Fig. 4. Their emission energies are fitted by a simple relation, $E_F \times \text{size}^{-1/3}$, predicted by the jellium model. These clusters are termed as free falling clusters [2] since they are grown inside the cavities of dendrimers. There is another class of clusters called thiolated clusters, which are protected by various thiols, and there exists a covalent bond between thiols and the gold core. These groups of clusters emit in the NIR region with relatively low quantum yield. For example, $\text{Au}_{25}\text{SG}_{18}$, a well-studied and the most stable cluster among the glutathione-protected gold clusters, shows a quantum yield of 1×10^{-3} (0.1%). These contrasted photoluminescence properties show the effect of thiolate passivation on the electronic structures and photophysical properties of small gold clusters. Since quantum clusters are highly fluorescent and biocompatible due to the lower metallic content, they hold great promise as ultra bright, biocompatible biolabels and light-emitting sources in nanoscale and hence can be used in imaging, detection, and so on, in conjunction with therapeutics. Unlike organic dyes, they are photostable [12], a quality that widens the scope of their potential applications. These clusters can be readily conjugated with several biological molecules, which

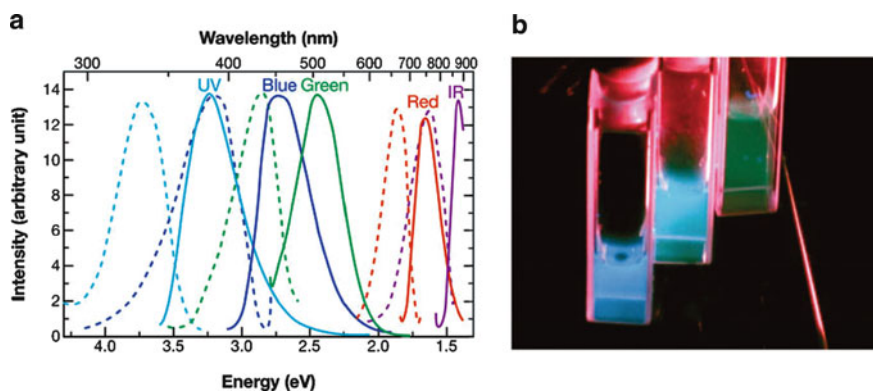


Fig. 4 (a) Excitation (*dashed*) and emission (*solid*) spectra of different Au nanoclusters. Excitation and emission maxima shift to longer wavelength with increasing nanocluster size. (b) Emission from the three shortest wavelength-emitting Au-nanocluster solutions (from left to right) under UV irradiation (366 nm) [1]

further enhance their application potential. They also exhibit electroluminescence at room temperature and hence provide facile routes to produce strong single-photon emitters. The photoluminescence of quantum clusters arises due to their molecular-like electronic structure. The emission originates from radiative intraband transitions within the *sp* bands, across the HOMO–LUMO gap. As the size of the cluster decreases, the spacing between the discrete states increases. This leads to a blue shift in the emission of smaller clusters when compared with the larger analogues.

7.1 Photostability

Quantum clusters are highly photostable when compared with organic fluorophores. A study was conducted to check the photostability of clusters in comparison to organic fluorophores and semiconductor quantum dots [12]. Photostability of a gold cluster capped with dihydrolipoic acid (AuNC@DHHLA) was compared with polymer coated CdSe/ZnS semiconductor quantum dots and two different organic fluorophores namely fluorescein and rhodamine 6G (Fig. 5). For the study, 20 μ l of fluorescent AuNC@DHHLA was dissolved in sodium borate buffer of pH 9. The sample was loaded into a quartz cuvette and was exposed to blue-light (480 nm)

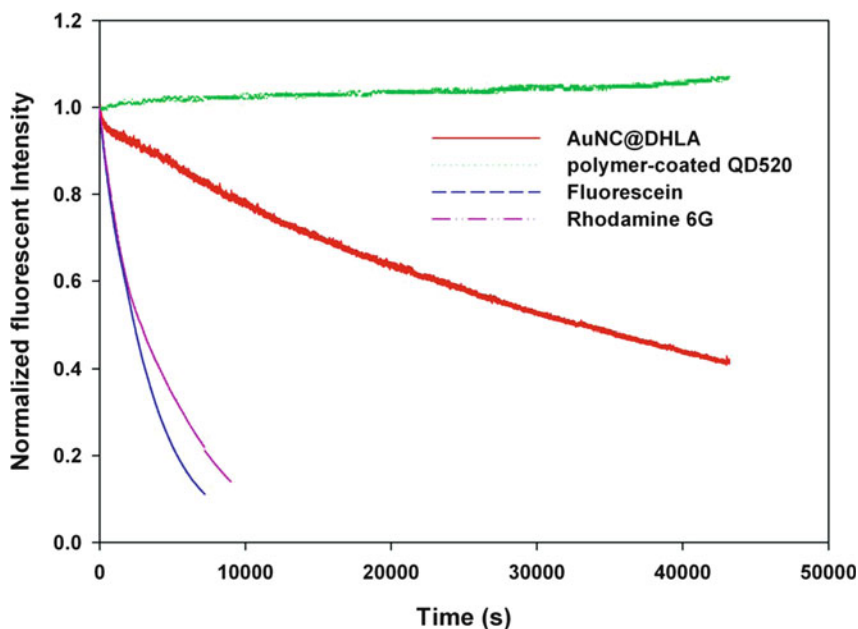


Fig. 5 Photostability of fluorescent Au nanoclusters (AuNC@DHHLA) compared with semiconductor quantum dots (polymer-coated QD 520 from Invitrogen) and organic fluorophores (fluorescein, rhodamine 6G) [12]

excitation from the Xenon lamp of the used fluorometer. Luminescence intensity at 680 nm was recorded over time. Quantum dots, Rhodamine 6G, and fluorescein were also exposed to the same condition. Organic fluorophores showed fast photobleaching as expected. Fluorescent Au nanoclusters exhibited a much slower photobleaching rate than the organic fluorophores although it was not as good as that of the semiconductor quantum dots. The half life of AuNC@DHLA in comparison to the organic dye is around 13 times more.

7.2 Luminescence Enhancement During Aqueous to Organic Phase Transfer

Luminescence of a material depends on its surrounding environment such as solvents. An enhancement in luminescence is observed when glutathione capped Au₂₃ clusters were phase transferred from water to toluene by TOABr [15]. The phase-transferred cluster is believed to be protected with glutathione monolayer and covered by TOA⁺. This covering of TOA⁺ makes the cluster hydrophobic and results in its transfer from the aqueous to the toluene layer. The quantum yield of the cluster after phase transfer was increased from 1.3% to 5%. This increase can be observed by eye as well (Fig. 6). Both the radiative (k_r) and nonradiative (k_{nr}) rates of the cluster are altered on phase transfer, thus indicating a change in the kinetics

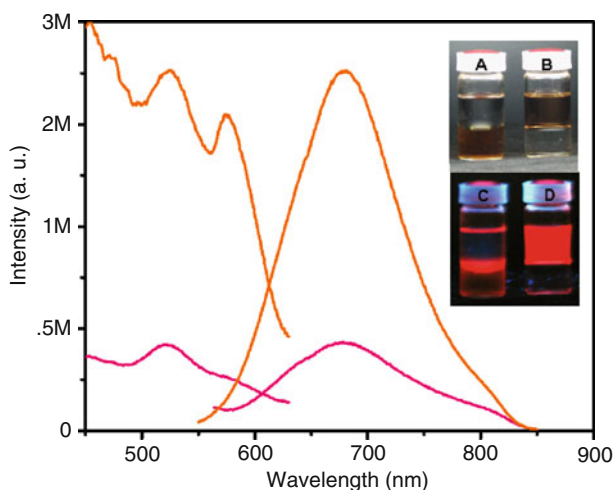


Fig. 6 Luminescent profile of Au₂₃ cluster before (*pink trace*) and after (*orange trace*) phase transfer. Emission of the cluster enhances considerably after phase transfer. Photographs of the aqueous–toluene mixture containing the cluster before and after phase transfer under white light (A and B, respectively) and UV light (C and D, respectively). In C, only the interface is illuminated as the UV radiation is attenuated as the sample was irradiated from the top [15]

of electron–hole recombination. The decrease in k_{nr} rate is significant upon phase transfer to an organic medium and can be explained as follows. The ability of thiols to act as hole-traps is well known. In the organic phase, further passivation of the cluster by TOA^+ makes the glutathione (thiols) less active and hence the decrease in nonradiative decay can be attributed to the reduced ability of thiols to act as hole-traps for the cluster.

7.3 Fluorescence Resonance Energy Transfer

Fluorescence resonance energy transfer is an ideal tool to measure the separation between an excited donor (D) and an acceptor (A) as the extent of such dipole interactions is a sensitive measure of the D–A distance. For more details about FRET, please refer [26]. FRET between the metal core and the ligand in $\text{Au}_{25}\text{SG}_{18}$ (SG–glutathione thiolate) is demonstrated using dansyl chromophores attached to the cluster core through glutathione linkers [22]. Efficient energy transfer from the dansyl donor to the Au_{25} core is manifested by way of the reduced lifetime of the excited state of the former and drastic quenching of its luminescence as shown in Fig. 7. Dansyl chromophore was attached to the Au_{25} core by two different routes as mentioned earlier. In the first route, dansyl chloride was reacted at the amino group of the glutamate residue of some of the glutathione ligands (–SG) anchored on Au_{25} . In the second route, some of the glutathione ligands of the cluster underwent exchange by the classical ligand exchange method with dansyl

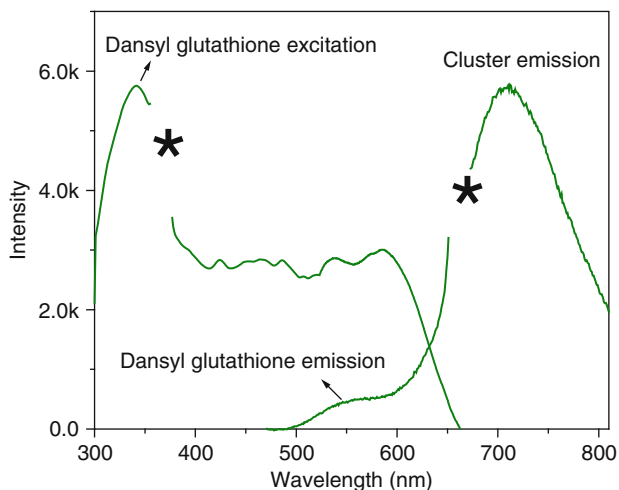


Fig. 7 Steady state excitation and emission spectra of Au_{25} after dansyl functionalization. Note that the emission of donor which appears ~ 550 nm quenched significantly. Asterisks (*) correspond to regions where higher order lines of the grating mask the spectrum [22]

glutathione (–SG–D) when the $\text{Au}_{25}\text{SG}_{18}$ was stirred with dansyl glutathione. Both the methods led to the formation of Au_{25} protected with a mixture of glutathione and *N*-dansyl glutathione. The donor–acceptor separation observed in the two synthetic routes reflects the asymmetry in the ligand binding on the cluster core, which is in agreement with the recent theoretical and experimental results on the structure of Au_{25} .

7.4 Two-Photon Emission

Two-photon emission is a process in which electronic transition between quantum levels occurs through the simultaneous emission of two photons. [27] presents more details about two-photon emission. Since metal clusters emit in the near-infrared region, they can be made useful for two-photon imaging with infrared excitation. Two-photon emission of Au_{25} clusters is observed at 830 nm by exciting at 1,290 nm (Fig. 8).[23] Two-photon absorption (TPA) cross-section of Au_{25} at 1,290 nm in hexane was determined to be 2,700 GM, which is superior to the TPA cross-sections of many organic chromophores with emission in the near-infrared region. In addition to the near-infrared luminescence for Au_{25} clusters, additional luminescence in the visible region with a maximum around 510 nm was observed, which is also two-photon allowed (excited at 800 nm). Present measurements on Au_{25} gold clusters suggest that they can be used as multiphoton imaging agents with near-infrared luminescence.

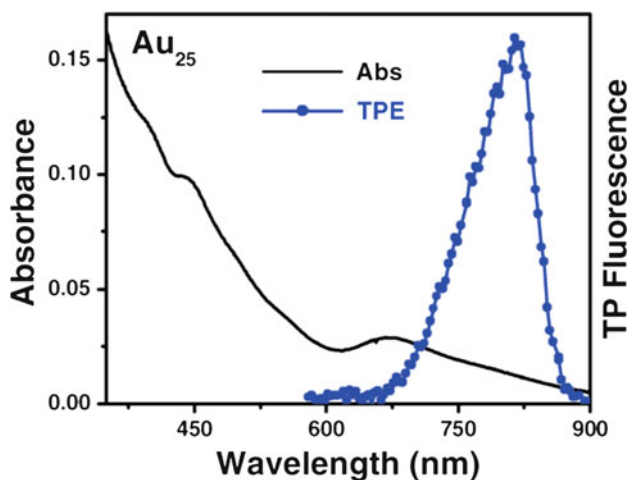


Fig. 8 Optical absorption of Au_{25} and two-photon emission spectrum after excitation at 1,290 nm for Au_{25} clusters [23]

7.5 Photon Antibunching

Photon antibunching is a quantum phenomenon that occurs during luminescence, in which the emission of one photon reduces the probability that another photon will be emitted immediately afterward. Unlike single atoms, metal nanoparticles exhibit collective oscillations of free electrons and produce bunched photons. On the one hand, antibunched photons cannot be observed from metallic nanoparticles since they possess continuous-band structure. On the other hand, since the electronic nature of quantum clusters is molecule-like and also possesses discrete energy levels, it is possible to observe antibunched photons from them. Antibunched luminescence from a single Au₂₃ cluster was observed when excited at 632.8 nm [1]. Photons arriving at each of two detectors show a decreased probability of two photons arriving simultaneously as shown in Fig. 9. The rise time of the antibunched signal matches the Au₂₃ lifetime.

7.6 Photoreactivity at Single-Cluster Level

Reactivity of metal clusters can be studied using spectroscopic techniques. By means of single molecule luminescence spectroscopy, we can observe individual clusters. Photoreactivity of gold clusters synthesized using a photochemical method

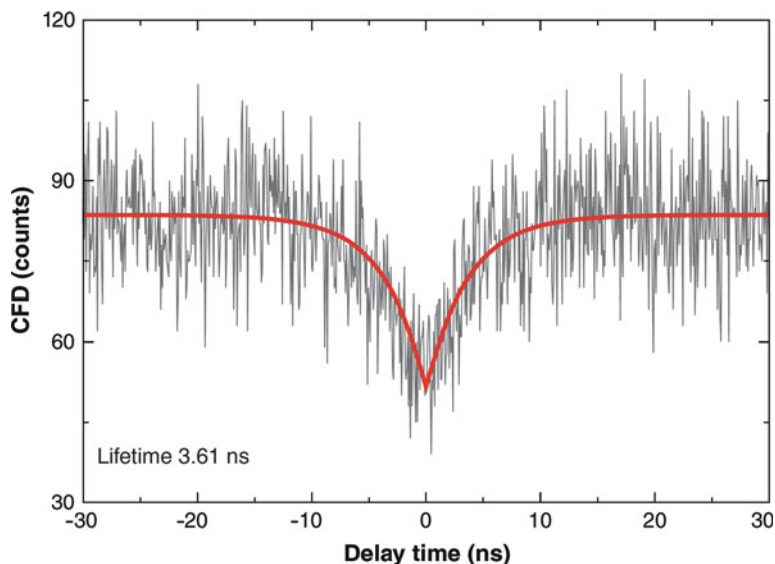


Fig. 9 Antibunched luminescence from a single Au₂₃ cluster, excited at 632.8 nm. Photons arriving at each of two detectors show a decreased probability of two photons arriving simultaneously (at zero interphoton delay) [1]

in a polymer matrix was studied at the single-cluster level [24]. The formation of individual clusters can be viewed in real-time by a single molecule luminescence spectroscopy (SMS) image. The sample for SMS was fabricated by spin coating a solution of the polymer containing a radical precursor (2-hydroxy-4'-(2-hydroxyethoxy)-2-methylpropiophenone) and HAuCl_4 . Upon photoexcitation, the radical precursor yields radicals via a Norrish-type-I R-cleavage. These radicals work as reducing agents for the Au ions to generate gold clusters. Initially, no luminescence was observed, with successive laser excitation, an increase in individually blinking fluorescent species with a long off-time was observed. A reversible and irreversible quenching of luminescence from this ligand-free gold clusters using O_2 was observed. Number of fluorescent species decreased dramatically when the samples were exposed to O_2 . The observed decrease was recovered by 50% by removing O_2 . Electron transfer played an important role in the luminescence quenching of photoluminescence of gold clusters. The luminescence spectra and the histogram of the luminescence maxima did not change significantly after the recovery. Therefore, it was concluded that there were two different quenching processes, that is, a reversible process and an irreversible process. Luminescence quenching by O_2 was prohibited by capping the clusters with octadecanethiol, inferring that access of O_2 to the surface of gold clusters played a key role in quenching. Relevant data are presented in Fig. 10.

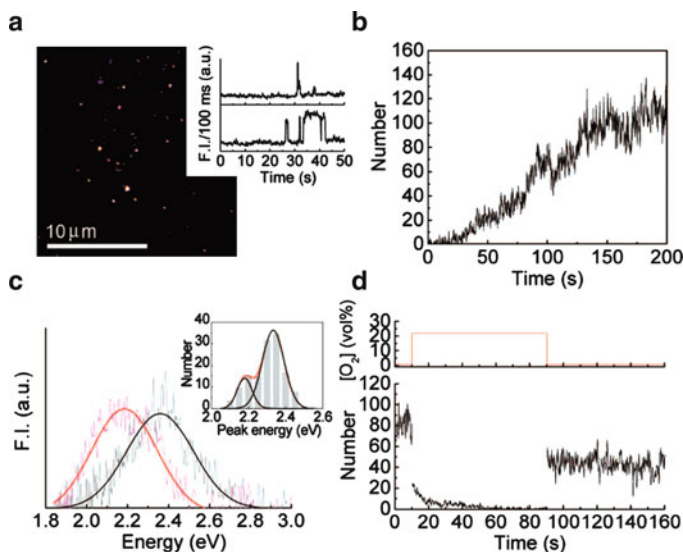


Fig. 10 (a) SMS image under excitation of a 405-nm laser for 60 s showing the photofabricated gold clusters. Inset shows the typical luminescence trajectories observed for a single gold cluster. (b) Time-dependent change in the number of fluorescent species. (c) Single-cluster luminescence spectra. Inset shows the histogram of single-cluster emission peak. Emission maxima for typical single gold cluster are ca. 2.2 and >2.4 eV. (d) Dependence of the change in the number of fluorescent species on O_2 concentration ($[\text{O}_2]$) [24]

7.7 Quantum Clusters as Metal Ion Sensors

The inherent luminescence of the clusters can be used as a sensing-tool for metal ions. The luminescence effect of glutathione capped Au_{23} in the presence of various metal ions was studied [15]. The ions selected were Au^{3+} , Ag^+ , Cu^{2+} , Ni^{2+} , Ca^{2+} , Mg^{2+} , Na^+ , Pb^{2+} , Hg^{2+} , and Cd^{2+} as their nitrates or chlorides. Next, 50 ppm of the aqueous solutions of Au_{23} was treated with metal ions so that its final concentration was 10 ppm, and the emission of the clusters was measured immediately after the addition of the ions. Au_{23} was found to be reactive toward Cu^{2+} . The emission of the cluster quenched significantly. Although cluster emission enhanced a bit in the presence of Ag^+ ions, it remained unaltered in the presence of other metal ions. Figure 11 is the plot of cluster-emission intensity against the metal ions added. Inset of the figure is a photograph of the aqueous solutions of Au_{23} under UV light after the addition of various metal ions. The specific reactivity toward Cu^{2+} can be used as a detection tool to find the presence of Cu^{2+} ions. Luminescence quenching in the presence of Cu^{2+} may be due to the aggregation of clusters by the addition of Cu^{2+} ions. However, Au_{23} did not show any particular reactivity toward anions.

7.8 Quantum Clusters for In Vitro Imaging

Since highly fluorescent water soluble gold clusters have been synthesized by various routes, they can be used in biology-related experiments such as imaging. These clusters may possess additional benefits over organic fluorophores and fluorescent semiconductor quantum dots. Organic fluorophores are prone to photobleaching,

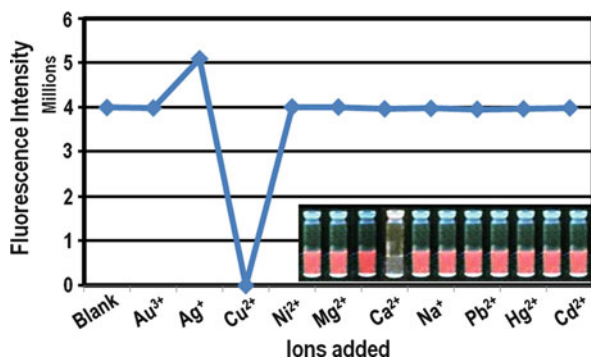


Fig. 11 Plot of the luminescence intensity of an aqueous solution of Au_{23} against the ions added externally to the solution. The concentration of Au_{23} was the same for all the experiments. Clusters showed specific reactivity toward Cu^{2+} ions with significant quenching of luminescence. Photographs of the aqueous solution of Au_{23} in the presence of externally added ions under UV light irradiation are also given. The photograph was collected immediately after the addition of metal ions [15]

whereas clusters are photostable [12]. Fluorescent semiconductor quantum dots are generally composed of elements such as Cd and Pb and they have to be coated with other inorganic or biological molecules to reduce their toxicity. Clusters composed of gold atoms, on the other hand, are likely to be biocompatible. Moreover, the cytotoxicity of the clusters is very low because of the low metallic content. In one study [25], highly luminescent gold clusters (Au-BSA) were synthesized by controlled reduction of Au^+ ions, stabilized in bovine serum albumin (BSA), using ascorbic acid (vitamin-C). For targeted imaging of cancer cells, the clusters were conjugated with folic acid (FA) through amide linkage with the BSA shell of the clusters. The bioconjugated clusters (Au-BSA-FA) show excellent stability over a wide range of pH from 4 to 14 and quantum yield of $\sim 5.7\%$ at pH 7.4 in phosphate buffered saline (PBS). The clusters show bright luminescence with a peak maximum at ~ 674 nm with the spectral profile covering NIR region, making it possible to image clusters at 700–800 nm emission window where the tissue-absorption of light is minimum. The gold clusters are nontoxic up to relatively higher concentrations of 500 $\mu\text{g/ml}$, as evident from the cell viability and reactive oxygen toxicity studies. Receptor targeted cancer detection using the Au-BSA-FA clusters is demonstrated on FR+ve oral squamous cell carcinoma (KB), where the FA conjugated gold clusters were found internalized in significantly higher concentration compared with the negative control cell lines, FR-ve lung carcinoma A549 (Fig. 12). This study demonstrates the potential of using

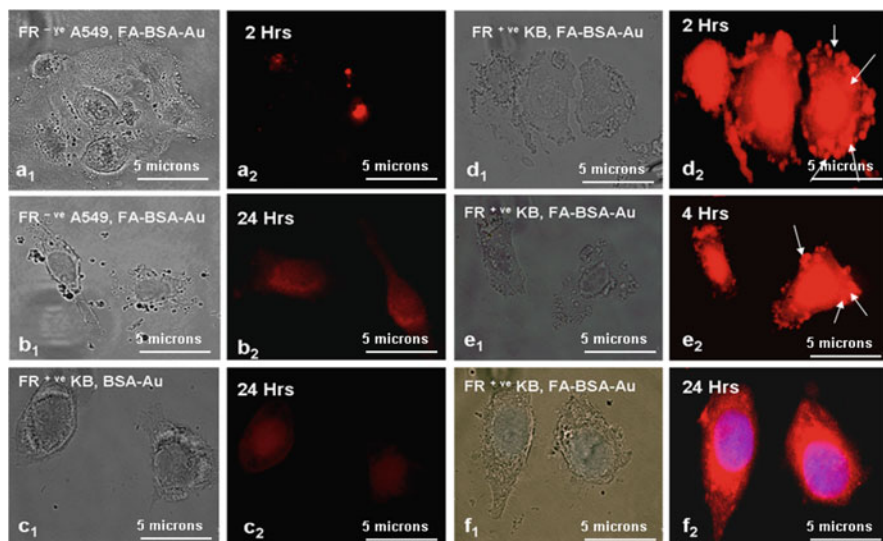


Fig. 12 Fluorescent microscopic images showing interaction of Au-BSA-FA NCs with different types of cell lines: (a1–a2) FR-ve lung carcinoma A549 after 2 h of incubation, (b1–b2) FR-ve lung carcinoma A549 after 24 h of incubation, (c1–c2) FR+ve KB cells with unconjugated Au clusters, (d1–d2) FR+ve KB cells with FA conjugated Au clusters at 2 h, (e1–e2) 4 h and (f1–f2) 24 h of incubation[25]

nontoxic fluorescent Au nanoclusters for the targeted imaging of cancer. There are also other reports of cell imaging using gold clusters [12, 15].

8 Conclusion

Quantum clusters are a new class of nanomaterials composed of very few atoms, with a core size in the subnanometer regime. Owing to the subnanometer core size, they cannot possess continuous density of states but have discrete electronic energy levels. They show “molecule-like” optical transitions in absorption and emission and are termed as molecular clusters. Because of their high luminescence, photostability, and low metallic content, they hold great promise as ultra bright, biocompatible biolabels and light-emitting sources in nanoscale, and hence can be used in imaging, detection, and so on, in conjunction with therapeutics. Some of these properties of clusters have been used in bio-labeling experiments. A brief overview of such efforts is presented. It is expected that many more studies will happen in the near future.

References

1. Zheng J, Nicovich PR, Dickson RM (2007) Highly fluorescent noble-metal quantum dots. *Annu Rev Phys Chem* 58:409–431
2. Negishi Y, Nobusada K, Tsukuda T (2005) Glutathione-protected gold clusters revisited: bridging the gap between gold(I)-thiolate complexes and thiolate-protected gold nanocrystals. *J Am Chem Soc* 127:5261–5270
3. Díez I, Ras RHA (2010) Few-atom silver clusters as fluorescent reporters. In: Demchenko (ed) *Advanced fluorescence reporters in chemistry and biology. II*. Springer Ser Fluoresc 9:307–332
4. Bartlett PA, Bauer B, Singer S (1978) Synthesis of water-soluble undecagold cluster compounds of potential importance in electron microscopic and other studies of biological systems. *J Am Chem Soc* 100:5085–5089
5. Schmis G, Boese R, Pfeil B et al (1981) $\text{Au}_{55}[\text{P}(\text{C}_6\text{H}_5)_3]_{12}\text{Cl}_6^-$ a gold cluster of an exceptional size. *Chem Ber* 114:3634–3642
6. Schaaff TG, Knight G, Shafiqullin MN et al (1998) Isolation and selected properties of a 10.4 kDa gold:glutathione cluster compound. *J Phys Chem B* 102:10643–10646
7. Zheng J, Zhang CW, Dickson RM (2004) Highly fluorescent, water-soluble size-tunable gold quantum dots. *Phys Rev Lett* 93:077402 (1–4)
8. Zhu M, Lanni E, Garg N et al (2008) Kinetically controlled, high-yield synthesis of Au_{25} clusters. *J Am Chem Soc* 130:1138–1139
9. Xie J, Zheng Y, Ying JY (2009) Protein-directed synthesis of highly fluorescent gold nanoclusters. *J Am Chem Soc* 131:888–889
10. Habeeb Muhammed MA, Ramesh S, Sinha SS et al (2008) Two distinct fluorescent quantum clusters of gold starting from metallic nanoparticles by pH-dependent ligand etching. *Nano Res* 1:333–340
11. Duan H, Nie S (2007) Etching colloidal gold nanocrystals with hyperbranched and multivalent polymers: a new route to fluorescent and water-soluble atomic clusters. *J Am Chem Soc* 129:2412–2413

12. Lin C-AJ, Yang T-Y, Lee C-H et al (2009) Synthesis, characterization, and bioconjugation of fluorescent gold nanoclusters toward biological labeling applications. *ACS Nano* 3:395–401
13. Shichibu Y, Negishi Y, Tsukuda T (2005) Large-scale synthesis of thiolated Au₂₅ clusters via ligand exchange reactions of phosphine-stabilized Au₁₁ clusters. *J Am Chem Soc* 127: 13464–13465
14. Shichibu Y, Negishi Y, Tsunoyama H (2007) Extremely high stability of glutathionate-protected Au₂₅ clusters against core etching. *Small* 3:835–839
15. Habeeb Muhammed MA, Verma PK, Pal SK et al (2009) Bright, NIR-emitting Au₂₃ from Au₂₅: characterization and applications including biolabeling. *Chem Eur J* 15:10110–10120
16. Balasubramanian R, Guo R, Mills AJ (2005) Reaction of Au₅₅(PPh₃)₁₂Cl₆ with thiols yields thiolate monolayer protected Au₇₅ clusters. *J Am Chem Soc* 127:8126–8132
17. Briant CE, Theobald BRC, White JW et al (1981) Synthesis and X-ray structural characterization of the centered icosahedral gold cluster compound [Au₁₃(PPhMe₂)₁₀Cl₂](PF₆)₃; the realization of a theoretical prediction. *Chem Commun* 5:201–202
18. Schmid G, Pfeil R, Boese R et al (1981) Au₅₅[P(C₆H₅)₃]₁₂Cl₆ – a gold cluster of unusual size. *Chemische Berichte* 114:3634–3642
19. Zhu M, Aikens CM, Hollander FJ (2008) Correlating the crystal structure of a thiol-protected Au₂₅ cluster and optical properties. *J Am Chem Soc* 130:5883–5885
20. Habeeb Muhammed MA, Pradeep T (2007) Reactivity of Au₂₅ clusters with Au³⁺. *Chem Phys Lett* 449:186–190
21. Jadzinsky PD, Calero G, Ackerson CJ et al (2007) Structure of a thiol monolayer – protected gold nanoparticle at 1.1 Å resolution. *Science* 318:430–433
22. Habeeb Muhammed MA, Shaw AK, Pal SK et al (2008) Quantum clusters of gold exhibiting FRET. *J Phys Chem C* 112:14324–14330
23. Ramakrishna G, Varnavski O, Kim J et al (2008) Quantum-sized gold clusters as efficient two-photon absorbers. *J Am Chem Soc* 130:5032–5033
24. Sakamoto M, Tachikawa T, Fujitsuka M et al (2009) Photoreactivity of as-fabricated Au clusters at the single-cluster level. *J Am Chem Soc* 131:6–7
25. Archana R, Sonali S, Deepthy M et al (2010) Molecular receptor specific, non-toxic, near-infrared emitting Au cluster–protein nanoconjugates for targeted cancer imaging. *Nanotechnology* 21:055103(1–12)
26. Demchenko AP (2010) Comparative analysis of fluorescence reporter signals based on intensity, anisotropy, time resolution and wavelength-ratiometry. In: Demchenko (ed) *Advanced fluorescence reporters in chemistry and biology. II.* Springer Ser Fluoresc 9:107–132
27. Przhonska OG, Webster S, Padilha LA et al (2010) Two-photon absorption in near-IR conjugated molecules: design strategy and structure-property relations. In: Demchenko (ed) *Advanced fluorescence reporters in chemistry and biology. II.* Springer Ser Fluoresc 8:105–147

Part V

Conjugated Polymers

Structure, Emissive Properties, and Reporting Abilities of Conjugated Polymers

Mary A. Reppy

Abstract A review of the emissive conjugated polymers used in sensing, their structures, optoelectronic properties, and material forms is presented here. The discussion includes an emphasis on the mechanisms of signal generation in chemical and biological sensing, identification of key design principles for the development of improved sensing materials and illustrative examples.

Keywords Conjugated polymer · Fluorescent sensor · FRET · Turn-off · Turn-on

Contents

1	Introduction	357
2	Polymer Structures	358
3	OptoElectronics of Conjugated Polymers	360
4	Material Forms	362
4.1	Materials for Aqueous Applications	364
5	Signal Transduction	366
5.1	Turn-Off Sensing	366
5.2	Turn-On Sensing	375
5.3	Emission Wavelength Shifts and FRET	379
6	Conclusion	382
	References	383

1 Introduction

The field of emissive conjugated polymers, designed and used for the detection of chemical and biological species, is well established and continues to grow. There has been considerable research performed since the 1980s on the design, synthesis,

M.A. Reppy
Abacalab, Inc., Wilmington, DE, USA
e-mail: reppy@alum.mit.edu

photophysical properties, material forms, and sensing applications of these polymers. There are many useful reviews available, including seminal summations by Swager and co-workers [1–3] and Bunz [4] on poly(arylene ethylenes) and sensing, a comprehensive review on polydiacetylene (PDA) materials for sensing [5], and more topical reviews on conjugated polymer molecular wires for metal ion detection [6], and on conjugated polyelectrolytes for detection of proteins [7] and DNA hybridization [8, 9]. The aim of this chapter is not to reproduce these reviews or the myriad papers described in them, but to explain the salient photophysical features and material forms of conjugated polymers and the basis of the emission changes used as signals in conjugated polymer chemical and biological sensors and illustrate these principles with appropriate examples.

Sensitivity, selectivity, reversibility, and response speed are major considerations in designing a sensing material. The specific application determines which of these factors are critical. For environmental sensing, such as detection of heavy metal ions in waste streams or biological agents in water, selectivity is key to avoiding false positives, while sensitivity needs to cover the range of concentration of interest for the target. For chemical contaminants, there will usually be a minimum concentration of concern that determines the sensitivity requirement. In drug discovery assays, selectivity may not be so important because the assay conditions can be controlled, but high sensitivity may be desirable to conserve precious reagents. Signal reversibility is important if the sensor is to be reused; if it is disposable, then reversibility is not needed and may not even be desired. A requirement for swift response is yet another sensor attribute that is application driven; for example, in the detection of chemical or biological warfare agents, a swift response may be critical, while in an assay setting, the development of a signal over a longer period may be tolerable. In addition, the form of the material must be suitable for incorporation in the device or assay format – films or coatings for environmental sensing devices, solutions or suspensions for high throughput assays. When considering the research and development of fluorescent conjugated polymer sensors, it is important to keep these factors in mind as they will determine whether a new material is simply a laboratory curiosity or actually has the potential to become a fully developed sensor.

2 Polymer Structures

The backbone structures of conjugated polymers used for fluorescence sensing have common motifs. With the exception of PDA, emissive conjugated polymers include aromatic or hetero-aromatic rings in the backbone, either linked directly or via double or triple bonds (Fig. 1). Para linkages between aromatics are the most common, but meta linkages have been used to improve backbone flexibility and enhance solubility [10, 11]. The rings have side groups which are chosen to give the polymer solubility or to prevent aggregation or to control π -stacking, etc. The side groups are often also chosen to interact with the target. In some cases,

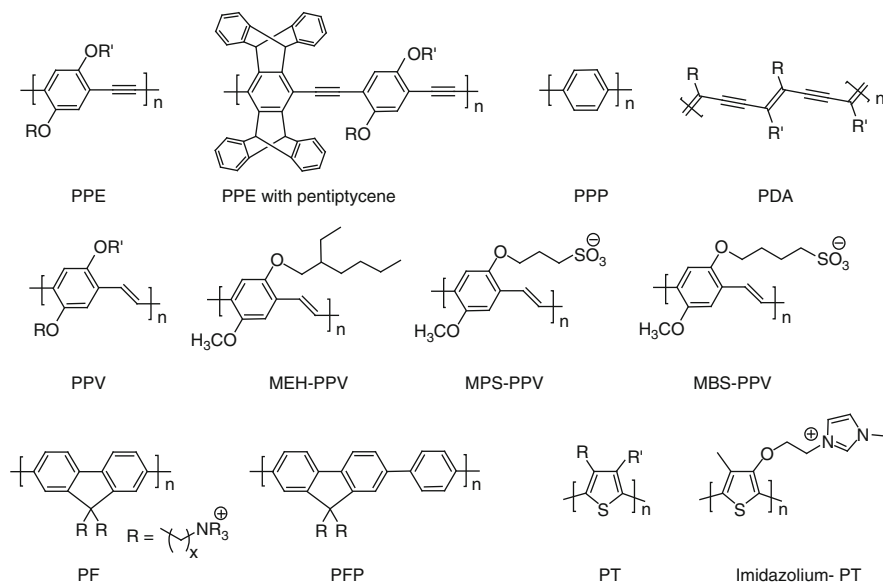


Fig. 1 Examples of emissive conjugated polymer structures

the target-binding groups, for example, bipyridines, are incorporated in the backbones. PDA is unusual in that the backbone does not contain any aromatic rings but is formed from alternating double and triple bonds.

Poly(arylene ethynylene)s (PAEs), aromatic rings linked by triple bonds, are a major class of emissive polymer used in sensing and have been extensively reviewed by Bunz [4] and by Swager et al. [2, 3]. Poly(phenylene ethynylene)s (PPEs) are a common subclass. These polymers are rigid rods and often have high quantum yields. Side chains are usually attached via ether groups and have been designed to introduce binding groups into the polymer and to add charge to make the polymer a polyelectrolyte and water soluble [12, 13]. Pentiptycene has been incorporated into the polymer backbone by Swager and co-workers to control interchain distances in polymer films [14] and 3-D structures [15]. The two side-chain groups may form a cyclophane such as crown ether and be used to capture ions or small organic molecules. PAEs have been designed with different alternating aryl groups between the triple bonds to control the density of binding groups [1, 6]. Standard PAEs are electron-rich and suitable for the detection of electron-poor targets. Electron-deficient PAE derivatives have been prepared by incorporating electron-withdrawing groups, such as CF_3 , along the backbone for the detection of electron-rich targets [3].

Other common emissive conjugated polymers with aromatic ring backbones are poly(phenylene vinylenes) (PPVs), poly(fluorenes) (PFs) – usually formed as copolymers such as poly(fluorene-*co*-phenylene)s (PFPs), and, more rarely, poly(*p*-phenylene)s (PPPs). Hetero-aromatic based polymers and copolymers alternating

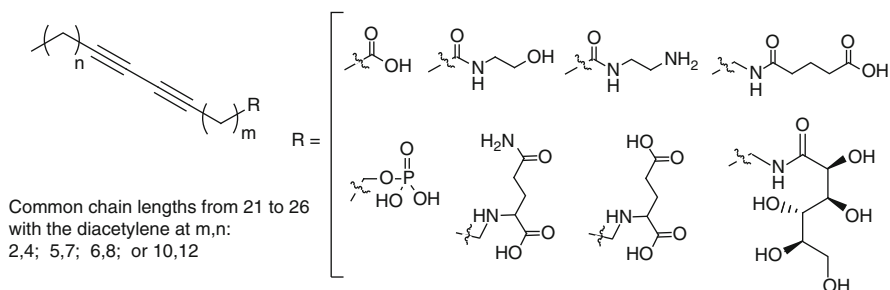


Fig. 2 Examples of diacetylene monomers showing diversity of head groups

phenyl groups with heteroatom aromatics are other types of conjugated sensing polymers. Poly(thiophene)s (PTs) are the most common class but nitrogen-containing conjugated polymers such as poly(benzoxazole)s [16] are known. A common approach in developing polymers for ion detection is to copolymerize nitrogen-containing aromatics with carbon aromatic units, examples include: polyfluorene (PF) copolymers with oxadiazole [17–20] and benzothiadiazole (BT) [8] units, PAEs incorporating quinoline [21] and quinoxaline [22] units, and PPVs with phenothiazylene and pyridylene [23] groups in the backbone. As with PAEs, side chains are added to affect solubility, chain structure and packing, as well as to add binding functionality.

PDA has a backbone of alternating double and triple bonds with side chains coming off the double bonds [5]. Diacetylene monomers can have a wide variety of charged and polar head groups (Fig. 2). Their amphiphilic nature allows self-assembly in water; the self-assembled structures are then photopolymerized to create the polymer *in situ*. Early studies on PDA were performed on chains formed in diacetylene crystals and then dissolved; however, for sensing applications, PDA is commonly prepared as self-assembled (in water) 2-D (films) or 3-D (liposomes, tubules, etc.) materials. For most PDA materials, the polymer backbone is isolated from the target by multiple methylene units; the notable exceptions are materials based on 2,4-diacetylenes. PDA was originally used for colorimetric biosensing [24]; realization that there was a concomitant emission change, that could be exploited for sensing, was developed later [25, 26] and has been adopted gradually by many groups in the PDA field [5, 27].

3 OptoElectronics of Conjugated Polymers

The optical properties of conjugated polymers primarily arise from the π -bonds in the polymer backbone. Alignment of π -bonds leads to electron delocalization, also referred to as conjugation or π -conjugation. Theoretically, backbone π -electrons can be delocalized along the entire length of the polymer if the π -bonds are all aligned; however, twists in the backbone and defects in the polymer structure at

room temperature lead to reduced delocalization and conjugation lengths. The π -bond system can contain double or triple bonds and aromatic rings. It should be noted that there are examples of emissive α -conjugated polymers with Si and Ge backbones used in sensing [28–30], but these are relatively rare and this chapter will focus on carbon-conjugated polymers.

Delocalization of π electrons leads to the absorbance and emission properties of the conjugated polymer. These optical properties are analogous to those of small-molecule fluorophores; however, the extended physical structures of the polymers lead to more varied and complicated excited state relaxation and energy transfer pathways than in small-molecule fluorophores. Molecular orbital (MO) theory and valence band gap models have been used to describe the electronic states and transitions of conjugated polymers. Brédas and co-workers have reviewed modeling conjugated polymers with MO theory [31, 32] and describe how Hückel theory and configuration interaction analysis (CI) are used for modeling oligomers. Quantum mechanical predictions for conjugated polymers are achieved by performing calculations on oligomer series and extrapolating the results to an extended polymer; interchain interactions have also been modeled [31, 33]. Comparisons between theoretical predictions and experimental results, and discussion of the possible pitfalls in these techniques, have been reviewed by Gierschner et al. [33].

Conjugated polymers have also been described using valence band gap theory, developed for infinite solids, with the filled π -orbitals making up a valence band with an energy gap to a conduction band. When the polymer is excited via photon absorption, an electron is promoted from the valence to the conduction band creating a positively charged hole in the valence band paired with the electron in the conduction band. The electron/hole pair forms an exciton, which can migrate along the conjugated backbone; the exciton is destroyed when it encounters a perturbation in the valence gap and the electron returns to the ground state via a radiative or nonradiative process to recombine with the hole (Fig. 3). In some polymers, the hole and electron decouple and the electron migrates as a free-carrier creating charge separation – this usually results in nonradiative return of the

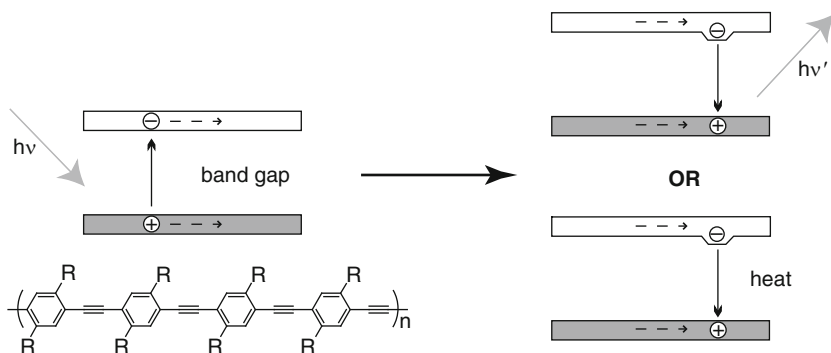


Fig. 3 Cartoon of exciton formation, migration, and recombination (radiative and nonradiative)

electron to the ground state. The formation and fate of excitons are affected by the extent of polarization and conjugation of the polymer. Greater polarizability of the polymer increases the likelihood of free-carrier generation, which also reduces emission [1].

In “real world” applications there are many factors affecting the fate of the polymer excited state and hence its emission. Conjugated polymers consist of different length segments of conjugated bonds with twists or other defects separating the segments. Such polymers can therefore be viewed as a collection of structurally related fluorophores strung together. There have been extensive spectroscopic studies of MEH-PPV examining their electronic states, driven primarily by interest in the optoelectronic properties of MEH-PPV and its use in light-emitting organic materials [34–37]. Exciton travel in these polymers is portrayed as the exciton hopping along chromophore segments of 5–10 monomer units, generally moving down a “funnel” of segments of decreasing energy, eventually arriving at a low-energy segment which acts as an exciton trap and leads to emission [34]. As the polymer chain coils or bends back on itself, the conjugated segments may align allowing transfer between noncontiguous chain segments; this has been referred to as interchain transfer, despite the segments being part of same chain. Polymer chains can also aggregate in solution and are adjacent in solid materials, again affecting the exciton migration and lifetime by allowing transfer between two chains. Intercchain transfer has been shown to be faster than exciton travel down adjacent chain segments [38].

To act as fluorescent transducers in sensing, the emission of conjugated polymers must be affected by external environmental triggers. An emissive polymer may be quenched (turn-off), a nonemissive polymer may become emissive (turn-on), energy from the polymer excited state may be transferred to another fluorophore, which then emits, or the polymer emission itself may shift wavelength. The target can interact with pendant groups off the backbone through electrostatics, hydrogen bonding and host–guest interactions, or by participating in a chemical reaction. The target may interact with the backbone directly if binding groups (for example, bipyridine) are incorporated in the backbone. These interactions may alter the valence energy leading to the formation or the removal of an exciton trap, cause conformational changes to the backbone thus increasing or decreasing the conjugation length, and/or cause changes in the polymer aggregation state.

4 Material Forms

Development of a commercial sensor or assay requires incorporation of the sensing elements into materials appropriate for device manufacture. Some assay applications use solution-phase materials only; this is more common for drug discovery assays and diagnostic testing than in environmental sensing. Polymers are less soluble than small molecules; however, with appropriate choice of side chains

and restriction to lower molecular weights, polymer chains can be dissolved. In some cases, the polymers are not strictly in solution but in suspension. The solvent will affect the polymer morphology, particularly for more flexible polymers. Changes in polymer chain structure from extended rigid-rod to coiled (or vice versa), changes in aggregation, and changes in solubility arising from interaction with a target have all been used in signal transduction. These changes in microstructure affect the optical properties of the polymer by allowing or disallowing new paths for the exciton during its lifetime: interchain transfer becomes possible with chain aggregation or precipitation, and changes in backbone geometry affect conjugation length and exciton delocalization and hence the energy gap between excited and ground state.

Many sensors particularly environmental sensors, have a solid/liquid or solid/vapor interface, with the detection elements in the solid and the liquid or vapor containing the target. The binding or other event that causes the signal occurs at the interface. In the case of small-molecule fluorophores, the presence of the detection element is achieved by incorporating the fluorophores in a matrix or attaching them to a surface. Sensing polymers offer the possibility of forming films or coatings, or 3-D structures made entirely from the detection element. It should be noted that the solid/liquid interface itself affects the interaction with the target as the surfaces of solids have different dielectric properties from bulk solids, solvent molecules are organized at the interface differently than from the bulk liquid and steric effects may come into play. As a result, electrostatic and hydrogen-bonding interactions of groups can be profoundly affected by being present at the interface [39–42] and predictions based on the properties measured for isolated species in solution may be significantly off when the same species is at an interface.

“Proof of concept” conjugated polymer sensing demonstrations are often performed with linear polymers, referred to as molecular wires. For sensors that depend on exciton traps for signal generation (as discussed below in Sect. 5.1), this approach is appropriate for initial work and testing of different chain compositions, lengths, etc. Solutions of molecular wires, however, are not as suitable for device design as the corresponding 2-D or 3-D materials both because of the difficulties of incorporating solutions into the devices and the inherent limitation in the sensitivity of the 1-D material. The exciton in its random progress along the 1-D molecular wire backbone will resample sites that it has already visited, reducing the number of distinct receptors it visits during its lifetime and hence the detection sensitivity [2]. Careful design of films and solids formed from molecular wire polymers can provide the exciton with a longer migration path and chances to sample more unique potential quenching sites.

Conjugated polymer films can be prepared by spin coating, evaporative deposition, Langmuir techniques, layer-by-layer deposition, reaction with active surfaces, and stamping to form patterns. Films have the disadvantage that the interchain energy transfer pathways, made accessible by the close packing of the chains, may reduce and shift the emission of the materials; this can be avoided by the incorporation of spacing groups off the polymer backbone [15]. A useful insight from the extensive studies on PPV films for LED applications is that the solution state of a

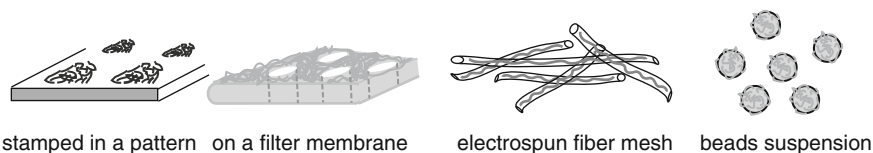


Fig. 4 Cartoon of polymers on different surface types

polymer (e.g., coiled, extended, aggregated, etc.) can strongly influence the behavior in a cast film; PPV films cast from a good solvent have morphology and emission yields significantly different from PPV films cast from a poor solvent [36]. Sensing polymers have been attached to various kinds of surfaces: planar surfaces such as wells of microplates and glass slides; fibers; filter membranes; and particles/beads (Fig. 4). Beads offer the option of suspending the sensing material (on the bead) in solution, improving mixing; beads can also be arrayed to create sensing chips [43, 44]. Conjugated polymers have also been combined with nanoparticles to exploit the quenching abilities of the nanoparticles [45, 46]. Attaching the sensing polymer to a filter membrane offers the option of pulling the target solution past the sensing surface and increasing exposure of the sensing polymer to the target [47, 48]. Conjugated polymers have been deposited on electrospun nanofiber films to increase the surface area and to prevent π - π stacking aggregation [49, 50].

4.1 Materials for Aqueous Applications

Detection of biological targets usually requires sensing in water. One technique is to synthesize the polymer as a polyelectrolyte with charged side chains so that it becomes more water soluble. Nonspecific interactions are a perennial problem in these systems for several reasons: (1) the hydrophobic nature of the polymer backbones makes the chains aggregation prone; (2) many biological species (proteins, nucleic acids, etc.) are charged and will form hydrogen bonds or electrostatically interact with the polymers affecting emission and/or causing aggregation [3]; and (3) buffer salts will potentially affect the microstructure of the polymer and, through charge screening, electrostatic interaction with the target. The ionic environment along the polymer is significantly different than in the bulk solution; for example, it has been shown that the pH in the vicinity of a weak polyelectrolyte is 3 units higher than the bulk solution pH [51].

Surfactants can be added to improve the behavior of polyelectrolytes. Early work with anionic PPV showed that the addition of surfactants changed polymer aggregation and morphology, and increased the polymer quantum yield by reducing self-quenching and increasing the conjugation length [52]. Bunz and co-workers have shown how choice of surfactant can be made to tune emissive properties of

PPEs in water and prevent aggregation and self-quenching [53]. Heeger and co-workers paired anionic PPV with a nonconjugated cationic polymer to form a charge-neutral complex and saw both reduction of nonspecific effects and some loss in sensitivity in protein detection [54]. Polyelectrolytes may be best used in assay schemes, such as DNA hybridization assays or drug discovery screens, where the assay conditions are well controlled and nonspecific interactions reduced or avoided.

Another approach for biological sensing materials is to prepare the conjugated polymer in biomimetic forms, such as liposomes (vesicles) or films that imitate cell membranes. PDA is particularly well known for being suitable for forming biomimetic materials [5]. Amphiphilic diacetylene monomers with a variety of head groups are dispersed in water or buffer by sonication where they self-assemble into liposomes, tubules, fibers, etc.; these are photopolymerized to form the polymer in situ (Fig. 5). PDA liposomes have been patterned on glass [55, 56] and attached to fiber membranes [57, 58] for fluorescence assay applications where liposomes tend to aggregate [5, 59]. Diacetylene films have been prepared by Langmuir techniques and photopolymerized; PDA coatings on filters have been prepared by the capture of diacetylene liposomes on filter membranes followed by polymerization [47, 59, 60]. Non-diacetylene species such as phospholipids can be incorporated at high percentages in diacetylene precursor materials without preventing the PDA formation [61]; domains form separating the monomers (and hence the polymers) from the added lipids [62]. Peptides and proteins can be inserted into the membranes or conjugated to the surfaces either before or after polymerization. The PDA domains are rigid unlike cell membranes; however, the lipid domains can incorporate

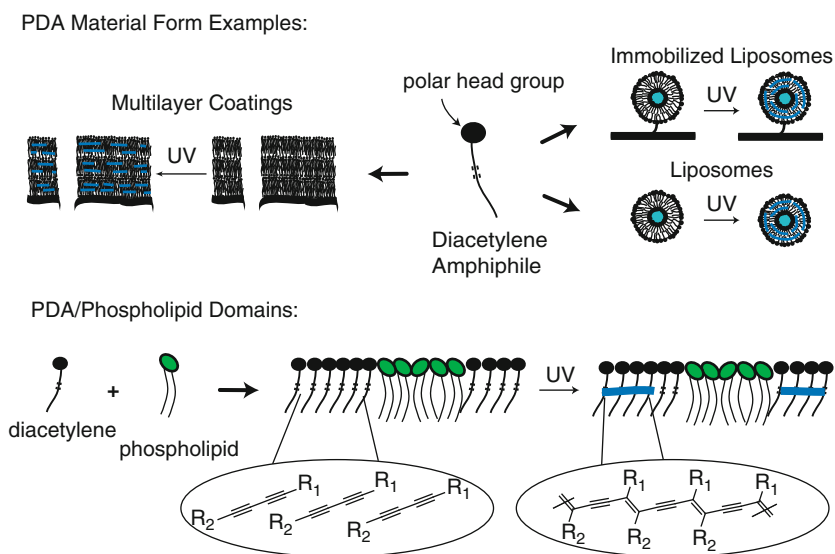


Fig. 5 Polydiacetylene self-assembled sensing material examples. PDA materials with phospholipids (or other natural lipids) may have separate domains

phospholipids with transition temperatures (T_m s) below room temperature [59, 61] allowing the possibility of forming fluid domains with more biomimetic character in the material.

5 Signal Transduction

Fluorescence signal generation can be sorted into three rough categories: reduction or quenching of emission by the target (“turn-off”), increase or restoration of emission (“turn-on”), and changes in the emission wavelength arising from the conformational changes in the polymer or energy transfer to another fluorophore. More than one signal may be present in a sensing system; in some cases, the signal with the largest change is measured and, in others, a ratio of signals may be used.

5.1 Turn-Off Sensing

Quenching of emission by a target is a well-known phenomenon in fluorescence sensing. In conjugated polymer systems, there are three major ways that quenching occurs in the presence of a target analyte: (1) the analyte quenches the polymer emission directly; (2) the analyte causes aggregation of the polymer chains leading to self-quenching; and (3) the analyte changes the polymer backbone conjugation and decreases the emission (Fig. 6). Direct quenching and aggregation often occur together leading to enhanced quenching as described below. Aggregation also can accompany the third path to quenching, in particular, in cases where the presence of the analyte changes the polymer microstructure from coils to rigid-rods, which then aggregate.

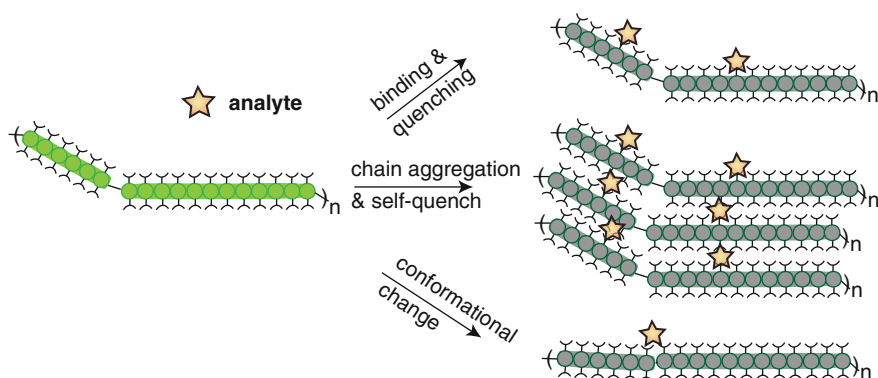


Fig. 6 Illustration of three quenching pathways

Quenching mechanisms are discussed in detail by Lakowicz in *Principles of Fluorescence Spectroscopy*. Interaction of the fluorophore and the quencher leads to nonradiative return to the ground state of the fluorophore via several different mechanisms [6, 63]. A quencher such as oxygen may induce the singlet excited state of the fluorophore to undergo intersystem crossing to the triplet state, which then undergoes nonradiative decay. The excited state of a fluorophore can exchange pairs of electrons with a quencher in close proximity (allowing MO overlap) in a Dexter exchange, dissipating the excited state as heat. Alternatively, the quencher and fluorophore may undergo photoinduced electron transfer (PET) where an electron is transferred either from the quencher to the excited state of the fluorophore or from the excited fluorophore to the quencher. Energy transfer from the excited state of the fluorophore to a chromophore can also occur via a Förster mechanism, as discussed below in Sect. 5.3; if the acceptor is not emissive, this leads to quenching of the system.

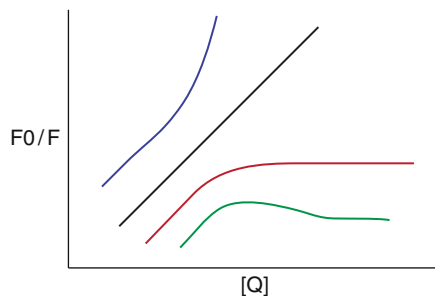
For small molecules, quenching often occurs through collisions between the quencher and the excited fluorophore (dynamic quenching). Conjugated polymers usually do not have excited states with sufficiently long lifetimes to allow dynamic quenching; however, quenching can occur through binding of the quencher (before excitation) creating a nonemissive species (static quenching). The Stern–Volmer equation is used to determine the efficiency of the quenching and can be expressed in terms of relative emission or as changes in lifetime. In dynamic quenching, a reduction in fluorescence lifetime is seen as the interaction with the quencher happens during the excited state lifetime cutting it short. In static quenching, the fluorophore/quencher complex is nonemissive and therefore while a reduction in emission is seen, there is no change in lifetime. The Stern–Volmer static quenching equation is:

$$F_0/F = 1 + K_{SV}[Q]$$

where F_0 is the emission without the quencher present, F is the emission with the quencher, $[Q]$ is the concentration of the quencher, and K_{SV} is the static Stern–Volmer constant. With perfect Stern–Volmer static quenching behavior, a plot of $[Q]$ vs. F_0/F yields a straight line with a slope of K_{SV} . The more effectively the emission of the fluorophore population is quenched, the higher K_{SV} will be.

Needless to say, real-life Stern–Volmer plots for quenching of conjugated polymers often show deviations from linearity over some portion of the $[Q]$ range. Upward curvature (Fig. 7, blue line) can be caused by the aggregation of the polymer. Aggregation can enhance quenching in two ways: through extending the exciton path so that it can sample more binding sites, and by stacking and self-quenching of polymer chains. Upward curvature has also been attributed to the sphere of action mechanism, which proposes that there is a volume around a fluorophore where quenching will always occur [64]. As quencher concentration increases, the probability that this volume will have a quencher in it goes up, adding to the observed quenching. Swager and co-workers in their 2007 review argue, however, that upward curvature seen in conjugated polymer systems is due to

Fig. 7 Static Stern–Volmer plots. The black line is the ideal Stern–Volmer response, the colored lines illustrate deviations from linearity



aggregation effects and not sphere of action [3]. In addition, contributions from dynamic quenching mechanisms will lead to upward curvature of the static quenching Stern–Volmer plot; studies of excited state lifetimes can determine whether dynamic quenching is occurring as well as static quenching. Saturation of the quenching response (Fig. 7, red line) is seen with a leveling of the curve at higher $[Q]$ concentrations. Occasionally, the Stern–Volmer plot has a downward curvature (Fig. 7, green line) showing a reduction in quenching with higher quencher concentrations. This can be attributed to the quencher causing a change in polymer conformation or aggregation state that reduces quencher access to the fluorophore or decreases the exciton sampling of quenching sites.

Many conjugated polymer molecular wire sensors exhibit what Whitten and co-workers have called “super-quenching” [12, 13]; binding of one target creates an exciton trap which quenches an entire polymer (in theory), or more realistically, quenches an extended segment of the polymer over which an exciton can travel. The term “super-quenching” is, however, somewhat misleading. A conjugated polymer has many more capture groups for the quenching target per “fluorophore” than a small molecule. In a small molecule, the excited state is localized, and usually there can only be one or two groups to capture the target on each molecule, whereas in the conjugated polymer the exciton can travel up and down the backbone and sample many binding sites. If any binding site is occupied, it can destroy the exciton and quench the emission of the whole conjugated segment (Fig. 8). Enhanced sensitivity therefore depends on the polymer having many binding sites, often one or more site per repeat unit combined with extensive exciton delocalization. Polymers that do not have extensive exciton delocalization do not show the enhanced sensitivity to the quenching target [3]. Sensitivity to quenchers can be increased by altering the polymer structure to increase exciton lifetime [65], allowing it to sample more binding sites [66, 67], and by choosing polymers with higher fluorescence efficiency.

It should also be noted that comparison of quenching efficiency of conjugated polymers with small-molecule fluorophores is complicated and oversimplification can lead to misleading claims of exceptional sensitivity enhancements. In their 2007 review, Swager and co-workers discuss cases where the charge state of the small molecule used for comparison differed fundamentally from the polymer and exceptional quenching efficiencies were inappropriately attributed to super-quenching alone [3]. In addition, a polymer will create a different local

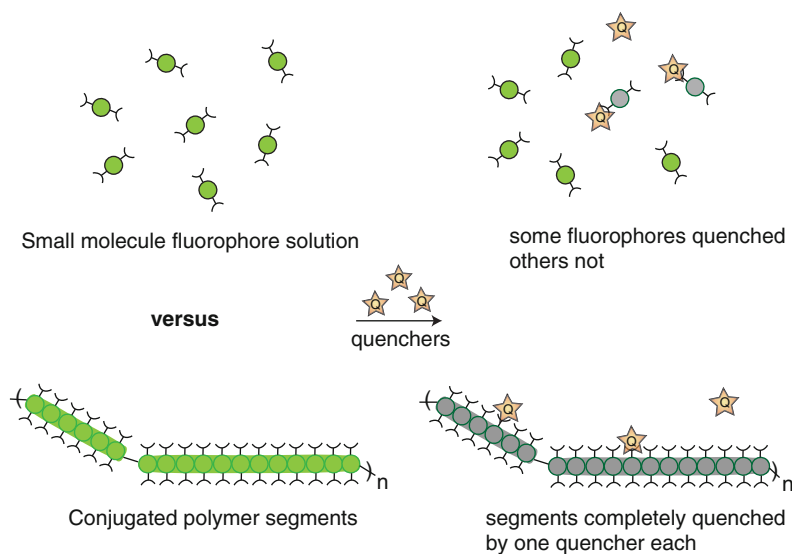


Fig. 8 Comparison of quenching of small-molecule fluorophores vs. conjugated polymers

environment for target binding than a small molecule, which can affect the binding affinity. Frequently, researchers overlook that the emissive species for a conjugated polymer is a collection of repeat units, and thus treat the polymer as though each repeat unit is an individual fluorophore. Analysis of whether there is an enhancement of binding to the polymer when compared with the small molecule needs to take into account the exciton delocalization length to estimate how many binding groups there are per emissive species. In the early work by Zhou and Swager, this was achieved by synthesis of a series of polymers of increasing molecular weight and examination of their Stern–Volmer quenching constants [66]. The K_{SV} values rose with increased polymer length and then plateaued, leading the researchers to conclude that the exciton was traveling on average over 134 repeat units. Since every repeat unit had a binding group, the fact that the K_{SV} of the polymer was 60-fold greater than that of a comparison small-molecule fluorophore with one binding group is not surprising.

Creating a polymer with many binding sites is more easily achieved for small molecules and ion targets that can be captured by cyclophanes, bi- and tri-pyridines and other binding units that are readily incorporated in the polymer, than for biological targets that may require relatively large (and expensive) biomolecules such as peptides, antibodies, or aptamers for target capture. If the target size is of a scale comparable to the polymer (e.g., a protein) or larger, then the advantages of super-quenching may be reduced, as the target can bind more small-molecule fluorophores than macromolecule fluorophores (Fig. 9a). Another consequence of the “super-quenching” mechanism is while the materials are often extremely sensitive it can also be easy to saturate the sensor (Fig. 9b) [3].

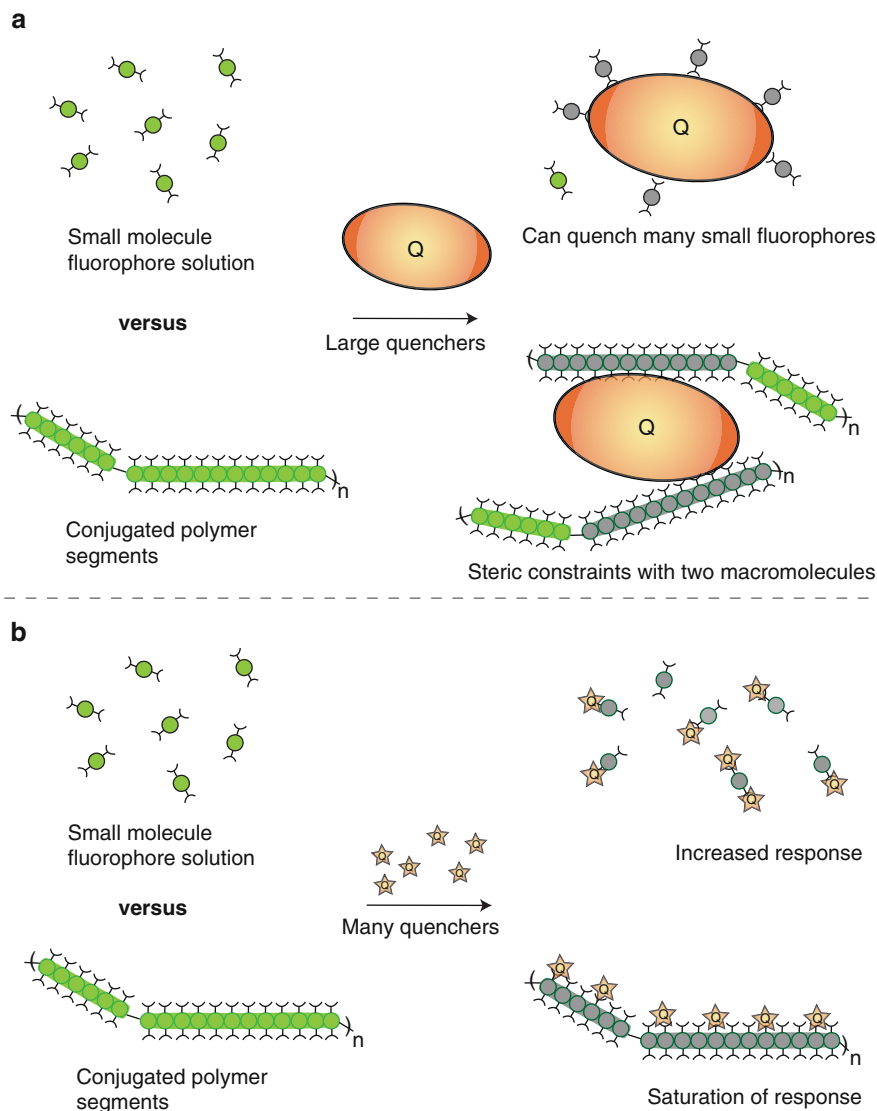


Fig. 9 Small-molecule and conjugated polymer quenching comparison: (a) with large quenchers and (b) at high quencher concentration

5.1.1 “Turn-Off” Detection of Small-Molecules

There are many examples in the literature of turn-off (or quenching) sensors based on conjugated polymers. Small organic molecules, metal ions, and various biological species have all been detected through turn-off sensing. Many initial studies of conjugated polymer quenching have been performed with electron-poor organic

molecules such as paraquat and methyl viologen (MV^{2+}); Thomas and Swager's 2007 review describes many of these studies in detail [3]. While these studies are illustrative and provide information relevant to the design of sensing polymers and in some cases identify factors such as aggregation that affect the sensing response, they do not represent detection of species of real interest. Electron-poor nitroaromatics used in explosives, in contrast, are targets of considerable interest. Swager and co-workers developed PAE sensing materials for the detection of trinitrotoluene (TNT) and dinitrotoluene (DNT) [68, 69]. These materials have been developed into sensors for land mines by Nomadics Inc., and represent one of the few examples of a fluorescent conjugated polymer sensing material being developed into a commercial device.

The research and development work on PAEs for nitroaromatic detection is important both as an example of how a fluorescent conjugated polymer sensor can be used to address a significant real-world problem, such as explosives detection, and also as a platform for the development of design principles that can be applied to other fluorescent conjugated polymer sensing systems. The principle that increasing exciton travel will improve quenching sensitivity was demonstrated in the development of these materials. Swager and co-workers first prepared PAE films, with the chains carefully designed with pentyptycene group spacers to avoid π - π stacking of the chains and self-quenching [68]. Subsequently, they incorporated chiral chains as side groups in PPEs and investigated the role of polymer molecular weight and aggregation in solution in preparing spin-coated films with increased sensitivity to TNT [15]. The combination of chiral side chains and pentyptycene groups led to the polymer chains aggregating in a chiral grid preventing the self-quenching that arises when the chain aggregate in a collinear geometry, while still allowing exciton migration through the three dimensions of the films. These films showed a fourfold increase in quenching efficiency over the previously prepared PPE with pentyptycene groups alone. In another interesting approach to sensitivity enhancement, Bulovic, Swager, and co-workers developed a lasing PPV, with the PPV backbone protected from photodegradation by side groups made up of phenyls with branched side chains, for quenching-based detection of nitroaromatics [70]. The quenching action of the nitroaromatics decreased the exciton lifetime and raised the lasing threshold thus preventing light generation through lasing; this approach was more sensitive than direct exciton quenching, showing a 30-fold enhancement.

Sugars are another class of small molecules that have been detected by emissive conjugated polymers. Unlike nitroaromatics or MV^{2+} , sugars are not electronic quenchers, so other quenching mechanisms come into play. Monosaccharides have been detected by several different conjugated polymer platforms that exploit the reaction between boronic acids and sugar diols. One approach depends on H^+ generated by the addition of sugar to boronic acid to aggregate pH-sensitive conjugated polymer chains, which results in quenching [71]. Another recent approach used PT polymers functionalized with boronic acid groups [72]. Binding of sugars to the boronic acids quenched the PT emission; quenching was attributed to conformational changes in the backbone arising from multivalent interactions

between the boronic acids and the sugars. The work with sugars illustrates how turn-off sensing can be achieved even though the target is not intrinsically a quencher.

5.1.2 “Turn-Off” Detection of Ions

Developing emissive conjugated polymers for ion detection, primarily of cations, is a significant research area [3, 6]. Quenching of conjugated polymer emission by cations [6, 73] occurs by Dexter and PET electron transfer mechanisms, by through space energy transfer (Förster), and by ion-induced aggregation [74]. There are far fewer examples of detection of anions by conjugated polymers, and the examples that exist tend to be either of fluoride, which has specific reactivity [20, 75, 76], or of anionic transition metal complexes, or consist of nonselective sensors that respond to a range of anionic species [3].

Polymers for cation detection have been designed both with the binding group incorporated in the backbone [77] and with the binding group as a side group. Designing the polymer with the binding group as a side chain allows more variation in the choice of binding group, as the binding group does not have to have the π structure required for participation in the conjugation of the backbone. Incorporation of the binding group into the polymer backbone, however, can increase sensitivity [78]. The nature of the linker between the backbone and the binding group [73] has been shown to affect sensitivity with a vinyl linker leading to greater quenching than an ether linker [79]. Similarly, when the binding group is incorporated in the backbone, the nature of the linker between units also affects performance, for example, fluorene/bipyridine copolymers showed greater sensitivity when there was a lower barrier to chelation-induced rotation of the bipyridine group [80].

The quenching effect of cations on conjugated polymer sensors is often amplified by cation-induced aggregation of the polymer chains [3]. Quenching may also occur purely as a result of aggregation in cases where the target itself cannot undergo electron or energy transfer with the polymer. K^+ , for example, was detected by conjugated polymers with crown ethers attached as side chains; the crown ethers sandwiched the K^+ , brought the chains together and induced self-quenching [74, 81].

It should be noted that most conjugated polymer ion sensors suffer from lack of selectivity. Even when the polymer responds to a particular ion with greater sensitivity than to other ions at the same concentration, it does not guarantee that the polymer will be effective in a real-world setting where environmental samples can contain many ions at a wide variety of concentrations. In cases where a few ion species are present at much higher concentrations than the target ions, the sensor response may be misleading. It is standard to invoke using sensor arrays (“tongues” and “noses”) as a technique to avoid this issue; however, such claims should be approached with some skepticism, as multivariate analysis of samples with ten or more species is considerably more difficult than analysis of standard example

systems with only 3–5 species. Sample processing steps can be used to remove interferents and/or concentrate target species; however, addition of these steps complicates sensor device design.

5.1.3 “Turn-Off” Detection of Biological Targets

Turn-off sensing has also been used for the detection of biological targets: enzymes, other proteins, and DNA hybridization. Conjugated polyelectrolyte turn-off sensing has been used for the detection of DNA hybridization and the identification of complementary strands through direct [82] and indirect bead-based assays [83] though these materials lack the exceptional sensitivity shown by PT DNA hybridization sensors developed by Leclerc and colleagues [84, 85] and discussed in Sect. 5.2.2.

Sensing schemes for detecting enzymes depend on using the enzymatic action – bond cleavage or functional group modification – to create a quencher. In one example of enzymatic sensing, rhodamine-110 diarginine amide was mixed with PPE with carboxylate side chains and nanomolar papain added [86]. The protease cleaved one arginine amide, creating the positively charged Rhodamine–Arg molecule that associated electrostatically with the negative PPE and quenched its emission through singlet–singlet energy transfer. A similar approach from Whitten and co-workers deployed beads coated with polyelectrolyte conjugated polymers and avidin proteins combined with a biotin–peptide–quencher [87]. Reduction in quenching signaled protease activity as cleavage of the peptide by proteases severed the connection between the biotin and the quencher and prevented quenching of the polymer upon the biotin binding to the avidin (Fig. 10). Interestingly, it was necessary to carry out the peptide/protease reactions before adding the beads – the enzymes were not able to cleave bead-bound peptide sequences. Kinase detection via quenching was achieved with PPE/carboxylate side chains on a bead loaded with Ga^{3+} ions [88]. The beads were mixed with a kinase substrate labeled with rhodamine; when the kinase phosphorylated the peptide the PO_3^- groups bound to the Ga^{3+} ions, bringing the quencher into proximity of the polymer and quenching its emission.

Nonenzymatic proteins have also been detected with turn-off conjugated polymer sensors. Unlike enzymatic assays, these assays do not depend on the protein having an action on a substrate. For redox-active proteins, the proteins themselves can act as the quenching agent; for example, Heeger and co-workers showed that sulfonated PPV can be quenched by cytochrome C (cyt C) [89]. Interestingly, a later study by Waldeck and co-workers, using anionic PPP mixed with cyt C, myoglobin and polyamidoamine dendrimer, showed that quenching does not require that the protein (or protein analog) engage in electron transfer but can occur because of conformational changes caused by electrostatic-driven aggregation. Bunz and co-workers have studied the nonspecific interactions of positive, neutral, and negative proteins with PPEs containing carboxylate sidechains and their effects on emission [90]. The different proteins studied quenched the polymer emission by varying combinations

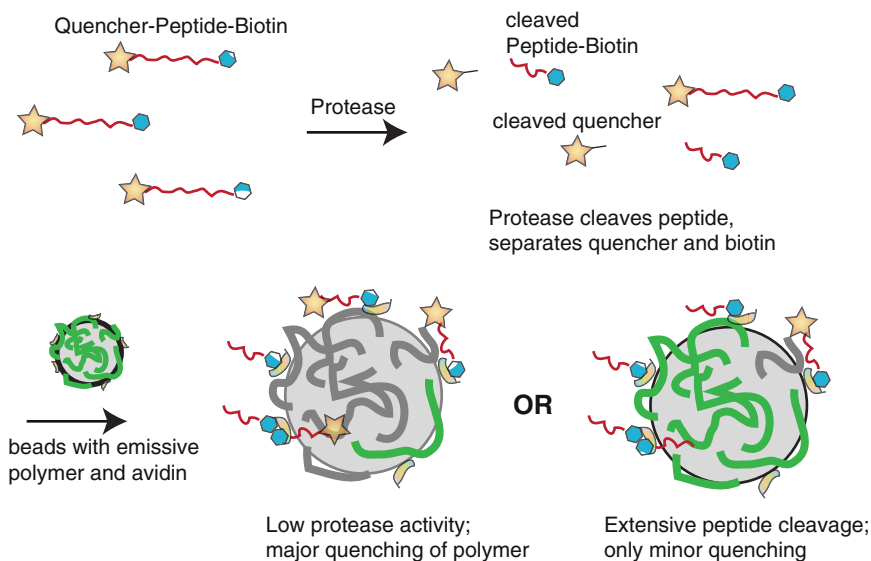


Fig. 10 Protease assay using beads with emissive polymer and avidin [87] cartoon. Emissive polymer is represented by *green lines*; quenched polymer by *grey*

of energy transfer, charge transfer, and aggregation mechanisms. Bovine serum albumin (BSA) was a notable exception; addition of BSA led to emission increases, which was attributed to the BSA acting as a surfactant and reducing the self-quenching by reducing the polymer aggregation. Proteins can also form complexes with multiple polymer chains; these complexes have been shown to have enhanced quenching when exposed to other targets [91, 92].

These examples illustrate some of the complications of detecting proteins with fluorescent polymers. The interplay between the two macromolecules will be directed by nonspecific hydrophobic or electrostatic interactions that can lead to aggregation of the polymer and nonspecific quenching. These interactions are particularly important in biological sensing because many biological samples of interest contain proteins that are not the actual targets; for example, serum samples have significant amounts of albumins and gamma globulins, and many enzyme- and antibody-based assays in drug discovery are run at low concentrations of active protein with BSA added to stabilize the active protein. Biological assays are also performed in buffers, and the buffer salts may interfere with electrostatic interactions between the polymer and the target.

In summary, emissive conjugated polymers are good materials for quenching-based sensing schemes because most of them are synthesized in the emissive state (PAEs, PPPs, PPVs, PFs) and exciton delocalization leads to sampling of many binding sites per excitation allowing detection of low levels of analytes. It should be noted, however, that high sensitivity is not always desirable; problems will ensue if the detection range of interest is above the sensor saturation point. The sensing materials described above are usually reversible – in most cases, if the target is

unbound the exciton trap disappears and emission is restored. Aggregation plays a role in many quenching assays and may be deliberately incorporated in the sensing scheme design, as it can amplify the signal through extending the exciton pathway and through enabling polymer self-quenching.

5.2 Turn-On Sensing

The complement to turn-off sensing is turn-on sensing – situations where the polymer emission goes up as a result of a target. Turn-on sensing may be achieved by preparing a conjugated polymer with a quenching group that is removed by the target, by changing the aggregation state of the polymer and thus reducing self-quenching, or by using a conjugated polymer that has intrinsically emissive and nonemissive states related by backbone twisting (Fig. 11). Ideally, the polymer is in a completely nonemissive state before being exposed to the target; the presence of initial emission lowers the sensitivity of the sensor. As seen below, however, obtaining a nonemissive state of many types of conjugated polymers is difficult, and as a result, the turn-on sensors are often less sensitive than turn-off sensors. Less-sensitive sensors, however, complement ultra-sensitive sensors and are useful for applications where the target is present in concentrations where an ultra-sensitive sensor is saturated. Another important consideration is that the

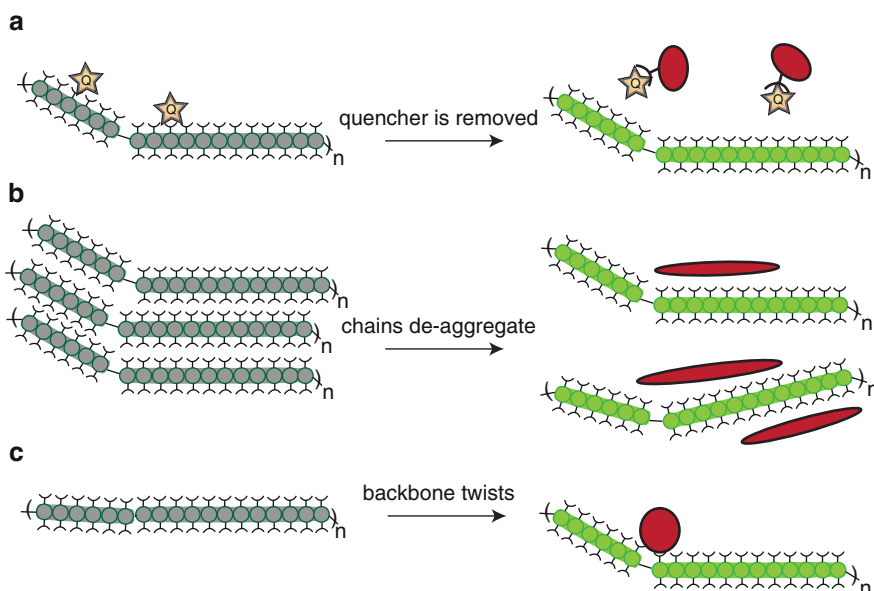


Fig. 11 Cartoons of “turn-on” mechanisms. The target (*in red*) may (a) remove a quencher, (b) deaggregate chains, or (c) twist the backbone, leading to increases in emission

aggregation of the polymer during turn-on assays can confuse the signal if the chains begin to self-quench, lowering the emission, while interaction with the target simultaneously raises it.

5.2.1 “Turn-On” From Quencher Displacement

The flip side of the super-quenching phenomenon seen with conjugated polymer molecular wires is that to use these polymers in a sensing scheme where a quenching species is removed as part of target identification has the disadvantage that all the binding sites along the exciton path have to be vacated or otherwise altered for the polymer to become fluorescent. This requirement points to using polymers, such as PPV, which have shorter conjugation lengths. Conversely, another problem with this approach is background emission from insufficiently quenched polymer segments. This has been addressed by pretreating polymers with effective quenchers, such as Cu(II), to reduce initial emission. The quenchers are removed during the assay; this approach was the basis for sensitive and selective detection of Fe²⁺ [93].

Quencher displacement has also been used for the detection of biological targets. One approach is for the quencher to be removed by an entity that competitively binds to it. For example, Whitten and co-workers developed a system where the biotin–avidin interaction was used to remove a biotin–MV²⁺ quencher from sulfonated PPV [12]. Subsequent studies by Bazan and co-workers on similar systems, however, showed that nonspecific protein interactions with the polyelectrolyte also led to increases in the emission of the quenched complex. In a buffer that promotes avidin–biotin binding, addition of avidin actually increased quenching. They attributed this to the avidin–biotin–quencher complex associating more strongly with the polymer in buffer than the biotin–quencher alone [94]. In another model study, Heeger and co-workers demonstrated using antibodies to remove quenchers from a sulfonated PPV complexed with a cationic (nonconjugated) polyelectrolyte system – the cationic polymer reduced the nonspecific interactions with the PPV [54]. Interestingly, both positive and negative quenchers interacted with the PPV/cationic polymer complex quenching the PPV emission. Addition of antibodies specific to the quenchers led to increase in the PPV emission. In a demonstration of detection of a more interesting target, Whitten and co-workers preloaded sulfonated PPV with Cu²⁺ to reduce emission then added a oligohistidine-tagged anti-hepatitis C antibody to form a complex with Cu²⁺, which quenched the emission further [95]. Addition of hepatitis C antigen led to the restoration of the emission. Quencher displacement has also been used to detect protease activity [7, 86] using conjugated polyelectrolytes and peptide substrates of opposite charge linked to quenchers. Cleavage of the substrate leads to the disassociation of the (neutral) quencher, which then diffuses away, turning on the emission.

A related type of turn-on assay has also been developed using competition between a quencher and a target for binding sites associated with the emissive polymer. The more target presented, the less the quenchers can interact with the polymer – this registers as a rise in emission. An illustration of how a turn-off

quenching assay can be turned into this type of turn-on assay can be found in the work of QTL Biosystems [44]. A turn-on high-throughput commercial (QTL Lightspeed™) assay variation was developed of the Whitten and co-workers' kinase detection turn-off scheme described above in Sect. 5.1.3. The turn-off assay detected quenching of polymer–Ga³⁺ beads by phosphorylation peptide kinase substrates labeled with quenchers to signal kinase activity (Fig. 12a) [88]. In the commercial form of the assay, a protein substrate phosphorylated by the kinase competes with a nonsubstrate “probe” peptide labeled with a quencher and a PO₃⁻ group (Fig. 12b). As the kinase phosphorylates its substrate, the extent of quenching by the probe is decreased and the emission of the overall sample increases.

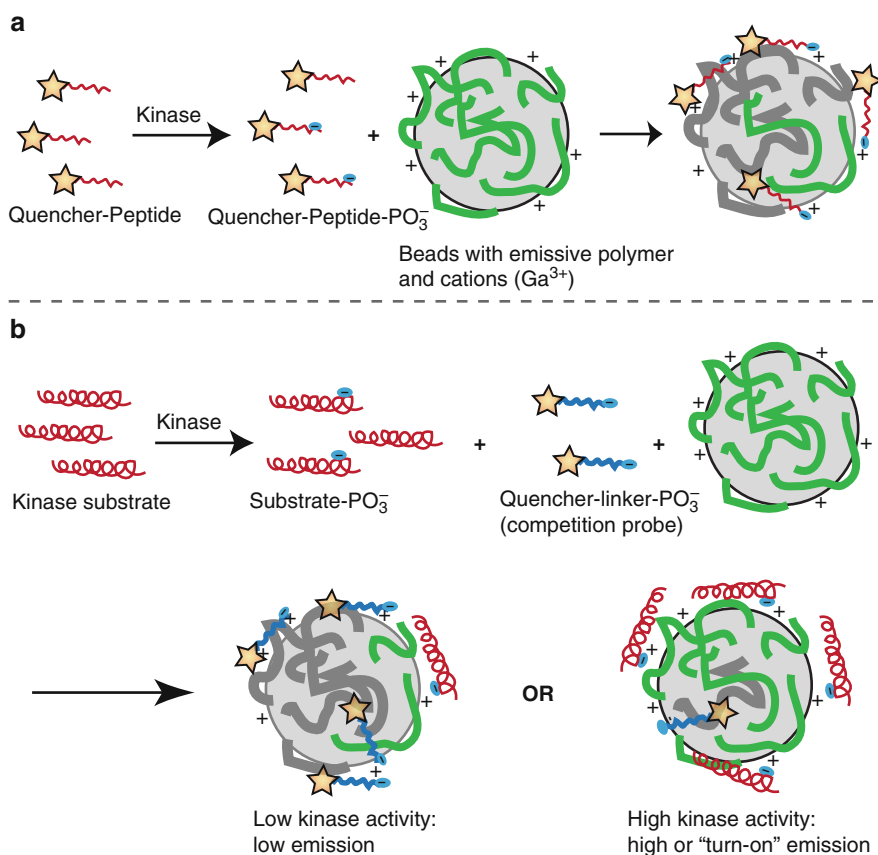


Fig. 12 Cartoon representing two versions of a kinase assay. **(a)** The “turn-off” version is a direct assay; the extent of phosphorylation of the substrate is reflected in the binding of the quencher to the bead and hence to the quenching [88]. **(b)** The “turn-on” version is a competition assay: increased phosphorylation of the substrate leads to it competing with the quencher in binding to the beads, and hence to increased emission [44]. Emissive polymers are represented by *green lines*; quenched polymers by *grey lines*

A related approach to quencher displacement for turn-on sensing is quencher modification. A simple approach is to design a system where the quencher and the polymer interact electrostatically causing the target to change the charge of the quencher and thus removing the attraction between the quencher and the polymer. An illustration of this approach was developed by Schanze, Lackowicz, and co-workers, who used sulfonated PPE complexed with a boronic acid functionalized methyl viologen analog for monosaccharide detection [96]. When sugars reacted with the boronic acid, they neutralized the quencher and it diffused away, turning-on the polymer emission. Another approach is to chemically modify the quencher. For example, Thomas and Swager developed reversible hydrazine turn-on sensing materials by preparing emissive PAE films [97] with alternating bis(alkylamino)phenylene and pentiptycene units. Upon exposure to hydrazine vapor, the emission increased. The authors hypothesized that the hydrazine reduced exciton traps formed from the oxidation of the polymer. Photobleaching before hydrazine exposure, to increase the number of exciton traps, increased the sensitivity of the material. Another example is the work of Lippard and co-workers who developed a selective NO sensor from a PPV with bipyridine units in the backbone [98]. The polymer was exposed to Cu(II) which quenched its emission. NO reacted with Cu(II) to form Cu(I); Cu(I) also quenched the polymer emission but not as strongly as Cu(II), so the overall emission rose.

5.2.2 “Turn-On” From Change in Conjugation Length

The discussion so far has focused on emission changes arising from the introduction, removal or modification of species that quench the polymer through some form of energy transfer. Changes in conjugation length of the polymer backbone affect both the absorbance and emission spectra; increases in conjugation lead to redshifts in absorbance, while the effect of conjugation length/exciton delocalization on overall emission is a more complicated issue. Greater delocalization (conjugation) generally reduces the energy gap which leads to an increase of nonradiative pathways, shortening the excited state lifetime and reducing the emission. For some classes of polymers, such as PDA and PT, the polymer's emission decreases or is eliminated at longer conjugation lengths, while the emission increases with backbone twisting that breaks conjugation. Changes in the conjugation length of PPVs and PAEs are also known [99] but are less commonly reported, possibly because of the relative rigidity of their backbones. For PPV polymers, with relatively short conjugation lengths and exciton delocalization over approximately 5–10 units [34, 37], increases in conjugation length have been reported to lead to increases in emission [52, 100, 101].

Leclerc, Ho, and co-workers have developed many sensing systems for different targets using cationic PT and exploiting the differences in emission and color between the extended conjugation form and the coiled form. The basis of these assays is that the polymer microstructure and conformation change as it interacts with the target. For example, in DNA hybridization assays, imidazolium–PT (see

Fig. 1) first forms a low emission complex with a single DNA strand where the polymer backbone is in the extended form [85, 102]. Upon DNA hybridization, the cationic PT wraps around the helix, kinking the backbone, reducing conjugation and increasing its emission. To increase sensitivity further, Leclerc and co-workers labeled the capture strand with a fluorophore that accepts energy from emissive PT via FRET – this allowed the detection of as few as five strands in 3 mL [84]. The photophysics leading to the exceptional sensitivity of this assay was further explored by Leclerc et al. and attributed to aggregation of the duplexes prior to target transfer, so that when the DNA hybridized the nonemissive PT in the triplex has multiple fluorophores nearby to accept energy [103]. Variations of this approach have also been used for the detection of K^+ [104] and thrombin [105] and have been adapted for microarray screening of nucleic acids [43, 106]. Nilsson and co-workers have used a zwitterionic PT [107] in a similar approach for probing protein conformations; again, the PT chain conformation changes in response to changes in the target 3-D shape [108]; this and related work is described in more detail in [109].

PDA has also been used as the basis for colorimetric and fluorescent sensing materials. Spectroscopic studies of PDA show that the blue, planar PDA undergoes ultrafast relaxation of the excited state [110], making it effectively nonemissive. The conversion of blue to red PDA is accompanied by a change in emission that has been shown to be more responsive than the change in absorbance [5, 26], and this change has been used for the detection of enzymes, bacteria, and other biological targets [5]. PDA materials can be formed with lipophilic binding groups and substrates incorporated or they can be added later through insertion or surface reactions. Interaction of the target with binding groups, substrate, etc. at the PDA interface leads to changes in the polymer backbone translated via the methylene groups between the surface and the polymer chain. While changes in the PDA emission have been used for detection, a more common approach is to use energy transfer to a small-molecule fluorophore, as discussed below. Emissive PDA has a relatively low quantum yield (0.02 at room temperature for a red PDA film [111]) and the overall emissive output can be increased by the choice of an appropriate acceptor fluorophore [112]. It should be noted that the conformational changes in PT chains are often reversible, while for a PDA material, the switch from non-emissive to emissive is usually not reversible after a certain amount of conversion has taken place. This is a general consequence of the thermodynamic strain present in the nonemissive form of PDA. This strain is a result of polymer formation through a sterically demanding two-electron process, and is reduced by the backbone twisting that makes the polymer emissive [5].

5.3 Emission Wavelength Shifts and FRET

In the discussion of detection signals above, the focus has been primarily on increases or decreases in the polymer emission at one wavelength. It is also possible for the emission wavelength of the polymer itself to shift as result of interaction

with a target. Changes in backbone conformation and polymer aggregation can cause shifts in emission wavelength as well as changes in emission intensity; both aggregation and increases in conjugation lead to redshifts in fluorescence. In the cases where the polymer is emissive pre- and post-target interaction, the shifts and ratios of peak intensities can be used to gain more information and to distinguish between possible targets. For example, the influential 1997 paper by Wang and Wasielewski in the area of metal ion sensing described a PPV–bipyridine copolymer that had redshifted emission in the presence of ions that flattened the bipyridine units increasing conjugation, blueshifted emission with ions that twisted the backbone upon binding reducing conjugation, and quenched emission for a third set of ions [77].

Resonance energy transfer (RET) from the excited state of a donor fluorophore/chromophore to an acceptor fluorophore/chromophore, is a well-known phenomenon in small-molecule fluorescence that has analogs in the field of emissive conjugated polymer sensing. RET between small molecules is generally described by the Förster (FRET) mechanism. The Förster mechanism involves point dipole to point dipole coupling of the excited state of the donor to the ground state of an acceptor leading to the donor returning to the ground state and the acceptor being excited [63]; this transfer has a $1/r^6$ distance dependence and is referred to as “through space” energy transfer. If the acceptor molecule is not fluorescent, this energy transfer will lead to quenching as seen above, but if the acceptor is a fluorophore, it can emit at a lower-energy (redshifted) wavelength compared to the donor emission. This leads to an increase in the Stokes shift of the sensing system and opportunities for “multi-color” and ratiometric emissive-based sensing. The extent of spectral overlap between the emission spectrum of the donor and the absorbance spectrum of the acceptor is often used as a quick guide as to whether FRET will occur. An in-depth discussion of the factors affecting FRET transfer and competition from PET is presented in [113]. It should be noted that though the Förster mechanism is frequently invoked to describe conjugated polymer to small-molecule fluorophore energy transfer, the mechanism does not always predict the behavior accurately as the chromophoric segments of conjugated polymers are frequently too large to be convincingly modeled as point dipoles [112, 114, 115]. Energy can also be transferred from donor to acceptor via the Dexter mechanism, described in Sect. 5.1. The Dexter mechanism involves direct orbital overlap and operates at close distances, while the Förster mechanism can operate at either relatively far or very close distances.

FRET is a good technique for sensing schemes where the target affects the distance between the donor and acceptor. The simplest approach is to label a target that then binds to the polymer; this is an appropriate approach for competition assays but not for sensing situations where target modification is not practical. Other design schemes that deploy FRET include: (1) the target reducing the donor–acceptor distance to “turn-on” FRET, (2) the target displacing a labeled species and thus “turning-off” FRET, or (3) the target altering the macromolecular structure of the polymer thus turning it into a donor (or acceptor) by changing its excited state behavior. FRET-based quenching-sensing schemes have been used in

the detection of proteins [7] and FRET-based emission has been used in the detection of DNA hybridization [3, 9, 84, 103].

FRET has also been used as the basis for multicolor emissive sensing as demonstrated by Bazan and co-workers with a cationic PF with 5% BT developed for DNA hybridization assays [8]. At high polymer dilution, the emission was dominated by the PF segments (blue). At polymer concentrations above 1 μM , the chains aggregated and BT emission (green) appeared from energy transfer from PF segments to lower energy BT segments. Addition of ssDNA strands also led to green BT emission as the DNA aggregated the polymer chains. The third color (red) was added through the addition of Cy-5 attached to a peptide nucleic acid (PNA) probe. Examination of the different emission wavelengths gave a picture of the mix of species in the assay. Addition of the PNA/Cy-5 probe strand alone did not affect polymer emission, so the emission was blue (Fig. 13a); while addition of noncomplementary DNA together with the probe left DNA free (as there was no hybridization), so aggregation occurred and the emission shifted to green (Fig. 13b). Addition of a complementary DNA strand led to DNA–PNA/Cy5 hybridization, this complex then associated with polymer, which acted as a FRET donor for the Cy-5 leading to red emission (Fig. 13c).

Swager and co-workers have observed that energy transfer from conjugated polymers to other fluorophores does not always go by a Förster mechanism.

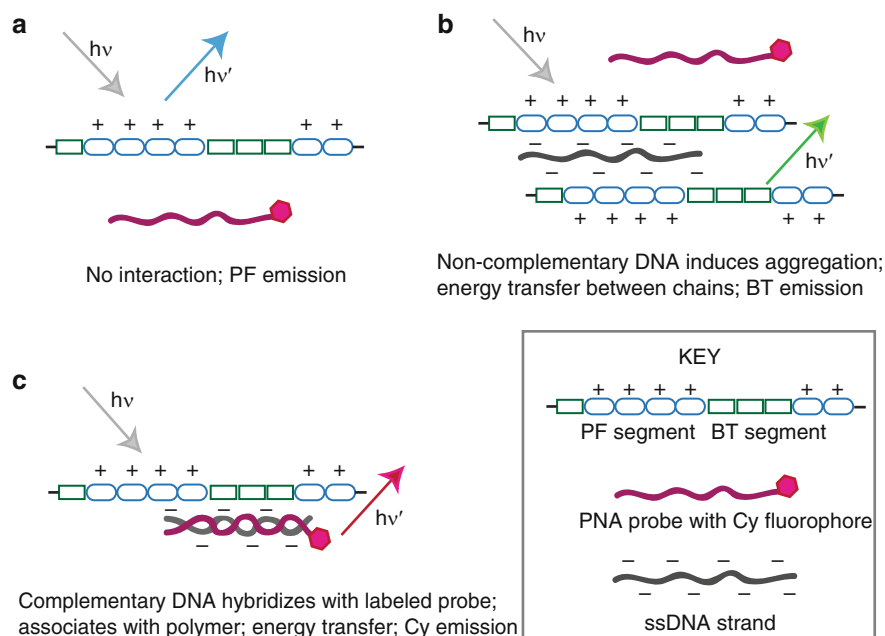


Fig. 13 Three-emission system cartoon. (a) poly(PF/BT) with neutral probe; (b) poly(PF/BT) with noncomplementary DNA and probe; (c) poly(PF/BT) with complementary DNA and probe

A 2004 study of the emission of PPE–biotin polymers mixed with fluorophore–streptavidin showed that energy transfer did not occur for the fluorophore with best spectral overlap but rather for the more planar hydrophobic fluorophore, which could stack with the polymer backbone and allow direct orbital overlap [116]. Kim and Swager developed a sensing approach for the detection of fluoride ion, which relied on the Dexter mechanism rather than the Förster for energy transfer [75]. A PAE polymer was prepared with alternative rings linked to a coumarin precursor via a thiophene group. In the presence of F^- , the precursor cyclized to form coumarin, the coumarin lowered the band gap and formed an exciton trap, and the emission peak shifted from the blue emission characteristic of the polymer to a blue–green emission characteristic of coumarin. This approach showed that the PAE “molecular wire” amplified the signal compared to the rise in emission from the formation of plain coumarin (without the polymer attached) from its precursor.

Energy transfer from PDA to fluorophores [26, 59, 112], and from fluorophores to PDA [26, 117, 118], has proven an effective way to improve the signal characteristics of PDA sensors [5]. As noted above, PDA has a relatively low emission. The overall quantum yield of PDA liposomes has been shown to be increased by incorporation of a fluorophore that accepts energy from emissive PDA [26]. A study of diacetylene/PDA liposomes with fluorophores, polymerized to different extents, suggest that energy transfer between PDA chains competes with energy transfer to fluorophores and that at greater polymerization extents the fluorophore emission is greatly reduced or eliminated [112]. The density of PDA chains in a material can be controlled by the UV dose used to form the polymer. In sensing schemes involving PDA and energy transfer to fluorophores it is important to balance the desire for greater conversion of monomers to polymer for material stability, and the need for lower polymer densities to facilitate energy transfer to amplifying fluorophores.

6 Conclusion

Emissive conjugated polymers have shown considerable potential as the basis for sensors for both biological and chemical targets. These macromolecular fluorophores have features arising from the delocalized electronic states created by the extended conjugation of the backbone that are not found in localized small-molecule fluorophores and lead to high sensitivities. For example, in quenching-based detection the exciton travels past many binding sites allowing it to sample and respond to targets captured by any site along its path, effectively allowing the conjugated polymer segment to behave as a fluorophore with many binding groups rather than the one or two found on small molecules. Changes in the polymer microstructure, e.g., from coil to rod, affect backbone conjugation and can be used for signal generation. Many complicating factors in using emissive conjugated polymer for sensing, arising from unanticipated microstructure changes and chain aggregation that can affect emission, go hand in hand with the advantages of these macromolecular materials. In addition, there is considerable variation between

the optoelectronic and structural properties of different types of conjugated polymers, so insights gained from studying one system should be applied cautiously when designing another. Nonetheless, there have been some notable successes in developing fluorescent conjugated polymers for TNT detection, enzyme assays, and DNA hybridization assays, and the understanding gained from the careful studies of many research groups will lead to even more effective designs in the future.

References

1. McQuade DT, Pullen AE, Swager TM (2000) Conjugated polymer-based chemical sensors. *Chem Rev* 100:2537–2574
2. Zheng J, Swager TM (2005) Poly(arylene ethynylene)s in chemosensing and biosensing. *Adv Polym Sci* 177:151–179
3. Thomas SW, Joly GD, Swager TM (2007) Chemical sensors based on amplifying fluorescent conjugated polymers. *Chem Rev* 107:1339–1386
4. Bunz UHF (2000) Poly(aryleneethynylene)s: syntheses, properties, structures, and applications. *Chem Rev* 2000:1605–1644
5. Reppy MA, Pindzola BA (2007) Biosensing with polydiacetylene materials: structures, optical properties and applications. *Chem Commun* 42:4317–4388
6. Fan L-J, Zhanga Y, Murphy CB, Angell SE, Parker MFL, Flynn BR, Jones WE Jr (2009) Fluorescent conjugated polymer molecular wire chemosensors for transition metal ion recognition and signaling. *Coord Chem Rev* 253:401–422
7. Ambade AV, Sandanara BS, Klaikherd A, Thayumanavan S (2007) Fluorescent polyelectrolytes as protein sensors. *Polym Int* 56:474–481
8. Liu B, Bazan GC (2004) Interpolyelectrolyte complexes of conjugated copolymers and DNA: platforms for multicolor biosensors. *J Am Chem Soc* 126:1942–1943
9. Liu B, Bazan GC (2009) Homogeneous fluorescence-based DNA detection with water-soluble conjugated polymers. *Chem Mater* 16:4467–4476
10. Liu B, Wang S, Bazan GC, Mikhailovsky A (2003) Shape-adaptable water-soluble conjugated polymers. *J Am Chem Soc* 125:13306–13307
11. Tan C, Pinto MR, Kose ME, Ghiviriga I, Schanze KS (2004) Solvent-induced self-assembly of a meta-linked conjugated polyelectrolyte. Helix formation, guest intercalation, and amplified quenching. *Adv Mater* 16:1208–1212
12. Chen L, McBranch DW, Wang H-L, Helgeson R, Wudl F, Whitten DG (1999) Highly sensitive biological and chemical sensors based on reversible fluorescence quenching in a conjugated polymer. *Proc Natl Acad Sci* 96:12287–12292
13. Achyuthan KE, Bergstedt TS, Chen L, Jones RM, Kumaraswamy S, Kushon SA, Ley KD, Lu L, McBranch D, Mukundan H, Rininsland F, Sh X, Xia W, Whitten DG (2005) Fluorescence superquenching of conjugated polyelectrolytes: applications for biosensing and drug discovery. *J Mater Chem* 15:2648–2656
14. McQuade DT, Kim J, Swager TM (2000) Two-dimensional conjugated polymer assemblies: interchain spacing for control of photophysics. *J Am Chem Soc* 122:5885–5886
15. Zahn S, Swager TM (2002) Three-dimensional electronic delocalization in chiral conjugated polymers. *Angew Chem Int Ed* 41:4225–4230
16. Lee JK, Lee TS (2005) Newly synthesized polybenzoxazole derivative with an adjacent hydroxyphenyl ring for optical sensing. *J Polym Sci A Polym Chem* 43:1397–1403
17. Yang NC, Chang S, Suh DH (2003) Synthesis and optically acid-sensory properties of novel polyoxadiazole derivatives. *Polymer* 44:2143–2148

18. Yang NC, Jeong JK, Suh DH (2003) A new conjugated polymer chemosensor functionalised with 2, 6-bis(1, 3, 4-oxadiazole-2-yl)pyridine for metal ion recognition. *Chem Lett* 32:40–41
19. Kim TH, Kim HJ, Kwak CG, Park WH, Lee TS (2006) Aromatic oxadiazole-based conjugated polymers with excited-state intramolecular proton transfer: their synthesis and sensing ability for explosive nitroaromatic compounds. *J Polym Sci A Polym Chem* 44:2059–2068
20. Zhou G, Cheng Y, Wang L, Jing X, Wang F (2005) Novel polyphenylenes containing phenol-substituted oxadiazole moieties as fluorescent chemosensors for fluoride ion. *Macromolecules* 38:2148–2153
21. Bangcuyo CG, Rampey-Vaughn ME, Quan LT, Angel SM, Smith MD, Bunz UHF (2002) Quinoline-containing, conjugated poly(aryleneethynylene)s: novel metal and H⁺ responsive materials. *Macromolecules* 35:1563–1568
22. Bangcuyo CG, Ellsworth JM, Evans U, Myrick ML, Bunz UHF (2003) Quinoxaline-based poly(aryleneethynylene)s. *Macromolecules* 36:546–548
23. Wu T-Y, Chen Y (2004) Poly(phenylene vinylene)-based copolymers containing 3,7-phenothiazylene and 2, 6-pyridylene chromophores: fluorescence sensors for acids, metal ions, and oxidation. *J Polym Sci A Polym Chem* 42:1272–1284
24. Okada S, Peng S, Spevak W, Charych DH (1998) Color and chromism of polydiacetylene vesicles. *Acc Chem Res* 31:229–239
25. Reppy MA, Sporn SA, Saller CF (2000) Method for detecting an analyte by fluorescence US Patent 6,984,528
26. Reppy MA (2002) Signal generation from switchable polydiacetylene fluorescence. *Mater Res Soc Symp Proc* 723:O5_9_1–O5_9_6
27. Yoon B, Lee S, Kim J-M (2009) Recent conceptual and technological advances in polydiacetylene-based supramolecular chemosensors. *Chem Soc Rev* 38:1958–1968
28. Saxena A, Fujiki M, Rai R, Kim S-Y, Kwa G (2004) Highly sensitive and selective fluoride ion chemosensing, fluoroalkylated polysilane. *Macromol Rapid Commun* 25:1771–1775
29. Toal SJ, Magde D, Trogler WC (2005) Luminescent oligo(tetraphenyl)silole nanoparticles as chemical sensors for aqueous TNT. *Chem Commun* 43:5465–5467
30. Sohn H, Sailor MJ, Magde D, Trogler WC (2003) Detection of nitroaromatic explosives based on photoluminescent polymers containing metalloles. *J Am Chem Soc* 125:3821–3830
31. Brédas J-L, Cornil J, Beljonne D, Santos DAD, Shuai Z (1999) Excited-state electronic structure of conjugated oligomers and polymers: a quantum-chemical approach to optical phenomena. *Acc Chem Res* 32:267–276
32. Brédas J-L, Beljonne D, Coropceanu V, Cornil J (2004) Charge-transfer and energy-transfer processes in π -conjugated oligomers and polymers: a molecular picture. *Chem Rev* 104:4971–5003
33. Gierschner J, Cornil J, Egelhaaf H-J (2007) Optical bandgaps of π -conjugated organic materials at the polymer limit: experiment and theory. *Adv Mater* 19:173–191
34. Yu J, Hu D, Barbara PF (2000) Unmasking electronic energy transfer of conjugated polymers by suppression of O₂ quenching. *Science* 289:1327–1330
35. Huser T, Yan M, Rothberg LJ (2000) Single chain spectroscopy of conformational dependence of conjugated polymer photophysics. *Proc Natl Acad Sci* 97:11187–11191
36. Schwartz BJ (2003) Conjugated polymers as molecular materials: how chain conformation and film morphology influence energy transfer and interchain interactions. *Annu Rev Phys Chem* 54:141–172
37. Lin H, Tabaei SR, Thomsson D, Mirzov O, Larsson P-O, Scheblykin IG (2008) Fluorescence blinking, exciton dynamics, and energy transfer domains in single conjugated polymer chains. *J Am Chem Soc* 130:7042–7051
38. Nguyen T-Q, Wu J, Doan V, Schwartz BJ, Tolbert SH (2000) Control of energy transfer in oriented conjugated polymer-mesoporous silica composites. *Science* 288:652–656
39. Sakurai M, Tamagawa H, Inoue Y, Ariga K, Kunitake T (1997) Theoretical study of intermolecular interaction at the lipid–water interface. 1. Quantum chemical analysis using a reaction field theory. *J Phys Chem B* 101:4810–4816

40. Sakurai M, Tamagawa H, Inoue Y, Ariga K, Kunitake T (1997) Theoretical study of intermolecular interaction at the lipid–water interface. 2. Analysis – based on the Poisson–Boltzmann equation. *J Phys Chem B* 101:4817–4825
41. Onda M, Yoshihara K, Koyano H, Ariga K, Kunitake T (1996) Molecular recognition of nucleotides by the guanidinium unit at the surface of aqueous micelles and bilayers. A comparison of microscopic and macroscopic interfaces. *J Am Chem Soc* 118:8524–8530
42. Sakurai M, Tamagawa H, Furuki T, Inoue Y, Ariga K, Kunitake T (1995) A theoretical interpretation of remarkable enhancement of intermolecular binding at the lipid–water interface. *Chem Lett* 11:1001–1002
43. Yang X, Zhao X, Zuo X, Wang K, Wen J, Zhang H (2009) Nucleic acids detection using cationic fluorescent polymer based on one-dimensional microfluidic beads array. *Talanta* 77:1027–1031
44. Rininsland F, Stankewicz C, Weatherford W, McBranch D (2005) High-throughput kinase assays with protein substrates using fluorescent polymer superquenching. *BMC Biotechnol* 5:16
45. Bajaj A, Miranda OR, Kim I-B, Phillips RL, Jerry DJ, Bunz UHF, Rotello VM (2009) Detection and differentiation of normal, cancerous, and metastatic cells using nanoparticle–polymer sensor arrays. *Proc Natl Acad Sci* 106:10912–10916
46. Guan H, Zhou P, Zhu X, He Z (2008) Sensitive and selective detection of aspartic acid and glutamic acid based on polythiophene–gold nanoparticles composite. *Talanta* 77:319–324
47. Pindzola BA, Nguyen AT, Reppy MA (2006) Antibody-functionalized polydiacetylene coatings on nanoporous membranes for microorganism detection. *Chem Commun* 8:906–908
48. Dai J, Baker GL, Bruening ML (2006) Use of porous membranes modified with polyelectrolyte multilayers as substrates for protein arrays with low nonspecific binding. *Anal Chem* 78:135–140
49. Wang X, Kim Y-G, Drew C, Ku B-C, Kumar J, Samuelson LA (2004) Electrostatic assembly of conjugated polymer thin layers on electrospun nanofibrous membranes for biosensors. *Nano Lett* 4:331–334
50. Long Y, Chen H, Yang Y, Wang H, Yang Y, Li N, Li K, Pei J, Liu F (2009) Electrospun nanofibrous film doped with a conjugated polymer for DNT fluorescence sensor. *Macromolecules* 42:6501–6509
51. Wang S, Granick S, Zhao J (2008) Charge on a weak polyelectrolyte. *J Chem Phys* 129:1–4
52. Chen L, Xu S, McBranch D, Whitten D (2000) Tuning the properties of conjugated polyelectrolytes through surfactant complexation. *J Am Chem Soc* 122:9302–9303
53. Lavigne JJ, Broughton DL, Wilson JN, Erdogan B, Bunz UHF (2003) “Surfactochromic” conjugated polymers: surfactant effects on sugar-substituted PPEs. *Macromolecules* 36:7409–7412
54. Wang D, Gong X, Heeger PS, Rininsland F, Bazan GC, Heeger AJ (2002) Biosensors from conjugated polyelectrolyte complexes. *Proc Natl Acad Sci* 99:49–53
55. Kim J-M, Lee YB, Yang DH, Lee J-S, Lee GS, Ahn DJ (2005) A polydiacetylene-based fluorescent sensor chip. *J Am Chem Soc* 127:17580–17581
56. Shim H-Y, Lee SH, Ahn DJ, Ahn K-D, Kim J-M (2004) Micropatterning of diacetylenic liposomes on glass surfaces. *Mater Sci Eng C* 24:157–161
57. Reppy MA, Pindzola BA (2006) Polydiacetylene liposomes attached to glass fibers for bioassays. *Mater Res Soc Symp Proc* 942(0942):W13-10
58. Reppy MA, Pindzola BA, Sharma B, Zecher M (2007) Supported polydiacetylene 3-D arrays for fluorescent or phosphorescent detection US Patent Application 20,070,248,950
59. Reppy MA, Pindzola BA (2009) Solid supported polydiacetylene materials for detection of biological targets, Ch. 13. In: Nagarajan R, Zukas W, Hatton, TA, Lee S (ed) *Nanoscience and nanotechnology for chemical and biological defense*, ACS symposium series, vol 1016, American Chemical Society, Washington DC

60. Reppy MA, Pindzola BA, Hussey SL (2008) Preparation of polydiacetylene coatings. US Patent Application 20,080,171,191
61. Reppy MA, Saller CF (2003) Method for evaluating drug candidates. US Patent 20,040,023,303
62. Kolusheva S, Wachtel E, Jelinek R (2003) Biomimetic lipid/polymer colorimetric membranes: molecular and cooperative properties. *J Lipid Res* 44:65–71
63. Lakowicz JR (2006) Mechanisms and dynamics of fluorescence quenching, Chapter 9. In: *Principles of fluorescence spectroscopy*, 3rd edn. Springer, New York
64. Lakowicz JR (2006) Quenching of fluorescence, Chapter 8. In: *Principles of fluorescence spectroscopy*, 3rd edn. Springer, New York
65. Rose A, Lugmair CG, Swager TM (2001) Excited-state lifetime modulation in triphenylene-based conjugated polymers. *J Am Chem Soc* 123:11298–11299
66. Zhou Q, Swager TM (1995) Fluorescent chemosensors based on energy migration in conjugated polymers: the molecular wire approach to increased sensitivity. *J Am Chem Soc* 117:12593–12602
67. Moon JH, Deans R, Kruegar E, Hancock LF (2003) Capture and detection of a quencher labeled oligonucleotide by poly(phenylene ethylene) particles. *Chem Commun* 1:104–105
68. Yang J-S, Swager TM (1998) Fluorescent porous polymer films as TNT chemosensors: electronic and structural effects. *J Am Chem Soc* 120:11864–11873
69. Yang J-S, Swager TM (1998) Porous shape persistent fluorescent polymer films: an approach to TNT sensory materials. *J Am Chem Soc* 120:5321–5322
70. Rose A, Zhu Z, Madigan CF, Swager TM, Bulović V (2005) Sensitivity gains in chemosensing by lasing action in organic polymers. *Nature* 434:876–879
71. Xu Q, An L, Wang S (2008) Design and synthesis of a new conjugated polyelectrolyte as a reversible pH sensor. *Macromol Rapid Commun* 29:390–395
72. Xue C, Cai F, Liu H (2008) Ultrasensitive fluorescent responses of water-soluble, zwitterionic, boronic acid-bearing, regioregular head-to-tail polythiophene to biological species. *Chem Eur J* 14:1648–1653
73. Murphy CB, Zhang Y, Troxler T, Ferry V, Martin JJ, Jones WE Jr (2004) Probing Förster and Dexter energy-transfer mechanisms in fluorescent conjugated polymer chemosensors. *J Phys Chem B* 108:1537–1543
74. Kim J, McQuade DT, McHugh SK, Swager TM (2000) Ion-specific aggregation in conjugated polymers: highly sensitive and selective fluorescent ion chemosensors. *Angew Chem Int Ed* 39:3868–3872
75. Kim T-H, Swager TM (2003) A fluorescent self-amplifying wavelength-responsive sensory polymer for fluoride ions. *Angew Chem Int Ed* 42:4803–4806
76. Qu Y, Hua J, Yiang Y, Tian H (2009) Novel side-chain naphthalimide polyphenylacetylene as a ratiometric fluorescent chemosensor for fluoride ion. *J Polym Sci A Polym Chem* 47:1544–1552
77. Wang B, Wasielewski MR (1997) Design and synthesis of metal ion-recognition-induced conjugated polymers: an approach to metal ion sensory materials. *J Am Chem Soc* 119:12–21
78. Liu X, Zhou X, Shu X, Zhu J (2009) A polymer-based ultrasensitive metal ion sensor. *Macromolecules* 42:7634–7637
79. Zhang Y, Murphy CB, Jones WE Jr (2002) Poly[p-(phenyleneethynylene)-alt-(thienyleneethynylene)] polymers with oligopyridine pendant groups: highly sensitive chemosensors for transition metal ions. *Macromolecules* 35:630–636
80. Liu B, Yu W-L, Pei J, Liu S-Y, Lai Y-H, Huang W (2001) Design and synthesis of bipyridyl-containing conjugated polymers: effects of polymer rigidity on metal ion sensing. *Macromolecules* 34:7932–7940
81. Béra-Abérem M, Ho H-A, Leclerc M (2004) Functional polythiophenes as optical chemo- and biosensors. *Tetrahedron* 60:11169–11173

82. Kushon SA, Ley KD, Bradford K, Jones RM, McBranch D, Whitten D (2002) Detection of DNA hybridization via fluorescent polymer superquenching. *Langmuir* 18:7245–7249
83. Kushon SA, Bradford K, Marin V, Suhrada C, Armitage BA, McBranch D, Whitten D (2003) Detection of single nucleotide mismatches via fluorescent polymer superquenching. *Langmuir* 19:6456–6464
84. Ho HA, Doré K, Boissinot M, Bergeron MG, Tanguay RM, Boudreau D, Leclerc M (2005) Direct molecular detection of nucleic acids by fluorescence signal amplification. *J Am Chem Soc* 127:12673–12676
85. Doré K, Dubus S, Ho H-A, Lévesque I, Brunette M, Corbeil G, Boissinot M, Boivin G, Bergeron MG, Boudreau D, Leclerc M (2004) Fluorescent polymeric transducer for the rapid, simple, and specific detection of nucleic acids at the zeptomole level. *J Am Chem Soc* 126:4240–4244
86. Pinto MR, Schanze KS (2004) Amplified fluorescence sensing of protease activity with conjugated polyelectrolytes. *Proc Natl Acad Sci* 101:7505–7519
87. Kumaraswamy S, Bergstedt T, Sh X, Rininsland F, Kushon S, Xia W, Ley K, Achyuthan K, McBranch D, Whitten D (2004) Fluorescent-conjugated polymer superquenching facilitates highly sensitive detection of proteases. *Proc Natl Acad Sci* 101:7511–7515
88. Rininsland F, Xia W, Wittenburg S, Shi X, Stankewicz C, Achyuthan K, McBranch D, Whitten D (2004) Metal ion-mediated polymer superquenching for highly sensitive detection of kinase and phosphatase activities. *Proc Natl Acad Sci* 101:15295–15300
89. Fan C, Plaxco KW, Heeger AJ (2002) High-efficiency fluorescence quenching of conjugated polymers by proteins. *J Am Chem Soc* 124:5642–5643
90. Kim I-B, Dunkhorst A, Bunz UHF (2005) Nonspecific interactions of a carboxylated-substituted PPE with proteins. A cautionary tale for biosensor applications. *Langmuir* 21:7985–7989
91. Phillips RL, Kim I-B, Carson BE, Tidbeck B, Bai Y, Lowary TL, Tolbert LM, Bunz UHF (2008) Sugar-substituted poly(p-phenyleneethynylene)s: sensitivity enhancement toward lectins and bacteria. *Macromolecules* 41:7316–7320
92. Kim I-B, Phillips R, Bunz UHF (2007) Forced agglutination as a tool to improve the sensory response of a carboxylated poly(p-phenyleneethynylene). *Macromolecules* 40:814–817
93. Fan L-J, Jones WE Jr (2006) Studies of photoinduced electron transfer and energy migration in a conjugated polymer system for fluorescence “turn-on” chemosensor applications. *J Phys Chem B* 110:7777–7782
94. Dwight SJ, Gaylord BS, Hong JW, Bazan GC (2004) Perturbation of fluorescence by nonspecific interactions between anionic poly(phenylenevinylene)s and proteins: implications for biosensors. *J Am Chem Soc* 126:16850–16859
95. Whitten D, Jones R, Bergstedt T, McBranch D, Chen L, Heeger P (2001) From superquenching to biodetection: building sensors based on fluorescent polyelectrolytes. In: Ramamurthy V, Schanze KS (eds) *Optical sensors and switches*. Marcel Dekker Inc, New York
96. DiCesare N, Pinto MR, Schanze KS, Lakowicz JR (2002) Saccharide detection based on the amplified fluorescence quenching of a water-soluble poly(phenylene ethynylene) by a boronic acid functionalized benzyl viologen derivative. *Langmuir* 18:7785–7787
97. Thomas SW, Swager TM (2006) Trace hydrazine detection with fluorescent conjugated polymers: a turn-on sensory mechanism. *Adv Mater* 18:1047–1050
98. Smith RC, Tennyson AG, Lim MH, Lippard SJ (2005) Conjugated polymer-based fluorescence turn-on sensor for nitric oxide. *Org Lett* 7:3573–3575
99. Pinto MR, Kristal BM, Schanze KS (2003) A water-soluble poly(phenylene ethynylene) with pendant phosphonate groups. Synthesis, photophysics, and layer-by-layer self-assembled films. *Langmuir* 19:6523–6533
100. Gu Z, Bao Y-J, Zhang Y, Wang M, Shen Q-D (2006) Anionic water-soluble poly(phenylenevinylene) alternating copolymer: high-efficiency photoluminescence and dual electrochromism. *Macromolecules* 39:3125–3131

101. Montañó GA, Dattelbaum AM, Wang H-L, Shreve AP (2004) Enhanced photoluminescence from poly(phenylene vinylene): dendrimer polyelectrolyte assemblies in solution. *Chem Commun* 2490–2491
102. Ho H-A, Boissinot M, Bergeron MG, Corbeil G, Doré K, Boudreau D, Leclerc M (2002) Colorimetric and fluorometric detection of nucleic acids using cationic polythiophene derivatives. *Angew Chem Int Ed* 41:1548–1551
103. Doré K, Leclerc M, Boudreau D (2006) Investigation of a fluorescence signal amplification mechanism used for the direct molecular detection of nucleic acids. *J Fluoresc* 16:259–265
104. Lévesque I, Leclerc M (1996) Ionochromic and thermochromic phenomena in a regioregular polythiophene derivative bearing oligo(oxyethylene) side chains. *Chem Mater* 8:2843–2849
105. Ho H-A, Leclerc M (2004) Optical sensors based on hybrid aptamer/conjugated polymer complexes. *J Am Chem Soc* 126:1384–1385
106. Raymond FR, Ho H-A, Peytavi R, Bissonnette L, Boissinot M, Picard FJ, Leclerc M, Bergeron MG (2005) Detection of target DNA using fluorescent cationic polymer and peptide nucleic acid probes on solid support. *BMC Biotechnol* 5:10
107. Nilsson KPR, Rydberg J, Baltzer L, Inganäs O (2003) Self-assembly of synthetic peptides control conformation and optical properties of a zwitterionic polythiophene derivative. *Proc Natl Acad Sci* 100:10170–10174
108. Nilsson KPR, Inganäs O (2004) Optical emission of a conjugated polyelectrolyte: calcium-induced conformational changes in calmodulin and calmodulin–calcineurin interactions. *Macromolecules* 37:9109–9113
109. Simon RA Nilsson P (2010) Optical reporting by conjugated polymers via conformational changes. In: Demchenko AP (ed) *Advanced fluorescence reporters in chemistry and biology. II*. Springer Ser Fluoresc 9:389–416
110. Yasuda A, Yoshizawa M, Kobayashi T (1993) Fluorescence spectrum of a blue-phase polydiacetylene obtained by probe saturation spectroscopy. *Chem Phys Lett* 209:281–286
111. Olmstedt JJ, Strand M (1983) Fluorescence of polymerized diacetylene bilayer films. *J Phys Chem* 87:4790–4792
112. Reppy MA (2008) Enhancing the emission of polydiacetylene sensing materials through fluorophore addition and energy transfer. *J Fluoresc* 18:461–471
113. Pu K-Y, Liu B Fluorescence reporting based on FRET between conjugated polyelectrolyte and organic dye for biosensor applications. In: Demchenko AP (ed) *Advanced fluorescence reporters in chemistry and biology. II*. Springer Ser Fluoresc 9:417–453
114. Schlindler F, Lupton JM, Feldmann J, Scherf U (2004) A universal picture of chromophores in π -conjugated polymers derived from single-molecule spectroscopy. *Proc Natl Acad Sci* 101:14695–147000
115. Wong KF, Bagchi B, Rossky PJ (2004) Distance and orientation dependence of excitation transfer rates in conjugated systems: beyond the Förster theory. *J Phys Chem A* 108:5752–5763
116. Zheng J, Swager TM (2004) Biotinylated poly(p-phenylene ethynylene): unexpected energy transfer results in the detection of biological analytes. *Chem Commun* 2798–2799
117. Ma G, Muller AM, Bardeen CJ, Cheng Q (2006) Self-assembly combined with photopolymerization for the fabrication of fluorescence “turn-on” vesicle sensors with reversible “on-off” switching properties. *Adv Mater* 18:55–60
118. Ma G, Cheng Q (2006) Manipulating fret with polymeric vesicles: development of a “mix-and-detect” type fluorescence sensor for bacterial toxin. *Langmuir* 22:6743–6745

Optical Reporting by Conjugated Polymers via Conformational Changes

Rozalyn A. Simon and K. Peter R. Nilsson

Abstract Conjugated polymers have many unique photophysical properties that make them useful for a variety of applications within the fields of chemistry, molecular biology, and medicine, specifically their ability to produce a conformation-dependent spectral signature reflective of changes in their local environment. This physical property makes conjugated polymers an indispensable tool in the toolbox of fluorescent reporters, and within this chapter, their utilization as molecular probes for studying protein structure and conformation is emphasized.

Keywords Biochromism · Conjugated polymers (CPs) · Optical properties

Contents

1	Introduction	390
1.1	Conjugation and Conformation-Dependent Optical Properties	390
2	Chromism	392
2.1	Thermochromism and Solvatochromism	392
2.2	pH Induced Chromic Transitions	393
3	Covalent Ligand Sensors	394
3.1	Ion Sensors	396
3.2	Biosensors	397
4	Noncovalent Ligand Sensors	399
4.1	Nucleic Acid Detection	400
4.2	Protein Detection	402
5	Direct Detection: CPs as Probes	404
5.1	Conformational Changes of Synthetic Peptides	404
5.2	Protein Aggregates	406
5.3	Novel Molecular Scaffolds for In Vivo Imaging	412
6	Concluding Remarks	414
	References	414

R.A. Simon and K.P.R. Nilsson (✉)

Department of Physics, Chemistry and Biology, Linköpings Universitet, SE-581 83 Linköping, Sweden

e-mail: petni@ifm.liu.es

1 Introduction

The art of detection is the heart of developing technologies within all scientific fields. What can be “seen” serves as an indicator or parameter to measure variable or invariable behavior. Within the fields of chemistry, biology, and medicine, the detection of small molecules, specific proteins, and biological events are of central importance. This has mainly been accomplished through means such as the use of fluorophore-labeled antibodies specific for distinct biomolecules. Such molecules integrate a sensing element (antibody) with a transducer (fluorophore), the component responsible for reporting a change in status of the sensing element and thus allowing for direct quantification of a distinct bimolecular target.

Conjugated polymers (CPs) represent a useful and interesting class of materials well known for their abilities as transducers in the form of colorimetric and fluorometric reporting. The CP can serve as a transducer covalently or noncovalently associated with the biological component or in some instances the CP itself can act to detect and transduce the signal. CPs provide various means of probing via a change in their conductivity, potential, color, or fluorescence. Because fluorescence measurements provide a number of parameters for observing a change in the system – e.g., changes in intensity, wavelength, energy transfer, and emission lifetime – the coupling of such measurements with the unique fluorescence reporting capabilities of CPs has been successful in a number of systems and continues to develop as a means for “seeing” the unseen. In this chapter, we will attempt to provide an intuitive and intentionally simplistic description of CPs and their unique conformation-dependent optical properties. A brief review of their use in fluorescence detection of small molecules and a diversity of biological processes will then follow.

1.1 Conjugation and Conformation-Dependent Optical Properties

CPs are in many ways similar to conventional plastics but because of their unique electronic configuration, they exhibit additional properties that make them useful in a variety of applications ranging from organic electronics to biosensors. In nonconjugated “conventional” organic polymers, the carbon chain consists of sp^3 hybridized carbon atoms with single σ bonds (Fig. 1a). Conjugated “conducting” polymers consist of alternating single and double bonds and are thus characterized by sp^2 hybridized carbon atoms with overlapping π orbitals (Fig. 1b). These overlapping π orbitals allow for delocalization of electrons along the backbone of the polymer chain (Fig. 1c), similar to the free motion of electrons within a metal.

The movement of these electrons along the backbone of the polymer can be facilitated or hindered depending on the ease with which the electron can migrate from orbital to orbital. When the p_z orbitals are aligned or “in-plane” and directly overlapping (Fig. 2, top), electron movement is facilitated. However, when the

Fig. 1 (a) Nonconjugated hydrocarbon polymer. (b) Conjugated polymer with alternating double and single bonds. (c) Conjugated polymer showing continuous conjugation along the polymer backbone

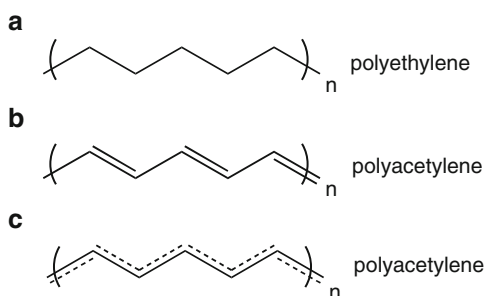
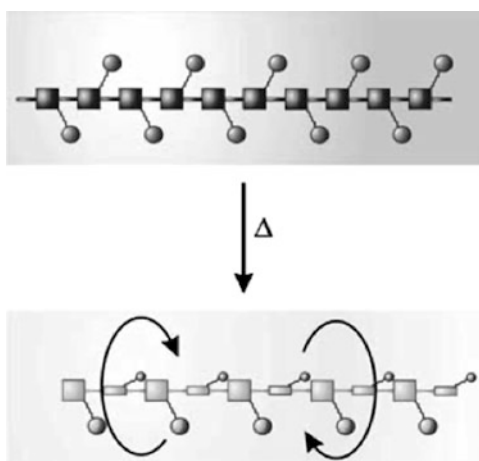


Fig. 2 (top) Planar regioregular polymer with directly overlapping pi orbitals vs. twisted backbone with π orbitals out-of-plane [1]



backbone of the molecule is twisted, i.e., the p_z orbitals are out-of-plane with one another, the electrons become confined, or localized to smaller segments of the material. These segments or stretches of polymer where the p_z orbitals are in-plane with one another can be referred to as conjugation lengths. Hence, planarization of the polymer backbone will give rise to an increase in effective conjugation length, whereas a twisting of the backbone will lead to a decrease in the effective conjugation length. This planar to twisted transition can be observed as a blue-shift of the absorption spectrum of the CP toward shorter wavelengths (Fig. 2, bottom). The extent to which a polymer's π orbitals are in conjugation is therefore dependant upon the torsion angle of the backbone, and when a polymer is optically excited, the restriction of the backbone torsion angles can have an impact upon the polymer's available optical modes and relaxation lifetimes, resulting in chromic transitions and changes in emission wavelengths. Another interesting characteristic of CPs is a tendency to aggregate or stack under planar or unfavorable solvent conditions. Aggregation can cause quenching or a decrease in fluorescence intensity, and can thus serve as an additionally useful parameter in fluorescence reporting.

2 Chromism

The appearance of color is the result of a material's reflection of electromagnetic radiation between the wavelengths of 380 and 740 nm. The perceived color of an object is due to the nature of the configuration and energy transitions of electrons within that material. Generally, materials that appear to be colored have weakly bound or delocalized electrons. In these systems, the energy difference between the lowest unoccupied molecular orbital (LUMO) and the highest occupied molecular orbital (HOMO) correspond to energetic transitions within the visible region of the spectra. Not surprisingly, a majority of dyes and brightly colored materials contain conjugated systems with loosely bound, freely moving electrons having energy transitions within the visible light spectrum. In the case of CPs, many chromic transitions can be induced by such changes as temperature, solvent, concentration of ions, or biomolecules. These phenomena have been termed thermochromism, solvatochromism, ionochromism, and biochromism, respectively. The underlying reason for most of these chromic transitions can be correlated with changes in the geometry of the polymers backbone and effective conjugation lengths. The following sections will give examples of how these changes in polymer geometry can be induced by a variety of means. We will first exemplify how conformation-dependent optical properties are affected by temperature or solvent; we will then continue with sensors based on CPs utilizing these optical properties for detection of ions and biomolecules.

2.1 *Thermochromism and Solvatochromism*

Owing to their delocalization of electrons, CPs often have interesting chromic properties, which can be manipulated through the use of charge, ion concentration, solvent, and temperature, to name only a few. Any of these changes in conditions can influence the conformation of the polymer's backbone and therefore the conjugation length, allowed electron energy transitions, and finally, color.

Such color transitions were illustrated by Leclerc and coworkers via temperature changes in the case of a substituted polythiophene (Fig. 3).

Through a combination of X-ray crystallography and solid-state NMR studies, they were able to correlate chromic transitions with motion, and an increase in disorder within the backbone of the polymer [1]. As the temperature increased, so did disorder within the polymer, resulting in a blue-shift of the UV-vis spectra (Fig. 4).

As the conjugation lengths within a polymer are shortened by the twisting of the backbone, the available states for relaxation are reduced causing the energy of the electrons within that segment to increase and therefore the UV-vis and fluorescent signals shift to a higher energy and shorter wavelength.

Another example of correlating conformation with spectral changes was conducted by Rothberg and coworkers. They studied thin films of poly[2-methoxy,

Fig. 3 Regioregular poly [3-(2-methyl-1-butoxy)-4-methylthiophene] (PMBMT) synthesized via oxidative electropolymerization

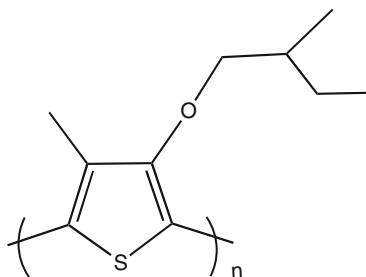
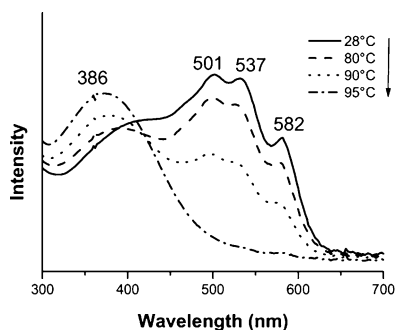


Fig. 4 Temperature dependant UV-vis absorption spectra of a PMBMT thin film [1]



5-(2'-ethylehexyloxy)-*p*-phenylene-vinylene] (MEH-PPV) spun from solution in either toluene or chloroform [2]. The polar MEH-PPV polymer in nonpolar toluene tends to stack as a coil to reduce solvent interactions whereas in chloroform it takes on a more extended chain formation. They demonstrated that the films cast from toluene exhibited intermittent fluorescence with rapid intervals of abruptly changing intensity. This behavior was attributable to defects quenching excitations along the chain (e.g., π -stacking between adjacent coils). π -stacking and intra-chain emissions could account for the lower fluorescence yields and the red-spectral shift when compared with the films cast from chloroform. Various studies conducted on the topic of conformation and chromic transitions agree upon the notion that conformational changes within the polymer backbone result in the alteration of the optical properties of CPs [2–8]. These chromic changes have been used to create sensing systems based on the conformation of the polymer and its associated optical changes.

2.2 pH Induced Chromic Transitions

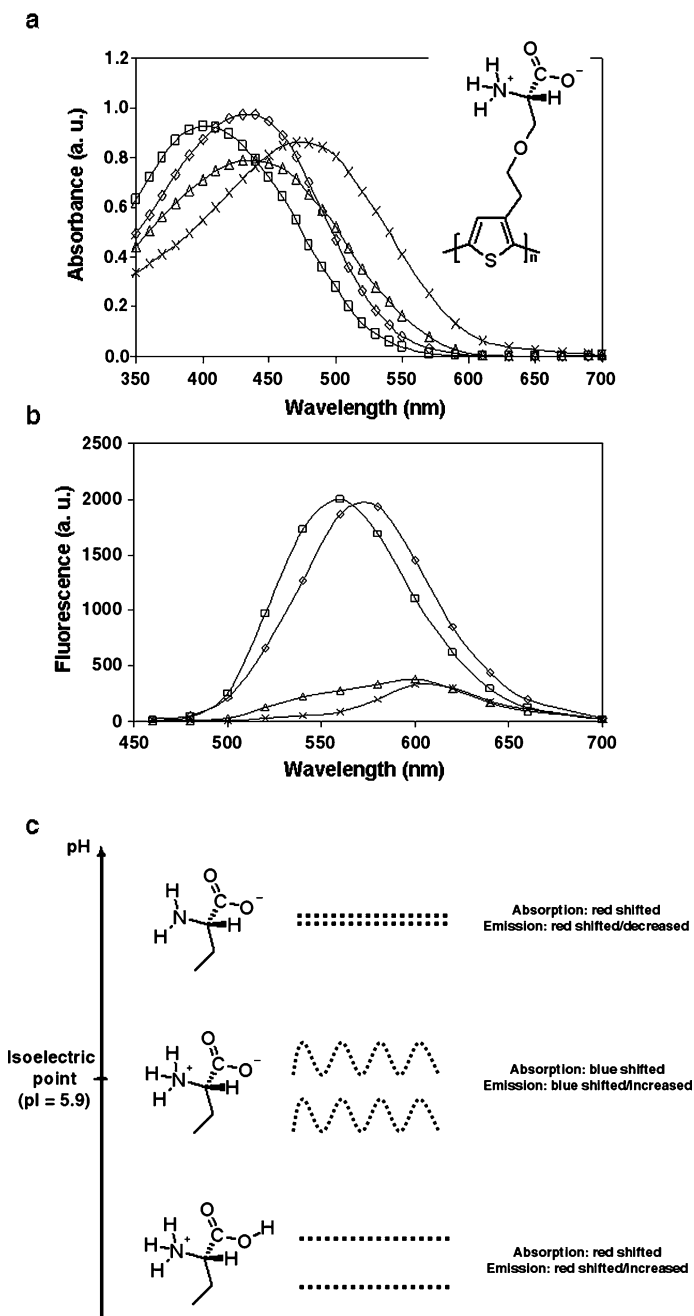
Optical transitions of CPs can also be induced by switching the net charge of the polymer side chain. By using a zwitter-ionic polythiophene derivative, POWT, Nilsson and co-workers were able to induce different chromic transitions by

changing the pH of the polymer solution [9]. The absorption spectra of POWT in different buffer systems are shown in Fig. 5a. At pH 5, where most of the side chains are zwitter-ionic (both negatively and positively charged), the polymer backbone is in a nonplanar helical conformation, associated with a blue-shifted absorption spectrum. When the pH is increased or decreased, the backbone of the CP adopts a more planar conformation, seen as a red shift of the absorption maximum. A closer look at the spectra for POWT in pH 2 and pH 8 buffer solutions (Fig. 5a) reveals an interesting observation. The absorption maximum is similar but the spectrum recorded for POWT in the pH 8 buffer solution has a shoulder in the region at 570 nm, indicating that an aggregation of polymer chains (stacking of the thiophene rings) takes place at alkaline pH but not at acidic pH.

The emission of POWT is also dependent on the geometry of the polymer backbone, especially the separation or aggregation of polymer chains. Studies of thin films of POWT have shown that the intensity of the fluorescence for the aggregated phase of POWT is weaker by approximately one order of magnitude compared with the fluorescence for the single chain state [10, 11]. As the polymer chains were separated, the photoluminescence maximum was also blue-shifted by approximately 105 nm, compared to the dense packing of the polymer chains. Similar changes also occur when placing POWT in different buffer solutions [9]. At pH 5, when the polymer side chains largely have a neutral net charge, the polymer chains adopt a nonplanar conformation and the chains are separated, seen as a blue-shifted emission maximum and an increase in the intensity of the emitted light. In more alkaline pH (pH 8), the POWT emits light with a longer wavelength and with decreased intensity, related to a more planar backbone and aggregation of polymer chains. At acidic pH, light with a slightly longer wavelength is emitted, but the intensity of the fluorescence is not decreasing in the same way as observed for POWT in alkaline buffer solution. Consequently, an acidic pH seems to favor a more rod shape conformation of the polymer chains, but aggregation of the polyelectrolyte chains is presumed to be absent. A schematic drawing of the polymer chain conformations for POWT in different buffer solutions and the conformation-induced optical transitions relating to these geometrical changes are shown in Fig. 5c.

3 Covalent Ligand Sensors

The first generation of chromic sensors based on CPs was generally utilizing ligand-functionalized CPs. Hence, the receptor (sensing element) was covalently attached to the CP backbone (the transducer) and this receptor-functionalized CP undergoes a colorimetric transition (coil-to-rod transition of the conjugated backbone) upon interaction with a receptor molecule of interest. The specificity in this first generation of CP-based biosensors is due to the covalent integration of distinct ligands on the side chains of the CPs, and this technique has been employed mainly for the detection of specific ions and a wide range of biological targets.

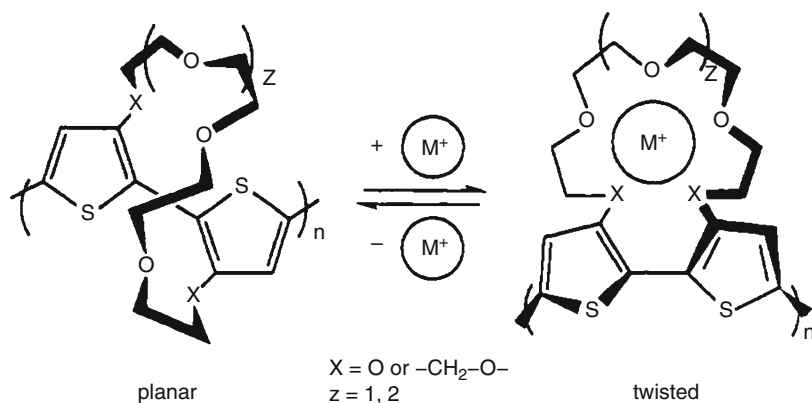


3.1 Ion Sensors

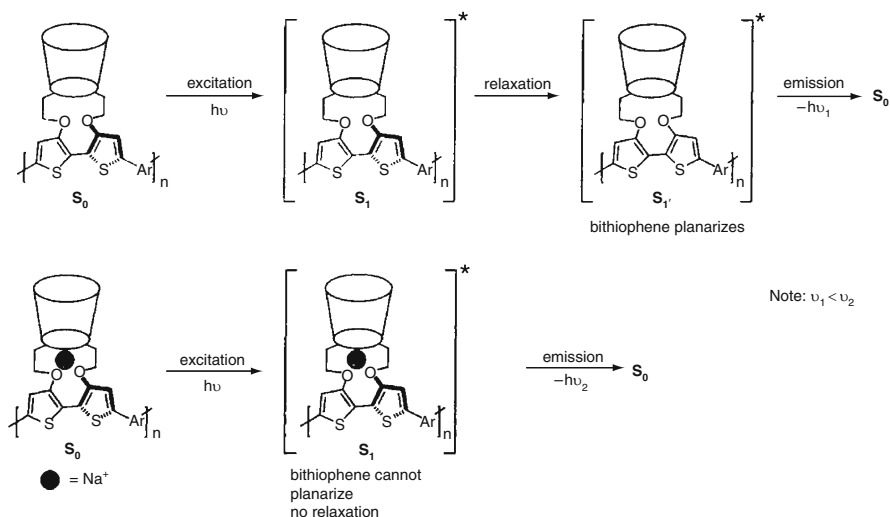
One of the early examples exploiting this chromic transition for sensing was the development of a metal ion sensor by Marsella and Swager [12].

The sensor covalently joined a bithiophene unit with a crown ether macrocycle as the monomeric unit for polymerization (Scheme 1). The spatial distribution of oxygen coordination sites around a metal ion causes planarization of the backbone in the bithiophene, eliciting a red-shift upon metal coordination. They expanded upon this bithiophene structure by replacing the crown ether macrocycle with a calixarene-based ion receptor, and worked with both a monomeric model and a polymeric version to compare ion-binding specificity and behavior [13]. The monomer exhibited less specificity for Na^+ than the polymer. However, with the gradual addition of Na^+ , the monomer underwent a steady blue shift in fluorescence emission whereas the polymer appeared to reach a critical concentration where the spectra rapidly transitioned to a shorter wavelength. Scheme 2 illustrates the proposed explanation for blue shift with increasing ion concentration.

The first scheme shows a normal process of excitation (in the absence of Na^+), reorganization, and planarization because of excitation and subsequent emission and relaxation at a lower energy. The second scheme shows that when the Na^+ ion binds, it locks the bithiophene into position and the reorganization of the backbone becomes restricted resulting in higher energy fluorescence emission. This experiment is a simple and clear example of how the restriction of torsional freedom within a CP's backbone can affect fluorescence emission and thus provide a probing mechanism for binding events.

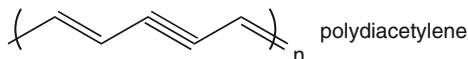


Scheme 1 Bithiophene crown ether in planar conformation with π orbital overlapping in the absence of bound metal. After the chelation of the metal ion, the bithiophene is forced out plane and the π orbitals no longer have maximal overlapping [12]



Scheme 2 A calixarene-based ion receptor with bithiophene backbone. The *top* scheme shows excitation of the receptor in the absence of coordinated ion with normal planarization and relaxation. The *bottom* scheme shows how ion binding restricts planarization and relaxation resulting in higher energy emission [13]

Fig. 6 Polydiacetylene with alternating double, single, and triple bonds along the polymer backbone

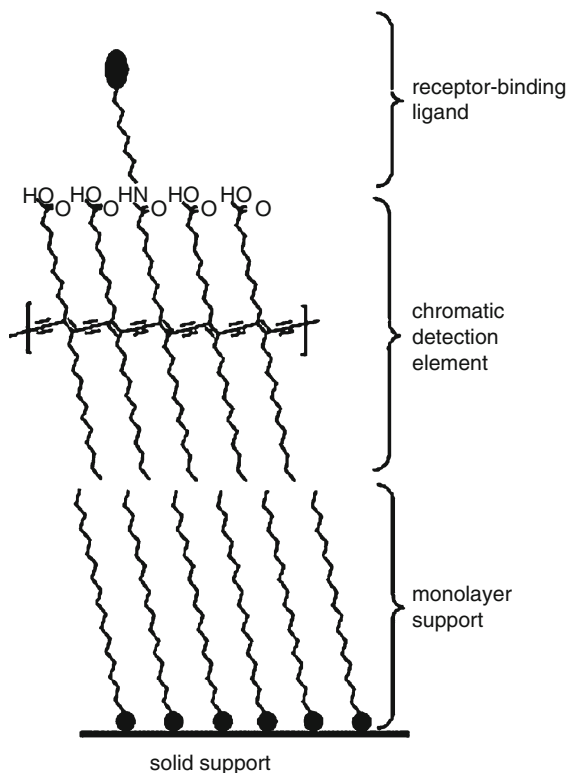


3.2 Biosensors

In addition to simple ions, CPs can be used to detect larger, potentially bio-active materials. An early example of such a system employed the polymer polydiacetylene (PDA) (Fig. 6) for viral detection [14].

A colorimetric detector was generated from a bilayer of octadecyltrichlorosilane (OTS) and polydiacetylene (PDA) with the potential for viral molecular recognition. In a living system, the infectious particles of the influenza virus are encapsulated within a lipid bilayer to which the hemagglutinin (HA) lectin is anchored. When cells come into contact with the virus capsules, the HA lectin binds to α -glycosides of sialic acid on the cell's surface, resulting in endocytosis of the virus and subsequent infection. In the biosensor, lipid chains functionalized with sialic acid, an established carbohydrate for viral influenza recognition, were prepared as Langmuir-Blodgett films, polymerized by UV radiation for PDA cross-linking, and then lifted onto glass slides prepared with a monolayer of self-assembled OTS (Fig. 7).

Fig. 7 PDA–OTS viral detection systems incorporating OTS monolayer with polydiacetylene linked backbone, lipid side chains, and surface ligand for receptor binding [14]



These glass slides, which appear blue upon fabrication, turned red upon interaction or exposure to the influenza virus. As evident in Fig. 7, any change in packing, conformation, or position of the receptor-binding ligand translates into a similar change in the packing of the polydiacetylene side chains. This, in turn, results in a change in polymer backbone configuration and therefore both conjugation length and color. In addition, the resultant color change was directly proportional to the amount of virus present, allowing for possible quantification of viral load.

First, the above-mentioned sensors have major drawbacks, as the detection and recognition event is a function of the nature and characteristics of the side chains, and the side chain functionalization of the CP requires advanced synthesis and extensive purification of numerous monomeric and polymeric derivatives. Second, this generation of sensors primarily employed optical absorption as the source for detection, resulting in lower sensitivity when compared with other sensing systems for biological processes. However, the use of fluorescence detection within these sensing systems could justify continued development. More recent examples include a fluorescent polythiophene derivative with carbohydrate functionalized side chains for the detection of different bacteria [15] and novel synthesis schemes for ligand-functionalization of polythiophenes [16].

4 Noncovalent Ligand Sensors

The sensors discussed so far are based on ligands covalently bound to the polymer backbone. Other methods of detection – often referred to as “mix and detect” methods – work by simple noncovalent incorporation of the polymer with the ligand of interest. Reichert et al. generated liposomes of polydiacetylene with sialic acid for the same purpose of detection as Charych’s surface-bound polymers, but realized that covalent functionalization of the polymer was not necessary [17]. Through simple mixing of the lipid-bound sialic acid with the polymer before sonication and liposome formation, they were able to form a functional colorimetric recognition system (Fig. 8).

The surface glycogen was displayed easily enough for binding to the HA lectin. This interaction sufficiently altered the conformation of the polymer, resulting in an observable color change [17]. Using a similar concept and polydiacetylene as the signal transducing CP, Charych and Okada went on to develop additional strategies for the molecular recognition of *Escherichia coli* enterotoxin, cholera toxin, botulinum neurotoxin, and an assay for phospholipase A₂ inhibitors [7, 18].

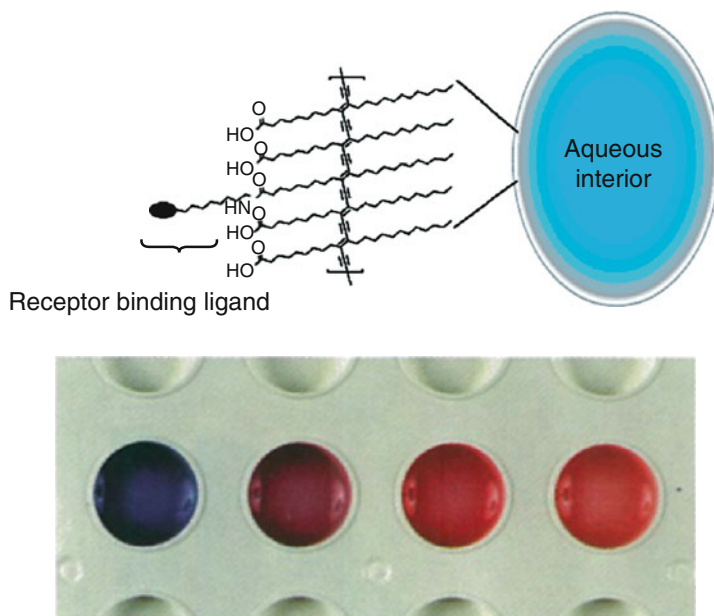


Fig. 8 (top) Liposome with polydiacetylene linked monolayer mixed with ligand for receptor detection. (bottom) Colorimetric detection of influenza virus using polymerized liposomes to which have been added increasing amounts of influenza virus from left to right. [18]

4.1 Nucleic Acid Detection

Although some of the first reports using CPs as molecular probes only took advantage of their colorimetric properties (i.e., the polymer's absorption signature), later studies, spearheaded by Mario Leclerc's group, began using fluorescence (i.e., the polymer's emission signature) for its inherent detection sensitivity. The initial focus was primarily on the use of polythiophene backbones, and in work reported by Ho et al., they synthesized water soluble cationic derivatives of polythiophene for the sequence-specific detection of nucleic acids [19]. Nucleic acid detection is important for the identification of DNA in forensics, infectious agents, and for the determination and detection of genetic mutations. Their polymer-based detection system provided a twofold advantage over other detection schemes: signal amplification by the polymer increased sensitivity, and the ease with which the polymer can be mixed with a sequence-specific probe bypassed the need for covalent tagging of biological molecules.

In their system, the positively charged polymer is dissolved in solution with an anionically charged single strand of DNA forming a "duplex". The duplex then acts to bait the complementary DNA of interest, forming a "triplex". To revisit the conjugation length effects discussed previously, in this experiment the disorganized polymer alone in solution (Fig. 9, left) has a far blue-shifted spectra indicating shorter lengths of conjugation (Fig. 10a). After the polymer associates with the nucleic acid probe strand, forming a "duplex" (Fig. 9), it adopts a more linear conformation and the conjugation is extended resulting in a more red-shifted spectra (Fig. 10b). Finally, upon DNA hybridization with the nucleic acid being detected, the DNA forms a double helix "triplex", which includes the associated polymer (Fig. 9, right). This helical conformation of the polymer causes twisting in

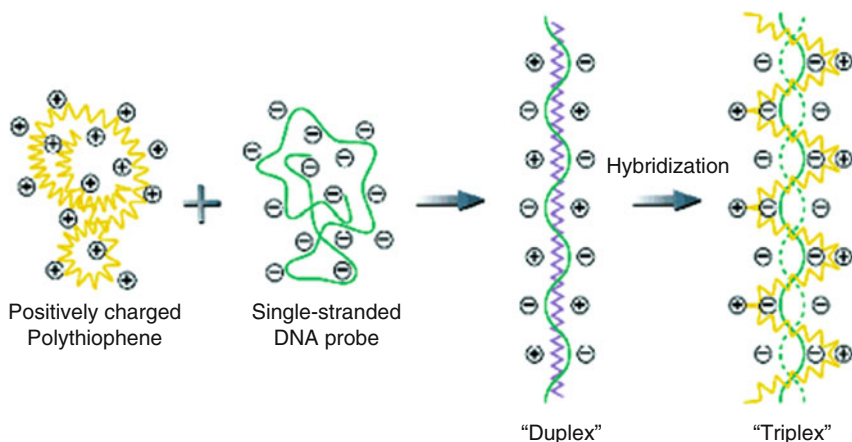


Fig. 9 Illustration of interaction between polymer and DNA single stranded "bait" to form the "duplex" to which the DNA binds to form a double helix "triplex" resulting in colorimetric and fluorometric DNA detection [19]

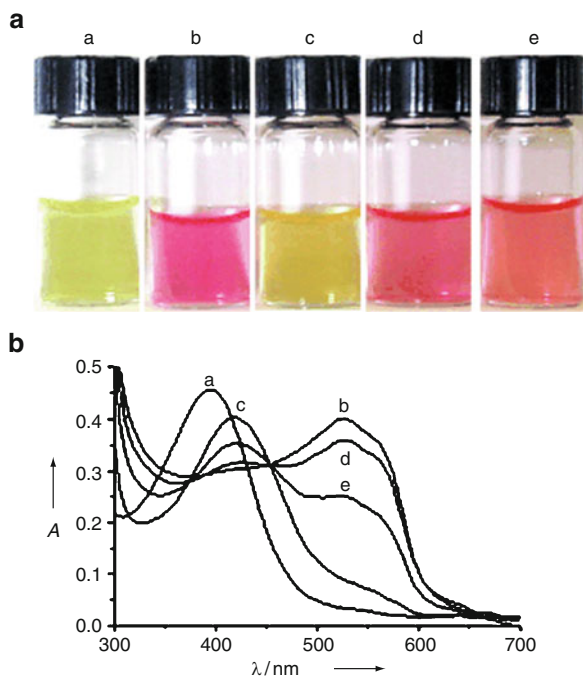


Fig. 10 (a) Photos of colorimetric changes in solutions of (7.9×10^{-5} M, on a monomer unit basis) (b) a) polymer b) polymer/DNA probe c) polymer/DNA probe/complementary DNA sequence d) polymer/DNA probe/1 base mismatched DNA sequence e) polymer/DNA probe/2 base mismatched DNA sequence after 5 min mixing at 55°C in 0.1 M NaCl/ H_2O . B) UV-vis spectra of the above corresponding samples [19]

the backbone, shortening of effective conjugation lengths, resulting in a spectral shift back toward blue (Fig. 10c).

Ho et al. were able to verify the α -helical shape of the polymer by circular dichroism (CD) spectra. No structural elements were observed until the formation of the double helical DNA at which point they observed a right-handed α -helix in the polythiophene backbone. Their work demonstrates the power of fluorometric detection as they noted a seven order of magnitude increase in detection sensitivity (20 fM in 200 μl) simply through the use of fluorometric detection as opposed to UV-vis absorption. The polymer in solution has a high fluorescence yield with a maximum at 530 nm (Fig. 11a). Upon formation of the “duplex” the fluorescence is significantly quenched (Fig. 11b), while with the addition of the complementary DNA and “triplex” formation, the fluorescence intensity is enhanced by a factor of 5 (Fig. 11c). The inherent sensitivity of the spectral shift even allowed distinction between DNA with only one and two mismatched bases (Fig. 10bd, e).

In addition this seminal work, other groups have utilized – and improved upon – such fluorometric polymer-based detection schemes. Using a slightly modified system, Dorè et al. were able to improve the detection sensitivity down to

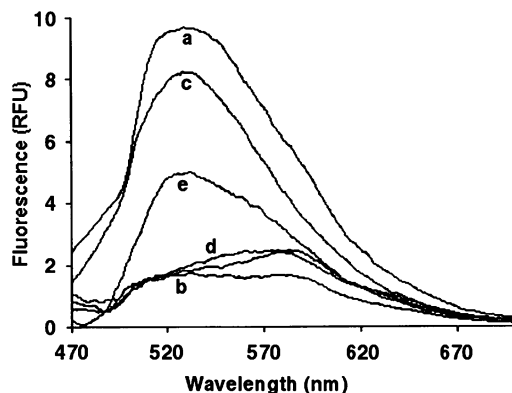


Fig. 11 Fluorescence spectra in solution (200 nM, on a monomer unit basis): a) polymer, b) polymer/DNA probe “duplex”, c) polymer/DNA probe/complementary DNA sequence “triplex”, d) polymer/DNA probe/1 base mismatched DNA sequence “triplex”, and polymer/DNA probe/1 base mismatched DNA sequence “triplex” (100 equivalents mixture), e) polymer/DNA probe/2 base mismatched DNA sequence “triplex” mixture at 55 °C in 10 mM Tris buffer containing 0.1 M NaCl (pH 8) [19]

zeptomolar concentrations [20]. Meanwhile, Raymond et al. modified the detection platform to be used on glass slides and microarrays for the purpose of high-throughput nucleic acid detection [21]. Research conducted in the labs of Inganäs and Bazan have improved solubility and handling as well as detection methods using fluorescence energy resonance transfer (FRET) for nucleic acid detection [22, 23]. The latter will be discussed in details in the following chapter.

4.2 Protein Detection

Ho and Leclerc continued their work on sensing systems by utilizing the established binding capabilities of artificial nucleic acid aptamers [24]. Aptamers are known for their ability to specifically bind to ions, proteins, and other small molecules. In their study, they synthesized two ss-DNA aptamers: X1, 5'-GGTTGGTGTGGTTGG-3', specific for binding to thrombin protein and X2, 5'-GGTGGTGTGGTGGT-3', a known nonbonding sequence. Once more employing a noncovalently-bound combination of probe with polymer transducer, they demonstrated a color change upon interaction with the ligand of interest. The choice of the X1 aptamer enabled binding to both potassium ions and the α -thrombin protein.

Figure 12 shows the difference in absorption spectra of the polymer's colorimetric changes upon interaction with the different ions. Note that the absorption wavelength for the polymer/aptamer complex with potassium is distinct from the other ions, all of which have a similar shift. Fluorescence spectra of the polymer/aptamer transducing complex with the α -thrombin ligand (Fig. 13) indicates a change

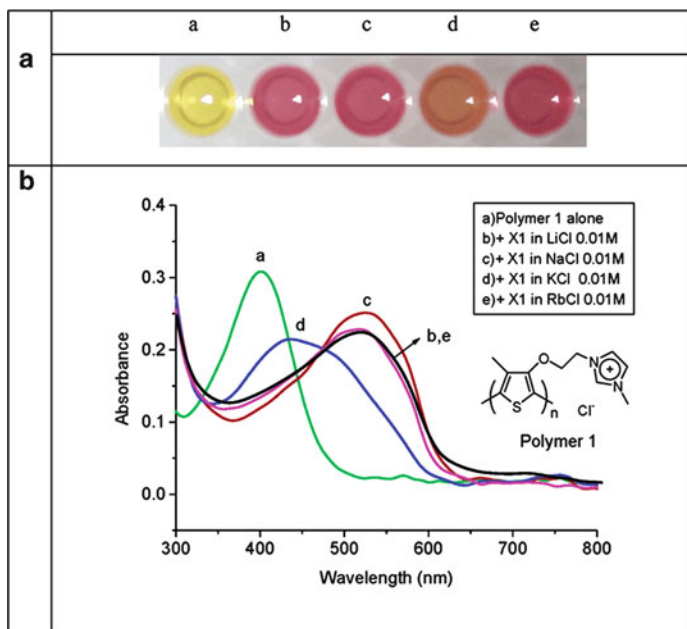


Fig. 12 (a) Photos of wells labeled in graph B exhibiting colorimetric changes. (b) UV-vis absorption spectra of polymer 1 (2.9×10^{-9} mol on a monomer unit basis) in the presence of X1 DNA aptamer (1.9×10^{-10} mol of the 15-mer) and different salts in 100 μ l of water at 25 $^{\circ}$ C [24]

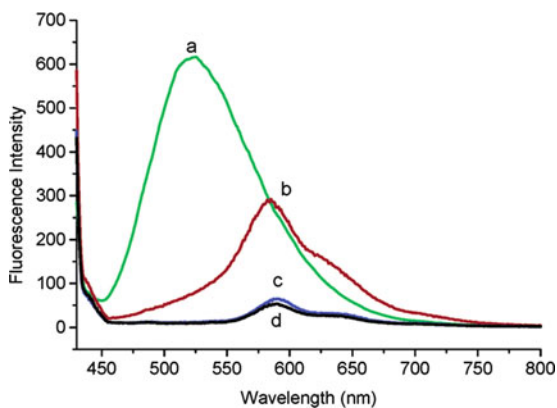


Fig. 13 Fluorescent spectra of (a) polymer 1, (b) human thrombin/X1 aptamer/polymer 1, (c) human thrombin/X2 aptamer/polymer 1 mixture, and (d) X1/polymer 1 complex in water, measured at 50 $^{\circ}$ C [24]

in fluorescence intensity based upon complexes with specific and nonspecific aptamers and the polymer. These differences in fluorescence intensity are most likely due to quenching that occurs as the polymer in the planar form tends to aggregate, causing a lower fluorescence intensity due to intra-chain de-excitation events [25]. The α -thrombin was able to be detected at a concentration of 10 pM in 200 μ l.

A similar approach for detecting the presence of specific proteins has also been reported by Nilsson and coworkers [26]. In this study, a complex between a calmodulin, a small calcium-binding protein, and the zwitter-ionic polythiophene POWT was used to detect the presence of calcineurin. The interaction between the POWT-calmodulin complex and calcineurin changed the emission profile from POWT, and no observable changes were observed upon exposure of the complex human serum albumin, suggesting that the complex could be used for the specific detection of calcineurin.

5 Direct Detection: CPs as Probes

The polymers used for fluorescence detection discussed thus far have all used either a synthetically linked polymer as the signal transducer for enhanced detection or some type of hybridization of the polymer with a receptor for ligand–receptor binding signaling. One of the most notable aspects of CPs is their ability to act as direct reporters for the detection of small molecules, or for conformational changes and protein aggregates.

5.1 Conformational Changes of Synthetic Peptides

Nilsson et al. designed an experiment to test the ability of a polymer to directly detect conformational changes within peptide/protein structure [27]. Using the zwitterionic polythiophene derivative, POWT, they succeeded in detecting the distinct conformations of synthetic peptides. The mechanism was concluded to be based on the polymer side chains' charged interactions and hydrogen bonding with the proteins.

They proceeded by synthesizing two peptides that, alone, formed random coils but upon association in solution produced a dimerized four-helix bundle (Fig. 14a). The POWT polymer in solution with the negatively charged peptide took on a planar conformation resulting in a red-shifted spectrum, while with the positively charged peptide, they observed a blue-shift (Fig. 14b). In a solution containing both of the peptides – and the subsequently formed four-helix bundle – the associating polymer displayed a slight red-shift and an increase in fluorescence intensity from its normal spectra free in solution. These data provided evidence that the polymer could in fact act as a reporter on a biological process (protein conformation) – in the absence of any additional binding complex – based solely on conformational changes within the polymer's backbone and charged side-chain interactions.

Following these initial results, POWT was employed in the detection of protein conformational changes after a binding event. The protein used, calmodulin, is relatively small and functions as an intracellular calcium sensor in eukaryotic cells [26]. When calmodulin interacts with calcium, a large conformational change

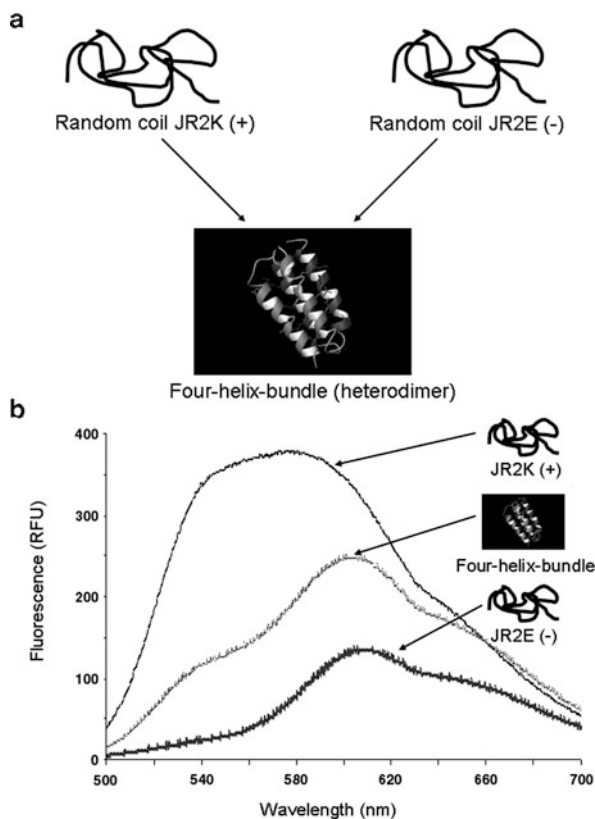


Fig. 14 (a) Schematic drawing of the conformational changes of the synthetic peptides JR2E (negatively charged), JR2K (positively charged) and the JR2K–JR2E heterodimer. (b) Fluorescence spectra of POWT being bound to JR2E, JR2K or the JR2K–JR2E heterodimer [27]

occurs where the protein goes from a compacted form to a more extended shape. This change in conformation was reflected in the POWT fluorescence spectra by a slight blue shift and an increase in fluorescence intensity, indicating a decrease in polymer planarity and a separation between adjacent polymer chains. As described, this system could also be employed for the detection of a specific protein, calcineurin.

Their next step was to synthesize by chemical oxidation, a negatively charged polythiophene acetic acid (PTAA)-Li for direct association with the previously discussed positively charged peptide JR2K [28]. It was found that the negatively charged carboxylic acid side chains of the polythiophene helped to induce the formation of a helix in the JR2K peptide just as the negatively charged peptide had previously. The change from polymer in solution to helical conformation resulted in both a blue-shift and an increase in fluorescence intensity because of a twisting in the backbone, shorter conjugation lengths, and a reduction in aggregation and quenching from the previously more planar form. In this example, it was

found that the polymer could not only act to induce a conformational change but also to directly report that change in the proteins structure.

5.2 Protein Aggregates

Nilsson and coworkers went on to use the anionic polymer (PTAA) for detection of amyloid fibril formation of bovine insulin [29]. The aggregation of proteins into fibrillar assemblies is problematic in diseases such as Alzheimer's, spongiform encephalitis, Parkinson's, Huntington's, and even in such practical applications as pharmaceutical insulin storage and delivery in the treatment of diabetes. As the monomeric proteins denature or change from their determined native states, they aggregate and form a repeating β sheet structure that further extends to form fibrils verifiable by transmission electron microscopy (TEM) (Fig. 15), CD spectroscopy, and historically with the characteristic gold-green birefringence from congo red dye [30].

Use of the anionic CP allowed for detection of amyloid fibril formation in both bovine insulin and chicken lysozyme proteins (Fig. 16). The polymer in buffer

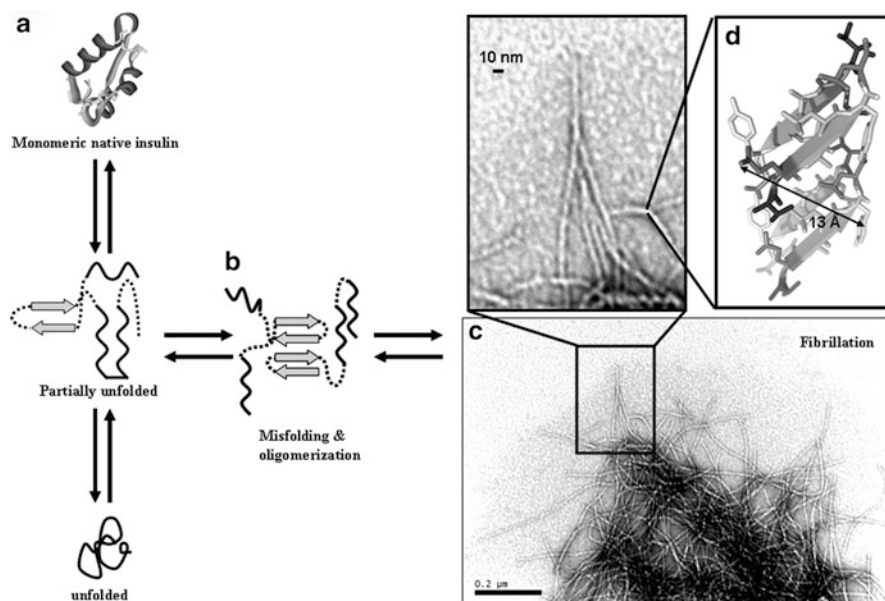


Fig. 15 Schematic drawing of the formation of amyloid fibrils. (a) Monomeric insulin having an α -helical conformation. (b) β -sheet (arrows) rich oligomers are being formed. (c) Amyloid fibrils having a diameter around 10 nm are being formed. (d) Higher magnification of the intrinsic repetitive β -pleated sheet structure of the amyloid fibril. The pictures were taken by transmission electron microscopy (TEM)

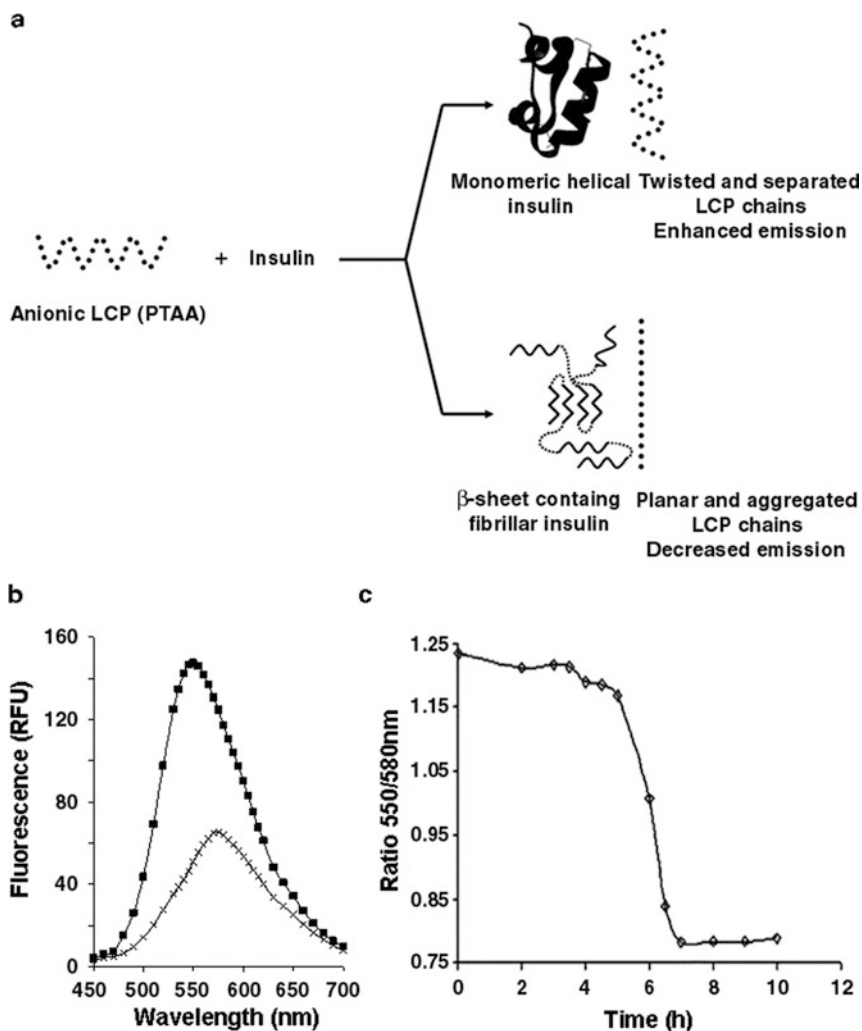


Fig. 16 (a) Description of the detection of amyloid fibrils in proteins with an anionic conjugated polymer, PTAA. (b) Emission spectra (*bottom*) of PTAA-Native bovine insulin (*filled square*) and PTAA-amyloid fibrillar bovine insulin (\times). (c) Kinetics of insulin amyloid fibril formation monitored by PTAA fluorescence [29]

solution had an absorption maximum of 446 nm, which was blue-shifted to 434 nm upon addition of the bovine insulin monomer and then red-shifted again with the formation of bovine insulin fibrils. The red-shift can again be associated with planarization of the polymer backbone and extended conjugation upon interaction with the β -sheet structure of the amyloid fibrils. A red shift was also seen for the emission spectra for PTAA bound to insulin fibrils (Fig. 16). The emission maximum was shifted from 550 to 580 nm and by plotting the ration of the emitted

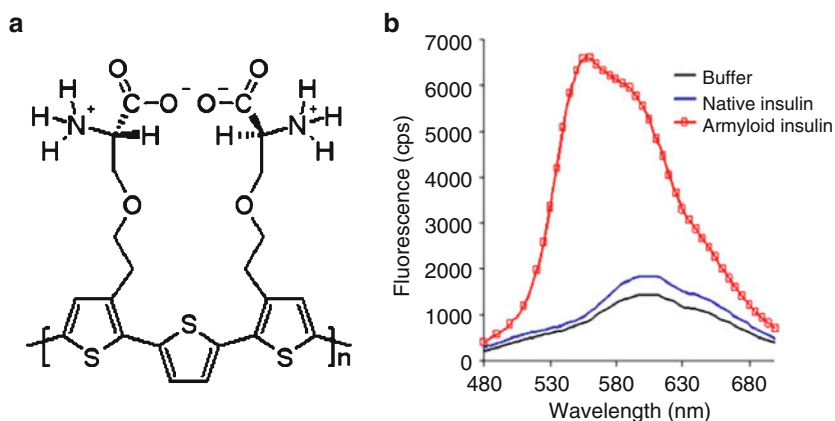


Fig. 17 (a) Chemical structure of polythiophene poly((3,3''-di[(S)-5-amino-5-carboxyl-3-oxapentyl]-[2,2';5'2'']-5-,5''-terthiophenylene hydrochloride), PONT. (b) Emission spectra of 6.5 μM PONT-HCl (on a chain basis) in 25 mM HCl (*black spectrum*), 25 mM HCl with 5.0 μM of native bovine insulin (*blue spectrum*), 25 mM HCl with 5.0 μM fibrillar bovine insulin (*red spectrum*). The emission spectra were recorded with excitation at 400 nm [31]

light at these wavelengths, Ration 550/580 nm, the kinetics of the fibrillation event could be followed (Fig. 16c). The ability to detect amyloid fibrils was demonstrated with both bovine insulin and chicken lysozyme to verify PTAA's usefulness as a conformation-sensitive probe. Hence, the PTAA emission profile was specific for the repetitive β sheet structure independent of the primary sequence of the protein used.

Later work, by Herland et al. synthesized a well-defined zwitterionic polythiophene, PONT, (Fig. 17a) [31]. On the basis of the previous work with serine substituted polythiophenes [9], Herland et al. synthesized regio-regular, well-defined molecules by chemical oxidation, which resulted in zwitter-ionic oligomeric thiophene derivatives from about 9 to 15 monomer units in length. This reduction in the distribution of chain lengths and polydispersity in the polymers helps to increase specificity of the probes and clarity in the interpretation of fluorescence data. Their application of choice was for the detection of amyloid fibrils of bovine insulin and chicken lysozyme. As shown in Fig. 17b, PONT showed a specific emission profile bound to amyloid fibrils, whereas the spectra for the polymer free in solution or mixed with native insulin were similar. The increased intensity of the emission and the blue-shift of the emission maximum upon binding to the amyloid fibrils are mainly due to separation of the polymer chains, whereas the decreased intensity and red-shift of the emission seen for PONT in acidic solvents or mix with native insulin correspond to planarization of the backbone, which causes aggregation or stacking of the polymers and interchain de-excitation between polymer chains. Hence, the authors were able to show that the regio-regular polymers could detect and identify amyloid fibrils specifically and reliably under the acidic conditions often required for *in vitro* fibrillization protocols. A recent study, comparing the amyloid selectivity of polythiophenes synthesized from monomeric or trimeric building blocks, has

also shown that the regioregular oligothiophenes are superior amyloid detectors when compared with their monomeric counterparts [32].

In the process of designing any tool for detection, the true test of value comes in working with complex biological samples, such as cells or tissue. Although the task of optimizing CPs for use with complex biological samples is daunting, there have been some successful results from the amyloid specific CPs in their use to discriminate between proteins of differing conformations. The proof of concept for the use of CPs as amyloid specific ligands was shown by Nilsson and coworkers in 2006 [33]. By using the previously described PTAA and PONT, and additionally cationic polythiophene, POMT, under proper staining conditions, they were able to obtain selective staining of amyloid deposits in a variety of tissues (Fig. 18). PONT and POMT were selective for amyloid deposits under acidic conditions, whereas PTAA was proven useful when alkaline staining conditions (pH 10) were used. Some indications that the unique conformation-dependent spectral signature from the CPs could be used for distinguish distinct types of amyloid deposits were also shown.

As a continuation of the previous study, Nilsson et al. were able to use CPs as histological stains to visualize A β protein aggregates in murine brain tissues [34]. Using the zwitterionic polythiophene derivative, tPTT (Fig. 19a), amyloid plaques were visible in histological stains verifiable through the use of the conventional amyloid ligands, congo red, and thioflavine T (ThT). Confocal microscopy techniques with spectral resolution allowed for determination of the polymers emission

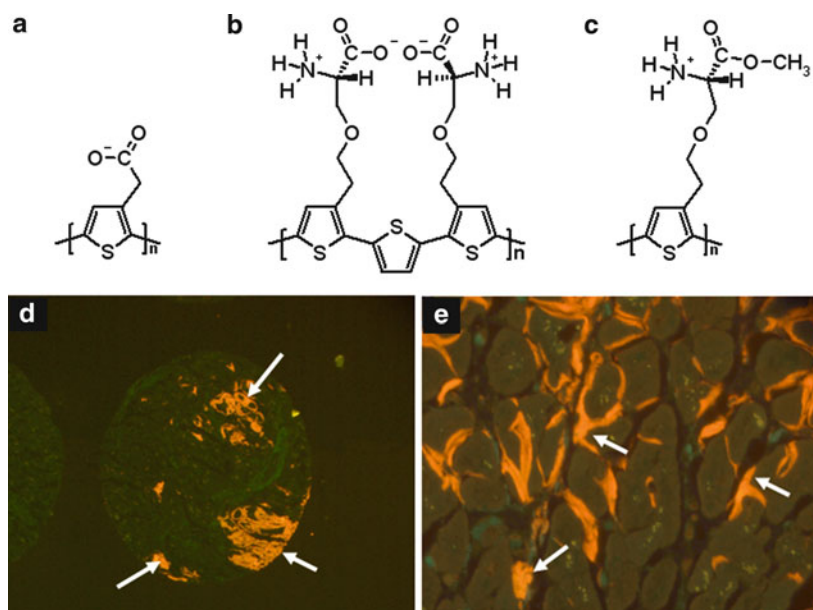


Fig. 18 Chemical structure of (a) PTAA, (b) PONT and (c) POMT. (d, e) Fluorescence images of amyloid deposits in tissue stained by PTAA. PTAA bound to amyloid deposits (white arrows) emits light with a yellow-red color [33]

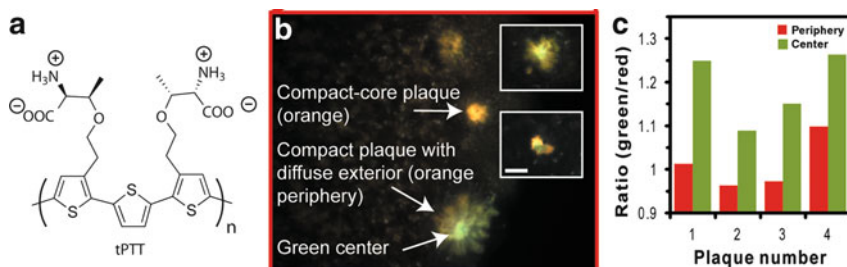


Fig. 19 (a) Chemical structure of the zwitter-ionic polythiophene derivative, tPTT. (b) Conformational heterogeneity of amyloid plaques in tPTT-stained mouse brain with A β deposits. Fluorescence microscope image showing localized distribution of amyloid plaques in the cerebral cortex. The compact plaques with diffuse exteriors show an *orange* periphery and a *green* center as indicated with *arrows*. In addition, a compact core plaque showing intense *orange* fluorescence is also visible. (c) Bar plot of the ratio of the fluorescence intensity of the *green* component (integrated between 543 and 564 nm) and the *red* component (integrated between 639 and 661 nm) of the spectra from the individual plaques 1–4. For all plaques, the periphery shows a larger *red* contribution than the center [34]

spectra over the region of distinct amyloid deposits (Fig. 19). The spectra revealed a range of colors from green to red appearing as though the packing conformation or the structural arrangement of the plaques varied from the plaque center to the periphery. To show that the polymer was actually able to distinguish between packing or conformational variation within the same peptide sequence, they showed that the polymer was able to show similar spectral distinctions between A β 1–42 fibrils formed under different conditions *in vitro*. Hence, the unique optical properties of CPs could be used to map the conformational heterogeneity in A β deposits both in tissue and solution. These findings could lead to novel ways of diagnosing Alzheimer's disease (AD) and also provide a new method for studying the pathology of the disease in a more refined manner. The technique has the potential to be valuable for establishing a correlation between the type of deposits and the severity of AD. However, further studies are necessary to understand the correlation of the spectroscopic read out from the LCP and the molecular structure of the protein aggregate. Nevertheless, the LCPs can be useful for comparison of heterogenic protein aggregates in well-defined experimental systems.

Heterogenic protein aggregates can also be found in other protein aggregation disorders, such as the infectious prion diseases. These diseases are caused by a proteinaceous agent called PrP^{Sc}, a misfolded and aggregated version of the normal prion protein. In addition, prions can occur as different strains, and the prion strain phenomenon is most likely encoded in the tertiary or quaternary structure of the prion aggregates. This belief was also verified when CP staining was applied to protein aggregates in brain sections from mice infected with distinct prion strains [35]. The LCPs bound specifically to the prion deposits and different prion strains could be differentiated due to a distinct spectral signature from the CP (Fig. 20). The anionic LCP, PTAA, was shown to emit light of different wavelengths when bound to distinct protein deposits associated with a specific prion strain, such as murine

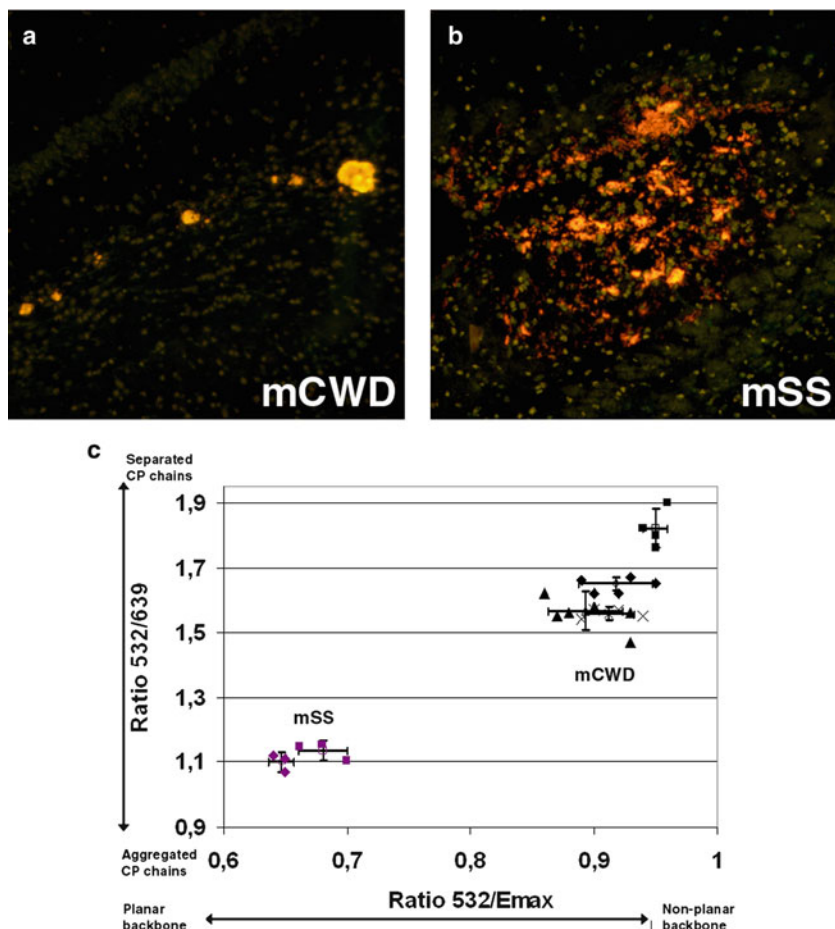


Fig. 20 Fluorescent images of prion deposits associated with distinct prion strains, murine chronic wasting disease (mCWD) (a) and murine sheep scrapie (mSS) (b), which has been stained by PTAA. (c) Correlation diagram of the ratios, $R_{532/639}$ and $R_{532/E_{max}}$, of the intensity of the emitted light from PTAA bound to prion deposits originating from individual mice infected with CWD (black symbols) or sheep scrapie (purple symbols) [35]

chronic wasting disease (mCWD) or murine sheep scrapie (mSS). Similar to the study described above, ratios of the intensity of the emitted light at certain wavelengths was used as an indicator of the geometry of the polymer chains. Nonplanar and separated CP chains emit light around 530–540 nm, whereas a planarization of the thiophene backbone will shift the emission maximum (E_{max}) toward longer wavelengths. A planar backbone might also give rise to stacking of the thiophene rings, seen as an increase of the intrinsic emission around 640 nm. When plotting the ratio $532/E_{max}$ and the ratio $532/639$ nm in a correlation diagram, prion aggregates associated with distinct prion strains, mCWD and mSS, were easily distinguished from each other, verifying the usefulness of spectral properties of LCPs for

classification of protein deposits (Fig. 20). These conformation- dependent spectral characteristics can only be afforded by LCPs and provide the opportunity to optically fingerprint protein aggregates correlating to distinct prion strains.

The study by Sigurdson et al. also provided evidence that the different spectral signatures obtained from PTAA were associated with distinct conformations of the prion aggregates [35]. Recombinant mouse prion protein (mPrP) was converted into two different types of amyloid fibrils by using varying conditions for fibrillation. As these two preparations of fibrils were chemically identical, having the same protein (mPrP), the spectral differences seen for PTAA was likely due to structural differences between the fibrils. Hence, the author showed that CPs provide structural insights regarding the morphology of individual protein deposits and that these molecular tools could be used as a complementary technique to conventional staining protocols for the characterization of protein deposits associated with individual prion strains. These findings might be of great value, as phenomena similar to those occurring in prion strains may be much more frequent than is now appreciated, and may extend to additional protein misfolding and aggregation disorders. As mentioned earlier, strain-like conformational variants can also be found for A β aggregates, the pathological hallmark of AD. LCPs might therefore aid in the fundamental understanding of conformational protein variants in a wide range of protein misfolding disorders.

5.3 *Novel Molecular Scaffolds for In Vivo Imaging*

As shown in the previous sections, CP materials that originate from electronics and solar cells have proven very useful as a novel class of fluorescent molecular dyes within the field of molecular biology and medicine. The spectral information from CPs could be useful to gain more information regarding the molecular details of the biological process and pathological events underlying a wide range of diseases, such as the protein aggregation diseases. However, there is still a great extent of basic research that must be performed to fully understand and properly utilize the CP-based technique for studying biological events.

One attractive possibility is to develop CPs that can be used for in vivo imaging of protein aggregates. In this regard, the synthesis of appropriately functionalized CPs that are able to cross the blood–brain barrier (BBB) has been exemplified [36]. Such dyes can be utilized in powerful multi-photon imaging applications as previously reported CPs have been shown to have an excellent cross-section area compared with small fluorescent dyes, making these molecules suitable for multi-photon applications [33, 37].

A novel thiophene-based molecular scaffold that could be used for optical in vivo imaging of protein aggregates was recently reported by Åslund et al. [36]. This chemically defined anionic pentameric thiophene derivative, p-FTAA (Fig. 21a), could be utilized for direct in vivo detection of A β deposit in the brain of a transgenic mouse model with AD pathology. The deposits were easily visualized by two-photon

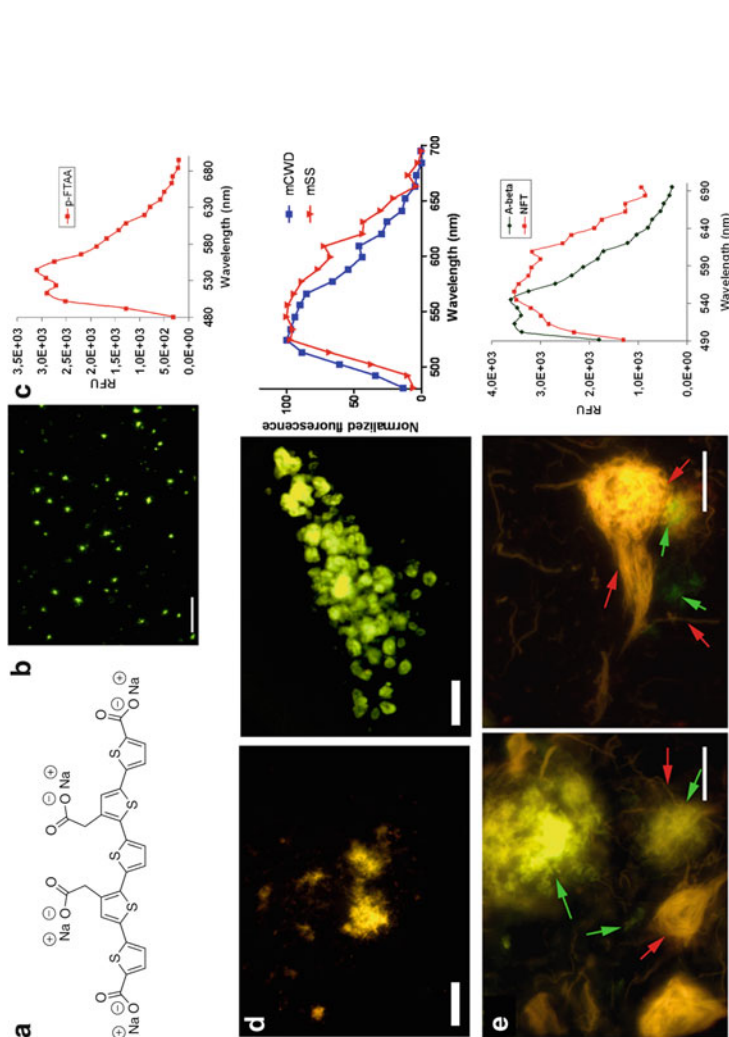


Fig. 21 (a) Chemical structure of the sodium salt of the anionic pentameric thiophene derivative, p-FTAA. (b) Fluorescence image of p-FTAA labeled A β deposits in brain tissue from a transgenic mouse model with AD pathology. (c) Emission spectrum of p-FTAA bound to A β deposits. (d) Ex vivo fluorescence image of p-FTAA-labeled prion deposits in mice infected with mouse-adapted sheep scrapie, mSS (left), or mouse-adapted chronic wasting disease, mCWD (middle), that have been intracerebrally injected with p-FTAA. Typical emission spectra from p-FTAA (right) upon binding to mCWD (blue) or mSS (red) deposits. Scale bars represent 50 μ m. (e) High resolution fluorescence images of human brain tissue with AD pathology showing an overview of the interplay between A β deposits (green arrows) and neurofibrillary tangles (NFTs, red arrows). Emission spectra of p-FTAA bond to A β aggregates (green spectrum) or NFTs (red spectrum) [36]

spectroscopy through a cranial window after an intravenous injection of the pentameric dye. Hence, p-FTAA was shown to cross the BBB rather efficiently and p-FTAA bound to A β deposits showed a characteristic emission spectrum with well-resolved substructures (Fig. 21c). This spectral feature is probably a result of conformational restriction of the thiophene backbone upon binding to the deposits. Furthermore, in a similar fashion to what was previously reported for the polydisperse PTAA [35], p-FTAA emission spectra could be used for assigning two differing strains of prions (Fig. 21d). Thus, p-FTAA was also shown to exhibit conformation-dependent optical properties comparable to the CPs described above. These properties could also be utilized for spectral separation of the two major pathological hallmarks of AD, namely neurofibrillary tangles (NFTs) and A β deposits. As shown in Fig. 21e, p-FTAA bound to A β -deposits emitted green light, whereas the NFTs showed a red-shifted spectrum for p-FTAA. Thus, the distinctive spectral signatures from p-FTAA bound to A β aggregates or tau deposits may be used to study the interplay between these entities in more detail. When compared with their larger, polymeric ancestors, these small chemically defined molecular probes with conjugated systems serve a much better chance for in vivo applications due to the ability of many to pass through cellular walls and across the blood–brain barrier.

6 Concluding Remarks

In conclusion, CPs and their oligomeric counterparts represent an interesting and diverse class of molecules that have proven to be useful in a number of applications in which their inherent fluorescent properties allow for very sensitive and precise detection using present technology in the field of fluorescence. The phenomenon of the spectral transition of CPs based upon planarity, backbone conjugation, and target association continues to prove useful in many new and diverse applications in fluorescence reporting. Future synthesis of novel, chemically defined oligomeric CPs will certainly realize combinatorial approaches for optimizing the CPs structure, which may provide more effective binders for different classes of biomolecular targets. To understand and correlate the spectral signature of the CPs to a distinct biological event, the focus must also be turned to the fundamental underlying photo-physical processes of CPs and their related oligomeric counterparts. As described in this chapter, CPs are being implemented in new areas of science and we foresee that these materials will continue to evolve and serve as practical research tools within the fields of biology and pathology.

References

1. Le Bouch N, Auger M, Leclerc M (2008) Structure and segmental motions in a substituted polythiophene: a solid-state NMR study. *Macromol Chem Phys* 209:2455–2462
2. Huser T, Yan M, Rothberg L (2000) Single chain spectroscopy of conformational dependence of conjugated polymer photophysics. *Proc Natl Acad Sci* 97:11187–11191

3. Shand M, Chance R, LePostollec M, Schott M (1982) Raman photoselection and conjugation-length dispersion in conjugated polymer-solutions. *Phys Rev B* 25:4431–4436
4. Orcharad B, Tripathy S (1986) Molecular-structure and electronic property modification of poly(diacetylenes). *Macromolecules* 19:1844–1850
5. Dobrosavljević V, Stratt R (1987) Role of conformational disorder in the electronic-structure of conjugated polymers: substituted polydiacetylenes. *Phys Rev B* 35:2781–2794
6. Yan M, Rothberg L, Papadimitrakopoulos F, Galvin M, Miller T (1994) Defect quenching of conjugated polymer luminescence. *Phys Rev Lett* 73:744–747
7. Okada S, Jelinek R, Charych D (1999) Induced color change of conjugated polymeric vesicles by interfacial catalysis of phospholipase A(2). *Angew Chem Int Ed* 38:655–659
8. Kim J, Swager TM (2001) Control of conformational and interpolymer effects in conjugated polymers. *Nature* 411:1030–1034
9. Nilsson KPR, Andersson MR, Inganäs O (2002) Conformational transitions of a free amino-acid-functionalized polythiophene induced by different buffer systems. *J Phys Condens Matter* 14:10011–10020
10. Andersson MR, Berggren M, Olinga T, Hjertberg T, Inganäs O, Wennerström O (1997) Improved photoluminescence efficiency of films from conjugated polymers. *Synth Met* 85:1383–1384
11. Berggren M, Bergman P, Fagerstrom J, Inganäs O, Andersson M, Weman H, Granström M, Stafström S, Wennerström O, Hjertberg T (1999) Controlling inter-chain and intra-chain excitations of a poly(thiophene) derivative in thin films. *Chem Phys Lett* 304:84–90
12. Marsella MJ, Swager TM (1993) Designing conducting polymer-based sensors – selective ionochromic response in crown-ether containing polythiophenes. *J Am Chem Soc* 115:12214–12215
13. Crawford K, Goldfinger M, Swager TM (1998) Na⁺ specific emission changes in an ionaphoric conjugated polymer. *J Am Chem Soc* 120:5187–5192
14. Charych DH, Nagy J, Spevak W, Bednarski M (1993) Direct colorimetric detection of a receptor-ligand interaction by a polymerized bilayer assembly. *Science* 261:585–588
15. Disney M, Zheng J, Swager TM, Seeberger P (2004) Detection of bacteria with carbohydrate-functionalized fluorescent polymers. *J Am Chem Soc* 126:13343–13346
16. Bernier S, Garreau S, Bera-Aberem M, Gravel C, Leclerc M (2002) A versatile approach to affinitychromic polythiophenes. *J Am Chem Soc* 124:12463–12468
17. Reichert A, Nagy JO, Spevak W, Charych D (1995) Polydiacetylene liposomes functionalized with sialic-acid bind and colorimetrically detect influenza-virus. *J Am Chem Soc* 117:829–830
18. Charych D, Cheng Q, Reichert A, Kuziemko G, Stroh M, Nagy JO, Spevak W, Stevens RC (1996) A ‘litmus test’ for molecular recognition using artificial membranes. *Chem Biol* 3:113–120
19. Ho HA, Boissinot M, Bergeron MG, Corbeil G, Doré K, Boudreau D, Leclerc M (2002) Colorimetric and fluorometric detection of nucleic acids using cationic polythiophene derivatives. *Angew Chem Int Ed Engl* 114:1618–1621
20. Doré K, Dubus S, Ho HA, Lévesque I, Brunette M, Corbeil G, Boissinot M, Boivin G, Bergeron MG, Boudreau D, Leclerc M (2004) Fluorescent polymeric transducer for the rapid, simple, and specific detection of nucleic acids at the zeptomole level. *J Am Chem Soc* 126:4240–4244
21. Raymond FR, Ho HA, Peytavi R, Bissonnette L, Boissinot M, Picard FJ, Leclerc M, Bergeron MG (2005) Detection of target DNA using fluorescent cationic polymer and peptide nucleic acid probes on solid support. *BMC Biotechnol* 5:10
22. Nilsson KPR, Inganäs O (2003) Chip and solution detection of DNA hybridization using a luminescent zwitterionic polythiophene derivative. *Nat Mater* 2:419–424
23. Gaylord BS, Massie MR, Feinstein SC, Bazan GC (2005) SNP detection using peptide nucleic acid probes and conjugated polymers: applications in neurodegenerative disease identification. *Proc Natl Acad Sci USA* 102:34–39

24. Ho HA, Leclerc M (2004) Optical sensors based on hybrid aptamer/conjugated polymer complexes. *J Am Chem Soc* 126:1384–1387
25. Nguyen TQ, Doan V, Schwartz BJ (1999) Conjugated polymer aggregates in solution: control of interchain interactions. *J Chem Phys* 110:4068–4078
26. Nilsson KPR, Inganäs O (2004) Optical emission of a conjugated polyelectrolyte: calcium-induced conformational changes in calmodulin and calmodulin–calcineurin interactions. *Macromolecules* 37:9109–9113
27. Nilsson KPR, Rydberg J, Baltzer L, Inganäs O (2003) Self-assembly of synthetic peptides control conformation and optical properties of a zwitterionic polythiophene derivative. *Proc Natl Acad Sci USA* 100:10170–10174
28. Nilsson KPR, Rydberg J, Baltzer L, Inganäs O (2004) Twisting macromolecular chains: self-assembly of a chiral supermolecule from nonchiral polythiophene polyanions and random-coil synthetic peptides. *Proc Natl Acad Sci USA* 101:11197–11202
29. Nilsson KPR, Herland A, Hammarström P, Inganäs O (2005) Conjugated polyelectrolytes: conformation-sensitive optical probes for detection of amyloid fibril formation. *Biochemistry* 44:3718–3724
30. Sipe JD, Cohen AS (2000) Review: history of the amyloid fibril. *J Struct Biol* 130:88–98
31. Herland A, Nilsson KPR, Olsson JDM, Hammarström P, Konradsson P, Inganäs O (2005) Synthesis of a regioregular zwitterionic conjugated oligoelectrolyte, usable as an optical probe for detection of amyloid fibril formation at acidic pH. *J Am Chem Soc* 127:2317–2323
32. Åslund A, Herland A, Hammarström P, Nilsson KPR, Jonsson BH, Inganäs O, Konradsson P (2007) Studies of luminescent conjugated polythiophene derivatives: enhanced spectral discrimination of protein conformational states. *Bioconjug Chem* 18:1860–1868
33. Nilsson KPR, Hammarström P, Ahlgren F, Herland A, Schnell EA, Lindgren M, Westermark GT, Inganäs O (2006) Conjugated polyelectrolytes-conformation-sensitive optical probes for staining and characterization of amyloid deposits. *Chem Bio Chem* 7:1096–1104
34. Nilsson KPR, Åslund A, Berg I, Nyström S, Konradsson P, Herland A, Inganäs O, Stabo-Eeg F, Lindgren M, Westermark GT, Lannfelt L, Nilsson LNG, Hammarström P (2007) Imaging distinct conformational states of amyloid-beta fibrils in Alzheimer's disease using novel luminescent probes. *ACS Chem Biol* 2:553–560
35. Sigurdson CJ, Nilsson KPR, Hornemann S, Manco G, Polymenidou M, Schwarz P, Leclerc M, Hammarström P, Wuthrich K, Aguzzi A (2007) Prion strain discrimination using luminescent conjugated polymers. *Nat Methods* 4:1023–1030
36. Åslund A, Sigurdson CJ, Klingstedt T, Grathwohl S, Bolmont T, Dickstein DL, Glimsdal E, Prokop S, Lindgren M, Konradsson P, Holtzman DM, Hof PR, Heppner FL, Gandy S, Jucker M, Aguzzi A, Hammarström P, Nilsson KPR (2009) Novel pentameric thiophene derivatives for in vitro and in vivo optical imaging of a plethora of protein aggregates in cerebral amyloidoses. *ACS Chem Biol* 4:673–684
37. Stabo-Eeg F, Lindgren M, Nilsson KPR, Inganäs O, Hammarström P (2007) Quantum efficiency and two-photon absorption cross-section of conjugated polyelectrolytes used for protein conformation measurements with applications on amyloid structures. *Chem Phys* 336:121–126

Fluorescence Reporting Based on FRET Between Conjugated Polyelectrolyte and Organic Dye for Biosensor Applications

Kan-Yi Pu and Bin Liu

Abstract Conjugated polyelectrolytes (CPEs), with highly delocalized electronic backbones and charged ionic side chains, are naturally robust light-harvesting antenna for fluorescence resonance energy transfer (FRET) applications. This chapter describes FRET-based biosensors using CPEs as energy donors from the viewpoint of sensing mechanism, donor–acceptor selection and detection targets. Important information on how to design CPE structures and assay schemes is elucidated, and examples for DNA and protein detection are discussed.

Keywords Conjugated polyelectrolyte · DNA · Energy transfer · Fluorescence · Protein · Sensor

Contents

1	Introduction	418
2	DNA Biosensor	421
2.1	Assay Design	421
2.2	Influencing Factors for FRET	428
2.3	Molecular Design for Efficient FRET	430
3	Protein Biosensor	437
3.1	Antibody–Antigen Based Sensor	437
3.2	Aptamer-Based Sensor	440
3.3	CPE Complex Based Sensor	444
4	Summary	447
	References	448

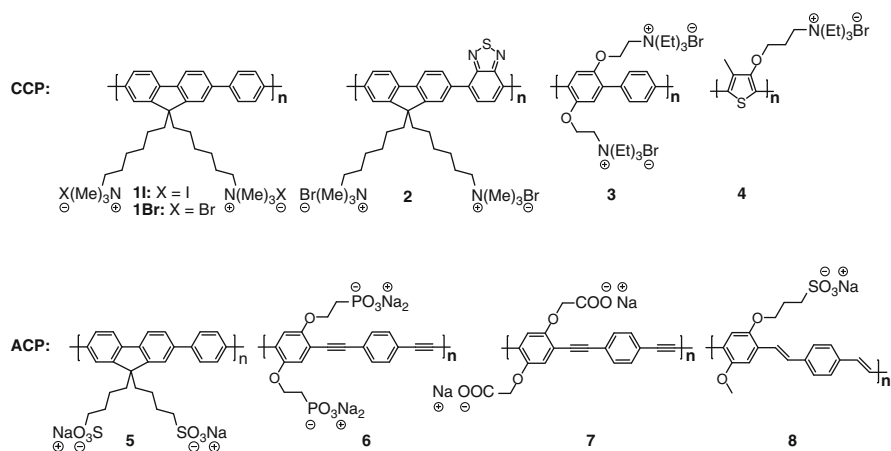
K.-Y. Pu and B. Liu (✉)

Department of Chemical and Biomolecular Engineering, 4 Engineering Drive 4, National University of Singapore, Singapore, Singapore 117576,
e-mail: cheliub@nus.edu.sg

1 Introduction

Conjugated polymers (CPs) are unsaturated rigid-rod macromolecules with sp^1 - or sp^2 -hybridized backbones. CPs in their neutral states are organic semiconductors that exhibit efficient absorption and emission. Their band gaps can be desirably fine-tuned by backbone structures, allowing emission ranging from ultraviolet to near-infrared. During the past decades, CPs have been extensively investigated for applications in optoelectronic devices, such as light-emitting diodes [1], photovoltaic cells [2], organic field-effect transistors [3], and organic lasers [4]. Recently, CPs have been proven useful for trace detection of analytes in a variety of environments [5], which benefit from their easily perturbed properties, including charge transport [6], conductivity [7], emission [8, 9], and absorption [10]. In particular, their delocalized electronic structures impart efficient electronic coupling among optoelectronic segments, leading to rapid intramolecular and intermolecular energy/charge transfer [11]. As compared to small-molecule fluorophores, CPs have larger absorption cross-section and unique collective optical response, making them superior in the transduction of optical signals.

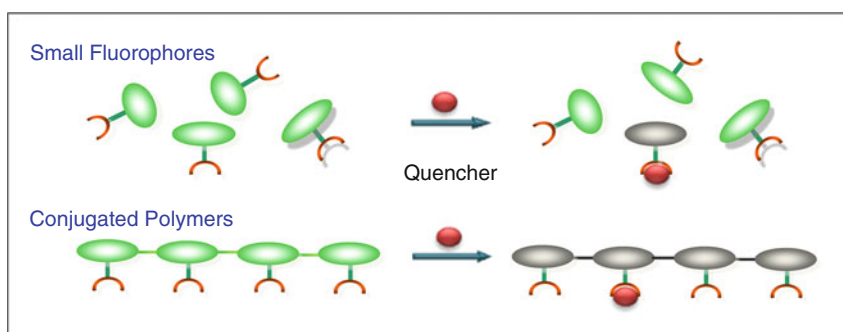
Water solubility, a prerequisite for fluorescent materials to interrogate biomolecules in physiological environments, necessitates the development of water-soluble CPs. Conjugated polyelectrolytes (CPEs) are CPs with water-soluble ionic side chains [12]. These polymers combine optoelectronic properties of CPs with charge-mediated behaviors of polyelectrolytes, providing a unique platform for the construction of chemical and biological sensors [13]. According to the charge sign, water-soluble CPEs can be simply divided into two categories, cationic CPs (CCPs) and anionic CPs (ACPs). The chemical structures of some typical CPEs are summarized in Scheme 1. Cationic groups of CCPs are usually quaternary ammonium (CCPs 1–4), while anionic groups of ACPs are carboxylate (7), phosphonate (6) or sulfonate (5 and 8). The water-solubility of CPEs is not only dependent on the



Scheme 1 Chemical structures of some typical CPEs

ionic side groups but also affected by the hydrophobic aromatic backbones [14]. More importantly, the presence of charged side groups in CPEs results in electrostatic attractions between CPEs and a myriad of biomolecules, which emerge as indispensable driving forces to bring them into close proximity to change the optical properties of CPEs. Owing to the aromatic backbones of CPEs, the hydrophobic interactions usually coexist with electrostatic attractions to participate in the sensing processes [15].

Most traditional CPE-based sensors rely on the polymer fluorescence decrease upon binding to an analyte, known as fluorescence quenching [16–18]. The first example of CP-based fluorescence quenching sensing was demonstrated by Swager's group in 1995 [19]. The significant finding of this report is that fluorescence quenching of CPs upon binding to strong electron-withdrawing quenchers (such as explosives) is much more effective than that of their small-molecule counterparts. This phenomenon is termed as “molecular wire effect” or “super-quenching” as illustrated in Scheme 2, which results from the CP's delocalized electronic structure that facilitates efficient charge transfer over a long distance to the quencher. Taking advantage of this principle, Whitten's and Schanze's groups have developed a series protein assays based on the reversible fluorescence quenching of CPEs in the presence of quencher-tether-ligand [20–23]. In contrast to direct quenching between CPEs and quenchers, nonquenching analytes may also indirectly cause fluorescence quenching through inducing polymer aggregation via electrostatic/hydrophobic interactions, leading to self-quenching of polymer fluorescence [24]. Fluorescence self-quenching occurs between an excited molecule and a ground-state molecule of the same type that induces nonradiative deactivation of the excited state [25]. Such aggregation-induced quenching behaviors of CPEs have been used to detect biomolecules without significant optoelectronic characters, such as concanavalin A [26], multicationic amines [27], oxalic acid [28], and glucose [29]. Water-soluble poly(phenylene ethynylene) (PPE) derivatives (5 and 7) were frequently used for these assays because of their more sensitive fluorescence responses toward environment variations relative to other CPEs.



Scheme 2 Illustration of “molecular wire effect” using fluorescence quenching of CPs as an example

Colorimetric assays have also been developed based on CPEs. Although the absorption characteristics of CPs are strongly determined by local electronic structure, the correlation between the band gap and the polymer conformation provides a useful channel to create colorimetric sensors. CPE-based colorimetric biosensors have been well established on water-soluble polythiophenes (PT) by Leclerc's and Inganäs's groups [30–32], which take advantage of the ultrasensitive conformation-dependent optical properties of PT for DNA detection. For the DNA assays reported by Leclerc's group, electrostatic attraction efficiently induces the formation of interpolyelectrolyte complexes between the oppositely charged cationic PT (**4**) and DNA, within which the polymer conformation is different in the presence of double-stranded DNA (dsDNA) and single-stranded DNA (ssDNA) [33]. DNA hybridization event, hence, could be monitored by colorimetric transition of the polymer from deep violet (absorption maximum at ~ 550 nm) to bright yellow (absorption maximum at ~ 425 nm), as a result of the polymer conformation variation from coplanar rigid rod to twisted random coil upon hybridization. Inganäs's group used a zwitterionic PT, which also showed absorption spectrum shift in the presence of ssDNA and dsDNA. In these assays, hydrogen bonding together with electrostatic attraction contribute to the DNA detection [31]. Similarly, water-soluble PTs have also been used to detect other chemicals and biomolecules, such as protein [33], peptide [34], adenosine triphosphate (ATP) [35], amines [36], and folic acid [37].

CPE-based sensors involving Förster resonance energy transfer (FRET) are of growing scientific interest and importance owing to their vital advantages over fluorescence quenching and colorimetric sensors, such as detection versatility and multichannel signal collection [38–40]. FRET is a well-known photophysical process whereby individual chromophores communicate their electronic states, providing means for transferring excitons from a donor to an acceptor [41]. Since FRET is sensitive to intra- and intermolecular distance in the range of < 10 nm, it has been widely adopted as a reliable pathway of signal transduction in biochemical research [42]. The application of CPEs in FRET biosensors were motivated by two main concerns. On the one hand, the strong distance-dependent FRET is especially effective in CPE-based sensing because changes in the distance between CPE and chromophore or chromophore-labeled probe can be facilely correlated with the recognition events and subsequently converted into measurable fluorescence signals from both acceptor and donor emission intensities. On the other hand, CPEs having efficient light-harvesting properties and high extinction coefficients are natural high-performance energy donors, allowing for amplified fluorescence of energy acceptors to yield high sensitivity with low signal-to-noise ratio. In 2002, Gaylord, Bazan and Heeger reported for the first time a CPE-based FRET assay to detect specific DNA sequences using a dye-labeled PNA probe [43]. Cationic poly[9,9-bis(6'-*N,N,N*-trimethylammonium)-hexyl]-fluorene phenylene) diiodide (**11**) was chosen as the donor molecule in view of its high-energy emission and sufficient photoluminescence (PL) quantum yield in aqueous media. This important report paves the way for the succeeding work concerning chemical and biological detection using CPEs as energy donors.

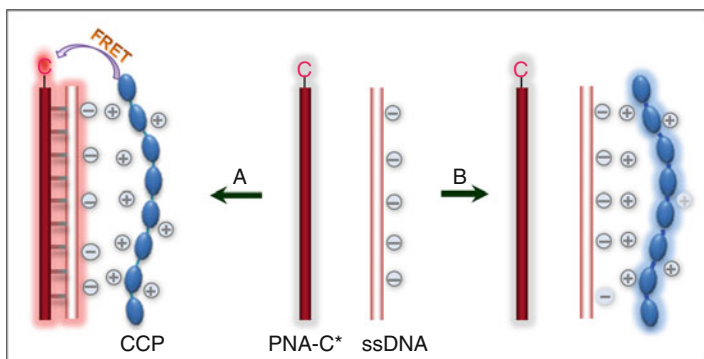
In this chapter, fluorescent sensors based on FRET between CPEs and organic fluorophores are introduced. In particular, DNA biosensors are described in details to illustrate the assay design and operation mechanism. Considering that FRET is a crucial process that generates the signal and determines the signal intensity, factors influencing FRET between CPEs and organic fluorophores are discussed using DNA biosensor as an example. To provide a brief view about how to obtain high FRET efficiency and in turn maximum detection sensitivity, molecular design of CPEs with respect to dye-labeled DNA is also elucidated. After acquiring knowledge of these vital issues in CPE-based FRET sensors, other representative protein assays are depicted in a case-by-case manner. This chapter intends to draw attention from researchers working with fundamental fluorescence technologies in chemistry and biology, and also to guide new researchers into this booming field. It is also expected that this chapter would help to inspire the specialists to have an evolutionary critical thinking about how to further optimize and advance such powerful sensory systems.

2 DNA Biosensor

Reliable methods for DNA detection are under intense investigation because of their vital applications in clinical diagnosis, environmental monitoring, forensic analysis and antiterrorism [44]. Effective DNA sensors require selectivity to identify single-nucleotide polymorphism (SNPs), and sensitivity to provide information from the small quantities of naturally occurring DNA molecules. A variety of DNA assays have been developed based on different transduction mechanisms, including fluorescence [45], electrochemical [46], microgravimetric [47], enzymatic [48], and nanostructure based methods [49]. In general, DNA detection is constrained by the levels of targets available in a particular sample. Thereby, the assay has to rely on the aid of enzymatic sample replication (polymerase chain reaction) to increase the concentration of specific nucleic sequences to detectable levels or turn to complex labeling steps (dye multiplicity) or enhanced optical (or instrumentation) systems. Such remedies are often reagent and instrumentation intensive, inciting high levels of complexity and cost. With these considerations, CPE-based DNA sensors have been developed to show reasonably high detection sensitivity with minimal DNA modifications.

2.1 Assay Design

The working mechanism of cationic conjugated polymer (CCP) based DNA assay using FRET protocol is illustrated in Scheme 3. [43]. This assay comprises two ingredients: (a) a light-harvesting CCP and (b) a probe oligonucleotide attached by a fluorescent signaling chromophore (C*). Emission of light characteristic of the



Scheme 3 Schematic illustration of the working mechanism of CCP/PNA-C*/DNA sensor

signaling C*, upon excitation of the CCP, indicates the presence of the target oligonucleotide. Transduction by electrostatic interactions triggered FRET is an essential procedure of the general strategy. A dye-tagged peptide nucleic acid (PNA-C*) sequence is used as the probe. Since PNA is neutral, there are no electrostatic interactions between CCP and PNA-C*, and thus the average CCP/PNA-C* distance is too large for effective FRET. In the presence of ssDNA, two situations may occur. Situation A: hybridization of the neutral PNA-C* to the complementary ssDNA causes the formation of PNA-C*/ssDNA duplex and in turn the incorporation of C* onto a macromolecular assembly with net negative charges. As such, electrostatic attraction between the PNA-C*/ssDNA duplex and CCP occurs to bring the dye sufficiently close to the CCP to favor FRET, leading to intense emission from C*. Situation B: in the presence of a noncomplementary ssDNA, hybridization does not occur and the CCP binds preferentially to ssDNA. One determines whether the target strand is complementary to the PNA probe by monitoring the C* emission upon CCP excitation.

Scheme 3 was first tested using a water-soluble CCP **II** and a PNA probe (5'-Fl-CAG TCC AGT GAT ACG-3', PNA₁-Fl) [43]. The absorption and emission spectra of **II** and PNA₁-Fl are shown in Fig. 1a. Good overlap between the emission of **II** and the absorption of Fl ensures FRET. Energy transfer was optimized by varying the ratio of **II** to PNA-C*. Fig. 1b shows the PL spectra of the solution of PNA₁-Fl (2.5×10^{-8} M, based on the PNA strand) and **II** (2.5×10^{-8} M, based on polymer chain) in the presence of ssDNA upon excitation of **II** at 380 nm. Intense Fl emission is induced in the presence of the complementary ssDNA₁ (sequence: 5'-CGT ATC ACT GGA CTG-3'), whereas only a minor signal is observed for the noncomplementary ssDNA₂ (sequence: 5'-ACT GAC GAT AGA CTG-3'). The amplified signal upon excitation of CCP at 380 nm is ~ 25 times higher than that upon direct excitation of Fl at its absorption maximum (480 nm). This leads to a detection limit of 10 pM with a standard fluorometer. The Fl emission in the presence of ssDNA₂ can be further decreased by using a solution containing 10% ethanol. Under the identical experimental conditions used (as given in Fig. 1b),

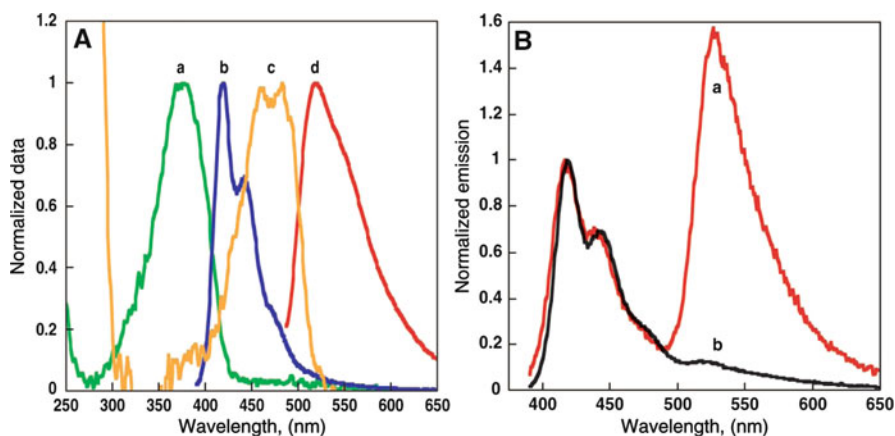
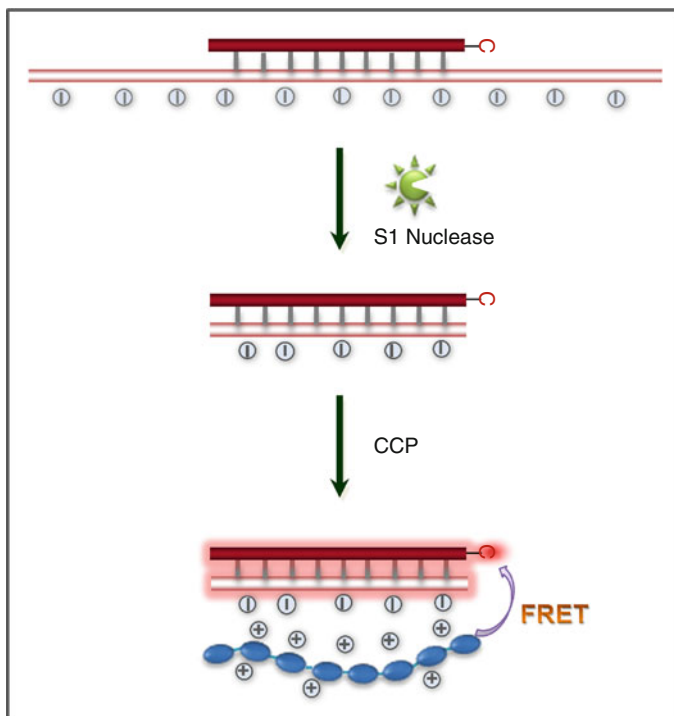


Fig. 1 (A) Absorption ((a) green and (c) orange) and emission ((b) blue and (d) red) spectra of CCP **II** and PNA₁-FI, respectively. Fluorescence was measured by exciting at 380 and 480 nm, for **II** and PNA₁-FI, respectively. (B) PL spectra of PNA-C* in the presence of complementary ((a) red) and noncomplementary ((b) black) DNA by excitation of CCP **II**. Conditions are in water at pH = 5.5. The spectra are normalized with respect to the emission of CCP **II** [43]

the presence of organic solvent weakens hydrophobic interactions between PNA₁-FI and CCP, consequently reducing FI emission by a factor of 3 in the presence of ssDNA₂, making the signal almost undetectable with a standard fluorometer.

Scheme 3 was also extended for single nucleotide polymorphisms (SNPs) detection with the aid of S1 nuclease enzyme by Bazan's group in 2005 [50]. The detection relies on the fact that PNA molecules are inherently resistant to nucleases and proteases, and PNA can protect the complementary DNA from S1 nuclease digestion. In this case, S1 nuclease could digest ssDNA, overhanging ssDNA segments that extend beyond the region of PNA/DNA duplex, and any unbound mismatches within a duplex. The targeted SNP was responsible for an arginine to tryptophan substitution at amino acid position 406 in the microtubule-associated protein tau. The mutant was linked to frontotemporal dementia. The probe strand was PNA₂-F1 (5'-FI-OO-TCC ACG GCA TCT CA-EE-3') that targets the R406W mutation. The detection was carried out by the addition of CCP **1Br** into the solution of the PNA/DNA solutions after enzymatic reaction as shown in Scheme 4. Excitation of **1Br** at 380 led to the selective FRET for only the perfectly complementary pair, while no obvious FRET occurred for samples containing even one mismatch (R406W mutation) because of the loss of electrostatic attraction afforded by the negatively charged DNA target after digestion. This method allows for straightforward discrimination of strand-specific SNP sites on short and long DNA target sequences.

Scheme 3 was subsequently modified to use chromophore-labeled ssDNA (ssDNA-C*) as the signaling probe, instead of PNA-C*, considering that ssDNA-C* is more common and cost-effective than PNA-C* [51]. In this case, ssDNA₃-F1



Scheme 4 Illustration of S1 nuclease mediated digestion of the duplex of long ssDNA target and the PNA probe, and subsequent FRET between the intact regions bound to the PNA probe

(5'-F1-GTA AAT GGT GTT AGG GTT GC-3') was used as the dye-labeled nucleic acid probe, and energy transfer was examined for the complementary ssDNA₄ (5'-GCA ACC CTA ACA CCA TTT AC-3') and the noncomplementary ssDNA₅ (5'-GAC TCA ATG GCG TTA GAC TG-3'). A direct comparison of FI emission (upon excitation at 380 nm) with [ssDNA₃-F1] = 2.1×10^{-8} M and [II] = 5.1×10^{-7} M is shown in Fig. 2. Electrostatic attraction between ssDNA-F1 and CCP (II) does occur, giving rise to background dye emission in the presence of noncomplementary ssDNA. Nevertheless, the FI emission intensity in the presence of ssDNA₄ is threefold higher than that in the presence of ssDNA₅. The difference in FRET is attributed to a closer proximity between F1 and II in the presence of ssDNA₄ as compared to that in the presence of ssDNA₅. This study indicates that utilization of ssDNA-C*, instead of PNA-C*, as the probe is less effective for DNA detection. This strategy was also examined by Leclerc's group using a cationic PT in conjunction with ssDNA labeled with Alexa Fluor 546, where a detection limit of 3 zM was achieved [52]. In addition, Wang et al. also used a similar scheme for SNP detection and allele frequency determination in association with probe extension reaction, where a DNA fragment as a part of p53 exon8 containing a polymorphic site (Arg282Trp) was effectively discriminated according to the difference in FRET [53].

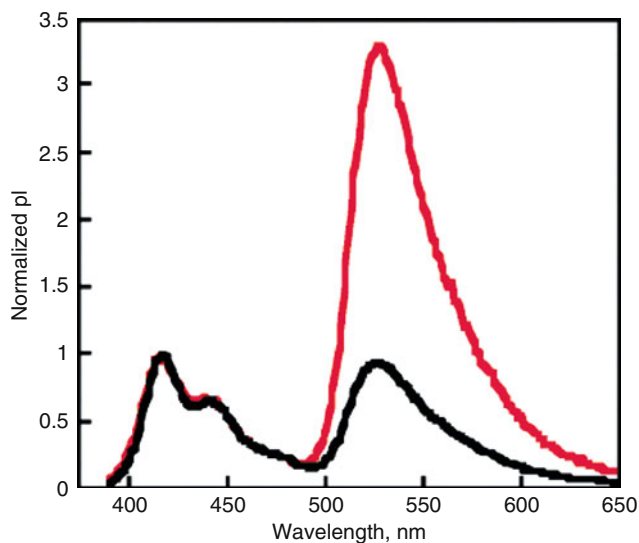
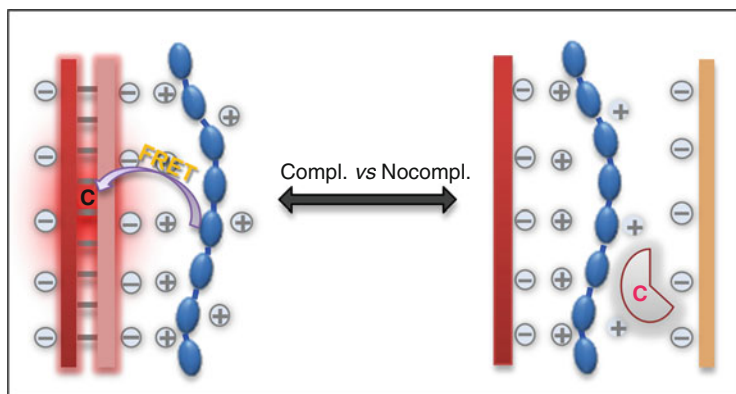


Fig. 2 PL spectra of **II** with complementary ssDNA₃-F1/ssDNA₄ (*red*) and noncomplementary ssDNA₃-F1/ssDNA₅ (*black*) in saline-sodium citrate buffer. The spectra were normalized to the polymer emission [50]

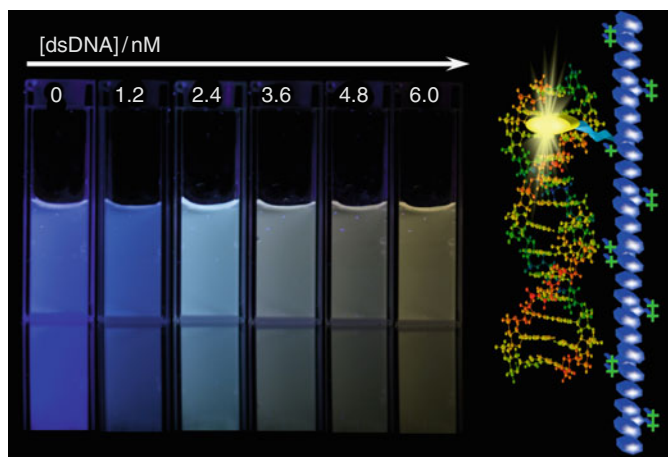


Scheme 5 Schematic illustration of the working mechanism of CCP/intercalating dye/DNA sensor

To overcome the nonspecific interactions between ssDNA-C* and CCP, Fan et al. introduced a magnetic microparticle assisted assay [54], which allows DNA detection in human serum with 0.1 nM sensitivity. In addition, DNA intercalating dyes were introduced for DNA detection as shown in Scheme 5. These special dyes have much higher fluorescence quantum yields upon intercalation with dsDNA relative to those in the presence of ssDNA or in their free states. As a result, when complementary ssDNA strands (target and probe) are present, the intercalating dye

is bound to the resulting dsDNA, giving rise to high fluorescence. Addition of CCP into the solution results in complex formation between CCP/dsDNA/intercalating dye, subsequently leading to the amplified dye emission. In contrast, in the presence of noncomplementary ssDNA strands, the fluorescence of intercalating dye is very weak because of the inefficient FRET and the intrinsically low quantum yield of free interlacing dye. However, this assay scheme is strongly dependent on the choice of intercalating dye as well as CCP. For instance, neglectable FRET was observed when ethidium bromide (EB) was used as the intercalating dye and **II** as the donor [55], while sufficient FRET occurred between DNA-bound thiazole orange (TO) and **II** [56]. It was suggested that the arrangement of donor and acceptor transition dipole moments played an important role in controlling such FRET processes [57]. In addition, our recent work shows that attachment of TO into the side chain of **II** affords an efficient multicolor light-up probe (PFPTO) that can distinguish dsDNA from ssDNA in serum media, which benefits from the stronger affinity of TO toward dsDNA as compared to other biomolecules [58]. As shown in Scheme 6, in the absence of DNA, the fluorescent color of PFPTO solution is blue. The blue fluorescence retains in the presence of ssDNA, while it gradually changes to brown with increasing [dsDNA]. Consequently, naked-eye discrimination of dsDNA from ssDNA in a mixed biological sample is feasible by using PFPTO as a multicolor indicator. The dsDNA concentration can be qualitatively estimated according to fluorescent color change of the polymer solution. This finding also indicates that Scheme 5 could work in biological media.

On the basis of Scheme 5, we recently realized label-free sequence-specific DNA detection with SNP selectivity with the aid of S1 nuclease [59]. In this assay, **1Br** and TO are chosen as the energy donor and acceptor, respectively.



Scheme 6 Photographs of fluorescence for PFPTO solutions at $[RU] = 2 \mu\text{m}$ in the presence of dsDNA with (DNA) ranging from 0 to 6.0 nM at intervals of 1.2 nM in $1 \times \text{PBS}$ containing 10 vol % serum under a hand-held UV lamp with $\lambda_{\text{max}} = 365 \text{ nm}$

When the target DNA is complementary to the PNA probe, the DNA/PNA duplexes remain after S1 nuclease digestion, which allows TO intercalation to give fluorescence. Addition of CCP to this solution results in enhanced TO emission due to FRET from **1Br** to TO. In contrast, in the presence of even one base mismatched DNA or dsDNA molecules, S1 nuclease can effectively digest the DNA strands into small fragments and thus no dye intercalation occurs, leading to very weak dye emission upon excitation of **1Br**. This method allows visual detection of target DNA with a detection limit of 5 μM according to the fluorescence color of the solution, which paves the way for the future exploration of real-time instrument-free SNP diagnosis.

DNA hybridization assays in heterogeneous formats have become increasingly common and powerful concomitant with the advancement of gene chip and DNA microarray technologies [60]. These systems allow for high-throughput screening of hundreds to thousands of genes in a single experiment [61]. Scheme 3 thus was applied in the solid state using a yellow light-emitting CCP (**2**) with two absorption bands centered at 330 and 444 nm as the light-harvesting donor [62]. This polymer can be excited at 488 nm and thereby is compatible with the excitation source used in commercial DNA microarray readers. The assay scheme was carried out with the PNA-modified surfaces (PNA₂: NH₂-O-O-TCC ACG GCA TCT CA) which were treated with Cy5-labeled complementary ssDNA (ssDNA₆-Cy5: 5'-Cy5-TGA GAT GCC GTG GA-3') and Cy5-labeled noncomplementary ssDNA (ssDNA₇-Cy5: 5'-Cy5-ATC TTG ACT GTG TGG GTG CT-3'), respectively. Treatment of the PNA-containing surface with complementary ssDNA results in an increase of the surface-negative charge, allowing **2** to bind to the surface. Excitation of the polymer thus induces FRET to the reporter dye, leading to strong Cy5 emission. In contrast, in the presence of the noncomplementary ssDNA, the reporter dye is not incorporated onto the surface, ultimately giving rise to neglectable Cy5 emission. In addition to this electrostatic interaction-based strategy, Kim's group has reported a kind of DNA-chips fabricated by DNA synthesis on a thin film of *organosoluble* CPs [63]. In these chips, the CP thin film serves as a signal amplifying surface to enhance the fluorescence of dye-labeled ssDNA. This method has been proven equally effective for the label-free DNA assay using SYBR green I as the intercalating dye [64].

Similar to the use of dye-labeled PNA or DNA as a signaling probe, dye-labeled RNA has also been used to study the interaction between tectoRNA molecules [65]. In addition, specific RNA/peptide interaction has been utilized for HIV-1 study [66]. The concept has been illustrated using the binding of the transactivator (Tat) peptide to the transactivation responsive element RNA sequence (TAR RNA) of HIV-1. In one study, the RNA and protein chosen were the HIV-1 mRNA fragment, TAR RNA, and its specific Tat polypeptide [66]. The bulge structure in TAR RNA is essential for Tat binding. A nonspecific polypeptide sequence labeled with FI at the N-terminus (SH3-FI*) and a three-base mutation dTAR RNA were also chosen for comparison. When **II** serves as the donor, intense FI emission is only observed for Tat-FI*/TAR RNA pair, indicating good selectivity of the assay for RNA detection.

2.2 Influencing Factors for FRET

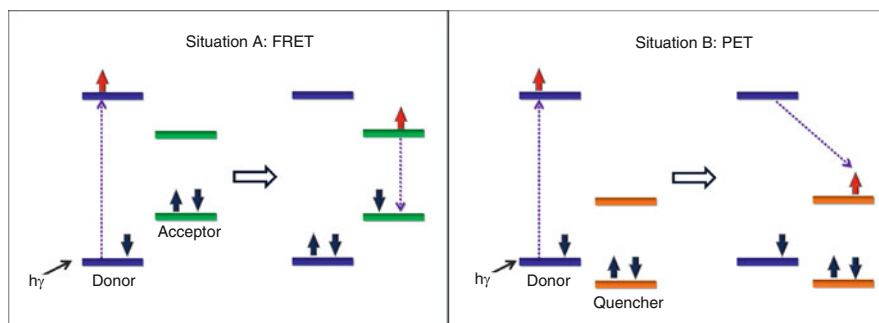
Amplification of C* emission upon excitation of CPE, relative to that upon direct excitation of C* is an important advantage of CPE-based FRET sensors, which benefits from the rapid intrachain and interchain energy migration from CPE to C* via FRET. The detection sensitivity of CCP-based DNA sensor thus is enhanced to an extent dependent on the signal amplification of C* emission. *Amplification factor* is defined as the intensity ratio of the saturated CCP-sensitized C* emission to the intrinsic C* emission in the absence of CCP. To acquire large signal amplification, it is necessary to review the factors affecting the FRET process from CCP to C*. Equation (1) describes the calculation of FRET rate (K_{FRET}) [67]:

$$K_{\text{FRET}}(r_{\text{DA}}) \propto \frac{1}{\tau_{\text{D}}} \left(\frac{R_0}{r_{\text{DA}}} \right)^6 \quad (1)$$

$$R_0 = \left[\frac{9000(\ln 10) Q_{\text{D}} \kappa^2 J(\lambda)}{128 \pi^5 N n^4} \right]^{1/6}, \quad J(\lambda) = \frac{\int_0^{\infty} F_{\text{D}}(\lambda) \varepsilon_{\text{A}}(\lambda) \lambda^4 d\lambda}{\int_0^{\infty} F_{\text{D}}(\lambda) d\lambda}$$

where r_{DA} is the donor–acceptor distance, τ_{D} is the lifetime of donor in the absence of acceptor, and R_0 is known as the Förster distance. Q_{D} is the quantum yield of the donor in the absence of acceptor, N is Avogadro's number, n is the refractive index of the medium, and κ is the orientation factor. The overlap integral, $J(\lambda)$, expresses the degree of spectral overlap between the donor emission $F_{\text{D}}(\lambda)$, and the absorption of acceptor $\varepsilon_{\text{A}}(\lambda)$.

The Förster equation is valid for ideal FRET processes when the donor and acceptor have well-matched energy levels. Otherwise, a competing process to FRET, photoinduced electron transfer (PET), is likely to occur. Although PET is a favorite mechanism for fluorescence quenching assays, it constitutes an undesirable energy-wasting channel in FRET assays that significantly reduces the intensity of signal output and in turn the overall sensitivity. Scheme 7 represents two



Scheme 7 Effect of relative orbital energy levels preferred for FRET and PET

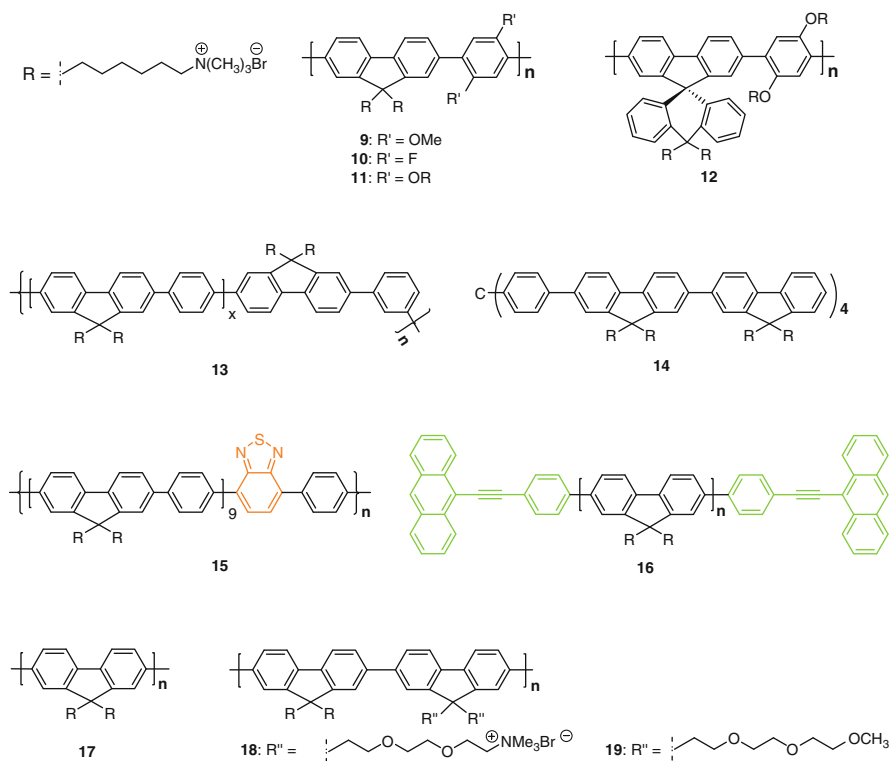
possible situations upon excitation of the polymer donor. Situation A refers to the ideal situation for FRET, where the highest occupied molecular orbital (HOMO) and lowest unoccupied molecular orbital (LUMO) energy levels of the acceptor are well contained within the orbital energy levels of the donor. Upon excitation of the donor, FRET to the acceptor occurs to induce an emissive process. Moreover, direct excitation of the acceptor under situation A does not quench the acceptor emission. This character is particularly useful for monitoring whether PET process exists in the system and how strong it could be. On the contrary, situation B favors PET, where both the electron affinity and the ionization potential are higher in one of the optical partners [68]. As shown in Scheme 7, excitation of the donor would lead to PET to the acceptor, while excitation of the acceptor would result in a similar charge-separated state via hole transfer to the donor. Although Scheme 7 is widely used for choosing suitable optical partners for a specific application, it becomes less accurate for intermediate cases because of the neglect of the contributions from the exciton binding energy, the intermolecular charge transfer state energy, and the stabilization of the charged species by the medium [69]. The mechanism for the competition between FRET and PET is complex and less understood for the CCP/C* pairs, but it is still probable to minimize the PET process by molecular design of CCP and the careful choice of donor/acceptor pairs.

Concomitant with these progresses in CCP-based DNA assays, it is gradually recognized that interactions within the CCP/DNA complexes are crucial for signal amplification [70]. Electrostatic attraction between positively charged CCP and negatively charged phosphate groups in DNA/PNA-C* or DNA/DNA-C* plays a vital role in bringing CCP and C* into close proximity to meet the FRET distance requirement. Different from ideal FRET systems, where the distance between the donor and the acceptor is fixed, the distance between CCP and C* varies because of the dynamic complex structures of CCP/DNA/PNA-C* (or DNA-C*). Thus, FRET between CCP and C* is much more complicated than ideal FRET process. Within the macromolecular complexes, there are cross-interaction between CCP and C* and self-interaction among C* or CCPs. Close association between CCP and DNA/PNA-C* or DNA/DNA-C* favors FRET; whereas, self-interaction among CCPs leads to polymer aggregation, which reduces the polymer quantum yield in solution. Self-interaction among C* causes dye fluorescence quenching, ultimately leading to reduced signal amplification.

According to this understanding, it is possible to optimize the FRET conditions to achieve high signaling emission, such as to increase the donor quantum yield (Q_D), to improve the spectral overlap ($J(\lambda)$), to optimize the molecular orientation (k), and to shorten the distance between donor/acceptor pairs (r_{DA}). In addition, it is also important to select donor–acceptor pairs with well-matched energy levels to minimize PET, and to develop strategies to solve the fluorescence self-quenching of both CCP and C* upon CCP/DNA-C* complexation. However, it is noteworthy to mention that the fluorescence quenching of CCP may not always have negative impact on CCP-sensitized dye emission [71].

2.3 Molecular Design for Efficient FRET

Intensive effort has been devoted to the optimization of CCP structures for improved fluorescence output of CCP-based FRET assays. The inherent optoelectronic properties of CCPs make PET one of the most detrimental processes for FRET. Before considering the parameters in the Förster equation, it is of primary concern to reduce the probability of PET. As the competition between FRET and PET is mainly determined by the energy level alignment between donor and acceptor, it can be minimized by careful choice of CCP and C*. A series of cationic poly(flourene-*co*-phenylene) (PFP) derivatives (**1Br**, **9**, **10** and **11**, chemical structures in Scheme 8) was synthesized to fine-tune the donor/acceptor energy levels for improved FRET [70]. F1 or Tex Red (TR) labeled ssDNA₈ (5'-ATC TTG ACT ATG TGG GTG CT-3') were chosen as the energy acceptor. The emission spectra of **1Br**, **9**, **10** and **11** are similar in shape with emission maxima at 415, 410, 414 and 410 nm, respectively. The overlap between the emission of these polymers and the absorption of F1 or TR is thus similar. Their electrochemical properties were determined by cyclic voltammetry experiments. The calculated HOMO and LUMO



Scheme 8 Chemical structures of the CCPs designed for DNA biosensors

levels are (-5.6 eV, -2.8 eV) for **1**, (-5.4 eV, -2.6 eV) for **9**, (-5.8 eV, -2.7 eV) for **10**, and (-5.4 eV, -2.6 eV) for **11**, respectively. Fluorine substitution raises the energy levels by ~ 0.2 eV, while the methoxy groups lower the levels by ~ 0.2 eV, relative to those of **1Br**. The LUMO energy of Fl (-3.6 eV) is well located within the band gap of these polymers. However, the HOMO energy of Fl (-5.9 eV) is lower than that of **1Br** (-5.6 eV), **9** (-5.4 eV) and **11** (-5.4 eV). As a result, PET process could occur between **1Br**, **9** or **11**, and Fl, and to less extent between **10** and Fl. The HOMO energy of TR (-5.4 eV) is higher than that of **1Br** and **10**, and is close to that of **9**. From the HOMO–LUMO energy level point of view, TR matches these polymers better than Fl. FRET experiments between **1Br**, **9** and **10** and ssDNA₈-Fl or ssDNA₈-TR were performed by monitoring dye emission upon excitation of **1Br** (385 nm), **9** (365 nm), and **10** (365 nm). The polymer concentrations were based on polymer repeat unit (RU). As shown in Fig. 3a, the most intense Fl emission was observed for **10**/ssDNA₈-Fl, which is approximately twofold more intense than that for **1Br**/ssDNA₈-Fl and is over an order of magnitude higher than that for **9**/ssDNA₈-Fl. For **10**/ssDNA₈-Fl, the integrated Fl emission is approximately fivefold greater than that obtained by direct excitation of Fl at its absorption maximum (495 nm) in the absence of CCPs. In contrast to the low Fl emission for **9**/ssDNA₈-Fl, TR emission from **9**/ssDNA₈-TR is much higher (Fig. 3b). This is due to better matched energy levels between **9** and TR than that for **9**/Fl. This study indicates the importance of energy level alignment between the donor and acceptor in determining the CCP-sensitized dye emission.

On the other hand, it is known that PET is essentially a contact process described by an exponential distance dependence, which functions effectively at a donor–acceptor distance considerably shorter than that for FRET processes [72]. Thus, it is also feasible to increase donor–acceptor distance to reduce PET. A poly(flourene-*alt*-1,4-phenylene) derivative with spiroanthracenyl groups (**12**) was synthesized

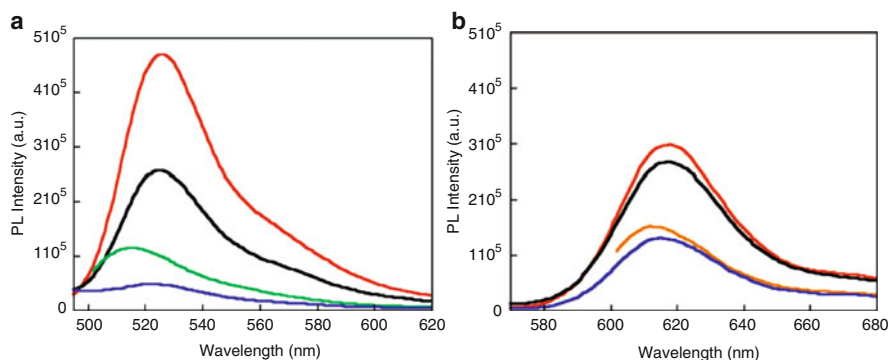


Fig. 3 PL spectra of ssDNA₁-Fl (a) and ssDNA₁-TR (b) in the presence of **1Br** (black), **9** (blue), and **10** (red) in 25 mM phosphate buffer at (ssDNA₁-Fl or ssDNA₁-TR) = 2×10^{-8} M and [RU] = 4×10^{-7} M. The excitation wavelengths are 385 nm for **1Br** and 365 nm for **9** and **10**. Direct excitation of ssDNA₁-Fl and ssDNA₁-TR prior to polymer addition is also shown in green and orange, respectively [71]

for this purpose [73]. The 10*H*-spiroanthracenyl groups are orthogonal to the main backbone vector but do not contribute to electron delocalization of the backbone, which also serve as “molecular spacers” to effectively shield the backbone and increase the donor–acceptor distance upon complexation with dye-labeled nucleic acid. FRET between **12** and ssDNA₈-Fl was studied and compared with **11** which have nearly the same energy levels as **12**. These polymers have similar polymer fluorescence quenching upon addition of ssDNA₈, while the polymer-sensitized Fl emission is totally different. As shown in Fig. 4, excitation of **11** results in negligible Fl emission, whereas strong Fl emission is obtained by using **12** as the energy donor. Likewise, Woo et al. have shown that changing the counterions of **1Br** from bromide into tetraphenylborate can also minimize PET process, which was attributed to increased donor–acceptor distance owing to the increased size of counterions [74].

To optimize the molecular orientation (*k*), nonlinear CCP and star-shaped CCP oligomer were synthesized. The introduction of *m*-phenyl groups into **1Br** leads to a CCP (**13**, Scheme 8) with nonlinear “kinks” along the backbone [75]. It was found that although there is a progressive blueshift in absorption with increasing *m*-phenyl content, FRET efficiency is increased, leading to twofold more intense polymer-sensitized fluorescence of dsDNA₈-Fl (dsDNA₈-Fl was obtained by hybridization of the ssDNA₈-Fl with ssDNA₉: 5'-AGC ACC CAC ATA GTC AAG AT-3') as compared to that of **1Br**. A water-soluble cationic tetrahedral molecule **14** was also synthesized, and the energy transfer from **14** to dsDNA₈-Fl was studied and compared with its arm and **1Br** [76]. The results show that **14** provides the highest Fl emission intensity. Fig. 5 shows the comparison of FRET between **1Br** and **14** to

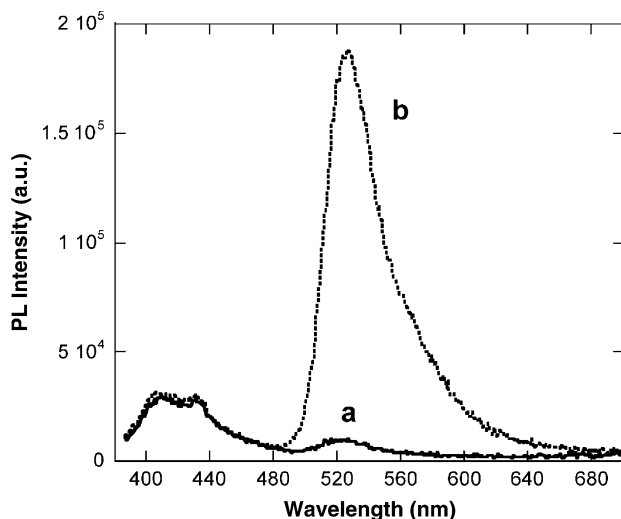
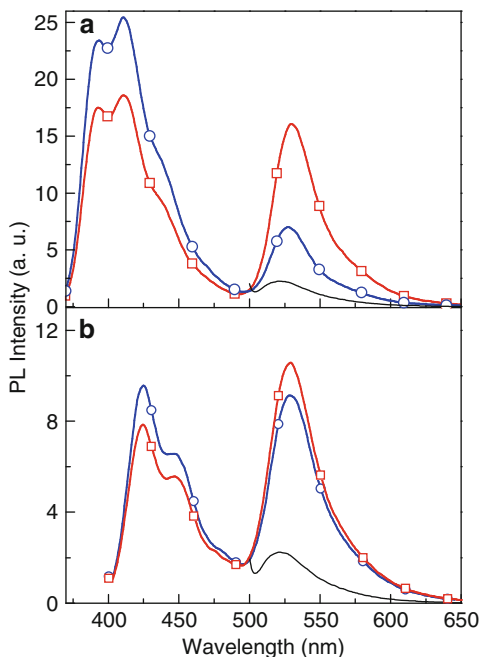


Fig. 4 PL spectra of (a) **11**/ssDNA₈-Fl and (b) **12**/ssDNA₈-Fl in water at pH = 8: ([ssDNA₈-Fl] = 1.5×10^{-8} M, [**12**] = [**11**] = 3×10^{-7} M); excitation at 380 nm. The spectra are not normalized according to the polymer emission [73]

Fig. 5 PL spectra from solutions containing **14**/ssDNA₈-Fl (**a**, circles), **14**/dsDNA₈-Fl (**a**, squares), **1**/ssDNA₈-Fl (**b**, circles), and **1Br**/dsDNA₈-Fl (**b**, squares) in 25 mM phosphate buffer. Excitation wavelength is 352 nm for **14** and 385 nm for **1**: [ssDNA₈-Fl or dsDNA₈-Fl] = 2.0×10^{-8} M, [FU] = 1.2×10^{-6} M. The emission spectrum of dsDNA₈-Fl upon direct excitation of Fl at 490 nm in the absence of the donor is shown in black



dsDNA₈-Fl and ssDNA₈-Fl at [ssDNA₈-Fl or dsDNA₈-Fl] = 2.0×10^{-8} M at [Fluorene Unit] ([FU]) = 1.2×10^{-6} M. The integrated FI emission from **14**/dsDNA-Fl is over twofold more intense than that from **14**/ssDNA₁-Fl, and there is no significant difference observed between **1Br**/ssDNA₁-Fl and **1Br**/dsDNA-Fl. These results indicate that **14** has improved selectivity between dsDNA and ssDNA as compared to **1Br**. The improvement in the signal amplification for **13** and **14** should arise from the fact that they have multiple-transition dipole moment orientations relative to the linear counterpart polymer **1Br**.

To match the biosensors using different acceptor chromophores, the emission spectra of CCPs were turned to improve the spectral overlap ($J(\lambda)$). Previous reports have shown that interchain FRET within CPs is more efficient than intrachain FRET due to stronger electronic coupling and increased transfer dimensionality for interchain relative to intrachain interactions [77]. Complex formation between the polymer and oppositely charged DNA molecules induces polymer aggregation and increases the local concentration of 2,1,3-benzothiadiazole (BT) units, leading to enhanced interchain contacts and improved electronic coupling between optical partners. The fundamental information inspired the design of CCPs with donor-acceptor architecture for improved spectral overlap with dye-labeled nucleic acid [78]. A cationic poly(fluorene-*alt*-1,4-phenylene) derivative containing 5 mol% BT units (**15**) was synthesized. In dilute solutions, the polymer emits blue with an emission maximum at 380 nm. Upon addition of ssDNA, green emission ranging from 500 to 650 nm dominates the solution fluorescence because of the enhanced

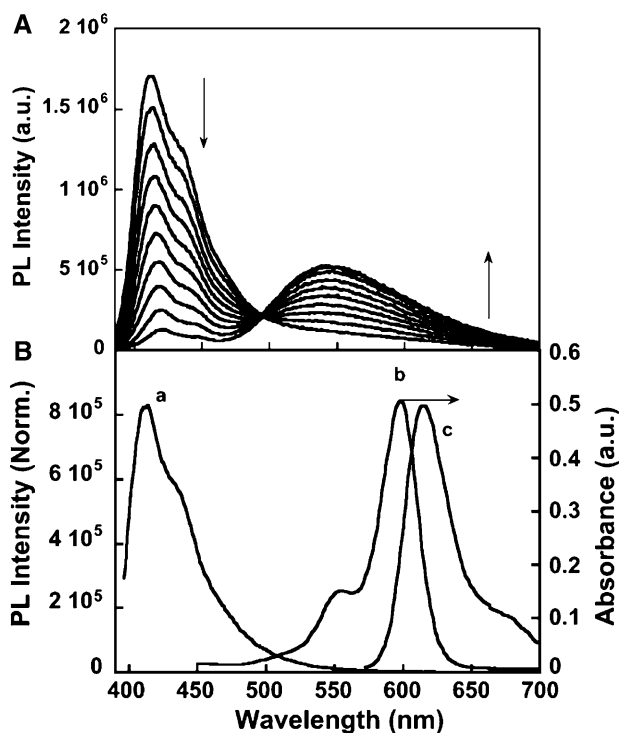


Fig. 6 (A) PL spectra of **15** in water as a function of [ssDNA] ([RU] = 5×10^{-7} M, [ssDNA] = 0 M to 2.7×10^{-8} M in 3.0×10^{-9} M increments; excitation at 380 nm. (B) (a) Normalized PL spectra of **1**, (b) absorption and (c) emission spectra of ssDNA₁-TR in water [77]

FRET within DNA/**15** complexes as shown in Fig. 6. Thus, the spectral overlap between the polymer and TR-labeled nucleic acid is improved relative to that of **1Br**, allowing for efficient FRET to red light-emitting dyes. In addition, in conjunction of a PNA₁-Cy5, where Cy5 is a standard red-emitting dye, a multicolor DNA sensor was obtained. Depending on the solution content, the colors of solution fluorescence are blue, green, and red in the absence of DNA, and in the presence of the noncomplementary ssDNA (ssDNA₂) and the complementary DNA (ssDNA₁), respectively, as demonstrated in Fig. 7.

Apart from copolymerization of low-energy sites into the backbones of CCPs, end-capping was used to construct intramolecular energy transfer architectures for CCPs. A cationic phenylethynyl anthracene (PEA) end-capped cationic polyfluorene (PF) (**16**) was synthesized [79]. Efficient energy migration from the bulky high-energy backbone to the minority low-energy end-cappers within this polymer was witnessed by the strong fluorescence at 452 nm (end-capper) and the weak fluorescence at 425 nm (backbone) in dilute aqueous solution. In addition, the end-capper emission tends to increase in the presence of DNA because the complexation between DNA and **16** induces polymer aggregation and thus enhances intramolecular and

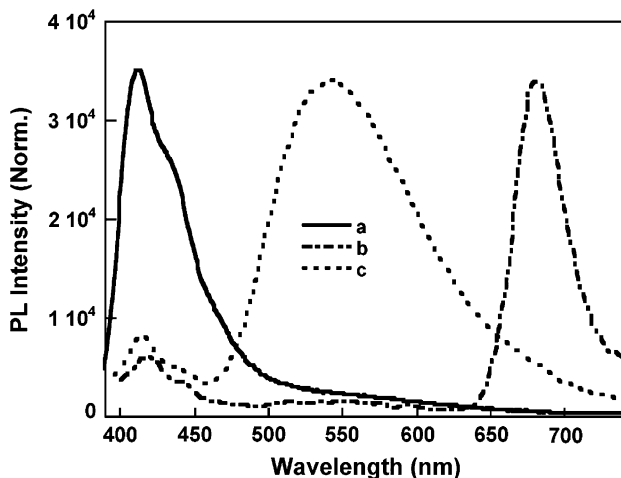


Fig. 7 Normalized PL spectra in water of (a) **15**/PNA₁-Cy5, (b) **15**/ss-DNA₁/PNA₁-Cy5, and (c) **15**/ss-DNA₂/PNA₁-Cy5: (PNA₁-Cy5) = 2.0×10^{-8} M, [RU] = 1.6×10^{-7} M; excitation at 380 nm [77]

intermolecular FRET from the fluorene backbone to the end-cappers. As a consequence, the aggregates of **16** have a better spectral overlap with the acceptor absorption as compared to its uncapped counterpart **17**. Thus, the polymer-sensitized dye emission of ssDNA₈-F1 for **16** is five fold stronger than that for **17**, which ultimately results in better fluorescence contrast between complementary and non-complementary DNA for **16** relative to that for **17**.

In addition to the modulation of the backbone structure of CCPs for improved FRET, we find that the side chains also have an impact on the donor and acceptor self-quenching upon complexation. The effect of CCP charge density on polymer-sensitized dye emission was investigated using three cationic PF derivatives (**17**, **18** and **19**) [80]. The facile functionality at fluorene C-9 position enables to vary the side chains of cationic PFs without substantially changing their optoelectronic properties (energy levels). On the basis of previous studies, ssDNA₈-TR was chosen as the signaling probe to minimize the interference of PET process and to facilitate the study of charge density effect. The absorption and emission spectra of **17**, **18** and **19** in water are similar because of the same electronic backbone structure. The emission maxima for **17**, **18**, and **19** are 426, 421 and 426 nm, respectively. Thereby, similar overlap between the polymer emission and TR absorption is present. Polymers **17**, **18**, and **19** also have similar quantum yields in water, which were measured to be 0.46, 0.50, and 0.50, respectively. Energy transfer studies between these polymers and ssDNA₈-TR were conducted in water at fixed [ssDNA₈-TR] = 2×10^{-8} M (based on strands) with φ (φ is the ratio of polymer positive charges relative to ssDNA negative charges) ranging from 0 to 1.05. The largest difference in TR emission intensity for **19**/ssDNA₈-TR relative to **17**/ssDNA₈-TR and **18**/ssDNA₈-TR is observed at $\varphi = 1.05$ where [RU] = 2.1×10^{-7} M. The

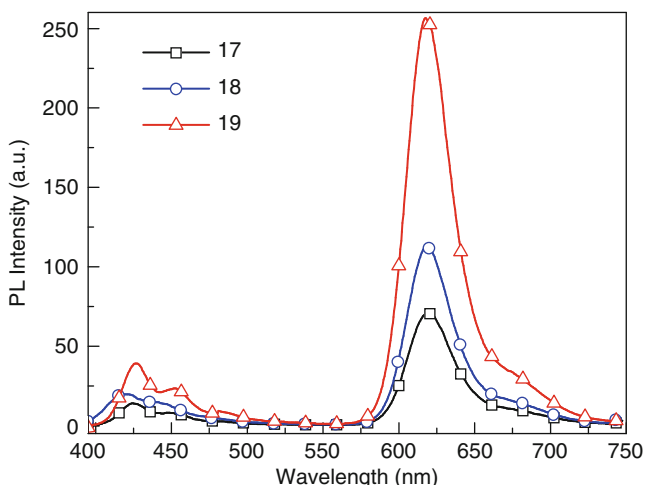


Fig. 8 The emission spectra of CCP/ssDNA₈-TR mixtures in water with [ssDNA₈-TR] = 2×10^{-8} M, and (FU) = 2.1×10^{-7} M (excitation at 385 nm)

PL spectra at this saturation point are shown in Fig. 8. The sensitized TR emission from **19**/ssDNA₈-TR is 2.3-fold more intense than that for **18**/ssDNA₈-TR, and is 3.6-fold more intense than that for **17**/ssDNA₈-TR. Detailed study of the TR fluorescence quenching upon ssDNA₈-TR/CCP complex formation reveals that the fluorescence quenching of TR emission is the lowest for ssDNA₈-TR/**19**. The reduced TR fluorescence quenching originates from the decreased local dye concentration within the **19**/ssDNA₈-TR complexes. These data highlight that reduction of the CCP charge density can lead to increased CCP-sensitized C* emission mainly as a result of the reduced C* fluorescence quenching within the CCP/DNA-C* complexes.

According to the above examples, to optimize FRET between CCPs and dye-labeled nucleic acid from the viewpoint of molecular structure, it is first necessary to examine the donor/acceptor energy levels and the fluorescence behaviors of the donor or the acceptor within the CCP/PNA-C* or DNA-C* complexes in addition to spectral overlap, orientation and distance between the donor and the acceptor. Mismatched energy levels can lead to PET that competes with the FRET process, leading to low or even neglectable CCP-sensitized dye emission. The probability of PET process can be minimized by the introduction of functional groups on the polymer backbone to fine-tune the HOMO and LUMO energy levels of the donor or the incorporation of molecular spacer to slightly increase the donor-acceptor distance. With the same electronic backbone structure, further improvement in CCP-sensitized dye emission can be accomplished by reducing the charge density of CCPs, which mitigates the acceptor quenching within CCP/DNA complexes.

In addition to optimization of molecular structures, small variations in the assay operation conditions can also induce similar effects for improved polymer-sensitized dye emission [40]. For instance, introduction of organic solvent into buffer can discourage PET owing to decreased dielectric constant of the solvent

mixture as compared to that of buffer [81]; dilution of dye-labeled probe using unlabeled ssDNA or cationic surfactant can relax the compaction of the complex structures, leading to minimized acceptor self-quenching [82]; addition of nonionic surfactant increases the quantum yields of donors and reduces donor self-quenching upon complexation with DNA as a result of the incorporation of CCP molecules into the surfactant micelles [83, 84]; and utilization of silica nanoparticles (NPs) as the sensing venue to immobilize DNA can further reduce acceptor quenching and also allow excess DNA probes on the NP surface to capture CCPs, leading to increased local concentration of donor units [85, 86].

3 Protein Biosensor

Since many diseases do not have a specific genetic signature, but rather have a variation in protein expression, biosensors for protein detection are of particular significance in medical diagnostics and pathogen recognition [87]. However, proteins are much more complex and sensitive than oligonucleotides, which merit additional severe considerations in the course of assay design [88]. Immunoassays are conventional methods based on specific antibody–antigen recognition for protein detection. Enzyme immunosorbent assay (ELISA) is the most widely used immunoassay in clinics, which requires antibodies to be immobilized on the substrate to capture antigens and the secondary antibodies [89]. The enzymes attached to the secondary antibodies serve as the catalyst to generate detection signals. Despite its high sensitivity, ELISA demands tedious protein modification, surface immobilization, blocking and washing and is limited by the availability of commercial antibodies. Thus, there is an ever-growing and urgent demand for developing new protein detection strategies that are simple and economical, with high selectivity and sensitivity.

CPEs have been explored for protein detection based on nonspecific interaction induced perturbation in their photophysical properties. Fluorescence quenching of CPEs in the presence of proteins via electron transfer or aggregation mechanisms allowed protein discrimination according to the pattern of Stern–Volmer quenching constants [90–92], and a protein sensor array has been built with six water-soluble poly(*p*-phenylene ethynylene)s (PPEs) by Bunz’s group [93]. These works provide important fundamental information about how proteins interact with CPEs and in turn affect the polymer fluorescence, which form a reference basis to be consulted during the design of CPE-based protein sensor involving FRET protocols.

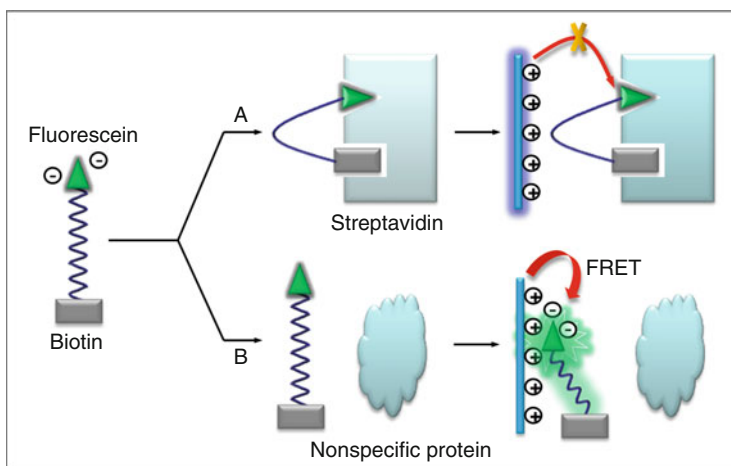
3.1 Antibody–Antigen Based Sensor

FRET-based protein biosensors have been developed using CPEs as the light-harvesting donors in conjugation of “lock–key” recognition. Streptavidin is a

tetrameric protein that binds up to four molecules of biotin with the dissociation constant estimated to be 4×10^{-14} M. In 2004, Zheng and Swager reported FRET experiments between a biotin-substituted PPE and three different dye-labeled streptavidins [94]. Among these dye-labeled streptavidins, TR-labeled streptavidin showed the highest FRET-induced dye fluorescence upon excitation of the biotin-substituted PPE, which was followed by rhodamine B-labeled streptavidin and then FI-labeled donor streptavidin. Of significance is the fact that a structurally similar PPE without biotin groups gave no observable FRET-induced dye emission, indicating the importance of specific antibody–antigen interaction in controlling FRET.

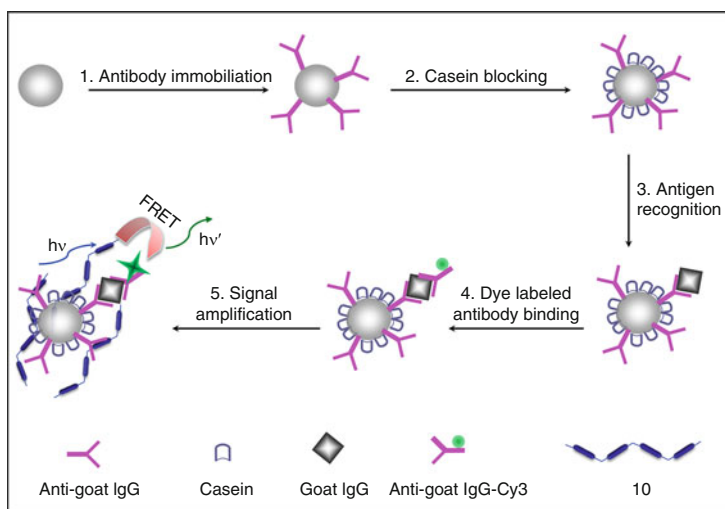
In 2006, Wang et al. reported a specific streptavidin assay using **1Br** as the light-harvesting donor and F1-labeled biotin (F1-B) as the acceptor probe [95]. The working mechanism of this assay is illustrated in Scheme 9. Addition of analyte proteins into the solution of F1-B leads to two situations. Situation A refers to the target protein, streptavidin. The biotin moiety of F1-B strongly associates with streptavidin and F1 is deeply buried in the adjacent vacant binding sites. Thus, after the addition of **1Br** into the mixture solution, although there are strong electrostatic interactions between **1Br** and the F1-B/streptavidin complexes, the distance between **1Br** and F1-B does not meet the requirement for FRET. As a result, the F1 fluorescence is weak. Situation B corresponds to a nonspecific protein, such as BSA. Under these conditions, F1-B remains separated from the protein. Therefore, electrostatic attraction between oppositely charged **1Br** and F1-B can bring them into close proximity, leading to efficient FRET from **1Br** to **F1** and thus strong F1 fluorescence. The discrepancy in F1 emission intensity thus allows one to distinguish streptavidin from other proteins.

Recently, we reported a CPE-amplified silica NP-based immunoassay for IgG detection [96]. Silica NPs (100 nm) were used as the substrate in view of their small size and high surface-to-volume ratio for maximum protein loading, which could



Scheme 9 Schematic illustration of streptavidin assay operation

provide improved assay performance relative to those based on planar microwells or glass substrates [97]. In addition, the antibody-immobilized silica NPs allowed for efficient target capture and thorough interference isolation by simple centrifugation, washing–redispersing procedures. CCP **10** and Cy3-labeled anti-goat IgG were chosen as the donor and acceptor, respectively. The assay scheme is shown in Scheme 10. Antigoat IgG–NP is first prepared by conjugating anti-goat IgG onto triazine-functionalized silica NPs. The free triazine groups on the NP surface are further blocked by casein to minimize the nonspecific interaction between antigoat IgG–NP conjugates and interference proteins. Goat IgG is then captured by antigoat IgG–NP conjugates, which is followed by the formation of a sandwich structure with the signaling antigoat IgG–Cy3 to afford fluorescent NPs. CCP **10** is then introduced into the NP suspension. Electrostatic attractions between the protein and **10** bring Cy3 and the polymer into close proximity to allow for efficient FRET, consequently yielding amplified Cy3 emission. On the contrary, in the presence of nonspecific proteins, the NPs remain nonfluorescent because of the inexistence of the sandwich structure, and thus no FRET occurs upon addition of the polymer. Fig. 9 shows the PL spectra of antigoat IgG–NP after incubation with goat IgG, thrombin, and BSA in the presence of **10** upon excitation at 370 nm. Intense Cy3 fluorescence at 575 nm is observed for the NP suspension incubated with goat IgG, while very weak Cy3 fluorescence is observed for NPs with thrombin and BSA treatment. The fluorescence intensities at 575 nm of anti-goat IgG NPs incubated with nonspecific proteins (BSA and thrombin) are less than 6% of that generated by goat IgG, resulting in a high signal-to-noise ratio of ~ 17 . The limit of detection for IgG is calculated to be ~ 1.1 ng/mL, which is comparable to other NP-based fluoroimmunoassay containing multiple dye molecules [98]. In addition, a seven-fold improvement in the limit of detection is achieved in the presence of **10** as



Scheme 10 Schematic illustration of the CCP-amplified NP-based fluoroimmunoassay

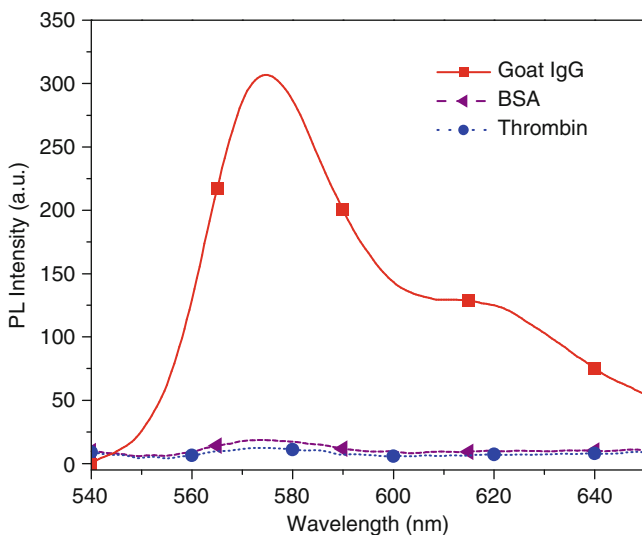
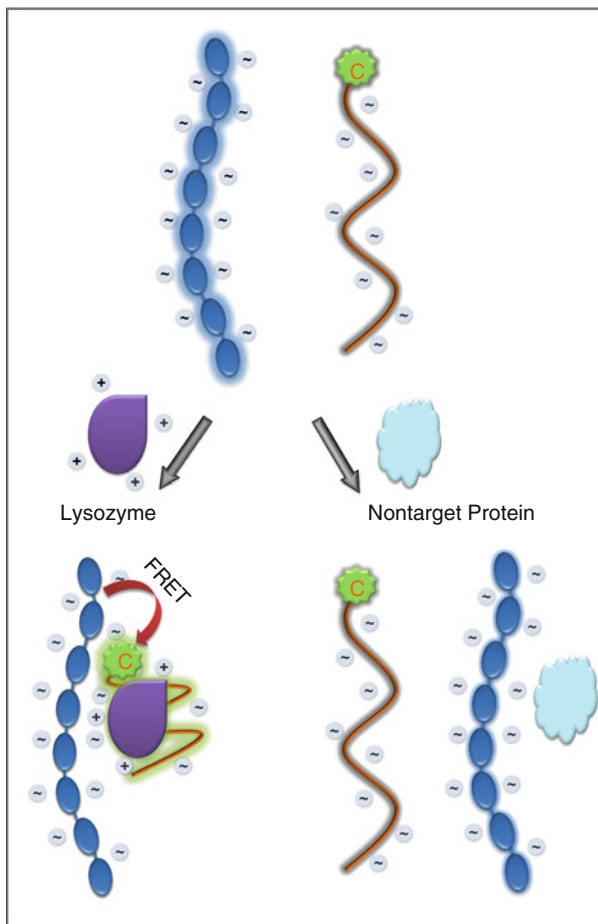


Fig. 9 PL spectra of the NP suspension in the presence of **10** (8 μM) for antigoat IgG-NPs (0.2 mg) incubated with various proteins (1 $\mu\text{g}/\text{mL}$) and subsequent treatment with antigoat IgG-Cy3 (0.18 mg/mL), excitation at 370 nm

compared to that upon direct excitation of Cy3 in the absence of **10**, as a result of efficient FRET. This study highlights that utilization of CPE as the energy donor can impart signal amplification and eliminate cross-talking fluorescence for protein immunoassays, which provides an opportunity to minimize the experimental errors and to improve the detection sensitivity.

3.2 Aptamer-Based Sensor

The specific aptamer-protein interaction has recently been used for protein detection with high selectivity [99]. Aptamers are artificial nucleic acids selected in vitro with high affinity to proteins and other biological compounds. In comparison with traditional specific antibody-antigen recognition, the application of aptamer as the probe has several advantages, which include easy preparation, stability, reusability and general availability for almost any protein. Recently, we reported a strategy for lysozyme detection that took advantage of specific aptamer/protein interaction and aptamer/protein complexation mediated FRET between an ACP and a dye-labeled aptamer [100]. The working mechanism for the assay is displayed in Scheme 11, which involves poly[9,9-bis(4'-sulfonatobutyl)fluorene-co-alt-1,4-phenylene] sodium salt (**5**) and a 6-carboxylfluorescein (FAM) labeled lysozyme aptamer as the energy donor and acceptor, respectively. ACP **5** was chosen as the light-harvesting molecule because of its high quantum yield in water (~ 0.9 in water) and



Scheme 11 The lysozyme detection mechanism (*left*) and the chemical structure (*right*) of poly [9,9-bis(4'-sulfonatobutyl)fluorene-co-alt-1,4-phenylene] sodium salt (**5**)

good emission spectral overlap with the absorption of FAM. The detection starts with a solution composed of **5** and FAM-labeled lysozyme aptamer. Since both the polymer and the aptamer are negatively charged, they separate from each other because of electrostatic repulsion and FRET does not occur in solution upon excitation of **5** at 370 nm. Thus, as shown in Fig. 10, there is no FAM emission initially. In the presence of lysozyme, the aptamer specifically binds to lysozyme, forming a complex with net positive charge. As a result, electrostatic attraction between **5** and the aptamer/lysozyme complex occurs to bring **5** and dye into close proximity for FRET to light up the FAM emission (Fig. 10). In the presence of nonspecific proteins, there is no recognition between the lysozyme aptamer and proteins, and the aptamer surface charge remains negative. The distance between the lysozyme aptamer and the polymer remains too far for

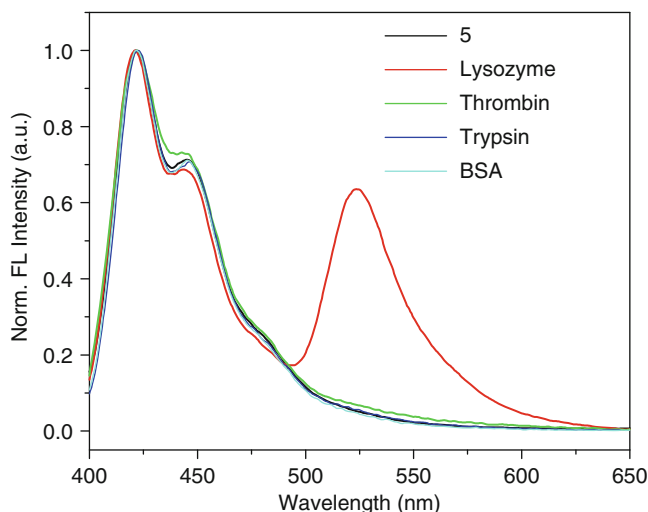
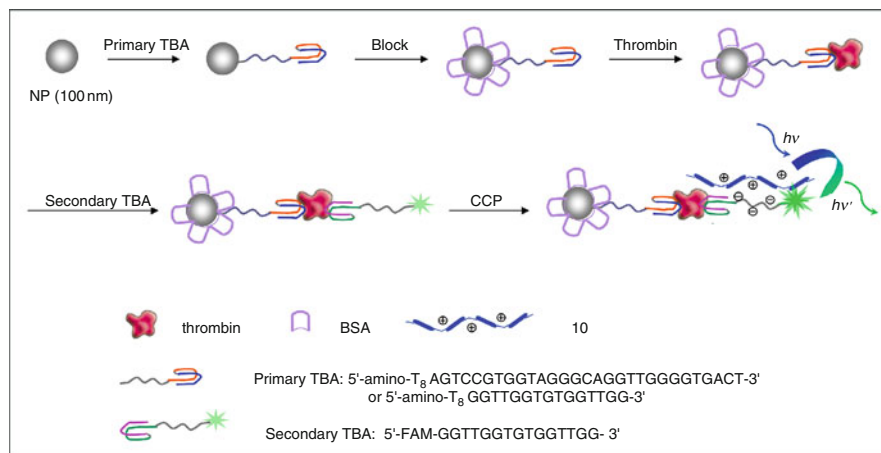


Fig. 10 Normalized PL spectra of **5** alone and **5** with FAM-labeled lysozyme aptamer preincubated with lysozyme, thrombin, trypsin and BSA, respectively: [FAM-labeled lysozyme-aptamer] = 4.5×10^{-8} M, [lysozyme] = 2.4 mg/mL in 5 mM Tris buffer; [**5**] = 4.6×10^{-7} M in 5 mM Tris buffer; Excitation at 370 nm

FRET to occur, and thus no FI emission is observed. The specificity of this assay was also examined for mixed samples. The mixed lysozyme samples were prepared in fetal bovine serum (FBS), human saliva and human urine. It was found that FAM emission was still visible upon addition of each mixed sample, implying that this assay has a great potential for the detection of real biological samples. This study illuminates that introduction of specific aptamer/protein interaction as the recognition event, and utilization of FRET as the signal transduction channel, is an effective way to develop CPE-based protein sensors with good specificity.

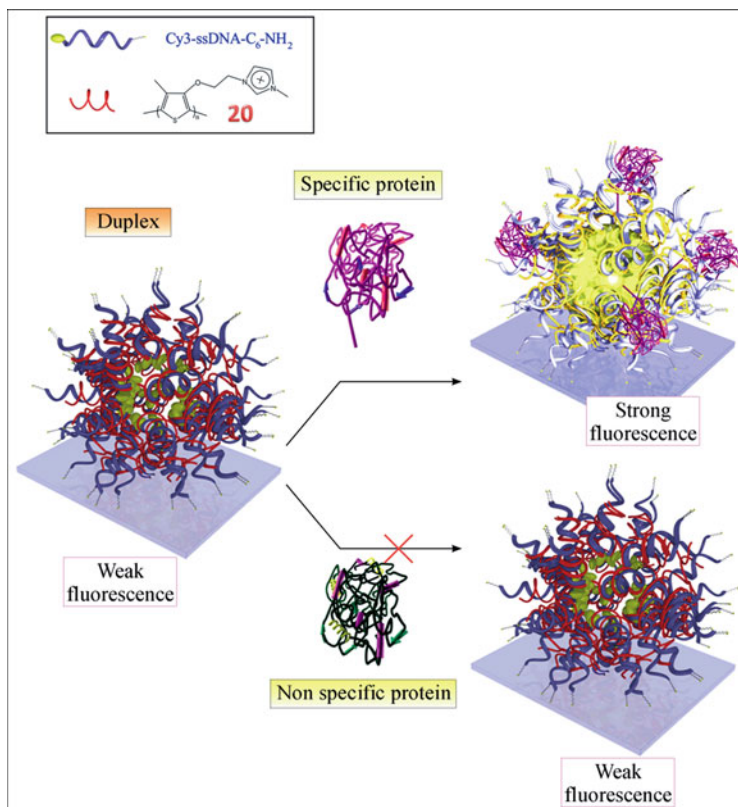
We also utilized CCP and aptamer-functionalized silica NPs to develop a sandwich assay for optical detection of thrombin in biological media with high sensitivity and selectivity [101]. CCP **10** and FI were chosen as the donor and the acceptor, respectively. The assay scheme is shown in Scheme 12. The primary thrombin-binding aptamer (TBA) is covalently attached to triazine-functionalized silica NPs, which is followed by BSA blocking on the free sites of NP surface. During the sensing process, TBA forms an intramolecular G-quartet (known as the guanine tetrad that consists of four guanine bases in a square planar array arranged in a cyclic hydrogen-bonding pattern, where each guanine is both the donor and acceptor of two hydrogen bonds) and recognizes the active site of thrombin, affording thrombin-bound TBA-NPs. The FI-labeled secondary TBA is then added to associate with the remaining thrombin binding sites, resulting in the dye-containing NPs. Finally, addition of CCP **10** into the NP suspension induces FRET, leading to amplified FI emission. In contrast, in the presence of nonspecific proteins, the primary TBA-immobilized NPs cannot capture the FI-labeled secondary TBA



Scheme 12 Working principle of CCP-amplified NP-based thrombin detection

and no polymer-sensitized FI emission is observed after addition of **10**. Therefore, thrombin detection can be easily realized by monitoring the amplified FI emission of NPs. On the basis of this assay, a thrombin detection limit of 1.06 nM is obtained. Moreover, the NP-based assay can be conducted in blood serum, which benefits from its solid-state detection platform that allows eliminating nonspecific adsorption through centrifugation–washing–redispersing circles. On the other hand, the successful detection of lysozyme in a similar manner also highlights the generality of this protein assay scheme.

Protein biochip for thrombin detection was also reported by Leclerc's group using the complex of a cationic polythiophene (**20**) and dye-labeled ssDNA aptamer as the FRET-based probe as illustrated in Scheme 13 [102]. The complex probe was prepared by stoichiometrically mixing CCP **20** with 3'-Cy3-labeled ssDNA aptamer. Two ssDNA sequences were used, one was the specific thrombin aptamer, ssDNA₉-Cy3 (5'-NH₂-C₆-GGTTGGTGTGGTTGG-Cy3-3'), and the other was the random ssDNA, ssDNA₁₀-Cy3 (5'-NH₂-C₆-GGTGGTGGTTGTGGT-Cy3-3'). The presence of amine group at the 5'-end of the ssDNA aptamer allows the complex of **20**/ssDNA to covalently binding onto treated glass slides to form the solid-state array. In the presence of thrombin, a significant fluorescence intensity increase is observed for the spots with **20**/ssDNA₉-Cy3 complexes (binding sequence). In the presence of two nonspecific proteins, BSA and immunoglobulin E (IgE), the fluorescence intensities of the spots remain low, revealing an excellent specificity of the detection with respect to the target. On the other hand, the spots with **20**/ssDNA₁₀-Cy3 complexes (nonbinding sequence) do not exhibit fluorescence enhancement for human thrombin, confirming the specificity of the detection in terms of the complex probe. Correlation of the fluorescence intensities as a function of protein concentration using the spots of **20**/ssDNA₉-Cy3 reveals a limit of detection of $\sim 1.5 \times 10^7$ molecules for human thrombin (i.e., 6.2×10^{-11} M in 0.4 μ L) together with a very good specificity. This work highlights that biochips can



Scheme 13 Illustration of the specific detection of target proteins by using the complex of a cationic polythiophene(21)/dye-labeled ssDNA aptamer on glass slides. Reproduced with permission from [102]

be established by taking advantage of CPEs in association with dye-labeled aptamers, which opens new feasibilities for simple and rapid multiplex analysis in proteomics.

3.3 CPE Complex Based Sensor

In addition to protein detection using specific antibody/antigen and aptamer/protein interactions, array detection was demonstrated based on nonspecific interactions between the CPE/dye-labeled ssDNA complexes and proteins [103]. The design concept is motivated by the fact that external agents can effectively perturb the electron coupling of optical units within the complex of CPE/ssDNA-C* and in turn vary the FRET-induced fluorescence of both CPE (donor) and C* (acceptor). Owing to discrepancies in local hydrophobic and charged domains of different

proteins, it is suggested that the concerted action of both the higher order aggregate structure and the ssDNA sequence/length would lead to differential responses to protein structures. A series complexes of a cationic conjugated oligomer (**21**, chemical structure in the inset of Fig. 11) and ssDNA–FAM with different sequences were used to form complex-based FRET probes to generate an array fluorescence response toward proteins. For detection, **21**/ssDNA–FAM solutions is prepared by mixing ssDNA–FAM (5.7×10^{-6} M, based on nucleotide bases) with **21** (1.0×10^{-6} M) in potassium phosphate/sodium hydroxide buffer solution (50 mM, pH = 7.4). The charge ratio between **21** and ssDNA is kept at 0.7 in order to avoid precipitation. As shown in Fig. 11, addition of proteins into the solution of **21**/ssDNA results in fluorescence intensity decreases in both the emission of **21** at 400 nm and the FRET sensitized FAM emission at 525 nm. More importantly, the FRET-induced fluorescence is sensitive to ssDNA sequence, allowing for cross-check of the detection reliability. The fluorescence response of **21**/ssDNA was also examined upon addition of other proteins, including myoglobin, lysozyme, hemoglobin, BSA, PS–BSA, PT–BSA, PY–BSA, streptavidin, proteinase K, T4 PNK, T4 DNA, DNA polymerase, and Taq polymerase. The resulting protein-dependent fluorescence changes were patterned and subjected to principle component analysis (PCA). PCA is a mathematical transformation used to extract variance between entries in a data matrix, by reducing the redundancy in the dimensionality

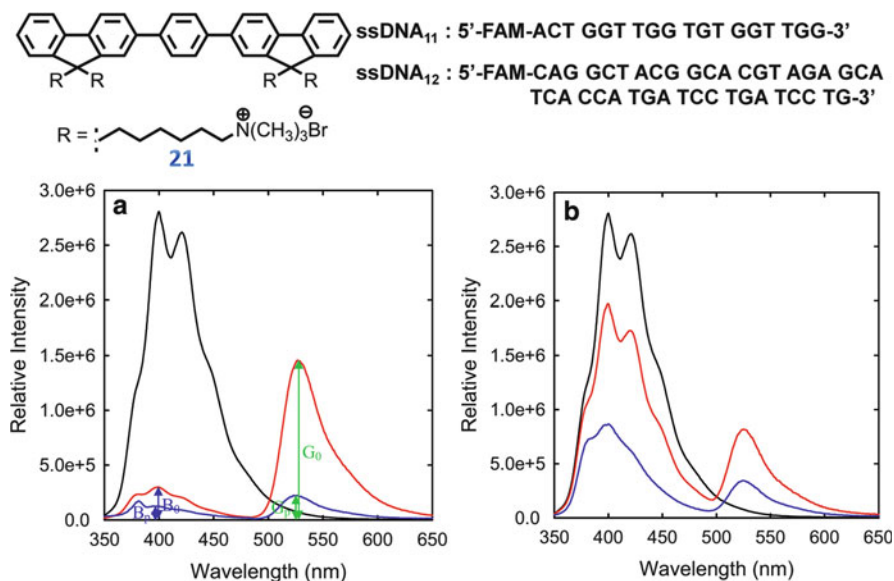
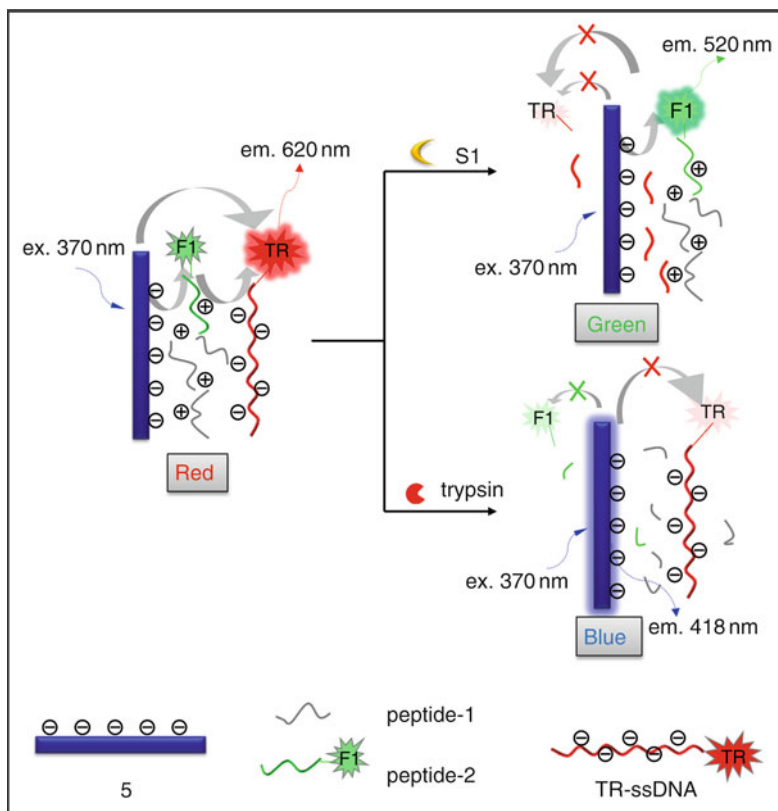


Fig. 11 Chemical structure of **21**, the sequences of ssDNA₁₁ and ssDNA₁₂, and PL spectra of **22** (1.0×10^{-6} M) before (black), after (red) the addition of (a) ssDNA₁₁-FAM and (b) ssDNA₁₂-FAM (5.7×10^{-6} M, nucleicbase), and after addition of 10 ng/mL thrombin (blue). Measurements were done in PBS (pH = 7.4) by excitation at 338 nm. Reproduced with permission from [103]



Scheme 14 Schematic representations of the assay for nucleases and protease detection based on the complex of ACP, DNA-TR and peptide-FI

of the data. The fluorescence pattern and the PCA score plots enabled to effectively distinguish 18 proteins from each other. Although this array cannot be used for protein quantification and is less suitable for mixed samples, it has good reliability and versatility for the detection of purified proteins.

Recently, we reported a complex-based FRET assay capable of detecting protease and nuclease in one solution, which relied on a peptide-mediated combinatorial FRET between an ACP and TR-labeled ssDNA [104]. The working mechanism of the assay is shown in Scheme 14. A solution of **5**, peptide-1 (Arg-Arg-Arg-Arg-Arg-Arg-Arg-Arg-Arg-Arg), peptide-2 (Arg-Arg-Arg-Arg-Arg-Arg-Arg-Arg-Arg-FI), and ssDNA₈-TR is prepared, within which FRET among **20**, FI, and TR occurs because of the formation of multicomponent complexes. Before enzyme digestion, excitation of **5** at 380 nm leads to dominant TR emission (red) in the solution fluorescence as shown in Fig. 12. In the presence of trypsin, the peptides are digested into fragments, giving rise to relatively weak electrostatic attraction between peptide fragments and **5**. Under these conditions, the complexes become

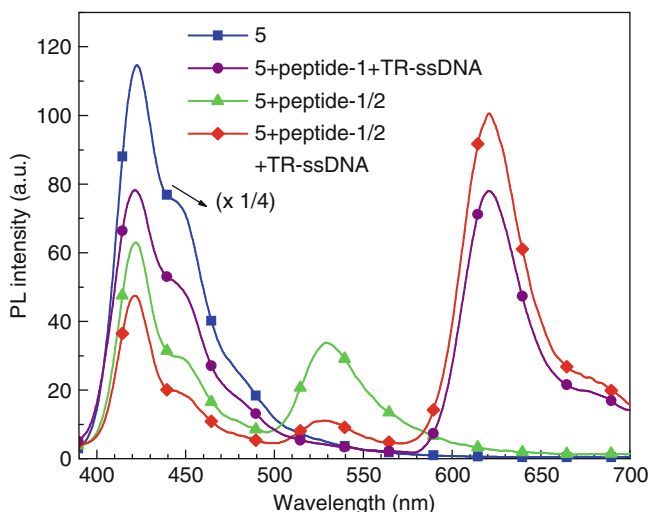


Fig. 12 PL spectra of **5**, **5**/peptide-1,2, **5**/peptide-1/TR-ssDNA and **5**/peptide-1,2/TR-ssDNA upon excitation at 370 nm. [**5**] = 1×10^{-7} M based on RU, [peptide-1] = 4.5×10^{-8} M, [peptide-2] = 5×10^{-9} M, [ssDNA₈-TR] = 2×10^{-9} M

loose, and thus TR emission gradually decreases, and finally the polymer emission dominates the solution fluorescence (blue). On the other hand, in the presence of S1 nuclease, ssDNA₈-TR is digested, which cause the release of TR from the complexes. In this case, the TR emission intensity progressively decreases while the emission intensity for both FI and **5** increases, ultimately leading to green fluorescence of the solution. Accordingly, the cleavage of peptide or DNA by trypsin or S1 nuclease can disturb the FRET within the complex of ACP/peptide-FI/DNA-TR, which allows the detection and monitoring of both protease and nuclease activity in the same solution.

4 Summary

In light of the sensory systems elucidated herein, it is clear that CPEs have formed an intriguing basis for the construction of advanced FRET-based biosensors capable of detecting a variety of chemical and biological substances. Facile modification of the molecular structures of CPEs provides opportunities to fine-tune their optoelectronic properties and charge natures to match specific sensory applications. Within these sensors, CPEs not only participate in the signal transduction to diagnostic fluorophores but also serve as powerful light-harvesting donors to amplify signaling fluorescence, ultimately leading to greatly enhanced sensitivity relative to small-molecular fluorophore assays. Both electrostatic and hydrophobic interactions between CPEs and dye-labeled probes or analytes play an

indispensable role in the control of distance-mediated signal transduction and in turn the operation of these FRET-based sensors. The differences in such interactions in the absence and presence of target species determine the signal-to-noise ratio and the detection reliability. Noteworthy is that different pairs of CPEs and biomolecules interact with each other differently according to their charge sign and hydrophobic natures. In addition, to obtain high FRET efficiency, the pair of CPE and acceptor fluorophore should be chosen in detailed consideration of their energy level alignment, molecular orientation, spectral overlap, distance and complex structure. It is believed that more and more biosensors based on FRET between CPEs and organic dyes will be established and brought into practical applications.

References

1. Friend RH, Gymer RW, Holmes AB, Burroughes JH, Marks RN, Taliani C, Bradley DDC, Dos SDA, Brédas JL, Lögdlund M, Salaneck WR (1999) Electroluminescence in conjugated polymers. *Nature (London)* 397:121–128
2. Yu G, Gao J, Hummelen JC, Wudl F, Heeger AJ (1995) Polymer photovoltaic cells: enhanced efficiencies via a network of internal donor–acceptor heterojunctions. *Science* 270:1789–1791
3. Sirringhaus H, Tessler N, Friend RH (1998) Integrated optoelectronic devices based on conjugated polymers. *Science* 280:1741–1744
4. Hide F, Díaz-García MA, Schwartz BJ, Andersson M, Pei Q, Heeger AJ (1996) Semiconducting polymers: a new class of solid-state laser materials. *Science* 273:1833–1836
5. McQuade DT, Pullen AE, Swager TM (2000) Conjugated polymer-based chemical sensors. *Chem Rev* 100:2537–2574
6. Weber SE (1990) Photon-harvesting polymers. *Chem Rev* 90:1469–1482
7. Korri YH, Garnier F, Srivastava P, Godillot P, Yassar A (1997) Toward bioelectronics: specific DNA recognition based on an oligonucleotide-functionalized polypyrrole. *J Am Chem Soc* 119:7388–7389
8. Bunz UHF (2000) Poly(aryleneethynylene)s: syntheses, properties, structures, and applications. *Chem Rev* 100:1605–1644
9. Kim K, Bouffard J, Kooi SE, Swager TM (2005) Highly emissive conjugated polymer excimers. *J Am Chem Soc* 127:13726–13731
10. Faïd K, Leclerc M (1998) Responsive supramolecular polythiophene assemblies. *J Am Chem Soc* 120:5274–5278
11. Swager TM (1998) The molecular wire approach to sensory signal amplification. *Acc Chem Res* 31:201–207
12. Pinto MR, Schanze KS (2002) Conjugated polyelectrolytes: synthesis and applications. *Synthesis* 9:1293–1309
13. Thomas SW III, Joly GD, Swager TM (2007) Chemical sensors based on amplifying fluorescent conjugated polymers. *Chem Rev* 107:1339–1386
14. Liu B, Gaylord BS, Wang S, Bazan GC (2003) Effect of chromophore-charge distance on the energy transfer properties of water-soluble conjugated oligomers. *J Am Chem Soc* 125:6705–6714
15. Xu QH, Gaylord BS, Wang S, Bazan GC, Moses D, Heeger AJ (2004) Time-resolved energy transfer in DNA sequence detection using water-soluble conjugated polymers: the role of electrostatic and hydrophobic interactions. *Proc Natl Acad Sci USA* 101:11634–11639

16. Wang D, Gong X, Heeger PS, Rininsland F, Bazan GC, Heeger AJ (2002) Biosensors from conjugated polyelectrolyte complexes. *Proc Natl Acad Sci USA* 109:49–53
17. Fan C, Plaxco KW, Heeger AJ (2002) High-efficiency fluorescence quenching of conjugated polymers by proteins. *J Am Chem Soc* 124:5642–5643
18. Kim IK, Bunz UHF (2006) Modulating the sensory response of a conjugated polymer by proteins: an agglutination assay for mercury ions in water. *J Am Chem Soc* 128: 2818–2819
19. Zhou Q, Swager TM (1995) Fluorescent chemosensors based on energy migration in conjugated polymers: the molecular wire approach to increased sensitivity. *J Am Chem Soc* 117:12593–12602
20. Chen L, McBranch DW, Wang HL, Helgeson R, Wudl F, Whitten DG (1999) Highly sensitive biological and chemical sensors based on reversible fluorescence quenching in a conjugated polymer. *Proc Natl Acad Sci USA* 96:12287–12292
21. Kumaraswamy S, Bergstedt T, Shi X, Rininsland F, Kushon S, Xia WS, Ley K, Achyuthan K, McBranch D, Whitten DG (2004) fluorescent conjugated polymer superquenching facilitates highly sensitive detection of proteases. *Proc Natl Acad USA* 101:7511–7515
22. Pinto MR, Schanze KS (2004) Amplified fluorescence sensing of protease activity with conjugated polyelectrolytes. *Proc Natl Acad Sci USA* 101:7505–7510
23. Achyuthan KE, Bergstedt TS, Chen L, Jones RM, Kumaraswamy S, Kushon SA, Ley KD, Lu L, McBranch D, Mukundan H, Rininsland F, Shi X, Xia W, Whitten DG (2005) Fluorescence superquenching of conjugated polyelectrolytes: applications for biosensing and drug discovery. *J Mater Chem* 15:2648–2656
24. Kim J, McQuade DT, McHugh SK, Swager TM (2000) Ion-specific aggregation in conjugated polymers: highly sensitive and selective fluorescent ion chemosensors. *Angew Chem Int Ed* 39:3868–3872
25. Turro NJ (1991) *Modern molecular photochemistry*. University Science Books, Sausalito, CA
26. Phillips RL, Kim IB, Tolbert LM, Bunz UHF (2008) Fluorescence self-quenching of a mannosylated poly(p-phenyleneethynylene) induced by concanavalin A. *J Am Chem Soc* 130:6952–6954
27. Satrijo A, Swager TM (2007) Anthryl-doped conjugated polyelectrolytes as aggregation-based sensors for nonquenching multicationic analytes. *J Am Chem Soc* 129:6020–6028
28. Sun H, Feng F, Yu M, Wang S (2007) Analyte-induced aggregation of a water-soluble conjugated polymer for fluorescent assay of oxalic acid. *Macromol Rapid Commun* 28:1905–1911
29. Xue C, Cai F, Liu H (2007) Ultrasensitive fluorescent responses of water-soluble, zwitterionic, boronic acid-bearing, regioregular head-to-tail polythiophene to biological species. *Chem Eur J* 14:1648–1653
30. Ho HA, Boissinot M, Bergeron MG, Corbeil G, Doré K, Boudreau D, Leclerc M (2002) Colorimetric and fluorometric detection of nucleic acids using cationic polythiophene derivatives. *Angew Chem Int Ed* 41:1548–1551
31. Nilsson KPR, Inganäs O (2003) Chip and solution detection of DNA hybridization using a luminescent zwitterionic polythiophene derivative. *Nat Mater* 2:419–424
32. Ho HA, Najari A, Leclerc M (2008) Optical detection of DNA and proteins with cationic polythiophenes. *Acc Chem Res* 41:168–178
33. Ho HA, Leclerc M (2004) Optical sensors based on hybrid aptamer/conjugated polymer complexes. *J Am Chem Soc* 126:1384–1387
34. Nilsson KPR, Rydberg J, Baltzer L, Inganäs O (2003) Self-assembly of synthetic peptides control conformation and optical properties of a zwitterionic polythiophene derivative. *Proc Natl Acad Sci USA* 110:10170–10174
35. Li C, Numata M, Takeuchi M, Shinkai S (2005) A sensitive colorimetric and fluorescent probe based on a polythiophene derivative for the detection of ATP. *Angew Chem Int Ed* 44:6371–6374

36. Maynor MS, Nelson TL, Sullivan CO, Lavigne JJ (2007) A food freshness sensor using the multistate response from analyte-induced aggregation of a cross-reactive poly(thiophene). *Org Lett* 9:3217–3220
37. Yao Z, Li C, Shi G (2008) Optically active supramolecular complexes of water-soluble achiral polythiophenes and folic acid: spectroscopic studies and sensing applications. *Langmuir* 24:12829–12835
38. Liu B, Bazan GC (2004) Homogeneous fluorescence-based DNA detection with water-soluble conjugated polymers. *Chem Mater* 16:4467–4476
39. Bazan GC (2007) Novel organic materials through control of multichromophore interactions. *J Org Chem* 72:8615–8635
40. Pu KY, Liu B (2009) Optimizing the cationic conjugated polymer-sensitized fluorescent signal of dye labeled oligonucleotide for biosensor applications. *Biosens Bioelectron* 24:1067–1073
41. Van der Meer BW, Coker G III, Chen SYS (1994) Resonance energy transfer theory and data. VCH, New York
42. Jares-Erijman EA, Jovin TM (2003) FRET imaging. *Nat Biotechnol* 21:1387–1395
43. Gaylord BS, Heeger AJ, Bazan GC (2002) DNA detection using water-soluble conjugated polymers and peptide nucleic acid probes. *Proc Natl Acad Sci USA* 99:10954–10957
44. Wang J (2000) From DNA biosensors to gene chips. *Nucleic Acid Res* 28:3003–3010
45. Sutherland G, Mulley J, Symons RH (1989) In nucleic acid probes. CRC, Gainesville, FL
46. Fan C, Plaxco KW, Heeger AJ (2003) Electrochemical interrogation of conformational changes as a reagentless method for the sequence-specific detection of DNA. *Proc Natl Acad Sci USA* 100:9134–9137
47. Mannelli I, Minunni M, Tombelli S, Mascini M (2003) Quartz crystal microbalance (QCM) affinity biosensor for genetically modified organisms (GMOs) detection. *Biosens Bioelectron* 18:129–140
48. Patolsky F, Lichtenstein A, Willner I (2001) Detection of single-base DNA mutations by enzyme-amplified electronic transduction. *Nat Biotechnol* 19:253–258
49. Nam JM, Thaxton CS, Mirkin CA (2003) Nanoparticle-based bio-bar codes for the ultrasensitive detection of proteins. *Science* 301:1884–1886
50. Gaylord BS, Massie MR, Feinstein SC, Bazan GC (2005) SNP detection using peptide nucleic acid probes and conjugated polymers: applications in neurodegenerative disease identification. *Proc Natl Acad Sci USA* 102:34–39
51. Gaylord BS, Heeger AJ, Bazan GC (2003) DNA hybridization detection with water-soluble conjugated polymers and chromophore-labeled single-stranded DNA. *J Am Chem Soc* 125:896–900
52. Ho HA, Doré K, Boissinot M, Bergeron MG, Tanguay RM, Boudreau D, Leclerc M (2005) Direct molecular detection of nucleic acids by fluorescence signal amplification. *J Am Chem Soc* 127:12673–12676
53. Duan X, Li Z, He F, Wang S (2007) A sensitive and homogeneous SNP detection using cationic conjugated polymers. *J Am Chem Soc* 129:4154–4155
54. Xu H, Wu H, Huang F, Song S, Li W, Cao Y, Fan C (2005) Magnetically assisted DNA assays: high selectivity using conjugated polymers for amplified fluorescent transduction. *Nucleic Acids Res* 33:e83
55. Wang S, Gaylord BS, Bazan GC (2004) Fluorescein provides a resonance gate for FRET from conjugated polymers to DNA intercalated dyes. *J Am Chem Soc* 126:5446–5451
56. Liu B, Bazan GC (2007) Energy transfer between a cationic conjugated poly(flourene-cophenylene) and thiazole orange for DNA hybridization detection involving G-rich sequences. *Macromol Rapid Commun* 28:1804–1808
57. Xu QH, Wang S, Korystov D, Mikhailovsky A, Bazan GC (2005) The fluorescence resonance energy transfer (FRET) gate: a time-resolved study. *Proc Natl Acad Sci USA* 102:530–535

58. Pu KY, Liu B (2008) Intercalating dye harnessed cationic conjugated polymer for real-time naked-eye recognition of double-stranded DNA in serum. *Adv Funct Mater* 19:1371–1378
59. Li K, Liu B (2009) Conjugated polyelectrolyte amplified thiazole orange emission for label free sequence specific DNA detection with single nucleotide polymorphism selectivity. *Anal Chem* 81:4099–4105
60. Service RF (1998) Microchip arrays put DNA on the spot. *Science* 282:396–399
61. Southern EM (1996) DNA chips: analyzing sequence by hybridization to oligonucleotides on a large scale. *Trends Genet* 12:110–115
62. Liu B, Bazan GC (2005) Methods for strand-specific DNA detection with cationic conjugated polymers suitable for incorporation into DNA chips and microarrays. *Proc Natl Acad Sci USA* 102:589–593
63. Lee K, Rouillard JM, Pham T, Gulari E, Kim J (2007) Signal-amplifying conjugated polymer–DNA hybrid chips. *Angew Chem Int Ed* 46:4667–4670
64. Lee K, Maisel K, Rouillard JM, Gulari E, Kim J (2008) Sensitive and selective label-free DNA detection by conjugated polymer-based microarrays and intercalating dye. *Chem Mater* 20:2848–2850
65. Liu B, Baudrey S, Jaeger L, Bazan GC (2004) Characterization of TectoRNA assembly with cationic conjugated polymers. *J Am Chem Soc* 126:4076–4077
66. Wang S, Bazan GC (2003) Optically amplified RNA–protein detection methods using light-harvesting conjugated polymers. *Adv Mater* 15:1425–1428
67. Lakowicz JR (1999) Principles of fluorescence spectroscopy. Kluwer Academic/Plenum, New York
68. Marcus RA (1993) Electron transfer reactions in chemistry: theory and experiment. *Angew Chem Int Ed* 32:1111–1121
69. Bédas JL, Beljonne D, Coropceanu V, Cornil J (2004) Charge-transfer and energy-transfer processes in π -conjugated oligomers and polymers: a molecular picture. *Chem Rev* 104:4971–5004
70. Liu B, Bazan GC (2006) Optimization of the molecular orbital energies of conjugated polymers for optical amplification of fluorescent sensors. *J Am Chem Soc* 128:1188–1196
71. Tan CY, Atas E, Müller JG, Pinto MR, Kleiman VD, Schanze KS (2004) Amplified quenching of a conjugated polyelectrolyte by cyanine dyes. *J Am Chem Soc* 126:13685–13694
72. Turro NJ (1997) Modern molecular photochemistry. University Science Books, Mill Valley, CA
73. Woo HY, Vak D, Korystov D, Mikhailovsky A, Bazan GC, Kim DY (2007) Cationic conjugated polyelectrolytes with molecular spacers for efficient fluorescence energy transfer to dye-labeled DNA. *Adv Funct Mater* 17:290–295
74. Kang M, Nag OK, Nayak RR, Hwang S, Suh H, Woo HY (2009) Signal amplification by changing counterions in conjugated polyelectrolyte-based FRET DNA detection. *Macromolecules* 42:2708–2714
75. Liu B, Wang S, Bazan GC, Mikhailovsky A (2003) Shape-adaptable water-soluble conjugated polymers. *J Am Chem Soc* 125:13306–13307
76. Liu B, Dan TTT, Bazan GC (2007) Collective response from a cationic tetrahedral fluorene for label-free DNA detection. *Adv Funct Mater* 17:2432–2438
77. Beljonne D, Pourtois G, Silva C, Hennebicq E, Herz LM, Friend RH, Scholes GD, Setayesh S, Müllen K, Bredas JL (2002) Interchain vs. intrachain energy transfer in acceptor-capped conjugated polymers. *Proc Natl Acad Sci USA* 99:10982–10987
78. Liu B, Bazan GC (2004) Interpolyelectrolyte complexes of conjugated copolymers and DNA: platforms for multicolor biosensors. *J Am Chem Soc* 126:1942–1943
79. Dishari SK, Pu KY, Liu B (2009) Combinatorial energy transfer between an end-capped conjugated polyelectrolyte and chromophore-labeled PNA for strand-specific DNA detection. *Macromol Rapid Commun* 30:1645–1650

80. Pu KY, Fang Z, Liu B (2008) Effect of charge density on energy-transfer properties of cationic conjugated polymers. *Adv Funct Mater* 18:1321–1328
81. Liu B, Bazan GC (2007) Tetrahydrofuran activates fluorescence resonant energy transfer from a cationic conjugated polyelectrolyte to fluorescein-labeled DNA in aqueous media. *Chem Asian J* 2:499–504
82. Pu KY, Pan SYH, Liu B (2008) Optimization of interactions between a cationic conjugated polymer and chromophore-labeled DNA for optical amplification of fluorescent sensors. *J Phys Chem B* 112:9295–9300
83. Hameed AAA, Andy PM (2008) Effect of surfactant on FRET and quenching in DNA sequence detection using conjugated polymers. *Adv Funct Mater* 18:2498–2509
84. Hameed AAA, Jean N, Stephen O, Andy PM (2008) Improved single nucleotide polymorphisms detection using conjugated polymer/surfactant system and peptide nucleic acid. *Biosens Bioelectron* 23:1466–1472
85. Wang YS, Liu B (2007) Label-free single nucleotide polymorphism detection using a cationic tetrahedralfluorene and silica nanoparticles. *Anal Chem* 79:7214–7220
86. Wang YS, Liu B (2007) Silica nanoparticle assisted DNA assays for optical signal amplification of conjugated polymer based fluorescent sensors. *Chem Commun* 34:3553–3555
87. Kodadek T (2001) Protein microarrays: prospects and problems. *Chem Biol* 8:105–115
88. Wright AT, Anslyn EV (2006) Differential receptor arrays and assays for solution-based molecular recognition. *Chem Soc Rev* 35:14–28
89. Lai S, Wang SN, Luo J, Lee LJ, Yang ST, Madou MJ (2004) Design of a compact disk-like microfluidic platform for enzyme-linked immunosorbent assay. *Anal Chem* 76:1832–1837
90. Kim IB, Dunkhorst A, Bunz UHF (2005) Nonspecific interactions of a carboxylate-substituted PPE with protein: a cautionary tale for biosensor applications. *Langmuir* 21:7985–7989
91. You CC, Miranda OR, Gider B, Ghosh PS, Kim IB, Erdogan B, Krovi SA, Bunz UHF, Rotello VM (2007) Detection and identification of proteins using nanoparticle–fluorescent polymer ‘chemical nose’ sensors. *Nat Nanotechnol* 2:318–323
92. Zhang Y, Liu B, Cao Y (2008) Synthesis and characterization of a water-soluble carboxylated polyfluorene and its fluorescence quenching by cationic quenchers and proteins. *Chem Asian J* 3:739–745
93. Miranda OR, You CC, Phillips R, Kim IB, Ghosh PS, Bunz UHF, Rotello VM (2007) Array-based sensing of proteins using conjugated polymers. *J Am Chem Soc* 129:9856–9857
94. Zheng J, Swager TM (2004) Biotinylated poly(p-phenylene ethynylene): unexpected energy transfer results in the detection of biological analytes. *Chem Commun* 24:2798–2799
95. An L, Tang Y, Wang S, Li Y, Zhu D (2006) A fluorescence ratiometric protein assay using light-harvesting conjugated polymers. *Macromol Rapid Commun* 27:993–997
96. Wang Y, Liu B (2009) Conjugated polymer as a signal amplifier for novel silica nanoparticle-based fluoroimmunoassay. *Biosens Bioelectron* 24:3293–3298
97. Santra S, Zhang P, Wang KM, Tapeç R, Tan WH (2001) Conjugation of biomolecules with luminophore-doped silica nanoparticles for photostable biomarkers. *Anal Chem* 73:4988–4993
98. Yang HH, Qu HY, Lin P, Li SH, Ding MT, Xu JG (2003) Nanometer fluorescent hybrid silica particle as ultrasensitive and photostable biological labels. *Analyst* 128:462–466
99. Kirby R, Cho EJ, Gehrke B, Bayer T, Park YS, Neikirk DP, McDevitt JT, Ellington AD (2004) Aptamer-based sensor arrays for the detection and quantitation of proteins. *Anal Chem* 76:4066–4075
100. Wang J, Liu B (2009) Fluorescence resonance energy transfer between an anionic conjugated polymer and a dye-labeled lysozyme aptamer for specific lysozyme detection. *Chem Commun* 17:2284–2286
101. Wang Y, Liu B (2009) Conjugated polyelectrolyte sensitized fluorescent detection of thrombin in blood serum using aptamer-immobilized silica nanoparticles as the platform. *Langmuir* 25:12787–12793

102. Béra-Abérem M, Najari A, Ho HA, Gravel JF, Nobert P, Boudreau D, Leclerc M (2006) Protein detecting arrays based on cationic polythiophene–DNA aptamer complexes. *Adv Mater* 18:2703–2707
103. Li H, Bazan GC (2009) Conjugated oligoelectrolyte/ssDNA aggregates: self-assembled multicomponent chromophores for protein discrimination. *Adv Mater* 21:964–967
104. Zhang Y, Wang Y, Liu B (2009) Peptide-mediated energy transfer between an anionic water-soluble conjugated polymer and Texas red labeled DNA for protease and nuclease activity study. *Anal Chem* 81:3731–3737

Index

A

ABAN, 287
Acetomethoxymethyl (AM) ester, 23
Adenovirus, 79
Aggregate dimension, 141
Aggregation, 17
Aggregation-cased quenching, 295
Aggregation-induced enhanced emission (AIEE), 285, 291, 294
 γ -Aminobutyric acid, 53
3-(2-Aminoethylamino)propyltrimethoxy silane (APTMOs), 324
3-Aminophthalic acid, 73
Ammonia sensors, 213
Amplification, 3
Anions, 61, 174
Antibody–antigen based sensor, 437
Approved indocyanine green (ICG), 19
Aptamers, 161, 180, 440
Au-BSA, 351

B

Beads, 193
 stained, 203
Benzimidazolocarbocyanine, 141
Benzothiadiazole (BT), 360
BINOL, 86
Biochromism, 389
Bioimaging, 174
Biolabeling, 333
Bioluminescence, 71
Bioluminescence resonance energy transfer (BRET), 87, 92
Biomembranes, 135, 143
Biomolecules, coupling, 21
 extra-/intracellular targeting, 23

Biotin–peptide–quencher, 373
2,2'-Bipyridyl, 44
Bithiophene crown ether, 396
BODIPY dyes, 13, 27
Botulinium neurotoxin, 399
Bovine serum albumin (BSA), 153

C

C-reactive protein (CRP), 213
Calcium phosphate nanoparticles, 183
Calixarene-based ion receptor, 397
Calixarenes, 160
Cancer cells, photosensitizer, 221
Capping, 160
Carbon dioxide sensors, 89, 213
5-Carboxyfluorescein (FAM), 28
Cascade energy transfer, 119
Cascade, directed excited-state energy transfer, 119
Cationic conjugated polymer (CCP), 421
Cell penetrating peptides (CPPs), 24
Cellulose acetate (CAc), 195
Charge transfer (CT), 13, 46, 286
Chemiluminescence, 71
Chemodosimeter, 66
Chemosensors (indicator), 43, 178
Cholera toxin, 399
Chromism, 392
Chromophores, comparison, 14
CN-MBE 287, 295
Cocaine, 90, 91, 182
Coelenterazine, 92
Combinatorial synthesis, 57
Communication channels, 57
Composite materials, dye-doped beads, 214
Concanavalin A, 201, 419

- Concentration quenching, 295
 Concentrational quenching (self-quenching), 117
 Conjugated polyelectrolytes (CPEs), 417, 418
 Conjugated polymers (CPs), 82, 357, 389
 Coumarin based cyanide chemodosimeter, 68
 Coumarins, 47, 198
 Crown-ethers, 160
 Cu²⁺, 66
 Cucurbiturils (CBs), 160, 167
 Cyanines, 27, 159, 180
 Cyclam, 256, 275
 Cyclodextrins, 160, 161
 Cytochrome C, 373
 Cytotoxicity, 19, 198
- D**
- DAP, 287
 DASPE, 287, 298
 Davydov free excitons, 113
 Dendrimers, 80, 84, 180, 253, 321
 Dendrons, coordinating focal point, 270
 2,4-Diamino-5-(3,4,5-trimethoxybenzyl)
 pyrimidine (trimethoprim/TMP), 23
 Dicytlyl phosphate (DCP), 145
 Dichloro-3,3'-diethyl-9-
 phenylthiacarbocyanine chloride, 144
 4,4'-Difluoro-4-bora-3a,4a-diaza-*s*-indacenes
 (BODIPY dyes), 13, 27
 Difluoroboron dibenzoylmethane, iodine-
 substituted, 208
 1,2-Dilauroyl-*sn*-glycero-3-phosphocholine
 (DLPC), 145
 9,10-Dimethylantracene, 52
 Dimethylindole red, 180
 1,2-Dimyrystoyl-*sn*-glycero-3-phosphocholine
 (DMPC), 145
 2,4-Dinitrotoluene (DNT), 83, 371
 Dioctadecyldimethylammonium bromide, 145
 Dioxetandione, 73
 Directed energy transfer, 118
 Displacement assays, 74
 Dithiothreitol (DTT), 18
 DNA, 77, 135, 417
 assay, CCP, 421
 biosensor, 421
 detection, 400
 hybridization, 373
 J-aggregates, 146
 oligonucleotides, 311
 DNA alkyltransferase, 23
 DNazymes, 70
 Donor-acceptor stilbenes, 47
 Dual lifetime referencing (DLR), 206
- Dyes, 193
 aggregation, biomembrane-induced, 143
 dye-aptamer, 161
 Dye-cucurbiturils, 167
 Dye-doped beads, 194
 polymeric, 206
 Dye-doped silica nanoparticles (DDSNs), 229
 Dye-macromolecule complexes, 180
 Dye-rotaxanes, 160
- E**
- Electrochemiluminescence (ECL), 72
 Electron exchange interactions, 113
 Emission wavelength shifts, 379
 Encapsulation, 159
 Energy transfer, 417
 red-edge effects, 121
 Energy-transfer cassettes, 28
 Enzyme immunosorbent assay (ELISA), 437
 Ethylcellulose (EC), 195
 Europium(III) chelates, 200
 Excimers, 107, 112
 Exciplexes, 54, 112
 Excited-state intramolecular proton transfer
 (ESIPT), 44
 Exciton delocalization length, 138
- F**
- F-IDAs, 74
 Fluorescein, 19, 198
 Fluorescein diacetate (FDA), 80
 Fluorescein isothiocyanate, 80
 Fluorescence, 229
 lifetimes, 175
 quantum yield, 42
 Fluorescence enhancement factor (FEF), 48
 Fluorescence in situ hybridization (FISH), 42
 Fluorescence lifetime imaging microscopy
 (FSIM), 42
 Fluorescence recovery after photobleaching
 (FRAP), 42
 Fluorescent markers, 307
 Fluorescent nanocrystals, 80
 Fluorescent organic nanoparticles, 285
 Fluorescent reporter/sensors, 3, 135, 357
 Fluoride sensing, coumarin leuko dye, 68
 Fluorophores, 3
 binding site, 44
 catalytic production, 69
 resonance interactions, 113
 Förster resonance energy transfer (FRET), 3, 5,
 26, 88, 113, 205, 346, 357, 379, 430
 FRET-gating, 120

G

Glucarate, 53
Glucose indicator, 211
Gold, 333
Green fluorescent protein (GFP), 20, 125
Guanidine triphosphate (GTP), 76

H

Hemagglutinin (HA) lectin, 397
Hetero-FRET, 118
Hexaphenylsilole (HPS), 287, 296
Hg²⁺, 67
Homo-transfer, 117
Human serum albumin (HSA), 152
Hydrogen bonding, ground/excited states, 111
2-(2-Hydroxyphenyl)benzothiazole (HBT), 297
1-Hydroxypyrene-3,6,8-trisulfonate, 75, 198, 209
8-Hydroxy-1,3,6-pyrene trisulfonate, 76
8-Hydroxyquinoline, 44

I

Imaging, 193
 collective effects, 125
Immunoassay, 185
Indicator displacement assays (IDAs), 74
 definition, 43
Inositol-triphosphate, 75
Intermolecular interactions, 107, 109
Intramolecular charge transfer (ICT), 13, 46, 110
Intramolecular rotation, restriction, 285
Ion association, 285, 290
Ion sensors, 396

J

J-aggregates, 135, 137
JC-1/JC-9, 154

K

Kinase assay, 377

L

Labels, 3, 6, 159
 definition, 43, 108
 dye-doped beads, 212
Lanthanides, 12, 31, 269
 chelates, 3, 199
Layer-by-layer (LbL) technique, 80
Leuko dye, 66
Lifetimes, 112, 175, 229
 multiplexing, 28
Light-harvesting (antenna) effects, 107, 120
Limits of detection (LODs), 79
Liposomes, 80, 399

Localized surface plasmon resonance (LSPR), 12

Luciferase, 74, 89
Luminescence, 7, 193, 333
Luminescent sensors, 253
Luminol, 72
Lysozyme, 153

M

Magnetic beads, dye-doped polymeric, 218
Magnetic optical sensor particles (MOSePs), 220
Magnetite nanoparticles, 201
Mandelic acid, 86
Membrane potential-sensitive aggregates, 154
Mercury chemodosimeters, sulfur-based, 69
Merocyanines, 145
Metabolites, nanobiosensors, 211
Metal cations, 58
Metal cluster, 311
Metal complexes, 253
Metal-enhanced fluorescence, 184
Metal ion selectivity, 45
Metal ion sensors, quantum clusters, 350
Metal ions, 253
Metal ligand complexes, 13
Metal nanoparticle, 311
Metal quantum dots, 311
Metal-to-ligand charge transfer, 13
Metalloporphyrins, 198
Methyl viologen, 371
Microbeads, 194
 dye-doped, 204
Microparticles, 79
Mitochondria, imaging, 154
Molar absorption coefficient at the excitation wavelength, 42
Molecular aggregates, 136
Molecular sensors, 109
 silver clusters, 325
Molecular wire effect, 419
Molecule packing structure, 137
Monosaccharides, 371
Morin, 44
Multifluorophore, 54
Multiplexing, 3

N
Nanobeads, 194
Nanoclusters/nanodots, 307
Nanoparticles (NPs), 3, 79, 182
 labels, 6
Nanoscale metals, 307

- Nanosensors, water-dispersible, 207
 Nanotoxicity, 19
 Naphthalimides, 198
 Naphthoxyquinone, 62
 Ni-nitriloacetic acid (NTA), 23
 Nile Blue, 20
 Noncovalent ligand sensors, 398
 Nucleic acids, 79, 400
- O**
- O6-alkylguanine-DNA alkyltransferase, 23
 Octadecyltrichlorosilane (OTS), 397
 Oligonucleotides, 213, 311
 Organic dye nanoparticles, 285
 Organic dyes, 13
 Ormosil beads, 205, 208, 213
 Ouzo effect, 290
 Oxygen sensors, 207
 Oxyluciferin, 74
 Oxymercuration, 69
- P**
- Paraquat, 371
 quencher, 83
 Pd/Pt, 70, 198
 Peptide transduction domains (PTDs), 24
 Peptides, 317
 Perylene, 287
 pH, chromic transitions, 393
 sensors/nanosensors, beads, 209
 Phenoxazines, 198
 Phenyl-thiocarbocyanine (PTC), 152
 Phospholipase A2 inhibitors, 399
 Phosphorescent platinum(II) porphyrin (PtTFPP), 213
 Photodynamic therapy (PDT), 206
 Photoinduced charge transfer (PCT), 46
 Photoluminescence, 7
 Photon antibunching, 348
 Photosensitization, 291
 Photostability, 197, 229
 Plasmonic enhancement, 123, 200
 Plasticizers, 201
 Platinum(II) octaethylporphyrin, 208
 Poly(acrylonitrile) (PAN), 206
 Poly(acrylonitrile-*co*-acrylic acid) (PAN-AA), 195
 Poly(allylamine hydrochloride), 80, 211
 Poly(amidoamine) (PAMAM) dendrimer, 321
 Poly(arylene ethynylene)s (PAEs), 359
 Poly(decyl methacrylate), 208, 210
 Poly(9,9-dihexylfluorene), 208
 Poly(ethylene-terephthalate), 67
 Poly(fluorene-*co*-phenylene)s (PFPs), 359
 Poly(fluorenes) (PFs), 359
 Poly(*N*-isopropylacrylamide), 211
 Poly(lactic acid), 209
 Poly(methacrylic acid) (PMAA), 322
 Poly[2-methoxy-5-(*-2'*-ethylehexyloxy)-*p*-phenylene-vinylene] (MEH-PPV), 392
 Poly[3-(2-methyl-1-butoxy)-4-methylthiophene] (PMBMT), 393
 Poly(methyl methacrylate-*co*-methacrylic acid) (PMMAMA), 195, 208
 Poly(NIPAM-AA-HEA), 322
 Poly(PF/BT), 381
 Poly(phenylene ethynylene)s (PPEs), 359
 Poly(phenylene vinylenes) (PPVs), 359
 Poly(*p*-phenylene)s (PPPs), 359
 Poly(*p*-phenylene ethynylene)s (PPEs), 83, 437
 Poly(sodium 4-styrenesulfonate), 80, 211
 Poly(styrene-*b*-vinylpyrrolidone) (PS-PVP), 195, 203, 208
 Poly(styrene-*co*-maleic acid) (PS-MA), 195
 Poly(styrene-*co*-maleic anhydride), 208
 Poly(thiophene)s (PTs), 360
 Poly(vinylidene chloride-*co*-acrylonitrile), 206
 Polyacrylamide (PAAm), 195
 beads, 207, 209
 Polyacrylonitrile (PAN), 195, 214
 Polydiacetylene (PDA), 358, 397
 self-assembled sensing material, 365
 Polyethyleneimine (PEI), 18
 Polyfluorene (PF), 360
 Polylysine dendrimer, 84
 Polymers, 193
 Polymethylmethacrylate beads, 195, 203
 Polyphenylene dendrimer, 181
 Polystyrene beads, 203
 Polysulfone (PSulf), 195
 Polyvinylchloride (PVC), 195
 Porphyrin-ketones, 199
 Porpholactones, 198
 POWT, 393
 Probes, 159
 definition, 43, 109
 Protease assay, 374
 Protein biosensors, 437
 Proteins, 135, 317, 417
 aggregate formation, 151
 Pseudoisocyanines, 141, 146
 Pseudorotaxane, 160, 173
 Pt detection, 70
 PtOEP, 211
 Pyrenes, 112
 Pyrophosphate, 75

Q

- Q-FRET, 90
- Quality assurance, 30
- Quantum clusters, 333, 350
- Quantum dots, 3, 108, 307
- Quantum yields, 175, 229
- Quencher displacement, 376
- Quenching, 325
 - pathways, 366

R

- Radiative decay engineering (RDE), 184
- Reactive oxygen species (ROS), 20, 68, 211
- Red-edge effects, 107, 114
- Reporters, 6
 - fluorescent, 3
- Reprecipitation, 285, 289
- Reproducibility, 29
- Resonance energy transfer (RET), 86, 107, 380
- Resonant dyes, 286
- Rhodamines, 27, 66, 198
- RNA aptamer, 180
- Rotaxanes, 160, 169
- Ruthenium(II) polypyridyl, 198
- Ruthenium(II) tris(bipyridine), 72
- Ruthenium(II) tris(4,7-diphenyl-1,10-phenanthroline disulfonic acid dichloride), 211

S

- Scandium 1,8-bis(3-*tert*-butyl-9-acridyl)naphthalene-*N,N'*-dioxide, 77
- Semiconductor nanoparticles (quantum dots), 108
- Semiconductor QDs, 7
- Seminaphthorhodofluors, 198
- Sensor arrays, 215
- Signal amplification, 29, 41, 65
- Signal transduction, 366
- Silica nanoparticles, 229
- Silver clusters, 307
- Silver island films (SIFs), 184
- Single binding site-single fluorophore, 50
- Single-nucleotide polymorphism (SNPs), 421
- Size-dependent optical properties, 285
- Solubility, 17
- Solvation energy, 109
- Spacer-separated binding site, 50
- Spectral multiplexing, 27
- Squaraine rotaxanes, 169
- Squaraines, 159
 - cyclobut-2-enone, 67

- Squaraine-zeolite, 182
- Stabilization energy, 109
- Stain, definition, 43
- Streptaphage, 24
- Streptavidin assay, 24, 438
- Sugars, 371
- Superquenching, 107, 117, 121, 368
- Surface plasmons, 123
- Surface types, 364
- Surface-enhanced immunoassay, 185
- Suspension array, 215

T

- Tag (label), definition, 43, 108
- Tandem dyes, 28
- Terbium(III) chelates, 200
- Tetra(pentafluorophenyl) porphyrin, 199
- Tetrabenzoporphyrins, 199
- Tetracene, 287, 291
- Tetrakis(*p*-sulfonatophenyl) porphine (TSPP), 153
- Tetralactam macrocycles, anthracene-containing, 171
- Tetranaphthoporphyrins, 199
- Tetraphenylborate (TPB), 290
- Thioflavin T 319
- Total internal reflection fluorescence (TIRF) microscopy, 42
- Toxicity, 19, 198
- Transition metal complex, 3
- 2,4,6-Trinitrotoluene (TNT), 83, 371
- TRITC 19
- Turn-off/turn-on sensing, 357, 366
- Twisted intramolecular charge transfer (TICT), 298
- Two-photon emission, 347

V

- Vesicles, 143
- Virus, adenovirus, 79
 - detection systems, 397

W

- Water transfer, 10
- Wavelength converting/shifting, 107, 118, 327

Z

- Zeolites, 182
- Zinc, 84
- Zinc(II)-dipicolylamine (Zn-DPA), 171